Westfälische
Wilhelms-Universität
Münster

institut für
theoretische physik

Lattice simulation of light fermionic degrees of freedom with Wilson fermions

als Habilitationsschrift
dem
Fachbereich Physik
der
Westfälischen Wilhelms-Universität zu Münster

vorgelegt von
Federico Farchioni

2008

A Franziska

Contents

Foreword **ix**

Introduction **1**
0.1. From QED to QCD . . . 1
0.2. From QCD to lattice QCD . . . 4
0.2.1. The Wilson discretization . . . 5
0.3. Monte Carlo simulation of lattice QCD . . . 8
0.3.1. Lattice expectation values . . . 9
0.3.2. The update . . . 11
0.4. Simulation of light fermionic degrees of freedom . . . 13

I. Simulations of QCD **19**

1. Algorithmic studies **21**
1.1. Beyond Hybrid Monte Carlo . . . 21
1.2. The Two-Step Multi-Boson Algorithm (TSMB) . . . 23
1.2.1. Local update . . . 23
1.2.2. Polynomial approximation . . . 24
1.2.3. Noisy correction . . . 25
1.2.4. Measurement correction . . . 26
1.2.5. Sign of the fermion measure . . . 27
1.2.6. Optimization . . . 27
1.3. Simulation tests of TSMB with light fermions [Alg] . . . 28
1.3.1. Cost figure . . . 30
1.3.2. Results for the cost figure with TSMB . . . 31
1.3.3. Eigenvalue spectrum of the fermion matrix . . . 32
1.3.4. Chiral logs? . . . 33

2. Lattice QCD and chiral perturbation theory **35**
2.1. Chiral Perturbation Theory (ChPT) . . . 36
2.1.1. Gasser-Leutwyler coefficients from phenomenology . . . 39
2.2. Gasser-Leutwyler coefficients from lattice QCD . . . 40
2.2.1. Partially quenching . . . 41

2.2.2. Including lattice artifacts . . . 43
2.3. Determination of the Gasser-Leutwyler coefficients [Chi-1,Chi-2,Chi-3] . 46
2.3.1. Setup . . . 48
2.3.2. Strategy . . . 49
2.3.3. Numerical results . . . 51
2.3.4. Discussion . . . 53

3. Simulation of twisted mass QCD (TMQCD) 57
3.1. Introduction . . . 57
3.2. Twisted mass Wilson fermions . . . 58
3.2.1. Positivity of the fermion measure . . . 60
3.2.2. $O(a)$ improvement . . . 60
3.3. The phase structure of lattice QCD with Wilson fermions . . . 63
3.3.1. ChPT predictions . . . 64
3.3.2. Adding the twisted mass term . . . 66
3.4. Study of the phase diagram of TMQCD [Wil-1, Wil-2, dbW-1, dbW-2] 67
3.4.1. Algorithmic developments . . . 68
3.4.2. Wilson plaquette action [Wil-1] . . . 69
3.4.3. Scaling of the phase diagram [Wil-2] . . . 70
3.4.4. DBW2 gauge action [dbW-1, dbW-2] . . . 72
3.4.5. Tree-level Symanzik improved gauge action . . . 74
3.5. Determination of the twist angle ω [dbW-1,dbW-2] . . . 75
3.5.1. Numerical determination of ω . . . 76
3.5.2. Renormalization constants . . . 77
3.5.3. Physical quark mass and pion decay constant . . . 77
3.6. Large-scale simulations of $N_f = 2$ TMQCD [tlS-1] . . . 78
3.6.1. Simulation and analysis . . . 79
3.6.2. ChPT analysis . . . 80
3.6.3. Isospin breaking . . . 80
3.7. First simulations of $N_f = 2{+}1{+}1$ TMQCD [tlS-2] . . . 81
3.7.1. Lattice formulation for the split doublet . . . 83
3.7.2. Simulation algorithm . . . 83
3.7.3. Tuning . . . 84
3.7.4. Physical fields and currents . . . 86
3.7.5. Numerical simulations . . . 87
3.7.6. Conclusions . . . 88

Summary and conclusions of part I 91

II. Simulations of $\mathcal{N} = 1$ SYM and one flavor QCD 95

4. Simulation of $\mathcal{N} = 1$ SYM and one flavor QCD **97**
4.1. $\mathcal{N} = 1$ SUSY Yang-Mills theory (SYM) . . . 98
4.1.1. The model . . . 99
4.1.2. Euclidean theory . . . 101
4.2. Quantum features of $\mathcal{N} = 1$ SYM . . . 101
4.2.1. $\mathrm{U}(1)_\mathrm{R}$ symmetry and its fate . . . 101
4.2.2. Color confinement and bound states spectrum . . . 103
4.3. Lattice formulation of $\mathcal{N} = 1$ SYM . . . 105
4.3.1. The Curci-Veneziano lattice action . . . 107
4.3.2. First studies . . . 109
4.4. SUSY Ward identities on the lattice [SYM-1] . . . 109
4.4.1. Lattice SUSY Ward identities . . . 110
4.4.2. Renormalization . . . 111
4.4.3. Insertion operators . . . 113
4.4.4. Simulation . . . 114
4.4.5. Results from the SUSY Ward identities . . . 115
4.5. Volume source technique revisited [SYM-2] . . . 116
4.5.1. Improved volume source technique (IVST) . . . 116
4.5.2. Comparing IVST with stochastic source methods . . . 117
4.6. Study of the bound state spectrum of $\mathcal{N} = 1$ SYM [SYM-3] . . . 118
4.6.1. Gauge samples . . . 119
4.6.2. Gluino mass and massless limit . . . 119
4.6.3. Spectrum . . . 120
4.7. One flavor QCD . . . 122
4.8. First study of the bound state spectrum of one flavor QCD [Nf1] . . . 123
4.8.1. Simulation . . . 124
4.8.2. Hadron spectrum . . . 125
4.8.3. Partially quenched viewpoint . . . 125

Summary and conclusions of part II **127**

Bibliography **131**

Publications **145**
[Alg] *Numerical simulation tests with light dynamical quarks* . . . 147
[Chi-1] *Partially quenched chiral perturbation theory and numerical simulations* . . . 149
[Chi-2] *Quark mass dependence of masses and decay constants of the pseudo-Goldstone bosons in QCD* . . . 151
[Chi-3] *Quark mass dependence of pseudoscalar masses and decay constants on a lattice* . . . 153
[Wil-1] *Twisted mass quarks and the phase structure of lattice QCD* . . . 155
[Wil-2] *Lattice spacing dependence of the first order phase transition for dynamical twisted mass fermions* . . . 157

[dbW-1] *The phase structure of lattice QCD with Wilson quarks and renormalization group improved gluons* 159
[dbW-2] *Numerical simulations with two flavors of twisted-mass Wilson quarks and DBW2 gauge action* 161
[tlS-1] *Dynamical twisted mass fermions with light quarks* 163
[tlS-2] *Numerical simulation of QCD with u, d, s and c quarks in the twisted-mass Wilson formulation* 165
[SYM-1] *The supersymmetric Ward identities on the lattice* 167
[SYM-2] *The volume source technique for flavor singlets: A second look* . . . 169
[SYM-3] *The low-lying mass spectrum of $\mathcal{N} = 1$ SU(2) SUSY Yang-Mills theory with Wilson fermions* 171
[Nf1] *Hadron masses in QCD with one quark flavour* 173

Foreword

This work covers recent advances in the Monte Carlo simulation of lattice gauge field theories containing light fermionic degrees of freedom. This aspect assumes special relevance in the lattice simulation of QCD, the non-Abelian gauge theory describing the dynamics of quark color at the basis of strong interactions.

The lattice approach represents the only way to access important quantities in hadron physics which cannot otherwise be computed by standard analytical techniques. Past lattice simulations of QCD were however confined to unphysically large values for the *up* and *down* quark masses. In nature, these are the two lightest quarks, with mass much lighter than the typical energy-scale of the underlying theory. The low-energy dynamics of strong interactions is heavily affected by this feature of QCD and must be therefore reproduced in an accurate way by simulations; large systematic errors are otherwise introduced in the final estimates. Unfortunately, the lightness of the *up* and *down* quarks besides being a distinctive feature of QCD also introduces non-trivial technical difficulties in the simulation process. The simulation of QCD in realistic conditions emerges as a computational challenge.

A dramatic progress has been witnessed in recent years in this field and now, for the first time, lattice simulations of QCD with light quark masses near, or even at, their physical values are possible. At the basis of this important achievement is not only an increased computing power available for lattice computations, but also, and this is the main point of this review, a substantial progress in the optimization of the lattice formulations and of the simulation algorithms. These aspects are considered in the first part of the review, which focuses on the simulation of QCD with light *up* and *down* quarks, in the original Wilson formulation first (Chapters 1 and 2) and thereafter in the so-called "twisted mass" formulation (Chapter 3). First simulations with the inclusion of the heavier *strange* and *charm* quarks are reviewed in the last section of this part.

The second part of the review is dedicated to the simulation of two "exotic" models, in the sense that they do not find application in the real world. The first is a gauge field theory characterized by supersymmetry, the supersymmetric Yang-Mills model (SYM); the second is a modification of QCD in which just one quark species, or "flavor", is included, "one flavor QCD". These two theories are in some sense related: the first is obtained from the second by replacing the Dirac spinor of the quark with a Majorana spinor. This affinity can be made more rigorous in a generalization of the two theories with a large number of colors: an exact equivalence can indeed be proven in the limit of infinite number of colors.

As is well known, supersymmetry is expected to play a role in particle physics at high energies, while it is broken at low energies. Non-perturbative effects in supersymmetric gauge theories, not accessible to analytical techniques, are nevertheless relevant since they can provide the necessary symmetry breaking at low energies. The supersymmetric Yang-Mills model offers a simplified framework in which such non-perturbative effects can be studied. The relationship between SYM and one flavor QCD on the other side, could help in understanding non-perturbative mechanisms in a non-supersymmetric (and therefore less symmetric) theory as QCD.

The simulation of light fermionic degrees of freedom represents a central issue in this second part of the review as well. Supersymmetry must be softly broken on the lattice by a small gluino mass and recovered in the limit of a massless gluino. In this limit the distinctive features of the theory related to supersymmetry, such as specific patterns in the particle mass spectrum, can be verified. On the basis of the above mentioned equivalence, "relics" of supersymmetry are expected in one flavor QCD, with three colors of massless quarks, in particular in the low-lying hadron spectrum.

The following Introduction contains a brief overview on (lattice) QCD and the basics of its Monte Carlo simulation. We refer to the standard monographs on the argument, for example [139], for more details about the Wilson lattice formulation of QCD and its Monte Carlo simulation. The last section of the Introduction presents a brief excursus on some aspects related to the simulation of light fermionic degrees of freedom, from which a more extended motivation for the main topic of this review should emerge.

The original publications, on which this review is based, are reported in the Appendix and are marked in the text with special reference labels ([Alg], [Chi-1], etc.). Each of the four chapters of this write-up contains an introductory part, which is intended to provide a wider perspective for these works. More space has been devoted to those aspects which are not (yet) standard in the lattice literature, such as for example details on the multi-boson simulation algorithm, chiral perturbation theory, the twisted mass formulation, the main features of SYM and its lattice formulation. A summary of the main results of the different works is given in specific sections towards the end of each chapter. A brief overall summary is also given at the end of each part.

The material presented here is the result of a collaboration work. I thank all my coauthors, the members of the Hamburg-Münster-Rome, qq+q and European Twisted Mass collaborations for pleasant and stimulating collaboration work. I wish to thank in particular István Montvay for having introduced me to the challenges of dynamical simulations and Gernot Münster and all the members of our research group for the nice work atmosphere at the Institute for Theoretical Physics of the WWU University of Münster. Last but not least, a special thank goes to my wife Franziska for continuous encouragement and endless patience during the completion of this work.

Münster, May 2008 Federico Farchioni

Introduction

0.1. From QED to QCD

Quantum field theories based on a gauge principle appear to be extraordinarily successful in describing quantum phenomena in high-energy physics. The first, simplest, and perhaps most striking example is given by Quantum Electro-Dynamics (QED), the theory of quantum phenomena in electromagnetism. A theory of this kind is expected to apply for the nuclear or "strong" interactions, too.

As is well known, QED is a quantum field theory characterized, like its classical counterpart, by gauge invariance and is therefore a gauge theory. The classical Lagrangian density describing photon-electron interactions,[1]

$$\mathcal{L}_{QED}(x) \;=\; -\frac{1}{4}F_{\mu\nu}(x)F^{\mu\nu}(x) \;+\; \bar{\psi}(x)\,[\gamma^{\mu}\,(i\partial_{\mu} \;+\; e\,A_{\mu}(x)) - m]\psi(x)\;, \tag{0.1}$$

is invariant under gauge transformations of the electron and photon fields

$$\psi(x) \;\;\rightarrow\;\; \mathrm{e}^{ie\alpha(x)}\,\psi(x)\;, \tag{0.2}$$

$$A_{\mu}(x) \;\;\rightarrow\;\; A_{\mu}(x) + \partial_{\mu}\alpha(x)\;. \tag{0.3}$$

The transformation of the electron field can be interpreted as a local, namely depending upon the space-time coordinate x, transformation under the Abelian group U(1); QED is an *Abelian* gauge theory.

A candidate for the underlying fermionic degree of freedom of the nuclear forces was independently proposed by M. Gell-Mann and G. Zweig in 1964, the "quark" [93, 199]. Particles observed in cosmic rays and collisions, the "hadrons", could be interpreted as composite bound states of the strong interactions, formed by two or three quarks, mesons and baryons respectively. Three *flavors* of quarks, "up" (u), "down" (d) and "strange" (s), could explain the approximate multiplet structure of the hadron spectrum in the so-called "Eightfold Way" [92, 149] on the basis of symmetry arguments.

Compared with the relatively simple case of electromagnetism, however, strong interactions soon emerged as a theoretically much more challenging problem. Indeed, nuclear forces appeared to encompass two seemingly contradictory features as *confinement* and *asymptotic freedom*. Quarks could not be observed as isolated particles: the strong interactions "confine" them inside the hadrons; however, as confirmed by a famous experiment at the Stanford Linear Collider in 1968 [30], the quarks, or spin-1/2

[1] We use natural units throughout this write-up, for which $\hbar = c = 1$.

"partons", behave as almost free particles inside the hadrons in high-energy collisions: in this regime strong interactions become weak. A decisive step towards a fundamental theory of strong interactions was therefore represented by the discovery made in 1973 by D. Gross, H. Politzer and F. Wilczek,[2] that gauge field theories with a *non-Abelian* gauge group can account for the mysterious property of asymptotic freedom, and at the same time make confinement plausible.

In the non-Abelian case, gauge transformations act on an internal quantum number of the fundamental fields. Already before Gross, Politzer and Wilczek's discovery, it was clear that, in order to be able to account for the complete hadron structure by symmetry arguments, the quarks had to possess such an "hidden" quantum number [98], the "color" [85]. Quarks with *three* different colors fitted into this scenario [100].

The theory of strong interactions emerging from these phenomenological indications is therefore a non-Abelian gauge theory with an SU(3) gauge group; the quark is assumed to transform in the *fundamental* representation of the group. The U(1) gauge transformation of the electron (0.2) is replaced in the case of the quark field by a local SU(3) transformation:

$$\psi_{qi}(x) \;\rightarrow\; \sum_{j=1}^{3} \left[\mathrm{e}^{ig_0 \sum_{c=1}^{8} \alpha_c(x) T^c} \right]_{ij} \psi_{qj} \;, \quad i = 1, \ldots, 3 \;, \tag{0.4}$$

where $T^c, c = 1, \ldots, 8$, are the eight generators of SU(3), i, j denote the colors, and g_0 is the universal coupling constant of the strong interactions, analogous to the electric charge in electromagnetism.

The puzzle of the strong interactions was completed with the observation, made in 1973 by H. Fritzsch, M. Gell-Mann and H. Leutwyler [85], that the gauge field of nuclear forces, analogous to the four-potential of QED, should transform in the *adjoint* representation of the gauge group SU(3). This implies that *eight* different colors are associated to it. It is convenient to write in this case the gauge field $A^a_\mu(x), a = 1, \ldots, 8$, in a matrix notation:

$$A_\mu(x) \;=\; \sum_{c=1}^{8} A^c_\mu(x) T^c \;; \tag{0.5}$$

the transformations for the matrix field read:

$$A_\mu(x) \;\rightarrow\; g(x) A_\mu(x) g^{-1}(x) - \frac{i}{g_0} (\partial_\mu g(x)) g^{-1}(x) \;, \tag{0.6}$$

with

$$g(x) \;=\; \mathrm{e}^{ig_0 \sum_{c=1}^{8} \alpha_c(x) T^c} \;. \tag{0.7}$$

Observe that (0.6) can be seen as a generalization of (0.3) in the case of a non-Abelian group. The particles described by the gauge fields, known as *gluons*, are in analogy with the photons of QED the carriers of the nuclear forces; they are responsible for the binding of the quarks inside hadrons.

[2] 2004 Nobel laureates in physics.

We see, therefore, that a fundamental theory of the strong interactions is a theory of the dynamics of the color quantum number, which assumes here the role of the electric charge in electromagnetism. In analogy with QED, it is given the name of "Quantum Chromo-Dynamics" (QCD).

The QCD Lagrangian is the straightforward generalization of the Lagrangian (0.1) for the case of a non-Abelian gauge group:

$$\begin{aligned}
\mathcal{L}_{QCD}(x) &= \mathcal{L}^g_{QCD}(x) + \sum_{q=u,d,s,\ldots} \mathcal{L}^q_{QCD}(x) \ , \qquad (0.8)\\
\mathcal{L}^g_{QCD}(x) &= -\frac{1}{4}\sum_{c=1}^{8} F^c_{\mu\nu}F^{c\,\mu\nu} \ , \ F^c_{\mu\nu}(x) = \partial_\mu A^c_\nu(x) - \partial_\nu A^c_\mu(x) + g_0 f_{cde} A^d_\mu(x) A^e_\nu(x) \ ,\\
\mathcal{L}^q_{QCD}(x) &= \sum_{i,j=1}^{3} \bar{\psi}_{qi}(x)\left[\gamma^\mu\left(i\delta_{ij}\partial_\mu + g_0\left[A_\mu(x)\right]_{ij}\right) - m_q\,\delta_{ij}\right]\psi_{qj}(x) \ .
\end{aligned}$$

Peculiar to the non-Abelian case is the presence in the field strength tensor of terms which are bilinear in the gauge fields and proportional to the structure constants of the Lie algebra associated with the gauge group f_{abc}; from these terms stem self-interactions of the gauge fields which have no counterpart in the Abelian case.

We have previously mentioned that quarks are characterized, besides color, by another quantum number, the *flavor*. It is in the meanwhile clear that *six* different quark flavors exist in nature: besides u, d and s, "charm" (c), "bottom" (b) and "top" (t). Observe that the different quark flavors appear essentially in the same way in the QCD Lagrangian, the only difference being represented by the mass m_q associated with each flavor. The latter mass is characterized by a pronounced hierarchy; indeed, one finds (approximately)

$$m_u : m_d : m_s : m_c : m_b : m_t = 1 : 2 : 40 : 500 : 1{,}700 : 74{,}000 \ . \qquad (0.9)$$

The u and d quark masses turn out to be small compared to the typical QCD energy scale, Λ_{QCD}; this means that the dynamics of the two lightest quarks plays a decisive role down to the lowest end of the QCD particle spectrum. In opposition, the b and t quarks are heavy and their role is less pronounced at low energies; the s and c quarks occupy an intermediate position; in particular the s quark is expected to give a sizeable contribution to the low-energy dynamics.

The QCD Lagrangian assumes an extra symmetry when some of the quark flavors become massless. With N_0 massless quark flavors, the QCD Lagrangian is invariant under unitary transformations mixing the different N_0 massless flavors with a definite chirality (chiral multiplet); independent transformations associated to, respectively, the left-handed (L) and right-handed (R) massless flavors define the *chiral symmetry*

group:

$$\mathrm{SU}(N_0)_L \ : \ \begin{cases} \psi_q^L \to \sum_{q'=1}^{N_0} [g_L]_{qq'}\, \psi_{q'}^L \\ \bar{\psi}_q^L \to \sum_{q'=1}^{N_0} \bar{\psi}_{q'}^L\, [g_L^{-1}]_{q'q} \end{cases} \qquad \mathrm{SU}(N_0)_R \ : \ \begin{cases} \psi_q^R \to \sum_{q'=1}^{N_0} [g_R]_{qq'}\, \psi_{q'}^R \\ \bar{\psi}_q^R \to \sum_{q'=1}^{N_0} \bar{\psi}_{q'}^R\, [g_R^{-1}]_{q'q} \end{cases} , \tag{0.10}$$

where $q = 1, \ldots, N_0$ runs over the massless flavors and $g_{L(R)} \in \mathrm{SU}(N_0)_{L(R)}$.

The behavior of the theory at low energies is strongly influenced by the fact that, in the massless limit, the $\mathrm{SU}(N_0)_L \times \mathrm{SU}(N_0)_R$ chiral symmetry (0.10) is *spontaneously broken* by the vacuum state. The chiral symmetry of massless QCD, and the spontaneous breaking thereof, allow to draw conclusions about the interactions of the dominating degrees of freedom at low-energies. These are given by the pseudoscalar mesons (pions, kaons and eta meson). In the resulting low-energy effective theory, different properties of these particles, as for example the masses, can be determined by an expansion in the light u, d and s quark masses, which are assumed to be small, around the chiral-symmetric case. This analytical approach, known in the literature as *chiral perturbation theory* [189, 88], allows in particular to determine the functional dependence of the meson properties upon the light quark masses, when the latter are considered as external tunable parameters. As we will see in the following, this information can be used in lattice QCD in order to extrapolate lattice determinations in hadron physics, obtained for quark masses heavier than in nature for which simulations are technically feasible, to the physical u and d quark masses. The interplay between lattice QCD and chiral perturbation theory will be discussed in more detail in Chapter 2.

0.2. From QCD to lattice QCD

As we have seen, hadrons can be interpreted as bound states of quarks and gluons, whose interactions are described by QCD. In the quantized theory, hadrons are eigenstates of the QCD Hamiltonian. The QCD Lagrangian (0.8) contains therefore all the information required for the determination of hadron properties, once the few free parameters of the renormalized theory are fixed. These are given by the renormalized quark masses and coupling constant at some given energy-scale; the latter can be replaced by the more natural QCD mass-scale parameter Λ_{QCD}. The values of these seven free parameters can be fixed by requiring that QCD predictions fit with the experimental results for an equal number of hadron properties. A necessary step of this program is *solving* QCD, which however turns out to hide formidable difficulties.

One possible approach to the solution of QCD, well known from QED, is based on an expansion in the coupling constant g_0 (weak-coupling perturbation theory). The method is very successful in QED, where it allows to obtain very precise determinations. The perturbative approach is however not applicable to many relevant hadron

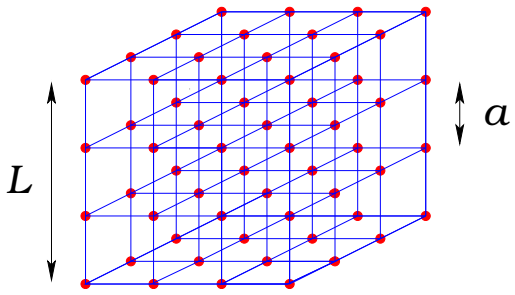

Figure 0.1.: Three-dimensional slice of an hyper-cubic lattice.

properties, starting with the masses. For such quantities indeed, QCD predicts a *non-analytical* dependence on the gauge coupling, with an essential singularity at $g_0 = 0$: in this case all the coefficients of the perturbative expansion vanish. Masses are generated in QCD by a special dynamical mechanism, known as "dimensional transmutation", which is inherently *non-perturbative*.

In a situation in which standard analytical methods fail, numerical methods may help. As we will see in the following, this is the case in a *lattice formulation* of QCD. In the lattice formulation, quark and gluon fields are no longer functions of the continuous space-time variable x: a four-dimensional Euclidean lattice manifold is introduced

$$\Lambda \equiv \{x \in \mathbb{R}^4 : \; x_\mu = a n_\mu, \; n_\mu \in \mathbb{N}, \; \mu = 1,2,3,4\} \quad (a = \text{lattice spacing}) \; ; \tag{0.11}$$

similarly to a spin system, particle fields are associated only to sites (or links) of this lattice. Since we want to deal with a finite number of total degrees of freedom, we consider here a *finite* lattice; the lattice size L should be in this case larger than the typical hadron length scale (see also in the following). Fig. 0.1 shows a three-dimensional "slice" of a 4^4 lattice.

0.2.1. The Wilson discretization

We consider here the first lattice discretization of QCD introduced by K. Wilson in 1974 [195]. In this formulation, a quark field is associated to each site of the lattice Λ; the gauge field $A_\mu(x)$ is replaced by a "link variable", a color SU(3) matrix defined through the path-ordered exponential of the gauge field along a link of the lattice:

$$A_\mu(x) \; \rightarrow \; U_\mu(x) \; = \; P \exp\left\{ i g_0 \int_x^{x+a\hat{\mu}} A_\mu(x)\, dx_\mu \right\} \; \in \; \text{SU(3)} \; ; \tag{0.12}$$

Fig. 0.2 gives a pictorial representation of the lattice quark field and link variables. With the introduction of the link variables, playing the role of parallel transporters for gauge transformations, the gauge invariance of QCD can be easily extended to the discrete case. From (0.6) and the definition (0.12) the transformation property of the link variables follows:

$$U_\mu(x) \; \rightarrow \; g(x + a\hat{\mu})\, U_\mu(x)\, g^\dagger(x) \; . \tag{0.13}$$

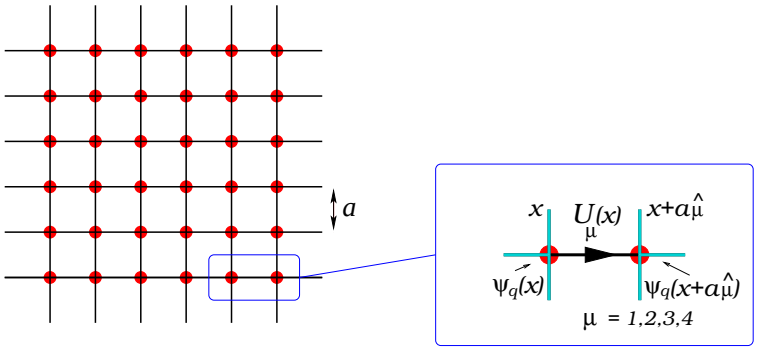

Figure 0.2.: Lattice quark fields and link variables.

The simplest lattice object of the link variables invariant under gauge transformations is the *plaquette variable*, namely the color-trace of the product of link variables along a $a \times a$ loop on the lattice (plaquette):

$$U_\Box \;=\; U_\nu^\dagger(x)\, U_\mu^\dagger(x + a\hat{\nu})\, U_\nu(x + a\hat{\mu})\, U_\mu(x) \;, \tag{0.14}$$

where μ, ν, $\mu < \nu$, define the oriented loop. See Fig. 0.3 for a pictorial representation.

Gauge invariant interactions of the link variables are constructed in terms of the plaquettes variables $U_\Box$; the action associated to the Lagrangian density $\mathcal{L}^g_{QCD}(x)$ in (0.8), containing the self-interactions of the gluon fields, is replaced on the lattice by the *plaquette action*:

$$\int dx\; \mathcal{L}^g_{QCD}(x) \;\rightarrow\; S^g_{WQCD} \;=\; \beta \sum_\Box \left(1 \;-\; \frac{1}{3}\,\Re\,\mathrm{Tr}\, U_\Box\right) \;, \quad \beta = \frac{6}{g_0^2} \;, \tag{0.15}$$

where the sum extends over all possible lattice plaquettes. Gauge invariance follows trivially from (0.13). In the limit $a \to 0$, the lattice plaquette action converges to the gluon action of QCD (in the Euclidean formulation)

$$S^g_{WQCD} \;\stackrel{a\to 0}{\longrightarrow}\; \int dx\; \mathcal{L}^g_{QCD}(x) \;=\; \int dx\; \frac{1}{4} F^a_{\mu\nu}(x) F^a_{\mu\nu}(x) \;. \tag{0.16}$$

The construction of the lattice action for the quarks relies on the definition of a gauge covariant difference operator, replacing the covariant derivative of the continuum:

$$D_\mu[A]\,\psi_q(x) \;\equiv\; [\partial_\mu \;-\; i g_0\, A_\mu(x)]\,\psi_q(x) \;; \tag{0.17}$$

on the lattice:

$$D_\mu[A]\,\psi_q(x) \;\rightarrow\; \frac{1}{a}\left[U_\mu^\dagger(x)\,\psi_q(x + a\hat{\mu}) - \psi_q(x)\right] \;\equiv\; \nabla_\mu[U]\,\psi_q(x) \;. \tag{0.18}$$

The fermion lattice action for a single quark flavor reads:

$$\begin{aligned} S^q_{WQCD} = a^4 \sum_x \bar{\psi}_q(x) \frac{\gamma_\mu}{2} (\nabla_\mu + \nabla^*_\mu) \psi_q(x) \;+\; m_{q0}\, \bar{\psi}_q(x) \psi_q(x) \\ - \underbrace{a\,\frac{r}{2}\, \bar{\psi}_q(x) \nabla^* \nabla \psi_q(x)}_{\text{“Wilson term”}} \;, \end{aligned} \tag{0.19}$$

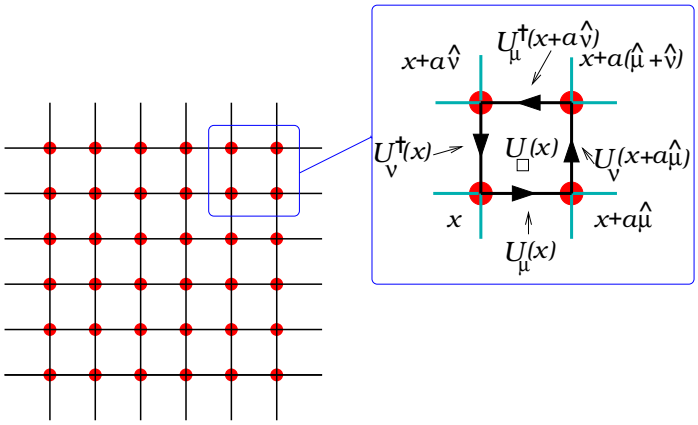

Figure 0.3.: Lattice plaquette variables.

with

$$\nabla^*_\mu[U]\,\psi_q(x) \;\equiv\; \frac{1}{a}\left[\psi_q(x) - U_\mu(x-a\hat{\mu})\,\psi_q(x-\hat{\mu})\right] \;.$$

Observe that the last term in the quark lattice action ("Wilson term") has no equivalent in the continuum theory. It is needed in order to realize the decoupling, in the limit $a \to 0$, of unphysical degrees of freedom otherwise present in the lattice theory ("doublers"). The parameter r can be set arbitrarily in the range $0 < r \leq 1$ with both signs: each value corresponds to a different lattice formulation of QCD.[3]

A more explicit expression of the quark lattice action is:

$$S^q_{WQCD} = a^4 \sum_x \frac{1}{2a} \sum_{\mu=\pm1}^{\pm4} \left[r\,\bar{\psi}_q(x)\psi_q(x) - \bar{\psi}_q(x+a\hat{\mu})U_\mu(x)(\gamma_\mu + r)\psi_q(x)\right] + m_{q0}\,\bar{\psi}_q(x)\psi_q(x) \;, \quad (0.20)$$

where we define $U_{-\mu}(x) \equiv U^\dagger_\mu(x-a\hat{\mu})$ and $\gamma_{-\mu} \equiv -\gamma_\mu$. Another parametrization, useful for numerical simulations, only involves dimensionless quantities

$$S^q_{WQCD} \;= \sum_{xy} \bar{\psi}^L_q(y)\,Q^{(q)}[U]_{yx}\,\psi^L_q(x) \;; \quad (0.21)$$

$\psi^L_q(x)$, $\bar{\psi}^L_q(x)$ are the dimensionless quark fields

$$\psi^L_q(x) \;=\; a^{3/2}(m_{q0}a + r)^{1/2}\,\psi_q(x) \;, \quad \bar{\psi}^L_q(x) \;=\; a^{3/2}(m_{q0}a + r)^{1/2}\,\bar{\psi}_q(x) \;, \quad (0.22)$$

$Q^{(q)}_{yx}$ is the *fermion matrix*, whose indices run over the sites of the lattice (color and Dirac indices are implicit):

$$Q^{(q)}[U]_{yx} \;=\; \delta_{y,x} \;-\; \kappa_q \sum_{\mu=\pm1}^{\pm4} U_\mu(x)\,(\gamma_\mu + r)\,\delta_{y,x+a\hat{\mu}} \;; \quad (0.23)$$

[3]It is normally set to one in lattice computations.

the dimensionless *hopping parameter* κ_q is related to the quark mass parameter m_{q0} by

$$\kappa_q \;=\; \frac{1}{2(m_{q0}a + 4r)} \;. \tag{0.24}$$

The Wilson term in the quark lattice action (0.19) breaks the chiral symmetry (0.10) of QCD in an explicit way. Even if the latter is expected to be recovered in the continuum limit, the symmetry breaking at finite lattice spacing introduces several (unwanted) effects in the lattice theory. One of these effects is an *additive renormalization* of the quark mass: the (bare) quark mass m_q, analogous to the quantity appearing in the continuum Lagrangian (0.8), is related to the lattice action parameter m_{q0} by:

$$m_q \;=\; m_{q0} - m_{0c} \;, \tag{0.25}$$

where $m_{0c} = f(g_0)/a$ is the additive mass renormalization diverging for $a \to 0$.

Another inconvenience deriving from the explicit breaking of the chiral symmetry in the lattice formulation is represented by large discretization errors, scaling linearly with the lattice spacing, in physical quantities. In Chapter 3 a slight modification of the Wilson discretization of QCD will be presented, which alleviates some of these problems. The fermion action associated to this new formulation is an example of an $O(a)$ *improved action*; this is a lattice formulation for which discretization errors linear in the lattice spacing are absent and only small $O(a^2)$ errors remain in lattice determinations.

After Wilson's breakthrough, different alternative lattice formulations of QCD have been devised. Another formulation often applied in lattice computations is the Kogut-Susskind formulation relying on the so-called *staggered lattice fermions* [125]. More complicated lattice discretizations of QCD with an exact chiral symmetry have been in the meanwhile constructed (Ginsparg-Wilson formulations) [95, 103, 151].

0.3. Monte Carlo simulation of lattice QCD

In the quantized lattice theory, the lattice spacing assumes the role of a regulator of the ultraviolet divergences typical of a continuum quantum field theory: taking the continuum limit of the lattice theory corresponds to removing the ultraviolet cutoff $\sim 1/a$. The renormalization group governs the dependence of the bare parameters of the (lattice) theory for fixed physical renormalized parameters. It dictates therefore how the "bare" gauge coupling g_0 should be varied with the ultraviolet cutoff $\sim 1/a$ at "constant physics". The result is a relationship between g_0 and the lattice spacing a which also involves the mass-scale parameter Λ_{QCD}: $g_0 = g_0(a\Lambda_{QCD})$.[4] By inverting this relation, one sees that the lattice spacing can be adjusted by properly varying the bare gauge coupling. Asymptotic freedom of QCD implies that the continuum limit corresponds to the weak coupling of the lattice theory $g_0 \to 0$.

[4] In a *mass independent* renormalization scheme this relation does not contain any dependence upon the quark masses.

The lattice spacing represents the natural dimensional scale on the lattice and replaces in this role Λ_{QCD}. Lattice computations deliver results for dimensionful quantities in units of the lattice spacing. In order to convert the lattice results into physical units, the lattice scale must be fixed by external input. One possibility for example is to require that the nucleon mass assumes the experimental value once translated into physical units; an analogous procedure must be applied to fix the quark masses, which can be considered as free parameters in the QCD Lagrangian.

The mathematical objects to be computed in the quantum theory in order to get information about hadron properties, are in general expectation values on the ground state, namely the vacuum state, of composite operators of the fields. The numerical techniques to be reviewed in the following are based on the Feynman quantization, in which these expectation values assume the form of path integrals over the fields. On a discrete space-time manifold, the Feynman path integrals reduce to ordinary integrals, in which each field attached to a lattice site represents an integration variable. The total amount of variables in these multiple-variable integrals, proportional to the number of lattice sites N_s, is typically very large $O(10^6 - 10^8)$ and increasing with the lattice resolution. Only a "Monte Carlo" evaluation of these integrals, with an attached statistical error, is possible in practice.

0.3.1. Lattice expectation values

The lattice expectation value of a lattice operator $O^L[U;\bar{\psi}_q,\psi_q]$, corresponding to the vacuum expectation value of a composite operator of the fields in the Euclidean theory, can be written:

$$\langle O^L \rangle \;=\; \frac{1}{\mathcal{N}} \int \prod_{x\in\Lambda} \prod_{\mu} dU_\mu(x) \prod_{q=u,d,\ldots} d\bar{\psi}_q(x) d\psi_q(x)\; \mathrm{e}^{-S_{WQCD}[U;\bar{\psi}_q,\psi_q]}\; O^L[U;\bar{\psi}_q,\psi_q] \tag{0.26}$$

where the normalization is given by

$$\mathcal{N} \;=\; \int \prod_{x\in\Lambda} \prod_{\mu} dU_\mu(x) \prod_{q=u,d,\ldots} d\bar{\psi}_q(x) d\psi_q(x)\; \mathrm{e}^{-S_{WQCD}[U;\bar{\psi}_q,\psi_q]} \quad . \tag{0.27}$$

The fermion fields, which are Grassmann variables, cannot be included in the simulation in a direct way; however they can explicitly integrated out. The Gaussian integral over the Grassmann variables delivers (up to trivial factors) the determinant of the fermion matrix (0.23)

$$\int \prod_{x\in\Lambda} d\bar{\psi}_q(x) d\psi_q(x)\; \mathrm{e}^{-S^q_{WQCD}[U;\bar{\psi}_q,\psi_q]} \;=\; \mathrm{det}Q^{(q)}[U] \;\in\; \mathbb{R}\;, \tag{0.28}$$

the so-called *fermion determinant*. The result is therefore

$$\langle O^L \rangle \;=\; \frac{1}{\mathcal{N}} \int \prod_{x\in\Lambda\,,\mu} dU_\mu(x) \prod_{q=u,d,\ldots} \mathrm{det}Q^{(q)}[U]\;\; \mathrm{e}^{-S^g_{WQCD}[U]}\; \tilde{O}[U]\;, \tag{0.29}$$

where $\tilde{O}[U]$ is an appropriate function of the lattice link variables[5]. Observe that the fermion determinant keeps track of the quark dynamics in this effective theory of the lattice links.

Assuming positivity of the quark measure resulting from the product of the fermion determinants, the expression on the RHS of Eq. (0.29) can be interpreted as a *statistical expectation value* of $\tilde{O}[U]$ with multivariate probability density

$$P[U] \;=\; \frac{1}{\mathcal{N}} \prod_{q=u,d,\ldots} \mathrm{det}Q^{(q)}[U] \;\; \mathrm{e}^{-S^g_{WQCD}[U]} \;, \tag{0.30}$$

or, equivalently,

$$P[U] \;=\; \frac{1}{\mathcal{N}} \, \mathrm{e}^{-S_{eff}[U]} \;, \tag{0.31}$$

where

$$S_{eff}[U] \;=\; S^g_{WQCD}[U] \;-\; \sum_{q=u,d,\ldots} \ln\left(|\mathrm{detQ^{(q)}[U]}|\right) \tag{0.32}$$

is the effective action of the link system also including the contribution of the quark dynamics.

A Monte Carlo evaluation of the RHS of Eq. (0.29) by *importance sampling* can be obtained by generating a set of N lattice link configurations (gauge configurations)

$$\{U^{(i)}_\mu(x);\; x \in \Lambda;\; \mu = 1,2,3,4;\; i = 1,\ldots,N\} \tag{0.33}$$

distributed according to the probability (0.30). An unbiased estimator of the RHS of Eq. (0.29) is given by the average value of $\tilde{O}[U]$ over this set of configurations (ensemble):

$$\langle O^L \rangle \;=\; \langle \tilde{O}[U] \rangle|_{P[U]} \;\simeq\; \frac{1}{N} \sum_{i=1}^{N} \tilde{O}[U^{(i)}] \;\equiv\; \bar{\tilde{O}}|_N \;. \tag{0.34}$$

The sample average $\bar{\tilde{O}}|_N$ can be assumed to be a Gaussian-distributed stochastic variable, in which case the statistical error attached to the estimate is inversely proportional to the square root of the sample statistic N: $\delta(\bar{\tilde{O}}|_N) \sim 1/\sqrt{N}$. The *sign* of the fermion measure cannot be included in the importance sampling, which requires positivity of the weight function. As we will see in the following in this review, positivity is only guaranteed in special situations, as for example two quark flavors with equal mass. This means that in general the sign of the fermion determinant has to be taken into account explicitly in the final average with potential efficiency loss of the sampling.

Having found a viable numerical procedure for the estimation of the multiple-variable integrals, the next problem to face, aiming at a precise determination of the quantity (0.29), the ultimate goal of a lattice computation, is how to generate in an efficient way a large number of statistically independent configurations distributed according to the probability density (0.30). These configurations of the link system represent the basis for any lattice determination in hadron physics by lattice computations.

[5]Build in terms of the *inverse* fermion matrix (quark propagator).

0.3.2. The update

In the case of many degrees of freedom, as the one we are considering here, a Markov stochastic process turns out to be the most effective method for generating samples of configurations of the link system. In this approach, one starts from some initial link configuration $\{U_\mu^{(0)}(x)\}$, for example the "trivial" configuration

$$U_\mu^{(0)}(x) \;=\; \mathbb{1} \;, \quad \forall\ \mu \text{ and } x \in \Lambda \;; \tag{0.35}$$

a chain of configurations is produced by a *stochastic* iterative process[6]

$$U_\mu^{(i-1)}(x) \;\longrightarrow\; U_\mu^{(i)}(x) \;, \tag{0.36}$$

or *update*, characterized by a transition probability

$$P_{trans}[U \to U'] \;. \tag{0.37}$$

The set of procedures defining the transition probability (0.37), and resulting in the so-called *simulation algorithm*, must be chosen such that the target distribution (0.30) is left invariant by the update. This latter condition is usually substituted with the stronger one, but easier to prove, of *detailed balance*. Under reasonable conditions on the algorithm, this ensures that, after a transient, the configurations of the lattice system along the Markov chain are distributed according to the target probability density.

From Eq. (0.30) it is clear that any approach to this problem must involve some estimation of the fermion determinant for a given link configuration, which represents the quark contribution to the link dynamics. An *exact* computation of the fermion determinant in the update is however not affordable. Indeed, the fermion matrix is a huge matrix with order $12 \times N_s \simeq 10^7$ or larger, and the computation should be repeated many times during the update.

The first solution found to this problem, which will be briefly discussed in the following, is based on the *pseudofermion representation* of the fermion determinant [191]. In this case, one uses a relation similar to (0.28) but with an integration over *bosonic* fields instead

$$\int \prod_{x\in\Lambda} d\bar{\phi}_q(x) d\phi_q(x)\ \mathrm{e}^{-\bar{\phi}_q (Q^{(q)}[U])^{-1} \phi_q} \;=\; \mathrm{det} Q^{(q)}[U] \;; \tag{0.38}$$

observe that in the case of bosonic fields, the *inverse* matrix appears in the exponent. The pseudofermion field variables $\phi_q(x), \bar{\phi}_q(x)$ carry formally the same quantum numbers of the quark fields but assume ordinary complex values and therefore can be interpreted as random variables. Eq. (0.38) is at the basis of Monte Carlo methods with a *stochastic* evaluation of the fermion determinant, a computationally feasible task. A different representation, also allowing a stochastic evaluation of the fermion

[6] Observe that computer-based algorithms cannot be exactly stochastic; the resulting error (bias) is however normally negligible.

determinant, is the *multi-boson* representation [132]. This latter approach solves in a radical way the problem of the non-locality introduced by the inverse fermion matrix in the exponent of (0.38); it will be discussed in more detail in Chapter 1.

Due to the huge number of involved degrees of freedom, the computational costs attached to the update of the lattice system are typically very large. These costs turn out to increase very fast with the target accuracy of the computation. Two immediate sources of systematic errors in lattice computations are represented by the finite size of the four-dimensional domain and by the discretization of the space-time. As one can intuitively understand, finite-size errors can be kept under control if the lattice size L is taken to be (considerably) larger than the typical hadron scale ~ 1 fm (1 fm = femtometer = 10^{-15} or "Fermi"). Lattice computations are currently performed for $L \simeq 2 - 3$ fm. On the other side, discretization errors are small if the lattice spacing a is much smaller than the hadron size; this means normally $a \lesssim 0.1$ fm. This requires therefore four-dimensional lattices with at least $N_s = 160{,}000$ sites and 5,120,000 degrees of freedom, increasing with the lattice resolution.

Another important factor influencing the computational cost of a lattice simulation of QCD, and we are now approaching the central issue of this review, turns out to be the *lightness* of the fermionic degrees of freedom. As a result of different physical and algorithmic effects, which will be analyzed in some detail in the following, the computational cost of a simulation increases when the values of the quark masses *inserted in the simulation* are reduced (recall that the quark mass can be tuned by changing m_{0q} in the lattice QCD action (0.19)). Limitations in computational resources confined past lattice simulations to values of the u and d quark masses much heavier than in nature and in fact nearer to the physical s quark mass[7]. As a matter of fact, the extrapolation of the lattice results to the physical situation where the light quarks assume their actual masses is affected in this case by large, essentially uncontrolled systematic errors.

Recently, considerable advance has been achieved in the optimization of the algorithms with a substantial reduction of the simulation costs; new lattice formulations of QCD have been conceived with small discretization errors. Thanks to these recent progresses, the lattice community is now for the first time in a position to make realistic estimates about the computational costs required for accurate determinations in hadron physics. The general expectation is that the multi-teraflop[8] supercomputers becoming now accessible to lattice computations will allow to reach this goal.

The next and last section of this Introduction contains an excursus on the aspects related to the simulation of QCD in physical conditions. The motivation for the investigation of new simulation algorithms and lattice formulations for QCD and related

[7]Recall (0.9); as we have seen, the u and d represent in nature the lightest quarks with $m_q \ll \Lambda_{QCD}$ and, because of this feature, they are expected to strongly affect QCD dynamics down to low energies.

[8]The teraflop is a measure of computing power, corresponding to 10^{12} floating point operations per second; a typical scale for lattice computations in realistic conditions is the teraflop year, corresponding to about $3 \cdot 10^{19}$ floating point operations.

theories will hopefully emerge.

0.4. Simulation of light fermionic degrees of freedom

Including the dynamics of light fermionic degrees of freedom in lattice simulations of QCD and related theories turns out to be one of the most challenging problems in today's computational physics. The basic difficulties originate from an interplay between features of the underlying theory (and the lattice version thereof) on the one hand, and from algorithmic and computational limitations on the other. As a result, QCD had to be simulated in the past with unphysically heavy masses for the two lightest u and d quarks, larger than in nature. The systematic effects deriving from this basic artifact of lattice QCD represented the main source of theoretical uncertainty in lattice determinations in hadron physics.

The problem of the lightness of the quarks in the lattice simulation has gained more and more attention from the lattice community in recent years, becoming today one of the central issues, if not *the* central issue, of the general discussion. Developments in computer technique have also played an important role in this context: with the recent introduction of multi-teraflop supercomputers a substantially larger amount of computing power is now available for lattice calculations.

At the time of the first lattice simulations of QCD in the early 80's, the very inclusion of the dynamics of the quarks was regarded as an almost intractable problem; for a long time, a popular approach was to consider the light quarks as static (namely infinitely heavy) and to disregard them *tout court* from the simulation. This is the well-known "quenched approximation" [99]. The first problem to tackle at the time of those first simulations was the high non-locality of the interactions among the lattice links introduced by the fermion determinant. The latter, we recall, represents the fermionic contribution to the partition function of the lattice theory, to be included in the Monte Carlo simulation. The introduction later on of the idea of the *stochastic* evaluation of the fermion determinant by pseudofermion auxiliary fields [191] opened the way to modern Monte Carlo simulations of QCD with full inclusion of the dynamics of the fermions. The next aspect to face was however the *lightness* of the simulated fermions.

We confine the discussion to the case of Wilson fermions described in Sec. 0.2, which are characterized by special features in the light quark regime. Early simulations with Wilson fermions only included the two lightest quarks; these are taken for simplicity to be *degenerate*, namely with equal masses ($N_f = 2$ QCD). A simulation algorithm using pseudofermion fields, applicable and widely applied for simulations of two degenerate Wilson fermions, is the so-called Hybrid Monte Carlo algorithm (HMC) [62]. In HMC one considers the lattice links as canonical variables of an appropriate Hamiltonian function. The transition in the Markov chain is realized by a hybrid Langevin–molecular-dynamics evolution, in a fictitious time, of the canonical system of the lattice links and of their conjugate momenta; a final Metropolis correction renders the al-

gorithm exact. As it turns out, HMC with Wilson fermions[9] efficiently updates the system only for relatively heavy quarks. This fact limited past large-scale simulations of QCD with Wilson fermions in a region of unphysically heavy u and d quark masses near the s quark mass[10] (see for example [7] and [110]).

A turning point in the discussion within the lattice community was marked in the Lattice conference held in Berlin in 2001, where a first estimate of the computational costs attached to simulations with light quarks was attempted. The main conclusion was that, due to the fast increase of the computational load, the light quark masses necessary for accurate determinations in hadron physics could not be attained in the next foreseeable future, even taking into account mid-term evolution in computer technique (see for example [184]).

Some of the difficulties in the light quark regime originate actually from peculiarities of the Wilson formulation, and in particular from its explicit breaking of the chiral symmetry at finite lattice spacing. As a consequence of the chirality breaking, which causes the additive renormalization of the quark mass, the fermion matrix can become (almost) singular during the Monte Carlo update; this results in large fluctuations of the fermion determinant, which cannot be properly handled by the stochastic estimate in HMC. A dramatic efficiency depletion and instable behavior in correspondence of special configurations of the lattice links ("exceptional configurations") is the consequence.

Another fundamental limitation of past lattice computations of QCD was the absence of the s quark, which is however expected to contribute at low energies. The inclusion of the s quark dynamics, another top issue of modern lattice simulations, and more in perspective physical u and d quark masses with $m_u \neq m_d$, necessarily requires going beyond HMC. Indeed, in its first conception, HMC can only accommodate pairs of *degenerate* quarks.

In this write-up, different approaches for tackling these new challenges in lattice QCD will be reviewed. A variety of setups will be considered, including QCD with one quark flavor ($N_f = 1$ QCD), with two degenerate light quark flavors ($N_f = 2$ QCD), with the addition of two heavier s and c quarks ($N_f = 2 + 1 + 1$ QCD); moreover a supersymmetric gauge field theory, the $\mathcal{N}$=1 supersymmetric Yang-Mills theory, will be discussed; here the fermionic degree of freedom, the superpartner of the gluon (gluino), is described by a Majorana spinor which effectively corresponds to "half" flavor of quarks.

The first step towards more effective algorithms for dynamical fermions is historically represented by M. Lüscher's idea [132] of a *multi-boson* representation of the fermion determinant. In opposition to the pseudofermion representation of HMC, the multi-boson representation produces a *local* effective action for the system of lattice links and pseudofermions including the dynamics of the quarks. Thanks to the locality of the action, the instabilities associated to exceptional configurations typical of

[9] Or modifications thereof with or without $O(a)$ improvement, or additional terms in the gauge action.

[10] With pion masses $M_\pi \gtrsim 500$ MeV.

HMC are avoided. A large part of the simulations reviewed in this work is based on a particular variant of Lüscher's multi-bosonic algorithm developed by I. Montvay: the Two-Step Multi-Boson algorithm (TSMB) [136]. The latter is specifically optimized for simulations in the light fermion regime. The first two chapters of this review in particular will be devoted to simulations of $N_f = 2$ QCD. In this context TSMB allowed to attain a substantial decrease of the quark masses applicable for simulations with Wilson fermions.

An important aspect of the simulation of QCD with light quarks is the application of chiral perturbation theory [189, 88]. Chiral perturbation theory indeed predicts the dependence of hadron properties upon the light quark masses in a theoretically well-founded framework and with control over systematic effects, coming essentially from the neglected higher orders in the chiral expansion. The resulting formulae can be used to extrapolate the lattice data for hadron properties to the physical point of the quark masses: light quark masses in the simulation result in small systematic uncertainties in the extrapolated values. In the present situation, in which the increased computing power allows for the collection of large statistics, these systematic effects often represent the main source of uncertainty in the final determinations. Simulations with light quarks are therefore crucial.

A first check in a simulation with light quarks is, therefore, whether lattice data do follow predictions from chiral perturbation theory. Another point of view [39, 169] is that lattice data can provide the needed input for the determination of the unknown coefficients in the chiral expansions, the so-called Gasser-Leutwyler coefficients. The knowledge of these quantities is very important in hadron phenomenology, since it allows to put non-trivial constraints in low-energy hadron physics.

In Chapter 1, TSMB is introduced and preliminary algorithmic tests performed in [Alg] are reviewed. Simulations of $N_f = 2$ QCD with light quarks [Chi-1, Chi-2, Chi-3] are reviewed in Chapter 2; lattice data for the pion sector are compared with predictions from chiral perturbation theory. In consideration of the rather large lattice spacings of the simulations in [Chi-1, Chi-2, Chi-3], $a \sim 0.2 - 0.3$ fm, lattice corrections were included in the chiral perturbation theory formulae according to the so-called "Wilson chiral perturbation theory" [170, 159]. These studies produced early determinations of the Gasser-Leutwyler coefficients with Wilson fermions.

Designing lattice actions in view of an optimal simulation process for light quarks is a new trend in modern lattice computations (a typical example in this sense is represented by the recently introduced fermion actions with "Stout-links" [142]). A minimal modification of the Wilson action for two degenerate quarks turns out to solve one fundamental problem of this formulation, namely the possibility for special link configurations of a singular fermion matrix with vanishing fermion determinant. In this new approach, proposed by R. Frezzotti and others in 1999 [76] and known as "twisted mass" QCD (TMQCD), an additional chirally twisted mass term is added in the standard Wilson action for the *u-d* chiral doublet.[11] For non-vanishing "twisted mass"

[11] This term is obtained by transforming the *u-d* fields in the mass term of Wilson lattice QCD, see (0.19), by a chiral transformation of the type (0.10) with $N_0 = 2$.

the fermion matrix of the two flavor theory is strictly positive, and the determinant cannot get extremely small in the update. An additional, even more important benefit of the twisted mass formulation is the "automatic" cancellation of $O(a)$ discretization errors for all physical quantities when the standard "untwisted" mass is tuned to zero, namely at *maximal twist*. TMQCD is expected to ensure small lattice artifacts and stable simulations within the conceptually simple framework of the Wilson discretization and therefore represents a competitive approach for lattice determinations with small systematic effects.

A program of large-scale simulations with twisted mass fermions has been recently initiated. These will be reviewed in Chapter 3. In particular, in [tlS-1] a region of light quark masses could be accessed[12], for which chiral perturbation theory formulae including leading order corrections are supposed to deliver reliable extrapolations to the physical quark masses. A novel Europe-wide lattice collaboration, the "European Twisted Mass" (ETM) collaboration was created especially for this purpose.

An important issue emerging when simulating QCD in presence of light quarks is the phase structure of the underlying lattice theory. In QCD, the latter is tightly related to the pattern of chiral symmetry breaking. As long as the quarks are sufficiently heavy for a given lattice spacing, chirality is essentially broken by the quark masses and the breaking from the Wilson term does not play a primary role: in this case the phase structure of the continuum theory is reproduced by the lattice theory up to small $O(a)$ deviations. Thanks to the recent progresses in the numerical simulation however, regions of parameter space can be now accessed where the chirality breaking of the discretization potentially drives the phase structure of the lattice theory [122]. The consequence is a large deviation from the continuum picture: the "Aoki phase" [12] at strong coupling [108] or, at weak coupling towards the continuum limit [Wil-1], an unphysical first order phase transition [170] near zero quark mass.

The important question is, therefore, which maximal lattice spacing can support a program of simulations towards light quark masses with small deviations from the continuum picture.

This question was addressed in [Wil-1, Wil-2, dbW-1, dbW-2], for different lattice formulations in the gluon sector. The resulting information allowed to select the safe regions of parameter space of the lattice theory for the subsequent large-scale simulations of [tlS-1].

We considered up to now simulations with two degenerate quark flavors where the dynamics of heavier quarks is neglected. As mentioned above, the inclusion of the s quark in the simulation is another important issue in today's lattice simulations of QCD. A crucial observation from our point of view is that the twisted mass formulation can also accommodate a doublet of quarks with different masses [82]. The way to simulations of TMQCD with the inclusion of the s quark is therefore open. Since the c quark has to be included as well in order to complete the twisted mass doublet with the s quark, one arrives at $N_f = 2{+}1{+}1$ TMQCD.

First simulations in this setup [tlS-2] will be reviewed. Large-scale simulations

[12]Corresponding to $M_\pi \simeq 300$ MeV, with a lattice spacing $a \simeq 0.09$ fm.

within the ETM collaboration are in preparation [42]. An important goal of the preparatory study [tlS-2] was to provide a feasible setup for tuning the theory to maximal twist and to the physical values of the s and c quark masses.

The second part of this review is mainly devoted to the problem of the lattice simulation of a supersymmetric model. Supersymmetry is expected to play a role in particle physics but, as is well known, is not observed in low-energy phenomenology. In a theoretically attractive scenario, the mechanism responsible for the (necessary) breaking of supersymmetry takes place at a energy scale where supersymmetric interactions become strong and therefore non-perturbative. This theoretical expectation motivates the extensive study of strongly interacting supersymmetric gauge theories in a lattice framework.

An immediate difficulty in this program is that supersymmetry cannot be preserved on a lattice (at least not in its original form), so it must be broken in any lattice formulation; however it can be recovered in the continuum limit similarly to chiral symmetry in Wilson lattice QCD.

We consider here the case of the $\mathcal{N} = 1$ supersymmetric Yang-Mills theory (SYM). This is the minimal supersymmetric version of the gauge theory only describing the self-interactions of gluons (this means, quarks are not included). The fermionic degree of freedom is given in this case by the gluon superpartner, the gluino, which is described by Majorana spinor. For reasons similar to those also applying to QCD and extensively discussed above, supersymmetry must be broken on the lattice by a small gluino mass. Also in this case, we consider a lattice formulation based on Wilson fermions [49], in which chirality is also explicitly broken, at finite lattice spacing, by the Wilson term.

We discover here a parallelism with the typical themes of standard simulations of QCD: the applied techniques and simulations costs are comparable as well. Also in the case of SYM, the main challenge, with similar difficulties, is the simulation of the lattice theory for *light* fermion masses: the supersymmetric case is realized in the limit of a *massless* gluino.

SYM presents nevertheless peculiar features which are absent in the familiar example of QCD. In SYM, indeed, the additional (super)symmetry imposes peculiar patterns in the hadron mass spectrum: the supermultiplets. The latter represent a fingerprint of restored supersymmetry in the continuum limit.

SYM represents a natural application target for TSMB, which is flexible in relation to the spinorial structure of the fermion (as mentioned, Majorana spinors effectively correspond to "half" Dirac fermion). Actually, the simulation of supersymmetric models was historically the first motivation for TSMB [136].

In this work, the most recent developments of a long-standing project for the simulation of SYM with the TSMB algorithm are reviewed [SYM-1, SYM-2, SYM-3]. We concentrate here on the simulation of a simplified version of the theory with two colors only (namely with color group SU(2)).

A crucial question in the case of Wilson fermions is the simultaneous restoration of

the chiral symmetry and supersymmetry for massless gluino in the continuum limit. As shown in [SYM-1], supersymmetry restoration can be studied in a numerical framework by considering the associated supersymmetric Ward identities. The latter put constraints on expectation values of certain composite operators of the fields; these constraints can be verified by lattice calculations. The studies [SYM-2, SYM-3] address the numerical investigation of the low-lying bound states spectrum, for which, as mentioned above, supermultiplets are expected in the supersymmetric limit with massless gluino.

$\mathcal{N} = 1$ SYM presents similarities with a special formulation of QCD where just one quark flavor is included. In both cases, indeed, a continuous chiral symmetry is absent due to a quantum anomaly. In fact, one flavor QCD can be obtained from $\mathcal{N} = 1$ SYM just by replacing the Majorana spinor describing the gluino with the Dirac spinor describing the quark. These similarities find a rigorous framework when one considers the theories in the limit of *infinite number of colors* N_c. At the lowest order (planar level) of the so-called orientifold large N_c expansion [17], the exact equivalence of the two theories can be proven. One flavor QCD, with three colors, is expected therefore to contain some "relics" of supersymmetry. The second part of this review will also cover first numerical simulations of QCD with one light quark flavor [Nf1]. The focus is in particular on the low-lying bound states spectrum, where relics of supersymmetry are expected to emerge.

Part I.

Simulations of QCD

1. Algorithmic studies

The Hybrid Monte Carlo (HMC) algorithm [62] represented in the past the standard algorithm for dynamical-fermion simulations of $N_f = 2$ QCD (u and d quarks with equal masses). HMC is based on the Hamiltonian evolution of a dynamical system in which the lattice links $U_\mu(x)$ assume the role of dynamical variables. The Hamiltonian evolution ("trajectory") is solved after discretization of the fictitious time parameter ("Monte Carlo time") in a hybrid Langevin–molecular-dynamics setup (we refer to [139] for an exhaustive discussion of themes related to the Monte Carlo simulation of lattice theories with fermions). After a transient, the gauge field configurations, sampled at regular time separations along the Monte Carlo evolution, result to be distributed with probability density $P[U] \sim \exp\{-S_{eff}[U]\}$, where the effective action $S_{eff}[U]$ (0.32) also includes the contribution of the quarks to the link dynamics, the fermion determinant.

HMC, in its original formulation [62], is characterized by conceptual clarity and straightforward implementation, which to some extent explains its popularity in lattice simulations of QCD with two degenerate Wilson fermions. However, as we will briefly discuss below, it turns out to be affected by severe limitations in the light fermion regime and therefore unsuitable for a program of simulations down to small quark masses. Moreover, it cannot be applied to the general case of a theory with non-degenerate Dirac fermions, or to fermions with peculiar spin structures. The second case is relevant for the $\mathcal{N}$=1 supersymmetric Yang-Mills theory (SYM), object of investigation in Chapter 4 (a brief introduction to SYM is contained in the first three sections of Chapter 4). The first applies for example to QCD including heavier quarks: in Chapter 3 a theory with such a flavor structure, namely $N_f = 2{+}1{+}1$ QCD, will be considered. Another case where standard HMC cannot be applied, also considered in Chapter 4, is QCD with a single quark flavor.

These limitations of HMC motivate the search for alternative algorithms for simulations of dynamical fermionic degrees of freedom in QCD and related theories.

1.1. Beyond Hybrid Monte Carlo

The basic limitation of HMC to degenerate pairs of Wilson fermions (or quartets of Kogut-Susskind [125] fermions) can be simply understood by considering the design of the algorithm. Its inefficiency in the light fermion regime is a less trivial subject which deserves a separate discussion.

As a matter of fact, HMC turns out to be extremely sensitive to roundoff-error accumulation along the time evolution. This aspect is critical in the case of light

fermionic degrees of freedom (see [112] and references therein for an early review on the topic, for more recent results see also [117, 9, 147]). In extreme cases [114] the HMC dynamics assumes chaotic features where small deviations from the proper trajectory of the Hamiltonian time evolution get exponentially amplified (with an associated Liapunov exponent). In this case the algorithm in no longer exact, as signalled by loss of reversibility in the Hamiltonian evolution.

A second aspect is related to the discretization of the time parameter in the Hamiltonian evolution, which necessarily introduces deviations from the exact classical trajectory. The consequent violation of the energy-conservation at the end of the trajectory must be compensated in HMC by a Metropolis accept-reject test with acceptance probability $\sim \mathrm{e}^{-\Delta E}$, where ΔE is the energy-variation. It has been observed in [117, 147] that a critical value of the time step-size exists, above which the dynamics of the system switches from a (normal) elliptic behavior to a diverging hyperbolic one. In this case, the energy-conservation violation becomes large and the acceptance rate of the new link configuration in the Metropolis test very small. The critical step-size depends on the magnitude of the driving force, which increases when the fermion mass is decreased. This latter feature is especially critical in the case of the Wilson lattice formulation of fermions, where due to the $O(a)$ breaking of the chiral symmetry, an infrared cutoff is missing for the eigenvalue spectrum of the lattice Dirac operator. Even for non-zero quark masses, the Wilson-Dirac operator can become almost singular on special configurations ("exceptional configurations"). On these configurations the fermionic contribution to the driving force in HMC can get extremely large[1]: "spikes" are observed in the Monte Carlo time-history of this quantity [147]. As a result, the acceptance of the Metropolis correction becomes practically zero and the system is never updated.

In the case of simulations of QCD, the instability of HMC becomes critical for values of the light quark masses m_q below the reference value $m_s/2$ [117, 9, 147], while "safe" simulations are confined to quite large values (see [7, 8] for representative simulations in this regime, and [110] for a more recent example). This clashes with an analysis in chiral perturbation theory in the pseudoscalar meson sector [169]; the latter indicates that extrapolations to the physical value of the u and d quark masses with full control over theoretical errors, coming from neglected higher order corrections, requires *simulated* light quark masses as light as $m_q \simeq m_s/5$.

In consideration of these limitations, we conclude that HMC cannot really bridge the gap between lattice QCD in the Wilson setup and nature, where $m_{ud} \simeq (3-5)$ MeV.

An efficient algorithm in the regime of light fermionic degrees of freedom is of course also required for lattice supersymmetric models: for example in SYM, supersymmetry is recovered in the limit of zero gluino mass. As already mentioned, however, HMC cannot be applied in this case due to more fundamental algorithmic limitations.

Algorithms alternative to HMC can be designed by recurring to a *multi-boson representation* [132] of the fermion measure in the path-integral. The resulting dynamical-fermion algorithms are radically different from HMC, since they are based on con-

[1] According to [117] proportionally to $1/m_f^{\alpha}$, with α a positive exponent.

ventional *local* update techniques. These procedures can be optimized for the case of light fermion masses and are, due to their locality, free from the instability features of HMC. In addition, they are flexible in relation to the spin structure of the fermions. Simulations of $N_f = 2$ QCD with a multi-boson algorithm [136] will be reviewed in the present and in the next two chapters, while the case of SYM will be considered in Chapter 4.

In a different, more recent, line of algorithmic development, the underlying hybrid Langevin–molecular-dynamics structure of HMC is maintained and different improvements are introduced in order to stabilize and speed-up the algorithm in the light quark regime [55, 166, 34, 102, 133]. However, these improvements do not really directly address the problem of the exceptional configurations; the intrinsic limitation to degenerate flavor pairs also remains. In Chapter 3 we will see how the first of these two issues can be solved by slightly modifying the Wilson formulation in the fermion sector. The limitation of HMC to particular flavor configurations can be overcome by introducing a polynomial expansion in the pseudofermion representation of the fermion measure ("Polynomial Hybrid Monte Carlo", PHMC [52, 78]). Applications of a PHMC algorithm [140] to QCD with a split-mass quark doublet, and to QCD with a single quark flavor will be considered in Chapters 3 and 4, respectively.

1.2. The Two-Step Multi-Boson Algorithm (TSMB)

A large part of the simulations discussed in this review are based on the Two-Step Multi-Boson Algorithm (TSMB), a variant of Lüscher's multi-boson algorithm [132]. TSMB was developed in [136] and successively improved in the course of its practical applications in the various setups considered in this review. In order to keep the discussion self-contained, we give in the following a brief account of its main features.

1.2.1. Local update

TSMB is based on the multi-boson representation [132] of the fermion determinant. In the most general setup considered in [136] the starting point is the relation:

$$\left|(\mathrm{det}Q)^{2\alpha}\right| \;=\; \mathrm{det}(Q^\dagger Q)^\alpha \;\simeq\; \frac{1}{\mathrm{det}P_n(Q^\dagger Q)}\;. \tag{1.1}$$

In the above equation, Q denotes the fermion matrix in the Wilson setup (0.23), or "Wilson-Dirac operator", $n_f = 2\alpha$ is the number of *degenerate* fermions of a given mass present in the theory, and $P_n(x)$ is an order n polynomial approximating the target function $f(x) = x^{-\alpha}$:

$$\lim_{n\to\infty} P_n(x) \;=\; x^{-\alpha}\;. \tag{1.2}$$

Observe that the quantity in the LHS of Eq. (1.1) represents in general only the *absolute value* of the fermion measure for $n_f = 2\alpha$ degenerate fermions; indeed, the fermion determinant can be negative implying negative fermion measure for odd n_f.

The relation (1.1) can be expressed in terms of the squared *Hermitian* matrix $\tilde{Q} = \gamma_5 Q$ since due to the γ_5-Hermiticity of the Wilson-Dirac operator $\gamma_5 Q \gamma_5 = Q^\dagger$ one has[2]

$$Q^\dagger Q \;=\; \tilde{Q}^2 \;. \tag{1.3}$$

Inserting the root decomposition of the polynomial $P_n(x)$ using explicitly the symmetry of the roots under complex-conjugation,[3]

$$P_n(x) \;=\; \prod_{i=1}^{n} (\sqrt{x} - \rho_i^*)(\sqrt{x} - \rho_i) \;, \tag{1.4}$$

into the last term in (1.1) also using (1.3), one obtains

$$|\mathrm{det} Q|^{2\alpha} \;\simeq\; \prod_{i=1}^{n} \frac{1}{\mathrm{det}(\tilde{Q} - \rho_i^*)(\tilde{Q} - \rho_i)} \;=$$
$$\int \prod_{j=1}^{n} [d\bar{\Phi}^{(j)}][d\Phi^{(j)}] \;\exp\{-\sum_{i=1}^{n} \sum_{xy} \bar{\Phi}_y^{(i)} \left[(\tilde{Q}[U] - \rho_i^*)(\tilde{Q}[U] - \rho_i)\right]_{yx} \Phi_x^{(i)}\} \;, \tag{1.5}$$

where the fields $\Phi_x^{(i)}, i = 1 \ldots n$ describe n species of bosonic particles carrying the same quantum numbers of the original fermion fields.

The multi-boson action (1.5) contains interactions between the link variables and the n species of boson fields with a finite range in lattice units[4]. Consequently, the contribution to the total probability density $P[U]$ given by the last term in (1.1) can be reproduced by means of conventional *local* updating procedures.

1.2.2. Polynomial approximation

Lüscher's original proposal [132], designed for the case $f(x) = 1/x$ ($n_f = 2\alpha = 2$), is based on Chebyshev polynomials for the approximation (1.2). In this case the maximal relative error $|xP_n(x) - 1|_\infty$ (L_∞ norm) is minimized for a given n and approximation interval $[\epsilon, \lambda]$. The general scheme of [136], applicable to a generic value of α, relies on the minimization of the quadratic relative deviation (L_2 norm) with a weight $w(x)$:

$$\text{minimize } \delta^2 \;, \quad \delta^2 \;=\; \int_\epsilon^\lambda dx\, w(x)\, (x^{-\alpha} - P_n(x))^2 \;. \tag{1.6}$$

It is useful to consider the spectral decomposition of Eq. (1.1) on the eigenvalues of the Hermitian matrix $\tilde{Q}^2 = Q^\dagger Q$. In this way, one sees that the limits of the

[2] A non-Hermitian multi-boson algorithm, in which the argument of the polynomial is the non-Hermitian fermion matrix Q, can also be conceived [33].

[3] It is assumed that all roots are complex, which is possible if the polynomial order n is chosen to be even.

[4] Observe that the different species do not interact among themselves.

optimization interval $[\epsilon, \lambda]$ in (1.6) should be chosen such that the spectrum of the positive semidefinite Hermitian matrix $\tilde{Q}^2$ lies inside it[5].

The two minimization criteria with L_∞ and L_2 norm differ in the way they treat the approximation errors. The L_∞ norm leads to an almost constant error in the bulk of the spectrum and the location of an optimal value of ϵ becomes non trivial in the case of small eigenvalues [33]. The L_2 norm criterion (1.6), in opposition, is characterized by smaller deviations in the bulk at the price of larger errors at the boundaries of the approximation interval. This is more advantageous for simulations of light fermions [137].

The general scheme defined by Eqs. (1.1), (1.5) and (1.6) is applicable to a generic model with fermion measure, in modulus, $|\det(Q)|^{2\alpha}$ where α is real and positive. This includes supersymmetric models ($\alpha = 1/4$) and, in QCD, a single non-degenerate quark (for example the s quark, with $\alpha = 1/2$). Moreover algorithmic improvements based on the "breakup" of the fermion determinant [101], where fractional powers of are required, can be easily implemented, see Subsec. 1.2.6.

1.2.3. Noisy correction

In the original conception of the multi-boson algorithm [132], the theory is simulated with the multi-boson representation of the fermion determinant with a given polynomial order n. The deviations from the canonical probability density of the gauge ensemble $P[U] \sim \exp\{-S_{eff}[U]\}$ produced by the polynomial approximation for finite n is corrected in a second step by reweighting the gauge sample when building the sample averages of the lattice operators. However, how one can easily infer, this procedure becomes extremely inefficient in the case of light fermions. For small bare fermion masses, indeed, the associated fermion matrix usually assumes large condition numbers[6]. With almost singular matrices, large polynomial orders n are required in the polynomial expansion (1.1), since the target function diverges at the origin. Large values of n produce in turn large autocorrelations in the lattice system with n species of bosons (1.1) and, consequently, a slowing down of the update algorithm [6]

A solution to this problem was put forward in [33] where a Metropolis test in the update with a better polynomial approximation was proposed. This method is feasible from the point of view of the computational load, since the correction factor can be stochastically evaluated by a single noisy estimator while preserving detailed balance [123] of the update algorithm. Here, a version [136] of the Metropolis test is considered which is valid in the general case given by (1.1).

The idea is to replace the polynomial approximation (1.2) with a two-step approximation where a second polynomial $P^{(2)}_{n_2}(x)$ corrects for small deviations:

$$\lim_{n_2\to\infty} P^{(1)}_{n_1}(x) P^{(2)}_{n_2}(x) = x^{-\alpha} \ . \tag{1.7}$$

[5] An optimal choice turns out to be $\epsilon \lesssim \lambda_{min}/3 - \lambda_{min}/2$ [Alg] .

[6] In the case of a positive semidefinite Hermitian matrix, such as $\tilde{Q}^2$, the condition number is given by the ratio between the largest and the smallest eigenvalue.

The correction to the fermion measure given by

$$\frac{1}{\det P_{n_2}^{(2)}(Q^\dagger Q)} \tag{1.8}$$

is taken into account by a global Metropolis correction. A random vector η is generated according to the normalized distribution

$$P(\eta) \;\sim\; e^{-\eta^\dagger P_{n_2}^{(2)}(\tilde{Q}^2[U])\eta} \;; \tag{1.9}$$

the test configuration $[U']$, generated in the local update $[U] \to [U']$, is submitted to a Metropolis test, with acceptance probability[7]

$$\min\{1, A(\eta; [U] \to [U'])\} \;, \tag{1.10}$$

where

$$A(\eta; [U] \to [U']) \;=\; \exp\left\{-\eta^\dagger P_{n_2}^{(2)}(\tilde{Q}^2[U'])\eta + \eta^\dagger P_{n_2}^{(2)}(\tilde{Q}^2[U])\eta\right\} \;. \tag{1.11}$$

The noise vector η is obtained from a Gauss-distributed vector η_g

$$\eta = [P_{n_2}^{(2)}(\tilde{Q}^2[U])]^{-\frac{1}{2}} \;\eta_g \;. \tag{1.12}$$

The inverse square root on the right hand side of (1.12) is again estimated by polynomial approximation. The latter approximation is the only possible source of systematic errors in TSMB, even if high precision can be easily achieved by choosing the lower limit of the approximation interval few order of magnitude smaller than ϵ in (1.6).

The main advantage of this second approximation step is that the order of the polynomial approximation in the local update n_1, the first approximation step, can be kept down to moderate values. The Metropolis step automatically corrects for deviations from the target distribution during the update. Of course, a poor first polynomial approximation results in low acceptances for the Metropolis step, so a balance must be found: an optimal value of n_1 corresponds to an acceptance $\gtrsim 50\%$ [Alg].

1.2.4. Measurement correction

For finite values of n_2, the correction (1.8) is normally not sufficient to render the TSMB algorithm exact within the precision of the computer arithmetics, and a third step is required[8]. A third polynomial $P_{n_3}^{(3)}(x)$ is introduced such that

$$\lim_{n_3\to\infty} P_{n_1}^{(1)}(x) P_{n_2}^{(2)}(x) P_{n_3}^{(3)}(x) = x^{-\alpha} \;, \qquad x \in [\epsilon', \lambda] \;. \tag{1.13}$$

[7] The multi-boson field configuration is always accepted. In this way the storage of the initial configuration is not required; one can easily argue that this procedure does not affect the distribution of the gauge fields.

[8] Exactness can be achieved, in the particular case $n_f = 2$, by considering a non-Hermitian version of the polynomial approximation [33].

In this case ϵ' can be chosen to coincide with zero, in which case the algorithm becomes exact in the limit $n_3 \to \infty$. After reweighting, the expectation value of a quantity A is given by the unbiased estimator

$$\langle A \rangle = \frac{\langle A \exp\{\eta^\dagger [1 - P_{n_4}^{(4)}(Q^\dagger Q)]\eta\}\rangle_{U,\eta}}{\langle \exp\{\eta^\dagger [1 - P_{n_4}^{(4)}(Q^\dagger Q)]\eta\}\rangle_{U,\eta}} \ , \tag{1.14}$$

where η is a Gaussian noisy vector. Stochastic noise is reduced by increasing the number of stochastic estimators, while n_4 can be easily taken very large, such that the violation of the detailed balance is below the machine precision. In practice, reweighting is only needed in the case of exceptionally small eigenvalues. A non-exact first step of approximation is actually welcome since it enhances, in the dynamical part of the update, the crossing of topological sectors. These crossings are normally associated with small eigenvalues of the fermion matrix and therefore suppressed by the fermion determinant. In the algorithmic studies of TSMB for light fermions, both in SYM [SYM-1] and in $N_f = 2$ QCD [Alg], the effect of the reweighting was generally negligible.

1.2.5. Sign of the fermion measure

Only the *absolute value* of the fermion measure can be reproduced by Monte Carlo methods (see Eq. (1.1)). The presence of a sign (or phase) must be taken into account explicitly in the sample average, with possible cancellation effects. This is potentially an issue in QCD for an odd number of light unpaired quarks; interesting cases are $N_f = 1 + 1$ QCD (non-degenerate u and d quarks), $N_f = 3$ QCD considered in [69][9], $N_f = 1$ QCD considered in [Nf1]; the sign can represent a problem in supersymmetric models in general, where the *Pfaffian* of the fermion matrix takes the place of the determinant (see also Chapter 4, Subsec. 4.3.1). Experiences with SYM [SYM-1], $N_f = 2$ QCD [Alg] and $N_f = 3$ QCD [69] show that the sign change is a rare event even in presence of relatively light fermions if the lattices are fine enough, but it can become an issue on coarse lattices and/or with extremely light quark masses.

1.2.6. Optimization

The local part of the update in TSMB consists in a sequence of heat-bath and over-relaxation sweeps for the gauge and the boson fields. In the case of SYM, heat-bath cannot be applied for the gauge field since the fermion action is *quadratic* in the link variable, see Eq. (4.32) in the following Chapter 4, and the less effective Metropolis algorithm has to be used[10]. For details about the general implementation of the TSMB

[9] The interest in this setup is motivated by comparison with ChPT, see the Introduction to the next chapter.

[10] In heat-bath, the new link variable does not depend on the old variable on that site, while this is the case for the Metropolis algorithm. As a result the autocorrelation length increases by up to a factor two.

in SYM and QCD we refer to the publications [35] and [Alg], respectively[11].

TSMB can be optimized in various ways. Even/Odd (EO) preconditioning of the fermion matrix [116] was applied already in [35]. The resulting reduction of the condition number of the fermion matrix by almost a factor two allows to lower the order of the first polynomial approximation n_1 by the same factor.

Global heat-bath in the "approximate" version of [51] (global quasi-heat-bath) was introduced in [Alg] for the boson fields. A speedup of the algorithm results in this case from the almost perfect decorrelation of the boson fields. The latter are generally responsible for long tails in the autocorrelations of measured quantities along the Monte Carlo history.

Finally, determinant breakup [101] was introduced in [71] and applied in subsequent simulations with TSMB. In this case the fermion measure is decomposed in the product of n_{DB} terms

$$|\mathrm{det}Q|^{2\alpha} = \prod_{k=1}^{n_{DB}} |\mathrm{det}Q|^{2\alpha/n_{DB}} \ , \tag{1.15}$$

each of which is expanded according to (1.1). The determinant breakup allows reduces the fluctuations of the stochastic correction, Eqs. (1.9)-(1.12), with a consequent increase of the acceptance rate. The general setup of the TSMB considered here allows a straightforward implementation of this technique.

1.3. Simulation tests of TSMB with light fermions [Alg]

Both QCD and SYM contain light fermionic degrees of freedom, the u and d quarks in QCD and the gluino in SYM (in this latter case exactly massless in the supersymmetric limit of the theory). However numerical simulations cannot access the massless limit of these theories, and in the case of SYM, supersymmetry has to be softly broken with a Majorana mass term. Simulations can only be performed until a minimal fermion mass and the physical point must be reached by extrapolation. Even not considering possible instability phenomena, as the ones outlined in Sec. 1.1, the computational load of a dynamical-fermion simulation increases dramatically when the masses of the light fermions are reduced. One factor of this increase is represented by the depleted performance of a generic simulation algorithm for large condition numbers of the fermion matrix, which for example in the case of TSMB imply higher orders in the polynomial approximation[12].

An additional difficulty in the light fermion regime emerges in the particular case of QCD. Here, the massless quark limit corresponds to restoration of the chiral symmetry and the mass gap of the theory vanishes as an effect of the spontaneous breaking of this symmetry. For light quarks, the low-energy physics is dominated by almost massless

[11] For more details, see also [177, 91, 162].

[12] In the case of HMC, the algorithm providing the solution of the lattice Dirac equation, the typical problem in the molecular-dynamics evolution, becomes more and more inefficient.

particles, the would-be Goldstone bosons coming from the spontaneous breaking of the symmetry. In the case of $N_f = 2$ QCD, these pseudo-Goldstone bosons can be identified with the lightest particles of the theory, the pions. The dependence of physical quantities upon the quark masses can be determined in the framework of Chiral Perturbation Theory (ChPT) [189, 88]. As we will see in more detail in the next chapter, ChPT formulae provide a guidance for the extrapolation of lattice data to the physical value of the light quark masses.

A consequence of the vanishing of the mass gap is the enhancement of finite-size effects towards the chiral limit (the light pions "do not fit" in the finite volume enclosed by the lattice). Moreover, and this is the relevant point for the present discussion, HMC and local algorithms as TSMB have to face a *critical slowing down* produced by the light pions, whose Compton wavelength sets the scale for the propagation of the information throughout the lattice; as a result, the autocorrelation time τ in the Monte Carlo update increases as an inverse power the quark mass[13].

The situation is somewhat alleviated in the case of SYM, where the mass gap persists in the supersymmetric limit: the dependence of physical observables upon the gluino mass is expected to be analytic with exponentially suppressed finite size effects for large lattices. Slowing down is not critical since a diverging length scale in the massless gluino limit is absent.

We have previously argued that TSMB, by its construction, can support the simulation of very light fermion masses. First experience for light fermions, namely with large $O(10^5)$ condition numbers of the fermion matrix, was accumulated for the case of SYM in [SYM-1]. This situation roughly corresponds to $m_q \simeq m_s/4$ in QCD [69]. In the case of SYM, proper tuning of the algorithm parameters allowed to keep simulation costs down to low levels for increasing condition numbers (see Chapter 4 and Subsec. 4.4.4 in particular for a more detailed discussion, also including the physical setup).

As already argued, the case of QCD is potentially more challenging and the behavior of the algorithm for light quarks must be carefully tested. An important objective of the study [Alg] was in particular to estimate the dependence of the simulation costs upon the quark mass for $N_f = 2$ QCD with Wilson fermions. Unprecedently light quarks $m_q \gtrsim m_s/5$ were covered by the simulations, although on a relatively coarse lattice with $a \simeq 0.27$ fm. This region of parameter space is orthogonal to that of a previous benchmarking of HMC with Wilson fermions [184] with $a \lesssim 0.1$ fm and $m_q > m_s/2$.

Further interesting aspects investigated in [Alg] are the influence of light dynamical quarks on the eigenvalue spectrum of the non-Hermitian fermion matrix and the comparison of lattice estimates for mesonic quantities with ChPT predictions.

[13] Assuming random walk for the propagation of the information, one has $\tau \sim 1/M_\pi^2$; since $M_\pi^2 \sim m_q$ one concludes $\tau \sim m_q^{-1}$. This sets a lower limit for the critical exponent $\tau \sim m_q^{-z}$, $z \geq 1$ in the case of local algorithms.

1.3.1. Cost figure

The computational "cost" C associated with the production of a a sample of n_s *independent* gauge configurations is given by

$$C \;=\; n_s \cdot \tau\,(f.p.o.)\;, \tag{1.16}$$

where $\tau\,(f.p.o.)$ denotes the autocorrelation time along the Monte Carlo evolution in terms of the corresponding number of floating point operations. For a given algorithmic setup and criterion for the definition of τ (namely which quantity τ refers to), the "cost figure" C is univocally determined by the simulation parameters. In the simplest setups (including $N_f = 2$ QCD and SYM) these are given by the lattice coupling constant β, the hopping parameter κ and the lattice extension in lattice units L/a. For a given value of L, the parameters β and κ can be replaced by any physical scale which, expressed in lattice units, fix the position of the lattice model in the parameter space. Typical dimensionless scales are given for example by the quark mass and the Sommer scale parameter [176] in lattice units, am_q and r_0/a. It is generally assumed that an analytic dependence of $\tau\,(f.p.o.)$ upon these parameters applies. In this case, Eq. (1.16) can be rewritten (we specialize the discussion to $N_f = 2$ QCD):

$$C = F\;(r_0 m_q)^{-z_{m_q}} \left(\frac{L}{a}\right)^{z_L} \left(\frac{r_0}{a}\right)^{z_a}\;. \tag{1.17}$$

(F is a proportionality constant). In the above formula, the lattice spacing dependence of C for fixed L/a is entirely contained in the last factor, and the quark mass appears in units of the (inverse) Sommer scale parameter. The ratio between the pion and the ρ meson mass M_π/M_ρ is sometimes used in place of the quark mass (see for example [184]).

In [Alg] it was argued that a better operational definition of the quark mass is given by the quantity

$$M_r \equiv (r_0 M_\pi)^2\;; \tag{1.18}$$

this latter quantity can be more easily determined in a region of light quark masses where the ρ meson can potentially decay into pions. In terms of M_r, the cost formula reads:

$$C = F'\;M_r^{-z} \left(\frac{L}{a}\right)^{z_L} \left(\frac{r_0}{a}\right)^{z_a}\;. \tag{1.19}$$

An alternative definition of the quark mass is given in the two flavor theory by the "Partially-Conserved Axialvector-Current" (PCAC) relation:

$$m_q^{PCAC} \equiv \frac{\partial_\mu \langle \bar\psi \gamma_\mu \gamma_5 \frac{\tau^a}{2} \psi(x)\;\mathcal{O}(y)\rangle}{2\langle \bar\psi \frac{\tau^a}{2} \gamma_5 \psi(x)\;\mathcal{O}(y)\rangle}\;, \tag{1.20}$$

where $\mathcal{O}(y)$ is a suitable composite operator of the quark fields. A dimensionless quantity can be defined in units of the Sommer scale

$$\mu_r \equiv r_0 m_q^{PCAC}\;. \tag{1.21}$$

Observe that the definition (1.18) reproduces the usual definition of the quark mass only for asymptotically light quarks masses; on the other side, the connection of (1.21) with the physical quark mass requires the knowledge of a renormalization factor.

In the case of HMC, the definition of the cost figure in units of the number of fermion-matrix-vector multiplications instead of floating point operations [77] has the advantage of being independent of the details of the algorithmic implementation for a given computer platform; moreover the trivial volume factor $(L/a)^4$ is rescaled away. In [Alg] this definition of C was adapted to the case of TSMB and chosen for the estimate of the computational cost[14].

TSMB is a complex algorithm with many tunable parameters and therefore an exact theoretical prediction about the dependence of the cost figure on the simulation parameters is not available. In the local part of the update, the slowing down for light quark masses is enhanced by the increased number (n_1) of the boson fields required for the more accurate polynomial approximation. In the most pessimistic case, one has [6]

$$\tau\,(updates) \sim n_1/m_q\ . \tag{1.22}$$

On the other hand, in order to keep the approximation error down to low values, n_1 has to be rescaled with m_q: $n_1 \sim \ln V/m_q$. After restoration of the lattice units, and neglecting logarithmic volume terms, one gets

$$\tau\,(f.p.o.)\ \sim\ n_1 \left(\frac{L}{a}\right)^4 \tau\,(updates)\ \sim\ \frac{1}{(am_q)^3}\left(\frac{L}{a}\right)^4\ , \tag{1.23}$$

corresponding to $z_{m_q} = z_a = 3$ and $z_L = 4$ in the parametrization (1.17). The above estimate is however incomplete since it does not include the stochastic step of the Metropolis test. Global updates of the multi-boson fields may also play a role (global quasi-heat-bath).

1.3.2. Results for the cost figure with TSMB

The study [Alg] is based on simulations on $8^3 \cdot 16$ lattices at a single value of the lattice spacing $a \simeq 0.27$ fm ($L \simeq 2.4$ fm). Autocorrelations were measured for the average plaquette value and for other basic physical quantities as the pion mass M_π and decay constant F_π. An appropriate estimate of the autocorrelation length for non primary quantities as M_π and F_π is obtained by applying the linearization method proposed in [77] (or "Γ-method" [197]). The traditional procedure based on jackknife and binning is usually not reliable in the case of marginal statistics.

In order to single out the dependence of the cost figure C upon the quark mass, see (1.17), the simulation parameters β and κ were tuned to an approximate constant value of r_0/a; the final results were obtained by interpolation at the reference value $r_0/a = 1.8$. The quark masses range in the region $m_s/5 - m_s$ ($M_\pi = 300 - 900$ MeV).

[14] The simulation costs with TSMB are not dominated by fermion-matrix-vector multiplications. An "effective" fermion-matrix-vector multiplication number can be however defined and related to the TSMB parameters of the simulation, see Eq. (13) of [Alg].

When the average plaquette is used as a reference quantity for the computation of the autocorrelations, the cost figure (1.19) results to increase towards small quark masses with a critical exponent $z \simeq 2$. This indicates that the additional slowing down from the increased number of boson fields (see Eqs. (1.22) and (1.23)) is compensated by the optimization of the algorithm in the non local part of the update. The more popular parametrization in terms of the ratio between the pion and ρ meson mass, $C \sim (M_\pi/M_\rho)^{-z_{\pi\rho}}$, gives $z_{\pi\rho} \simeq 6$ in agreement with the estimates of [184] obtained however for $m_q > m_s/2$ and smaller lattice spacings.

One important result of [Alg] is that TSMB displays a stable behavior down to the smallest tested quark mass ($m_q \simeq m_s/5$). The absolute cost figure for the lightest quark mass is compatible with the extrapolated value from heavier quark masses with the HMC algorithm [184]. We recall however that HMC would not be really able to simulate such small quark masses due to the aforementioned instability problems.

TSMB was tested in [Alg] on rather coarse lattices. Tests of TSMB for smaller values of the lattice spacing ($a \simeq 0.06$ fm in QCD units) and larger condition numbers $O(10^6)$ (corresponding in QCD to $m_q \simeq m_s/4$) are available for SYM [SYM-1]. Also in this case, TSMB displays a satisfactory behavior.

An interesting question is how the cost figure scales with the lattice size [71]. The order of the first polynomial n_1 only increases with the *logarithm* of the volume (due to the denser eigenvalue spectrum); further polynomial orders n_2 and n_3 do not need to be rescaled at all, as long as the smallest eigenvalue of $\tilde{Q}^2$ is unchanged (which is the case for large enough volumes). So the deviation from the trivial scaling law with $z_L = 4$ in (1.17) can only come from an increased autocorrelation of the tested quantity in update units. Comparison with a larger $16^3 \cdot 32$ lattice shows indeed a volume scaling of the simulation costs compatible, or even slightly below, the $z_L = 4$ scaling law.

1.3.3. Eigenvalue spectrum of the fermion matrix

In the regime of small quark masses, the dynamics of the light quarks is expected to show up in different contexts. An aspect, which is important also in relation to the simulation process, is the eigenvalue spectrum of the Wilson-Dirac operator.

A clear effect is observed in the eigenvalue spectrum of the non-Hermitian matrix, namely a depletion of the number of eigenvalues close to the origin of the complex plane. This is expected, since configurations with small fermion determinants are disfavored in the sampling process (recall (0.30)). A special role is played by the *real* eigenvalues, which, being unpaired, can assume extremely small values. In particular the smallest real eigenvalue sets a limit for the lightness of the quark mass in partially quenched computations, see in the next chapter. Real eigenvalues are also responsible for the flip of the determinant sign. This is of course an issue only in the case of unpaired light flavors. An example is given by $N_f = 1$ QCD, where the determinant sign plays a special role in connection to a possible phase transition [43], see also Sec. 4.7 in Chapter 4. In the case of $N_f = 2$ dynamical fermions considered in [Alg] a negative determinant sign tuns out to be a rare event even for the lightest investigated

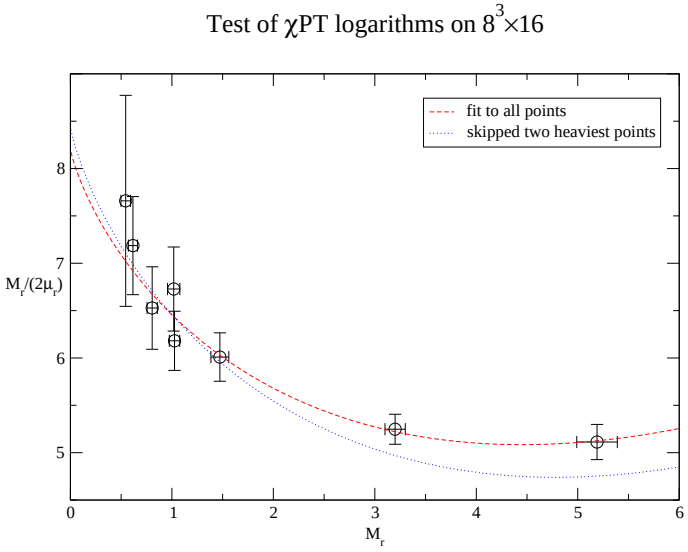

Figure 1.1.: *Fits of the squared pseudoscalar meson mass with the one-loop ChPT formula. The reported ratio is constant in tree-level ChPT. For the definition of M_r and μ_r, see Eqs. (1.18) and (1.21), respectively.*

quark mass.

Monitoring the spectrum of the *Hermitian* (squared) matrix is important in relation to the algorithmic performance. TSMB tends to stall on configurations with very small eigenvalues. The representativity of such configurations in the canonical ensemble is however marginal, as can be verified by measuring the associated correction factors.

1.3.4. Chiral logs?

Effects of the light quarks can also be observed in the functional dependence of hadron quantities on the quark mass. An interesting case is represented by the pion mass and decay constant. ChPT formulae for these quantities are characterized at next-to-leading by a non-analytic dependence on the quark mass, the so-called "chiral logs". This feature qualifies the special pattern of chirality breaking in the massless limit of QCD. More information about ChPT in relation to lattice computations will be given in the next chapter.

A behavior compatible with next-to-leading ChPT corrections can be observed in the data of [Alg]. The ratio $M_r/2\mu_r$ reported in Fig. 1.1 taken from [70] is independent of the quark mass in leading-order ChPT; so, the observed deviation from the constant behavior can be interpreted as an effect of the chiral logs.

Finite volume effects on the pion mass can potentially play a role in the behavior of $M_r/2\mu_r$. In the present case with $M_\pi L \gtrsim 3.4$, however, these are expected to be small. For example for the point at the lightest quark mass, lattice size and pion mass are $L \simeq 2.2$ fm and $M_\pi \simeq 300$ MeV, respectively; ChPT predicts in this case [40] an effect for F_π and M_π below the statistical precision. Due to the relatively large lattice spacing, however, discretization errors could play a role: the inclusion of discretization

effects in ChPT formulae will be discussed in full detail in the next chapter.

The comparison of the data from [Alg] with ChPT predictions is not really simple, since different quark masses are analyzed at different values of β in that work: this strategy was motivated by the necessity of keeping r_0/a fixed in the cost formula (1.17). Of course, a better strategy in view of ChPT studies would be to analyze the quark mass dependence at a *fixed value* of the coupling constant. In a mass independent scheme, indeed, the renormalization constants only depend on β and the quark mass dependence of the hadron quantities is explicit up to an overall renormalization constant. This strategy will be pursued in the next chapter.

2. Lattice QCD and chiral perturbation theory

For the reasons explained in the previous chapter, lattice QCD must be presently simulated for values of the u and d quark masses which are heavier than in nature. As already mentioned, Chiral Perturbation Theory (ChPT) [189, 88] can provide the necessary formulae for the extrapolation of the computed physical quantities to the physical point, where the u and d quarks assume their actual masses.

In ChPT, constraints coming from the (spontaneously broken) chiral symmetry of QCD are used for establishing relationships among different observables in hadron physics. The missing information is contained in *unknown* low-energy constants and coefficients appearing in the ChPT formulae. The latter can be fixed by additional input from hadron physics.

For the hadron quantities considered here, the pion mass and decay constant, the chiral expansion produces power-series in the light quark masses m_q (also containing a non-analytic dependence, the "chiral logs" mentioned in the previous chapter). These series have (most likely) an *asymptotic* character. This implies that the accuracy of the estimates *for a fixed quark mass* does not necessarily improve when higher order terms are included in the expansion; on the other hand, this is expected at a given order of the expansion, if the quark mass m_q is reduced to low enough values. The latter statement may sound rather formal at this level, since in nature the masses of quarks cannot be varied. However, in lattice QCD m_q is a tunable parameter and this issue must be taken into account when performing the extrapolations.

Due to proliferation of free parameters in the chiral formulae for increasing order of the expansion, one has usually to rely on the next-to-leading order (NLO) approximation. In this case, two low-energy constants are relevant, F_0 and B_0, and few low-energy coefficients, known in the literature as Gasser-Leutwyler coefficients (GLC).

As it turns out, the program of closing the ChPT relations involving physical quantities and the light quark masses cannot be completely accomplished, since chiral symmetry is not able to provide all the required constraints. In particular, at NLO, transformations of the light quark masses and of some low-energy coefficients can be found, which leave the ChPT formulae invariant: as noticed by D. Kaplan and A. Manohar [119], the light quark masses *and* the low-energy coefficients cannot be univocally fixed by the phenomenological input.

The above mentioned ambiguity, known in the literature as the Kaplan-Manohar ambiguity, was actually the first motivation for considering ChPT in the framework of lattice computations [39, 169]. In lattice QCD, the quark masses can be *fixed* as

external parameters, and, therefore, the missing information for determining of the low-energy coefficients and thus for closing the ChPT relations is provided. Moreover, since in lattice QCD all quark masses can be in principle lowered to arbitrarily small values (with some limitations), higher order ChPT corrections can be made negligible. As we will see, a special lattice technique (partial quenching) can be exploited in order to enhance the level of information about the quark mass dependence of hadronic observables.

The values of the GLC, beyond being interesting for themselves, can also be used for extrapolating the lattice data to the physical point for the light u and d quarks (the starting point of this discussion). An unsettled issue in this context is the role of the s quark. In nature the latter is considerably heavier than the u and d quarks and it is not obvious at all that it can be viewed as "light" (the K and η masses are not extremely small when compared to the typical cut-off scale of ChPT). In view of very accurate lattice determinations, the amount of systematic uncertainty injected in the final estimates by the ChPT formulae used for the extrapolations can potentially represent an issue. A conservative approach in this sense would be to simulate the s quark at the physical value of the mass and use chiral formulae for two light quarks for the extrapolations in the and u and d quark masses. On the other hand, simulation of the theory very near or even at the physical point for the two lightest quarks seems to be now at reach.

In Section 2.3 of this chapter, first lattice determinations of the low-energy coefficients in $N_f = 2$ QCD will be presented. This represents an approximation of the physical case where the dynamics of heavier quarks is also involved. The next two sections will be devoted to a brief overview of ChPT and of its applications in lattice QCD.

2.1. Chiral Perturbation Theory (ChPT)

Chiral Perturbation Theory (ChPT)[1] is an effective theory of the strong interactions and therefore characterized by an intrinsic energy cut-off, conventionally denoted with $\Lambda_\chi \simeq 1$ GeV. For energies $E < \Lambda_\chi$ and up to a given precision $O((E/\Lambda_\chi)^n)$, a finite number of counterterms must be introduced in the chiral Lagrangian for the computation of physical quantities. In opposition to a fundamental theory, however, the number of counterterms (and related free parameters) needed for an arbitrary precision increases indefinitely.

We recall here the few basic assumptions which are at the basis of ChPT.

i) In the case of N_f *massless* quarks the fundamental underlying theory (QCD) is invariant under the chiral group

$$G = \mathrm{SU}(N_f)_L \times \mathrm{SU}(N_f)_R \tag{2.1}$$

(see also (0.10), here $N_0 \equiv N_f$).

[1] A brief introduction to ChPT can be found for example in [41].

ii) The vacuum breaks spontaneously the chiral symmetry into its diagonal subgroup

$$\mathrm{SU}(N_f)_L \times \mathrm{SU}(N_f)_R \;\rightarrow\; \mathrm{SU}(N_f)_V \;; \tag{2.2}$$

the bosonic massless states postulated by the Goldstone theorem are identified with the octet of the pseudoscalar mesons for $N_f = 3$ (with the isotriplet of the pions in the case $N_f = 2$). For non-vanishing quark masses, these states are not exactly massless; they are however light compared to the typical hadron mass scale and dominate the low-energy dynamics of strong interactions.

iii) The masses of the light quarks can be treated as a small perturbation around the chiral limit.

Since we only consider pion properties, the discussion can be restricted to the sector of the pseudo-Goldstone bosons.

The interactions among pseudo-Goldstone bosons is the ideal application field of ChPT; here the discussion is particularly well-defined. The transformation properties of the fields under the chiral group can be derived from assumption ii); these build a non linear realization of G [188]. Once the transformation properties are established, assumption i) can be used to constrain the interaction terms. Chiral invariance forces the introduction of a growing number of derivatives at higher orders in the chiral Lagrangian: a derivative expansion of the strong interactions is in this way obtained; correspondingly, the amplitudes of the interactions are expanded in the external momenta p of the mesons: at zero momentum the interactions vanish.

It is convenient to parametrize the meson fields in a flavor $\mathrm{SU}(N_f)$ matrix transforming linearly under G:

$$U \xrightarrow{G} g_{_R} U g_{_L}^{-1} \;. \tag{2.3}$$

Explicitly:

$$\begin{aligned} U(x) &= e^{i\sqrt{2}\Phi(x)/F_0}, \\ \Phi &= \frac{1}{\sqrt{2}}\sum_{i=1}^{8}\phi^i\lambda_i = \begin{bmatrix} \frac{\pi^0}{\sqrt{2}} + \frac{\eta_8}{\sqrt{6}} & \pi^+ & K^+ \\ \pi^- & -\frac{\pi^0}{\sqrt{2}} + \frac{\eta_8}{\sqrt{6}} & K^0 \\ K^- & \bar{K}^0 & -\frac{2\eta_8}{\sqrt{6}} \end{bmatrix} ; \end{aligned} \tag{2.4}$$

in the above formula λ_i are the Gell-Mann matrices generating SU(3) and the first free parameter F_0 has been introduced, coinciding (as can be *a posteriori* inferred) with the decay constant of the pseudo-Goldstone boson in the chiral limit. At leading order (LO) in the chiral expansion, $O(p^2)$, just one term exists[2]

$$\mathcal{L}_2^{\chi} \;=\; \frac{F_0^2}{4}\langle \partial_\mu U \partial_\mu U^\dagger \rangle \;; \tag{2.5}$$

[2]Here and in the following, the formulae appropriate for the Euclidean theory are reported.

$\langle \cdots \rangle$ denotes the trace over the flavor indices.

In the case of explicit chiral symmetry breaking by a non-zero quark mass, the chiral transformations must be supplemented with a transformation of the quark mass matrix $\mathcal{M}$ in order to maintain the invariance under the chiral group (spurion symmetry). These transformations can be read-off from the (chirality-breaking) mass term in the QCD Lagrangian

$$\mathcal{L}_M^{QCD} \;=\; \bar{\psi}_L \mathcal{M} \psi_R \;+\; h.c.\,, \quad \mathcal{M} = \mathrm{diag}(m_u, m_d, m_s)\;; \tag{2.6}$$

the required transformations follow:

$$\mathcal{M} \xrightarrow{G} g_{_L} \mathcal{M} g_{_R}^{-1}\;. \tag{2.7}$$

The most general LO term invariant under this generalized symmetry is

$$\mathcal{L}_2^\chi = \frac{F_0^2}{4} \langle \partial_\mu U \partial_\mu U^\dagger - X U^\dagger - U X^\dagger \rangle\;, \qquad X = 2B_0 \mathcal{M}\;, \tag{2.8}$$

where B_0 is a second arbitrary low-energy constant.

In the $N_f = 3$ case, twelve terms appear at next-to-leading (NLO) order $O(p^2)$ [89]; these can be reduced to eight when external fields describing electroweak interactions are set to zero and contact terms neglected[3]:

$$\begin{aligned} \mathcal{L}_4^\chi \;=\; & -L_1 \langle \partial_\mu U^\dagger \partial_\mu U \rangle^2 - L_2 \langle \partial_\mu U^\dagger \partial_\nu U \rangle \langle \partial_\mu U^\dagger \partial_\nu U \rangle - L_3 \langle \partial_\mu U^\dagger \partial_\mu U \partial_\nu U^\dagger \partial_\nu U \rangle \\ & + L_4 \langle \partial_\mu U^\dagger \partial_\mu U \rangle \langle X^\dagger U + X U^\dagger \rangle + L_5 \langle \partial_\mu U^\dagger \partial_\mu U (X^\dagger U + X U^\dagger) \rangle \\ & - L_6 \langle X^\dagger U + X U^\dagger \rangle^2 - L_7 \langle X^\dagger U - X U^\dagger \rangle^2 - L_8 \langle X^\dagger U X^\dagger U + X U^\dagger X U^\dagger \rangle\;. \end{aligned} \tag{2.9}$$

The coefficients L_i, known in the literature as "Gasser-Leutwyler coefficients" (GLC), together with the low-energy constants F_0 and B_0, encode the missing information from QCD at high energies above the cut-off scale Λ_χ.

As an example of application of ChPT we take here, and for the different extensions of ChPT which will be considered in the following, the mass of the pseudo-Goldstone bosons in presence of N_f light quarks with equal mass [88]. The chiral expansion delivers in this case a correction to the Gell-Mann–Oaks–Renner formula [94]:

$$\begin{aligned} M^2/F_0^2 \;&=\; \chi\,(1 \,+\, \delta_{NLO,loop}) \,+\, \delta_{NLO,tree} \,+\, O(\chi^3)\;, \\ \delta_{NLO,loop} \;&=\; \frac{1}{16\pi^2 N_f}\,\chi\,\ln\frac{\chi}{16\pi^2}\;, \\ \delta_{NLO,tree} \;&=\; 8[N_f(2L_6 - L_4) + (2L_8 - L_5)]\,\chi^2\;, \end{aligned} \tag{2.10}$$

where, in view of the future lattice applications, we have introduced the "dimensionless quark mass"

$$\chi \;=\; \frac{2B_0 m_q}{F_0^2}\;. \tag{2.11}$$

[3] In the case $N_f = 2$ some of the terms are redundant.

As in any standard quantum field theory, the ultraviolet divergences from the virtual pseudo-Goldstone boson loops call for renormalization. This means that the GLC appearing in estimates like (2.10) are *renormalized* at some (arbitrary) scale[4]; the above formula applies to the $\overline{MS}$-scheme with renormalization scale fixed at a conventional value

$$L_i \equiv L^r(\mu_{ren}) \; ; \quad \mu_{ren} = \Lambda_\chi \equiv 4\pi F_0 \; . \tag{2.12}$$

Observe that the correction to the squared pseudo-Goldstone boson masses coming from the virtual loops, $\delta_{NLO,loop}$, is characterized by the already anticipated non-analytic dependence upon the quark masses. This important prediction of ChPT, related to the peculiar pattern of the chiral symmetry breaking, can be verified in lattice QCD.

2.1.1. Gasser-Leutwyler coefficients from phenomenology

As already briefly mentioned in the introduction to this chapter, due to the Kaplan-Manohar ambiguity, phenomenological input and ChPT formulae alone are not sufficient to fix all the GLC. This ambiguity derives from an invariance of the NLO chiral Lagrangian under redefinition of the quark masses and of some low-energy coefficients [89]

$$\begin{aligned} X &\rightarrow X + \delta \, \frac{16}{F_0^2} \, (\mathrm{det}X) X^{-1} \\ L_6 &\rightarrow L_6 - \delta, \quad L_7 \rightarrow L_7 - \delta, \quad L_8 \rightarrow L_8 + 2\delta \; , \end{aligned} \tag{2.13}$$

where δ is an arbitrary dimensionless parameter. Quantities which, expressed in terms of GLC and quark masses, are *not* invariant under (2.13) cannot be fully determined in ChPT [119].

One of such quantities is the NLO correction to the quark mass ratios. Relations similar to (2.10), and phenomenological input for the pseudoscalar meson sector, can in principle put constraints on the quark masses realized in nature. In particular, a relation can be found between the two quark mass ratios m_u/m_d and m_s/m_d. In order to pin down the mass ratios themselves, however, the NLO order correction is needed

$$\Delta_M \; = \; \frac{8}{F_0^2} (M_K^2 - M_\pi^2) \, (2L_8 - L_5) \; + \; \text{chiral logs} \; . \tag{2.14}$$

Since the combination of GLC contained in Δ_M is not invariant under (2.13), this quantity is affected by the Kaplan-Manohar ambiguity. The value of the ratio m_u/m_d is theoretically relevant; in particular, the vanishing of the m_u would solve the so-called *strong CP problem*. (See [20] for a review on the subject. However, see also [46] for a criticism to this solution of the strong CP problem.)

The example of Δ_M shows that chiral symmetry alone cannot, in some cases, fully constrain physical quantities in hadron phenomenology. One possible solution to this

[4] In order to keep the notation as simple as possible, we use for these renormalized coefficients the same notation as for the bare ones appearing in the Lagrangian.

problem is to introduce some additional information from the fundamental theory of strong interactions (see [130] for a discussion on this topic). A combination of phenomenological and large N_c constraints can be used for example to fix all the GLC [65]. This additional information is however subject to large theoretical uncertainties, which spoil the accuracy the determinations. For the GLC needed for Δ_M, one obtains in this way the estimates (see for example [109])

$$L_8 = (0.6 \pm 0.3) \cdot 10^{-3} , \tag{2.15}$$
$$L_5 = (0.4 \pm 0.5) \cdot 10^{-3} . \tag{2.16}$$

These values of the GLC imply a small and positive Δ_M:

$$0 < \Delta_M \leq 0.13 . \tag{2.17}$$

On the other hand, a massless u quark requires [39]

$$L_8 = (-0.7 \pm 0.3) \cdot 10^{-3} . \tag{2.18}$$

implying a large negative NLO correction Δ_M. This second scenario is theoretically disfavored since it implies too large breaking effects of the SU(3) flavor symmetry [130]. However, due to the large uncertainties in the determinations (2.15), the question is not yet completely settled.

An accurate determination of the GLC is in general important in order to constrain QCD predictions. The intrinsic systematic errors on ChPT estimates coming from the neglected NNLO corrections (assuming exact knowledge of the NLO GLC) are generally smaller than the uncertainties deriving from the present, rather poor, knowledge of the GLC (a recent review of GLC determinations from phenomenology can be found in [64]). As we will see in the following in this chapter, lattice QCD can provide the additional information needed for a determination of the GLC with full control over systematic errors.

2.2. Gasser-Leutwyler coefficients from lattice QCD

Lattice computations of hadron properties can be used for the determination of the low-energy constants in NLO ChPT (see [97] for an early discussion). In lattice simulations the quark mass represents an external parameter which can be arbitrarily fixed and the Kaplan-Manohar ambiguity, expressed by (2.13), is resolved. In this approach, the GLC are determined by fitting the light quark mass dependence of the different hadron properties with the functional form predicted by NLO ChPT.

In the following we briefly discuss the main systematic uncertainties affecting this methodology. For the regime of moderate quark masses of the simulations considered here, the systematic effects produced by the finite volume can be kept under control. On the other side, the contribution of the neglected NNLO corrections in the chiral formulae can be relevant. As we will see in the following when discussing the numerical studies, this turns out to be the dominating source of systematic error.

A separate discussion must be reserved to the lattice discretization effects. Ideally, the chiral fits should be performed after the extrapolation of the lattice data in the continuum, where ChPT formulae apply. An alternative procedure consists in fitting the lattice data at finite lattice spacing and extrapolating the resulting fitted parameters in the continuum. This can be improved by including in the chiral formulae the leading corrections coming from the explicit chirality breaking of the lattice discretization. A general discussion of the lattice corrections in ChPT is possible in the so-called "Wilson chiral perturbation theory", to be discussed in the following in this section. Even in this improved approach however, a continuum extrapolation of the fitted parameters is eventually required, because of the neglected sub-leading discretization effects. The convergence to the continuum is however faster, with a reduction of the systematic uncertainties attached to the determinations of the low energy constants.

2.2.1. Partially quenching

The information about the light quark mass dependence of hadron properties is at the basis of the determination of the GLC from the lattice. As noticed in [39, 169] the possibility in lattice simulations to assign different masses to *valence* and *sea* quarks allows to enhance this information.

Given a generic lattice operator of the lattice quark fields $\bar{\psi}, \psi$ and the gauge links U, $O^L[U; \bar{\psi}, \psi]$, its vacuum expectation value can be written (recall the discussion in Subs. 0.3.1)

$$\langle O^L \rangle \;=\; \frac{1}{\mathcal{N}} \int \prod_{x\in\Lambda\,,\mu} dU_\mu(x) \prod_{q=u,d,\ldots} \mathrm{det} Q^{(q)}[U; m_q]\, \mathrm{e}^{-S^g_{WQCD}[U]}\; \tilde{O}[U; m_q]\;, \tag{2.19}$$

where the effective operator $\tilde{O}[U, m_q]$ is a complicated functional of the gauge links, resulting after the explicit integration over the lattice quark field Grassmann variables. In (2.19) the dependence of the vacuum expectation value upon the light quark masses has been made explicit, in a collective notation, for future convenience.

It is possible to compute a generalization of the expectation value (2.19), in which the *valence* and *sea* quarks have different masses; the sea mass is contained in the fermion determinant contributing to the effective action of the link system, while the valence mass applies for the effective operator. In formulae:

$$\mathcal{F}(m_{sea}, m_{val}) = \frac{1}{\mathcal{N}} \int \prod_{x\in\Lambda\,,\mu} dU_\mu(x) \prod_{q=u,d,\ldots} \mathrm{det} Q^{(q)}[U; m_{q,sea}]\; \mathrm{e}^{-S^g_{WQCD}[U]}\; \tilde{O}[U; m_{val}] \;\equiv$$
$$\langle\, \tilde{O}[U, m_{val}]\, \rangle_{P[U; m_{sea}]}\;. \tag{2.20}$$

The most expensive part of a lattice computation is generally represented by the generation of the canonical ensemble of lattice gauge configurations $\{U\}$ distributed according to the multivariate probability density

$$P[U; m_{sea}] \;=\; \frac{1}{\mathcal{N}} \prod_{q=u,d,\ldots} \mathrm{det} Q^{(q)}[U; m_{q,sea}]\;\; \mathrm{e}^{-S^g_{WQCD}[U]}\;. \tag{2.21}$$

On the other hand, the computation of $\tilde{O}[U, m_{val}]$ for each configuration of the gauge sample is comparably less demanding. This suggests that more information about the functional dependence upon the light quark masses of the hadron vacuum expectation value (2.19) can be obtained in a relatively "cheap" way by computing the generalized version (2.20) for different values of m_{val} at a fixed m_{sea}.

If the step from (2.19) to (2.20) is trivial in the effective action formalism exploited in lattice QCD, it requires more thought at the level of the (continuum) fundamental theory. Here, the introduction of bosonic ghost quark fields $\tilde{\psi}_q$ is required in order to cancel the fermion determinant of the valence quarks [141]. The resulting theory is no longer unitary. In the case of two valence quarks having masses m_{V1}, m_{V2} and N_f sea quarks with masses $(m_{S_1}, \cdots, m_{S_{N_f}})$ for example, one is in presence of an extended quark multiplet

$$\psi = (\psi_{qV1}, \psi_{qV2};\, \psi_{qS1}, \ldots, \psi_{qSN_f};\, \tilde{\psi}_{qV1}, \tilde{\psi}_{qV2}) \;; \tag{2.22}$$

the mass matrix in the generalized QCD Lagrangian is given by

$$\mathcal{M} = \mathrm{diag}(m_{V1}, m_{V2};\, m_{S1}, \ldots, m_{S_{N_f}};\, m_{V1}, m_{V2}) \;. \tag{2.23}$$

The low-energy theory of this generalization of the QCD Lagrangian gives rise to a "partially quenched" ChPT [26].

As an illustration of this partially quenched ChPT we consider the generalization of (2.10) with N_f degenerate sea quark masses $m_{S1} = m_{S2} = \ldots = m_{S_{N_f}} = m_S$ and valence quark masses (m_A, m_B) [167]:

$$\begin{aligned} M_{AB}^2/F_0^2 &= \frac{1}{2}(\chi_A + \chi_B)(1 + \delta_{NLO,loop}) + \delta_{NLO,tree} + O(\chi^3) \;, \\ \delta_{NLO,loop} &= \frac{1}{16\pi^2 N_f}\left[(\chi_S - \chi_A)\chi_A \ln\frac{\chi_A}{16\pi^2} - (\chi_S - \chi_B)\chi_B \ln\frac{\chi_B}{16\pi^2}\right]\frac{1}{(\chi_B - \chi_A)} \;, \\ \delta_{NLO,tree} &= 4N_f(2L_6 - L_4)\chi_S(\chi_A + \chi_B) + 2(2L_8 - L_5)(\chi_A + \chi_B)^2 \end{aligned} \tag{2.24}$$

(χ is the dimensionless quark mass defined in (2.10)). The basic point when using (2.24) and analogous partially quenched ChPT formulae is that [39, 169] the quark mass dependence in the chiral Lagrangian is *only explicit*, and in particular the GLC appearing in (2.24) are those of the unitary theory with $m_{val} = m_{sea}$ and the *same number of sea quarks* N_f.

That the partially quenched analysis provides more information than the standard one is apparent already in (2.24): in this case, in opposition to the "unquenched" case (2.10), the combination of GLC $(2L_8 - L_5)$ can be disentangled from the other combination $(2L_6 - L_4)$. Notice that exactly this combination of GLC is required in order to settle the question of the vanishing of the u quark mass, see (2.14). When the decay constants are included in the partially quenched analysis as well [105], all four GLC L_4, L_5, L_6 and L_8 can be separately determined.

Another advantage of partially quenching is a faster convergence of the chiral formulae for $m_{val} < m_{sea}$ [169]; in particular, NLO corrections below 10% require light quark masses m_q as light as one eight of the physical strange quark mass [169].

2.2.2. Including lattice artifacts

The artifacts of the lattice discretization introduce corrections in the ChPT formulae. These corrections can be computed in a systematic way in Wilson ChPT [170, 159].

As shown by K. Symanzik [179], the lattice artifacts of Green functions in Wilson lattice QCD are described in a synthetic way by a continuum *local effective Lagrangian* (LEL) $\mathcal{L}^{eff}$. The latter can be written in form of an expansion in which the lattice spacing a plays the role of an external expansion parameter:

$$\mathcal{L}^{eff} \;=\; \mathcal{L}_0^{eff} + a\mathcal{L}_1^{eff} + a^2\mathcal{L}_2^{eff} + \cdots \;. \tag{2.25}$$

The first, dimension four, term of the expansion $\mathcal{L}_0^{eff}$ coincides with the continuum QCD Lagrangian $\mathcal{L}^{QCD}$, while further higher dimensional terms account for the lattice corrections. The residual symmetries of Wilson lattice QCD restrict the possible form of these operators. Some of them are obtained by multiplying lower dimensional operators with powers of the quark mass and only produce a renormalization of the quark mass and of the coupling constant. Since these operators do not introduce a lattice-specific breaking of the chiral symmetry, they do not generate new terms in the chiral expansion[5].

At $O(a)$ one is left with two operators [173], which *on shell* reduce to one; this is the Pauli term

$$\mathcal{L}_1^{eff} \;=\; c_{SW}\,\bar{\psi}\sigma_{\mu\nu}F_{\mu\nu}\psi \;. \tag{2.26}$$

The coefficient c_{SW} is in general a function of the lattice coupling constant and of the Wilson parameter r. It can be formally promoted to a matrix in flavor space (analogous to the mass matrix $\mathcal{M}$ in Eq. (2.6)), in this way, we see that the pattern of flavor breaking of the Pauli term is analogous to that of the mass term (2.6), producing the same breaking terms in the chiral Lagrangian.

$O(a^2)$ terms in the effective action (2.25) introduce further breaking parameters [21] associated with dimension six operators $\mathcal{L}_2^{eff}$. All these breaking parameters can be treated as spurion fields with appropriate transformation properties under the chiral group G (see Sec. 2.1) and the corresponding contributions to the low-energy Lagrangian evaluated in a spurion analysis.

We have now essentially *two* dimensionless expansion parameters

$$\epsilon \;\sim\; \frac{p^2}{\Lambda_\chi^2} \sim \frac{2B_0 m_q}{\Lambda_\chi^2} \;, \qquad \delta \;\sim\; \frac{2W_0 a}{\Lambda_\chi^2} \;; \tag{2.27}$$

W_0 is a low-energy constant with mass dimension three, related to the discretization effects, and analogous to B_0, whose precise meaning will become clear in a while.

At this point the question arises about the appropriate power counting scheme. If the magnitude of the breaking effects coming from the lattice discretization is comparable to that of the chirality breaking from the quark mass, synthetically $m_q = O(a)$

[5] In the case of the quark mass, these lattice artifacts can be reabsorbed in a lattice definition of the quark mass, see (3.17).

or $\epsilon \sim \delta$, the correct criterion for collecting terms in the LO and NLO Lagrangian is [159] (we use the notation $\mathcal{L}^W$ for the effective low-energy Lagrangian of the Wilson theory):

$$\begin{aligned} \text{LO:} \quad \mathcal{L}_2^W &\sim O(\epsilon, \delta) \ , \\ \text{NLO:} \quad \mathcal{L}_4^W &\sim O(\epsilon^2, \epsilon\delta, \delta^2) \ . \end{aligned} \tag{2.28}$$

A different power counting, more appropriate in the case of a small quark mass and dominating $O(a)$ breaking effects, is [12]

$$\begin{aligned} \text{LO:} \quad \mathcal{L}_2^W &\sim O(\epsilon, \delta, \delta^2) \ , \\ \text{NLO:} \quad \mathcal{L}_4^W &\sim O(\epsilon\delta, \delta^3) \ ; \end{aligned} \tag{2.29}$$

in this case it is assumed $m_q = O(a^2)$. We will consider here an application of the first power counting scheme (2.28). In this scheme, the LO and NLO lattice terms only come from the chirality breaking parameters, since the chiral-symmetric corrections coming for example from the lattice gauge action, but also from the fermion action, are $O(p^2a^2)$ and NNLO.

The generalization of the LO chiral Lagrangian (2.8) is simply obtained by making the replacement

$$X \to X + R \ , \qquad R = 2W_0\mathcal{A} \ , \tag{2.30}$$

where, in order to highlight the formal analogy with the breaking from the quark mass, the lattice spacing has been transformed into a matrix in flavor space $\mathcal{A}$, to be set eventually to $\mathcal{A} = aI$. In this way we get:

$$\mathcal{L}_2^W = \frac{F_0^2}{4}\langle \partial_\mu U \partial_\mu U^\dagger - (X+R)U^\dagger - U(X^\dagger + R^\dagger)\rangle \ . \tag{2.31}$$

New terms appear in the NLO Lagrangian [159, 21]

$$\begin{aligned} \mathcal{L}_4^W \ = \ & \mathcal{L}_4^\chi \ + \ W_4 \left\langle \partial_\mu U^\dagger \partial_\mu U \right\rangle \left\langle R^\dagger U \ + \ R U^\dagger \right\rangle \ + \ W_5 \left\langle \partial_\mu^\dagger U \partial_\mu U (R^\dagger U + R U^\dagger) \right\rangle \\ & - W_6 \left\langle X^\dagger U + X U^\dagger \right\rangle \left\langle R^\dagger U + R U^\dagger \right\rangle \ - \ W_7 \left\langle X^\dagger U - X U^\dagger \right\rangle \left\langle R^\dagger U - R U^\dagger \right\rangle \\ & - W_8 \left\langle R^\dagger U X^\dagger U + \text{h.c.} \right\rangle \ - \ W_6' \left\langle R^\dagger U + R U^\dagger \right\rangle^2 \ - \ W_7' \left\langle R^\dagger U - R U^\dagger \right\rangle^2 \\ & - W_8' \left\langle R^\dagger U R^\dagger U + \text{h.c.} \right\rangle \ , \end{aligned} \tag{2.32}$$

with associated lattice low-energy coefficients W_i, W_i' ("Wilson Gasser-Leutwyler Coefficients", Wilson GLC).

The main dependence upon the lattice spacing in the NLO Wilson ChPT Lagrangian, $O(a)$ and $O(p^2a, m_q a, a^2)$, is *explicit*. In particular, the GLC in $\mathcal{L}_4^\chi$ are the ones of the continuum theory. This means that the Wilson ChPT formulae can be used in order to determine the GLC from (Wilson) lattice data with leading discretization errors $O(m_q^2 a, m_q a^2, a^3)$.

Since the Wilson GLC, as the GLC, contain information about the high energy details of the underlying lattice theory, their actual value depends on the precise way

the theory is discretized, the gauge sector included. For example in the case of an $O(a)$ improved fermion action, the LO Lagrangian coincides with the continuum one and $W_4, \dots W_8 = 0$. Moreover the left-over discretization errors in the physical quantities are in this case $O(m_q a^2, a^3)$.

On the other hand, using NLO Wilson ChPT with the unimproved Wilson action for the extraction of physical quantities from lattice data is almost equivalent, from the point of view of the lattice artifacts, to a standard ChPT analysis with a non-perturbatively $O(a)$ improved action. The only difference in the residual lattice artifacts is indeed represented by the absence in the latter case of the (presumably small) $O(m_q^n a), n \geq 2$, corrections.

It should be recalled at this point that the chirality breaking parameters in the Symanzik effective action depend in general upon the lattice bare coupling constant g_0 (and the Wilson parameter r), in particular, $c_{SW} = c_{SW}(g_0, r)$. This dependence is in general inherited by the lattice low-energy constant W_0 and by the Wilson GLC. The renormalization group dictates on the other hand a weak dependence of g_0 on the lattice spacing for fixed renormalized theory: at leading order $g_0 \sim \ln(a\Lambda_{QCD})$. This means that the dependence of the lattice low-energy constants upon g_0 can be seen as a residual, not explicit, dependence of the Wilson ChPT Lagrangian upon the lattice spacing.

We conclude this introductory section about Wilson ChPT with an example of how lattice artifacts modify ChPT predictions. In the case of the pseudo-Goldstone boson mass considered in Eq. (2.10) for example, one gets [21]

$$\begin{aligned} M^2/F_0^2 &= (\chi+\rho)(1 + \delta^W_{NLO,loop}) + \delta^W_{NLO,tree} + O(\chi^3, \chi^2\rho, \chi\rho^2, \rho^3) \ , \quad (2.33) \\ \delta^W_{NLO,loop} &= \frac{1}{16\pi^2 N_f}(\chi+\rho)\ln[(\chi+\rho)/16\pi^2] \ , \\ \delta^W_{NLO,tree} &= \delta_{NLO,tree} + 8[N_f(2W_6 - W_4 - L_4) + 2W_8 - W_5 - L_5]\,\chi\rho + \\ &\quad +8[N_f(2W_6' - W_4) + (2W_8' - W_5)]\,\rho^2 \ , \end{aligned}$$

where we define here, in analogy with (2.11), a dimensionless lattice breaking parameter:

$$\rho = \frac{2W_0 a}{F_0^2} \ . \quad (2.34)$$

Observe that, due to (2.30), the LO and NLO loop corrections are simply obtained by making the replacement $\chi \to \chi + \rho$ in the corresponding terms in the ChPT result (2.10), while the tree-level NLO correction can be trivially derived from the Lagrangian (2.32) by analogy with the continuum terms. For the sake of the completeness we also quote the partially quenched result, namely the lattice-corrected version of (2.24):

$$\begin{aligned} M^2_{AB}/F_0^2 &= [\frac{1}{2}(\chi_A+\chi_B)+\rho](1 + \delta^W_{NLO,loop}) + \delta^W_{NLO,tree} + O(\chi^3, \chi^2\rho, \chi\rho^2, \rho^3) \ , \\ \delta^W_{NLO,loop} &= \frac{1}{16\pi^2 N_f}\left\{(\chi_S - \chi_A)(\chi_A+\rho)\ln[(\chi_A+\rho)/16\pi^2]\right. \end{aligned}$$

$$
\begin{aligned}
& - (\chi_S - \chi_B)(\chi_B + \rho) \ln[(\chi_B + \rho)/16\pi^2] \Big\} \, \frac{1}{(\chi_B - \chi_A)} \; , \\
\delta^W_{NLO,tree} \;\; = \;\; & \delta_{NLO,tree} \; + \; 8N_f(W_6 - L_4)\, \chi_S \rho \; + \\
& 4[N_f(W_6 - W_4) + 2W_8 - W_5 - L_5]\, \rho(\chi_A + \chi_B) \; + \\
& + 8[N_f(2W'_6 - W_4) + (2W'_8 - W_5)]\, \rho^2 \; .
\end{aligned} \tag{2.35}
$$

2.3. Determination of the Gasser-Leutwyler coefficients [Chi-1,Chi-2,Chi-3]

After the theoretical breakthrough of [39, 169], where the potentiality of lattice simulations for the determination of the GLC was realized, several groups started numerical investigations. In the first paper on the subject [105] ($N_f = 2$ Wilson formulation in the quenched approximation) the inclusion of the decay constants together with the masses in the pseudo-Goldstone boson sector was suggested. These quantities can be determined on the lattice with extremely high statistical precision. In [105] the advantage of using in the analysis *ratios* of hadron quantities computed at different valence (or sea) quark masses, was also pointed out. In the case of the pseudo-Goldstone boson mass, with N_f degenerate quarks, one may consider for example the combination [105]

$$
Rn_{AB} = \frac{M^2_{AB}/(\chi_A + \chi_B)}{M^2_{SS}/2\chi_S} \; . \tag{2.36}
$$

Since the quantities in numerator and denominator are highly correlated, the ratio Rn_{AB} can be determined with high statistical precision for different values of the valence quark masses $m_{A,B}$. An additional advantage is that, in a mass independent renormalization scheme, the renormalization constants (of the quark mass in the above case) cancel out between numerator and denominator. Mass independent discretization effects cancel out, too, see in the following.

We consider here as an example the continuum partially quenched ChPT representation of the pseudo-Goldstone boson mass ratio [167] (see also [Chi-2])

$$
Rn_{VV} = 1 + 8(\xi - 1)\chi_S(2L_{S8} - L_{S5}) + \frac{\chi_S}{16\pi^2 N_f}[\xi - 1 + (2\xi - 1)\log\xi] + \text{NNLO} \; , \tag{2.37}
$$

where ξ denotes the ratio between the valence and the sea quark mass

$$
\xi = \frac{\chi_V}{\chi_S} \tag{2.38}
$$

and we have introduced the GLC L_{Si} renormalized at the sea quark mass scale

$$
L_{Si} \;\; : \quad \mu_{ren} \; = \; \sqrt{2B_0 m_S} \; = \; \sqrt{\chi_S} F_0 \; ; \tag{2.39}
$$

with this choice, the sea quark mass dependence of the chiral logs is reabsorbed in the renormalization scale[6]. In the case of Eq. (2.37), the sea quark mass plays the role of

[6]The L_{Si} are related to the standard GLC L_i, renormalized at the scale $\mu = 4\pi F_0$, by a renormalization group transformation, see for example [Chi-1], Eqs. (5-13).

a *reference quark mass*, while the valence quark mass is varied (*valence quark mass analysis*).

If several quark masses are available, one can choose one of the sea masses (say the largest one) as reference quark mass and study the mass ratios as a function of the remaining sea quark masses (*sea quark mass analysis*). In this case the relevant formula is (see [Chi-2]):

$$Rn_{SS} \equiv \frac{M_{SS}^2/\chi_S}{M_{RR}^2/\chi_R} = \tag{2.40}$$
$$1 + 8(\sigma-1)\chi_R(2N_f L_{R6} + 2L_{R8} - N_f L_{R4} - L_{R5}) + \frac{\chi_R}{16\pi^2 N_f}\sigma\log\sigma + \text{NNLO} ,$$

where now the label R refers to the *reference sea quark mass* and the ratio σ is defined as

$$\sigma = \frac{\chi_S}{\chi_R} ; \tag{2.41}$$

in this case the GLC L_{Ri} have been renormalized at the appropriate reference scale

$$L_{Ri} \; : \quad \mu_{ren} = \sqrt{2B_0 m_R} = \sqrt{\chi_R} F_0 . \tag{2.42}$$

The two procedures can be of course combined. In the case of $p > 1$ simulation points, with $m_{S0} > m_{S1} > \ldots > m_{Sp}$, one can define several σ variables $\sigma_0, \ldots, \sigma_p$. Taking m_{S0} as reference quark mass, $m_{S0} \equiv m_R$, one has of course $\sigma_0 \equiv 1$, while a generic valence quark mass for the ith simulation point is related to the reference quark mass by

$$m_V = \xi\,\sigma_i\, m_R ; \tag{2.43}$$

the same relation holds for the dimensionless quark masses χ_V and χ_R.

The parameters ξ and σ can be easily determined by computing ratios of the appropriate PCAC quark masses (1.20). The left-over parameter χ_R can be determined by using the LO formula

$$\chi_R = \frac{M_{RR}^2}{F_0^2} \tag{2.44}$$

(the NLO correction to the above formula enters at NNLO) and inserting for M_{RR} the measured value of the pseudo-Goldstone boson mass at the reference quark mass and for F_0 the phenomenological value of $F_0 = 87$ MeV [105]; this procedure however requires fixing the lattice scale. Alternatively, this is the procedure considered here, χ_R can be viewed as an unknown parameter and fitted together with the GLC.

The method proposed in [105] foresees a prior continuum extrapolation of the hadron ratios at fixed values of χ_R, ξ, σ.[7] After continuum extrapolation, partially quenched continuum ChPT formulae such as (2.37) can be applied.

[7] The dimensionless ratios (2.36), and other ratios with different combinations of the quark masses (for example valence-sea "VS"), are after the continuum extrapolation *universal* functions of the dimensionless parameters (χ_R, ξ, σ).

The optimal strategy would be to extrapolate the lattice data at a fixed value of the quark mass. In this way, in particular, one can avoid large lattice artifacts occurring when the quark mass is lighter than the typical mass scale of the chirality breaking at finite lattice spacing ($\chi \ll \rho$). In this regime the phase structure, of the lattice theory is expected to depart from the continuum one (these aspects will be discussed in more detail in the next chapter and in particular in Sec. 3.3).

Performing the continuum extrapolation before the chiral fits can be however very expensive in terms of computing time, especially in the case of light dynamical quarks. An alternative procedure, which we consider here, consists in fitting the ChPT formulae at *fixed lattice spacing*.[8]

As we have seen in the previous section, the application of Wilson ChPT at NLO allows to reduce the discretization errors in the determination of the low-energy constants to $O(m_q^2 a)$ in the unimproved theory. The dimensionless lattice scale ρ and the Wilson ChPT coefficients $W_4, \ldots, W_8$, which describe the main lattice artifacts linear in a, enter as additional fit parameters (see for example (2.33)).

Observe that, since the mass independent cut-off effects cancel out in the ratios, the primed Wilson GLC do not appear in the corresponding Wilson ChPT formulae. For light quark masses, it is legitimate to assume that the residual $O(m_q^2 a)$ corrections are equivalent to the $O(m_q a^2)$ corrections affecting the standard analysis with a (non-perturbatively) $O(a)$ improved fermion action.

2.3.1. Setup

The analyzes of [Chi-1, Chi-2, Chi-3] are based on sets of configurations ($N_f = 2$ theory) on lattices with extension in the space direction $L_s = 16$ and extensions in the time direction $L_t = 16$ [Chi-1,Chi-2] and 32 [Chi-3]. Lattice QCD in the Wilson setup was simulated by the TSMB algorithm in the configuration described in Sec. 1.2. Two values of β were considered, $\beta = 4.8$ in [Chi-1] corresponding to $a(4.8) \simeq 0.27$ fm and $\beta = 5.1$ in [Chi-2] and [Chi-3] corresponding to a smaller lattice spacing $a(5.1) \simeq 0.19$ fm. The analysis at $\beta = 4.8$ includes only one, fairly light, sea quark mass $m_S \simeq m_s/4$ ($M_\pi \simeq 360$ MeV); this point reflects one simulation point of [Alg], where a behavior of hadron properties in the pseudo-Goldstone boson sector compatible with ChPT predictions was observed, see discussion in Subsec. 1.3.4. The simulations of [Chi-2] and [Chi-3] include several values of the quark mass, with m_S ranging between $m_s/3$ and $m_s/2$ ($M_\pi = 380 - 680$ MeV). The simulations of [Chi-3] differ from those of [Chi-2] for a doubled extension in the time direction, $L_t = 32$, which allows for an accurate determination of the hadron quantities; a fourth simulation point was included at an intermediate value of the quark mass.

The valence analysis includes valence quark masses both lighter and heavier than the sea mass. On the coarser lattice, ξ (see definition (2.38)) could not be lowered below the value 0.9 due to the appearance of exceptional configurations. On the finer

[8] In this case one has to make sure that, at the give regime of quark masses, the phase structure of the lattice theory still reflects the continuum theory, see also Sec. 3.3.

lattice and with heavier sea masses, ξ could be lowered down to ~ 0.5 with a maximal value $\xi \sim 2$.

The physical lattice extension is large in the $\beta = 4.8$ simulation, $L_s \simeq 4.5$ fm, while for the $\beta = 5.1$ simulations, $L_s \simeq 3$ fm. This must be compared with the lightest pion masses. In the present case, finite volume effects reside in the permille region and can be safely neglected (see for example Tables 3 and 4 of [40]).

The evaluation of the remaining two main systematic effects, the discretization errors and the contribution from NNLO terms in ChPT, is less straightforward. The discretization effects can only be estimated by comparing simulations at different lattice spacings and fixed remaining parameters, which is not possible in the present case. An indirect estimate can be obtained from the evaluation of the breaking terms in the Wilson ChPT formulae. The latter estimate relies however on the validity of the lattice-corrected formulae for the given regime of lattice spacings and quark masses. As we will see in the following section, this second indirect estimate points to small lattice artifacts. The impact of the NNLO corrections will be estimated by including a subset of NNLO terms in the chiral fits. The NNLO corrections turn out to be essential for the quality of the fits in the case of the heavier sea masses.

2.3.2. Strategy

The chiral fits of [Chi-1,Chi-2,Chi-3] include various ratios of pseudo-Goldstone boson masses and decay constants. We give in the following an overview. In the sea sector:

$$Rn_{SS} = \frac{M_{SS}^2}{\sigma M_{RR}^2} \ , \qquad Rf_{SS} = \frac{F_{SS}}{F_{RR}} \ . \tag{2.45}$$

In the valence sector, starting with the single ratios:

$$Rn_{VV} = \frac{M_{VV}^2}{\xi M_{SS}^2} \ , \qquad Rf_{VV} = \frac{F_{VV}}{F_{SS}} \ , \tag{2.46}$$

$$Rn_{VS} = \frac{M_{VS}^2}{\xi M_{SS}^2} \ , \qquad Rf_{VS} = \frac{F_{VS}}{F_{SS}} \ . \tag{2.47}$$

In order to better constrain the fits, it is convenient to consider in addition *double ratios* in which the dependence on the GLC cancels out:

$$RRn = \frac{4\xi M_{VS}^4}{(\xi+1)^2 M_{VV}^2 M_{SS}^2} \ , \tag{2.48}$$

$$RRf = \frac{F_{VS}^2}{F_{VV} F_{SS}} \ . \tag{2.49}$$

The double ratio (2.49) was proposed in [104] with the motivation that it delivers, within NLO ChPT, a parameter-free prediction of the quark mass dependence in the pseudo-Goldstone boson sector. The latter can be easily tested against lattice data (with a negative result in that case of [104]).

As an illustration, we report the representation in NLO Wilson ChPT of Rn_{VV}, now also including lattice corrections (compare with (2.37))[9]; observe that the $O(a^2)$ mass independent corrections cancel out in the ratios:

$$\begin{aligned} Rn_{VV} \equiv \frac{M_{VV}^2}{\xi M_{SS}^2} &= 1 - \eta\frac{(\xi-1)}{\xi} \\ &+8(\xi-1)\chi_S(2L_{S8}-L_{S5}) + 8N_f\frac{(\xi-1)}{\xi}\eta\chi_S(L_{S4}-W_{S6}) \\ &+\frac{\chi_S}{16\pi^2 N_f}\frac{(\xi-1)}{\xi}(\xi+\eta) - \frac{\chi_S}{16\pi^2 N_f}(1+2\eta)\log(1+\eta) \\ &+\frac{\chi_S}{16\pi^2 N_f}\frac{(2\xi^2-\xi-\eta+3\eta\xi)}{\xi}\log(\xi+\eta)\ , \end{aligned} \tag{2.50}$$

where

$$\eta \ \equiv \ \frac{\rho}{\chi_S} \ = \ \frac{W_0 a}{B_0 m} \tag{2.51}$$

parametrizes the lattice breaking effects.

The Wilson ChPT formula for the double ratio of the pseudo-Goldstone boson masses reads:

$$\begin{aligned} RRn \equiv \frac{4\xi M_{VS}^4}{(\xi+1)^2 M_{VV}^2 M_{SS}^2} &= 1 - \frac{\eta(\xi-1)^2}{\xi(\xi+1)} \\ &+\frac{\chi_S(\xi^2+\xi+\eta+3\eta\xi^2)\log(\xi+\eta)}{16\pi^2 N_f\xi(\xi+1)} - \frac{\chi_S(2\eta+1)\log(1+\eta)}{16\pi^2 N_f} \\ &-\frac{\chi_S(\xi-1)(\xi+\eta)}{16\pi^2 N_f\xi} + \frac{8N_f\chi_S\eta(\xi-1)^2}{\xi(\xi+1)}(L_{S4}-W_{S6})\ . \end{aligned} \tag{2.52}$$

In [Chi-2, Chi-3], the ratios (2.45)-(2.49) could not be fitted with satisfactory results for the whole spectrum of the valence quark masses. Consequently, a subclass of (continuum) ChPT NNLO corrections, quadratic in the quark masses, had to be included in the theoretical formulae. These corrections correspond to tree-level diagrams in the perturbative expansion. In the valence sector, the quadratic corrections introduce two additional parameters for each ratio. The correction for the ratio X ($X \equiv R_{nVV}$, etc.) reads

$$\delta_{NNLO,tree} = D_X\,\chi_S^2 \ + \ Q_X\,\chi_S^2(\xi-1)^2\ . \tag{2.53}$$

Constraints from ChPT reduce the number of free parameters [Chi-2].

The Wilson ChPT representations of the ratios used in the valence analysis (2.46)-(2.49) contain two "reference parameters" χ_R and η, two combinations of GLC, $2L_8 -$

[9] See [Chi-2], Eqs. (3-4), (10-11), (12-13) and (22-23), for the Wilson ChPT formulae of all the considered ratios.

Table 2.1.: *Parameters entering in the NLO chiral formulae for the different ratios (in boldface the combinations with physical relevance).*

Ratio	Continuum	Lattice Correction
Sea Analysis		
Rn_{SS}	$\mathbf{2L_8 + 4L_6 - 2L_4 - L_5}$	$2W_8 + 4W_6 - 2W_4 - W_5 - 2L_4 - L_5$
Rf_{SS}	$\mathbf{2L_4 + L_5}$	$2W_4 + W_5$
Valence Analysis		
$Rn_{VV,VS}$	$\mathbf{2L_8 - L_5}$	$L_4 - W_6$
$Rf_{VV,VS}$	$\mathbf{L_5}$	-
RRn	-	$L_4 - W_6$
RRf	-	-

L_5 and L_5 and the combination, associated with the mass-dependent NLO lattice artifacts, $L_4 - W_6$. In Table 2.1, an overview of the combinations of GLC and Wilson GLC contained in the NLO chiral representations of the various ratios is given. Observe that in the valence analysis, due to the cancellation of lattice artifacts in the ratios, lattice corrections only introduce two additional parameters (η and $L_4 - W_6$).

One possible strategy, followed in [Chi-1], consists in determining the combinations of (Wilson) GLC by performing a sequence of single or double parameter fits. One starts with determining η and χ_R from the double ratio RRf (whose Wilson ChPT representation does not contain additional free parameters, see Table 2.1). The so obtained values of η and χ_R are then inserted in the fits for the remaining ratios. The latter allow to determine the combinations of GLC in the second column ("Continuum") of Table 2.1.

In [Chi-2, Chi-3], global fits including all the available ratios were performed[10]. The quadratic NNLO corrections (2.53) considered in [Chi-2, Chi-3] introduce eight (or six, considering ChPT constraints) additional parameters in the fits.

2.3.3. Numerical results

Wilson ChPT formulae depend linearly upon all unknown parameters with the exception of η, see (2.50)-(2.52). As it turns out, the chi-square associated with the (linear) fits of the remaining twelve parameters is characterized by a weak dependence upon η: the chi-square presents a swallow minimum in correspondence of a small value $\eta \lesssim 0.1$ (Fig. 4 of [Chi-3]). This indicates that, in spite of the rather large lattice spacing, the lattice corrections play a minor role at least within the assumed form of the quark mass dependence. As a consequence of this observation, lattice corrections were not included in the fits of [Chi-3].

By contrast, the NNLO corrections play a major role. These are, as expected,

[10] In [Chi-2] χ_R was determined from the analysis of RRn.

Table 2.2.: *Overview of the results for the Gasser-Leutwyler coefficients from the hereby reviewed and other works in the $N_f = 2$ Wilson setup (sea quark mass analysis).*

Ref.	a(fm)	m_q/m_s	Λ_3/F_0	Λ_4/F_0	$\bar{l}_3$	$\bar{l}_4$
[Chi-2]	0.19	0.28	6.51 ± 0.57	22.9 ± 1.5	2.86 ± 0.17	5.38 ± 0.13
[Chi-3]	0.19	0.28	8.21 ± 0.27	21.4 ± 1.5	3.32 ± 0.07	5.24 ± 0.14
[tlS-1]	0.10	0.16	9.66 ± 0.58	14.8 ± 0.4	3.65 ± 0.12	4.52 ± 0.06
Cern [56]	0.08	0.29	7.0 ± 1.7	–	3.0 ± 0.5	–

more relevant for the larger sea quark masses and in the region $m_V > m_S$, see Fig. 3 of [Chi-2].

In [Chi-2, Chi-3] several simulations at different quark masses were performed, three and four respectively, and a sea quark mass analysis was also possible[11]. Also in this case, *ratios* of the meson quantities were considered, see Eq. (2.45); this reduces to two and three, respectively, the number of available data points.

This sea-quark analysis allows to determine two additional combinations of the GLC, see Table 2.1. It is convenient to introduce the two universal low-energy scales (see for example [131]) defined by

$$\Lambda_3 = 4\pi F_0 \exp[-8(4\pi)^2(4L_6 - L_5 + 2L_8 - 2L_4)] , \quad (2.54)$$

$$\Lambda_4 = 4\pi F_0 \exp[2(4\pi)^2(2L_4 + L_5)] \quad (2.55)$$

(here the L_i are renormalized at $\mu_{ren} = \Lambda_\chi \equiv 4\pi F_0$). The fits allow to determine the dimensionless ratios $\Lambda_{3,4}/F_0$. In order to be able to compare with other results present in the literature (for a recent summary, see [129]), it is convenient to translate these scales into the dimensionless coefficients

$$\bar{l}_{3,4} = \log(\frac{\Lambda^2_{3,4}}{M^2_\pi}) , \quad (2.56)$$

where M_π is the physical pion mass. The physical values of F_0 and M_π are used as an input for the conversions in (2.54)-(2.56).

An overview of the results is given in Tables 2.2 and 2.3, and in Fig. 2.1. The lattice convention for the GLC is:

$$\alpha_i = 8(4\pi)^2 L_i . \quad (2.57)$$

Results from other determinations present in the literature in the $N_f = 2$ Wilson setup are also reported (Del Debbio et Al. [56], Irving et Al. (UKQCD) [109]); we also report results obtained from a subsequent work [tlS-1], see in the next Chapter. The reported errors on the determinations of [Chi-1, Chi-2, Chi-3, tlS-1] are statistical only.

[11] In this case, due to the low number of points at disposal, quadratic corrections were not included in the fits.

Table 2.3.: *Overview of the results for the Gasser-Leutwyler coefficients (valence quark mass analysis).*

Ref.	a(fm)	m_q/m_s	α_5	$2\alpha_8 - \alpha_5$
[Chi-1]	0.28	0.25	1.6 ± 0.3	0.58 ± 0.03
[Chi-2]	0.19	0.28	2.2 ± 0.2	0.76 ± 0.05
[Chi-3]	0.19	0.28	2.1 ± 0.4	0.58 ± 0.05
UKQCD [109]	0.10	0.67	1.2 ± 0.6	0.36 ± 0.24

2.3.4. Discussion

The relative dispersion of the different lattice determinations in Tables 2.2 and 2.3, in some cases larger than the statistical error, is to be attributed to relevant systematic effects. Indeed, the collective fit for a given quantity always delivers chi-square/d.o.f. $>$ 2. The observations made in [Chi-2, Chi-3] support the hypothesis that, for the considered regime of light quark masses, the neglected NNLO contributions in the chiral expansion could play a major role.[12]

Nevertheless, all determinations of $2\alpha_8 - \alpha_5$ are compatible with the "standard" phenomenological value [28] supporting a massive u quark, see Fig. 2.1, lower right panel. It should be recalled, however, that the dynamics of the s quark was not included in these lattice simulations.

The main result of the studies [Chi-2, Chi-3] is that, for the analyzed regime of quark masses ($m_s/3 \leq m_q \leq 2m_s/3$), higher order corrections in the chiral expansion dominate over lattice corrections. A direct verification of this conclusion can be obtained by considering the quantity

$$RRn \, + \, 2RRf \, - 3 \, = \left\{ \begin{array}{c} \mathrm{NNLO} \\ O(a) \end{array} \right. ,$$

which vanishes in the continuum up to NLO order and, therefore, could be either described by NNLO or $O(a)$ terms. The two fits are shown in Fig. 5 of [Chi-3] for the lightest sea quark mass. The chi-square of the fit is 1.3 for chiral fits including some of the NNLO corrections and 7.2 for NLO fits with $O(a)$ corrections. This indicates that the NNLO corrections dominate. The systematic inclusion of all NNLO corrections [27] in the fits, however, does not appear to be a viable possibility, since it would involve too many free parameters.

We conclude that a light quark mass $m_q \simeq m_s/3$ is still outside the domain of validity of NLO ChPT. This outcome motivates the simulation of lighter quarks. In

[12] In [150] a similar analysis was performed, in the $N_f = 3$ staggered-fermion formulation, only for the pseudo-Goldstone boson masses. For $2\alpha_8 - \alpha_5$ values in the range $0.4 - 0.5$ were found in the region of quark masses considered here. For lighter quark masses, the value of $2\alpha_8 - \alpha_5$ tends to decrease. Since the GLC depend non trivially upon N_f, a quantitative comparison of these results with the $N_f = 2$ case is not possible.

the next chapter we will present a different formulation of QCD with Wilson lattice fermions and new simulations algorithms which allow to make substantial progresses in this direction. The experience accumulated in the course of these studies will be useful in future applications with lighter quarks.

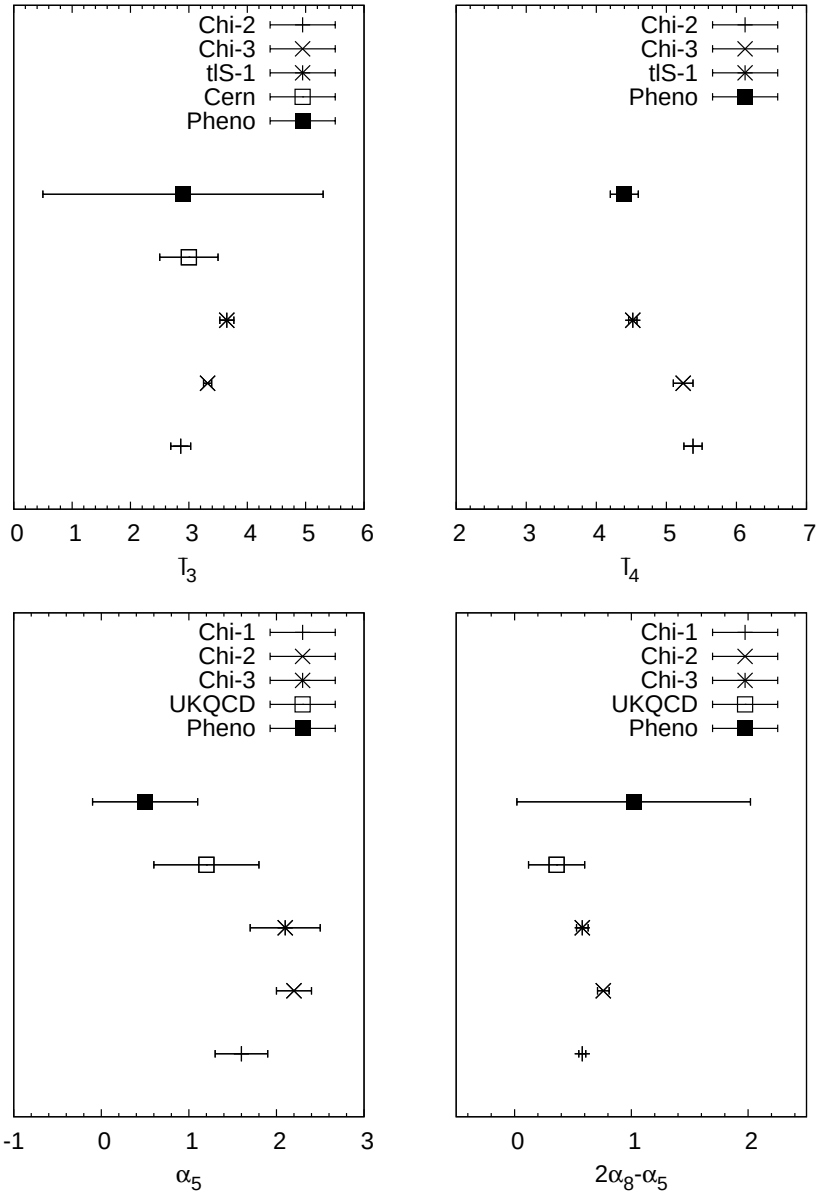

Figure 2.1.: *Comparison of lattice and phenomenological determinations of low-energy constants, from the sea analysis (upper panels) and from the valence analysis (lower panel)*

3. Simulation of twisted mass QCD (TMQCD)

In this chapter, a recently discovered phenomenon in Wilson lattice QCD in the regime of light quarks will be discussed, characterized by the appearance of metastable vacua in the phase structure of the lattice theory. This feature of the Wilson formulation is theoretically well understood and related to the explicit breaking of the chiral symmetry.

Moreover, a modification of the original Wilson formulation will be introduced, known as "twisted mass" lattice QCD (TMQCD) [76]. TMQCD solves in a rather simple way the two main problems of the Wilson formulation, infrared instability and large cut-off effects, while maintaining the important advantages of simplicity and theoretical soundness. TMQCD seems therefore to provide a suitable framework for large-scale simulations of QCD in view of precise determinations in hadron physics. The first steps taken in this direction will be reviewed in this chapter.

The two above outlined topics of the chapter are actually interrelated: any lattice simulation towards the chiral limit requires, as a preliminary step, the investigation of the phase structure of the underlying lattice theory. This investigation turns out to be easier in the twisted mass formulation due to the presence of an additional tunable parameter.

3.1. Introduction

As we have seen previously in this review, the lattice simulation of QCD with light quarks presents several difficulties. In this chapter, a new aspect of the light quark mass regime in Wilson QCD will be discussed; its relevance in numerical simulations has only recently been pointed out [Wil-1]. This aspect is actually quite general and is related to the explicit breaking of chiral symmetry present in any non Ginsparg-Wilson formulation of lattice fermions. An useful theoretical framework in this context is provided by chiral perturbation theory with the inclusion of lattice corrections [170]. Wilson chiral perturbation theory applying for the Wilson formulation was discussed in the previous Chapter.

At finite lattice spacing and for light quarks, the explicit chiral symmetry breaking can dominate over the soft breaking produced by the quark masses and a faithful reproduction of the physical phase structure of QCD is not guaranteed in the lattice theory. In particular, unphysical metastable states can appear. In the case of Monte Carlo algorithms characterized by local ergodicity, as TSMB and HMC, the link con-

figuration of the system can fluctuate for a rather long time during the update around the local minimum represented by a "wrong vacuum". Another unpleasant implication of this unphysical regime is that the pion mass cannot be decreased below a certain minimal value, a potential obstruction for the chiral limit.

As already anticipated, in this chapter a new formulation for lattice fermions, TMQCD, will be introduced. It is obtained by a slight modification of the Wilson formulation, which however introduces several substantial improvements. The modification consists in the introduction of a new (chirally twisted) mass term for the quarks, which provides the already anticipated infrared regulator for the eigenvalue spectrum of the Wilson-Dirac operator. The sharp infrared cut-off is expected to be important in the simulation process and in the measurement of low-energy hadron quantities, which are known to be affected by the fluctuations in the spectrum of the Wilson-Dirac operator. In the twisted mass theory the standard "untwisted" mass can be tuned to zero: in this case the theory is $O(a)$ improved. The improvement follows from a symmetry of the action and does not require additional improvements of the operators.

After briefly introducing TMQCD for the $N_f = 2$ case in Sec. 3.2, the review will concentrate on the phase diagram with Wilson fermions. In Sec. 3.3, the theoretical picture will be given. Its numerical verification is contained in [Wil-1, Wil-2, dbW-1, dbW-2], which will be reviewed in Sec. 3.4. The numerical results about the phase structure of the lattice theory provided the basis for the large-scale simulations of $N_f = 2$ TMQCD of [tlS-1] reviewed in Sec. 3.6. In Sec. 3.5 the methodology for the numerical determination of the twist angle ω associated with the twisted theory is explained.

QCD with only two light degenerate quark flavors has been considered until now in this review. This formulation, however, is just an approximation of the physical case where also heavier quarks are included. Inclusion of additional quark flavors in the twisted mass formulation is not completely trivial, since reality of the fermion action and improvement at maximal twist must be maintained. New flavors have to be introduced in quark pairs forming isospin doublets. This means that, together with the s quark, also the next heavier c quark has to be included. In Sec. 3.7 we will discuss a twisted mass formulation accommodating a split-mass doublet describing the s and c quarks ($N_f = 2{+}1{+}1$ QCD). First simulations and the preliminary study of the phase structure of this lattice theory [tlS-2] will be discussed.

3.2. Twisted mass Wilson fermions

The lattice action for two degenerate flavors of twisted mass Wilson quarks, arranged in the isospin doublet

$$\chi \equiv \begin{pmatrix} \chi_1 \\ \chi_2 \end{pmatrix} , \tag{3.1}$$

can be written [76]

$$S^q = a^4 \sum_x \frac{1}{2a} \sum_{\mu=\pm 1}^{\pm 4} [r\,\overline{\chi}(x)\chi(x) - \overline{\chi}(x+a\hat{\mu})U_\mu(x)(\gamma_\mu + r)\chi(x)] + \overline{\chi}(x)[m_0 + i\mu_0\,\gamma_5\tau_3]\chi(x)\ , \tag{3.2}$$

where we define as usual $U_{-\mu}(x) = U_\mu^\dagger(x - a\hat{\mu})$ and $\gamma_{-\mu} = -\gamma_\mu$, τ_3 is the third Pauli matrix (in flavor space). When comparing with the original Wilson action for the quark sector, Eq. (0.20), we realize that lattice fermion action (3.2) contains, besides the standard mass term for a degenerate doublet

$$m_0\,\overline{\chi}(x)\chi(x)$$

(m_0 will be referred in the following as to the *untwisted mass*), an unconventional mass term (twisted mass term)

$$i\mu_0\,\overline{\chi}(x)\gamma_5\tau_3\chi(x)\ . \tag{3.3}$$

An important point to notice here is that, in the continuum limit, the renormalized theory associated to twisted mass lattice QCD only differs from the corresponding renormalized theory of (conventional) Wilson lattice QCD by a redefinition of the fermion fields by an axial chiral transformation [76]. This implies that the two theories are equivalent in the continuum limit and both are expected to reproduce QCD. In particular, the isospin and parity breakings introduced by the twisted mass term disappear in the continuum limit: they represent discretization effects similar to, for example, breaking of Lorentz invariance present in any lattice version of QCD.

More precisely, the renormalized theory associated to (3.2) may be identified with QCD if the physical quark fields ψ, $\bar{\psi}$ are identified according to:

$$\chi \to \psi \equiv \mathrm{e}^{i\frac{\omega}{2}\gamma_5\tau_3}\,\chi\ , \quad \bar{\chi} \to \bar{\psi} \equiv \bar{\chi}\,\mathrm{e}^{i\frac{\omega}{2}\gamma_5\tau_3}\ , \quad \omega = \arctan\left(\frac{\mu}{m}\right)\ . \tag{3.4}$$

The quantities m and μ in the above relations denote the renormalized counterparts of the untwisted and twisted masses in the continuum limit; these are related to the lattice Lagrangian parameters $(m_0\,, \mu_0)$ by

$$m = Z_{S^0}^{-1}\,(m_0 - m_{0c}) \tag{3.5}$$

$$\mu = Z_P^{-1}\mu_0\ ; \tag{3.6}$$

here, Z_{S^0} and Z_P are the multiplicative renormalization constants of the scalar singlet and pseudoscalar non-singlet fermion bilinears $S^0 = \bar{\chi}\chi$, $P^a = \bar{\chi}\gamma_5\tau^a\chi$ $(a = 1, 2, 3)$, respectively; $m_{0c} = f(g_0)/a$ is the additive mass renormalization of standard Wilson lattice QCD.

Another important point to observe here, is that the validity of the identification stated by Eqs. (3.4)-(3.6) strongly relies on the independence of the renormalization scheme (defining the renormalized theory) of the actual value assumed by the quark

masses (including both the untwisted and twisted masses in the twisted theory). Particularly convenient is the *massless scheme*, where the renormalization constants are computed for vanishing quark masses. In this case twisted mass and standard ($N_f = 2$) QCD trivially coincide and the renormalization constants in (3.5) can be computed, for the given value of the lattice coupling g_0, in the standard Wilson theory.

The *physical* quark mass m_q is given in the twisted theory by the *length* of the two-dimensional vector defined by the two components (untwisted, twisted) of the quark mass:

$$m_q = \sqrt{m^2 + \mu^2} \; ; \tag{3.7}$$

observe that the *twist angle* ω in (3.4) corresponds to the *polar angle* associated to this "mass vector".

Even if the chiral twist of the quark mass does not change the continuum limit of the lattice theory, it does have an effect at finite lattice spacing. Indeed, the Wilson term is *not* invariant under the chiral transformation (3.4). The two main improvements introduced in the lattice theory by the twisted mass term will discussed in detail in the following two subsections.

3.2.1. Positivity of the fermion measure

For $\mu_0 \neq 0$ the fermion measure resulting from the action (3.2), namely the determinant of the associated fermion matrix, is characterized by a sharp infrared cut-off [76].

The fermion matrix of the twisted mass theory with degenerate quarks can be written as (see Eq. (3.2))

$$Q_{TM} = Q \times \mathbb{1} \; + \; ia\mu_0 \, \gamma_5 \tau_3 \; , \tag{3.8}$$

where Q is the standard matrix for one flavor of Wilson lattice quarks defined in Eq. (0.23); $\mathbb{1}$ is the unity matrix in the two-dimensional flavor space. Starting from (3.8), one can quite simply derive the following relation for the fermion determinant of the twisted mass theory:

$$\det(Q_{TM}) = \det\left[(\gamma_5 Q)^2 + (a\mu_0)^2\right] \; , \tag{3.9}$$

where the determinant on the RHS is computed in the *one flavor* theory. The above equation shows that the determinant of Q_{TM} is strictly positive for $\mu_0 \neq 0$, and consequently eigenvalues with arbitrarily small modulus cannot occur in the spectrum. This feature of the twisted mass formulation, as discussed previously in this review, is expected to ensure stability in the dynamical evolution of the lattice system in Monte Carlo simulations.

3.2.2. $O(a)$ improvement

$O(a)$ improvement applies for the twisted mass theory [80] when the Lagrangian mass parameter m_0 is tuned to the critical value m_{0c} for which the renormalized untwisted

quark mass vanishes, $m = 0$, see Eq. (3.5). Improvement holds in this situation for any value of the twisted quark mass μ, which represents in this case the *total* quark mass (see also in the following); however, in a massless renormalization scheme m_{0c} must be in principle computed, for the given value of g_0, in the limit of vanishing (twisted) quark mass $\mu \to 0$. According to (3.4) $m = 0$ for $\mu \neq 0$ implies $\omega = \pi/2$, corresponding to *maximal twist*.

Summarizing briefly the argument of [80] (see also [79]), for $m = 0$ the lattice action (3.2) enjoys an extra symmetry which protects physical quantities from lattice corrections with an odd power of the lattice spacing, $O(a^{2k+1})$, $k \geq 0$. This ensures in particular $O(a)$ improvement of all quantities which can be expressed as expectation values of parity-even (multi)local operators[1]. The improvement at maximal twist is "automatic" [80], in the sense that the absence of $O(a^{2k+1})$ corrections only relies on the symmetry properties of the lattice action (and of the insertion operators) and the introduction of further counterterms in the action is not required. This has to be compared with the standard Symanzik improvement program, where the non-perturbative determination of the improvement coefficients for *each* composite field is necessary [134].

The definition of maximal twist by the vanishing of the renormalized untwisted quark mass $m = 0$ results in a natural way from the discussion of the cut-off effects in the Symanzik expansion [179]. In this expansion, the renormalized continuum counterpart of the quark mass appears. However, in the Wilson formulation of fermions, on which the twisted mass formulation relies, the untwisted quark mass is not protected from additive renormalizations due to the explicit breaking of the chiral symmetry[2]. This fact introduces an $O(a)$ ambiguity in the definition of the massless limit with Wilson fermions. The consequence is that only a looser condition $m = O(a\Lambda_{QCD}^2)$ can be enforced on the lattice without further action.

As already stated previously in this review, in an ideal approach the chiral extrapolation should be performed *after* the continuum limit. In this way, for fine enough lattices, the soft chiral symmetry breaking in the lattice action always dominates over the "sharp" $O(a)$ breaking from the Wilson term. On the basis of a simple dimensional analysis, one can conclude that the soft breaking introduces corrections of the order $\sim m_q \Lambda_{QCD}^3$, while the lattice breaking corrections $\sim a\Lambda_{QCD}^5$ (the proportionality coefficients can be reasonably assumed to be $\simeq 1$). The aforementioned "ideal situation" therefore applies if

$$m_q \gg a\Lambda_{QCD}^2 \ . \tag{3.10}$$

It can be argued [80] that in this regime of quark masses, the lattice ambiguity in the condition of vanishing untwisted quark mass does not spoil the argument of au-

[1] Automatic improvement includes all expectation values of parity-even (multi)local operators. Further action is required for lattice operators which are not trivially even under parity. An example is given by the projecting operators for states which are not at rest; in this case, an average over the two directions of the momentum may be required (parity-average). Observe that vacuum expectation values of parity-odd operators are in general non-zero and $O(a)$ (even at maximal twist) as a consequence of the parity breaking of the twisted mass formulation.

[2] This is instead the case for the twisted component.

tomatic improvement: the $O(a)$ ambiguity only affects the *even* cut-off effects in the lattice spacing (namely $O(a^2)$ or smaller). So, any "reasonable" lattice prescription is acceptable.

Very often however, the condition (3.10) cannot be realized in practice, since it implies very fine (and large) lattices for the light quark masses required for safe chiral extrapolations. More realistic regimes of quark masses are

$$m_q \simeq a\Lambda_{QCD}^2 \tag{3.11}$$

or even

$$m_q \simeq a^2\Lambda_{QCD}^3 \ll a\Lambda_{QCD}^2 \ . \tag{3.12}$$

In these regimes of quark masses not all prescriptions for maximal twist are equally good, since some of them may introduce large $O(a^2)$ discretization errors in the resulting maximally twisted theory. Improvement would be in this case spoiled [13]. These large discretization errors can be discussed in the Symanzik's effective Lagrangian framework by assuming a pion dominance at low-energies [79]. In this approach one concludes that *infrared enhanced* cut-off effects $O((a\Lambda_{QCD})^{2k}/\mu^h)$, $1 \leq h \leq 2k$ can indeed be produced at maximal twist by the $O(a)$ parity breaking term in the effective action. In a Wilson ChPT analysis [172] these terms are automatically resummed delivering infrared finite results [168]. Both approaches agree in the conclusion that lattice corrections become very large as soon as, at maximal twist, $\mu \simeq m_q = O(a\Lambda_{QCD}^2)$.

An effective $O(a)$ improvement, also holding in the regimes of quark masses (3.11), and even (3.12) [168], is obtained if an "optimal" definition of the critical quark mass is chosen [13, 168, 79]. For an optimal prescription of maximal twist, the infrared enhanced cut-off effects are reduced to $O((a\Lambda_{QCD})^{2k}/\mu^{k-1})$ effects [79]. This suppression can be understood in Wilson ChPT, where the leading cut-off effects are resummed: for an optimal prescription the *shifted* untwisted quark mass incorporating lattice corrections, see Eq. (3.17) in the following, vanishes with $O(a^3)$ precision, while it vanishes with only $O(a)$ precision [168] with a generic prescription. In the former case improvement is effective down to quark masses $m_q \gtrsim a^2\Lambda_{QCD}^3$. As it turns out, the $O(a)$ improvement breaks down when the quark mass is reduced to a critical value in the regime (3.12). At this point, as we will see in more detail in the next section, the phase structure of the lattice theory departs from the picture of the continuum [170].

An optimal prescription for maximal twist in the sense of the above discussion is obtained by requiring in the twisted theory the vanishing of matrix elements of operators which are *odd* under parity in the physical theory [79]. Such a prescription for tuning to maximal twist in numerical simulations was first proposed in [67] and [dbW-1] (see also [dbW-2]). Details will be given in Sec. 3.5. This prescription based on "parity restoration" is equivalent to imposing vanishing of the PCAC quark mass in the twisted theory (see in the following).

Two different strategies can be at this point conceived for the simulation of the theory at maximal twist; both turn out to ensure effective automatic improvement:

i) The theory is simulated, for different values of μ_0, at $m_0 = m_{0c}$ where m_{0c} is the critical mass extrapolated at $\mu_0 = 0$.

ii) The theory is tuned to maximal twist only for the lightest quark mass $\mu_{0,min}$ and the so obtained value of m_{0c} is used in all simulations at heavier quark masses.

Choice i) is consistent with a massless renormalization scheme, while choice ii) produces only small deviations in physical quantities $\sim a^2\mu_{0,min}\Lambda_{QCD} \ll 1$ [79].

The two different prescriptions were tested in quenched simulations [115, 1]; small lattice artifacts were indeed observed in both cases. The large-scale simulations with dynamical fermions of [tlS-1], to be described in the following, rely on the procedure ii).

For completeness, we mention that the question of the optimization of m_{0c} becomes immaterial if clover improvement [173] is performed in the twisted mass theory. In this case indeed, the mass independent $O(a)$ cut-off effects in the shifted untwisted mass are canceled by the improvement term and only residual $O(\mu^2 a^2)$ cut-off effects remain. This strategy, which however requires the tuning of an extra coefficient, was put forward in [23].

The freedom in the choice of the exact twisted formulation in the *valence* sector can be used to simplify the complicated mixing patterns of composite operators in the lattice theory; this is an important issue for example in the determination of the parameter B_K [81], relevant for the $B_0 - \bar{B}_0$ mixing (see also [157] for a different approach). A simple example of this advantage of the twisted mass theory can be already found in the unitary formulation given by (3.2): in the (maximally) twisted theory the physical axial-vector current corresponds to the vector current, for which an exactly conserved lattice version exists; no lattice renormalization is therefore involved in the determination of the pion decay constant F_π.

3.3. The phase structure of lattice QCD with Wilson fermions

In the continuum, the degeneracy of the QCD vacuum associated to the spontaneous breaking of the chiral symmetry is resolved by the quark mass, which plays the same role of an external magnetic field in a ferromagnet. The ground state corresponds to a local minimum of the potential, which is symmetric in the chiral limit with massless quarks. The properties of the resulting ground state, the vacuum, depend on the detailed way the mass term in the QCD Lagrangian deforms the potential of the theory. In the case of Wilson fermions, which we consider here, the quark mass does not represent the only source of chirality breaking, since chirality is also explicitly broken by the Wilson term (recall the discussion before Eq. (3.10)). Consequently, the phase structure of the lattice theory may depart from the expected continuum picture in regions of the parameter space in which the explicit breaking is comparable in size with the soft breaking. In this case, extremely large discretization effects are introduced in the lattice determinations.

The possible occurrence of such phenomena was realized already at a very early stage in the theoretical discussion of lattice gauge theories [122]. The existence of

an unphysical phase for the theory with more than one quark flavor was successively conjectured by S. Aoki [12] (see also [44]). Aoki's scenario corresponds to an extreme situation, in which the QCD vacuum becomes unstable and the true vacuum breaks both parity and flavor symmetry[3]. Numerical studies indicate [108] that the Aoki's scenario is realized in the strong-coupling regime of the lattice theory. In the more interesting regime of weak couplings, near to the continuum limit, a milder scenario is expected to apply. In this case, the lattice theory possesses a QCD-like vacuum, however additional metastable states, corresponding to local minima of the free energy, also appear in the phase structure of the theory. Findings in the numerical studies [31, 14, 15] may be interpreted as early evidences for the emergence of this latter scenario in the regime of light quark masses. Clearly, the knowledge of the phase diagram of the underlying lattice theory should be the prerequisite for any large-scale simulations program.

A detailed investigation of the phase diagram of lattice QCD with Wilson fermions and a twisted mass term was undertaken in [Wil-1, Wil-2, dbW-1, dbW-2, tlS-2] and [68] in view of large-scale simulations of TMQCD (to be discussed in Sec. 3.6). The objective of these studies was to map the "safe" region of parameter space, in which the maximally twisted lattice theory is characterized by *truly* small $O(a^2)$ discretization errors. In this section, a brief account of the underlying theoretical background is given. Numerical results will be discussed in the next section.

We stress here that the hereby discussed complications, originating from the interchange of the chiral and the continuum limits, are generic for any non Ginsparg-Wilson formulation which explicitly breaks the chiral symmetry. "Exotic" scenarios are also possible for example in the case of the staggered fermions [19].

3.3.1. ChPT predictions

Wilson ChPT (discussed in the previous chapter, Sec. 2.2) provides the theoretical background for the discussion of the phase structure of Wilson lattice QCD [170]. We illustrate here the application to the standard theory. The inclusion of the twisted mass term will be considered in the next subsection.

The vacuum of QCD is given by the absolute minimum of the potential, which at low-energies is assumed to be dominated by the (pseudo) Goldstone bosons. In our case, $N_f = 2$, these are given by the pions, whose fields can be parametrized as (see the definition (2.4))

$$U = \exp\left\{ i \sum_{a=1}^{3} \pi_a \sigma_a / F_0 \right\} \ . \tag{3.13}$$

On the basis of the vector symmetry ($g_L = g_R$ in (2.3)), preserved by the Wilson formulation, one can show that the potential must be a function of the flavor-trace

$$A = \frac{1}{4}\mathrm{Tr}(U + U^\dagger) \ , \quad -1 \leq A \leq 1 \ . \tag{3.14}$$

[3] In a different interpretation [29], this vacuum corresponds to one of the degenerate vacua associated to the (continuum) chiral phase transition, see also the discussion in [170].

In the continuum, the potential is a polynomial in A, of second order up to NLO or $O(m_q^2)$:

$$\mathcal{V} = -c_1 A + c_2 A^2 \ , \tag{3.15}$$

with $c_1 = 2F_0^2 B_0 m_q$, while the exact expression for $c_2 = O(m_q^2)$ contains a combination of Gasser-Leutwyler coefficients.

Inclusion of lattice corrections up to $O(a^2)$ in the sense of Wilson ChPT produces an $O(a)$ shift of the coefficient c_1, $c_1 = O(m_q, a)$, while the coefficient c_2 gets $O(am_q)$ and $O(a^2)$ corrections: $c_2 = O(m_q^2, am_q, a^2)$.[4] After rewriting (3.15) in the convenient form

$$\mathcal{V} = c_2(A-\epsilon)^2 + \text{const} \ , \quad \epsilon = \frac{c_1}{2c_2} \quad -1 \leq A \leq 1 \ , \tag{3.16}$$

one immediately concludes:

i) for $|\epsilon| \geq 1$ the potential has one (absolute) minimum at $A = \text{sgn}(c_1)$,

ii) for $|\epsilon| < 1$ and $c_2 < 0$ the potential has an absolute minimum at $A = \text{sgn}(c_1)$ and in addition a local minimum at $A = -\text{sgn}(c_1)$,

iii) for $|\epsilon| < 1$ and $c_2 > 0$ the potential has one minimum at $A = \epsilon$.

The scenario i) corresponds to the physical situation. This is what results from continuum NLO ChPT if the quark mass is not too large and ChPT is applicable (in the continuum one has $\epsilon \sim 1/m_q$). Scenarios ii) and iii) can only be realized, for small quark masses for which the NLO chiral expansion is applicable, if the $O(a)$ corrections play a major role. Notice that ϵ is a measure of the size of the LO term when compared to the NLO correction.

The coefficient c_1 gives a possible lattice definition of the quark mass

$$m_q' \sim c_1 \ , \qquad \text{with} \quad m_q' = m_q + O(a) \ . \tag{3.17}$$

The crucial point is that ϵ is not necessarily large if $m_q' \sim c_1 = O(a^2)$. This situation occurs when $m_q = O(a)$, also implying $c_2 = O(a^2)$: c_1 and c_2 are in this case of the same order of magnitude $O(a^2)$ and their ratio ϵ can be smaller than one. So, in this regime of quark masses one of the two unphysical scenarios ii) or iii) can potentially apply, depending on the sign of c_2.

Case ii) is the "mild" scenario anticipated at the beginning of this section. Here the metastable state corresponds to the vacuum appropriate for the *opposite* sign of the quark mass m_q'. For $m_q' = c_1 = 0$ the potential is symmetric in A and the two states with $A = \pm 1$ are degenerate as one would expect for vanishing quark masses. When c_1 (or m_q') changes sign the two vacua are switched. For $m_q' = 0$, due to $O(a)$ terms, a different lattice definition of the quark mass, as for example the PCAC quark mass (1.20), is expected not to vanish. The latter therefore changes sign and has a

[4] We omit here powers of Λ_{QCD} needed to restore the right mass dimensions.

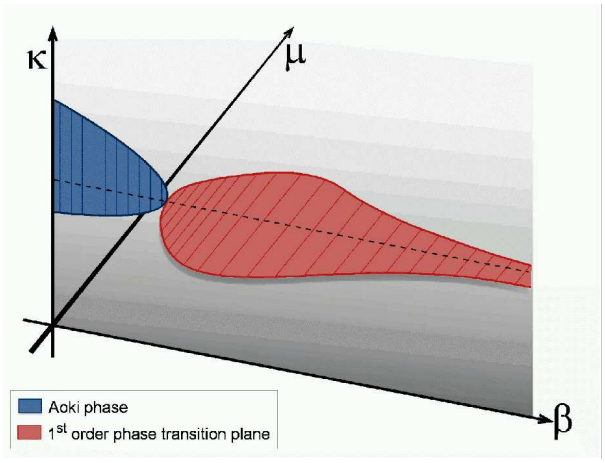

Figure 3.1.: *Phase structure of twisted mass lattice QCD.*

discontinuity at $m'_q = 0$. Similarly, the pion mass does not vanish at $m'_q = 0$, while assumes a (non-zero) *minimal value* [170]:

$$(M_\pi^{(min)})^2 \;=\; \frac{2|c_2|}{F_0^2} \;=\; O(a^2)\;. \tag{3.18}$$

Case iii), less relevant for us, corresponds to the "extreme" scenario of the Aoki phase. Here $|A_{\rm min}| < 1$, which in turn implies $U_{min} \neq \mathbb{1}$: the pion field must have a non-zero vacuum expectation value, see (3.13) and (3.14). This latter scenario seems to apply in a regime of strong couplings [108] and should not affect lattice simulations towards the continuum limit.

3.3.2. Adding the twisted mass term

A twisted mass term in the lattice action introduces a third direction μ in the parameter space of Wilson lattice QCD, besides the conventional untwisted quark mass and the coupling constant, or in lattice notation the hopping parameter $\kappa \equiv 1/2(m_0 + 4r)$ and $\beta \equiv 6/g_0^2$. The resulting parameter space is therefore three-dimensional as depicted in Fig. 3.1. The phase diagram of Wilson lattice QCD in this extended parameter space was studied within Wilson ChPT in [144, 165, 171]; we report in the following the main features relevant for the future discussion.

In the continuum limit and for fixed values of the quark mass in physical units, the twisted mass term just produces a chiral rotation of the vacuum, see Eq. (3.4), which is immaterial from the point of view of physics. The theory can be "rotated back" to standard QCD by proper redefinition of the quark fields. Lattice corrections produce in this case small $O(a)$ deviations if $|\epsilon| \geq 1$ (scenario i)). In this "safe" region of parameter space an effective $O(a)$ improvement can be realized at maximal twist, with small $O(a^2)$ discretization errors, if an optimal definition of maximal twist is chosen, see the discussion in Subsec. 3.2.2.

For a given lattice formulation in the gauge sector, the coefficient c_2 in (3.15), whose sign discriminates between the scenario ii) first order phase transition as in the continuum and iii) Aoki phase, is a function of β. As mentioned above, for low values of β (strong coupling) scenario iii), $c_2 > 0$, is expected to apply. In this case the unphysical phase disappears for non-zero twisted mass: it only extends in the untwisted mass (or κ) direction (this is the blue region in Fig. 3.1).

The case of interest ii), on the contrary, is expected to apply at weak couplings, on the right in the figure. Here the unphysical first order phase transition at $m'_q = 0$ (maximal twist) extends in the twisted mass (μ) direction: a critical segment appears, defined by[5]

$$|\mu| \;\leq\; \mu_c(\beta) \;=\; \frac{|c_2|}{B_0 F_0^2} = O(a^2) \;; \tag{3.19}$$

this is the red region in the figure.

The *charged* pion mass assumes on this segment the minimal value (3.18). The latter represents the absolute minimum for the charged pion mass in the (κ,$a\mu$)-plane for fixed β. The *neutral* pion mass vanishes at the endpoint of the first order phase transition at $\kappa = \kappa_c, |\mu| = \mu_c$, where the system undergoes, according to this discussion, a *second order phase transition*.

3.4. Study of the phase diagram of TMQCD [Wil-1, Wil-2, dbW-1, dbW-2]

As we have seen in the previous section ChPT predicts, for the Wilson lattice theory, strong deviations in the phase structure from the continuum picture, when the region of small quark masses $m_q = O(a)$ is entered. ChPT, however, does not predict the precise region of parameter space affected by the unphysical phases, nor discriminates between the two possible scenarios ii) and iii) of Sec. 2.1: the sign of the coefficient c_2 is a priori unknown. More in general, it is important to know whether the above described exotic scenarios apply for values of the lattice spacing and of the quark masses which are relevant in view of phenomenological applications. Open questions are the dependence of the phase diagram of the lattice theory upon the lattice spacing and the impact of the formulation for the gauge sector.

In [Wil-1] a microscopic interpretation for the first order phase transition was given. According to this interpretation, the phase transition is related to a massive rearrangement of the eigenvalues of the Wilson-Dirac operator in the infrared region. As will be explained in Subsec. 3.4.4, the introduction of extended loops in the definition of the gauge action is expected to produce an impact in this region of the Wilson-Dirac spectrum. Examples already considered in the literature contemplate the introduction of rectangular loops in the standard plaquette action (0.15); one can define a family

[5]Due to the symmetry of the lattice action, the sign of μ is irrelevant.

of lattice gauge actions:

$$S^g = \beta \left\{ b_0 \sum_{\square} \left(1 - \frac{1}{3} \Re \mathrm{Tr} U_{\square} \right) + b_1 \sum_{\mathrm{rec}} \left(1 - \frac{1}{3} \Re \mathrm{Tr} U_{\mathrm{rec}} \right) \right\} , \tag{3.20}$$

where the new variable U_{rec} result from the product of links along a $a \times 2a$ lattice loop; the normalization condition $b_0 = 1 - 8b_1$ ensures the reproduction of the correct continuum limit. The Wilson plaquette action corresponds to $b_1 = 0$. An optimal choice of b_1 in view of reduction of lattice artifacts can be obtained in tree-level weak-coupling perturbation theory. This leads to $b_1 = -1/12$ [192] corresponding to the tree-level Symanzik improved gauge action (tlSym). An alternative approach relies on the renormalization group theory: cases considered in the literature are the DBW2 gauge action [181], $b_1 = -1.4088$, and the Iwasaki action [111], $b_1 = -0.331$. The extension and strength of the unphysical first order phase transition in the resulting lattice theory will be considered as a further criterion for an optimal choice in the gauge sector.

3.4.1. Algorithmic developments

Two different simulation algorithms were employed for the study of the phase structure of Wilson lattice QCD: the TSMB algorithm described in Chapter 1 and a new version of the HMC algorithm optimized for high efficiency in the light quark regime; this is a multiple time-scale mass-preconditioned HMC (mtmp-HMC [185]). Cross-checking results from two different simulation algorithms was important in order to disentangle possible simulation artifacts from the observed emerging phenomena in the phase structure.

The TSMB algorithm was already described in Sec. 1.2. The mtmp-HMC algorithm differs from standard HMC of [62] by several improvements including mass-preconditioning [102] and a multiple time-scales integration scheme [166]. A detailed description of the algorithm can be found in [185], where a dramatic reduction of the simulation costs for Wilson fermions in the light quark regime was proven. The comparative tests of [Wil-1] show that mtmp-HMC is superior to TSMB in decorrelating configurations of the system for the considered regime of light quark masses.

This success of mtmp-HMC prompted further algorithmic developments: in [140] a polynomial version of the HMC algorithm (PHMC [52, 78]) was designed including the aforementioned improvements. In addition, some advanced features are inherited from TSMB, as for example the stochastic correction in the update (see Sec. 1.2). This optimized PHMC algorithm, which can be applied for arbitrary flavor structure, is a promising starting point in particular for the $N_f = 2{+}1{+}1$ twisted mass formulation including the s and c quarks (to be considered in Sec. 3.7). Applications of an analogous algorithm in SYM and in $N_f = 1$ QCD are also in progress [Nf1] [57, 72].

3.4.2. Wilson plaquette action [Wil-1]

In [Wil-1] first investigations of the phase diagram were performed with the plaquette action in the gauge sector, evidences for a first order phase transition were collected, and the identification of the latter with the phase transition predicted by Wilson ChPT [170] was put forward. The Wilson action was simulated in this case for a single value of the coupling constant $\beta = 5.2$, corresponding to $a(5.2) \simeq 0.15$ fm.[6] Both the untwisted theory and a non-zero twisted mass $a\mu_0 = 0.01$ were considered; the latter mass corresponds to $\mu \simeq 12$ MeV in physical units if renormalization factors are neglected.

Hysteresis cycles. In a preliminary survey, the thermal cycles of the plaquette as a function of the hopping parameters κ (driving the untwisted quark mass) were performed for different values of $a\mu_0$ on small lattices. Hysteresis phenomena were observed for small values of $a\mu_0$ (Fig. 1 of [Wil-1]). This observation supports a first order phase transition for $\mu < \mu_c$, as predicted by Wilson ChPT.

Metastability of the plaquette. The metastability of the plaquette was further investigated on larger $12^3 \cdot 24$ and $16^3 \cdot 32$ lattices. The existence of metastable vacua, typical of a first order phase transition, was observed. As we have seen in Sec. 3.3, for a given value of the twisted mass below the critical value (3.19), Wilson ChPT predicts the existence, in addition to the true vacuum, of a metastable vacuum. The latter becomes the true vacuum of the theory when the sign of the untwisted mass is reversed.

The technique for a systematic investigation of the metastable vacua is based on the observation that the vacuum associated with a negative quark mass is characterized by smoother gauge configurations (signaled by a larger value of the average plaquette). So the vacuum associated with the negative (positive) quark mass can be localized by starting the thermalization from a cold (hot) configuration: the expectation is that the local update algorithm remains in the metastable vacuum for a while before finding the true minimum. The two time histories of the average plaquette, from cold and hot start, are expected to display therefore different plateau values for intermediate Monte Carlo times, corresponding to the two different vacua. In Fig. 2 of [Wil-2] examples are shown. The full accomplishment of this procedure can be in practice very expensive, especially for large volumes where the tunnelling is less probable. As a matter of fact, the localization of the true minimum is in many cases not possible. An unpleasant aspect of this situation is that a complete simulation can be performed in the wrong vacuum.

Minimal pion mass. Further investigated quantities were the *charged* pion mass M_{π^+} and the *untwisted* PCAC quark mass. The latter is defined by the PCAC relation, holding for the charged axial-vector current in the twisted theory, with an appropriate

[6] The lattice spacing is estimated from the Sommer parameter after chiral extrapolation. However, due to the metastabilities, a massless renormalization scheme is not really well defined. This estimate and analogous ones given in the following should be interpreted therefore as indicative values.

insertion operator

$$m_\chi^{PCAC} \;=\; \frac{\partial_\mu \langle \bar\chi \gamma_\mu \gamma_5 \frac{\tau^+}{2} \chi(x)\; \bar\chi \gamma_5 \frac{\tau^+}{2} \chi(y) \rangle}{2 \langle \bar\chi \frac{\tau^+}{2} \gamma_5 \chi(x)\; \bar\chi \gamma_5 \frac{\tau^+}{2} \chi(y) \rangle} \tag{3.21}$$

($\tau^\pm = \tau_1 \pm i\tau_2$). m_χ^{PCAC} provides a lattice definition of the untwisted quark mass alternative to the rather abstract one of Eq. (3.17).

While decreasing the untwisted quark mass for a fixed twisted mass, a switch of the vacuum is at some point observed, signalled by the sign change of m_χ^{PCAC} (Fig. 4 of [Wil-1]). Consistently, the pion mass never vanishes but presents a minimum (Fig. 3 of [Wil-1]). These observations again support the picture of a first order phase transition predicted by Wilson ChPT.

The PCAC quark mass reabsorbs most of the $O(a)$ discretization effects in the quark mass dependence of the pion mass. In particular for $m_\chi^{PCAC} = 0$ the theory is at maximal twist and $O(a)$ corrections are absent in physical quantities (as also confirmed by NLO Wilson ChPT formulae [172]). This is illustrated by Fig. 5 of [Wil-1], where the pion mass is reported as a function of m_χ^{PCAC}: the extrapolated value of the pion mass at maximal twist is very small, consistent with the relatively light quark mass $\mu \simeq 12$ MeV. This observation has an academic value only, since, due to the metastabilities, the minimal *simulated* pion mass is rather large $M_{\pi^+}^{(min)} \simeq 550$ MeV: the chiral point can only be accessed after a rather long extrapolation. According to Wilson ChPT this value of the pion mass, which depends on the lattice spacing, sets an *absolute lower limit* for the lightness of the pion in lattice simulations.

Discussion. Hints for a bulk phase transition in Wilson lattice QCD were previously found in the $N_f = 3$ theory [14, 15] and in the $N_f = 2$ theory at finite temperature [31]. To what extent these observations are related to the present evidences of a first order phase transition is however not yet completely clear.

An important question left unanswered by [Wil-1] is how the phase transition *scales* with the lattice spacing, and in particular which is the largest lattice spacing suitable for light quarks and a short chiral extrapolation. Taking for example the benchmark value $M_\pi \simeq 300$ MeV, for which NLO ChPT is expected to give accurate predictions, a *maximal* lattice spacing $\bar a$ can be defined by inverting the condition

$$\bar a : \quad M_{\pi^+}^{(min)}(\bar a) = 300 \text{ MeV} \; . \tag{3.22}$$

An answer to this question is given in the study [Wil-2], which will be discussed in the next subsection.

3.4.3. Scaling of the phase diagram [Wil-2]

In order to probe the lattice spacing dependence of the phase diagram, the analysis of [Wil-1] was extended in [Wil-2] to a coarser ($\beta = 5.1$) and a finer ($\beta = 5.3$) lattice. Altogether the study includes three lattice spacings: $a(5.1) \simeq 0.17$ fm, $a(5.2) \simeq 0.15$ fm, $a(5.3) \simeq 0.12$ fm. The scaling test was performed at fixed physical conditions;

in particular, the parameter $a\mu_0$ was varied with β such that μ is roughly constant $\simeq 12$ MeV; the lattice extension is $L \simeq 2$ fm.

Estimate of the minimal lattice spacing. In Sec. 3.3 a definition of the minimal pion mass associated to the unphysical first order phase transition was given. This corresponds to the value assumed by the charged pion mass when the shifted quark mass m'_q (3.17) vanishes and the potential is symmetric. The precise value of the hopping parameter for which the two vacua are degenerate cannot be easily established in practice, however, and this definition cannot be directly implemented in numerical simulations.

A numerically more accessible, though not completely rigorous, estimate of the minimal pion mass is obtained by determining (by interpolation) the value of κ corresponding to equal values of aM_{π^+} in the two phases. The so obtained pion mass is taken as a definition of $M_{\pi^+}^{(min)}$. This procedure results, for the three lattice spacings considered in [Wil-2], in the following values: $M_{\pi^+}^{(min)}(5.1) \simeq 740$ MeV, $M_{\pi^+}^{(min)}(5.2) \simeq 640$ MeV and $M_{\pi^+}^{(min)}(5.3) \simeq 480$ MeV.

The benchmark lattice spacing $\bar{a}$ defined in (3.22) can now be obtained by extrapolation, assuming on the basis of (3.18) a linear dependence of $M_{\pi^+}^{(min)}$ on a. This results in $\bar{a} = 0.072 - 0.075$ fm, depending on the number of included points (2 or 3).

The given definition of the minimal pion mass $M_{\pi^+}^{(min)}$ is anyway academic: this value of the pion mass is obtained when the lattice theory is maximally metastable. A more useful benchmark, in view of the computation of physical quantities by numerical simulations, is given by the lightest pion mass which can be simulated *in absence* of metastable vacua, namely outside the critical region of untwisted quark masses centered at $m'_q = 0$. Only *positive* values of the untwisted mass should be taken into account in this case, since lattice simulations are usually performed in this region of quark masses (simulations with negative quark masses are generally subject to larger fluctuations). This kind of analysis delivers a somewhat larger range for the benchmark lattice spacing, $\bar{a} = 0.07 - 0.1$ fm (the lowest value appears to be more likely than the highest).

In view of these results, the Wilson plaquette action appears not to be well suited for lattice simulations in the light quark regime. The largest lattice spacing allowing stable simulations for light quarks is already rather demanding in terms of computational load. The finer lattices required for the continuum extrapolation would be even more demanding.

Scaling test. The work [Wil-2] also contains a scaling test for few elementary quantities as the charged pion mass and decay constant. Since a (rigorous) chiral extrapolation of the Sommer parameter is not possible due the metastabilities (see the footnote to Subsec. 3.4.2), the lattice scale was fixed at a non-zero *reference* quark mass by requiring $(M_{\pi^+} r_0)^2 = 1.5$. Given a quantity O (pion mass or decay constant) the dimensionless ratios

$$R_O = \frac{O}{O|_{ref}} \tag{3.23}$$

were considered. Neglecting the effect of the (small) twisted mass μ, R_O is a universal function of the dimensionless ratio of untwisted quark masses

$$\sigma = \frac{m_\chi^{PCAC}}{m_\chi^{PCAC}|_{ref}} \ . \tag{3.24}$$

The results reported in Figs. 5, 6 and 7 of [Wil-2] for the functional dependence of the dimensionless ratios R_O upon σ reveal surprisingly small scaling violations. Due the rather large values of the pion mass $M_{\pi^+} r_0 > 500$ MeV, the question arises, whether these good properties are maintained closer to the chiral limit. Moreover, the results could be affected by the first order phase transition. It would of course desirable to perform such a test in absence of metastabilities. As we will see in the following, this can be realized by using a different formulation in the gauge sector.

3.4.4. DBW2 gauge action [dbW-1, dbW-2]

As already mentioned at the beginning of this section, a gauge action with extended Wilson loops is expected to improve the behavior of the lattice theory in relation to the metastabilities. Prior observations [14, 15] indeed indicate reduction of metastabilities in the case of a RG improved action with a rectangular term (Iwasaki action). We consider here the DBW2 gauge action.

Simulation. Three values of β were studied with the DBW2 gauge action: $\beta = 0.55$ on a $8^3 \cdot 16$ lattice, $\beta = 0.67$ on a $12^3 \cdot 24$ lattice and $\beta = 0.74$ on a $16^3 \cdot 32$ lattice. The first lattice is a rather coarse one: $a(0.55) \simeq 0.3$ fm, while the two finer lattices correspond to $a(0.67) \simeq 0.18$ fm and $a(0.74) \simeq 0.13$ fm respectively. These two smaller lattice spacings are close to the ones considered for the Wilson gauge action ($a \simeq 0.12 - 0.17$ fm).

Also in this case, both vanishing and non-vanishing twisted masses were studied, $a\mu_0 = 0.01$ ($\beta = 0.67$) and $a\mu_0 = 0.0075$ ($\beta = 0.74$). The value of the twisted mass in physical units, $\mu = 0.11$ MeV, and the linear extension of the lattice, $L \simeq 2$ fm, roughly match those considered for the Wilson gauge action. The two consistent setups allow a direct comparison between the Wilson plaquette action and the DBW2 action.

The DBW2 action displays nice properties in the simulation process: smoother configurations are sampled and small real eigenvalues of the fermion matrix occur less frequently. This produces a sizeable speed up of the TSMB algorithm even in the untwisted theory.

In [dbW-2] the optimized HMC algorithm mtmp-HMC described in Subsec. 3.4.1 was compared with TSMB; the former algorithm appears to over-perform the latter by a factor 10 in computer time, confirming that an optimized HMC algorithm is the best choice for dynamical simulations in the light quark regime.

Phase transition. The expected improvement of the metastabilities is indeed observed with the DBW2 gauge action. They are observed in the untwisted runs, see in [dbW-1] the upper panels of Figs. 4 and 5. However for a non-zero twisted mass

they disappear already at the moderate lattice spacing $a(0.67) \simeq 0.18$ fm, see lower panels of the figures. A small effect, probably a residuum of a weak phase transition (or crossover) can be observed in the pion mass. The improvement is impressive, if one compares with the corresponding case at $\beta = 5.2$, compare for example with Fig. 1 of [Wil-2]. For the $\beta = 0.74$ case studied in [dbW-2], the relatively small twisted quark mass already brings the system to a safe region away from the phase transition. This can be seen in the smooth behavior of the PCAC quark mass in Fig. 4 of [dbW-2]. In the Wilson plaquette case for similar conditions ($\beta = 5.3$) the lattice model is still clearly in the metastable region.

A consistent picture of the results with the Wilson plaquette and DBW2 gauge actions can be obtained within Wilson ChPT (Secs. 3.3.1 and 3.3.2). In particular, the extension of the critical segment in the twisted mass direction (3.19) is given by the coefficient c_2, whose size depends on the size of W_0 and on a combination of Wilson GLC [171], see Eqs. (2.30)-(2.32). These quantities depend on the lattice gauge action and the extension of the critical region is probably reduced in the DBW2 action as an effect of the rectangular terms.

This is the right place to mention that, those discussed here are very special discretization effects: the (partial) improvement realized in the case of the potential is not guaranteed for other important quantities, for example in the gluon sector. This point will be further considered when discussing the choice of an optimal gauge action in the light quark mass regime.

Minimal pion mass. In absence of metastabilities, the minimal pion mass obtained at maximal twist corresponds, up to (small) $O(a^2)$ corrections, to the continuum value for the given value of $m_q \equiv \mu$. In particular, LO Wilson ChPT predicts for $\mu > \mu_c$ for the pion mass

$$(M_{\pi^+}^{(min)})^2 = 2B_0\mu \ + \ O(a^2) \qquad (m_\chi^{PCAC} = 0 \ , \ \ \mu > \mu_c) \tag{3.25}$$

(inside the critical region for $\mu < \mu_c$ the continuum value is exceeded by a factor μ_c/μ). So in the present case outside the metastable region, the most appropriate estimate of $M_{\pi^+}^{(min)}$ is obtained by fitting the lattice data for the pion mass with the Wilson ChPT formulae; see also in the following in this subsection and Figs. 9 and 10 of [dbW-2]. The results for the two values of β are similar (recall that μ is constant $\simeq 11$ MeV in physical units): $M_{\pi^+}^{(min)} = 270 - 280$ MeV. This result must be compared with the much larger values obtained with the Wilson plaquette action in a similar physical situation (480 MeV and higher, see in Subsec. 3.4.3).

The DBW2 action displays an extremely nice behavior in relation to the metastabilities: already for rather coarse lattices with $a \simeq 0.13$ fm, pion masses as small as $M_\pi \lesssim 300$ MeV can be simulated without any influence from the phase transition. In the case of the plaquette action, we recall, a lattice spacing as small as $a \simeq 0.07$ fm is required.

Chiral fits. Chiral fits have been performed in [dbW-2] on some of the pion properties in the charged sector, including the mass and decay constant. Differently from the studies described in Chapter 2, here the investigation is of qualitative nature

only. The main goal was to verify whether chiral formulae are applicable in the vicinity of or even across a phase transition, namely in a *metastable* vacuum. In particular, it turns out that the parametrization of pion properties in terms of the untwisted PCAC quark mass m_χ^{PCAC} (3.21) removes most of the discretization effects.

The fits of [dbW-2] include lattice corrections up to $O(a)$ precision. Wilson ChPT for the twisted formulation was developed in [145, 146, 172, 165]. The expansion of the pion mass in terms of the PCAC quark mass takes the form (compare with Eq. (2.33) where the pion mass is parametrized in terms of the *continuum* quark mass)

$$M_{\pi^\pm}^2/F_0^2 = \chi + \frac{1}{32\pi^2}\chi^2 \ln\frac{\chi}{(4\pi)^2} + \delta_{NLO,tree}^W \ , \tag{3.26}$$

$$\delta_{NLO,tree}^W = \delta_{NLO,tree} \ + \ 8(2W_6 + W_8 - 2W_4 - W_5 - 2L_6 - L_8 + 2L_4 + L_5)\,\rho\chi_{PCAC} \ ,$$

where $\delta_{NLO,tree}$ is the continuum correction given in Eq. (2.10). The dimensionless quark mass χ_{PCAC} (2.11) is in the present case defined in terms the renormalized untwisted quark mass

$$m = Z_A Z_P^{-1} m_\chi^{PCAC} \ , \tag{3.27}$$

while in χ the *full* quark mass is inserted:

$$m_q = Z_P^{-1}\sqrt{(Z_A m_\chi^{PCAC})^2 + \mu_0^2} \ . \tag{3.28}$$

The formula (3.26) can be used to fit lattice data *across* the phase transition. The minimal pion mass in absence of metastabilities can be determined by extrapolating (or interpolating) to $m_\chi^{PCAC} = 0$. This procedure is particularly interesting in the case of the simulation points with the Wilson plaquette action of Subsec. 3.4.2, which lie in the metastable region.

The chiral fits relative to the DBW2 gauge action, given in Table 10 of [dbW-2], give reasonable values for the physical quantities, even if with large fluctuations related to systematic effects. The results for the low-energy constant F_0 lie in the range $70 - 80$ MeV close to the phenomenological value $F_0 \simeq 86$ MeV.[7] The results for the low-energy constants Λ_3/F_0 and Λ_4/F_0 (see definition (2.54)) lie in the range 7-8 and 17-20 respectively, in agreement with the results of Chapter 2, Table 2.1. The determination of the low-energy coefficients describing the lattice artifacts is afflicted with large statistical uncertainties. This indicates that the lattice corrections have little significance for the basic description of the lattice data (this observation agrees with the results of Chapter 2).

3.4.5. Tree-level Symanzik improved gauge action

The phase structure of the lattice theory is one important criterion for the choice of the gauge action for large-scale simulations. As we have seen, a gauge action

[7] For comparison, the result obtained from the direct determination of the pion decay constant by Eq. (3.41), to be discussed in the next subsection, is $F_0 = 76(5)$ MeV.

containing a rectangular term with a negative coefficient (b_1) has better properties in this respect. We considered as a benchmark the maximal lattice spacing $\bar{a}$ allowing stable simulations with pions as light as 300 MeV. We found for the Wilson plaquette action ($b_1 = 0$) $\bar{a} \simeq 0.07$ fm, and for the DBW2 action ($b_1 = -1.4088$) $\bar{a} \simeq 0.13$ fm.

The metastabilities should not be however the *only* criterion for the choice of the gauge action. In particular, one could be worried about the relatively large coefficient attached to the rectangular term in the DBW2 action; large scaling violations could be injected somewhere else. In fact the DBW2 action is suspected of suppressing small size instantons and therefore of introducing large distortions in the hadron spectrum [54]. Bad scaling behavior for DBW2 was observed in the pure gauge theory in [148]. Finally, large corrections in weak-coupling perturbation theory were found in [107].

If the phase structure points towards a strictly negative value for b_1, some freedom is left in the range $-1.4088 < b_1 < 0$. A special point in this range is represented by $b_1 = -1/12$, where the pure gauge theory is improved at tree-level in weak-coupling perturbation theory [192] (tree-level improved Symanzik action, tlSym). Good scaling and fast convergence in perturbation theory are in this case expected, but the behavior in relation to the phase structure has to be checked.

The properties of the tlSym action in relation to the phase structure where studied in [68]. There, the phase transition was investigated for three values of β, corresponding to $a \simeq 0.1 - 0.13$ fm. The basic result of this analysis is that for $a \lesssim 0.1$ fm a pion as light as ~ 280 MeV can be simulated ($\mu \simeq 8$ MeV) in absence of metastabilities. On the basis of this result and of the other aforementioned expected good qualities, tlSym was taken as the gauge action of choice for the large-scale simulations of $N_f = 2$ TMQCD at maximal twist, to be discussed in Sec. 3.6.

3.5. Determination of the twist angle ω [dbW-1,dbW-2]

We recall that the twist angle ω is defined by Eq. (3.4) as the angle of the chiral rotation transforming, in the continuum limit, the twisted theory back to ordinary QCD. In [dbW-1, dbW-2] (see also [67]) a methodology was proposed for the numerical determination of the twist angle from the analysis of certain correlators of the chiral currents in the twisted mass theory. As we will explain below, this methodology is based on the requirement that, after the chiral rotation, the chiral currents assume the expected symmetry properties valid in ordinary QCD.

The physical chiral currents of QCD can be related to the bilinears of the χ-fields in the twisted mass formulation,

$$V^a_\mu(x) = \overline{\chi}(x)\frac{1}{2}\tau_a\gamma_\mu\chi(x) \ , \quad A^a_\mu(x) = \overline{\chi}(x)\frac{1}{2}\tau_a\gamma_\mu\gamma_5\chi(x) \ , \tag{3.29}$$

by re-expressing the χ-fields in terms of the physical fields ψ (3.4) [76]. In the case of the charged currents ($a = 1, 2$) the relation assumes the simple form

$$\hat{V}^a_\mu(x) \ = \ Z_V V^a_\mu(x)\,\cos\omega \,+ \epsilon_{ab}\, Z_A A^b_\mu(x)\,\sin\omega \ , \tag{3.30}$$

$$\hat{A}^a_\mu(x) \;=\; Z_A A^a_\mu(x)\,\cos\omega \,+\epsilon_{ab}\,Z_V V^b_\mu(x)\,\sin\omega\;. \tag{3.31}$$

The lattice renormalizations $Z_V(g_0)$ and $Z_A(g_0)$ are needed in order to enforce the correct normalization of the bilinears of the χ-fields[8].

As shown in [dbW-1, dbW-2], for a given choice of the lattice parameters m_0 and μ_0 the twist angle ω can be determined by requiring that the physical currents $\hat{V}^a_\mu(x)$ and $\hat{A}^a_\mu(x)$ reproduce the correct transformation properties under the symmetries of (continuum) QCD. Two conditions are required due to the presence in (3.30), (3.31) of unknown lattice renormalization factors. Considering for example the symmetry under parity, two possible conditions are:

$$\langle\, 0\,|\,\hat{V}^+_0(x)\,|\,\pi^-,\vec{p}=0\,\rangle \;=\langle\, 0\,|\,\hat{A}^+_i(x)\,|\,\rho^-,\vec{p}=0\,\rangle \;=\; 0\;. \tag{3.32}$$

At maximal twist $\omega = \pi/2$, the parity of the chiral currents is swapped in the χ-basis, see Eqs. (3.30) and (3.31), and the first condition in (3.32) reads

$$\langle\, 0\,|\,A^+_0(x)\,|\,\pi^-,\vec{p}=0\,\rangle \;=0\;. \tag{3.33}$$

The meaning of this condition becomes more transparent if one considers an equivalent condition[9]

$$\langle\, 0\,|\,\nabla_\mu A^+_\mu(x)\,|\,\pi^-,\vec{p}=0\,\rangle \;=0\;, \tag{3.34}$$

which is equivalent to imposing vanishing of the untwisted PCAC quark mass (3.21):

$$m_\chi^{PCAC}=0\;. \tag{3.35}$$

As pointed out in [168, 79], the definition of maximal twist given by (3.33) and the equivalent condition (3.35) are *optimal* in the sense of the discussion of Subsec. 3.2.2.

Observe also that Eqs. (3.32) ensure parity restoration in the continuum limit only, where Eqs. (3.30), (3.31) become exact. At finite lattice spacing, residual $O(a)$ isospin and parity violations, $O(a^2)$ at maximal twist, are expected. The verification of the relevance of these effects in lattice computations is therefore of utmost importance (for first studies in the quenched approximation, see [1, 113].

3.5.1. Numerical determination of ω

By inserting Eqs. (3.30), (3.31) into the conditions (3.32), relations involving hadron correlators and containing the two unknown "auxiliary angles"

$$\omega_V=\arctan(Z_A Z_V^{-1}\tan\omega)\;,\quad \omega_A=\arctan(Z_V Z_A^{-1}\tan\omega) \tag{3.36}$$

are obtained. The two auxiliary angles ω_V,ω_A can be directly related to ratios of hadron correlators of the twisted theory (Eqs. (22) and (23) of [dbW-2]); a typical example of such a determination can be found in Fig. 2 of [dbW-2]. The angle ω

[8] In a massless scheme, these lattice renormalization coincide with those of standard QCD.

[9] Equivalence of the two conditions has been verified numerically: see Fig. 3 of [dbW-2].

is determined, together with the ratio of the renormalization constants Z_A/Z_V, by inverting the relations (3.36):

$$\omega = \arctan\left(\sqrt{\tan\omega_V \tan\omega_A}\right) \ , \quad \frac{Z_A}{Z_V} = \sqrt{\tan\omega_V / \tan\omega_A} \ . \tag{3.37}$$

Fig. 6 of [dbW-1] shows the dependence of ω_V upon the untwisted quark mass for fixed μ_0; the sharp, cross-over-like change of the twist angle around maximal twist $\omega_V = \pi/2$ is probably explained by the nearby phase transition (the twist angle has a jump across the critical segment and never assumes the value $\pi/2$). As one can see from Table 4 of [dbW-2], one run at $\beta = 0.74$ is practically at maximal twist (with $a \simeq 0.13$ fm and $M_\pi \simeq 300$ MeV).

3.5.2. Renormalization constants

The enlarged parameter space of the twisted mass formulation opens new possibilities for the non-perturbative determination of the renormalization constants of composite operators (this also applies for the $N_f = 2{+}1{+}1$ formulation to be discussed in Sec. 3.7). In a massless renormalization scheme, the latter renormalization constants are obtained after the chiral extrapolation and coincide with the corresponding renormalizations of Wilson lattice QCD.

As noticed in [dbW-1], the dependence of the twist angle upon the untwisted quark mass allows to determine the ratio Z_P/Z_S – we have already shown how Z_A/Z_V can be determined from the analysis of the twist angle. The twisted mass formulation also opens a clean channel for the determination of Z_V. For $\mu \neq 0$ the bilinear $V_0^a(x)$ (see (3.29)) projects onto the pion state, and Z_V can be obtained by

$$Z_V = \frac{\langle 0|\tilde{V}_0^+(x)|\pi^-, \vec{p}=0\rangle}{\langle 0|V_0^+(x)|\pi^-, \vec{p}=0\rangle} \ , \tag{3.38}$$

where $\tilde{V}$ is the conserved version of the current [32]. At $\mu = 0$ the analogous procedure has to rely on the noisier matrix elements of the vector current (with spatial indices) or on more complicated three-point functions. By putting together the above determination of Z_A/Z_V and the determination of the absolute normalizations Z_V (3.38), Z_A can also be determined [dbW-1, dbW-2].

3.5.3. Physical quark mass and pion decay constant

The *physical* PCAC quark mass m_q^{PCAC} (not to be confused with the *untwisted* PCAC quark mass m_χ^{PCAC} of Eq. (3.21)) and pion decay constants are defined in terms of the physical currents (3.30), (3.31), which can be determined from the bilinears of twisted theory once the angle ω is known. One can for example show (Sec. 3.3 of [dbW-2]):

$$m_q^{PCAC} = \frac{-i}{2\sin\omega} \frac{\langle \partial_\mu^* \tilde{V}_\mu^+(x) P^-(y)\rangle}{\langle P^+(x) P^-(y)\rangle} = \frac{\mu_0}{\sin\omega} \ , \tag{3.39}$$

while the *untwisted* PCAC quark mass can be expressed as

$$m_\chi^{PCAC} = Z_A^{-1} m_q^{PCAC} \cos\omega \ . \tag{3.40}$$

Analogously, the pion decay constant F_π is given by

$$F_\pi = M_\pi^{-1} \langle 0|\hat{A}_0^+(x)|\pi^-, \vec{p}=0\rangle = -i(M_\pi \sin\omega)^{-1} \langle 0|\tilde{V}_0^+(x)|\pi^-, \vec{p}=0\rangle \ . \tag{3.41}$$

By using the conserved current, a determination of the F_π free of lattice renormalizations is obtained [84].

The dependence of F_π upon m_q^{PCAC} is shown in Figs. 7 and 8 of [dbW-2] (diamonds). Consistently with many observations in the literature, F_π shows a pretty linear behavior for decreasing quark mass[10]. A (naive) linear extrapolation to $am_q^{PCAC} = 0$ is not far from the phenomenological value $(F_0 r_0)_{phen} = 0.308$:

$$F_0 r_0(0.67) = 0.333(10) \ , \quad F_0 r_0(0.74) = 0.274(20) \ . \tag{3.42}$$

Observe that these estimates are off maximal twist and consequently *not* $O(a)$ improved.

At maximal twist, one has $\omega = \pi/2$ by construction. However in some conditions (for example in the approach ii) for tuning to maximal twist discussed in Subsec. 3.2.2) the maximal twist condition cannot be exactly maintained for all simulation parameters. The deviation from maximal twist can be corrected by "back-rotating" results to maximal twist using formulae similar to (3.30), (3.31).

3.6. Large-scale simulations of $N_f = 2$ TMQCD [tIS-1]

The numerical studies of the previous sections (together with the cited theoretical works) form the basis for a program of large-scale simulations of twisted mass lattice QCD in view of accurate determinations in hadron physics.

As stressed already several times in this review, a basic prerequisite for accurate determinations in lattice QCD are simulations with light quarks. The sharp infrared regulator of the twisted mass formulation ensures smooth simulations in this regime. Algorithmic advances (Subsec. 3.4.1) also play a fundamental role. The knowledge of the main features of the phase structure of the lattice theory for light quark masses is also important: regions of parameter space of the lattice theory, where lattice data contain large lattice artifacts, can in this way avoided.

The $O(a)$ improvement of the twisted mass formulation at maximal twist is expected to reduce systematic uncertainties in the continuum extrapolation. The procedure for tuning the theory to maximal twist, with small $O(a^2)$ effects, is supported by theoretical arguments and its applicability has been verified in the simulations of Secs. 3.4 and 3.5,

[10]The lightest point on the coarse lattice is probably still affected by the nearby phase transition.

Since the accomplishment of a large-scale simulation program, and of the related analysis program, calls for substantial human and computational resources, a new Europe-wide collaboration was founded: the "European Twisted Mass" (ETM) collaboration [66]. The first step in the aforementioned program was taken in [tlS-1], where the maximally twisted theory with two quark flavors was simulated and its basic properties investigated. Only the simplest quantities in the pion sector are included in this first study.

The finite-volume effects are expected to become a critical aspect, for $L \gtrsim 2$ fm, in the regime of light quarks when $M_\pi \lesssim 300$ MeV. ChPT NLO formulae can correct for them, however at the price of introducing new systematic effects (which are not totally under control). The latter can be reduced by involving larger lattices in the computations.

Further systematic effects come from the neglected s quark in the Monte Carlo. The size of these effects are a priori unknown. A twisted mass formulation including the s quark and preserving all the advantages of the $N_f = 2$ formulation will be introduced in the last section of this Chapter, Sec. 3.7. The first steps in the numerical implementation will be presented there.

3.6.1. Simulation and analysis

In [tlS-1] the theory was simulated for one value of $\beta = 3.9$ by the mtmp-HMC algorithm briefly described in Subsec. 3.4.1. (Simulations for one lower and one higher value of β are under completion and results will soon be published [42].) Five values of the quark mass were simulated at this value of β (the corresponding lattice parameters are reported in the first column of Table 2 of [tlS-1]).

The lattice spacing was determined in two ways: from the Sommer scale parameter r_0 [176] extrapolated at the physical value of the light quark mass, giving $a \simeq 0.0958(4)$ with input value $r_0 = 0.5$ fm, and from the pion decay constant (see next section), giving a slightly lower value $a = 0.087(1)$. This latter value results in the estimate $r_0 = 0.454(7)$ fm[11]. Using the lattice scale from to the r_0-calibration, one arrives at the estimate[12] for the lightest quark mass ($a\mu_0 = 0.004$): $m_q \simeq 8$ MeV. This value is slightly below the reference value of the previous studies with the plaquette and the DBW2 action ($m_q \simeq 11 - 12$ MeV).

The theory was tuned to maximal twist at the lightest quark mass $a\mu_0 = (a\mu_0)_{min} \equiv 0.004$ by requiring the vanishing of the untwisted PCAC quark mass (3.21); the actual value

$$\kappa_c(\beta = 3.9, a\mu_0 = 0.004) = 0.160856 \tag{3.43}$$

was determined by interpolation. The effect of the non-vanishing twisted quark mass in the determination of $\kappa_c(\beta)$ is $O(a^2\Lambda_{QCD}\mu_{min})$. This results in a permille effect, if the actual values of the parameters ($\Lambda_{QCD} \simeq 300$ MeV) are inserted in the estimate.

[11] The phenomenological estimate or r_0 is affected by large uncertainties.
[12] Neglecting again the renormalization factor Z_P^{-1}.

As expected from the previous preparatory studies [68], no signs of metastability were observed during the simulation, confirming that the covered parameter space is outside the critical region.

The analysis also included the computation of the pion mass and decay constant. As a result of smooth simulations with an infrared cut-off in place, extremely precise determinations of these quantities in lattice units could be obtained, with an accuracy in the range $5-6$ permille even for the lightest quark mass, see Table 2 of [tlS-1].

3.6.2. ChPT analysis

The lattice determinations of the charged pion mass and decay constants were fitted against the predictions of NLO continuum ChPT. In this case, also finite volume effects [90] were taken into account. These amount to a multiplicative correction of the infinite volume formula, see (2.10) for the case of the pion; in that notation ($m_q \equiv \mu$ at maximal twist)

$$M_\pi^2(\mu, L) = M_{\pi,NLO}^2(\mu) \left[1 + \frac{\chi}{32\pi^2}\tilde{g}_1(\sqrt{\chi}F_0 L)\right]^2 , \quad \chi = \frac{2B_0\mu}{F_0^2} , \tag{3.44}$$

where $\tilde{g}_1(x)$ is a dimensionless function; an analogous formula can be written for $F_\pi(\mu, L)$. By fitting the lattice data with the NLO chiral formulae, one can match the quark mass to the physical point $\mu \equiv \mu_\pi$ where the ratio $M_{\pi,NLO}(\mu)/F_{\pi,NLO}(\mu)$ assumes its phenomenological value. The corresponding value of $aF_{\pi,NLO}(\mu_\pi)$ can be used to fix the lattice spacing a (the previously quoted value).

As a by-product of this analysis, the low-energy scales $\Lambda_{3,4}$, see Eq. (2.54), contained in the ChPT formulae for M_π and F_π could be determined. In terms of the low-energy constants $\bar{l}_{3,4}$, defined in Eq. (2.56), the result is

$$\bar{l}_3 = 3.65(12) \qquad \bar{l}_4 = 4.52(06) , \tag{3.45}$$

in agreement with previous lattice determinations for light quark masses recently appeared in the literature [129]. A comparison, also including the determinations discussed in Chapter 2, can be found in Table 2.2 and Fig. 2.1 of that chapter.

We see that the values obtained in Chapter 2 for the chiral fits in the untwisted theory are not very far form the present ones. In the case of $\bar{l}_4$, however, the light quarks seem to have a sizeable impact on the lattice estimate, the latter getting into agreement with the phenomenological one. The works reviewed in Chapter 2 are based on simulations with $M_\pi \gtrsim 380$ MeV, for which, we recall, the NNLO corrections in the ChPT formulae were found to be relevant; see the discussion in Subsec. 2.3.4.

The behavior predicted by the NLO ChPT formulae for the quark mass dependence of the pion mass is clearly visible in Fig. 2, left panel, of [tlS-1].

3.6.3. Isospin breaking

$O(a^2)$ isospin breaking in the twisted mass theory is expected to lift the mass-degeneracy between the charged and neutral pion. This effect is maximal in vicinity of

the phase transition endpoint, where the neutral pion mass vanishes while the charged pion remains massive, see the discussion near the end of Subsec. 3.3.2.

It is important to quantify the size of this effect. The determination of the neutral pion mass is particularly awkward in the twisted mass theory, where the neutral pion correlator contains disconnected diagrams. The computation of the latter diagrams requires the application of expensive stochastic techniques (analogous to the ones employed in the next Chapter for the computation of the bound state spectrum of SYM). In addition to this, the disconnected diagrams are intrinsically noisy and the precision of the determination of the mass poorer than in the charged case.

For the lightest quark mass the result of the computation is

$$aM_{\pi^\pm} = 0.1359(7) \qquad aM_{\pi^0} = 0.111(11) \ , \tag{3.46}$$

namely about a 10-30 % isospin breaking effect, even if the statistical errors on the determination of the neutral pion mass are large[13]. A lighter neutral pion is consistent with ChPT predictions in the first order phase transition scenario [144, 171] also confirmed by the numerical studies of Sec. 3.4.

The effect of this mass-split in the numerical determinations in the charged sector can be understood in ChPT, where the neutral pion enters as a virtual particle. Being lighter than the charged pion, its impact on the finite size scaling could be larger than predicted by continuum ChPT where it is assumed to be degenerate with the heavier charged pion. This shows that $O(a^2)$ effects are likely to play a relevant role at least in the finite volume effects. The inclusion of these corrections in the chiral fits is planned for future studies [42].

According to a theoretical argument [83], large $O(a^2)$ discretization errors in twisted mass QCD are confined in the neutral pion sector. Therefore the *charged* pion properties, and in general all hadron properties outside the neutral pion sector, are expected to contain small $O(a^2)$ errors, as expected from the discussion of subsection 3.2.2. In the present case of degenerate u and d quarks, the charged pion gives of course the most accurate determinations in the pion sector.

3.7. First simulations of $N_f = 2{+}1{+}1$ TMQCD [tlS-2]

After simulations with light dynamical u and d quarks, the next step towards realistic simulations of QCD is the inclusion of the s quark. The mass of the s quark is not extremely large compared to the typical energy scale of QCD and its dynamics is therefore expected to have an impact down to the lowest end of the QCD energy spectrum. The s quark is however much heavier than the light u, d quarks (a rough bound is $m_s/m_{ud} > 12$ [198]). The inclusion of the s quark, and possibly of the c quark ($m_{charm} \simeq 1.2$ GeV [198]), is therefore not expected to substantially increase the computational cost of the simulations, which as we have seen in Chapter 1 rapidly

[13] In this case, also (noisy) disconnected diagrams have to be taken into account.

decreases for increasing quark masses. Similarly, a relatively heavy quark is not expected to dramatically change the phase structure of the lattice theory (described in Sec. 3.3).

Including the s quark is however not completely trivial from point of view of the algorithm; for example, the basic structure of the HMC algorithm, also inherited by the optimized mtmp-HMC algorithm of the previous sections, foresees even numbers of *degenerate* quarks[14]. More work is required for tuning of the additional parameters of the lattice action associated with the new degrees of freedom (this aspect will be discussed in Subsec. 3.7.3).

As shown in [82], the s quark can be accommodated in the twisted mass setup while preserving reality and positivity of the fermion measure, and $O(a)$ improvement at maximal twist. As we will show in the next sections, the resulting lattice action, including u, d, s and c quarks all in principle with different masses, can be simulated in practice. For the near future, the ETM collaboration will concentrate on the four-flavor theory with degenerate light quarks, $N_f = 2{+}1{+}1$, where the number of free parameters is still manageable. The inclusion of (continuum) isospin breaking in the light quark sector is conceivable and easily applicable in the two flavor theory, $N_f{=}1{+}1$, while the case of four non-degenerate flavor requires a non trivial additional study of the parameter tuning.

A suitable HMC-based algorithm for the case of non-degenerate twisted flavors was developed in [140, 163] and an alternative one has been in the meanwhile completed [38]. First simulation tests of the $N_f = 2{+}1{+}1$ theory based on the former algorithm were performed in [tlS-2] and will be reviewed in the following sections (see also [68]). One of the objectives of [tlS-2] was the investigation, in this new context, of the phase transition already observed in the $N_f = 2$ lattice theory at small quark masses (Sec. 3.4).

A viable scheme for tuning the theory to the desired setup, namely light degenerate u and d quarks and s and c quarks at the physical point, was proposed in [tlS-2]. The unitary scheme is considered there, in which the same formulation is adopted in the *valence* and the *sea* sector. This implies that the quark propagator is not diagonal in the heavy quark sector[15]. The theoretical framework for the extraction of the hadron masses containing the s and the c quarks for this special case was also developed.

[14] The TSMB described in Chapter 1 can be easily applied to this case, but, as we have seen in the present chapter, optimized HMC-based algorithms appear to be more efficient in the light quark regime.

[15] Alternatively, one can consider a different, flavor-diagonal, twisted mass formulation in the *valence* sector. After proper matching *valence* and *sea* quark masses, the resulting unitarity violations, and flavor non-diagonal interactions, are $O(a^2)$ in the maximally twisted theory, see [81] and references therein for a theoretical discussion; a flavor-diagonal formulation was also put forward in [157]. A quenched study including the s quark in a flavor-diagonal formulation was performed in [2].

3.7.1. Lattice formulation for the split doublet

A *real* fermion determinant with a split-mass doublet (denoted with the label "h" in the following, since coinciding here with the heavy sector of the s and c quarks) can be obtained [82] if the mass splitting term is taken to be orthogonal in isospin space to the twist direction. Opting for a diagonal *untwisted* mass matrix with mass splitting term proportional to τ_3, the *twisted* mass term must be chosen in the τ_1 or τ_2 direction. The resulting action is therefore not flavor diagonal. We consider in the following the choice with twist in the τ_1 direction, in which case the action reads (compare with Eq. (3.2)):

$$S^h = a^4 \sum_x \frac{1}{2a} \sum_{\mu=\pm 1}^{\pm 4} [r\,\overline{\chi}_h(x)\chi_h(x) - \overline{\chi}_h(x+a\hat{\mu})U_\mu(x)(\gamma_\mu + r)\chi_h(x)] + \overline{\chi}_h(x)\left[m_{0h} + i\mu_\sigma\gamma_5\tau_1 + \mu_\delta\tau_3\right]\chi_h(x)\ . \quad (3.47)$$

With this choice for the twist/split direction, the twist can be rotated away in the continuum limit exactly as in the degenerate case (Sec. 3.2): the unphysical off-diagonal interactions are actually $O(a)$ effects, $O(a^2)$ in the maximally twisted theory (analogous to the unphysical isospin breaking in the degenerate theory). $O(a)$ improvement of the overall theory is obtained by tuning all doublets, in the present case (u,d) and (c,s), to maximal twist, see Subsec. 3.7.3 in the following for the exact definition in the non-degenerate case.

For a twisted mass split-mass doublet positivity of the fermion determinant is not guaranteed in the whole parameter space of the lattice theory[16]. A sufficient condition for positivity is given by the bound [82][17]

$$\mu_\sigma > \mu_\delta\ . \quad (3.48)$$

3.7.2. Simulation algorithm

Past experience (see in particular in Subsec. 3.4.1) indicates that an optimized HMC algorithm is the best option in term of simulation efficiency in the regime of light quarks. The fermion matrix Q associated with the action (3.47) is however not diagonal in flavor space. Consequently, the two flavors of the non degenerate quarks must be included explicitly in the update similarly to the a single flavor in standard QCD. This implies that standard HMC cannot be applied. The positive definite matrix $Q^\dagger Q$ is indeed needed for the update, see Subsec. 1.2.1 for the case of TSMB, and the fermion measure is given by the *square root* of its determinant $\sqrt{\det(Q^\dagger Q)}$. With n_{DB}-fold *determinant breakup* (Subsec. 1.2.6) the $(2n_{DB})$-th root of the determinant is required[18]:

$$(\det Q^\dagger Q)^{\frac{1}{2n_{DB}}}\ . \quad (3.49)$$

[16] This is expected, since in the continuum the fermion measure can be negative for two non-degenerate quarks.

[17] We always assume positive values of μ_σ and μ_δ.

[18] In the present case $n_{DB} = 2$.

Fractional powers of the fermion determinant (3.49) can be handled in a HMC algorithm by applying the idea of the polynomial expansion [132] as proposed in [52, 78]: the resulting algorithm is a *Polynomial Hybrid Monte Carlo* (PHMC) algorithm. The version used for the present simulations, developed in [140, 163], contains the optimizations of mtmp-HMC (E/O and mass-preconditioning, multiple time-scales). The error of the polynomial expansion is corrected by a stochastic step in the update (in general multi-step, see [140]) along the lines of the noisy correction of TSMB described in Subsec. 1.2.3, and, if needed, by measurement correction (Sec. 1.2.4).

3.7.3. Tuning

One of the main goals of the exploratory study [tlS-2] was to establish a practicable procedure for tuning the twisted mass theory with an additional split-mass doublet to maximal twist and realize the expected hierarchy of quark masses.

One possible method for tuning the degenerate twisted mass doublet to maximal twist relies on the discussion of the chiral currents (as done in Sec. 3.5). Equivalently, one can enforce vanishing of the *untwisted* PCAC quark mass (3.21). The direct generalization of this method to the split-mass doublet involves the discussion of the axial-vector Ward identities (defining in the degenerate case the PCAC quark mass (3.21)). The PCAC relation is however more complicated in the non-degenerate case:

$$\partial^*_\mu A^a_{h,\mu}(x) = 2am^{PCAC}_{\chi h}\, P^a_h(x) + \begin{cases} 2iZ_A^{-1}a\mu_\sigma S^0_h(x), & a=1 \\ 0, & a=2 \\ (-2i)Z_A^{-1}a\mu_\delta P^0_h(x), & a=3 \end{cases} \tag{3.50}$$

where, in analogy with the light sector, we define

$$\begin{aligned} A^a_{h,\mu}(x) &\equiv \overline{\chi}_h(x)\frac{1}{2}\tau_a\gamma_\mu\gamma_5\chi_h(x) \quad (a=1,2,3)\ , \\ S^0_h(x) &\equiv \overline{\chi}_h(x)\chi_h(x)\ , \quad P^0_h(x) \equiv \overline{\chi}_h(x)\gamma_5\chi_h(x)\ . \end{aligned} \tag{3.51}$$

The maximal twist condition in the heavy sector is given by

$$m^{PCAC}_{\chi h} = 0\ . \tag{3.52}$$

This way of tuning the heavy sector is however not a viable option in practice. Indeed, due to the flavor off diagonal terms in the quark propagator of the split-mass doublet, all hadron correlators needed for the analysis of the Ward identities contain disconnected diagrams (in the degenerate case these are present only for the neutral currents via a different mechanism). Even not considering this problem, the *simultaneous* tuning of the two untwisted mass parameters m_{0l} and m_{0h} such that

$$m^{PCAC}_{\chi l} = 0 \quad \wedge \quad m^{PCAC}_{\chi h} = 0\ , \tag{3.53}$$

could be in practice very complicated.

An alternative solution to the tuning problem was proposed in [tlS-2], and is based on the following argument. One can namely show that, when the untwisted Lagrangian mass parameters are equal in the two sectors

$$m_{0l} = m_{0h} \ , \tag{3.54}$$

the discrepancy between the respective untwisted PCAC quark masses is an $O(a)$ effect:

$$m_{0l} = m_{0h} = m_0 \quad \Rightarrow \quad m_{\chi h}^{PCAC} = m_{\chi l}^{PCAC} + O(a) \ . \tag{3.55}$$

This suggests to tune m_0 to the value where $m_{\chi l}^{PCAC} = 0$ while keeping $m_{0h} = m_{0l} = m_0$: in this situation $m_{\chi h}^{PCAC} = O(a)$. Observe that, since the twisted quark mass in the heavy sector is typically much larger than the one in the light sector, the $O(a)$ error is not expected to affect the maximal twist improvement in the sense of [80] (while it is critical to have good tuning in the light quark sector, recall the discussion in Subsec. 3.2.2). This can be checked by computing the twist angle in the heavy sector ω_h, as suggested in Subsec. 3.7.4, and verifying the accuracy of the condition $\omega_h \simeq \pi/2$.

On the basis of simple universality arguments, one can show that the *physical* quark masses of the split-mass doublet are expressed in terms of the bare twisted and untwisted quark masses by

$$m_{c,s} \ = \ Z_P^{-1} \sqrt{(Z_A \, m_{\chi h}^{PCAC})^2 + \mu_\sigma^2} \ \pm \ Z_S^{-1} \, \mu_\delta \ . \tag{3.56}$$

The above equation can be considered as a generalization of Eq. (3.7). At maximal twist $m_{\chi l}^{PCAC} = m_{\chi h}^{PCAC} = 0$ and

$$m_{c,s} = Z_P^{-1} \left(\mu_\sigma \ \pm \ \frac{Z_P}{Z_S} \, \mu_\delta \right) \ ; \tag{3.57}$$

one is left with two additional tunable parameters, μ_σ and μ_δ. The latter should be chosen such that

$$m_s \simeq (m_s)_{phys} \qquad m_c \simeq (m_c)_{phys} \ . \tag{3.58}$$

The second condition is not critical as long as

$$\Lambda_{\rm cut-off} \sim a^{-1} \ \lesssim \ (m_c)_{phys} \ \simeq \ 1.2 \ {\rm GeV} \ , \tag{3.59}$$

since in this case the c quark dynamics is anyhow distorted by discretization effects. On finer lattices, say $\Lambda_{\rm cut-off} \simeq 2$ GeV, however, the tuning of the c quark becomes an issue.

From Eq. (3.57) the relation for the relative split of the quark masses at maximal twist follows

$$\frac{(m_c - m_s)}{(m_c + m_s)} \ = \ \frac{Z_P}{Z_S} \, \frac{\mu_\delta}{\mu_\sigma} \ ; \tag{3.60}$$

the positivity bound (3.48) implies

$$\frac{(m_c - m_s)}{(m_c + m_s)} < \frac{Z_P}{Z_S} \ . \tag{3.61}$$

After inserting the phenomenological values of the quark masses [198], we see that the theory can be tuned to the desired configuration (maximal twist, physical quark masses), while remaining in the region where positivity is guaranteed, if [82]

$$\frac{Z_P}{Z_S} > 0.85 \ . \tag{3.62}$$

This condition potentially puts a lower bound for the values of β for which positivity is guaranteed (the ratio of normalizations converges to one for weak couplings).

3.7.4. Physical fields and currents

The discussion of Sec. 3.5 can be extended to the non degenerate case. In the degenerate case, the charged pion (light-light) sector was considered. Here, a natural option is given by the mixed heavy-light meson sector, the isospin doublets of the kaons and of the D-mesons (and charge-conjugated versions thereof)

$$K \equiv (K^+ , \ K^0) \quad \text{and} \quad D \equiv (D^0 , \ D^-) \ . \tag{3.63}$$

One considers bilinears in the twisted basis with the corresponding *nominal* flavor quantum numbers

$$V_{K^+,\mu}(x) \equiv \overline{\chi}_s(x)\gamma_\mu\chi_u(x) \ , \qquad A_{K^+,\mu}(x) \equiv \overline{\chi}_s(x)\gamma_\mu\gamma_5\chi_u(x) \ , \tag{3.64}$$

$$S_{K^+}(x) \equiv \overline{\chi}_s(x)\chi_u(x) \ , \qquad P_{K^+}(x) \equiv \overline{\chi}_s(x)\gamma_5\chi_u(x) \ , \tag{3.65}$$

$$V_{D^0,\mu}(x) \equiv \overline{\chi}_c(x)\gamma_\mu\chi_u(x) \ , \qquad A_{D^0,\mu}(x) \equiv \overline{\chi}_c(x)\gamma_\mu\gamma_5\chi_u(x) \ , \tag{3.66}$$

$$S_{D^0}(x) \equiv \overline{\chi}_c(x)\chi_u(x) \ , \qquad P_{D^0}(x) \equiv \overline{\chi}_c(x)\gamma_5\chi_u(x) \ ; \tag{3.67}$$

the hadron correlators of the above operators do not contain disconnected diagrams (present instead in the heavy-heavy sector). Here, each bilinear in a given doublet mixes not only with the corresponding operator with opposite parity (see Eqs. (3.30) and (3.31)), but also with the corresponding operator in the "partner" doublet. This means that the physical operators with definite *physical* flavor quantum numbers are related to the bare heavy-light bilinears (3.64-3.67) by a linear transformation given by a *four-by-four* matrix $\mathcal{M}$. The latter contains the rotation angles in the heavy and light sectors:

$$\hat{\mathcal{V}} = \mathcal{M}(\omega_l, \omega_h)\,\mathcal{V} \ , \qquad \bar{\hat{\mathcal{V}}} = \bar{\mathcal{V}}\,\mathcal{M}^{-1}(\omega_l, \omega_h) \ . \tag{3.68}$$

In the case of the (pseudo)scalar densities one can define

$$\mathcal{V} = \begin{pmatrix} Z_P P_{K^+} \\ Z_P P_{D^0} \\ Z_S S_{K^+} \\ Z_S S_{D^0} \end{pmatrix} \qquad \bar{\mathcal{V}} = (-Z_P P_{K^-}, -Z_P P_{\bar{D}^0}, Z_S S_{K^-}, Z_S S_{\bar{D}^0}) \tag{3.69}$$

(and similarly for the chiral currents). The exact form of the rotation matrix $\mathcal{M}$ can be found in Eq. (33) of [tlS-2].

The condition of restoration of the flavor and parity symmetries for suitable matrix elements of the physical operators, such as

$$\langle\, 0 \,|\, \hat{P}^{+}_{K^+}(x) \,|\, \bar{D}_0, \vec{p} = 0 \,\rangle \;= \langle\, 0 \,|\, \hat{S}^{+}_{K^+}(x) \,|\, \bar{D}_0, \vec{p} = 0 \,\rangle \;=\; 0 \tag{3.70}$$

(analogous to (3.32) in the pion sector), leads to the relation

$$Z_P^2/Z_S^2 = \frac{\langle S_{K^+} S_{\bar{D}^0}\rangle + \langle S_{D^0} S_{K^-}\rangle}{\langle P_{K^+} P_{\bar{D}^0}\rangle + \langle P_{D^0} P_{K^-}\rangle}\;, \tag{3.71}$$

and a constraint relating ω_h to ω_l, see Sec. 3 of [tlS-2] for details. These relations allow the determination of ω_h and of the ratio Z_S/Z_P from numerical data.

3.7.5. Numerical simulations

The $N_f = 2{+}1{+}1$ twisted mass theory defined by Eqs. (3.2), (3.47) in the fermion sector and with tlSym gauge action, the choice $b_1 = -1/12$ in Eq. (3.20), was simulated for two values of $\beta = 3.25$ ($12^3 \cdot 24$ lattice) and 3.35 ($16^3 \cdot 32$ lattice). The lattice spacing was estimated to be $a(3.25) = 0.2$ fm and $a(3.35) = 0.15$ fm. For each value of β, different values of the untwisted mass $m_{0l} = m_{0h} = m_0$ where investigated at fixed remaining parameters $\mu_0, \mu_\sigma, \mu_\delta$, see Table 2 and 3 of [tlS-2]. Different values of the untwisted mass were considered in order to investigate the metastabilities. The positivity bound $\mu_\sigma > \mu_\delta$ is satisfied in all cases.

The twisted mass parameter in the light sector was chosen such that its value in physical units was $\mu_l \simeq 10$ MeV approximately matching the one investigated in the two-flavor theory[19].

Metastabilities. The light sector is expected to drive the phase transition, since the heavy sector is characterized by a much larger twisted mass, $\mu_\sigma/\mu_l = 31.5$. However, the additional degrees of freedom may have an effect on the *strength* of the transition.

The first lattice, with $a \simeq 0.2$ fm, roughly corresponds to the DBW2 point at $\beta = 0.67$ studied in Subsec. 3.4.4. In that case, we recall, only a residual cross-over behavior was observed. In the present case, in opposition, strong metastabilities are present, signalized by the behavior of the plaquette (Fig. 1, left panel, of [tlS-2]). This can be explained on one side by the superior properties of the DBW2 action in relation to the phase transition, but could be an effect of the increased number of quark flavors as well. On the finer lattice, $a \simeq 0.15$ fm, a sudden jump of the plaquette value was observed when changing the untwisted quark mass, Fig. 2 of [tlS-2], which could indicate a residual cross-over or a weaker phase transition in the region not covered by the simulations. Direct comparison with the simulation tests of [68] for the $N_f = 2$ theory with tlSym gauge action (in particular the run at $\beta = 3.75$ with similar values of a and μ in physical units) reveals an analogous behavior for the

[19] As usual for these estimates renormalization factors are neglected.

plaquette (compare with the left panel of Fig. 5 of [68]); in the present case, however, the transition appears to be stronger.

Hadron masses. Few basic hadron quantities were measured, including the kaon and D-meson masses. On the basis of the symmetries of the lattice action in the present setup, it can be argued [tlS-2] that isospin breaking is absent in the heavy-light doublets (3.63), whose members are exactly degenerate.

The simulated pion masses are not particularly small: the smallest pion mass outside the metastable region (from positive quark masses) is $M_\pi \simeq 670$ MeV on the coarser lattice and $M_\pi \simeq 450$ MeV on the finer one. Assuming on the basis of the Wilson ChPT prediction (3.18) a linear dependence of the minimal pion mass upon the lattice spacing, it is possible to estimate the maximal lattice spacing ($\bar{a}$) allowing for safe simulations in the region $M_\pi \lesssim 300$ MeV (the benchmark lattice spacing of Eq. (3.22)). The result is $\bar{a} \simeq 0.1$ fm; the same result was obtained in the $N_f = 2$ theory (Subsec. 3.4.5).

The simulated kaons are heavier than in nature ($M_K \geq 850$ MeV), but in this case the mass can be easily reduced by properly tuning the mass parameters in the heavy sector μ_σ and μ_δ (the present study was performed at a single value of μ_σ and μ_δ for each β).

Twist angle ω_h and Z_P/Z_S. The twist angle in the heavy sector ω_h was determined, according to the method of Subsec. 3.7.4, for one simulation point of each lattice. One can see in this way that the condition $\omega_h = \pi/2$ is very well satisfied in the heavy sector, even when the light sector is still off maximal twist (recall that the untwisted masses are equal in the two sectors up to $O(a)$). We conclude that in the heavy quark sector, the tuning to maximal twist is not an issue at all.

The non-perturbative determination of the ratio Z_P/Z_S according to (3.71) reveals quite small values $Z_P/Z_S = 0.5 - 0.6$, which can explain the quite heavy kaons: the relative c-s mass-split is suppressed by this factor, see Eq. (3.60), and the resulting s mass is larger than in absence of renormalizations. Observe that the estimated values of $Z_P/Z_S = 0.5 - 0.6$ are below those ensuring the positivity of the measure in the heavy sector at maximal twist and for physical values of the c and s mass.

Chiral fits. In spite of the heaviness of the respective masses, LO continuum ChPT seems to describe quite well the lattice data *for the ratios* of the pion and kaon masses, see Fig. 6 of [tlS-2]. Interestingly, data from the two lattices ($\mu_\sigma \neq \mu_\delta$) lie on the same curve, confirming constant physics; moreover the interpolated value at maximal twist of the mass ratio is close to the physical value $M_\pi^2/M_K^2 \simeq 0.082$.

3.7.6. Conclusions

This exploratory study of the $N_f = 2{+}1{+}1$ theory demonstrates the feasibility of simulations of the twisted mass theory including a split-mass doublet. Tuning to maximal twist is not more difficult than in the $N_f = 2$ theory, while the tuning of the quark masses in the heavy sector appears to be practicable (the situation should

improve for smaller lattice spacings).

The relatively heavy masses obtained for the kaon can be explained by the large renormalization effects in the Wilson formulation. This issue could be less critical at weaker lattice couplings, for which large-scale simulations are planned [42]. The unphysical phase transition could be somewhat stronger than in the $N_f = 2$ theory, but present results do not allow to draw definite conclusions at this regard.

Summary and conclusions of part I

The first part of this review addressed the problem of the lattice simulation of QCD with light dynamical quarks. The difficulties encountered in this regime with the standard HMC algorithm motivated the search for alternative algorithms with better properties in the case of light quarks. The first simulations considered in this review are based on a multi-boson algorithm, TSMB [132, 136], which historically represents a first attempt towards an effective simulation of QCD at light quark masses. Only more recently [102] it has been shown how the HMC algorithm can be made efficient in this regime. Efficient HMC-based algorithms [185, 140] were employed for the simulations reviewed in the concluding sections of this part.

Chapter 1 was dedicated to the testing and benchmarking of the TSMB algorithm [Alg] in the case of $N_f = 2$ QCD. Simulations were considered down to relatively light quark masses: one fifth of the physical s quark mass corresponding to about $M_\pi \simeq 300$ MeV. In [Alg] the first example is given of a simulation with light pions in the case of Wilson fermions, in a time when the bulk of the simulations with Wilson fermions were confined in the region of pion masses $M_\pi \simeq 500 - 600$ MeV. Due to limitations in computer power however, only coarse $8^3 \cdot 16$ lattices could be considered in those tests, with a lattice spacing $a \simeq 0.27$ fm.

The main result of [Alg] from the algorithmic point of view, is a stable behavior of TSMB until the lightest simulated quark mass. The "cost figure", growing proportionally to the inverse squared quark mass, is consistent with extrapolations from values at larger quark masses obtained with HMC [184].

Hints for chiral logs could be found for the first time in the behavior of the lattice data for the pion mass and decay constant as a function of the light quark mass. This latter result prompted the systematic analysis of the meson sector with Chiral Perturbation Theory (ChPT) performed in [Chi-1, Chi-2, Chi-3] and reviewed in Chapter 2. The simulation point of [Chi-1], corresponding to one of the simulation points of [Alg], is characterized by a fairly light quark mass ($m_{ud} \simeq m_s/4$) and a quite coarse lattice (as mentioned above); in [Chi-2, Chi-3] a range of quark masses was simulated down to $m_{ud} \lesssim m_s/3$ on a finer lattice ($a \simeq 0.19$ fm).

The study of the meson sector, accomplished by comparing lattice data with partially quenched chiral perturbation theory at NLO, also including lattice corrections ("Wilson chiral perturbation theory" [170, 159]), allowed the determination of the low-energy constants $\bar{l}_3$ and $\bar{l}_4$ (in the sea quark sector analysis) and α_5, $2\alpha_8 - \alpha_5$ (in the valence quark sector analysis). The analysis highlights the presence of still relevant higher order (NNLO) corrections in the chiral formulae for the values of the quark

mass considered in [Chi-2, Chi-3]. These corrections cannot be included in a easy way in the fits and introduce relevant systematic effects in the lattice determinations of the low-energy constants. A more accurate determination of $\bar{l}_3$ and $\bar{l}_4$ could be obtained from the sea quark analysis of [tlS-1] at lower quark masses and with substantially higher statistics (see in the following).

The simulation of Chapters 1 and 2 are based on the original Wilson formulation of QCD. The fermion sector of this formulation is characterized by $O(a)$ discretization effects, which potentially introduce large systematic errors in the continuum extrapolation. Moreover the fermion measure is not protected by infrared singularities. In Chapter 3 a different lattice formulation in the fermion sector was considered, solving both problems: "twisted mass" lattice QCD (TMQCD).

The results on the phase structure of the lattice theory with different formulations in the gauge sector [Wil-1, Wil-2, dbW-1, dbW-2] prepared the way to the first large-scale simulations, performed in [tlS-1], of the maximally twisted mass theory, which is $O(a)$ improved. The main objective of the former works was to map the region of quark masses where, for a given lattice spacing, unacceptably large discretization effects are avoided. These effects manifest themselves in form of an unphysical first order phase transition and appearance of metastable vacua [170].

The comparison between the simple plaquette action [Wil-1, Wil-2] and the DBW2 gauge action [dbW-1, dbW-2] shows that gauge actions with a rectangular term are characterized by an improved behavior in relation to the metastabilities at small quark masses. An useful benchmark proposed in [Wil-2] is the maximal lattice spacing for which simulations down to $M_\pi \simeq 300$ MeV are possible in absence of metastabilities. For this value of the pion mass and lower, ChPT formulae at NLO are supposed to allow precise extrapolations to the physical value of the quark mass. In the case of the plaquette action the benchmark lattice spacing was estimated to be $\bar{a}_{Pl} \simeq 0.07$ fm, for the DBW2 action $\bar{a}_{DBW2} \simeq 0.13$ fm. An intermediate result was obtained with the tree-level Symanzik improved gauge action (tlSym), $\bar{a}_{tlSym} \simeq 0.1$ fm. These results show that the plaquette action is not a suitable choice in view of large-scale simulations. The tlSym action was finally chosen, in opposition to DBW2, because of its good scaling properties.

Another important aspect considered in some detail in [dbW-1, dbW-2] was the determination of the twist angle of the twisted mass theory for a given choice of the simulation parameters. The knowledge of the twist angle allows to extract physical results from the twisted mass theory off maximal twist. The proposed method is based on symmetry arguments and allows to obtain an "optimal" tuning of the theory to maximal twist [13, 168, 79]; the latter ensures small $O(a^2)$ effects in the maximally twisted mass theory down to light quark masses. A similar analysis also allowed to extract finite lattice renormalization constants or combinations thereof.

As already mentioned, the tlSym gauge action was finally chosen for the large-scale simulations at maximal twist of [tlS-1], since it ensures stable simulations already at $a \simeq 0.1$ fm. At five simulation points, with light quark masses down to one sixth of the physical s quark mass, precise determinations in the pion sector could be obtained with numerical accuracy of one percent and below.

These results could be achieved thanks to algorithmic developments as well [185]: the stochastic evaluation of the quark determinant with several pseudofermion fields (with different step-sizes in the molecular dynamics) appears to be the main ingredient at the basis of the speed-up and stabilization of HMC at low quark masses [102, 133].

In perspective, the simulations of TMQCD will include the s and c quarks in a N_f=2+1+1 formulation [42]. In [tlS-2], a framework for tuning the various parameters of the theory was set up: maximal twist and s and c quark masses at their respective phenomenological values. A negative (even if expected) result of [tlS-2] is the strengthening of the unphysical phase transition at small quark masses in comparison with the $N_f = 2$ case. This negative effects of this feature can be probably compensated by an optimization of the formulation in the gauge and/or fermion sector.

We conclude this part by acknowledging very important recent progresses in the simulation of light quarks in the Wilson framework, alternative to TMQCD and obtained by several improvements in the simulation algorithms and in the lattice formulation [133, 56, 96, 127, 63].

Part II.

Simulations of $\mathcal{N} = 1$ SYM and one flavor QCD

4. Simulation of $\mathcal{N} = 1$ SYM and one flavor QCD

Theoretical arguments support a picture in which supersymmetry (SUSY) plays a role in particle physics down to low energy scales. Since, however, no trace of it is observed in low-energy phenomenology, it must be broken at a higher scale by some, yet unknown, mechanism. Non-renormalization theorems holding for SUSY quantum field theories imply that such a breaking mechanism can occur either at tree-level by a proper tuning of the Lagrangian parameters, or dynamically by non-perturbative effects. In this latter case, the SUSY breaking has to take place at a scale where SUSY interactions become strong. This second, theoretically more attractive scenario provides the main motivation for studying non-perturbative aspects in SUSY gauge theories.

There are few analytical methods suitable for a non-perturbative analysis of SUSY gauge theories; they are based on general arguments (as for example the Witten index [196]), low-energy Lagrangians [187, 74], or explicit (sometimes exact) computations (for a comprehensive discussion for example of the instanton calculus in SUSY theories, see [175]). These analytical methods can shed light on some aspects of strongly interacting SUSY gauge theories. A systematic *ab initio* investigation of their properties, however, can only be obtained in the lattice framework.

The basic problem one has to face when trying to put this program into practice was already realized in the very first work on SUSY in a lattice quantum field theory [58]. It consists in the simple observation that in a discretized space-time manifold, SUSY cannot be formulated. Exact SUSY only emerges in the continuum limit. In the case of extended SUSY, the explicit breaking of the symmetry on the lattice can potentially bring to the proliferation of counterterms needed for the renormalization of the theory, in which case the recovery of SUSY in the continuum limit becomes a non-trivial issue. Different approaches partially coping with this problem have been in the meanwhile developed. In the case of extended SUSY, a prescription can be given for the construction of a lattice model with a residual exact symmetry[1] interchanging bosons and fermions [118, 36, 178]. The numerical implementation of these approaches is however not (yet) practicable in the case of physically interesting models.

In the case of minimal ($\mathcal{N}$=1) SUSY, the explicit SUSY breaking introduced by the space-time discretization is harmless (in the above mentioned sense) and a simple discretization of the theory, based on the Wilson formulation of QCD, can be

[1] Generated by some of the supercharges which are not related to infinitesimal space-time translations.

considered [49]. SUSY is in this case recovered in the continuum limit by a proper renormalization of few bare parameters. The simplest four-dimensional non-Abelian SUSY gauge theory with minimal SUSY will be considered here, the $\mathcal{N}$=1 SUSY Yang-Mills theory (SYM). Only one tunable parameter exists in the Wilson discretization of SYM, the bare gluino mass. The situation here is similar to the one applying for the Wilson lattice formulation of QCD, discussed in the previous chapters, where chirality is recovered in the continuum limit by properly tuning the bare quark mass.

The review will cover recent large-scale simulations of SYM with SU(2) gauge group ($N_c = 2$). The recovery of SUSY for vanishing gluino mass was verified in [SYM-1] by the numerical study of the lattice SUSY Ward identities. The works [SYM-2, SYM-3] focus on the bound state spectrum, where SUSY is expected to show up in form of supermultiplets. A previous review of some of these themes can be found in [138].

QCD, in the special formulation where only one quark flavor is considered ($N_f = 1$ QCD), shares many similarities with SYM. In particular, both theories lack a continuous chiral symmetry. This affinity can be put on more rigorous grounds in a particular "orientifold" large N_c expansion [17]. At the planar level of this expansion, an exact equivalence between SYM and $N_f = 1$ QCD can be established [17]. QCD with one quark flavor represents therefore the case of a non-supersymmetric theory in which relics of SUSY are expected [18].

One flavor QCD is interesting in itself, apart from the above mentioned equivalence with SYM. Open questions in this theory regard in particular the hadron bound state spectrum, the definition of the quark mass in absence of a (restored) chiral symmetry, and a possible *spontaneous* breaking of the CP symmetry [48]. The latter two issues also apply for the physical multi-flavor theory: they can be better understood in the simplified framework of QCD with a single flavor.

Surprisingly, in spite of these interesting aspects, a systematic lattice investigation of the model is still missing in the literature[2]. Here, first numerical simulations [Nf1] in a starting project trying to close this gap will be reviewed. The focus in this first study was on the low-lying bound states spectrum, where relics of SUSY can be verified.

This is the plan of the chapter. SYM is introduced in Sec. 4.1; Sec. 4.2 highlights the interesting non-perturbative aspects of this theory, deserving lattice investigation; the lattice formulation with Wilson fermions is given in Sec. 4.3; Secs. 4.4, 4.5 and 4.6 account for the numerical studies of SYM [SYM-1, SYM-2, SYM-3]. Sec. 4.7 and 4.8 are dedicated to QCD with one flavor; Sec. 4.7 contains a summary of open questions in the theory while in Sec. 4.8 the first numerical results about the hadron spectrum obtained in [Nf1] are described.

4.1. $\mathcal{N} = 1$ SUSY Yang-Mills theory (SYM)

SYM is the SUSY extension of the gauge theory describing the self-interactions of SU(N) gauge fields (gluons). The SUSY partner of the gluon is a spin 1/2 particle,

[2]With recent exceptions [53].

the gluino ($\tilde{g}$). The balance between fermionic and bosonic degrees of freedom implied by SUSY can only be fulfilled if gluinos are described by real neutral fields, namely Majorana spinors. Moreover, compatibility of SUSY with gauge invariance requires that the gluinos transform in the adjoint representation of the color group. We consider here the general case of a SU(N_c) color group (N_c = number of colors).

4.1.1. The model

A generalization of gluodynamics under the minimal assumptions of SUSY and gauge invariance is easily obtained in the superfield formalism [160].[3] The basic degree of freedom is represented in this case by a vector superfield $V(x, \bar{\theta}, \theta)$ satisfying the constraint $V^\dagger = V$ and transforming in the adjoint representation of the gauge group:

$$\exp\{V^g\} = \exp\{-i\Lambda^+\} \exp\{V\} \exp\{i\Lambda\} \ , \quad \Lambda\text{: chiral superfield} \ . \tag{4.1}$$

An action which is manifestly invariant under SUSY and gauge transformations can be easily obtained in terms of the SUSY field strength W_α, a chiral superfield:

$$\mathcal{L}_{SYM} = \frac{1}{16\pi k} \, \mathrm{Im} \, \{\tau \, \mathrm{Tr}_{color} \, (W^\alpha W_\alpha)_{\theta\theta}\} \ . \tag{4.2}$$

SUSY invariance follows from the fact that the $\theta\theta$ (or F) component of the chiral superfield $W^\alpha W_\alpha$ is SUSY invariant (up to a total divergence, see in the following). The factor k is conventional and related to the normalization of the generators of SU(N) in a generic representation: $\mathrm{Tr}(T^a T^b) = k \, \delta_{ab}$; τ is an arbitrary complex parameter which we identify with

$$\tau \ = \ \frac{\Theta}{2\pi} \ + \ \frac{4\pi i}{g_0^2} \ . \tag{4.3}$$

The number of component fields can be reduced by a partial gauge fixing (Wess-Zumino gauge). In terms of the ungauged fields the Lagrangian (4.2) reads[4]

$$\mathcal{L}_{SYM} = -\frac{1}{4} \, F^a_{\mu\nu} F^{a\mu\nu} + \frac{i}{2} \, \lambda^a \sigma^\mu \mathcal{D}^{ab}_\mu \bar{\lambda}^b + \frac{i}{2} \, \bar{\lambda}^a \bar{\sigma}^\mu \mathcal{D}^{ab}_\mu \lambda^b + \frac{1}{2} \, D^a D^a + i \frac{\Theta g_0^2}{32\pi^2} \tilde{F}^a_{\mu\nu} F^{a\mu\nu} \ , \tag{4.4}$$

where we indicate the color indices explicitly.

The D field decouples and can be neglected in the remainder. The calligraphic symbol $\mathcal{D}$ above denotes the covariant derivative in the *adjoint* representation:

$$\mathcal{D}^{ab}_\mu = \delta_{ab} \, \partial_\mu + g_0 \, f_{abc} \, A^c_\mu \tag{4.5}$$

and $F^a_{\mu\nu}$ is the conventional field strength tensor of A^a_μ.

[3] For details on SUSY and the superfield formalism, see for example [193, 190].

[4] We revert here to the conventional normalization of the fields, related to that of the component fields of the vector supermultiplet, see for example [193], by $\lambda \to \lambda/g_0$, $A_\mu \to A_\mu/g_0$.

We see from (4.4) that the Weyl spinor λ^a interacts with the vector fields by minimal coupling and gauge invariance is manifest. Observe that, as anticipated, the Lagrangian (4.4) can be naturally expressed in terms of a Majorana bispinor

$$\Psi = \begin{pmatrix} \lambda_\alpha \\ \bar{\lambda}^{\dot{\alpha}} \end{pmatrix} \ . \tag{4.6}$$

The Lagrangian assumes in this case the compact form (we set here and in the following $\Theta = 0$)

$$\mathcal{L}_{SYM} = -\frac{1}{4} F^a_{\mu\nu} F^{a\,\mu\nu} + \frac{i}{2} \bar{\Psi}^a \gamma^\mu D^{ab}_\mu \Psi^b \ . \tag{4.7}$$

The factor $1/2$ in the fermion action is characteristic for the SUSY formulation (compare with the case of the quarks, Eq. (0.8)).

The Lagrangian (4.7) is invariant, up to a surface term, under a *global* transformation

$$\begin{aligned} \delta_\xi A^a_\mu &= i\,\bar{\xi}\gamma_\mu \Psi^a \ , \\ \delta_\xi \Psi^a &= \frac{1}{2}\,\sigma^{\mu\nu} F^a_{\mu\nu} \xi \ , \\ \delta_\xi \bar{\Psi}^a &= -\frac{1}{2}\,\bar{\xi}\sigma^{\mu\nu} F^a_{\mu\nu} \ . \end{aligned} \tag{4.8}$$

We have

$$\delta_\xi \mathcal{L}_{SYM} \ = \ -\frac{i}{4}\,\partial_\mu (\bar{\xi}\gamma^\mu \sigma^{\nu\rho} F^a_{\nu\rho} \Psi^a) \ . \tag{4.9}$$

Considering the variation under a *local* SUSY transformation ($\xi = \xi(x)$), an expression for the variation of the Lagrangian similar to (4.9) is obtained, however with γ^μ and $\sigma^{\mu\nu} F^a_{\mu\nu}$ interchanged. The conserved Noether current associated with the transformations (4.8), the *supercurrent*, reads therefore

$$S_\mu \ = \ -\frac{1}{2}\,\sigma^{\nu\rho} F^a_{\nu\rho} \gamma_\mu \Psi^a \ . \tag{4.10}$$

For the following discussion, it is convenient to introduce a non-vanishing mass m for the gluino. This can be obtained by regarding the parameter τ in the action (4.2) as a chiral superfield [156]. A non zero vacuum expectation value of the F component of τ introduces a SUSY soft-breaking gluino mass term. The choice $F_\tau = i 8\pi m_{\tilde{g}}/g_0^2$ and the replacement

$$\tau \ \to \ \tau \ + \ F_\tau \theta\theta \tag{4.11}$$

results in a Majorana mass term for the gluino

$$\mathcal{L}^{(m_{\tilde{g}})}_{SYM} = -\frac{1}{4} F^a_{\mu\nu} F^{a\,\mu\nu} + \frac{i}{2} \bar{\Psi}^a \gamma^\mu D^{ab}_\mu \Psi^b \ - \frac{m_{\tilde{g}}}{2}\,\bar{\Psi}^a \Psi^a \ ; \tag{4.12}$$

in this case the SUSY Ward identities of the supercurrent contain a soft-breaking term

$$\partial_\mu S_\mu(x) = -\frac{i}{2}\, m_{\tilde{g}}\, \sigma^{\mu\nu} F^a_{\mu\nu} \Psi^a \ . \tag{4.13}$$

4.1.2. Euclidean theory

An Euclidean formulation of SYM is needed for a rigorous quantization of the theory in the functional integral scheme; it is also needed for the two relevant non-perturbative computational techniques in this context, instanton calculus and lattice field theory. Euclidization is however not completely trivial in the case of SUSY models [153] due to the presence of Majorana spinors. In Euclidean geometry indeed, real neutral spinors cannot be build, with the consequence that Hermiticity of the action must be abandoned if one wants to preserve the equivalence with the relativistic theory. The latter can be established as it is well known [164] by analytic continuation to imaginary times of the Green functions of the relativistic theory. In this approach the conjugated Euclidean Majorana field $\bar{\Psi}_E(x)$ is no longer an independent variable (as it is the case for Dirac spinors) but it *defined* by the Majorana condition

$$\bar{\Psi}_E \equiv -(\Psi_E)^T C \ , \tag{4.14}$$

where C is the spinorial representation of the charge conjugation operator. The functional integration is therefore performed over the Ψ_E fields only:

$$\langle Q[\bar{\Psi}_E, \Psi_E, A^\mu_E]\rangle = Z^{-1} \int [dA^\mu_E][d\Psi_E] Q[\bar{\Psi}_E, \Psi_E, A^\mu_E] \exp\{-S^E[\bar{\Psi}_E, \Psi_E, A^\mu_E]\} \ . \tag{4.15}$$

The Euclidean version of the action (4.12) is obtained by applying the usual prescriptions, with the result:

$$\mathcal{L}^{(m)}_{SYM,E} = \frac{1}{4} (F_E)^a_{\mu\nu} (F_E)^a_{\mu\nu} + \frac{1}{2} \bar{\Psi}^a_E \gamma^E_\mu D^{E\,ab}_\mu \Psi^b_E + \frac{m_{\tilde{g}}}{2} \bar{\Psi}^a_E \Psi_E{}^a \tag{4.16}$$

(with $\gamma^E_4 \equiv \gamma^0$ and $\gamma^E_i \equiv -i\gamma^i$, $i = 1, 2, 3$).

An Euclidean formulation for relativistic Weyl spinors as in (4.4), instead of Majorana spinors, is also possible, but notationally more cumbersome (the two formulations are of course equivalent). The calculation of matrix elements of products of Euclidean Majorana fields according to the prescription (4.14)-(4.15) can be greatly simplified by using an analogy with the corresponding matrix elements for Dirac spinors [136].

4.2. Quantum features of $\mathcal{N} = 1$ SYM

4.2.1. $\mathrm{U(1)_R}$ symmetry and its fate

Supersymmetric theories are characterized by a peculiar symmetry which does not leave the supercharges unchanged, the so-called R-symmetry. In the case of $\mathcal{N} = 1$ SYM, with just one supercharge, this symmetry is Abelian:

$$Q_\alpha \to \mathrm{e}^{i\phi} Q_\alpha \qquad \bar{Q}_\alpha \to \mathrm{e}^{-i\phi} \bar{Q}_\alpha \ . \tag{4.17}$$

In the superfield representation it corresponds to a U(1) transformation of the gluino field

$$\lambda_\alpha \to \mathrm{e}^{i\phi} \lambda_\alpha \qquad \bar{\lambda}_\alpha \to \mathrm{e}^{-i\phi} \bar{\lambda}_\alpha \ , \qquad \Psi \to \mathrm{e}^{i\phi\gamma_5} \Psi \ , \tag{4.18}$$

with associated Noether current

$$J^5_\mu = \bar{\Psi}^a \gamma_\mu \gamma_5 \Psi^a \ . \tag{4.19}$$

The $\mathrm{U(1)_R}$ symmetry is (partially) broken by the triangular anomaly, which for adjoint fermions reads

$$\partial^\mu J^5_\mu \ = \ 2N_c\, Q(x) \ , \qquad Q(x) = \frac{g_0^2}{32\pi^2}\, \tilde{F}^{a\,\mu\nu} F^a_{\mu\nu} \ . \tag{4.20}$$

In the Euclidean formulation, $Q(x)$ corresponds to the *topological charge density* of the gauge field. Due to the extra factor $2N_c$ in Eq. (4.20), originating from the adjoint representation of the gluino, the anomaly term does not break the R-symmetry completely. This can be seen by following Fujikawa's approach [87] to anomalies, after having temporarily reintroduced the Θ-term in the action of SYM, see Eq. (4.4). For the Euclidean theory, an anomalous rotation produces a shift of the Θ-parameter:

$$\mathcal{L}_{SYM}(x) \to \mathcal{L}_{SYM}(x) \ - \ 2N_c\, \phi \int dx\, Q(x) \ : \quad \Theta \to \Theta - 2N_c \Phi \ . \tag{4.21}$$

Since the topological charge is an integer corresponding to the winding number of the (Euclidean) gauge configuration, $\nu = \int \, dx\, Q(x) \in N$, rotations with angles

$$\phi \ = \ \phi_n \ \equiv \ n\, \frac{2\pi}{2N_c} \ , \quad n \in N \tag{4.22}$$

do not produce any effect in the functional integrals. This means that a *discrete* subgroup Z_{2N_c} is preserved by the anomaly.

Theoretical arguments indicate that the vacuum of SYM develops a non-vanishing gluino condensate $\langle \lambda^a_\alpha \lambda^{a\alpha} \rangle$, implying spontaneous breaking of the discrete chiral symmetry into Z_2 ($\lambda^a_\alpha \to -\lambda^a_\alpha$). A first indication for gluino condensation in SYM comes from the low-energy Lagrangian approach of [187], see also in the next section; a quantitative prediction for the magnitude of the condensate can be obtained by instanton computations. Instanton calculus for supersymmetric theories [155] is characterized by absence of perturbative corrections: the leading order of the saddle-point expansion gives already the exact result. On general grounds one expects

$$\left\langle \frac{g_0^2 (\lambda^a_\alpha \lambda^{a\alpha})}{16\pi^2} \right\rangle \ = \ C\, \Lambda^3 \, \exp\{2\pi i k / N_c\} \tag{4.23}$$

where $k = 0, \ldots, N_c - 1$ labels the N_c degenerate vacua related by transformations in the quotient group Z_{2N_c}/Z_2 and Λ is the dynamical scale developed, as in QCD, through dimensional transmutation. Two different instanton computations present in the literature come up however with two different values for C:

$$C = \frac{2}{((N_c-1)!(3N_c-1))^{1/N_c}}$$

in a "strong-coupling" computation (SCI) [154, 158, 11, 10, 86], $C = 1$ in a "weak-coupling" one (WCI) [86, 4, 5, 155, 174]. The discrepancy between the two results can be explained by introducing in the theory an "extra" chiral symmetric phase where the condensate vanishes [126] (however, see also the criticism expressed in [106] to this argument). A third approach, based on the connection of $\mathcal{N} = 1$ SYM with the exact Seiberg-Witten solution of the $\mathcal{N} = 2$ model, confirms the SCI result, $C = 1$ [106].

The chiral group Z_{2N_c} being discrete, the Goldstone theorem does not apply to the spontaneous breaking of this residual symmetry, and the mass gap of the theory persists for massless gluino. In an approximation of SYM, however, the spontaneous breaking of a continuous symmetry does occur: this is the Okubo-Zweig-Iizuka (OZI) approximation of the theory, in which Feynman diagrams containing disconnected gluino loops[5] are neglected. In this case the anomaly vanishes and $\mathrm{U(1)_R}$ is expected to be broken by a mechanism analogous to the one expected for the chiral symmetry in QCD [187]. This means that, in the OZI approximation, the theory should contain pseudoscalar states with negative parity, which are massless for vanishing gluino mass (the so-called "adjoint-pions", see also in the following).

4.2.2. Color confinement and bound states spectrum

The analogy with QCD suggests the occurrence of color confinement in SYM. The large N_c expansion supports similarities with QCD in this respect (see for example the discussion in [187]). The leading term of the expansion has indeed the same features of the corresponding term in QCD for fixed N_f [180][6]. Differently from QCD, where only gluonic and $\bar{q}q$ bound states survive for $N_c \to \infty$, hadron bound states associated with any combination of gluino and gluon fields are present in SYM. Observe that, the gluino transforming in the adjoint representation, gauge invariant composite operators can be built in SYM by taking the color trace of products of any number of gluino and gluon fields:

$$Q^{\alpha_1,\ldots,\alpha_m}_{\mu_1,\ldots,\mu_n}(x_1,\ldots,x_m;y_1,\ldots,y_n) = \mathrm{Tr}_{color}[\Psi_{\alpha_1}(x_1)\cdots\Psi_{\alpha_m}(x_m)\,A_{\mu_1}(y_1)\cdots A_{\mu_n}(y_n)]\ . \tag{4.24}$$

In consideration of the (partial) analogy with QCD, the question naturally arises whether SYM confines static color sources. In QCD, dynamical quarks are expected to screen the static fundamental charges so that the string tension vanishes. The situation is different in SYM, since the dynamical fermions are in the *adjoint* representation and are not expected to screen fundamental charges. It is therefore generally assumed that SYM confines static quarks with a non-vanishing string tension.

If SUSY is not broken at the dynamical level, the colorless bound states of the theory should form *supermultiplets*. The lowest end of the spectrum can be explored in particular by means of low-energy Lagrangians.

[5] Diagrams which can be disconnected by cutting gluon lines.

[6] In spite of the different counting of the fermionic degrees of freedom in the two theories ($\sim N_c$ in QCD and $\sim N_c^2$ in SYM).

Starting from the analogy with QCD, Veneziano and Yankielowicz [187] take as basic degree of freedom a superfield $S(x, \theta)$ containing the composite operators $\lambda^a \lambda^a \equiv \bar{\Psi}^a_R \Psi^a_L$ (and Hermitian conjugated) and $\tilde{F}^a_{\mu\nu} F^{a\mu\nu}$. The simplest choice is a chiral superfield also containing $F^a_{\mu\nu} F^{a\mu\nu}$ and $\sigma^{\mu\nu} F^a_{\mu\nu} \lambda^a$:

$$S(x,\theta) \sim \bar{\Psi}^a_R \Psi^a_L + i\theta\sigma^{\mu\nu} F^a_{\mu\nu} \Psi^a_L + \frac{1}{2}\theta^2 \left(F^a_{\mu\nu} F^{a\mu\nu} + i\tilde{F}^a_{\mu\nu} F^{a\mu\nu}\right) + \cdots \tag{4.25}$$

(the ellipsis indicates further terms not relevant for the following discussion). The last three operators in (4.25) correspond, respectively, to the superconformal, scale and $\mathrm{U(1)_R}$ anomalies of SYM. The kinetic term of the effective Lagrangian of the chiral superfield S is a Kähler potential of the form

$$\mathcal{L}_{kin} = \frac{9}{\alpha} \left(S^* S\right)^{1/3}_D , \tag{4.26}$$

where α is a free parameter. $\mathcal{L}_{kin}$ enjoys all the symmetries of the fundamental Lagrangian (4.4) at the classical level. The superpotential $W(S)$ is determined, on the other side, by requiring that the anomalous transformations reproduce the correct anomaly terms. This results in

$$W(S) = \frac{1}{3} \left(S \log S/\mu^3 - S\right)_F + \text{ Hermitian conjugated} . \tag{4.27}$$

The effective Lagrangian of the superfield S allows to determine the Green functions of the composite components fields, contained in (4.25), by a tree-level computation. Since these composite operators represent interpolating fields for the bound states of the theory, the mass spectrum of SYM follows immediately from the effective Lagrangian. In this, one assumes that S contains precisely those degrees of freedom which dominate the dynamics of the theory at low-energies.

Purely gluonic operators do not possess any kinetic term in the Kähler potential and consequently decouple in the Veneziano-Yankielowicz theory. The dynamical degrees of freedom are given by the gluino bilinear $\lambda^a \lambda^a$ and the gluino-glue operator $\sigma_{\mu\nu} F^a_{\mu\nu} \Psi^a_L$. They project over a Wess-Zumino supermultiplet containing two mesonic gluino states with both parities and one gluino-glue spin 1/2 state. This picture is obviously incomplete, since mixing with the states projected by the purely gluonic operators in (4.25) (glueballs) is expected.

Again starting from an analogy with QCD, where the scalar glueball can be coupled to the η' by a three-form potential $C_{\mu\nu\rho}$, the authors of [74] embedded the chiral superfield S in a three-form superfield U. The former can be obtained from the latter by the relation

$$\bar{D}^2 U = -\frac{1}{4} \left(S - \mu^3\right) , \tag{4.28}$$

which allows to re-express the Veneziano-Yankielowicz Lagrangian in terms of U. The superfield U contains all the components of S and in addition the tree-form potential $C_{\mu\nu\rho}$, a scalar operator interpolating the glueball with positive parity[7], and a

[7]The operator $F^a_{\mu\nu} F^{a\mu\nu}$ is not dynamical as in the Veneziano-Yankielowicz approach.

second Majorana spinor. The pseudoscalar glueball is described by the only physical component of the three-form potential $C_{\mu\nu\rho}$. The resulting low-energy spectrum is characterized in this new effective theory by two Wess-Zumino multiplets. The expected mixing between the two supermultiplets is obtained by introducing in the Veneziano-Yankielowicz Lagrangian a new interaction term of the form

$$\frac{1}{\delta}\left(-\frac{U^2}{(S^\dagger S)^{1/3}}\right)\Big|_D \ , \tag{4.29}$$

where δ is a free parameter. In the limit $\delta \to 0$ the mass-split and mixing between the two supermultiplets vanishes and the scalar states of the lower multiplet have a prevalent glueball component.

The problem of the inclusion of the glueballs in the bound state spectrum of SYM was also considered in [37] and [135]. A different point of view is put forward in [25], where the authors point out that the inclusion of glueballs in the spectrum of SYM necessarily requires dynamical breaking of SUSY, where no supermultiplets appear.

The mass spectrum of SYM with a small gluino mass was studied in [75] by extending the analysis of [74] . The effective Lagrangian of the theory with softly broken SUSY can be obtained by rephrasing the procedure for the introduction of a gluino mass term in the fundamental Lagrangian (see end of Subsec. 4.1.1).

The effects on the spectrum, resulting from this kind of analysis, are analytic in the gluino mass, with a first $O(m_{\tilde{g}})$ correction and higher order corrections suppressed by powers of $m_{\tilde{g}}/\mu$. The gluino mass removes in particular the degeneracy between the supermultiplet members. In the lower supermultiplet the ordering of the states is (with increasing mass): scalar, spin 1/2, pseudoscalar. The ordering is reversed in the higher multiplet. At $O(m_{\tilde{g}})$, the energy levels in the supermultiplets are equispaced; one has namely: $m_{1/2} = (m_{0^+} + m_{0^-})/2$. In Fig. 4.1, taken from [75], the qualitative behavior of the softly broken spectrum of SYM is given.

4.3. Lattice formulation of $\mathcal{N} = 1$ SYM

As already anticipated in the introduction to this chapter, SUSY cannot be defined in a straightforward way in a discretized space-time manifold. The basic problem already emerges in the simplest case of the Wess-Zumino model [194] describing the interactions of a chiral superfield ϕ. [8] In this model, the interactions are contained in a term $\sim \phi^3_{\theta\theta}$ and the SUSY invariance relies on the (non trivial) property that products of chiral superfields are themselves chiral superfields. Going back to the expression of the supercharge in superspace (we consider minimal SUSY)

$$Q_\alpha = \frac{\partial}{\partial\theta^\alpha} - i\sigma^\mu_{\alpha\dot{\alpha}}\bar{\theta}^{\dot{\alpha}}\partial_\mu \ , \tag{4.30}$$

one sees that any lattice definition of the supercharge requires in turn a lattice version of the differential operator ∂_μ. The presence of the latter operator in the supercharge

[8] We follow here the discussion in [58].

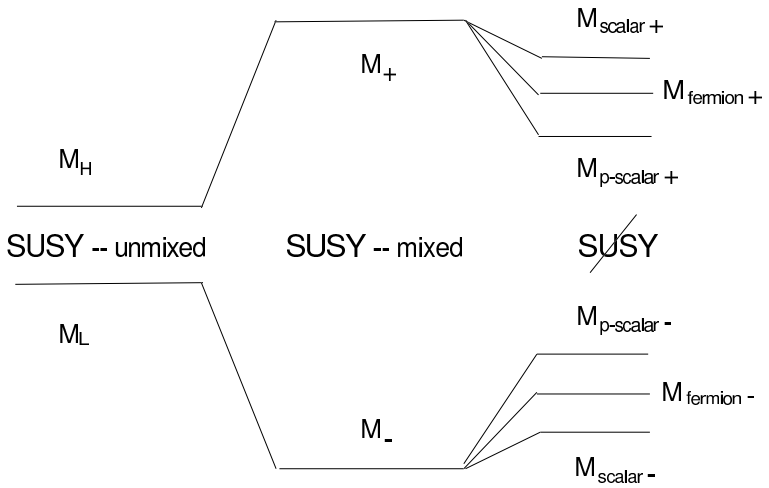

Figure 4.1.: *Qualitative behavior of the mass spectrum of SYM when passing from the exact SUSY model (unmixed and mixed cases, see in the text) to the softly broken model in the effective low-energy Lagrangian picture.*

comes from the superalgebra identity

$$\{Q_\alpha, \bar{Q}_{\dot{\beta}}\} \;=\; 2\,\sigma^{\mu}_{\alpha\dot{\beta}}\,P_\mu \;, \tag{4.31}$$

and the fact that in the superfield representation $P_\mu \equiv -i\partial_\mu$. The problem of the absence of infinitesimal translations on the lattice can be bypassed by considering a lattice version of the differential operator ∂_μ, O^L_μ, having the correct continuum limit. The lattice version of the supercharge according to (4.30), with $\partial_\mu \to O^L_\mu$, satisfies the identity (4.31) by construction[9].

The point is now that for any *local* definition of the lattice differential operator O^L_μ, the composite field ϕ^3 does not transform like a chiral superfield, and the interaction term $\phi^3_{\theta\theta}$, in particular, is not invariant under lattice SUSY transformations. The basic reason for this is that any local definition of the lattice derivative does not satisfy the *Leibniz rule*. Explicit invariance of a lattice Lagrangian under a lattice version of the SUSY transformation can only be obtained by introducing non local definitions of the lattice differential operator (for example the "SLAC derivative" [61, 60]) and, consistently, non local interaction terms in the action (a first attempt in this direction can be found for example in [22]). These formulations however violate Lorentz invariance in the continuum limit [121].

Even if not relevant for the present discussion were *minimal* SUSY is considered, we mention that, in the case of extended SUSY with several supercharges, lattice models with a partial exact SUSY can be constructed [118, 36, 178]. The residual SUSY is generated by supercharges which are not related to infinitesimal translations.

[9]However, the operator O^L_μ does not generate finite translations on the lattice, unless a non-local definition is used.

The motivation behind this line of research is that the residual exact symmetry may protect the renormalized theory from many relevant SUSY-violating terms.

As we will see in the next section, in the case of $\mathcal{N}$=1 SYM only one SUSY-violating term exists, associated with the gluino mass. The latter must be properly tuned in order to recover SUSY in the continuum limit.[10]

4.3.1. The Curci-Veneziano lattice action

In [49] Curci and Veneziano put forward a lattice formulation of SYM which rephrases the Wilson discretization of QCD.

In this original proposal the standard plaquette action is taken for the gluon sector. The Wilson discretization of the Euclidean fermion action (4.16) leads to (we omit here and in the following the label E referring to the Euclidean manifold):

$$S^{\tilde{g}} = a^4 \sum_x \mathrm{Tr}_{color} \Big\{ \frac{1}{2a} \sum_{\mu=\pm 1}^{\pm 4} \left[r\, \overline{\Psi}(x)\Psi(x) - \overline{\Psi}(x+a\hat{\mu}) U_\mu(x) (\gamma_\mu + r) \Psi(x) U_\mu^\dagger(x) \right] + m_0\, \overline{\Psi}(x)\Psi(x) \Big\} \ , \quad (4.32)$$

with $\Psi \equiv \Psi^a T^a$ (T^a are the generators of the fundamental representation of SU(N)), a the lattice spacing and m_0 the gluino bare mass, related to the hopping parameter by $am_0 = 1/2\kappa - 4r$; the bare gauge coupling g_0 is related to the lattice parameter β by the usual relation $\beta = 2N_c/g_0^2$. Observe the analogy with the Wilson action for quarks (0.20). The parallelism with the Wilson formulation of QCD becomes even more evident if an *adjoint link* is introduced:

$$V_\mu^{ab}(x) \ \equiv \ 2\,\mathrm{Tr}(U_\mu^\dagger(x) T^a U_\mu(x) T^b) \ = \ V_\mu^{ab}(x)^* \ = \ (V^{-1T})_\mu^{ab}(x) \ ; \quad (4.33)$$

in this case, the Curci-Veneziano action assumes the more familiar form (observe, again, the factor 1/2)

$$S^{\tilde{g}} = a^4 \sum_x \frac{1}{4a} \sum_{\mu=\pm 1}^{\pm 4} \left[r\, \overline{\Psi}^a(x)\Psi^a(x) - \overline{\Psi}^a(x+a\hat{\mu}) V_\mu^{ab}(x) (\gamma_\mu + r) \Psi^b(x) \right] \quad (4.34)$$

$$+ \frac{m_0}{2}\, \overline{\Psi}^a(x)\Psi^a(x) \ , \quad (4.35)$$

The adjoint link is a real orthogonal matrix; in this case $V_{-\mu}(x) \equiv V_\mu^T(x - a\hat{\mu})$ (and $\gamma_{-\mu} \equiv -\gamma_\mu$ as usual).

In Wilson QCD, a chirality-breaking counterterm is required in order to recover chiral symmetry in the renormalized theory in the continuum limit. Here similarly, as can be argued in an analysis in weak-coupling perturbation theory, the SUSY *and* anomalous $U_R(1)$ Ward identities are recovered in the renormalized theory if m_0 is

[10] Since the mass term breaks chirality too, this tuning is avoided in chiral-symmetric lattice formulations [152, 120].

tuned to a critical value $m_{0c}(g_0) \neq 0$ corresponding to massless gluino. Observe that, at finite lattice spacing, even for $m_0 = m_{0c}(g_0)$ no lattice version of the SUSY transformations (4.8) exists leaving the lattice action invariant. Assuming that the Curci-Veneziano lattice action belongs to the universality class of SYM, this means that features of SYM related with SUSY will only appear in the continuum limit, while at finite lattice spacing $O(a)$ deviations are expected. The same considerations hold for the U(1) R-symmetry. An analysis of these issues in a non-perturbative context will be reviewed in the Section 4.4.

Using relation (4.14), the fermion action (4.32) can be rewritten in terms of an antisymmetric matrix $M_{\alpha\beta}$, where the Greek indices refer collectively to space-time, color and Dirac indices

$$S^{\tilde{g}} \; = \; -\frac{1}{2}\Psi_\alpha M_{\alpha\beta}\Psi_\beta \; . \tag{4.36}$$

In this case the fermion measure reads:

$$\int \prod_\gamma d\Psi_\gamma \, \exp\{-\frac{1}{2}\Psi_\alpha M_{\alpha\beta}\Psi_\beta\} \; = \; \mathrm{Pf}(M) \; , \tag{4.37}$$

where

$$\mathrm{Pf}(M) \; \equiv \; \frac{1}{N!2^N}\epsilon_{\alpha_1\beta_1\ldots\alpha_N\beta_N} M_{\alpha_1\beta_1}\ldots M_{\alpha_N\beta_N} \; , \tag{4.38}$$

is the *Pfaffian* of the antisymmetric matrix M (N denotes its order). Similarly to QCD, a non-Hermitian and a Hermitian fermion matrix can be defined; respectively:

$$Q \; = \; C^{-1}M \qquad \tilde{Q} \; = \; \gamma_5 Q \; , \tag{4.39}$$

with the relation

$$\det(\tilde{Q}) \; = \; \det(Q) \; = \; \mathrm{Pf}(M)^2 \; . \tag{4.40}$$

Due to the property of $\tilde{Q}$, following from (4.39) and from the antisymmetry of M,

$$C^T \, \tilde{Q} \, C \; = \; \tilde{Q}^T \; , \tag{4.41}$$

the spectrum of $\tilde{Q}$ is doubly degenerate and, consequently, the fermion determinant is positive. Relation (4.40) implies in turn that $\mathrm{Pf}(M)$ is real[11]. One can thus write:

$$\mathrm{Pf}(M) \; = \; \sqrt{\det(Q)}\, \mathrm{sgn}(\mathrm{Pf}(M)) \; . \tag{4.42}$$

On the basis of (4.42), the TSMB algorithm described in Sec. (1.2) can be applied to SYM with the choice $\alpha = 1/4$, while the sign of the Pfaffian must be taken into account in the reweighting procedure (see in Sec. (1.2) and in [35] for more details). The situation is in this sense similar to $N_f = 1$ QCD with a light quark mass to be considered in the following in this chapter.

[11] If the Majorana representation of the gamma-matrices is used the matrix M itself is real.

4.3.2. First studies

A first numerical study of SYM with gauge group SU(2) and dynamical gluino was accomplished in [124], where the phase structure of the theory was studied by analyzing the gluino condensate for light gluino masses. In the continuum (Subsec. 4.2.1), a gluino condensate is expected to produce the spontaneous breaking of the discrete chiral symmetry: $Z_4 \to Z_2$ for gauge group SU(2). The gluino mass aligns the vacuum into one specific direction in Z_4/Z_2 and the condensate changes sign when the gluino mass becomes negative (Eq. (4.23)): a *first order phase transition* is expected for vanishing gluino mass[12]. In the Wilson formulation, the condensate is subject to an additive and a multiplicative renormalization and only a *jump* of the condensate can be detected directly from lattice data. It is not clear how lattice artifacts can change this scenario. In the case of QCD, as we have seen in Sec. 3.3, $O(a)$ effects can substantially modify the phase structure when $m \lesssim a\Lambda_{QCD}^2$; metastable vacua are in particular produced for light quark masses.

In [124] evidences for a first order phase transition with metastable vacua were found, with a double-peak structure of the sample-distribution of the gluino condensate. The method allowed to determine the critical value of the bare lattice gluino mass m_0 (vanishing gluino mass) corresponding to a symmetric distribution of the condensate. The simulation was performed on a relatively small $6^3 \cdot 12$ lattice and for one value of $\beta = 2.3$. As we will see in Sec. 4.6, this value of β corresponds to a lattice spacing $a \simeq 0.06$ fm when QCD units are used to fix the lattice scale (an explanation of the conversion to QCD units can be found in Sec. 4.6); this implies on the $6^3 \cdot 12$ lattice a spatial volume of only $(0.4 \text{ fm})^3$. The value found in [124] for the critical hopping parameter, $\kappa_c = 0.1955(5)$, is therefore expected to be affected by substantial finite volume effects.

A new analysis of the chiral phase transition in SU(2) SYM, based on a new PHMC simulation algorithm [140], see also in Subsec. 3.4.1, on larger volumes and several values of the lattice spacing is in preparation [57].

In [35] first large-scale simulations of the theory with the TSMB algorithm were realized at $\beta = 2.3$ and on $6^3 \cdot 12$, $8^3 \cdot 16$ and $12^3 \cdot 24$ lattices. In this case, the analysis focused on the inter-quark potential and the light bound state masses. The results of this study will be compared with new results to be discussed in Sec. 4.6.

4.4. SUSY Ward identities on the lattice [SYM-1]

According to the discussion in Sec. 4.3, the Wilson discretization of SYM is not left invariant by any lattice counterpart of the continuum SUSY transformations (4.8). From the analysis in weak-coupling perturbation theory of [49], SUSY is however expected to be recovered in the *continuum* renormalized theory. The situation is similar to the one applying for chiral symmetry in QCD, with a substantial difference,

[12] Recall that no Goldstone boson is associated with this spontaneous symmetry breaking and the mass gap of the theory does not vanish.

however. In QCD, a lattice version of the non-renormalization theorem for conserved currents [183] ensures the existence of the chiral currents in the continuum limit. The latter are obtained by a finite multiplicative renormalization of the lattice operators[13]. The chiral currents satisfy softly broken Ward identities if the quark mass is properly renormalized by an additive term $\sim a^{-1}$. A similar scenario is expected to apply to the SUSY Ward identities too, Eq. (4.13), but a rigorous proof is (still) missing. A non-perturbative verification of SUSY restoration, complementing the weak-coupling arguments of [49], is therefore of primary importance. A first non-perturbative study of the SUSY Ward identities with dynamical gluino was performed in [SYM-1], where also the theoretical issue of the renormalization was investigated in detail[14].

4.4.1. Lattice SUSY Ward identities

The SUSY Ward identities for lattice SYM are obtained by rephrasing the method introduced in [32] for the case of the chiral Ward identities in Wilson QCD. One considers the invariance of the vacuum expectation value of a local operator $Q(y)$ (insertion operator) under redefinition of the fields by a *local* SUSY transformation. The invariance of the vacuum expectation value under redefinition of the field variables at the site x implies

$$\langle -(\delta_x S)\, Q(y) \,+\, \delta_x Q(y) \rangle = 0 \;, \tag{4.43}$$

where $\delta_x S$ and $\delta_x Q(y)$ denotes the variation of the action and of the insertion operator, respectively. The variation of the symmetric part of the action results in the divergence of the spinorial Noether current $S_\mu(x)$ ("supercurrent"); so one can rewrite Eq. (4.43) in the form:

$$\langle \partial_\mu S_\mu(x)\, Q(y) \rangle \;=\; \langle \delta_x S_{break}\, Q(y) \rangle + \text{contact terms} \sim \delta(x-y) \;; \tag{4.44}$$

the contact term derives from the variation of the local insertion operator.

The first step is therefore to define a lattice analogous of the transformations (4.8)[15]. The lattice SUSY transformations should commute with the lattice gauge transformations, the discrete symmetries of the action (P, T) and preserve the Majorana condition for the gluino field (4.14). The simplest choice is

$$\begin{aligned}
\delta_\xi U_\mu(x) &= -\frac{ig_0 a}{2}(\overline{\xi}(x)\gamma_\mu U_\mu(x)\Psi(x) + \overline{\xi}(x+a\hat{\mu})\gamma_\mu \Psi(x+a\hat{\mu})U_\mu(x)) \;, \\
\delta_\xi U_\mu^\dagger(x) &= \frac{ig_0 a}{2}(\overline{\xi}(x)\gamma_\mu \Psi(x)U_\mu^\dagger(x) + \overline{\xi}(x+a\hat{\mu})\gamma_\mu U_\mu^\dagger(x)\Psi(x+a\hat{\mu})) \;, \\
\delta_\xi \Psi(x) &= \frac{1}{2} P_{\mu\nu}^{(cl)}(x)\sigma_{\mu\nu}\xi(x) \;, \\
\delta_\xi \overline{\Psi}(x) &= -\frac{1}{2}\overline{\xi}(x)\sigma_{\mu\nu}P_{\mu\nu}^{(cl)}(x) \;,
\end{aligned} \tag{4.45}$$

[13] The renormalization converges to one for $g_0 \to 0$.

[14] SUSY Ward identities for SYM in the quenched approximation were considered in [59].

[15] Observe, however, that the equations of Subsec. 4.1.1 were derived for the Minkowski manifold.

where $\xi(x)$, $\overline{\xi}(x)$ are infinitesimal Majorana fermionic parameters. $P^{(cl)}_{\mu\nu}(x)$ is a (clover-symmetrized) lattice version of the field strength tensor $F_{\mu\nu}$ which complies with P and T [SYM-1].

This results in the following Ward identities[16]

$$\sum_{\mu} \left\langle \left(\nabla_\mu S^{(ps)}_\mu(x)\right) Q(y) \right\rangle \;=\; m_0 \left\langle \chi(x) Q(y) \right\rangle + \left\langle X^{(ps)}(x) Q(y) \right\rangle - \left\langle \frac{\delta Q(y)}{\delta \overline{\xi}(x)} \right\rangle \;. \quad (4.46)$$

The meaning of the various terms will be explained in the following.

The lattice SUSY current $S^{(ps)}_\mu(x)$ is a point-split current [182]

$$S^{(ps)}_\mu(x) = -\frac{1}{2} \sum_{\rho\sigma} \sigma_{\rho\sigma}\gamma_\mu \mathrm{Tr}\Big(P^{(cl)}_{\rho\sigma}(x) U^\dagger_\mu(x) \Psi(x+a\hat{\mu}) U_\mu(x) \;+ \quad (4.47)$$

$$P^{(cl)}_{\rho\sigma}(x+a\hat{\mu}) U_\mu(x) \Psi(x) U^\dagger_\mu(x) \Big) \;;$$

∇^b is the backward lattice derivative $\nabla^b_\mu f(x) = (f(x) - f(x-a\hat{\mu}))/a$.

The first two terms on the RHS of Eq. (4.46) result from the fact that the lattice action is not invariant under a *global* SUSY transformations. In particular, the gluino mass term gives rise to the expected soft breaking term (compare with Eq. (4.13)):

$$\chi(x) = \sum_{\rho\sigma} \sigma_{\rho\sigma} \mathrm{Tr}\left(P^{(cl)}_{\rho\sigma}(x) \Psi(x) \right) \;. \quad (4.48)$$

The *explicit* SUSY breaking of the Curci-Veneziano action, including the one stemming from the Wilson term, gives rise to an additional SUSY-breaking term, denoted with $X^{(ps)}(x)$ in Eq. (4.46). The exact expression of $X^{(ps)}(x)$ [182] is not needed for the following discussion; it is enough to know that, in the naive continuum limit, $X_S(x) \simeq a O_{11/2}(x)$, where $O_{11/2}(x)$ is a dimension 11/2 operator.

The last contact term in (4.46) will be disregarded in the following, where $x \neq y$ will always be taken.

The lattice definition of the SUSY current is univocal up to $O(a)$ terms. In particular, a local choice for the current is also possible. The local current $S^{(loc)}_\mu(x)$ satisfies a Ward identities of the form (4.46), with a symmetric lattice derivative $\nabla^s_\mu f(x) = (f(x+a\hat{\mu}) - f(x-a\hat{\mu}))/2a$ (preserving P and T); the SUSY-breaking term, which depends on the details of the discretization, differs from the point-split version by $O(a)$ terms: $X^{(loc)} = X^{(ps)} + O(a)$.

4.4.2. Renormalization

Eq. (4.46) is a relation among *bare* correlators, while the continuum limit can only be taken after proper renormalization of the theory. The discussion of the renormalization of the lattice SUSY Ward identities is closely related to that of the chiral Ward

[16] In view of non-perturbative studies, only gauge invariant insertion operators are considered; in this case, SUSY-breaking gauge fixing terms in the action do not play any role.

identities in QCD [32, 183]. In particular, the mixing of the SUSY-breaking operator $X_S(x)$ with lower dimensional operators gives rise to logarithmically divergent renormalizations and power subtractions.

The renormalization pattern of the operator $O_{11/2}(x)$, related to the SUSY-breaking lattice term $X_S(x)$, is discussed in detail in Appendix B of [SYM-1]. By using the available symmetries of the lattice action (gauge invariance, C, P, T, hyper-cubic), one can make restrictions on the mixing pattern of $O_{11/2}$. In particular, hyper-cubic invariance excludes Lorentz violating mixing terms.

In the on-shell case, the resulting general mixing pattern involves operators with dimensions $7/2 \leq d \leq 11/2$:

$$\begin{aligned} O^R_{11/2}(x) \quad = \quad & \\ & Z_{11/2}\,\left[O_{11/2}(x) + a^{-1}(Z_S-1)\,\nabla_\mu S_\mu(x) + a^{-1} Z_T\,\nabla_\mu T_\mu(x) + a^{-2} Z_\chi\,\chi(x)\right] \\ & + \quad \sum_j Z^{(j)}_{11/2} O^{(j)\,R}_{11/2}(x)\ . \end{aligned} \tag{4.49}$$

An additional dimension 7/2 operator (besides the SUSY current) appears in (4.49), the *mixing current* $T_\mu(x)$. In the point-split case it may be defined as

$$\begin{aligned} T^{(ps)}_\mu(x) = \sum_\nu \gamma_\nu \mathrm{Tr}\Big(& P^{(cl)}_{\mu\nu}(x) U^\dagger_\mu(x) \Psi(x+a\hat{\mu}) U_\mu(x) \ + \\ & P^{(cl)}_{\mu\nu}(x+a\hat{\mu}) U_\mu(x) \Psi(x) U^\dagger_\mu(x) \Big)\ . \end{aligned} \tag{4.50}$$

The last term on the RHS of Eq. (4.49) reflects the mixing of the operator $O_{11/2}(x)$ with other bare operators $O^{(j)}_{11/2}(x)$ with the same dimension. Solving Eq. (4.49) for $O_{11/2}(x)$ and substituting it in the Ward identities (4.46), one gets the new *renormalized* Ward identities

$$Z_S\,\langle (\nabla_\mu S_\mu(x))\,Q(y)\rangle + Z_T\,\langle (\nabla_\mu T_\mu(x))\,Q(y)\rangle = m_S\,\langle \chi(x) Q(y)\rangle \ + \ O(a)\ , \tag{4.51}$$

where the subtracted mass m_S is given by

$$m_S = m_0 - a^{-1} Z_\chi\ . \tag{4.52}$$

In deriving Eq. (4.51) we have relied on the vanishing in the continuum limit of the correlation

$$a \left\langle [Z^{-1}_{11/2} O^R_{11/2}(x) - \sum_j Z^{(j)}_{11/2} O^{(j)\,R}_{11/2}(x)]\,Q(y) \right\rangle \ = \ O(a)\ , \tag{4.53}$$

which is valid on-shell, $x \neq y$ ($Z_{11/2}$, $Z^{(j)}_{11/2}$ are logarithmically divergent renormalizations).

By using general renormalization group arguments (see for example [183]) one can show that the power-subtraction coefficients Z_S, Z_T and Z_χ are independent of the renormalization scale. Dimensional considerations imply in this case:

$$Z_S = Z_S(g_0, m_0 a) \ , \quad Z_T = Z_T(g_0, m_0 a) \ , \quad Z_\chi = Z_\chi(g_0, m_0 a) \ . \tag{4.54}$$

In particular, the dependence of Z_S and Z_T on the gluino mass is vanishingly small in the continuum limit[17].

In QCD, the lattice chiral Ward identities lead to the definition of a *multiplicatively renormalized* chiral current. A rigorous argument [32, 183] shows in this case that the renormalized current coincides with the physical current in the continuum limit. It satisfies in particular the appropriate current algebra. The analogous quantity for SUSY would be (see Eq. (4.51)):

$$\hat{S}_\mu(x) \ = \ Z_S \, S_\mu(x) + Z_T \, T_\mu(x) \ . \tag{4.55}$$

As discussed in [SYM-1], an attempt to reproduce the QCD argument in the case of the SUSY current however fails. Explicit one-loop calculations in lattice perturbation theory may shed some light on this issue [182]. If the correctly normalized SUSY current coincides with $\hat{S}_\mu(x)$ (or is related to it by multiplicative renormalization), then Eq. (4.51) implies that it is conserved when m_S vanishes. In this case SUSY is restored in the continuum limit at $m_S = 0$.

The renormalized SUSY Ward identities (4.51) are the object of the numerical investigations which will be reviewed in the following. In particular, the Ward identities are used to determine, in a non-perturbative way, m_S. The issue of the renormalization of the supercurrent, which can only be settled by studying the continuum limit of lattice SYM, is beyond the scope of this analysis taking place at a single value of the lattice spacing.

4.4.3. Insertion operators

The choice of the insertion operator for the SUSY Ward identities (4.51) is not completely trivial due to the spinorial nature of the SUSY current. Since the Ward identities are considered at zero spatial momentum, the "orbital" angular momentum vanishes and rotational invariance requires that the insertion operator contains at least one spin 1/2 component ($O(a)$ corrections are neglected in the Ward identities, meaning that the more restrictive Lorenz invariance of the continuum applies). So, as one would naively expect, only insertion operators containing spin 1/2 representations of the rotational group result in non trivial Ward identities. It is possible to classify the representations of the Lorentz group having this property (Appendix C of [SYM-1]).

For the optimization of the signal-to-noise ratio, it is convenient to choose low dimensional composite operators. The best candidate according to these criteria is

[17] In simulations at fixed lattice spacing this dependence is treated as an $O(a)$ effect.

the dimension 7/2 operator confined on a time-slice

$$Q(x_0) = \sum_{\vec{x}} \chi^{(sp)}(\vec{x}, x_0) \equiv \sum_{\vec{x}, i<j} \sigma_{ij} \mathrm{Tr} \left[P_{ij}^{(cl)} \Psi(\vec{x}, x_0) \right] \ . \tag{4.56}$$

Another possible choice is given by the temporal component of the mixing current (4.50), which however is not confined on a time-slice.

Each spinorial dimension 7/2 operator delivers two independent equations when inserted in the Ward identities (4.51), corresponding to the two spin 0 components in the sink-source operator product. The two resulting Ward identities can be used to determine the bare soft-breaking gluino mass $Z_S^{-1} m_S$ and the combination of renomalization constants $Z_S^{-1} Z_T$.

4.4.4. Simulation

The investigation of [SYM-1] relies on samples of configurations on a $12^3 \cdot 24$ lattice at $\beta = 2.3$. Besides the set at $\kappa = 0.1925$ of [35], two further sets at lighter values of the gluino mass, $\kappa = 0.194$ and 0.1955, were generated. The motivation for simulating with a light gluino is of course that the restoration of SUSY can only be verified after an extrapolation to zero gluino mass.

From the algorithmic point of view, the simulation allowed to test for the first time the behavior of TSMB in the case of extremely light fermionic degrees of freedom. This was also important in view of the future applications in QCD, covered in the first three Chapters.

The possibility given by TSMB of tuning various algorithmic parameters allowed to avoid a dramatic increase of the autocorrelations for decreasing gluino mass, see Table 2 of [SYM-1]. A more detailed analysis of the behavior of TSMB for light quarks was given in Chapter 1.

A potential problem in lattice SYM is the fast fluctuation of the sign of the Pfaffian during the update. Such a behavior is expected in the vicinity of the chiral phase transition at zero gluino mass (Secs. 4.2.1 and 4.3.2). In the present case, up to the lightest simulated gluino mass, occurrence of sign flips turned out to be statistically negligible.

Missing any connection to phenomenology, in SYM it is not possible to fix the lattice scale; nevertheless one can exploit the analogy with the physical theory QCD in order to get qualitative indications. Using the Sommer scale parameter r_0 [176], extrapolated to zero gluino mass, to fix the scale (see Sec. 4.6 in the following) one obtains for the lattice spacing $a \simeq 0.06$ fm. This corresponds to a quite small lattice spacing in QCD computations. If analogy with QCD holds, $O(a)$ SUSY-breaking effects are not expected to play a major role at this β-value (even if the lattice theory is not improved). The physical volume is on the other hand relatively small: $(0.7 \text{ fm})^3$. In the case of SYM however the mass gap does not vanish in the massless gluino limit and the finite size scaling may be radically different from the one applying to QCD. In the case of the SUSY Ward identities, finite volume effects come into play through

the (SUSY-breaking) anti-periodic boundary conditions in the time direction for the fermions.

4.4.5. Results from the SUSY Ward identities

As mentioned above, the study of the SUSY Ward identities allows to determine the bare SUSY soft-breaking gluino mass $Z_S^{-1} m_S$ and the combination of finite renormalization constants $Z_S^{-1} Z_T$. The numerical results for these quantities in lattice units are reported in the Tables 4-7 of [SYM-1], for different lattice definitions of the currents and choices of the insertion operator (results as a function of the sink-source time separation are given in Figs. 4 and 5). The time-slice insertion operator (4.56) gives the most precise determinations; the following discussion is based on these results.

Local and point-split currents produce quite different values for $Z_S^{-1} Z_T$ (in particular the coefficient is close to zero in the case of the point-split current). This is expected, since this quantity is a pure lattice artifact and therefore sensitive to the exact lattice definition of the current. In the case of $Z_S^{-1} m_S$, a quantity with a continuum counterpart, different discretizations are expected to produce relatively small $O(g_0^2)$ deviations. This is well reflected by the numerical results.

Another observation consistent with theoretical expectations is that the dimensionless coefficient $Z_S^{-1} Z_T$ has a weak dependence upon κ; this dependence, according to the discussion of Subsec. 4.4.2, is an $O(a)$ effect. On the contrary, a strong dependence upon κ is observed for the soft-breaking gluino mass, which decreases for increasing κ. This is consistent with the picture of restored SUSY for $\kappa \to \kappa_c$, where the gluino mass vanishes. An independent check of this picture is obtained in the OZI approximation (briefly discussed near the end of Subsec. 4.2.1), predicting a massless adjoint-pion in the limit of restored (discrete) chiral symmetry at zero gluino mass. This aspect will be discussed more extensively in Sec. 4.6, when reviewing [SYM-3]. We anticipate that numerical results indicate that both the soft-breaking gluino mass and the adjoint-pion mass vanish at a common value of κ.

A simple linear extrapolation of $Z_S^{-1} a m_S$ as a function of $m_0 \sim 1/\kappa$ (based on the expectation of an analytic dependence of this quantity on the Lagrangian gluino mass parameter) allows to estimate the critical value of the hopping parameter where $m_S = 0$. The result is $\kappa_c = 0.19750(38)$ (point-split current) and $\kappa_c = 0.19647(27)$ (local). This result shifts the critical value to larger values compared with the previous estimate $\kappa_c = 0.1955(5)$ of [124] (Subsec. 4.3.2). Indeed, one of the simulations of [SYM-1] was exactly at $\kappa = 0.1955$. We conclude that the value $\kappa = 0.1925$ considered in [35] for the analysis of the bound states spectrum corresponds to a quite heavy gluino, for which soft breaking effects are still large. A new investigation of the spectrum deeper into the light gluino regime is therefore required for a verification SUSY in the mass spectrum of the theory. This will the subject of Sec. 4.6.

In summary, the results of [SYM-1] show the feasibility of a non-perturbative study of the SUSY ward identities in a SUSY gauge theory; the results are consistent with the renormalized SUSY Ward identities (4.51) and support a picture in which both SUSY

and the (discrete) chiral symmetry are restored (up to $O(a)$ corrections) if the bare gluino mass is tuned to a common critical value. SUSY restoration in the continuum limit can be verified for example in the bound state spectrum of SYM (Sec. 4.6).

4.5. Volume source technique revisited [SYM-2]

As we have seen in Subsec. 4.2.2, the interpolating operators of mesonic bound states of SYM consist of gluino bilinears. The correlators of these operators contain diagrams with two disconnected gluino loops. The numerical estimate of such disconnected diagrams is not trivial, since standard fermion-matrix inversion techniques are not applicable; in addition, the signal for the correlators is intrinsically noisy. A prerequisite for an accurate determination of the hadron masses in SYM is therefore the optimization of the computational techniques. In the following, as a preparation for the analysis of the bound state spectrum of SYM to be discussed in Sec. 4.6, a novel method for the evaluation of the disconnected diagrams of the mesonic correlators in SYM is proposed and compared with stochastic methods already available for QCD.

4.5.1. Improved volume source technique (IVST)

Interpolating operators of mesonic states in SYM are given, see also in Subsec. 4.2.2, by bilinears of the fermion fields $\lambda^a_\alpha \lambda^{a\alpha}$, $\bar{\lambda}^{a\dot{\alpha}} \bar{\lambda}^a_{\dot{\alpha}}$, or equivalently with Majorana spinors[18]:

$$\bar{\psi}(x) \Gamma \psi(x) \ , \quad \Gamma = \mathbb{1}, \gamma_5 \ . \tag{4.57}$$

The disconnected component of the meson correlators in the background of a gauge configuration $\{U\}$ can be written

$$C_{\Gamma,\mathrm{disc}}[U](x_0 - y_0) = \frac{1}{V_s} \mathrm{Tr}_{Dirac}[\Gamma S(x_0)] \, \mathrm{Tr}_{Dirac}[\Gamma S(y_0)] \, ; \tag{4.58}$$

$S(x_0)$ is the trace over color and spatial indices of the fermion propagator in the background of the gauge configuration $\{U\}$:

$$S_{\alpha\beta}(x_0) = \sum_{\vec{x}} \mathrm{Tr}_{color}[Q^{-1}_{x\alpha,x\beta}] \, . \tag{4.59}$$

The exact evaluation of the above time-slice sum is not feasible in practice, since it requires the computation of $Q^{-1}_{x\alpha,y\beta}$ for any x and y ("all-to-all" inversion problem).

The first solution found for this problem was based on a volume source [128] ("Volume Source Technique", VST). VST delivers an estimate of $S_{\alpha\beta}(x_0)$ at the price of a single inversion for each value of the color and the Dirac index. The inversion problem with the volume source ω_V reads

$$Q Z = {\omega_V}^{[a,\alpha]} \, , \quad (\omega_V^{[a,\alpha]})_{xb\beta} = \delta_{ab} \, \delta_{\alpha\beta} \ , \tag{4.60}$$

[18] The present discussion is general for any representation of the gauge group SU(N_c) and the usual symbols for the fermion fields are therefore used.

with solution

$$Z^{[a,\alpha]}_{xb\beta} = [Q^{-1}\omega^{[a,\alpha]}_V]_{xb\beta} = Q^{-1}_{xb\beta,xa\alpha} + \sum_{y\neq x} Q^{-1}_{xb\beta,ya\alpha} \ . \tag{4.61}$$

An estimate of the time-slice sum (4.59) is given by

$$\tilde{S}_{\alpha\beta}(x_0) \equiv \sum_{\vec{x},a} Z^{[a,\alpha]}_{xa\beta} = [Q^{-1}\omega^{[a,\alpha]}_V]_{xa\beta} \ , \tag{4.62}$$

where however the last term in (4.61) yields spurious, non gauge-invariant, contributions to the disconnected component of the correlator (4.58). In QCD and in general for a non real representation of SU(N), one can eliminate these spurious terms in the correlators by replacing $\tilde{S}$, for example in the source term, with its Hermitian conjugate (transposition in color and Dirac indices)

$$\tilde{C}_{\Gamma,\mathrm{disc}}[U](x_0-y_0) = \frac{1}{V_s}\mathrm{Tr}_{Dirac}[\Gamma\tilde{S}(x_0)]\,\mathrm{Tr}_{Dirac}[\Gamma\tilde{S}^\dagger(y_0)]\,; \tag{4.63}$$

after this replacement, the spurious contributions add up to zero in the average over the gauge sample, since they do not contain any gauge invariant component. The latter statement can be proven by considering that the product of fundamental representations of SU(3) does not contain the trivial representation. This argument holds more generally for the fundamental representation of SU(N_c) with $N_c > 2$.

As noticed in [SYM-2], however, in the case of gauge group SU(2), which has real representations only, and in the adjoint representation of SU(N_c) in general for any N_c, the above argument fails. For SU(2) the product of two fundamental representations contains the trivial one, which leads to non-vanishing contributions. The same is true in general for the adjoint representations of SU(N_c).

At this point the simple observation was made in [SYM-2], that the error term in the correlator, resulting from these spurious gauge invariant contributions, can be in general removed by replacing $\tilde{S}_{\alpha\beta}(x_0)$ with its gauge-average, since

$$\left\langle \tilde{S}_{\alpha\beta}(x_0) \right\rangle_{gauges} = S_{\alpha\beta}(x_0)\,. \tag{4.64}$$

In practice this is obtained by averaging $\tilde{S}_{\alpha\beta}(x_0)$ over a sufficiently large number N_g of gauge configurations obtained from the original one by a *random gauge transformation* $g(x)$; this defines the improved version of VST (IVST in the following). The stochastic input given by the random gauge transformation suggests an analogy with the stochastic estimator techniques (SET) often used for the computation of flavor-singlet correlators in QCD (see [161] for a recent review on the topic). A direct comparison of the efficiency of the two methods is therefore possible.

4.5.2. Comparing IVST with stochastic source methods

For the comparative study of IVST and SET in the case of SYM, a new set of configurations on a larger $16^3 \cdot 32$ lattice was generated with the TSMB algorithm at $\beta = 2.3$ and $\kappa = 0.194$.

For $\sim$ 200 uncorrelated gauge configurations, 50 estimates of the time-slice sum (4.59) were performed in IVST and 165 estimates in SET in the spin-explicit variant. In the latter case each estimate of the time-slice sum is obtained by inverting the fermion-matrix with source

$$(\omega_S^{[\alpha]})_{xb\beta} = \delta_{\alpha\beta}\,\eta_{xb}^{[\alpha]}\ , \tag{4.65}$$

where $\eta_{xb}^{[\alpha]}$ are independent stochastic variables chosen at random among $\frac{1}{\sqrt{2}}(\pm 1 \pm i)$ (complex Z_2).

The comparison of the two methods must be done in terms of *matrix inversions*, since the computational load per estimate is different in the two cases (one estimate with IVST is a factor of three more expensive than the corresponding one with SET). The two methods give in general consistent results for the expectation values of the condensates with both parities and for the mesons correlators (Figs. 2 and 5 of [SYM-2]).

A non trivial result of the study is that the two stochastic methods produce the same level of noise in the correlators. Indeed, see Fig. 4 of [SYM-2], the statistical error for the same number of inversions is comparable in the two cases. As expected from the discussion above, the unimproved VST introduces a systematic error in the correlators (Fig. 5); the latter is reflected by large fluctuations of the effective hadron mass for large time-separations, where the disconnected term dominates.

The main result of the study [SYM-2] is that the two stochastic methods for the determination of the disconnected diagrams, IVST and SET, are essentially equivalent and both give satisfactory results for the quantity of interest, the masses of the mesonic bound states of SYM. On the contrary, VST introduces large systematic effects in the correlators and in the estimates of the masses. In consideration of this result, IVST and SET were applied in the investigation of the light bound state spectrum of [SYM-3] (next section).

4.6. Study of the bound state spectrum of $\mathcal{N} = 1$ SYM [SYM-3]

As we have seen in Subsec. 4.2.2, the main features of the low-lying bound state spectrum of SYM are still under debate in the theoretical discussion. In particular, glueball states, which should naturally appear at low-energies, cannot be easily included in the low-energy effective Lagrangians.

On the other side, the numerical analysis of the spectrum of SYM presents non trivial difficulties. The involved bound state correlators are indeed intrinsically noisy and the extraction of the signal awkward. In the case of the glueball and mixed gluino-glue bound states, the noise originates from the gluon content of the interpolating operators. For the mesonic states, as discussed in the previous section, large fluctuations are introduced by the disconnected diagrams.

In [35], a first pioneering investigation of the spectrum of SYM was undertaken. However, the repositioning of the critical hopping parameter to a larger value operated in [SYM-1] implies that the gluino mass considered in that first work is probably too heavy; the soft breaking effects are still too large for a safe extrapolation of the data to the massless gluino limit. Another open question from [35] is the effect of the finite volume on the bound state masses: the spatial volume in the $12^3 \cdot 24$ lattice was estimated to be less than $(1 \text{ fm})^3$.

The new analysis of [SYM-3] tries to cope with these open questions. In order to obtain more precise results, a larger statistic was sampled for the computation of the masses. The accuracy for the meson masses was improved by recurring to the optimized analysis techniques described in the previous section. Finally, substantially lighter (up to a factor three) gluino masses and a larger volume were included in the analysis of the bound states mass spectrum.

4.6.1. Gauge samples

The analysis of [SYM-3] is based on three sets of configurations on a $12^3 \cdot 24$ lattice at $\beta = 2.3$, $\kappa = 0.1925$ [35], $\kappa = 0.194$ and $\kappa = 0.1955$ [SYM-1]. At $\kappa = 0.194$, a set of configurations on a larger $16^3 \cdot 32$ lattice was also included in the analysis (this set was already employed for the study [SYM-2] described in the previous section).

As already briefly mentioned, a characterization of the gauge sample can be obtained by the Sommer scale parameter r_0 [176] of the inter-quark potential. In [SYM-3] a definition of the lattice spacing was proposed obtained from the extrapolated value of r_0 at massless gluino. This corresponds to the massless renormalization scheme of QCD, where the lattice spacing only depends on the bare gauge coupling.

In the case of SYM, the lattice spacing cannot of course be translated into physical units. However, one can quote [SYM-3] the value of the lattice spacing corresponding to the phenomenological value of r_0, $r_0 = 0.5$ fm, appropriate for the case of QCD. This delivers for $\beta = 2.3$ in two-color SYM $a \simeq 0.06$ fm, a fairly small lattice spacing from the point of view of QCD simulations. Of course SYM and QCD are different theories and the discretization effects in the respective lattice formulations could be very different.

The study of the inter-quark potential allows to determine the string tension σ of static fundamental sources, which does not vanish in SYM (Subsec. 4.2.2). Finite volume effects play an important role here; the comparison of the string tension for $L_x = 12$ (~ 0.7 fm) vs. $L_x = 16$ (~ 1 fm) reveals a small deviation inside the statistical errors, as shown in Table 1 of [SYM-3]. The picture of confinement of static fundamental sources is substantially confirmed.

4.6.2. Gluino mass and massless limit

The (bare) gluino mass $m_{\tilde{g}}$ can be determined in a direct way from the study of the SUSY Ward identities ([SYM-1], Sec. 4.4). As noticed in [SYM-3] an indirect determination of $m_{\tilde{g}}$ is available in the OZI approximation of SYM (Subsec. 4.2.1).

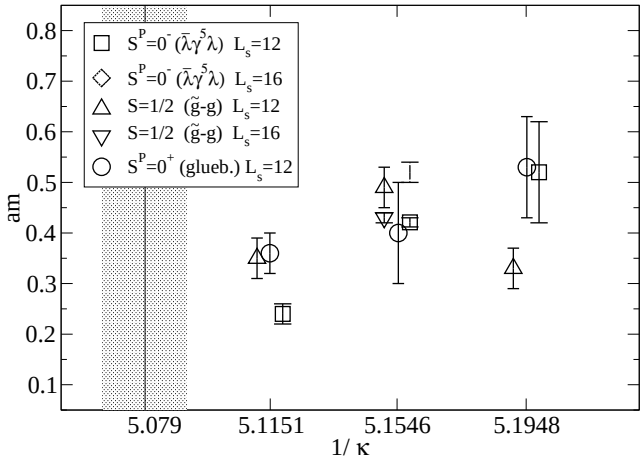

Figure 4.2.: *Low-energy hadron masses in* $\mathcal{N} = 1$ *SYM [SYM-3].*

In the OZI limit, the anomaly vanishes and the adjoint pion is the Goldstone boson associated to the spontaneous breaking of $\mathrm{U(1)_R}$. Assuming a linear behavior of the squared adjoint pion mass $M^2_{a\text{-}\pi}$ with $m_{\tilde{g}}$, one can use the dimensionless quantity $M_r = (M_{a\text{-}\pi} r_0)^2$ as *reference gluino mass* in analogy with the QCD case ([Alg], Sec. 1.3). The relation valid in QCD [Alg], $m_q = (M_r/3.1)\, m_s$, can be used for the conversion to physical units by replacing the quark mass m_q with the gluino mass $m_{\tilde{g}}$.

Numerically, the two definitions of the gluino mass, by the SUSY Ward identities and the OZI approximation, result in $m_{\tilde{g}} = 180 - 550$ MeV and $m_{\tilde{g}} = (1.3 - 4.4) m_s$, respectively. The two estimates are in rough agreement for $m_s \simeq 100$ MeV. The range of the adjoint pion mass in physical units is $M_{a\text{-}\pi} = 840 - 1800$ MeV.

Under the assumption of the analogy with QCD, these results indicate that the gluino mass is still too large, probably outside the domain of validity of the estimates of [75] in the effective Lagrangian approach (see end of Subsec. 4.2.2). We recall that in QCD, NLO chiral perturbation theory is expected to hold for fairly light quark masses $m_q \lesssim m_s/4 \simeq 20 - 25$ MeV or $M_\pi \lesssim 300$ MeV.

Nevertheless, the two definitions of the gluino mass seem to point towards a consistent massless limit, as suggested by Fig. 3 of [SYM-3].

4.6.3. Spectrum

We recall that the low-energy Lagrangians discussed in Subsec. 4.2.2 predict the presence of two Wess-Zumino supermultiplets at the lower end of the bound state mass spectrum of SYM. They also predict mixing between the states projected by the simplest interpolating operators for the given quantum numbers $(0^\pm, 1/2)$. As argued in [SYM-3] however, the masses of the *unmixed states* diagonalizing the Hamiltonian are determined in the standard methods relying on the asymptotic behavior of Euclidean correlators. In this kind of analysis, the second supermultiplet is formed by the *excited states* in the channel with given quantum numbers.

Unfortunately, two of the simplest operators in the spin zero sector, the 0^- glueball

operator ($\tilde{F}F$) and the 0^+ mesonic operator ($\bar{\Psi}\Psi$), are for different reasons affected by large statistical fluctuations. This means that one has to rely on the remaining operators, the 0^+ glueball (FF) and the 0^- meson ($\bar{\Psi}\gamma_5\Psi$), for the determination of the masses. Notice that in case of strong mixing, gluonic and mesonic operators are in principle equivalent.

The pseudoscalar mesonic operator delivers the most solid results for the masses. The quality of the data is displayed by Fig. 7 of [SYM-3], where the effective mass is plotted. The disconnected diagram of the meson correlator was determined in this case by the optimized stochastic method with complex Z_2 noise (SET) of Sec. 4.5 (SET and IVST are essentially equivalent). For the pseudoscalar and spin 1/2 particles it was possible to extract the excited state masses, which turned out to be $\simeq 1$ in lattice units.

An important test is the verification of the finite volume scaling of the masses. The comparison of the estimates when passing from the $\simeq 0.7$ fm of the $L_x = 12$ lattice to the $\simeq 1$ fm of the $L_x = 16$ lattice, reveals sizeable $(10 - 20)\%$ finite volume effects (Table 2 of [SYM-3]).

The behavior of the correlators reveals the presence of excited states with mass comparable to that of the ground state and large component in the projected state. This observation is compatible with a second nearby multiplet as predicted by the low-energy Lagrangian of [74].

For convenience, we report in Fig. 4.2 the determined bound state masses as a function of $1/\kappa$, which is proportional to the gluino mass up to a constant. One can observe a general tendency of the bound state masses to decrease with the gluino mass. At the lightest gluino mass, in particular, the 0^- state is the lightest particle (with mass $\simeq 800$ MeV). This contradicts the predictions of [75], where the lowest state contained in the softly broken supermultiplet has *positive* parity, Fig. 4.1. A possible explanation is that, as already argued, the gluino mass is still too heavy to allow for a comparison with those predictions.

A naive linear extrapolation of the pseudoscalar particle mass to massless gluino reveals a fairly light particle, with mass $\simeq 300$ MeV. The corresponding state of QCD, the η', is considerably heavier, $M_{\eta'} \simeq 1$ GeV. Interestingly, as we will see in the following in this chapter, a similar observation can be done in $N_f = 1$ QCD too. The above estimate about the pseudoscalar particle mass in SYM is however only qualitative, since, as already stated, the simulated gluino masses are probably too heavy for safe extrapolations to the SUSY limit.

The study [SYM-3] represents a first step towards an accurate analysis of the bound state spectrum of SYM. One indication from [SYM-3] is that the gluino mass should be further reduced in order to be able to see SUSY effects in the bound state spectrum. The large statistical fluctuations in the hadron correlators can be reduced by a substantial increase of the number of sampled configurations (at least by one order of magnitude). These goals can be probably achieved with a new Monte Carlo algorithm for SYM based on polynomial hybrid Monte Carlo along the lines of [140] (see also in Subsec. 3.4.1); such an algorithm is currently under development [57].

The main systematic errors on the determination of the masses are probably represented by the contamination from the excited states. This effect is particularly relevant in the case of the O^+ glueball projecting operator. In this case, due to the high level of noise, the investigation of large time separations was not possible. The introduction in the analysis of variational smearing methods based on an "optimized" interpolating operator, along the lines of [143], could improve the situation. In the mesonic sector, a better signal can probably be obtained by including explicitly the contribution of the lowest eigenmodes of the fermion matrix to the gluino propagator.

4.7. One flavor QCD

QCD with one flavor of quarks ($N_f = 1$ QCD) differs from QCD with two or more flavors in that chiral symmetry is absent: the Abelian chiral symmetry of the one flavor theory is washed out at the quantum level by the Adler-Bell-Jackiw anomaly [3, 24]. Only a vector symmetry remains, related to the conservation of the baryon number. As a consequence of this, the main features of the phase structure and mass spectrum of $N_f = 1$ QCD strongly deviate from those of ordinary QCD, characterized by the spontaneous breaking of the non-Abelian chiral symmetry.

$N_f = 1$ QCD is in this aspect nearer to $\mathcal{N} = 1$ SYM, where the Dirac spinor of the quark is replaced by the Majorana spinor of the gluino and a continuous chiral symmetry is also absent due to the anomaly (Subsec. 4.2.1)[19].

As recently shown, these differences between the two theories get weaker and weaker in a special large N_c limit preserving balance between fermionic and bosonic degrees of freedom (orientifold large N_c limit) [17]. The equivalence of the two theories can indeed be proven [17] at the planar level of this large N_c expansion[20].

Relics of SUSY are therefore expected in the massless quark limit of $N_f = 1$ QCD [18]. A prediction of the orientifold equivalence, already studied in the literature [53], concerns the size of the quark condensate which, as seen in Subsec. 4.2.1 can be computed analytically in SYM.

Another important place where relics of SUSY can be investigated, considered here in more detail, is the low-lying bound state spectrum [Nf1]. As we have seen (Subsec. 4.2.2) SUSY strongly constraints the hadron mass patterns in SYM. In particular a signature of SUSY is the presence at low energies of two degenerate scalar particles with opposite parity. In $N_f = 1$ QCD these two particles can be easily identified with the pseudoscalar η meson and the scalar σ meson, respectively; the former picks up a mass through the anomaly. On the basis of the planar equivalence, their mass ratio including $O(1/N_c)$ corrections is expected to be $m_\sigma/m_\eta = N_c/(N_c - 2)$ [16].

One flavor QCD turns out to be useful for a better understanding of different aspects

[19] In the latter case however, a residual discrete chiral symmetry is preserved by the anomaly. As we have seen in the previous sections of this chapter, the consequence is a richer vacuum structure with a phase transition corresponding to the spontaneous breaking of the discrete chiral symmetry at zero gluino mass, which however does not produce Goldstone bosons.

[20] The equivalence holds for any number of flavors and, also, for a massive fundamental fermion.

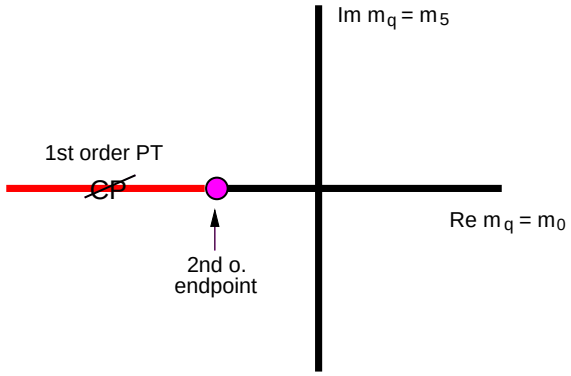

Figure 4.3.: *Expected phase diagram of one flavor QCD in the complex mass plane [45].*

of the multi-flavor theory. We refer here to the recent works of M. Creutz addressing open problems in QCD [46, 47]. These aspects are not directly related to the spontaneous breaking of the chiral symmetry and have therefore an equivalent in the single flavor theory: the latter represents therefore a simple setup for their investigation.

One question raised by Creutz [46], having a relevant phenomenological impact, is whether it is possible to define in an unambiguous way the case where *one* quark (say the u quark) becomes massless. The arguments against an unique definition of the massless limit [46] essentially rest upon the U(1) anomaly and should therefore hold *a fortiori* for the one flavor theory. A second aspect is the possibility of a spontaneous CP breaking in QCD for special choices of the quark masses, conjectured for the first time by Dashen [50]. According to the Vafa-Witten theorem [186] a prerequisite for the spontaneous breaking of a discrete symmetry is the non positivity of the fermion measure. For $N_f = 1$ QCD this is the case when the quark mass is negative. The transition line is indeed expected to be located [45] on the negative real quark mass axis in the extended complex parameter space, see Fig. 4.3. In the case of the physical theory, the transition is excluded for phenomenologically relevant values of the quark masses, but its nearby presence might nevertheless affect lattice numerical simulations [47]. In this sense, the interest to these phenomena is not purely academic.

In Sec. 4.8, first numerical simulations of one flavor QCD in a large volume and with light quark masses [Nf1] will be reviewed. In this region, relics of SUSY are expected in the hadron spectrum, see the discussion above. The study of the phase structure at negative quark masses will be the subject of a future work [72].

4.8. First study of the bound state spectrum of one flavor QCD [Nf1]

The study of the mass spectrum of hadron states of $N_f = 1$ QCD requires reasonably large physical volumes, in order to be able to accommodate the bound states, and small quark masses. Mesonic states of the single flavor theory are characterized, as in SYM,

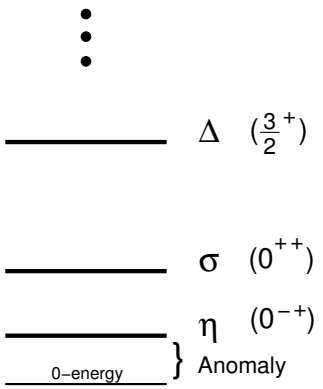

Figure 4.4.: *Expected low-energy spectrum of hadron masses in one flavor QCD.*

by disconnected contributions. These are intrinsically noisy and require large statistics for precise determinations. High statistics is also relevant for the computation of the glueball masses.

4.8.1. Simulation

The study [Nf1] is based on the Wilson lattice fermion action which, as we have already seen in different instances in this review, turns out to be suitable for this kind of investigations[21]. The tree-level improved Symanzik action (tlSym, see Eq. (3.20)) was taken in the gauge sector; tlSym was proven in [tlS-1] and [tlS-2] to speedup the Monte Carlo simulation as an effect of the reduced number of small eigenvalues of the fermion matrix. The same effect can be obtained by introducing a so-called "Stout-link" [142] in the lattice Wilson-Dirac operator. First experiences in this direction were collected in [73].

The simulation algorithm is the PHMC algorithm proposed in [140] and already applied in [tlS-2] for the N_f=2+1+1 twisted mass setup. Two lattices were considered in [Nf1]: $12^3 \cdot 24$ at $\beta = 3.8$ and $16^3 \cdot 32$ at $\beta = 4.0$, corresponding in QCD units to $a(3.8) = 0.186$ fm and $a(4.0) = 0.134$ fm. These lattice spacings are larger than the one applying for the simulations of two-color SYM, $a \simeq 0.06$ fm. This could explain the different behavior found in the two cases in relation to the sign of the fermion measure, see in the following.

As already briefly mentioned in the previous introductory section, the fermion measure in $N_f = 1$ QCD is not positive for all values of the quark masses. The sign of the quark determinant, analogous to the sign of the Pfaffian in SYM (Subsec. 1.2.5) is a sensitive issue in $N_f = 1$ QCD; in particular, a negative determinant could trigger a CP-violating phase transition. In the continuum, the fermion determinant is positive for positive quark mass. With Wilson lattice fermions for small quark masses, it can become negative on some configurations due to quantum fluctuations.

[21] Observe that a twisted mass formulation as the one given in Chapter 3 for the multi-flavor theory is not possible in the single flavor theory; a chiral singlet rotation would introduce a non-zero theta-term in the formulation.

The sign of the determinant was computed in [Nf1] by means of the spectral-flow method also employed in the case of SYM [SYM-1]. For the new analysis performed in [73], an alternative method was considered. In this case, the (complex) spectrum of the non-Hermitian matrix was computed, concentrating on the lowest real eigenvalues: sign changes are signaled by negative real eigenvalues. This latter method, which will be used for future investigations, delivers unambiguous results and can be simply automatized.

In most of the simulations of [Nf1] the (positive) quark mass was large enough to prevent sign changes and the occurrence of a negative determinant was a rare event. For the lightest simulated quark mass on the coarser lattice however ("run c" at $\beta = 3.8$ and $\kappa = 0.1710$) sign changes did occur (26 configurations out of 2884). The sign of the determinant had in this case a sizeable effect on the computed hadron masses.

4.8.2. Hadron spectrum

Due to the absence of the flavor symmetry, the hadron spectrum of $N_f = 1$ QCD is characterized by a simpler structure compared to the multi-flavor theory. A schematic picture of the expected spectrum of $N_f = 1$ QCD is given in Fig. 4.4. In particular, one finds only two states in the meson sector at low energies, the η (0^-) and the σ (0^+). At somewhat higher energies spin 3/2 baryons are expected corresponding to the Δ^{++} baryon in QCD.

The estimate of the meson masses in the single flavor theory requires the computation of disconnected diagrams. Here the spin-explicit variant of SET, also considered in SYM, was applied.

As mentioned in Sec. 4.7 relics of SUSY suggest approximate degeneracy of the two lightest mesons, while the first correction gives $m_\sigma/m_\eta = N_c/(N_c - 2)$; this means $m_\sigma/m_\eta = 3$ for $N_c = 3$ [16]. For the simulation points of [Nf1] this ratio turns out to be about 1.5. This results is below the estimate in [16], but the situation could improve in the massless quark limit where the prediction applies. The lightest Δ^{++} baryon is by about a factor of 3 heavier than the η meson. The scalar glueball was investigated as well: its mass turns out to lie between the σ meson and the baryon mass. A proper measurement of the glueball mass could not however achieved with the given statistics.

4.8.3. Partially quenched viewpoint

An observation made in [Nf1] is that $N_f = 1$ QCD can be embedded in a *partially quenched* multi flavor theory (see 2.2 for a brief introduction). A particularly symmetric choice consists in taking the N_{val} *valence* quark flavors degenerate with the *sea* quark: in this case the combined sea-valence sector is characterized by an exact non-Abelian SU($N_{val} + 1$) flavor symmetry.

In this fictitious multi-flavor theory a pion, also containing quenched valence quarks, can be defined. Similarly to the "adjoint pion" of SYM (Subsec. 4.2.1) its mass gives an useful indication on the lightness of the fundamental fermion (the quark in this case).

In particular, the run with the lightest quark mass in [Nf1] ("run c") corresponds to a pion with fairly small mass: $M_\pi \simeq 270\,\mathrm{MeV}$ in QCD units. A PCAC quark mass can also be defined as in Eq. (1.20) and taken as an operational definition of the quark mass for the single flavor theory. The behavior of the hadron masses as a function of this quark mass can be investigated, see Figs. 1 and 2 of [Nf1].

A *partially quenched chiral perturbation theory* can be setup, exactly as in the $N_f > 1$ case. The comparison of the lattice data with the chiral perturbation theory predictions allows in particular to extract the low-energy constants Λ_3 and Λ_4, defined in Eq. (2.54). Observe that these constants refer here to the $N_f = 1$ case: the dependence upon the number of flavors should be taken into account when comparing for example with the $N_f = 2$ case.

The values found in [Nf1] for the single flavor theory are:

$$\frac{\Lambda_3}{F_0} = 10.0 \pm 2.6 \tag{4.66}$$

$$\frac{\Lambda_4}{F_0} = 31.5 \pm 14.3\ . \tag{4.67}$$

These values are compatible, although with large errors, with the recent determinations for the two flavor theory at light quark masses in [tlS-1], see Table 2.2.

This first Monte Carlo investigation of $N_f = 1$ QCD in a large volume reveals the qualitative features of the low lying hadron spectrum of this theory. In general, the mass measurements have relatively large errors between 3–10%. In order to obtain more quantitative results, larger statistics and smaller quark masses are required. Progresses in both directions are expected with new simulations with Stout-smeared links in the fermion action [72].

The introduction of a partially quenched extension of the single flavor theory with valence quarks allows in particular to obtain a definition of the bare quark mass which is otherwise awkward in absence of chiral symmetry.

A further direction of investigation for the future [72] is the CP-violating phase transition expected at negative quark masses [45]. For this aspect of the single flavor theory the non-positivity of the fermion measure is expected to play an essential role.

In consideration of the planar orientifold equivalence, it would be interesting to directly compare lattice determinations in $N_f = 1$ QCD and SYM (in this comparison the fundamental fermion does not need to be massless). For this, the simulation of SYM with *three* colors is required (recall that the hereby described simulations of SYM apply for the $N_c = 2$ theory). This line of investigation is under consideration for future activities.

Summary and conclusions of part II

This second part of the review covered simulations of the $\mathcal{N} = 1$ supersymmetric Yang-Mills theory (SYM) with two colors, and of N_f=1 QCD with three colors. The two theories (for equal number of colors) share a similar structure in the fermionic sector: the first is obtained from the second by replacing the Dirac spinor of the quark by the Majorana spinor of the gluino. Both theories are in particular characterized by a non-positive fermion measure and are expected to spontaneously break a discrete symmetry [187, 43]. In a particular generalization of the theories with large number of colors an *exact* equivalence can be actually proven [17].

The lattice simulation of a SUSY gauge theory can shed light on non-perturbative mechanisms in non-Abelian gauge theories, where supersymmetry plays a distinctive role. One important aspect in view of phenomenological applications is of course the mechanism triggering a possible spontaneous breaking of SUSY. This phenomenon is however is not expected in SYM, which is at present the only four dimensional SUSY gauge theory accessible to large-scale lattice simulations.

Chapter 4 reviews first large-scale simulation of SYM [SYM-1, SYM-2, SYM-3]. The main focus was in this case on the restoration of SUSY in the Wilson fermion formulation for vanishing gluino mass and on the low-energy spectrum of the bound states. At the lower end, low-energy Lagrangians predict the presence of a chiral supermultiplet [187, 74].

One value of lattice coupling, $\beta = 2.3$, was considered in the Curci-Veneziano formulation [49] rephrasing the Wilson formulation for lattice QCD. This value of β corresponds, in QCD units, to a fairly small lattice spacing $a \simeq 0.06$ fm. Correspondingly, the volume is quite small $\simeq (1 \text{ fm})^3$, and finite volume effects could be large.

A lattice formulation of SYM necessarily breaks supersymmetry. In the Wilson approach considered here, also chiral symmetry (coinciding with the R-symmetry in the SUSY model, Subsec. 4.2.1) is explicitly broken. Both symmetries are expected to be recovered in the continuum limit. This important point was in particular addressed in [SYM-1], where the SUSY Ward identities were analyzed and the gluino mass of the soft-breaking term computed non-perturbatively. Chiral symmetry can be analyzed in the OZI limit of the theory where the U(1) anomaly disappears and a massless pion emerges ("adjoint pion") for vanishing gluino mass.

The analysis of [SYM-1] allowed in particular to compute the SUSY softly breaking gluino mass in a non-perturbative framework. Its behavior as a function of the hopping parameter indicates that, indeed, this mass parameter can be tuned to zero: in this

situation the theory is supersymmetric up to $O(a)$ lattice artifacts. Numerical results on the adjoint pion mass indicate restoration of chiral symmetry in this limit. This latter result could be better established by an analysis of the chiral phase transition in a large volume: for vanishing gluino mass the residual discrete Z_{N_c} chiral symmetry should be restored (see the discussion in Subsec. 4.2.1). This aspect is currently under study [57].

The study of the spectrum, and in particular of the mesonic states, requires the computation of disconnected diagrams. The techniques which are well known in QCD can also be applied in SYM, however with some care due to the different (adjoint) color representation of the gluino. This aspect was considered in [SYM-2] where the efficiency of different techniques was also compared (volume source vs. stochastic source).

The systematic analysis of the expected bound states at low-energy was undertaken in [SYM-3]. A negative outcome of this study is the relatively large content of noise of some of the states preventing a precise determination of the masses. The most solid determinations could be obtained for the spin 1/2 mixed gluino-glue states and the pseudoscalar meson. The latter is the lightest state for the smallest gluino mass. This outcome is in contrast with the predictions of low-energy Lagrangians at leading order in the soft SUSY breaking [75], which indicate a state with *positive* parity. A possible explanation is that higher order corrections could play a significant role for the relatively heavy gluino masses in the simulation. The lightest simulated gluino mass was indeed estimated to be $\simeq 150$ MeV (QCD units).

A general qualitative observation is that the bound states masses tend to cluster and get lighter when decreasing the gluino mass. Numerical data for the effective bound states masses indicate the presence of nearby excited states. These states are predicted by the low-energy Lagrangians and should form a second chiral supermultiplet.

For an improved analysis, a lighter gluino mass in a larger volume, and larger statistics for a more precise determination of the masses are essential [57]. In consideration of this latter aspect, the simulation of SYM with a more efficient polynomial HMC algorithm has been started.

The above mentioned polynomial HMC algorithm could be already applied in first simulations of single flavor QCD in a large volume [Nf1]. The Wilson formulation was again taken in the fermion sector and the tree-level Symanzik action in the gauge sector. In this case two relatively coarse lattices were considered, $a = 0.186$ fm at $\beta = 3.8$ and $a = 0.134$ fm at $\beta = 4.0$, and three different values of the quark mass down to $M_\pi \simeq 270\,\mathrm{MeV}$ (the pion is defined in a partially quenched setup). The volume $\simeq (2\ \mathrm{fm})^3$ is large enough to the accommodate the bound states of the hadrons.

Here all the masses expected at the lower end of the spectrum could be estimated with satisfactory accuracy. The approximate degeneracy of the pseudoscalar and scalar mesons, expected from the relics of SUSY in this model [18, 16], could be partially verified. The hierarchy of the hadron masses was established at a qualitative level. The role of the sign of the fermion determinant in the determination of the hadron masses for the lightest simulated quark mass was investigated.

Moreover, in [Nf1] a partially quenched set up for the one flavor theory was proposed, enabling the definition of a quark mass in absence of chiral symmetry and the comparison of lattice data for hadron properties with chiral perturbation theory. The estimated low-energy constants of the chiral Lagrangian are, even if with relatively large statistical errors, comparable to those for the $N_f = 2$ theory [tlS-1]; this outcome supports a weak dependence of the constants upon the number of flavors. More precise determinations will settle this issue.

Bibliography

[1] A. M. Abdel-Rehim, R. Lewis, and R. M. Woloshyn. Spectrum of quenched twisted mass lattice QCD at maximal twist. *Phys. Rev.*, D71:094505, 2005.

[2] A. M. Abdel-Rehim, R. Lewis, R. M. Woloshyn, and J. M. S. Wu. Lattice QCD with a twisted mass term and a strange quark. *Eur. Phys. J.*, A31:773–776, 2007.

[3] S. L. Adler. Axial vector vertex in spinor electrodynamics. *Phys. Rev.*, 177:2426–2438, 1969.

[4] I. Affleck, M. Dine, and N. Seiberg. Supersymmetry breaking by instantons. *Phys. Rev. Lett.*, 51:1026, 1983.

[5] I. Affleck, M. Dine, and N. Seiberg. Dynamical supersymmetry breaking in supersymmetric QCD. *Nucl. Phys.*, B241:493–534, 1984.

[6] C. Alexandrou, A. Borrelli, Ph. de Forcrand, A. Galli, and F. Jegerlehner. Full QCD with the Lüscher local bosonic action. *Nucl. Phys.*, B456:296–312, 1995.

[7] A. Ali Khan et al. Light hadron spectroscopy with two flavors of dynamical quarks on the lattice. *Phys. Rev.*, D65:054505, 2002.

[8] C. R. Allton et al. Effects of non-perturbatively improved dynamical fermions in QCD at fixed lattice spacing. *Phys. Rev.*, D65:054502, 2002.

[9] C. R. Allton et al. Improved Wilson QCD simulations with light quark masses. *Phys. Rev.*, D70:014501, 2004.

[10] D. Amati, K. Konishi, Y. Meurice, G. C. Rossi, and G. Veneziano. Nonperturbative aspects in supersymmetric gauge theories. *Phys. Rept.*, 162:169–248, 1988.

[11] D. Amati, G. C. Rossi, and G. Veneziano. Instanton effects in supersymmetric gauge theories. *Nucl. Phys.*, B249:1, 1985.

[12] S. Aoki. New phase structure for lattice QCD with Wilson fermions. *Phys. Rev.*, D30:2653, 1984.

[13] S. Aoki and O. Bär. Twisted-mass QCD, $O(a)$ improvement and Wilson chiral perturbation theory. *Phys. Rev.*, D70:116011, 2004.

[14] S. Aoki et al. Non-trivial phase structure of $N_f = 3$ QCD with $O(a)$-improved Wilson fermion at zero temperature. *Nucl. Phys. Proc. Suppl.*, 106:263–265, 2002.

[15] S. Aoki et al. Bulk first-order phase transition in three-flavor lattice QCD with $O(a)$-improved Wilson fermion action at zero temperature. *Phys. Rev.*, D72:054510, 2005.

[16] A. Armoni and E. Imeroni. Predictions for orientifold field theories from type $0'$ string theory. *Phys. Lett.*, B631:192–198, 2005.

[17] A. Armoni, M. Shifman, and G. Veneziano. Exact results in non-supersymmetric large N orientifold field theories. *Nucl. Phys.*, B667:170–182, 2003.

[18] A. Armoni, M. Shifman, and G. Veneziano. SUSY relics in one-flavor QCD from a new 1/N expansion. *Phys. Rev. Lett.*, 91:191601, 2003.

[19] C. Aubin and Q.-H. Wang. A possible Aoki phase for staggered fermions. *Phys. Rev.*, D70:114504, 2004.

[20] T. Banks, Y. Nir, and N. Seiberg. Missing (up) mass, accidental anomalous symmetries and the strong CP problem. In *Gainesville 1994, Yukawa couplings and the origin of mass*, 1994. E-Print: hep-ph/9403203.

[21] O. Bär, G. Rupak, and N. Shoresh. Chiral perturbation theory at $O(a^2)$ for lattice QCD. *Phys. Rev.*, D70:034508, 2004.

[22] J. Bartels and J. B. Bronzan. Supersymmetry on a lattice. *Phys. Rev.*, D28:818, 1983.

[23] D. Becirevic et al. Exploring twisted mass lattice QCD with the clover term. *Phys. Rev.*, D74:034501, 2006.

[24] J. S. Bell and R. Jackiw. A PCAC puzzle: $\pi_0 \to \gamma\gamma$ in the sigma model. *Nuovo Cim.*, A60:47–61, 1969.

[25] L. Bergamin and P. Minkowski. SUSY glue-balls, dynamical symmetry breaking and non-holomorphic potentials. E-Print: hep-th/0301155, 2003.

[26] C. W. Bernard and M. F. L. Golterman. Partially quenched gauge theories and an application to staggered fermions. *Phys. Rev.*, D49:486–494, 1994.

[27] J. Bijnens, N. Danielsson, and T. A. Lahde. The pseudoscalar meson mass to two loops in three-flavor partially quenched χPT. *Phys. Rev.*, D70:111503, 2004.

[28] J. Bijnens, G. Ecker, and J. Gasser. Chiral perturbation theory. In *The 2nd DAΦNE Physics Handbook:125-144*, 1994. E-Print: hep-ph/9411232.

[29] K. M. Bitar, U. M. Heller, and R. Narayanan. A new method to measure the chiral condensate in lattice QCD using Wilson fermions. *Phys. Lett.*, B418:167–172, 1998.

[30] E. D. Bloom et al. High-energy inelastic e p scattering at 6-degrees and 10-degrees. *Phys. Rev. Lett.*, 23:930–934, 1969.

[31] T. Blum et al. QCD thermodynamics with Wilson quarks at large κ. *Phys. Rev.*, D50:3377–3381, 1994.

[32] M. Bochicchio, L. Maiani, G. Martinelli, G. C. Rossi, and M. Testa. Chiral symmetry on the lattice with Wilson fermions. *Nucl. Phys.*, B262:331, 1985.

[33] A. Borici and Ph. de Forcrand. Systematic errors of Lüscher's fermion method and its extensions. *Nucl. Phys.*, B454:645–662, 1995.

[34] R. C. Brower, T. Ivanenko, A. R. Levi, and K. N. Orginos. Chronological inversion method for the Dirac matrix in hybrid Monte Carlo. *Nucl. Phys.*, B484:353–374, 1997.

[35] I. Campos et al. Monte Carlo simulation of SU(2) Yang-Mills theory with light gluinos. *Eur. Phys. J.*, C11:507–527, 1999.

[36] S. Catterall. Lattice supersymmetry and topological field theory. *JHEP*, 05:038, 2003.

[37] D. G. Cerdeno, A. Knauf, and J. Louis. A note on effective $\mathcal{N} = 1$ super Yang-Mills theories versus lattice results. *Eur. Phys. J.*, C31:415–420, 2003.

[38] T. Chiarappa, R. Frezzotti, and C. Urbach. Work in progress.

[39] A. G. Cohen, D. B. Kaplan, and A. E. Nelson. Testing $m_u = 0$ on the lattice. *JHEP*, 11:027, 1999.

[40] G. Colangelo, S. Dürr, and Ch. Haefeli. Finite volume effects for meson masses and decay constants. *Nucl. Phys.*, B721:136–174, 2005.

[41] G. Colangelo and G. Isidori. An introduction to ChPT. In *Frascati 2000, Nuclear, subnuclear and astroparticle physics, 333-376*, 2000. E-Print: hep-ph/0101264.

[42] European Twisted Mass Collaboration. Work in progress.

[43] M. Creutz. One flavor QCD. E-Print: hep-th/0609187, 2006.

[44] M. Creutz. Wilson fermions at finite temperature. E-Print: hep-lat/9608024, 1996.

[45] M. Creutz. Quark masses and chiral symmetry. *Phys. Rev.*, D52:2951–2959, 1995.

[46] M. Creutz. Ambiguities in the up-quark mass. *Phys. Rev. Lett.*, 92:162003, 2004.

[47] M. Creutz. Spontaneous violation of CP symmetry in the strong interactions. *Phys. Rev. Lett.*, 92:201601, 2004.

[48] M. Creutz. One flavor QCD. *Annals Phys.*, 322:1518–1540, 2007.

[49] G. Curci and G. Veneziano. Supersymmetry and the lattice: A reconciliation? *Nucl. Phys.*, B292:555, 1987.

[50] R.F. Dashen. Some features of chiral symmetry breaking. *Phys. Rev.*, D3:1879–1889, 1971.

[51] Ph. de Forcrand. Monte Carlo quasi-heatbath by approximate inversion. *Phys. Rev.*, E59:3698–3701, 1999.

[52] Ph. de Forcrand and T. Takaishi. Fast fermion Monte Carlo. *Nucl. Phys. Proc. Suppl.*, 53:968–970, 1997.

[53] Th. DeGrand, R. Hoffmann, S. Schaefer, and Z. Liu. Quark condensate in one-flavor QCD. *Phys. Rev.*, D74:054501, 2006.

[54] Th. A. DeGrand, A. Hasenfratz, and T. G. Kovacs. Improving the chiral properties of lattice fermions. *Phys. Rev.*, D67:054501, 2003.

[55] Th. A. DeGrand and P. Rossi. Conditioning techniques for dynamical fermions. *Comput. Phys. Commun.*, 60:211–214, 1990.

[56] L. Del Debbio, L. Giusti, M. Lüscher, R. Petronzio, and N. Tantalo. QCD with light Wilson quarks on fine lattices. I: First experiences and physics results. *JHEP*, 02:056, 2007.

[57] K. Demmouche, F. Farchioni, A. Ferling, I. Montvay, and G. Münster. Bound states masses and spontaneous breaking of a discrete chiral symmetry in SUSY Yang-Mills (in progress).

[58] P. H. Dondi and H. Nicolai. Lattice supersymmetry. *Nuovo Cim.*, A41:1, 1977.

[59] A. Donini, M. Guagnelli, P. Hernandez, and A. Vladikas. Towards $\mathcal{N} = 1$ Super-Yang-Mills on the lattice. *Nucl. Phys.*, B523:529–552, 1998.

[60] S. D. Drell, M. Weinstein, and S. Yankielowicz. Strong coupling field theories. 2. Fermions and gauge fields on a lattice. *Phys. Rev.*, D14:1627, 1976.

[61] S. D. Drell, M. Weinstein, and S. Yankielowicz. Variational approach to strong coupling field theory. 1. ϕ^4 theory. *Phys. Rev.*, D14:487, 1976.

[62] S. Duane, A. D. Kennedy, B. J. Pendleton, and D. Roweth. Hybrid Monte Carlo. *Phys. Lett.*, B195:216–222, 1987.

[63] S. Dürr et al. Scaling study of dynamical smeared-link clover fermions. E-Print: arXiv:0802.2706, 2008.

[64] G. Ecker. Chiral low-energy constants. In *Effective Theories of Colors and Flavors from EURODAPHNE to EURIDICE*, 2007. E-Print: hep-ph/0702263.

[65] G. Ecker, J. Gasser, A. Pich, and E. de Rafael. The role of resonances in chiral perturbation theory. *Nucl. Phys.*, B321:311, 1989.

[66] European Twisted Mass Collaboration (ETMC). http://www-zeuthen.desy.de/kjansen/etmc/.

[67] F. Farchioni et al. Exploring the phase structure of lattice QCD with twisted mass quarks. *Nucl. Phys. Proc. Suppl.*, 140:240–245, 2005.

[68] F. Farchioni et al. Dynamical twisted mass fermions. *PoS*, LATTICE 2005:072, 2006.

[69] F. Farchioni, C. Gebert, I. Montvay, and W. Schroers. QCD spectroscopy with three light quarks. *Nucl. Phys. Proc. Suppl.*, 106:215–217, 2002.

[70] F. Farchioni, C. Gebert, I. Montvay, and L. Scorzato. On the price of light quarks. E-print: hep-lat/0209142, 2002.

[71] F. Farchioni, C. Gebert, I. Montvay, and L. Scorzato. Lattice QCD with light dynamical quarks. *Nucl. Phys. Proc. Suppl.*, 119:344–349, 2003.

[72] F. Farchioni, I. Montvay, G. Münster, E. E. Scholz, T. Sudmann, and J. Wuilloud. Hadron masses and CP violation in QCD with one quark flavour (in progress).

[73] F. Farchioni, I. Montvay, G. Münster, E. E. Scholz, T. Sudmann, and J. Wuilloud. Hadron spectrum of QCD with one quark flavor. *PoS*, LATTICE 2007:235, 2007.

[74] G. R. Farrar, G. Gabadadze, and M. Schwetz. On the effective action of $\mathcal{N} = 1$ supersymmetric Yang-Mills theory. *Phys. Rev.*, D58:015009, 1998.

[75] G. R. Farrar, G. Gabadadze, and M. Schwetz. The spectrum of softly broken $\mathcal{N} = 1$ supersymmetric Yang-Mills theory. *Phys. Rev.*, D60:035002, 1999.

[76] R. Frezzotti, P. A. Grassi, S. Sint, and P. Weisz. Lattice QCD with a chirally twisted mass term. *JHEP*, 08:058, 2001.

[77] R. Frezzotti, M. Hasenbusch, U. Wolff, J. Heitger, and K. Jansen. Comparative benchmarks of full QCD algorithms. *Comput. Phys. Commun.*, 136:1–13, 2001.

[78] R. Frezzotti and K. Jansen. A polynomial hybrid Monte Carlo algorithm. *Phys. Lett.*, B402:328–334, 1997.

[79] R. Frezzotti, G. Martinelli, M. Papinutto, and G. C. Rossi. Reducing cutoff effects in maximally twisted lattice QCD close to the chiral limit. *JHEP*, 04:038, 2006.

[80] R. Frezzotti and G. C. Rossi. Chirally improving Wilson fermions. I: $O(a)$ improvement. *JHEP*, 08:007, 2004.

[81] R. Frezzotti and G. C. Rossi. Chirally improving Wilson fermions. II: Four-quark operators. *JHEP*, 10:070, 2004.

[82] R. Frezzotti and G. C. Rossi. Twisted-mass lattice QCD with mass non-degenerate quarks. *Nucl. Phys. Proc. Suppl.*, 128:193–202, 2004.

[83] R. Frezzotti and G.C. Rossi. $O(a^2)$ cutoff effects in Wilson fermion simulations. *PoS*, LAT2006, 2007 (arXiv:0710.2492 [hep-lat]).

[84] R. Frezzotti and S. Sint. Some remarks on $O(a)$ improved twisted mass QCD. *Nucl. Phys. Proc. Suppl.*, 106:814–816, 2002.

[85] H. Fritzsch, M. Gell-Mann, and H. Leutwyler. Advantages of the color octet gluon picture. *Phys. Lett.*, B47:365–368, 1973.

[86] J. Fuchs and M. G. Schmidt. Instanton induced Green functions in the superfield formalism. *Z. Phys.*, C30:161, 1986.

[87] K. Fujikawa. Path integral measure for gauge invariant fermion theories. *Phys. Rev. Lett.*, 42:1195, 1979.

[88] J. Gasser and H. Leutwyler. Chiral perturbation theory to one loop. *Ann. Phys.*, 158:142, 1984.

[89] J. Gasser and H. Leutwyler. Chiral perturbation theory: Expansions in the mass of the strange quark. *Nucl. Phys.*, B250:465, 1985.

[90] J. Gasser and H. Leutwyler. Light quarks at low temperatures. *Phys. Lett.*, B184:83, 1987.

[91] C. Gebert. *Light quark fields in lattige gauge theories.* PhD thesis, DESY, Germany, 2002.

[92] M. Gell-Mann. The eightfold way: A theory of strong interaction symmetry. Cal. Tech. Synchrotron Laboratory Report CTSL-20, 1961.

[93] M. Gell-Mann. A schematic model of baryons and mesons. *Phys. Lett.*, 8:214–215, 1964.

[94] M. Gell-Mann, R. J. Oakes, and B. Renner. Behavior of current divergences under SU(3)×SU(3). *Phys. Rev.*, 175:2195–2199, 1968.

[95] P. H. Ginsparg and K. G. Wilson. A remnant of chiral symmetry on the lattice. *Phys. Rev.*, D25:2649, 1982.

[96] M. Göckeler et al. A status report of the QCDSF $N_f = 2 + 1$ Project. *PoS*, LAT2007:041, 2007.

[97] M. Golterman. Connections between lattice gauge theory and chiral perturbation theory. E-Print: hep-th/9710468, 1997.

[98] O. W. Greenberg. Spin and unitary spin independence in a paraquark model of baryons and mesons. *Phys. Rev. Lett.*, 13:598–602, 1964.

[99] H. Hamber and G. Parisi. Numerical estimates of hadronic masses in a pure SU(3) gauge theory. *Phys. Rev. Lett.*, 47:1792, 1981.

[100] M. Y. Han and Y. Nambu. Three-triplet model with double SU(3) symmetry. *Phys. Rev.*, 139:B1006–B1010, 1965.

[101] M. Hasenbusch. Speeding up finite step-size updating of full QCD on the lattice. *Phys. Rev.*, D59:054505, 1999.

[102] M. Hasenbusch. Speeding up the Hybrid-Monte-Carlo algorithm for dynamical fermions. *Phys. Lett.*, B519:177–182, 2001.

[103] P. Hasenfratz. Lattice QCD without tuning, mixing and current renormalization. *Nucl. Phys.*, B525:401–409, 1998.

[104] S. Hashimoto et al. Chiral extrapolation of light-light and heavy-light decay constants in unquenched QCD. *Nucl. Phys. Proc. Suppl.*, 119:332–334, 2003.

[105] J. Heitger, R. Sommer, and H. Wittig. Effective chiral Lagrangians and lattice QCD. *Nucl. Phys.*, B588:377–399, 2000.

[106] T. J. Hollowood, V. V. Khoze, W.-J. Lee, and M. P. Mattis. Breakdown of cluster decomposition in instanton calculations of the gluino condensate. *Nucl. Phys.*, B570:241–266, 2000.

[107] R. Horsley, H. Perlt, P. E. L. Rakow, G. Schierholz, and A. Schiller. One-loop renormalisation of quark bilinears for overlap fermions with improved gauge actions. *Nucl. Phys.*, B693:3–35, 2004.

[108] E.-M. Ilgenfritz, W. Kerler, M. Müller-Preussker, A. Sternbeck, and H. Stüben. A numerical reinvestigation of the Aoki phase with $N_f = 2$ Wilson fermions at zero temperature. *Phys. Rev.*, D69:074511, 2004.

[109] A. C. Irving, C. McNeile, C. Michael, K. J. Sharkey, and H. Wittig. Is the up-quark massless? *Phys. Lett.*, B518:243–251, 2001.

[110] T. Ishikawa et al. Light hadron spectrum in 2+1 flavor full QCD by CP-PACS and JLQCD collaborations. *Nucl. Phys. Proc. Suppl.*, 140:225–227, 2005.

[111] Y. Iwasaki. Renormalization group analysis of lattice theories and improved lattice action. 2. Four-dimensional nonabelian SU(N) gauge model. UTHEP-118, 1983.

[112] K. Jansen. Recent developments in fermion simulation algorithms. *Nucl. Phys. Proc. Suppl.*, 53:127–133, 1997.

[113] K. Jansen et al. Flavour breaking effects of Wilson twisted mass fermions. *Phys. Lett.*, B624:334–341, 2005.

[114] K. Jansen and C. Liu. Kramers equation algorithm for simulations of QCD with two flavors of Wilson fermions and gauge group SU(2). *Nucl. Phys.*, B453:375–394, 1995.

[115] K. Jansen, M. Papinutto, A. Shindler, C. Urbach, and I. Wetzorke. Quenched scaling of Wilson twisted mass fermions. *JHEP*, 09:071, 2005.

[116] B. Jegerlehner. Improvements of Lüscher's local bosonic fermion algorithm. *Nucl. Phys.*, B465:487–506, 1996.

[117] B. Joo et al. Instability in the molecular dynamics step of hybrid Monte Carlo in dynamical fermion lattice QCD simulations. *Phys. Rev.*, D62:114501, 2000.

[118] D. B. Kaplan, E. Katz, and M. Unsal. Supersymmetry on a spatial lattice. *JHEP*, 05:037, 2003.

[119] D. B. Kaplan and A. V. Manohar. Current mass ratios of the light quarks. *Phys. Rev. Lett.*, 56:2004, 1986.

[120] D. B. Kaplan and M. Schmaltz. Supersymmetric Yang-Mills theories from domain wall fermions. *Chin. J. Phys.*, 38:543–550, 2000.

[121] L. H. Karsten and J. Smit. The vacuum polarization with SLAC lattice fermions. *Phys. Lett.*, B85:100, 1979.

[122] N. Kawamoto. Towards the phase structure of Euclidean lattice gauge theories with fermions. *Nucl. Phys.*, B190:617, 1981.

[123] A. D. Kennedy and J. Kuti. Noise without noise: A new Monte Carlo method. *Phys. Rev. Lett.*, 54:2473–2476, 1985.

[124] R. Kirchner, I. Montvay, J. Westphalen, S. Luckmann, and K. Spanderen. Evidence for discrete chiral symmetry breaking in $\mathcal{N} = 1$ supersymmetric Yang-Mills theory. *Phys. Lett.*, B446:209–215, 1999.

[125] J. B. Kogut and L. Susskind. Hamiltonian formulation of Wilson's lattice gauge theories. *Phys. Rev.*, D11:395, 1975.

[126] A. Kovner and M. A. Shifman. Chirally symmetric phase of supersymmetric gluodynamics. *Phys. Rev.*, D56:2396–2402, 1997.

[127] Y. Kuramashi. N_f=2+1 dynamical Wilson quark simulation toward the physical point. *PoS*, LAT2007:017, 2007.

[128] Y. Kuramashi, M. Fukugita, H. Mino, M. Okawa, and A. Ukawa. Eta-prime meson mass in lattice QCD. *Phys. Rev. Lett.*, 72:3448–3451, 1994.

[129] H. Leutwyler. π π scattering. E-Print: hep-ph/0612112, 2006.

[130] H. Leutwyler. Light quark effective theory. In *Erice 1996, Effective theories and fundamental interactions, 53-97*, 1996. E-Print: hep-ph/9609465.

[131] H. Leutwyler. Non-lattice determinations of the light quark masses. *Nucl. Phys. Proc. Suppl.*, 94:108–115, 2001.

[132] M. Lüscher. A new approach to the problem of dynamical quarks in numerical simulations of lattice QCD. *Nucl. Phys.*, B418:637–648, 1994.

[133] M. Lüscher. Schwarz-preconditioned HMC algorithm for two-flavour lattice QCD. *Comput. Phys. Commun.*, 165:199–220, 2005.

[134] M. Lüscher, S. Sint, R. Sommer, and P. Weisz. Chiral symmetry and $O(a)$ improvement in lattice QCD. *Nucl. Phys.*, B478:365–400, 1996.

[135] P. Merlatti and F. Sannino. Extending the Veneziano-Yankielowicz effective theory. *Phys. Rev.*, D70:065022, 2004.

[136] I. Montvay. An algorithm for gluinos on the lattice. *Nucl. Phys.*, B466:259–284, 1996.

[137] I. Montvay. Least-squares optimized polynomials for fermion simulations. In *Wuppertal 1999, Numerical challenges in lattice quantum chromodynamics, 153-165*, 1999. E-Print: hep-lat/9911014.

[138] I. Montvay. Supersymmetric Yang-Mills theory on the lattice. *Int. J. Mod. Phys.*, A17:2377–2412, 2002.

[139] I. Montvay and G. Münster. *Quantum Fields on a Lattice*. Cambridge University Press, 1994.

[140] I. Montvay and E. E. Scholz. Updating algorithms with multi-step stochastic correction. *Phys. Lett.*, B623:73–79, 2005.

[141] A. Morel. Chiral logarithms in quenched QCD. *J. Phys. (France)*, 48:1111–1119, 1987.

[142] C. Morningstar and M. J. Peardon. Analytic smearing of SU(3) link variables in lattice QCD. *Phys. Rev.*, D69:054501, 2004.

[143] C. J. Morningstar and M. J. Peardon. The glueball spectrum from an anisotropic lattice study. *Phys. Rev.*, D60:034509, 1999.

[144] G. Münster. On the phase structure of twisted mass lattice QCD. *JHEP*, 09:035, 2004.

[145] G. Münster and Ch. Schmidt. Chiral perturbation theory for lattice QCD with a twisted mass term. *Europhys. Lett.*, 66:652–656, 2004.

[146] G. Münster, Ch. Schmidt, and E. E. Scholz. Chiral perturbation theory for partially quenched twisted mass lattice QCD. *Europhys. Lett.*, 86:639–644, 2004.

[147] Y. Namekawa et al. Light hadron spectroscopy in two-flavor QCD with small sea quark masses. *Phys. Rev.*, D70:074503, 2004.

[148] S. Necco. Universality and scaling behavior of RG gauge actions. *Nucl. Phys.*, B683:137–167, 2004.

[149] Y. Ne'eman. Derivation of strong interactions from a gauge invariance. *Nucl. Phys.*, 26:222–229, 1961.

[150] D. R. Nelson, G. T. Fleming, and G. W. Kilcup. Is strong CP due to a massless up quark? *Phys. Rev. Lett.*, 90:021601, 2003.

[151] H. Neuberger. Exactly massless quarks on the lattice. *Phys. Lett.*, B417:141–144, 1998.

[152] H. Neuberger. Vector like gauge theories with almost massless fermions on the lattice. *Phys. Rev.*, D57:5417–5433, 1998.

[153] H. Nicolai. A possible constructive approach to super ϕ^3 in four dimensions. 1. Euclidean formulation of the model. *Nucl. Phys.*, B140:294, 1978.

[154] V. A. Novikov, M. A. Shifman, A. I. Vainshtein, and V. I. Zakharov. Instanton effects in supersymmetric theories. *Nucl. Phys.*, B229:407, 1983.

[155] V. A. Novikov, M. A. Shifman, A. I. Vainshtein, and V. I. Zakharov. Supersymmetric instanton calculus: Gauge theories with matter. *Nucl. Phys.*, B260:157–181, 1985.

[156] A. Parkes and P. C. West. Finiteness and explicit supersymmetry breaking of the $\mathcal{N}$=4 supersymmetric Yang-Mills theory. *Nucl. Phys.*, B222:269, 1983.

[157] C. Pena, S. Sint, and A. Vladikas. Twisted mass QCD and lattice approaches to the $\Delta I = 1/2$ rule. *JHEP*, 09:069, 2004.

[158] G. C. Rossi and G. Veneziano. Nonperturbative breakdown of the nonrenormalization theorem in supersymmetric QCD. *Phys. Lett.*, B138:195, 1984.

[159] G. Rupak and N. Shoresh. Chiral perturbation theory for the Wilson lattice action. *Phys. Rev.*, D66:054503, 2002.

[160] A. Salam and J. A. Strathdee. Supergauge transformations. *Nucl. Phys.*, B76:477–482, 1974.

[161] K. Schilling, H. Neff, and Th. Lippert. Computing the η and η' mesons in lattice QCD. *Lect. Notes Phys.*, 663:147–176, 2005.

[162] E. E. Scholz. *Light quark fields in QCD: numerical simulations and chiral perturbation theory.* PhD thesis, DESY, Germany, 2005.

[163] E. E. Scholz and I. Montvay. Multi-step stochastic correction in dynamical fermion updating algorithms. *PoS*, LAT2006:037, 2006.

[164] J. S. Schwinger. Euclidean quantum electrodynamics. *Phys. Rev.*, 115:721, 1959.

[165] L. Scorzato. Pion mass splitting and phase structure in twisted mass QCD. *Eur. Phys. J.*, C37:445–455, 2004.

[166] J. C. Sexton and D. H. Weingarten. Hamiltonian evolution for the hybrid Monte Carlo algorithm. *Nucl. Phys.*, B380:665–678, 1992.

[167] S. R. Sharpe. Enhanced chiral logarithms in partially quenched QCD. *Phys. Rev.*, D56:7052–7058, 1997.

[168] S. R. Sharpe. Observations on discretization errors in twisted-mass lattice QCD. *Phys. Rev.*, D72:074510, 2005.

[169] S. R. Sharpe and N. Shoresh. Physical results from unphysical simulations. *Phys. Rev.*, D62:094503, 2000.

[170] S. R. Sharpe and R. L. Singleton, Jr. Spontaneous flavor and parity breaking with Wilson fermions. *Phys. Rev.*, D58:074501, 1998.

[171] S. R. Sharpe and J. M. S. Wu. The phase diagram of twisted mass lattice QCD. *Phys. Rev.*, D70:094029, 2004.

[172] S. R. Sharpe and J. M. S. Wu. Twisted mass chiral perturbation theory at next-to-leading order. *Phys. Rev.*, D71:074501, 2005.

[173] B. Sheikholeslami and R. Wohlert. Improved continuum limit lattice action for QCD with Wilson fermions. *Nucl. Phys.*, B259:572, 1985.

[174] M. A. Shifman and A. I. Vainshtein. On gluino condensation in supersymmetric gauge theories. SU(N) and O(N) groups. *Nucl. Phys.*, B296:445, 1988.

[175] M. A. Shifman and A. I. Vainshtein. Instantons versus supersymmetry: Fifteen years later. In *ITEP Lectures in Particle Physics and Field Theory. Edited by M. Shifman. Singapore, World Scientific, 1999. Vol. 2, pp. 485-648*, 1999. E-Print: hep-th/9902018.

[176] R. Sommer. A new way to set the energy scale in lattice gauge theories and its applications to the static force and α_s in SU(2) Yang-Mills theory. *Nucl. Phys.*, B411:839–854, 1994.

[177] K. Spanderen. *Monte-Carlo-Simulationen einer SU(2) Yang-Mills-Theorie mit dynamischen Gluinos*. PhD thesis, University of Münster, Germany, 1998. In German.

[178] F. Sugino. A lattice formulation of super Yang-Mills theories with exact supersymmetry. *JHEP*, 01:015, 2004.

[179] K. Symanzik. Continuum limit and improved action in lattice theories. 1. principles and ϕ^4 theory. *Nucl. Phys.*, B226:187, 1983.

[180] G. 't Hooft. A planar diagram theory for strong interactions. *Nucl. Phys.*, B72:461, 1974.

[181] T. Takaishi. Heavy quark potential and effective actions on blocked configurations. *Phys. Rev.*, D54:1050–1053, 1996.

[182] Y. Taniguchi. One loop calculation of SUSY Ward-Takahashi identity on lattice with Wilson fermion. *Phys. Rev.*, D63:014502, 2001.

[183] M. Testa. Some observations on broken symmetries. *JHEP*, 04:002, 1998.

[184] A. Ukawa. Computational cost of full QCD simulations experienced by CP-PACS and JLQCD collaborations. *Nucl. Phys. Proc. Suppl.*, 106:195–196, 2002.

[185] C. Urbach, K. Jansen, A. Shindler, and U. Wenger. HMC algorithm with multiple time scale integration and mass preconditioning. *Comput. Phys. Commun.*, 174:87–98, 2006.

[186] C. Vafa and E. Witten. Restrictions on symmetry breaking in vector-like gauge theories. *Nucl. Phys.*, B234:173, 1984.

[187] G. Veneziano and S. Yankielowicz. An effective Lagrangian for the pure $\mathcal{N}$=1 supersymmetric Yang-Mills theory. *Phys. Lett.*, B113:231, 1982.

[188] S. Weinberg. Nonlinear realizations of chiral symmetry. *Phys. Rev.*, 166:1568–1577, 1968.

[189] S. Weinberg. Phenomenological Lagrangians. *Physica*, A96:327, 1979.

[190] S. Weinberg. *The Quantum Theory of Fields, Volume III: Supersymmetry*. Cambridge University Press, 2000.

[191] D. H. Weingarten and D. N. Petcher. Monte Carlo integration for lattice gauge theories with fermions. *Phys. Lett.*, B99:333, 1981.

[192] P. Weisz. Continuum limit improved lattice action for pure Yang-Mills theory. 1. *Nucl. Phys.*, B212:1, 1983.

[193] J. Wess and J. Bagger. *Supersymmetry and Supergravity*. Princeton University Press, 1983.

[194] J. Wess and B. Zumino. Supergauge transformations in four-dimensions. *Nucl. Phys.*, B70:39–50, 1974.

[195] K. G. Wilson. Confinement of quarks. *Phys. Rev.*, D10:2445–2459, 1974.

[196] E. Witten. Dynamical breaking of supersymmetry. *Nucl. Phys.*, B188:513, 1981.

[197] U. Wolff. Monte carlo errors with less errors. *Comput. Phys. Commun.*, 156:143–153, 2004.

[198] W.-M. Yao et al. Review of Particle Physics. *Journal of Physics G*, 33:1+, 2006.

[199] G. Zweig. An SU(3) model for strong interaction symmetry and its breaking. CERN preprint TH401, 1964.

Publications

[Alg]

Numerical simulation tests with light dynamical quarks

Eur. Phys. J. C26 237-251 (2002)

Eur. Phys. J. C 26, 237–251 (2002)
Digital Object Identifier (DOI) 10.1140/epjc/s2002-01057-6

THE EUROPEAN PHYSICAL JOURNAL C

Numerical simulation tests with light dynamical quarks

The qq+q Collaboration
F. Farchioni[1], C. Gebert[2], I. Montvay[2], L. Scorzato[2]

[1] Institut für Theoretische Physik, Universität Münster, Wilhelm-Klemm-Str. 9, 48149 Münster, Germany
[2] Deutsches Elektronen-Synchrotron DESY, Notkestr. 85, 22603 Hamburg, Germany

Received: 20 June 2002 / Revised version: 30 August 2002 /
Published online: 25 October 2002 –

Abstract. Two degenerate flavors of quarks are simulated with small masses down to about one fifth of the strange quark mass by using the two-step multi-boson (TSMB) algorithm. The lattice size is $8^3 \times 16$ with lattice spacing about $a \simeq 0.27\,\mathrm{fm}$ which is not far from the $N_t = 4$ thermodynamical cross-over line. Autocorrelations of different physical quantities are estimated as a function of the quark mass. The eigenvalue spectra of the Wilson–Dirac operator are investigated.

1 Introduction

The question of the computational cost of dynamical quark simulations is a central issue in lattice gauge theory. Existing unquenched simulations are typically done in a region where the quarks are not light enough, in most cases – especially in case of Wilson-type quarks – with two light quark flavors (u and d) having masses larger than half the strange quark mass ($m_{ud} > (1/2)m_s$). The physical masses of the u- and d-quarks are so small that in the foreseeable future simulations can only be carried out at somewhat higher masses. In order to extrapolate the results to the physical masses, chiral perturbation theory based on the low energy chiral effective Lagrangian can be used. However the systematic errors can only be controlled if the dynamical quark masses in the simulations are close enough to the physical point. For instance, in case of partially quenched simulations to determine the low energy constants in the chiral effective Lagrangian of QCD we would like to reach at least $m_{ud} \leq (1/4)m_s$ [1].

Going to light quark masses in unquenched QCD simulations is a great challenge for computations because known algorithms have a substantial slowing down towards small quark masses. The present status has been recently summarized by the contributors to the panel discussion at the Berlin lattice conference [2–7]. Inspired by the results presented there the computational cost of a simulation with two light quarks will be parametrized in the present paper as

$$C = F(r_0 m_\pi)^{-z_\pi} \left(\frac{L}{a}\right)^{z_L} \left(\frac{r_0}{a}\right)^{z_a}. \qquad (1)$$

Here r_0 is a physical length, for instance the Sommer scale parameter [8], m_π the pion mass, L the lattice extension and a the lattice spacing. The powers $z_{\pi,L,a}$ and the overall constant F are empirically determined. The value of the constant factor F depends on the precise definition of "cost" [9]. For instance, one can consider the number of floating point operations in one autocorrelation length of some important quantity, or the number of fermion-matrix-vector multiplications necessary for achieving a given error of a quantity. Of course, the cost also depends on the particular choice of lattice action and of the dynamical fermion algorithm which should be optimized.

An alternative parameterization can be obtained from the one in (1) by replacing the powers of $r_0 m_\pi$ by those of m_π/m_ρ. In fact, the results of the CP-PACS, JLQCD Collaboration have been presented by Ukawa at the Berlin lattice conference [6] in this form

$$C_U = F_U \left(\frac{m_\pi}{m_\rho}\right)^{-z_{\pi\rho}} \left(\frac{L}{a}\right)^{z_L} \left(\frac{r_0}{a}\right)^{z_a}, \qquad (2)$$

$$F_U = 5.9 \times 10^6\,\mathrm{flop}, \qquad (3)$$

$$z_{\pi\rho} = 6, \quad z_L = 5, \quad z_a = 2. \qquad (4)$$

Since the determination of the ρ meson mass is difficult for light quarks when the decay $\rho \to \pi\pi$ is allowed, we prefer the form in (1). Other parameterizations used for Wilson-type quarks [5,7] are given under the assumption that $z_\pi = z_a \equiv z_{a\pi}$ when in (1) the physical length parameter r_0 disappears.

In the present paper we report on the results of extended test runs with the simple Wilson fermion action using the two-step multi-boson algorithm [10] in order to determine the quark mass dependence of the computational cost of dynamical Monte Carlo simulations with two light flavors in the region $m_{ud} \geq (1/5)m_s$. For the definition of the quark mass the dimensionless quantity

$$M_r \equiv (r_0 m_\pi)^2 \qquad (5)$$

is used, which already appears in (1). This is a possible definition for small quark masses because for $m_q \to 0$ the pion mass behaves as $m_\pi \propto m_q^{1/2}$. For defining the value of M_r which corresponds to the strange quark mass one can use unquenched $N_f = 2$ lattice data. For instance, the experimental value of the Ω^- baryon mass $m_{\Omega^-} = 1.672\,\mathrm{GeV}$ and $r_0 = 0.5\,\mathrm{fm}$ give $r_0 m_{\Omega^-} = 4.237$. Interpolating the CP-PACS results [11] for the Δ baryon mass at their largest β value, $\beta = 2.20$, between $\kappa = 0.1363$ and $\kappa = 0.1368$ one can match $r_0 m_\Delta = 4.237$ if their pion mass is $r_0 m_\pi \simeq 1.76$. This gives for the strange quark mass $M_{r,\mathrm{strange}} \simeq 3.1$. Of course, there are also other ways to estimate $M_{r,\mathrm{strange}}$ which might give slightly different values. In the present paper, without attempting to really compute the strange quark mass, we shall stick to the operational definition

$$M_{r,\mathrm{strange}} \equiv 3.1. \tag{6}$$

The Monte Carlo simulations are done near the $N_t = 4$ thermodynamical cross-over line, that is for $a \simeq 0.27\,\mathrm{fm}$. The lattice size is $8^3 \times 16$ implying a physical lattice extension $L \simeq 2.2\,\mathrm{fm}$. Later on we shall also extend our investigations to $12^3 \times 24$ and $16^3 \times 32$ lattices. Our present studies can be considered as complementary to the ones on larger lattices (closer to the continuum limit) but at larger quark masses (typically $m_{ud} \geq (1/2)m_s$) [2–7].

In addition to obtaining estimates of autocorrelation lengths as a function of the quark mass we also performed a detailed study of the small eigenvalue spectra both for the hermitean and non-hermitean Wilson–Dirac fermion matrix. Besides giving important qualitative information about quark dynamics this also allows one to clear the issue of the *sign problem* of the quark determinant. For an odd number of Wilson-type quark flavors the fermion determinant can have both signs, because there might be some eigenvalues (of the non-hermitean fermion matrix) on the negative real axis. Since for importance sampling a positive measure is required, the determinant sign can only be taken into account in a measurement reweighting step. A strongly fluctuating determinant sign is a potential danger for the effectiveness of the Monte Carlo simulation because cancellations can occur resulting in an unacceptable increase of statistical errors. We actually study this question here with two degenerate quark flavors ($N_f = 2$) where in the path integral the square of the fermion determinant appears and hence the sign is irrelevant. But our two quarks are much lighter than the physical s-quark. Therefore the statistical insignificance of negative eigenvalues in this case hints towards the absence of the sign problem in the physical case of $N_f = 2 + 1$ quark flavors, when the sign of the s-quark determinant could, in principle, cause a problem.

The plan of this paper is as follows: in the next section we briefly introduce the parameters of the TSMB algorithm and give some details of our implementation on different computers. In Sect. 3 the autocorrelations are investigated for some basic quantities such as the average plaquette and the pion mass. Section 4 contains a detailed study of the small eigenvalue spectra of the fermion matrix. The last section is devoted to discussion and conclusions.

2 The TSMB algorithm

We use in this study the two-step multi-boson (TSMB) algorithm which has been originally developed for Monte Carlo simulations of the supersymmetric Yang–Mills theory [10], but that can also be applied more generally [12].

2.1 Algorithmic parameters

TSMB is based on a representation of the fermion determinant in the form

$$|\det(Q)|^{N_f} \simeq \frac{1}{\det P_{n_1}^{(1)}(\tilde{Q}^2)\,\det P_{n_2}^{(2)}(\tilde{Q}^2)}. \tag{7}$$

Here N_f denotes the number of fermion flavors and Q is the fermion matrix, which in the present paper is equal to the Wilson–Dirac matrix

$$\begin{aligned} Q_{ys,xr} &\equiv \delta_{yx}\delta_{sr} \\ &- \kappa \sum_{\mu=1}^{4} \left[\delta_{y,x+\hat{\mu}}(1+\gamma_\mu)U_{sr,x\mu} + \delta_{y+\hat{\mu},x}(1-\gamma_\mu)U^\dagger_{sr,y\mu}\right], \end{aligned} \tag{8}$$

with x, y denoting lattice sites, r, s color (triplet) indices, $\hat{\mu}$ the unit lattice vector in direction μ, $U_{x\mu} \in \mathrm{SU}(3)$ gauge link matrices and κ the hopping parameter. The hermitean Wilson–Dirac fermion matrix is defined as usual by

$$\tilde{Q} \equiv \gamma_5 Q = \tilde{Q}^\dagger. \tag{9}$$

The polynomial approximations in (7) satisfy

$$\begin{aligned} P_{n_1}^{(1)}(x) &\simeq x^{-N_f/2}, \\ \lim_{n_2\to\infty} P_{n_1}^{(1)}(x) P_{n_2}^{(2)}(x) &= x^{-N_f/2}, \quad x \in [\epsilon, \lambda], \end{aligned} \tag{10}$$

where the interval $[\epsilon, \lambda]$ covers the spectrum of the squared hermitean fermion matrix $\tilde{Q}^2$ on a typical gauge configuration. The first polynomial $P^{(1)}$ is a crude approximation with relatively low order. It is used in the multi-boson representation of fermion determinants [13]. The second polynomial $P^{(2)}$ is a correction factor which is taken into account in the gauge field updating by a global accept-reject step. For this a polynomial approximation of the inverse square root of $P^{(2)}$ is also needed:

$$P_{n_3}^{(3)}(x) \simeq P_{n_2}^{(2)}(x)^{-1/2}. \tag{11}$$

The limit $n_2 \to \infty$ can be taken in the computed expectation values if one produces several update sequences with increasing n_2 or, more conveniently, one can keep n_2 fixed at some sufficiently large value for a good approximation and introduce a further polynomial $P^{(4)}$ satisfying

$$\lim_{n_4\to\infty} P_{n_1}^{(1)}(x) P_{n_2}^{(2)}(x) P_{n_4}^{(4)}(x) = x^{-N_f/2}. \tag{12}$$

$P^{(4)}$ can be taken into account by reweighting the gauge configurations during the evaluation of expectation values. In most cases the order n_2 of $P^{(2)}_{n_2}$ can be chosen high enough such that the reweighting correction has a negligible effect on expectation values. In any case the evaluation of the reweighting factors is useful because it shows whether or not the two-step approximation in (10) is good enough. For a recent summary of some details of TSMB and for references see Sect. 3 of [14].

The Monte Carlo integration of the path integral is performed by averaging over a sequence (Markov chain) of multi-boson and gauge field configurations. The n_1 multi-boson fields (Φ) and gauge fields (U) are updated in repeated *update cycles* consisting of several sweeps over the multi-boson fields and gauge field. For the multi-boson fields we use (local) heatbath and overrelaxation as well as global quasi-heatbath [15] sweeps. For the gauge field update heatbath and overrelaxation sweeps are alternated. After several gauge field sweeps a global Metropolis accept–reject correction step is performed by the polynomials $P^{(2)}$ and $P^{(3)}$. The update sequence within a cycle is subject to optimization with the goal to decrease autocorrelations. We tried several kinds of update sequences within an update cycle. A typical sequence was 3 Φ-overrelaxations, 1 Φ-heatbath, 12 U-overrelaxation, global U-Metropolis, 3 Φ-overrelaxations, 1 Φ-heatbath, 6 U-heatbath, global U-Metropolis. In every 10th cycle the first Φ-overrelaxation–Φ-heatbath combination was replaced by a global quasi-heatbath.

2.2 Implementation and performance

We have implementations of the updating and measurement programs in TAOmille for the APEmille and in C++/MPI. The latter implementation is usable on many different architectures as long as they provide a C++ compiler and, in case of parallel computers, support MPI. In the updating program the computing time is dominated by the fermion-matrix-vector multiplications (MVMs); $2\times(n_2+n_3)$ of them are needed for the correction step and $\mathcal{O}(100\times n_1)$ for the global heatbath and quasi-heatbath [15]. Altogether they make up 60%–80% of the computing time. In the most interesting regions of small quark masses the program is dominated by the MVMs even more strongly. The same is true for the measurement program, where smearing and calculation of simple Wilson loops takes only a few percent of the time. It is therefore of the utmost importance to improve the performance of the MVM routines, both preconditioned (for the correction step and the measurements) and non-preconditioned (for the global heatbath). This has been done for the APEmille, the Cray T3E with the KAI C++ compiler, and for a multi-node Pentium-4 cluster here also exploiting the possibilities of SSE and SSE2 instructions. Results are given in Table 1. Note that an important feature of the SSE instructions is that in single precision the peak performance is doubled compared to double precision. The performance numbers in Table 1 are substantially influenced by the communication costs among computing nodes. Without communications the numbers both for APEmille and P4-cluster would be almost a factor of 2 higher. On larger volumes than those considered here communication will have less influence on the performance.

Table 1. Performance of the matrix-vector multiplication in MFlops and percent relative to peak performance on one board (8 nodes) on the APEmille and on 8 processors on the T3E and P4-cluster for a $8^3\times 16$ lattice

	APEmille	T3E-1200	P4-1700
32 bit	1008 (23.9%)	912 (9.5%)	4322 (7.9%)
64 bit	–	712 (7.4%)	2087 (7.7%)

Since the matrix multiplications dominate the computing time it is reasonable to express e.g. autocorrelations in units of MVMs. The remaining part of the computation is given by the local updates. These are composed of parts which can be essentially thought of as pieces of MVMs, too. As a result the following approximate formula for the total amount of MVMs needed for one update cycle is obtained:

$$N_{\mathrm{MVM}}/\mathrm{cycle} \simeq 6(n_1 N_\Phi + N_U) + 2(n_2+n_3)N_{\mathrm{C}} + I_{\mathrm{G}}F_{\mathrm{G}}. \tag{13}$$

Here N_Φ is the number of local bosonic sweeps per update cycle, N_U the number of local gauge sweeps, N_{C} the number global Metropolis accept–reject correction steps, and I_{G} and F_{G} give the number of MVMs and frequency of the global heatbath.

For data from APEmille and Cray the estimate of the cost of the local updates obtained from (13) agrees with the actual costs up to 5%. Therefore the final costs in units of MVM based on (13) are not much influenced by the approximation. This is not true for the data presented for the P4-1700 system, since in this case the matrix multiplication and the local updates are not treated homogeneously. Indeed the former is written in assembler using SSE/SSE2 instructions while our code for the local updates is written in C++ and compiled with the g++ compiler. As a result, the estimate for the cost of the local updates is in this case underestimated by about a factor 3. Still we take the above formula as a reference when tuning the parameters because the number of MVMs is more generally applicable as it does not depend on implementation details. In addition, in the future the local updates could be rewritten by using SSE/SSE2 instructions, too, thus eliminating the non-homogeneity with the MVMs.

It is sometimes interesting to convert the number of MVMs into the number of floating point operations. On our $8^3\times 16$ lattice this conversion is approximately

$$1\,\mathrm{MVM} \simeq 1.1\times 10^7\,\mathrm{flop}. \tag{14}$$

3 Autocorrelations at small quark masses

The bare parameters of the QCD lattice action with Wilson quarks (β for the SU(3) gauge coupling and κ for the hopping parameter of two degenerate quarks) have to be

Table 2. Bare couplings, parameters of the TSMB algorithm as defined in Sect. 2.1 and total statistics in 1000 update cycles (U_k) of our runs

Run	β	κ	n_1	n_2	n_3	n_4	λ	ϵ	U_k
(a)	5.28	0.160	20	40	70	100	2.8	1.75×10^{-2}	80
(b)	5.04	0.174	28	90	120	150	3.0	3.75×10^{-3}	33
(c)	4.84	0.186	38	190	240	300	3.6	1.44×10^{-3}	31
(d)	4.80	0.188	44	240	300	300	3.6	7.2×10^{-4}	12
(e)	4.76	0.190	44	360	380	500	3.6	2.7×10^{-4}	144
(f)	4.80	0.190	44	360	380	500	3.6	2.7×10^{-4}	224
(g)	4.72	0.193	52	600	750	800	3.6	0.9×10^{-4}	196
(h)	4.68	0.195	66	900	1200	1100	3.6	3.6×10^{-5}	200
(i)	4.64	0.197	72	1200	1500	1400	3.6	1.8×10^{-5}	110
(j)	4.64	0.1975	72	1200	1350	1400	4.0	2.0×10^{-5}	4

tuned properly in order to obtain the desired parameters in the Monte Carlo simulations. We are interested in the quark mass dependence of the simulation cost of hadron spectroscopy applications; therefore, we want to keep the physical volume of our lattices sufficiently large and (approximately) constant. For a $8^3 \times 16$ lattice, a lattice spacing $a \simeq 0.27\,\mathrm{fm}$ implies a lattice extension of $L \simeq 2.2\,\mathrm{fm}$ which is a reasonable starting point for spectroscopy. Previous Monte Carlo simulations with $N_f = 2$ Wilson quarks [16,17] showed that this kind of lattice spacing is realized near the $N_t = 4$ and $N_t = 6$ thermodynamical transition lines which, therefore, provide a good orientation. We started our simulations at a relatively large quark mass on the $N_t = 4$ transition line and then tuned β and κ towards smaller quark masses keeping r_0/a approximately constant. A summary of simulation points is given in Table 2, where some important algorithmic parameters of the TSMB are also collected.

Most of the runs have been done with 32-bit arithmetics. Exceptions are run (j) and about 10% of the statistics in run (h) where 64-bit arithmetics was used. In general, on the $8^3 \times 16$ lattice it is not expected that single precision makes any difference. In fact, the double precision results in run (h) were compatible within errors with the single precision ones.

3.1 Physical quantities

In order to monitor lattice spacing and quark mass one has to determine some physical quantities containing the necessary information. As discussed before, we define the physical distance scale from the value of the Sommer scale parameter r_0. Once r_0 in lattice units is known one can transform any dimensionful quantity, for instance the pion mass m_π, from lattice to physical units. Therefore a careful determination of r_0/a is important. For a dimensionless quark mass parameter one can use M_r as defined in (5): $M_r = (r_0/a \times a m_\pi)^2$. In addition, we also measured some other quantities like f_π, m_ρ and another definition of the quark mass m_q for obtaining a broader basis for orientation. In the next subsections the procedures for extracting these quantities will be described in detail.

3.1.1 Masses and amplitudes

In order to extract masses and amplitudes we compute the zero-momentum two-point functions depending on the time-slice distance $(x_0 - y_0)$:

$$C_{XY}(x_0 - y_0) = \frac{1}{V_s} \sum_{\mathbf{x},\mathbf{y}} \langle X^\dagger(x) Y(y) \rangle \ , \qquad (15)$$

with $x \equiv (x_0, \mathbf{x})$ and

$$\begin{aligned} X(x) = Y(x) = P_5(x) &\equiv \bar{q'}(x)\gamma_5 q(x) \\ &\quad (C_{PP}(x_0 - y_0)), \\ X(x) = Y(x) = A_0(x) &\equiv \bar{q'}(x)\gamma_5\gamma_0 q(x) \\ &\quad (C_{AA}(x_0 - y_0)), \\ X(x) = Y(x) = V_i(x) &\equiv \bar{q'}(x)\gamma_i q(x) \\ &\quad (C_{V_i V_i}(x_0 - y_0)); \end{aligned}$$

we also consider the mixed correlator with

$$X(x) = A_0(x), \quad Y(x) = P_5(x) \quad (C_{AP}(x_0 - y_0)).$$

Exploiting translation invariance we pick the source y in (15) at random over the lattice. Taking into account correlations between different time-slices, one sees that this procedure is optimal for the ratio computational cost/final statistical error for hadronic observables.

Masses and amplitudes are in general obtained from the asymptotic behavior of the correlators[1]:

$$C_{XY}(T) = \frac{\xi_{XY}^2}{2m_p}(\mathrm{e}^{-m_p T} + (-1)^{X+Y}\mathrm{e}^{-m_p(L_t - T)}), \qquad (16)$$

$$\xi_{XY} = \sqrt{\langle 0|X(0)|p\rangle\langle 0|Y(0)|p\rangle}, \qquad (17)$$

where $|p\rangle$ is the zero-momentum state of the particle associated with the operators $X(x)$ and $Y(x)$, m_p the corresponding mass and $(-1)^{X(Y)}$ the time-parity of $X(Y)(x)$. We determine parameters m_p and ξ_{XY} by global fitting

[1] Amplitudes are assumed to be real

Table 3. Results of runs specified in Table 2 for different physical quantities defined in the text. The values given in lattice units can be transformed to physical units by canceling the lattice spacing a with the help of the results for r_0/a and using $r_0 = 2.53\,\mathrm{GeV}^{-1}$

Run	r_0/a	af_π	am_π	am_ρ	m_π/m_ρ	M_r	μ_r
(a)	1.885(30)	0.3738(50)	1.2089(36)	1.2982(32)	0.9312(17)	5.19(20)	0.498(12)
(b)	1.715(20)	0.4321(23)	1.0428(41)	1.1805(38)	0.8834(14)	3.20(10)	0.305(6)
(c)	1.616(110)	0.4171(47)	0.7886(40)	1.0251(48)	0.7693(32)	1.61(24)	0.148(11)
(d)	1.903(159)	0.4199(75)	0.753(11)	0.999(12)	0.752(11)	2.05(40)	0.155(13)
(e)	1.697(46)	0.4191(20)	0.7151(20)	0.9941(19)	0.7187(16)	1.473(88)	0.1229(41)
(f)	1.739(33)	0.3658(34)	0.5825(34)	0.9089(47)	0.6431(33)	1.026(51)	0.0811(30)
(g)	1.772(41)	0.3791(39)	0.5695(38)	0.9116(33)	0.6256(31)	1.018(61)	0.0770(32)
(h)	1.765(37)	0.3668(54)	0.5088(51)	0.8983(35)	0.5675(42)	0.806(50)	0.0596(27)
(i)	1.812(46)	0.3575(48)	0.4333(48)	0.8616(80)	0.5002(60)	0.616(45)	0.0429(21)
(j)	1.756(128)	0.3377(48)	0.4205(54)	0.859(12)	0.4894(65)	0.545(47)	0.0363(38)

over a range of time-slice distances (after time-symmetrization) $T \in [T_{\min}, L_t/2]$. We find the optimal value for $T_{\min}$ by checking the behavior of the effective local mass $m_{\mathrm{eff}}(T)$. The latter is implicitly defined by the relation

$$\frac{C_{XY}(T)}{C_{XY}(T+1)} = \frac{\mathrm{e}^{-m_{\mathrm{eff}}(T)T} + (-1)^{X+Y}\mathrm{e}^{-m_{\mathrm{eff}}(T)(L_t-T)}}{\mathrm{e}^{-m_{\mathrm{eff}}(T)(T+1)} + (-1)^{X+Y}\mathrm{e}^{-m_{\mathrm{eff}}(T)(L_t-T-1)}}. \tag{18}$$

The value of $T_{\min}$ is fixed by the onset of the plateau for $m_{\mathrm{eff}}(T)$ as a function of T. The plateau value for the effective mass is always consistent with the result from the global fit procedure. The latter gives however the most precise determination.

A typical problem associated with small quark masses is a delayed asymptotic behavior for correlators (i.e. a larger $T_{\min}$) resulting in large errors for the hadronic observables. This problem was solved by applying Jacobi smearing [18] on both source and sink. Jacobi smearing was applied in a different context [19,20] in the same situation of light fermionic degrees of freedom, and it appeared to improve the overlap of the hadronic operators with the bound state. Amplitudes and decay constants have been determined from correlators with local operators.

We determine the pion mass m_π from the asymptotic behavior of the correlator $C_{PP}(T)$. From $C_{PP}(T)$ one can also extract the amplitude $g_\pi = \langle 0|P_5(0)|\pi\rangle$ by identifying $g_\pi = \xi_{PP}$. The ρ meson mass m_ρ is determined from the asymptotic behavior of the correlator

$$C_{VV}(T) = \frac{1}{3}\sum_{i=1}^{3} C_{V_iV_i}(T). \tag{19}$$

For the determination of the pion decay constant $f_\pi \equiv m_\pi^{-1}\langle 0|A_0(0)|\pi\rangle$ we apply two different methods. In the first, the amplitude $\langle 0|A_0(0)|\pi\rangle$ is obtained by fitting the asymptotic behavior of the correlator $C_{AA}(T)$, while the pion mass is the one coming from $C_{PP}(T)$. In the second method [21], we fit the amplitude ratio

$$r_{AP} = \frac{\langle 0|A_0(0)|\pi\rangle}{\langle 0|P_5(0)|\pi\rangle} \tag{20}$$

by using the asymptotic behavior

$$\frac{C_{AP}(T)}{C_{PP}(T)} = r_{AP}\tanh[m_\pi(L_t/2 - T)], \tag{21}$$

where m_π is fixed at the best-fit value from $C_{PP}(T)$. The determination of f_π is then obtained from the relation

$$f_\pi = m_\pi^{-1} r_{AP} g_\pi, \tag{22}$$

using for g_π the determination from $C_{PP}(T)$. In the region of large and moderate quark masses the second method gives by far the most precise determination of f_π. This is generally no more true for very light quarks where the data are highly correlated. Here the best determination was picked from the two different methods on a case-by-case basis.

Using the above determinations we can extract the quark mass defined by the PCAC relation

$$m_q^{\mathrm{PCAC}} = \frac{f_\pi}{2g_\pi} m_\pi^2. \tag{23}$$

The PCAC quark mass gives us a second definition of the physical quark mass as an alternative to (5):

$$\mu_r \equiv r_0 m_q^{\mathrm{PCAC}}. \tag{24}$$

We estimated statistical errors on hadron quantities by applying the Jackknife procedure on blocks of data of increasing size. The same procedure is applied also for the Sommer scale parameter (see next subsection). This method provides us with a definition of the *integrated autocorrelation* τ_{int} of the pion mass. Autocorrelations in general will be discussed in Sect. 3.2. The results for the hadronic quantities are listed in Table 3.

3.1.2 Sommer scale parameter

There are several phenomenological models that can be used to get an estimate for the Sommer scale parameter

r_0 in nature, and most of them point towards a value of $r_0 \simeq 0.49\,\mathrm{fm}$. On the lattice r_0/a can be calculated from the static quark potential, which is in turn determined from Wilson loops. The basic idea is simple, but since we want to match all our results to this parameter it is crucial to get a precise determination. To achieve this we follow the method proposed by Michael and collaborators [22, 23] and some details are found in [24].

Using the variational approach of [25] we get matrices $W_{ij}(r,t)$ consisting of $r \times t$ loops of smeared gauge links, where our smearing technique of choice is APE-smearing (the indices i,j label the level of smearing). We use for our determinations two and six or two, four and six levels of smearing and symmetrize the matrices W_{ij}. The ratio staple/link is set to $\alpha = 0.45$.

From the solutions to

$$W_{ij}(\mathbf{r},t)\phi(\mathbf{r})_j^{(k)} = \lambda^{(k)}(\mathbf{r};t,t_0)W_{ij}(\mathbf{r},t_0)\phi(\mathbf{r})_j^{(k)}, \quad i,j,k = 0,1(,2) \tag{25}$$

one gets the eigenvector $\phi(\mathbf{r})_j^{(0)}$ for the largest eigenvalue $\lambda^{(0)}(\mathbf{r};t=t_0+1,t_0)$. This equation is solved by transforming it into an ordinary eigenvalue equation, where several ways are possible:

$$W(\mathbf{r},t_0)^{-1}W(\mathbf{r},t)\phi = \lambda\phi, \tag{26}$$

$$W(\mathbf{r},t)W(\mathbf{r},t_0)^{-1}(W(\mathbf{r},t_0)\phi) = \lambda(W(\mathbf{r},t_0)\phi), \tag{27}$$

$$W(\mathbf{r},t_0)^{-1/2}W(\mathbf{r},t)W(\mathbf{r},t_0)^{-1/2}(W(\mathbf{r},t_0)^{1/2}\phi) = \lambda(W(\mathbf{r},t_0)^{1/2}\phi). \tag{28}$$

In the literature [25] the third version has been used. However this can only be done with extremely good statistics. Otherwise it is possible that, due to statistical fluctuations, the matrix W_{ij} gets negative eigenvalues making the (real) square root impossible. We checked that the first two versions give numerically exactly the same result. For the final determinations we choose the first version (26), where one has to be careful about the fact that $W(\mathbf{r},t_0)^{-1}W(\mathbf{r},t)$ has no longer to be symmetric, complicating the calculation of the corresponding eigenvectors.

Once the eigenvector $\phi(\mathbf{r})_j^{(0)}$ has been obtained, we can project the matrix W_{ij} to the ground state:

$$\tilde{W}_0(\mathbf{r},t) = \phi(\mathbf{r})_i^{(0)}W_{ij}(\mathbf{r},t)\phi(\mathbf{r})_j^{(0)}. \tag{29}$$

This correlator leads to good estimates of the ground state energy

$$\tilde{E}_0(\mathbf{r},t) = \ln\left(\frac{\tilde{W}_0(\mathbf{r},t)}{\tilde{W}_0(\mathbf{r},t+1)}\right). \tag{30}$$

The potential $V(\mathbf{r})$ is estimated by averaging $E_0(\mathbf{r},t)/t$ over time extensions t with $t \geq 1$ and weight given by the Jackknife error. Compared to some other methods this way of extracting the potential seems to give the most reliable estimates with smallest error bars.

The Sommer scale parameter is defined in terms of the potential as

$$r_0^2 \left.\frac{\mathrm{d}V}{\mathrm{d}r}\right|_{r_0} = 1.65. \tag{31}$$

Having a reliable static quark potential we can follow [26] by fitting the potential to

$$V(\mathbf{r}) = V_0 + \sigma r - e\left[\frac{1}{\mathbf{r}}\right] \tag{32}$$

with $r = |\mathbf{r}|$ and $[1/\mathbf{r}]$ being the tree-level lattice Coulomb term

$$\left[\frac{1}{\mathbf{r}}\right] = 4\pi\int_{-\pi}^{\pi}\frac{\mathrm{d}^3\mathbf{k}}{(2\pi)^3}\frac{\cos(\mathbf{k}\cdot\mathbf{r})}{4\sum_{j=1}^{3}\sin^2(k_j/2)}. \tag{33}$$

Due to the small lattice size we had to drop in (32) the additional correction term $f\times([1/\mathbf{r}]-(1/r))$, which could have been used to estimate $\mathcal{O}(a)$ effects, fixing $e = \pi/12$. Bringing together the above equations we extract r_0 from

$$r_0 = \sqrt{\frac{1.65-e}{\sigma}}. \tag{34}$$

3.2 Autocorrelations

The "cost" of numerical simulations can be expressed in terms of the necessary number of arithmetic operations for obtaining during the Monte Carlo update process a new "independent" gauge field configuration. The real cost can be then easily calculated once the price of e.g. a floating point operation is known. For a definition of the independence of a new configuration the *integrated autocorrelation* τ_{int} is used. (For a general reference see [27].) τ_{int} does depend on the particular quantity it refers to. Of course, it is reasonable to choose an "important" quantity as, for instance, the pion mass but simple averages characterizing the gauge field such as the plaquette average are also often considered.

In case of the TSMB algorithm a peculiar feature is the reweighting step correcting for the imperfection of polynomial approximations. As will be discussed in the next subsection, in most of our runs this correction is totally negligible but even in these cases it is important to perform the reweighting on a small subsample of configurations in order to check that the used polynomials are precise enough. In some cases, especially for very small quark masses, there are a few *exceptional configurations* with small eigenvalues of the squared hermitean fermion matrix ($\tilde{Q}^2$) which are practically removed from statistical averages by their small reweighting factors. In the calculation of expectation values these reweighting factors were always taken into account. For the autocorrelations the effect of the exceptional configurations is in most cases negligible.

3.2.1 Integrated autocorrelation of the pion mass

In case of secondary quantities such as the pion mass, or in general any function of the primary expectation values, the straightforward definition of the integrated autocorrelation τ_{int} for primary quantities is not directly applicable. In fact, there are several possibilities which we shall now shortly discuss.

(1) *Linearization.* As has been proposed by the ALPHA Collaboration [9], in the limit of high enough statistics the problem of the error estimate and of the autocorrelation for secondary quantities can be reduced to considering a linear combination of primary quantities. Let us denote the expectation values of a set of primary quantities by A_α, $(\alpha = 1, 2, \ldots)$. Their estimates obtained from a data sequence are $\overline{a}_\alpha$. For high statistics the estimates are already close to the true values: $|\overline{a}_\alpha - A_\alpha| \ll 1$. Therefore, if the secondary quantity is defined by a function $f(A)$ of primary quantities, we have

$$f(\overline{a}) - f(A) \simeq \sum_\alpha (\overline{a}_\alpha - A_\alpha) \frac{\partial f(A)}{\partial A_\alpha}. \tag{35}$$

The values of the derivatives are constants; therefore, on the right hand side there is a linear combination of primary quantities which can be handled in the same way as the primary quantities themselves. Since

$$\frac{\partial f(A)}{\partial A_\alpha} \simeq \left.\frac{\partial f(A)}{\partial A_\alpha}\right|_{A=\overline{a}} \equiv \bar{f}_\alpha, \tag{36}$$

one can consider the linear combinations

$$A_{\bar{f}} \equiv \sum_\alpha A_\alpha \bar{f}_\alpha, \quad \overline{a}_{\bar{f}} \equiv \sum_\alpha \overline{a}_\alpha \bar{f}_\alpha, \tag{37}$$

and the variance of the secondary quantity can be estimated as

$$\sigma_f^2 \simeq \left\langle (\overline{a}_{\bar{f}} - A_{\bar{f}})^2 \right\rangle. \tag{38}$$

(Note that here $\langle \ldots \rangle$ stands for the expectation value in an infinite sequence of identical measurements with the same statistics as the one under consideration.) According to (38) the integrated autocorrelation of the secondary quantity can be defined as the integrated autocorrelation of $A_{\bar{f}}$.

This way of obtaining error estimates and autocorrelations of secondary quantities is simple and generally applicable. Let us note that because of the reweighting even the simplest physical quantities are given by ratios of two expectation values and are, therefore, secondary quantities.

(2) *Blocking.* In case of sufficiently large statistical samples the integrated autocorrelations of secondary quantities can also be obtained by comparing statistical fluctuations of data coming from the measurement program before and after a blocking procedure. The blocking procedure eliminates for increasing block size the autocorrelations between data and the final error is the one for *uncorrelated data*. Since the latter is the true error of the measurement, it is appropriate to use this definition of $\tau_{\rm int}$ to estimate the real cost of a simulation. In the case of primary quantities such as the plaquette this definition coincides with the usual one.

For a generic quantity A one can define $\sigma_n^B(A)$ as the standard deviation of the data at blocking-level n. In the case of the pion mass, we determine this quantity by applying the jackknife procedure on the hadron correlators averaged over blocks of length n. In the limit of infinite statistics, for increasing n, $\sigma_n^B(A)$ should approach after a transient an asymptotic value corresponding to the standard deviation of the uncorrelated data $\sigma_{\rm unc}(A)$. For finite statistics, $\sigma_n^B(A)$ fluctuates around $\sigma_{\rm unc}(A)$. We determine $\sigma_{\rm unc}(A)$ by averaging $\sigma_n^B(A)$ over a range of block sizes n after the transient. The error on this determination is given by the mean dispersion of data around the average. Once $\sigma_{\rm unc}(A)$ is given the integrated autocorrelation is defined by

$$\tau_{\rm int} = \frac{1}{2} \left(\frac{\sigma_{\rm unc}(A)}{\sigma_1^B(A)} \right)^2. \tag{39}$$

Another way of writing the above formula is

$$N_{\rm unc} = \frac{N_{\rm stat}}{2\tau_{\rm int}} \tag{40}$$

where $N_{\rm stat}$ is the original statistics and $N_{\rm unc}$ is the number of uncorrelated configurations; so $2\tau_{\rm int}$ can be thought of as the distance between two uncorrelated configurations.

(3) *Covariance matrix.* In most cases it is a good approximation to assume that the probability distribution of the estimates $\overline{a}_\alpha$ of the primary quantities A_α is Gaussian:

$$P(\overline{a}) \propto \exp\left\{ -\frac{1}{2} \sum_{\alpha\alpha'} (\overline{a}_\alpha - A_\alpha)\, C^{-1}_{\alpha\alpha'}\, (\overline{a}_{\alpha'} - A_{\alpha'}) \right\}. \tag{41}$$

The covariance matrix is

$$\langle (\overline{a}_\alpha - A_\alpha)(\overline{a}_{\alpha'} - A_{\alpha'}) \rangle = \langle \overline{a}_\alpha \overline{a}_{\alpha'} \rangle - \langle \overline{a}_\alpha \rangle \langle \overline{a}_{\alpha'} \rangle = C_{\alpha\alpha'}. \tag{42}$$

The elements of the covariance matrix can be estimated from the data sequence by determining the integrated autocorrelations $\tau_{\rm int}^{(A_\alpha A_{\alpha'})}$:

$$C_{\alpha\alpha'} \simeq (\overline{a_\alpha a_{\alpha'}} - \overline{a}_\alpha \overline{a}_{\alpha'}) \, \frac{2\tau_{\rm int}^{(A_\alpha A_{\alpha'})}}{N_{\rm stat}}. \tag{43}$$

Once the probability distribution of the estimates $P(\overline{a})$ is known one can obtain an error estimate for any function of $\overline{a}_\alpha$ by generating a large number of estimates. From the error it is also possible to obtain an indirect estimate of the integrated autocorrelation from a formula like (39).

The integrated autocorrelation of the pion mass (and the error of the pion mass) can be obtained by any of these three methods and the results are generally consistent with each other. The method based on linearization is rather robust already at the level of statistics we typically have. The blocking method becomes easier unstable, especially for moderate statistics. This is understandable since the statistics in the individual blocks is reduced compared to the total sample. The method based on the covariance matrix needs sufficient statistics in order that the estimate of the covariance matrix be reliable. This is usually the case for effective masses derived from intermediate distances but – in our runs – this method sometimes fails for the largest distances.

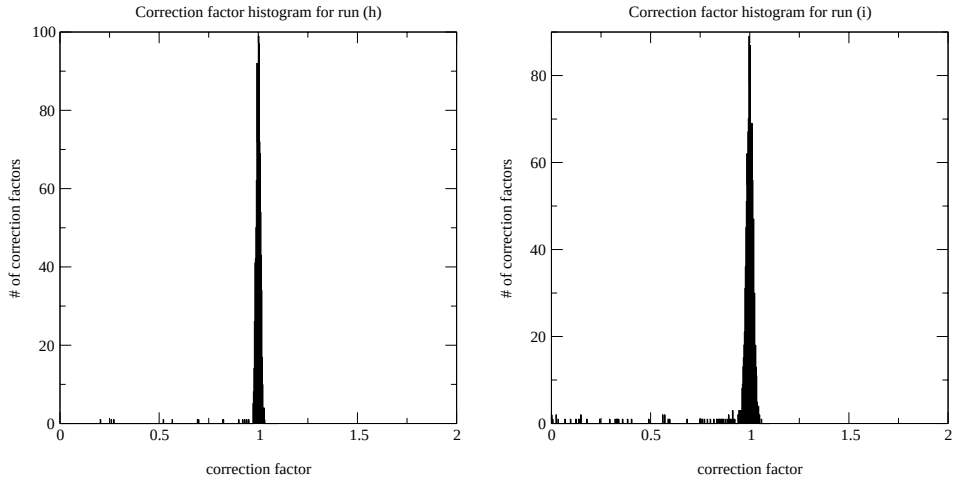

Fig. 1. Correction factors for run (h) (*left panel*) and (i) (*right panel*)

3.2.2 Correction factors

As has been described in Sect. 2.1 a fourth polynomial $P^{(4)}_{n_4}$ can be used to extrapolate to infinite polynomial order, therefore avoiding the need for several simulations with different orders of the second polynomial $P^{(2)}_{n_2}$. In our runs the evaluation of the reweighting factors was done in the way described in detail in [19]. Few smallest eigenvalues $\tilde{\lambda}^2$ of the squared hermitean fermion matrix $\tilde{Q}^2$, typically four, were explicitly determined and the corresponding correction factors were exactly taken into account. In the subspace orthogonal to the corresponding eigenvectors a stochastic estimate based on four Gaussian random vectors was taken. (Note that in the limit of infinite statistics a stochastic estimate always gives a correct result independently of the number of random vectors; no systematic error is introduced.)

As stated before, most of our results were obtained with second polynomials $P^{(2)}_{n_2}$ which gave already a good approximation of the fermionic measure. In this case the inclusion of the correction factors had nearly no influence on the final determinations since they were very close to one. Going to smaller quark masses the smallest eigenvalue starts to fluctuate more, and it is therefore no longer reasonable to try to use a second polynomial that is good enough for all cases. Such large fluctuations appeared in runs (h) and (i). The histograms of reweighting factors are illustrated by Fig. 1. It turned out that, as expected, the inclusion of the correction factors had the nice effect of reducing error bars. This is especially noticeable for fermionic quantities and in particular the pion mass which is highly correlated to the smallest eigenvalue.

Nevertheless, even in these cases the effect of reweighting was so small that the individual estimates with correction factors agreed within error bars with those without correction factors. As a whole, however, a minor systematic increase in the masses could be seen. Both histograms in Fig. 1 have a tail towards small values which are due to eigenvalues that could have been further suppressed by a better second polynomial. As the figure shows, this tail is more important in run (i) than in run (h). A closer look at

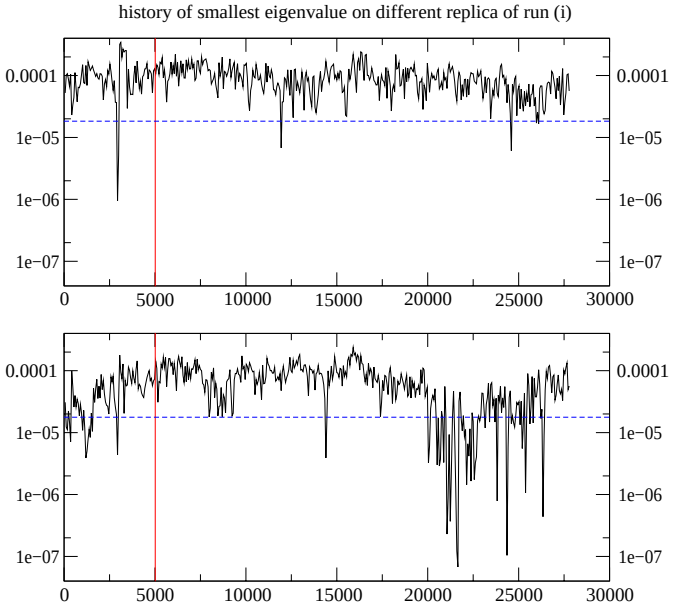

Fig. 2. Histories of the smallest eigenvalue at $\beta = 4.64$, $\kappa = 0.197$ for two independent lattices. The upper figure shows the typical case when the smallest eigenvalue stays most of the time above ϵ shown by the dashed line. The lower figure is the history with exceptionally small eigenvalues. The measurement of physical quantities was started at the vertical line

the smallest eigenvalue histories in run (i) reveals that the tail near zero was produced by one of the four independent parallel lattices when the smallest eigenvalue stayed for some time below the lower limit of the approximation interval ϵ (see Fig. 2).

Configurations with small eigenvalues $\tilde{\lambda}^2$ are interesting because exceptionally small values could indicate crossing of real eigenvalues of the Wilson–Dirac matrix Q to the negative axis. This could give a negative sign for the determinant of a single quark flavor. We systematically analyzed in all our runs configurations with small $\tilde{\lambda}^2$, searching for this effect. In the present study we found, for the first time in a QCD simulation with TSMB, configurations with real negative eigenvalues of the Wilson–Dirac

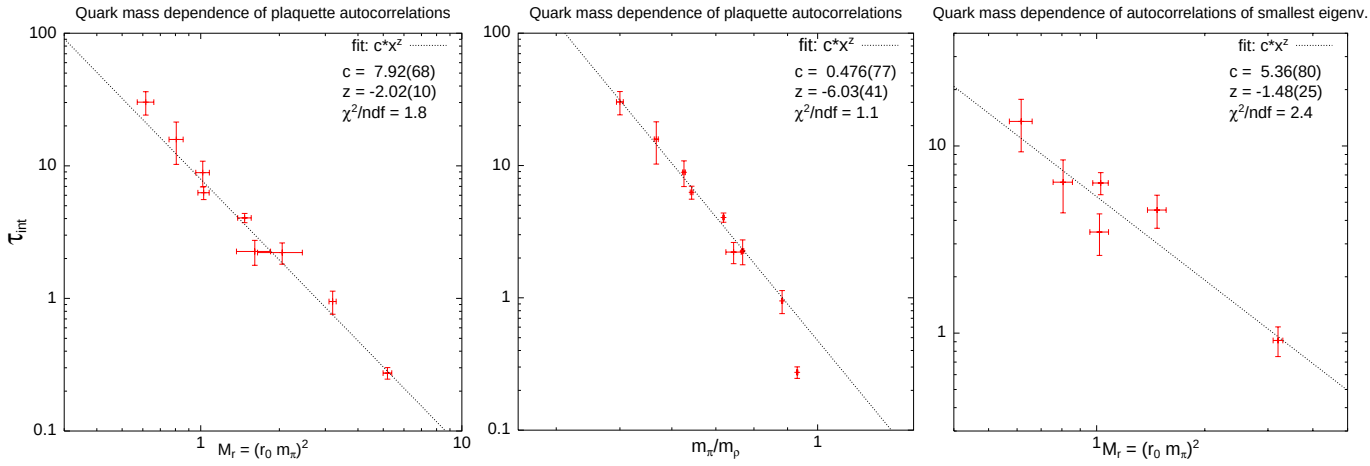

Fig. 3. *Left panel:* Power fit of the plaquette autocorrelation given in units of $10^6 \times$ MVM as a function of the dimensionless quark mass parameter M_r. The best fit of the form cM_r^z is at $c = 7.92(68)$, $z = -2.02(10)$. *Middle panel:* The same as a function of m_π/m_ρ. In this case the last point is omitted from the fit. The best fit of the form $c(m_\pi/m_\rho)^z$ is at $c = 0.476(77)$, $z = -6.03(41)$. *Right panel:* Power fit of autocorrelation for the smallest eigenvalue of $\tilde{Q}^2$ given in units of $10^6 \times$ MVM as a function of the dimensionless quark mass parameter M_r. The best fit of the form cM_r^z is at $c = 5.36(80)$, $z = -1.48(25)$

matrix. This happened namely in one run, run (i). The (three) configurations are however statistically insignificant, since the corresponding reweighting factors are extremely small: 2.7×10^{-2}, 8.2×10^{-4} and 3.0×10^{-4}. Statistically they represent less than 0.03 configurations in a sample with a total statistical weight of about 1600.

3.2.3 Results for autocorrelations

The analysis of the runs specified in Table 2 gives the results for physical quantities collected in Table 3. The integrated autocorrelations, where they could be determined, are given in Table 4.

The quoted errors of autocorrelations were estimated in different ways. For the determination of the autocorrelation of the pion mass we apply the blocking method explained in Sect. 3.2.1. In general, one has to say that in some cases our statistics is only marginal for a precise determination of the integrated autocorrelations. In some cases (run (a), (j)) we are not able to quote a reliable result for the autocorrelation of the pion mass.

In the high statistics runs with small quark masses (e), (f), (g), (h) and (i) we had four independent parallel update sequences which could be used for a crude estimate of the errors. In addition, whenever the runs were long enough, we used binning with increasing bin lengths for the error estimates.

In general, integrated autocorrelations of the average plaquette are longest. Those for the smallest eigenvalue are comparable but sometimes by a factor 2–3 shorter. The important case of $\tau_{\rm int}^{m_\pi}$ is the most favorable among the quantities we have considered: it is by a factor 2 to 10 shorter than $\tau_{\rm int}^{\rm plaq}$. Our experience was that the best values for $\tau_{\rm int}^{m_\pi}$ could be achieved in runs where the lower limit of the approximation interval ϵ was at least by a factor of 2–3 smaller than the typical smallest eigenvalue of $\tilde{Q}^2$

Table 4. Integrated autocorrelations in update cycles obtained from runs specified by Table 2. In the second column $C_{\rm cycle}$ gives the number of kMVMs (10^3 MVMs) per update cycle. The suffices min, plaq, $\pi 8$ and m_π refer to the minimal eigenvalue of $\tilde{Q}^2$, the average plaquette, the pion correlator at distance $d = 8$ and the pion mass, respectively

Run	$C_{\rm cycle}$	$\tau_{\rm int}^{\rm min}$	$\tau_{\rm int}^{\rm plaq}$	$\tau_{\rm int}^{\pi 8}$	$\tau_{\rm int}^{m_\pi}$
(a)	1.49	–	200(20)	–	–
(b)	2.45	340(60)	350(50)	152(20)	140(20)
(c)	4.35	–	420(80)	–	150(20)
(d)	5.05	$\simeq 310$	490(90)	–	170(90)
(e)	7.34	550(110)	490(40)	274(41)	207(33)
(f)	7.31	810(110)	800(90)	367(110)	187(63)
(g)	10.5	320(80)	820(180)	466(62)	188(13)
(h)	16.2	380(120)	940(330)	370(88)	186(40)
(i)	20.4	670(210)	1500(300)	283(67)	153(54)
(j)	17.4	$\simeq 390$	$\simeq 1050$	–	–

and the multi-boson fields were relatively often updated by the global quasi-heatbath.

Using the values given in Table 4 one can extract, for instance, the behavior of $\tau_{\rm int}^{\rm plaq}$ as a function of the dimensionless quark mass parameter M_r. Since, according to Table 3, the different runs are at slightly different values of r_0/a, one can correct the points with an assumed power $z_a = 2$ to a common value, say, $r_0/a = 1.8$. The resulting behavior is shown by Fig. 3 (left panel) where a two-parameter fit cM_r^z is also shown. The best fit is at $c = 7.92(68)$ (10^6 MVMs), $z = -2.02(10)$ with a χ^2 per number of degrees of freedom of $\chi^2/{\rm d.o.f.} = 1.8$. (The result for z remains the same if the common value of r_0/a is changed in the interval $1.6 \leq r_0/a \leq 2.0$.)

The alternative parameterization in (2) suggests a power fit as a function of m_π/m_ρ. A good fit can only be

obtained in this case if the last point with the largest quark mass is omitted (see Fig. 3, middle panel). The best-fit parameters are in this case $c = 0.476(77)$, $z = -6.03(41)$ with $\chi^2/\text{d.o.f.} = 1.1$. The obtained power agrees very well with $z_{\pi\rho} = 6$ in (2) given by the CP-PACS, JLQCD Collaboration although the latter value was obtained in a range of substantially larger quark masses on large lattices.

The data on the integrated autocorrelation of the smallest eigenvalues $\tau_{\text{int}}^{\text{min}}$ typically have larger errors. A fit of the form cM_r^z is shown in Fig. 3 (right panel) where $c = 5.36(80)$, $z = -1.48(25)$ with $\chi^2/\text{d.o.f} = 2.4$. A fit to the integrated autocorrelation of the pion mass $\tau_{\text{int}}^{m_\pi}$ gives similar parameters: $c = 1.99(16)$, $z = -1.47(16)$ with $\chi^2/\text{d.o.f} = 1.7$. This shows that for $\tau_{\text{int}}^{\text{min}}$ and $\tau_{\text{int}}^{m_\pi}$ the quark mass dependence is described by $z_\pi \simeq 3$ which is, of course, more favorable than $z_\pi \simeq 4$ for $\tau_{\text{int}}^{\text{plaq}}$.

Concerning the quality of fits one has to remark that the different points belong to individually different optimizations of the polynomial parameters which have not necessarily the same quality. This implies an additional fluctuation beyond statistics. In view of this the χ^2 per number of degrees of freedom values are reasonably good.

4 Eigenvalue spectra

The eigenvalue spectrum of the Wilson–Dirac matrix is interesting both physically and from the point of view of simulation algorithms. From the physical point of view the low-lying eigenvalues are expected to dominate the hadron correlators [28,29] and carry information about the topological content of the background gauge field [30–32]. Although, as already stressed, in the present work we consider rather coarse lattices, given the importance of the question, it is interesting to see the effect of the determinant of light quarks on the qualitative properties of the eigenvalue spectrum. From the algorithmic point of view knowledge of the low-lying eigenvalues is crucial for the optimization of polynomial approximations. Finally, since we plan to perform simulations with an odd number of flavors [33], we have to consider the possibility of negative (real) eigenvalues of the non-hermitean quark matrix Q, which would imply a negative determinant for a single quark flavor. For $N_f = 2$ the square of the determinant is relevant; therefore, the sign does not matter, but the absence (or statistical insignificance) of negative eigenvalues at very small quark masses would strongly support the assumption that for the heavier strange quark there will be no problem with the determinant sign.

In order to study the low-lying spectrum of the eigenvalues we used two methods: for the eigenvalues of the hermitean fermion matrix with small absolute value the one by Kalkreuther and Simma [34] and for small eigenvalues of the non-hermitean matrix the Arnoldi method [35, 36]. The determination of the eigenvalues of the hermitean matrix is in general much faster. However, the spectrum of the non-hermitean fermion matrix contains more information. First of all, the eigenvalues of Q depend trivially on the valence hopping parameter κ_{val}, because

$$Q = 1 - \kappa_{\text{val}} D. \tag{44}$$

This is not true for $\tilde{Q}$. Moreover, because of the symmetries

$$Q^\dagger = \gamma_5 Q \gamma_5, \quad ODO = -D, \tag{45}$$

where $O_{xy} = (-1)^{(x1+x2+x3+x4)}\delta_{xy}$, the spectrum of D is invariant under complex conjugation and sign change. As a consequence, it is sufficient to compute the low-lying spectrum of Q at an arbitrary value $\kappa_{\text{val}} = \bar{\kappa}_{\text{val}}$. Other κ_{val} are easily obtained by a shift. The value of $\bar{\kappa}_{\text{val}}$ is chosen such that it gives the best compromise of computation time and precision.

It turned out that the application of the Arnoldi algorithm is more efficient on the even–odd preconditioned matrix $\bar{Q}$ than on Q itself. The analytic relation between the eigenvalues of $\bar{Q}$ and Q can be used to transform the result back to Q. Indeed if Q is written in the form

$$Q = 1 - \kappa \begin{pmatrix} 0 & D_{\text{eo}} \\ D_{\text{oe}} & 0 \end{pmatrix}, \tag{46}$$

then $\bar{Q}$ is given by

$$\bar{Q} = 1 - \kappa^2 \begin{pmatrix} 0 & 0 \\ 0 & D_{\text{oe}} D_{\text{eo}} \end{pmatrix}. \tag{47}$$

If $v = (v_{\text{e}}, v_{\text{o}})$ is an eigenvector of Q with eigenvalues λ then it satisfies

$$(\lambda v_{\text{e}}, \lambda v_{\text{o}}) = (v_{\text{e}} - \kappa D_{\text{eo}} v_{\text{o}}, v_{\text{o}} - \kappa D_{\text{oe}} v_{\text{e}}) \tag{48}$$

and hence

$$(1 - \kappa^2 D_{\text{oe}} D_{\text{eo}}) v_{\text{o}} = v_{\text{o}} - (1-\lambda)^2 v_{\text{o}} = \lambda(2-\lambda) v_{\text{o}}. \tag{49}$$

As a result, the eigenvalues of $\bar{Q}$ are either 1 (in the even subspace) or they satisfy

$$\bar{\lambda} = \lambda(2-\lambda). \tag{50}$$

Because of the symmetries mentioned above, the solutions of (50) will give precisely all the eigenvalues of the matrix Q. This relation also gives a possibility to perform a non-trivial check of the Arnoldi code. (In addition, we also compared the algorithm with a direct computation of all the eigenvalues on a small 4^4 lattice by means of a NAG library routine.) All checks confirmed the high precision given as an output by the ARPACK code, which was, in our cases, always better than 10^{-4} (relative precision).

4.1 Small eigenvalues

As a first task we computed the low-lying eigenvalues from sample sets of 10 configurations for runs in decreasing order of quark masses, namely those labeled with (a) and (c)–(j) in Table 2. In order to have a better access to the most interesting regions of the spectrum we analyzed

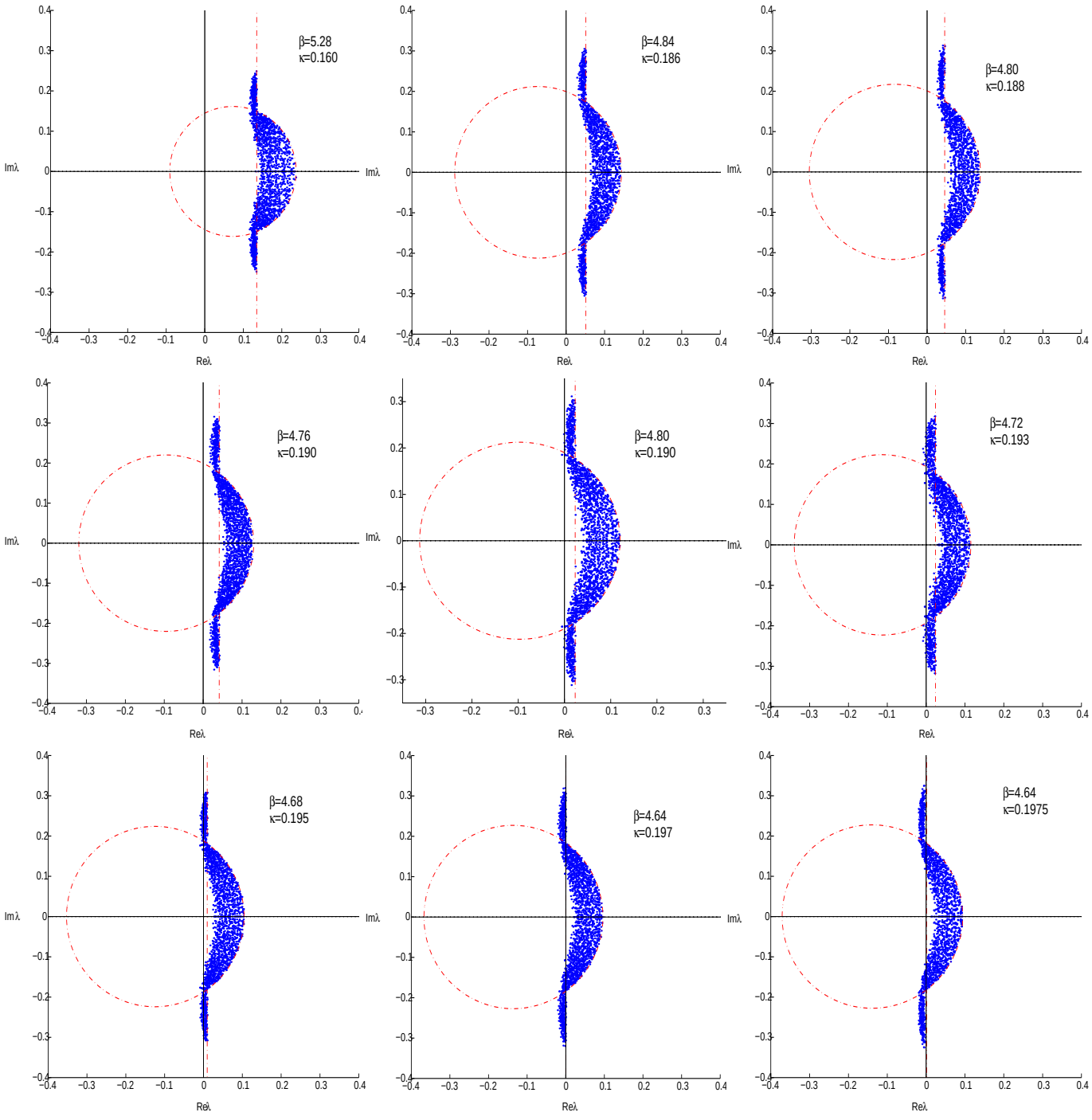

Fig. 4. Low-lying eigenvalues from a set of $\mathcal{O}(10)$ configurations for runs (a), (c) to (j)

each configuration from two different points of view. For each configuration we first determined the 150 eigenvalues of the preconditioned Wilson–Dirac matrix ($\bar{Q}$) with smallest modulus and then the 50 eigenvalues of the non-preconditioned one (Q) with smallest real part.

Both computations were performed at an auxiliary value of $\kappa_{\rm val} = 0.170$, where the Arnoldi algorithm performed better. By using the analytical relations (44) and (50) we transformed the eigenvalues to those of Q at the κ value of the dynamical updates ($\kappa \equiv \kappa_{\rm sea}$). The results are plotted in Fig. 4. The dashed vertical line shows the limit for the computation of the eigenvalues with smallest real part: only the part of the spectrum to the left of this line is known. In a similar way, by computing the eigenvalues with smallest modulus, we have access to the portion of the spectrum inside the dashed circle. The circle is deformed and not centered at the origin because it has been transformed together with the eigenvalues by using (50).

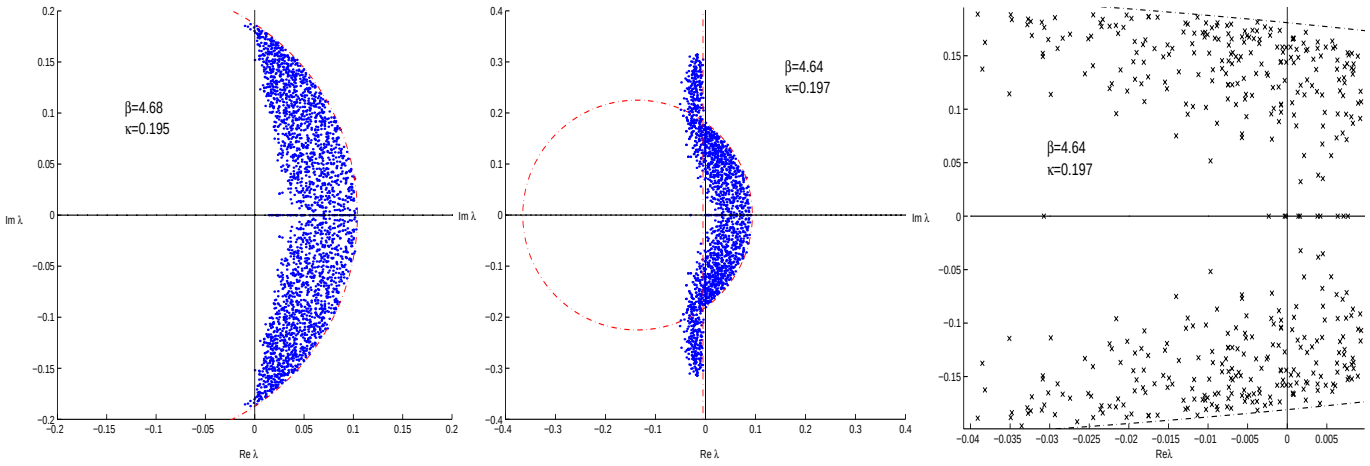

Fig. 5. Low-lying eigenvalues for a set of 10 configurations with exceptionally small eigenvalues, at $\beta = 4.68$ and $\kappa = 0.195$ (*left panel*), $\beta = 4.64$ and $\kappa = 0.197$ (*middle panel*), detail (*right panel*)

In summary, the spectrum is not known in those points of the complex plane which are both to the right of the vertical line *and* outside the circle.

Since the sequence from (a) to (j) corresponds to decreasing quark masses it is not a surprise that the eigenvalues have an increasing tendency to go to the left in the complex plane. At the same time they are pushed away from zero as an effect of including the fermionic determinant in the path integral measure. At very small quark masses a pronounced hole near zero is developing. For the continuum Dirac operator the spectrum is on a vertical line with some gap near zero. On our coarse lattices there is an additional horizontal spread of the eigenvalues and the picture is strongly deformed.

The size of the holes produced by the determinant is very important if we have in mind the possibility of computing observables at a *partially quenched* $\kappa_{\rm val}$ higher than $\kappa_{\rm sea}$ used in the update. The distance between the origin and the smallest real eigenvalue determines how much smaller masses (larger $\kappa_{\rm val}$) one can reach by partial quenching before encountering exceptional configurations. This question can be answered by studying configurations with exceptionally small eigenvalues. Of course, the reweighting factors discussed in Sect. 3.2.2 have to be taken into account in this analysis because they suppress such configurations to a large extent.

4.2 Negative eigenvalues

One of the purposes of the analysis of the eigenvalues was to determine whether there is a statistically significant presence of configurations with negative determinant. As already said, the sign of the determinant is easy to determine from the low-lying spectrum since it is negative if an odd number of real negative eigenvalues occurs. In fact, non-real eigenvalues always appear in conjugate pairs. In the randomly chosen set of configurations reported above we did not find a single real negative eigenvalue. However, a set of $\mathcal{O}(10)$ configurations is a rather small subsample.

Additional information on the presence or absence of negative eigenvalues in our samples is given by the distribution of reweighting factors. Crossing of eigenvalues to negative real axis implies small reweighting factors corresponding to very small eigenvalues of $\tilde{Q}^2$ below the lower bound of the interval $[\epsilon, \lambda]$. The calculation of reweighting factors, which was carried out on every configuration in the selected subsamples, is much cheaper than the analysis of small eigenvalues of the non-hermitean matrix Q. As we discussed in Sect. 3.2.2, the distribution of reweighting factors is strongly peaked near 1 in all runs, except for runs (h) and (i) which have high statistics at very small quark masses (see Fig. 1). In these cases there are a few configurations with reweighting factors close to zero. In order to see whether the small reweighting factors (and the corresponding small eigenvalues of $\tilde{Q}^2$) are associated to negative eigenvalues or not, we concentrated on configurations with particularly small eigenvalues of $\tilde{Q}^2$.

Note that there is no simple analytical relation between the lowest eigenvalues of the hermitean and the non-hermitean matrix, but it is reasonable to expect that small eigenvalues occur together. This expectation was confirmed in all cases we investigated. An interesting observation was that very small eigenvalues of the hermitean matrix seem to be usually associated to small *real* eigenvalues of the non-hermitean one. This is compatible with the fact that real eigenvalues do not need to be double degenerate and therefore they can afford one to approach closer to the origin than a complex conjugate pair.

In Fig. 5 two significant examples are reported. The first set of configurations in the figure corresponds to a moderately small quark mass (run (h)) and the second to a very small quark mass (run (i)). In both cases we selected the configurations with smallest eigenvalues of $\tilde{Q}^2$. Even in this way we could not find a single real negative eigenvalue for the first run (h). In the second case we found three configurations with negative eigenvalues. The (in total) four negative eigenvalues are visible in the detail in the right panel of Fig. 5. As stated before these configurations are statistically insignificant.

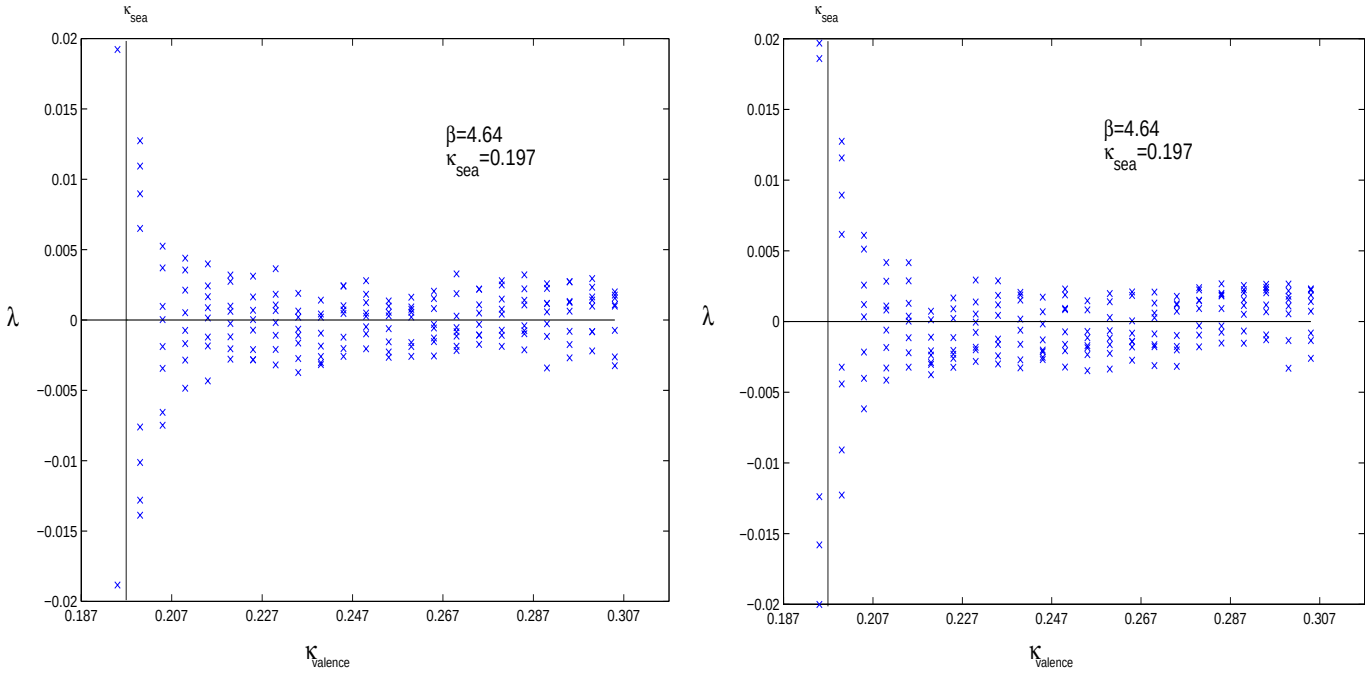

Fig. 6. Computation of 8 eigenvalues closest to zero of the hermitean Wilson–Dirac matrix for two configurations from the run at $\beta = 4.64$ and $\kappa = 0.197$

Some comments are in order. We have collected strong evidence that the presence of configurations with negative determinant is irrelevant at this stage. Of course it is not yet possible to tell how this picture will evolve on larger volumes and closer to the continuum limit. It will be necessary to keep monitoring the low part of the spectrum as we did here. Since, to that purpose, we only need to know a very small part of the spectrum, there is no reason to think that this task should become too difficult on large volumes.

As a last remark we should stress that we performed this analysis of the sign for very small quark masses. Even if (partially quenched) chiral perturbation theory is valid for any combination of the quark masses, it is probably not worth having an unpaired sea quark with a mass much smaller than the strange quark. Therefore, provided that the picture will not dramatically change on larger lattices, for all *physical* circumstances it seems very unlikely that the determinant sign could become a problem.

4.3 Flow of eigenvalues

By using the algorithm of Kalkreuther and Simma [34] we also explored the flow of the spectrum $\{\tilde{\lambda}\}$ of the hermitean matrix $\tilde{Q}$ for a wide range of valence κ values, going from zero bare quark mass to a large negative one. This is interesting in view of simulations of dynamical fermions with Neuberger's operator [37], where the inverse square root of $\tilde{Q}^2$ with negative valence mass has to be taken. The optimal valence mass should be chosen in a region where $\tilde{Q}$ has no eigenvalues extremely close to zero, namely where a "gap" is opening up in the spectrum near $\tilde{\lambda} = 0$. The results for two typical configurations are plotted in Fig. 6. For large negative masses we observed many sign changes, and the eigenvalue with smallest absolute value is always close to zero. It seems that for dynamical Wilson fermions on our coarse lattice there is no gap-opening near $\tilde{\lambda} = 0$.

A possible application of the eigenvalue flow is to monitor the number of negative eigenvalues at $\kappa = \kappa_{\rm sea}$ [38, 19]. This is substantially cheaper than the analysis of the spectrum of the non-hermitean matrix Q by the Arnoldi method. For instance, observing the eigenvalue flow one can easily exclude the absence of negative eigenvalues if there is no crossing of zero in the flow below $\kappa_{\rm sea}$ – which is the typical case. A more detailed (and more expensive) analysis can be restricted to the rare case when a crossing occurs.

5 Discussion

Our runs on $8^3 \times 16$ lattices with a lattice spacing of about $a \simeq 0.27\,\mathrm{fm}$ for $N_f = 2$ degenerate quarks display the dependence of simulation costs on the quark mass. Assuming the parameterization in (1) with $z_L = 5$ and $z_a = 2$, from the integrated autocorrelation of the average plaquette we obtain

$$z_\pi \simeq 4, \quad F \simeq 0.8 \times 10^9\,\mathrm{flop}. \tag{51}$$

The power for the quark mass dependence z_π comes out smaller than $z_{\pi\rho} = 6$ in the form (2) quoted by the CP-PACS, JLQCD Collaboration [6] but if we omit the point with largest quark mass and perform a fit with the parametrization (2), we also obtain $z_{\pi\rho} \simeq 6$ (see Fig. 3).

As shown by Fig. 3 (left panel), our data on the integrated autocorrelation of the average plaquette are well

fitted by $z_\pi = 4$ in the whole range $0.6 \leq M_r \leq 6$ which approximately corresponds to $(1/5)m_s \leq m_{ud} \leq 2m_s$. The data on the integrated autocorrelation of the smallest eigenvalue of the squared hermitean fermion matrix show an even weaker power $z_\pi \simeq 3$, but there the errors are larger and the fit is less convincing (see right panel in Fig. 3). The pion mass has the shortest autocorrelation; this also shows a power $z_\pi \simeq 3$. $z_\pi = 4$ corresponds to a behavior proportional to the inverse square of the quark mass. Qualitatively speaking, according to Table 4, one inverse quark mass power is due to the increase of the condition number of the fermion matrix and another inverse power comes from the increase of the autocorrelation in numbers of update cycles. Note that because of $(r_0 m_\pi)^2 \propto (r_0 m_q)$ the case of $z_\pi = 4$, $z_a = 2$ corresponds to a situation when the scale parameter r_0 cancels in the cost formula (1).

The overall factor F given in (51) is such that for our second smallest quark mass $M_r \simeq 0.6$ (run (i)) the cost in floating point operations turns out to be $C \simeq 2.3 \times 10^{14}$. As Table 4 shows, considering instead of the integrated autocorrelation of the average plaquette the one of the pion mass, the result is $C \simeq 0.4 \times 10^{14}$. The parameters in (2) give the same number. The other estimates for Wilson-type quarks in [5] and [7] in this point are $C_L \simeq 0.2 \times 10^{14}$ and $C_W \simeq 1.1 \times 10^{14}$, respectively. Taking into account that the numbers $C_{U,L,W}$ have been obtained under rather different circumstances concerning simulation algorithm, autocorrelations considered, quark mass range, lattice size and even lattice action, there is a surprisingly good order of magnitude agreement.

It is remarkable that in a rather broad range of quark masses $(1/5)m_s \leq m_{ud} \leq m_s$ (leaving out the point at $m_{ud} \simeq 2m_s$) two fits with $z_\pi = 4$ and $z_{\pi\rho} = 6$ work equally well (Fig. 3). This implies in this range of quark masses a peculiar dependence of m_π/m_ρ on M_r (see Fig. 7, where the relation between the two different quark mass parameters μ_r and M_r is also shown). However, the two parameterizations in (1) and (2) cannot be both correct in the vicinity of zero quark mass because there the two powers have to be equal: $z_{\pi\rho} = z_\pi$. Putting it differently, the extrapolations of the two fits below $m_{ud} = (1/5)m_s$ are different. The fit with $z_{\pi\rho} = 6$ gives a more dramatic slowing down near zero quark mass than the one with $z_\pi = 4$. The real asymptotics near $m_{ud} = 0$ could be disentangled by going to still smaller quark masses. With TSMB there is no serious obstacle for doing this – except for the increase in necessary computer time.

The value of the lattice spacing in this paper is chosen rather large in order to limit the computational costs for these tests. Our aim was to concentrate on the quark mass dependence in the range of light quarks. Further studies will be needed for investigating the cost as a function of the lattice spacing (in particular, the value of the exponent z_a) for smaller values of a. In this respect the experience of the DESY–Münster–Roma Collaboration in the supersymmetric Yang–Mills theory at much smaller lattice spacings ($a \simeq 0.06$fm) [19,20] shows already that TSMB has a decent behavior also closer to the continuum limit.

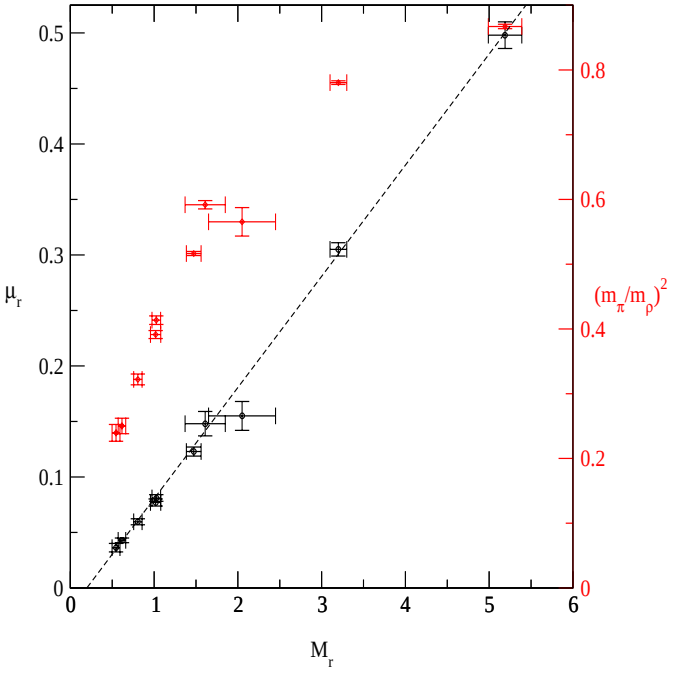

Fig. 7. The dependence of $(m_\pi/m_\rho)^2$ on M_r according to Table 3 (*right values*). The values of μ_r are also shown (*left*) together with a linear fit (*dashed line*)

Besides the quark mass dependence of simulation costs, the other interesting question we investigated in this paper is the distribution of the small eigenvalues of the fermion matrix and, in particular, the existence of negative fermion determinants of a single quark flavor. Our data show that the effect of the fermion determinant is rather explicit because of the strong suppression of the eigenvalue density near zero (see Figs. 4–5). The statistical weight of configurations with negative determinant is negligible even at our smallest quark masses. In fact after an extensive analysis we only found three configurations with negative determinant at our second smallest quark mass $M_r \simeq 0.6$ (run (i)) and none of them at other quark masses. Taking into account the small reweighting factors of the configurations with negative determinant, their relative statistical weight is $\mathcal{O}(10^{-5})$.

It is clear that it would be important to check the volume dependence of our results, both for simulation costs and small eigenvalues, on larger lattices and closer to the continuum limit. We plan to do this in the future.

Acknowledgements. The computations were performed on the APEmille systems installed at NIC Zeuthen, the Cray T3E systems at NIC Jülich and the PC clusters at DESY Hamburg. We thank H. Simma for help with APEmille programming and optimization, M. Lüscher for providing his SSE code, H. Wittig for useful discussions on various topics, T. Kovacs and W. Schroers for sharing with us their experience with the computation of eigenvalues, and R. Peetz for careful reading of the manuscript.

References

1. S.R. Sharpe, N. Shoresh, Phys. Rev. D **62**, 094503 (2000), hep-lat/0006017
2. N.H. Christ, Nucl. Phys. Proc. Suppl. **106**, 187 (2002)
3. S. Gottlieb, Nucl. Phys. Proc. Suppl. **106**, 189 (2002), hep-lat/0112039
4. K. Jansen, Nucl. Phys. Proc. Suppl. **106**, 191 (2002), hep-lat/0111062
5. TXL, Th. Lippert, Nucl. Phys. Proc. Suppl. **106**, 193 (2002), hep-lat/0203009
6. CP-PACS, JLQCD, A. Ukawa, Nucl. Phys. Proc. Suppl. **106**, 195 (2002)
7. H. Wittig, Nucl. Phys. Proc. Suppl. **106**, 197 (2002), hep-lat/0203021
8. R. Sommer, Nucl. Phys. B **411**, 839 (1994), hep-lat/9310022
9. ALPHA, R. Frezzotti, M. Hasenbusch, U. Wolff, J. Heitger, K. Jansen, Comput. Phys. Commun. **136**, 1 (2001), hep-lat/0009027
10. I. Montvay, Nucl. Phys. B **466**, 259 (1996), hep-lat/9510042
11. CP-PACS, A. Ali Khan et al., Phys. Rev. D **65**, 054505 (2002), hep-lat/0105015
12. I. Montvay, Nucl. Phys. Proc. Suppl. **83**, 188 (2000), hep-lat/9909020
13. M. Lüscher, Nucl. Phys. B **418**, 637 (1994), hep-lat/9311007
14. I. Montvay (2001), hep-lat/0112007
15. Ph. de Forcrand, Phys. Rev. E **59**, 3698 (1999), cond-mat/9811025
16. Y. Iwasaki, K. Kanaya, S. Sakai, T. Yoshie, Phys. Rev. Lett. **67**, 1494 (1991)
17. T. Blum et al., Phys. Rev. D **50**, 3377 (1994), hep-lat/9404006
18. UKQCD, C.R. Allton et al., Phys. Rev. D **47**, 5128 (1993), hep-lat/9303009
19. DESY–Münster, I. Campos et al., Eur. Phys. J. C **11**, 507 (1999), hep-lat/9903014
20. DESY–Münster–Roma, F. Farchioni et al. (2001), hep-lat/0111008
21. UKQCD, R.M. Baxter et al., Phys. Rev. D **49**, 1594 (1994), hep-lat/9308020
22. C. Michael, Nucl. Phys. B **259**, 58 (1985)
23. S. Perantonis, A. Huntley, C. Michael, Nucl. Phys. B **326**, 544 (1989)
24. UKQCD, C.R. Allton et al., Phys. Rev. D **65**, 054502 (2002), hep-lat/0107021
25. M. Lüscher, U. Wolff, Nucl. Phys. B **339**, 222 (1990)
26. R.G. Edwards, U.M. Heller, T.R. Klassen, Nucl. Phys. B **517**, 377 (1998), hep-lat/9711003
27. I. Montvay, G. Münster, (Cambridge, 1994), p. 491 (Cambridge monographs on mathematical physics)
28. T.L. Ivanenko, J.W. Negele, Nucl. Phys. Proc. Suppl. **63**, 504 (1998), hep-lat/9709130
29. H. Neff, N. Eicker, Th. Lippert, J.W. Negele, K. Schilling, Phys. Rev. D **64**, 114509 (2001), hep-lat/0106016
30. T. DeGrand, A. Hasenfratz, Phys. Rev. D **65**, 014503 (2002)
31. T.G. Kovacs (2001), hep-lat/0111021
32. QCDSF, R. Horsley, T.G. Kovacs, V. Linke, D. Pleiter, G. Schierholz, Nucl. Phys. Proc. Suppl. **106**, 569 (2002), hep-lat/0111030
33. F. Farchioni, C. Gebert, I. Montvay, W. Schroers, Nucl. Phys. Proc. Suppl. **106**, 215 (2002), hep-lat/0110130
34. T. Kalkreuter, H. Simma, Comput. Phys. Commun. **93**, 33 (1996), hep-lat/9507023
35. R.B. Lehoucq, D.C. Sorensen, C. Yang, 1997, http://www.caam.rice.edu/software/ARPACK/
36. K. Maschhoff, D.C. Sorensen, 1996, http://www.caam.rice.edu/software/ARPACK/
37. H. Neuberger, Phys. Lett. B **417**, 141 (1998), hep-lat/9707022
38. R.G. Edwards, U.M. Heller, R. Narayanan, Nucl. Phys. B **535**, 403 (1998), hep-lat/9802016

Note added in proof. After submitting this paper for publication we realized that the results on m_π and f_π in Table 3 – if plotted as $M_r/(2\mu_r)$ versus M_r and $f_\pi r_0$ versus M_r, respectively, – qualitatively show the expected behavior with chiral logarithms in chiral perturbation theory (see [39]).

39. F. Farchioni, C. Gebert, I. Montvay, L. Scorzato (2002), hep-lat/0209142

[Chi-1]

Partially quenched chiral perturbation theory and numerical simulations

Phys. Lett. B561 102-110 (2003)

Available online at www.sciencedirect.com
SCIENCE DIRECT®
PHYSICS LETTERS B
ELSEVIER
Physics Letters B 561 (2003) 102–110
www.elsevier.com/locate/npe

Partially quenched chiral perturbation theory and numerical simulations

qq + q Collaboration

F. Farchioni [a], C. Gebert [b], I. Montvay [b], E. Scholz [b], L. Scorzato [b]

[a] *Westfälische Wilhelms-Universität Münster, Institut für Theoretische Physik, Wilhelm-Klemm-Strasse 9, D-48149 Münster, Germany*

[b] *Deutsches Elektronen-Synchrotron, DESY, Notkestr. 85, D-22603 Hamburg, Germany*

Received 20 February 2003; received in revised form 7 March 2003; accepted 8 March 2003

Editor: P.V. Landshoff

Abstract

The dependence of the pseudoscalar meson mass and decay constant is compared to one-loop partially quenched chiral perturbation theory (PQChPT) in a numerical simulation with two light dynamical quarks. The characteristic behaviour with chiral logarithms is observed. The values of the fitted PQChPT-parameters are in a range close to the expectation in continuum in spite of the fact that the lattice spacing is still large, namely $a \simeq 0.28$ fm.

1. Introduction

In numerical Monte Carlo simulations of QCD chiral perturbation theory (ChPT) [1] is often used to guide the extrapolation to the physical values of the three light quark masses ($m_u \simeq m_d$ and m_s). In this procedure not only the lattice gauge theory results are established but also useful information is obtained about the values of the *Gasser–Leutwyler parameters* of ChPT. In fact, recently several groups explored this possibility in quenched [2] and unquenched simulations with Wilson-type [3] and staggered [4,5] quarks. (For a review see [6].)

In order to achieve small systematic errors the simulations themselves have to be performed in a range of quark masses where the applied one-loop (NLO) ChPT-formulas give a good approximation. In particular, the characteristic *chiral logarithms* have to appear in the quark mass dependence of different physical quantities. This applies both to original ChPT as well as to PQChPT [7,8]. However, in most recent simulations—especially with Wilson-type quarks—this condition is not fulfilled because they are performed in the range $m_{u,d} \geqslant \frac{1}{2}m_s$. Estimates based on present knowledge of the ChPT parameters indicate (see, for instance, [9]) that at least $m_{u,d} \leqslant \frac{1}{4}m_s - \frac{1}{5}m_s$ has to be reached. (See also the summary of the panel discussion at the Boston lattice conference [10].) Another

E-mail address: montvay@mail.desy.de (I. Montvay).

0370-2693/03/$ – see front matter
doi:10.1016/S0370-2693(03)00386-1

requirement is that the virtual effects of the s-quark also has to be taken into account by simulating with three light dynamical quarks.

Since the dynamical quarks in most unquenched simulations do not satisfy the above bound, it is not surprising that the chiral logarithms have not been observed [11–16]. This was the main motivation of our collaboration to start exploring the possibility of simulating QCD with light quarks in the range $m_{ud} \leqslant \frac{1}{2}m_s$ [17–21]. In these simulations we use the *two-step multi-boson* (TSMB) algorithm for dynamical fermions [22] and consider for the moment $N_s = 2$ dynamical "sea" quarks. The case of $N_s = 3$ is also under study [23]. Our first simulations were oriented towards the investigation of simulation costs as a function of the quark mass and were performed on modest size lattices (typically $8^3 \cdot 16$) with lattice spacings of the order $a \simeq 0.27$ fm—a value where continuum behaviour is not necessarily expected. Therefore, it came to us as a surprise that plotting the pseudoscalar ("pion") mass and decay constant as a function of the quark mass (in the form suggested by [24,25]) the chiral logarithmic behaviour has been qualitatively displayed [19,20].

Encouraged by this result we picked out a point with $m_{ud} \simeq \frac{1}{4}m_s$ and performed a high statistics run on 16^4 lattice in order to study the dependence on the valence quark mass in a sufficiently large physical volume. This has the advantage that by taking ratios of the masses and decay constants the Z-factors of renormalization cancel. This removes an uncertainty in [19,20] where the Z-factors have been neglected by setting them to $Z \equiv 1$. In our analysis of simulation data we applied PQChPT for Wilson lattice fermions [26] which take into account leading lattice artefacts of $\mathcal{O}(a)$.

The plan of this Letter is as follows: in the next section the one-loop PQChPT formulas for Wilson lattice fermions will be recapitulated. In Section 3 the numerical simulation data will be analyzed and discussed.

2. PQChPT formulas

Our analysis of the valence quark dependence of the pseudoscalar mass (m_π) and decay constant (f_π) is based on the one-loop PQChPT formulas for the Wilson lattice action as derived in [26]. Instead of the quantities with dimension mass-square χ_A and ρ_A of Ref. [26] we prefer to use the dimensionless ones

$$\chi_A \equiv \frac{2B_0 m_q}{f_0^2}, \qquad \rho_A \equiv \frac{2W_0 a c_{SW}}{f_0^2}. \tag{1}$$

Here m_q is the quark mass, a the lattice spacing, B_0 and W_0 are parameters of dimension mass and (mass)^3, respectively, which appear in the leading order (LO) chiral effective Lagrangian, c_{SW} is the coefficient of the $\mathcal{O}(a)$ chiral symmetry breaking term and f_0 is the value of the pion decay constant at zero quark mass. (Its normalization is such that the physical value is $f_0 \simeq 93\,\text{MeV}$.) In Ref. [26] the case of three non-degenerate quark flavours is considered. Here we consider a general number N_s of equal mass sea quarks.

The next to leading order (NLO) PQChPT formula for the pion decay constant is in this case:

$$\begin{aligned}
\frac{f_{AB}}{f_0} = 1 &- \frac{N_s}{128\pi^2}\Big\{(\chi_A+\chi_S+\rho_A+\rho_S)\log\Big(\frac{1}{2}(\chi_A+\chi_S+\rho_A+\rho_S)\Big) \\
&\qquad + (\chi_B+\chi_S+\rho_B+\rho_S)\log\Big(\frac{1}{2}(\chi_B+\chi_S+\rho_B+\rho_S)\Big)\Big\} \\
&+ \frac{1}{64N_s\pi^2}\Big\{\chi_A+\chi_B+\rho_A+\rho_B-2\chi_S-2\rho_S+(\chi_B-\chi_A+\rho_B-\rho_A)^{-1} \\
&\qquad \times\Big[2(\chi_A+\rho_A)(\chi_B+\rho_B)-(\chi_S+\rho_S)(\chi_A+\chi_B+\rho_A+\rho_B)\log\Big(\frac{\chi_A+\rho_A}{\chi_B+\rho_B}\Big)\Big]\Big\} \\
&+ 2\bar{L}_5(\chi_A+\chi_B)+2\overline{W}_5(\rho_A+\rho_B)+4N_s\bar{L}_4\chi_S+4N_s\overline{W}_4\rho_S.
\end{aligned} \tag{2}$$

Here A and B denote generic quark indices: S will be the label for the sea quarks V for valence quarks. For the pion mass squared we have:

$$\begin{aligned}\frac{m_{AB}^2}{f_0^2} &= \frac{1}{2}(\chi_A+\chi_B+\rho_A+\rho_B)+\frac{1}{32N_s\pi^2}\frac{(\chi_A+\chi_B+\rho_A+\rho_B)}{(\chi_B-\chi_A+\rho_B-\rho_A)}\\ &\quad\times\big\{(\chi_A+\rho_A)(\chi_S-\chi_A+\rho_S-\rho_A)\log(\chi_A+\rho_A)\\ &\qquad-(\chi_B+\rho_B)(\chi_S-\chi_B+\rho_S-\rho_B)\log(\chi_B+\rho_B)\big\}\\ &\quad+4N_s\big(2\bar{L}_6-\bar{L}_4\big)\chi_S(\chi_A+\chi_B)+2\big(2\bar{L}_8-\bar{L}_5\big)(\chi_A+\chi_B)^2\\ &\quad+4N_s\big(\overline{W}_6-\bar{L}_4\big)\chi_S(\rho_A+\rho_B)+4N_s\big(\overline{W}_6-\overline{W}_4\big)\rho_S(\chi_A+\chi_B)\\ &\quad+2\big(2\overline{W}_8-\overline{W}_5-\bar{L}_5\big)(\chi_A+\chi_B)(\rho_A+\rho_B).\end{aligned}\tag{3}$$

The NLO parameters $\bar{L}_k$ and $\overline{W}_k$ are related to L_k and W_k in Refs. [9,26] by

$$\bar{L}_k \equiv L_k - c_k\log\big(f_0^2\big),\qquad \overline{W}_k \equiv W_k - d_k\log\big(f_0^2\big),\tag{4}$$

where the coefficients of the logarithms are given by

$$c_4=\frac{1}{256\pi^2},\qquad c_5=\frac{N_s}{256\pi^2},\qquad c_6=\frac{(N_s^2+2)}{512N_s^2\pi^2},\qquad c_8=\frac{(N_s^2-4)}{512N_s\pi^2},\tag{5}$$

respectively,

$$d_4=\frac{1}{256\pi^2},\qquad d_5=\frac{N_s}{256\pi^2},\qquad d_6=\frac{(N_s^2+2)}{256N_s^2\pi^2},\qquad d_8=\frac{(N_s^2-4)}{256N_s\pi^2}.\tag{6}$$

The relations in (4) have the unpleasant feature that logarithms of a dimensionful quantity appear. One can avoid this by introducing

$$L_k' \equiv L_k - c_k\log\big(\mu^2\big),\qquad W_k' \equiv W_k - d_k\log\big(\mu^2\big),\tag{7}$$

where μ is the mass scale introduced by dimensional regularization. Since L_k and W_k depend on μ the choice of it in the logarithm is natural. In terms of L_k' and W_k' we have

$$\bar{L}_k = L_k' - c_k\log\left(\frac{f_0^2}{\mu^2}\right),\qquad \overline{W}_k = W_k' - d_k\log\left(\frac{f_0^2}{\mu^2}\right).\tag{8}$$

Note that the NLO parameters α_k in Ref. [7] are related to L_k' by

$$\alpha_k = 128\pi^2 L_k'.\tag{9}$$

The *universal low energy scales* $\Lambda_{3,4}$ in Refs. [24,25] can be expressed, in the case of $N_s=2$, by the following combinations of the coefficients $\bar{L}_k$:

$$-\frac{1}{256\pi^2}\log\frac{\Lambda_3^2}{f_0^2}=2\bar{L}_8-\bar{L}_5+4\bar{L}_6-2\bar{L}_4,\qquad \frac{1}{64\pi^2}\log\frac{\Lambda_4^2}{f_0^2}=2\bar{L}_4+\bar{L}_5.\tag{10}$$

In this Letter we are interested in the valence quark mass dependence of f_π and m_π^2 for fixed sea quark mass parameter χ_S. Therefore, it is natural to introduce the ratios of the other mass parameters to χ_S:

$$\xi\equiv\frac{\chi_V}{\chi_S},\qquad \eta\equiv\frac{\rho_S}{\chi_S},\qquad \zeta\equiv\frac{\rho_V}{\rho_S}=\frac{\rho_V}{\eta\chi_S}.\tag{11}$$

Once relations (11) are substituted in (2), (3), the logarithmic dependence on χ_S can be absorbed in the NLO parameters if one introduces

$$L_{Sk} \equiv \bar{L}_k - c_k \log(\chi_S) = L'_k - c_k \log\left(\frac{f_0^2}{\mu^2}\chi_S\right),$$
$$W_{Sk} \equiv \overline{W}_k - d_k \log(\chi_S) = W'_k - d_k \log\left(\frac{f_0^2}{\mu^2}\chi_S\right). \tag{12}$$

Let us note that the argument of the last logarithms here can also be written as

$$\frac{f_0^2}{\mu^2}\chi_S = \frac{2B_0 m_{qS}}{\mu^2}\,. \tag{13}$$

In this Letter we keep the sea quark mass (χ_S) fixed and vary the valence quark mass ($\chi_V = \xi\chi_S$). Expanding the ratio of decay constants up to first order in the one-loop corrections one obtains

$$Rf_{VV} \equiv \frac{f_{VV}}{f_{SS}} = 1 + 4(\xi-1)\chi_S L_{S5} - \frac{N_s\chi_S}{64\pi^2}(1+\xi+2\eta)\log\frac{1+\xi+2\eta}{2} + \frac{N_s\chi_S}{32\pi^2}(1+\eta)\log(1+\eta), \tag{14}$$

and similarly

$$Rf_{VS} \equiv \frac{f_{VS}}{f_{SS}} = 1 + 2(\xi-1)\chi_S L_{S5} + \frac{\chi_S}{64N_s\pi^2}(\xi-1) - \frac{\chi_S}{64N_s\pi^2}(1+\eta)\log\frac{\xi+\eta}{1+\eta}$$
$$- \frac{N_s\chi_S}{128\pi^2}(1+\xi+2\eta)\log\frac{1+\xi+2\eta}{2} + \frac{N_s\chi_S}{64\pi^2}(1+\eta)\log(1+\eta). \tag{15}$$

In case of the ratios of m_π^2 we expand up to first order in the "correction" which now also includes the $\mathcal{O}(a)$ terms of the tree-level expressions:

$$Rm_{VV} \equiv \frac{m_{VV}^2}{m_{SS}^2} = \xi + \eta - \eta\xi + 8\xi(\xi-1)\chi_S(2L_{S8} - L_{S5}) + 8N_s(\xi-1)\eta\chi_S(L_{S4} - W_{S6})$$
$$+ \frac{\chi_S}{16N_s\pi^2}(\xi-1)(\xi+\eta) - \frac{\chi_S}{16N_s\pi^2}\xi(1+2\eta)\log(1+\eta)$$
$$+ \frac{\chi_S}{16N_s\pi^2}\left(2\xi^2 - \xi - \eta + 3\eta\xi\right)\log(\xi+\eta), \tag{16}$$

and

$$Rm_{VS} \equiv \frac{m_{VS}^2}{m_{SS}^2} = \frac{1}{2}(1+\xi+\eta-\eta\xi) + 2(\xi+1)(\xi-1)\chi_S(2L_{S8} - L_{S5}) + 4N_s(\xi-1)\eta\chi_S(L_{S4} - W_{S6})$$
$$- \frac{\chi_S}{32N_s\pi^2}(\xi+1)(1+2\eta)\log(1+\eta) + \frac{\chi_S}{32N_s\pi^2}\left(\xi^2+\xi+\eta+3\eta\xi\right)\log(\xi+\eta). \tag{17}$$

In these expressions it is assumed that the $\mathcal{O}(a)$ mass terms ρ are the same for valence quarks and the sea quark, namely $\rho_V = \rho_S$. This is the case if only the hopping parameter κ is changed. Changing $\rho_V = \zeta\eta\chi_S$ can be investigated by changing the Wilson-parameter r in the Wilson fermion action, too.

Up to now we considered the valence quark mass dependence for unchanged sea quark masses. Let us remark that the formulas for the sea quark mass dependence can also be written in a similar form as Eqs. (14)–(17). In this case it is advantageous to fix a *reference sea quark mass* χ_R (see [2]) and introduce the variables

$$\sigma \equiv \frac{\chi_S}{\chi_R}, \qquad \omega \equiv \frac{\rho_R}{\chi_R}, \qquad \tau \equiv \frac{\rho_S}{\rho_R} = \frac{\rho_S}{\omega\chi_R}. \tag{18}$$

Instead of the NLO parameters in (12) the appropriate ones are then obviously

$$L_{Rk} \equiv L'_k - c_k \log\left(\frac{f_0^2}{\mu^2}\chi_R\right), \qquad W_{Rk} \equiv W'_k - d_k \log\left(\frac{f_0^2}{\mu^2}\chi_R\right). \tag{19}$$

3. Numerical results

We performed Monte Carlo simulations with $N_s = 2$ degenerate sea quarks on a 16^4 lattice at $\beta = 4.68$, $\kappa = 0.195$ and investigated the valence quark mass dependence at $\kappa = 0.1955, 0.1945, 0.1940, 0.1930, 0.1920$. The statistics corresponds to 1180 gauge field configurations. The error analysis was based on the *linearization method* [27]. Since $r_0/a = 1.76(6)$ the lattice spacing is $a \simeq 0.28$ fm. This means that the physical lattice extension is rather large: $L \simeq 4.5$ fm. The value of the quark mass parameter is given by $am_\pi = 0.519(1)$ as $M_r \equiv (r_0 m_\pi)^2 \simeq 0.83$. This is about $1/4$ of the value of M_r for the strange quark $M_r^{\text{strange}} \simeq 3.1$.

The ratios in Eqs. (14)–(17) as a function of the quark mass ratio (ξ) depend on five parameters, namely, $\chi_S, \eta, L_{S5}, (2L_{S8} - L_{S5})$ and $(L_{S4} - W_{S6})$. With our choice of the valence hopping parameters and with our statistics most of the multi-parameter fits were unstable, therefore, our analysis is based one a sequence of single or double parameter fits. The stability of the multi-parameter fits can be improved by optimizing the choice of valence quark mass values, which we did not exploit this time.

A very useful quantity is the double ratio of decay constants [14] which does not depend on any of the NLO coefficients. In other words there one can see the chiral logarithms alone. The NLO formula is:

$$RRf \equiv \frac{f_{VS}^2}{f_{VV} f_{SS}} = 1 + \frac{\chi_S}{32N_s\pi^2}(\xi - 1) - \frac{\chi_S}{32N_s\pi^2}(1+\eta)\log\frac{\xi+\eta}{1+\eta}. \tag{20}$$

Because of the $\mathcal{O}(a)$ contributions this has two parameters: χ_S and $\eta = \rho_S/\chi_S$. For performing two-parameter fits some timeslice distance pairs were chosen and the fits of the pion- and quark-mass were taken from them. Useful choices are, for instance, 4–5, 4–6 or 5–6. (The way physical quantities were obtained has been described in detail in [17].) The result of the two-parameter fit was (see Fig. 1):

$$\chi_S = 9.2 \pm 2.5, \qquad \eta = 0.14 \pm 0.30. \tag{21}$$

The value of χ_S has the right order of magnitude. Indeed, from the axial Ward identity we obtain $r_0 m_{qS} = 0.06 Z_q^{-1}$. Using this and the phenomenological estimates [25] $r_0 f_0 = 0.23$, $r_0 B_0 = 7.0$, where the value of B_0 refers to the $\overline{MS}$ scheme at $\mu = 2$ GeV, we deduce $\chi_S^{\text{estimate}} \simeq 16 Z_q^{-1}$. Here Z_q is an unknown Z-factor relating the bare lattice quark mass to the renormalized one at 2 GeV, which is typically of $\mathcal{O}(1)$. Another estimate can be obtained by using the tree-level ChPT formula $\chi_S^{\text{estimate}} \approx M_r/(r_0 f_0)^2 \simeq 15.7$.

After determining χ_S and $\eta = \rho_S/\chi_S$ from the double ratio RRf one can fit the other ratios to obtain estimates of the NLO coefficients. A nice linear combination of mass-squared ratios is:

$$\begin{aligned} LRm \equiv 2Rm_{VS} - Rm_{VV} = 1 - 4(\xi-1)^2\chi_S(2L_{S8} - L_{S5}) - \frac{\chi_S}{16N_s\pi^2}(\xi-1)(\xi+\eta) \\ - \frac{\chi_S}{16N_s\pi^2}(1+2\eta)\log(1+\eta) - \frac{\chi_S}{16N_s\pi^2}\left(\xi^2 - 2\xi - 2\eta\right)\log(\xi+\eta). \end{aligned} \tag{22}$$

This has only a single new parameter $(2L_{S8} - L_{S5})$ and the statistical errors are small, therefore, one can also perform a two-parameter fit of χ_S and $(2L_{S8} - L_{S5})$ with the result ($\eta = 0.05$ fixed, errors in last digits given in parentheses):

$$2L_{S8} - L_{S5} = -0.00203(5), \qquad 2\alpha_8 - \alpha_5 = 0.85(6), \qquad \chi_S = 5.2(1.1). \tag{23}$$

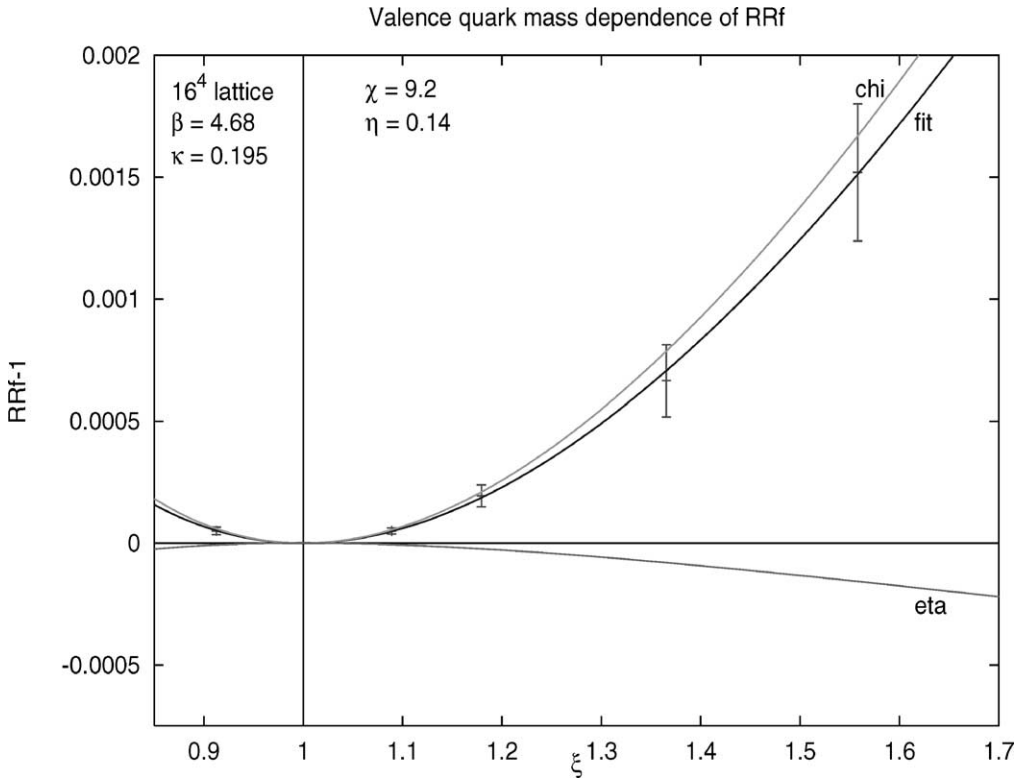

Fig. 1. The valence quark mass dependence of the double ratio of pion decay constants RRf. Besides the "fit" the two other curves show the $\mathcal{O}(a)$ contribution ("eta") and the physical contribution obtained at $\eta = 0$ ("chi").

α_k denote the NLO parameters in (9) taken at the renormalization scale $\mu = 4\pi f_0$. Fixing both $\chi_S = 10.0$ and $\eta = 0.10$ gives:

$$2L_{S8} - L_{S5} = -0.00177(3), \qquad 2\alpha_8 - \alpha_5 = 0.58(3). \tag{24}$$

As Fig. 2 shows, with these parameters the last point is not perfectly fitted. A perfect fit is obtained with the parameters in (23).

The value of L_{S5} can be determined from Rf_{VV}. (Rf_{VS} gives very similar results.) In this case the statistical errors are larger, therefore, only a single parameter fit is useful. The result for fixed $\chi_S = 10.0$ and $\eta = 0.10$ is (see Fig. 3):

$$L_{S5} = 0.0034(1), \qquad \alpha_5 = 1.55(24). \tag{25}$$

The errors given in (23)–(25) are the ones for the specified values of fixed parameters. The overall error is, of course, larger—as one can see, for instance, by comparing (23) and (24). The values of $(2\alpha_8 - \alpha_5)$ and α_5 are somewhat larger than the results of UKQCD [3]: $(2\alpha_8 - \alpha_5) = 0.36 \pm 0.10$ and $\alpha_5 = 1.22 \pm 0.11$ (only statistical errors quoted).

The double ratio of the pion mass squares [13]

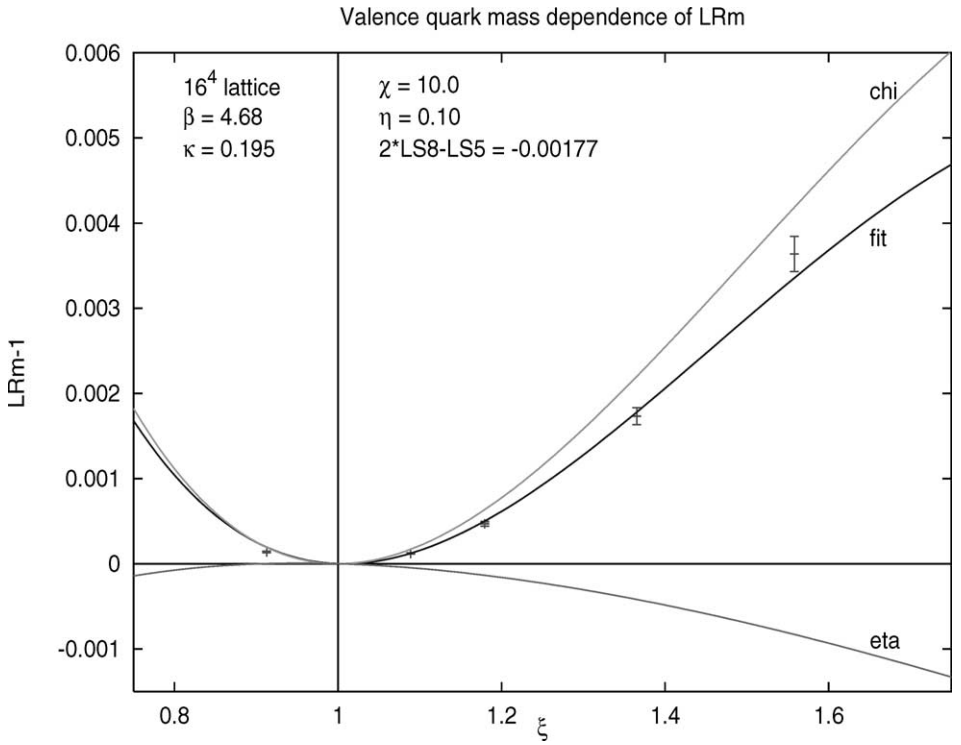

Fig. 2. The valence quark mass dependence of the linear combination of pion mass-squared ratios LRm. Besides the "fit" the two other curves show the $\mathcal{O}(a)$ contribution ("eta") and the physical contribution obtained at $\eta = 0$ ("chi").

$$RRm \equiv \frac{m_{VS}^4}{m_{VV}^2 m_{SS}^2} = \frac{(\xi+1)(\xi^2+\xi-\eta+2\eta\xi-\eta\xi^2)}{4\xi^2} + \frac{\chi_S(\xi+1)(\xi^2+\xi+\eta+3\eta\xi^2)\log(\xi+\eta)}{64N_s\pi^2\xi^2} - \frac{\chi_S(\xi+1)^2(2\eta+1)\log(1+\eta)}{64N_s\pi^2\xi} - \frac{\chi_S(\xi-1)(\xi+1)^2(\xi+\eta)}{64N_s\pi^2\xi^2} + \frac{2N_s\chi_S\eta(\xi+1)(\xi-1)^2}{\xi^2}(L_{S4}-W_{S6}) \tag{26}$$

can be used to determine the fifth parameter $(L_{S4} - W_{S6})$. In this case a single parameter fit with fixed $\chi_S = 10.0$ and $\eta = 0.10$ gives $(L_{S4} - W_{S6}) = 0.00358(6)$.

The conclusion of this Letter is that—once the quark masses are small enough—the qualitative behaviour of the low energy chiral effective theory with chiral logarithms is present even on coarse lattices. Since here ratios of pion masses and decay constants are considered the Z-factors of renormalization cancel, therefore the uncertainty about their β-dependence, which can influence the results of [17,19], is removed. The coefficients of the observed chiral logarithms and the fitted values of the Gasser–Leutwyler coefficients are close to expectation. This qualitative agreement of the results of a numerical simulation with (PQ)ChPT is quite satisfactory but for a quantitative determination of NLO ChPT parameters one has to perform extrapolations to $a \to 0$ and $m_q \to 0$. Since $\mathcal{O}(a)$ effects are taken into account in the analysis by the Rupak–Shoresh effective Lagrangian, the continuum limit will be reached asymptotically at the rate $\mathcal{O}(a^2)$.

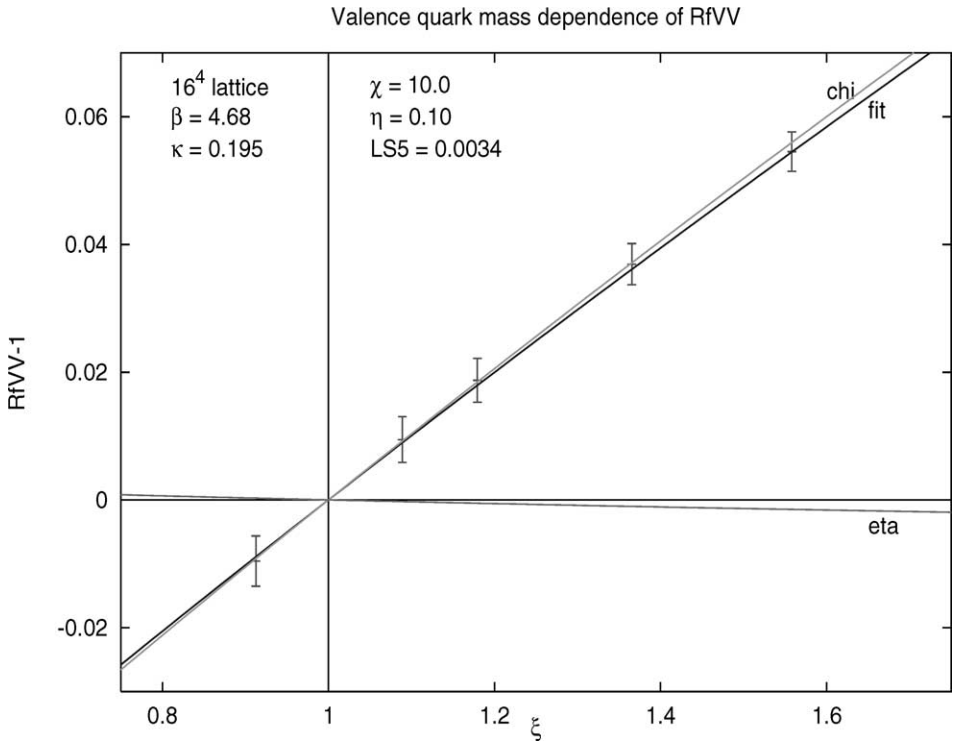

Fig. 3. The valence quark mass dependence of the ratio of pion decay constants Rf_{VV}. Besides the "fit" the two other curves show the $\mathcal{O}(a)$ contribution ("eta") and the physical contribution obtained at $\eta = 0$ ("chi").

Acknowledgements

The computations were performed on the APEmille systems installed at NIC Zeuthen, the Cray T3E systems at NIC Jülich and the PC clusters at DESY Hamburg. We thank Hartmut Wittig for helpful discussions on various topics and for careful reading of the manuscript. I.M. profited from enlightening discussions on the Asia-Pacific Mini-Workshop on Lattice QCD especially with Shoji Hashimoto, Yoichi Iwasaki, Yusuke Namekawa and Steve Sharpe.

References

[1] J. Gasser, H. Leutwyler, Ann. Phys. 158 (1984) 142.
[2] ALPHA Collaboration, J. Heitger, et al., Nucl. Phys. B 588 (2000) 377, hep-lat/0006026.
[3] UKQCD Collaboration, A.C. Irving, et al., Phys. Lett. B 518 (2001) 243, hep-lat/0107023.
[4] G.T. Fleming, D.R. Nelson, G.W. Kilcup, Nucl. Phys. B (Proc. Suppl.) 106 (2002) 221, hep-lat/0110112.
[5] G.T. Fleming, D.R. Nelson, G.W. Kilcup, hep-lat/0209141.
[6] H. Wittig, hep-lat/0210025.
[7] S.R. Sharpe, Phys. Rev. D 56 (1997) 7052, hep-lat/9707018;
S.R. Sharpe, Phys. Rev. D 62 (2000) 099901, Erratum.
[8] M.F.L. Golterman, K.-Ch. Leung, Phys. Rev. D 57 (1998) 5703, hep-lat/9711033.
[9] S.R. Sharpe, N. Shoresh, Phys. Rev. D 62 (2000) 094503, hep-lat/0006017.
[10] C. Bernard, S. Hashimoto, D.B. Leinweber, P. Lepage, E. Pallante, S.R. Sharpe, H. Wittig, hep-lat/0209086.
[11] CP-PACS Collaboration, A. Ali-Khan, et al., Phys. Rev. D 65 (2002) 054505, hep-lat/0105015.

[12] UKQCD Collaboration, C.R. Allton, et al., Phys. Rev. D 65 (2002) 054502, hep-lat/0107021.
[13] JLQCD Collaboration, S. Aoki, et al., Nucl. Phys. B (Proc. Suppl.) 106 (2002) 224, hep-lat/0110179.
[14] JLQCD Collaboration, S. Hashimoto, et al., hep-lat/0209091.
[15] CP-PACS Collaboration, Y. Namekawa, et al., hep-lat/0209073.
[16] JLQCD Collaboration, S. Aoki, et al., hep-lat/0212039.
[17] qq+q Collaboration, F. Farchioni, C. Gebert, I. Montvay, L. Scorzato, Eur. Phys. J. C 26 (2002) 237, hep-lat/0206008.
[18] qq+q Collaboration, F. Farchioni, C. Gebert, I. Montvay, L. Scorzato, hep-lat/0209038.
[19] qq+q Collaboration, F. Farchioni, C. Gebert, I. Montvay, L. Scorzato, hep-lat/0209142.
[20] C. Gebert, PhD Thesis, Hamburg University, 2002.
[21] I. Montvay, hep-lat/0301013.
[22] I. Montvay, Nucl. Phys. B 466 (1996) 259, hep-lat/9510042.
[23] F. Farchioni, C. Gebert, I. Montvay, W. Schroers, Nucl. Phys. B (Proc. Suppl.) 106 (2002) 215, hep-lat/0110130.
[24] H. Leutwyler, Nucl. Phys. B (Proc. Suppl.) 94 (2001) 108, hep-ph/0011049.
[25] S. Dürr, hep-lat/0208051.
[26] G. Rupak, N. Shoresh, Phys. Rev. D 66 (2002) 054503, hep-lat/0201019.
[27] ALPHA Collaboration, R. Frezzotti, M. Hasenbusch, U. Wolff, J. Heitger, K. Jansen, Comput. Phys. Commun. 136 (2001) 1, hep-lat/0009027.

[Chi-2]

Quark mass dependence of masses and decay constants of the pseudo-Goldstone bosons in QCD

Eur. Phys. J. C31 227-238 (2003)

Eur. Phys. J. C 31, 227–238 (2003)
Digital Object Identifier (DOI) 10.1140/epjc/s2003-01321-3

THE EUROPEAN PHYSICAL JOURNAL C

Quark mass dependence of masses and decay constants of the pseudo-Goldstone bosons in QCD

The $qq{+}q$ Collaboration

F. Farchioni[1], I. Montvay[2], E. Scholz[2], L. Scorzato[2]

[1] Westfälische Wilhelms-Universität Münster, Institut für Theoretische Physik, Wilhelm-Klemm-Strasse 9, 48149 Münster, Germany
[2] Deutsches Elektronen-Synchrotron DESY, Notkestr. 85, 22603 Hamburg, Germany

Received: 7 July 2003 /
Published online: 2 October 2003 –

Abstract. The dependence of the pseudo-scalar meson masses and decay constants on sea and valence quark masses is compared to next-to-leading order (NLO) chiral perturbation theory (ChPT). The numerical simulations with two light dynamical quark flavors are performed with the Wilson quark lattice action at gauge coupling $\beta = 5.1$ and hopping parameters $\kappa = 0.176,\ 0.1765,\ 0.177$ on a 16^4 lattice. $\mathcal{O}(a)$ lattice artifacts are taken into account by applying chiral perturbation theory for the Wilson lattice action. The values of the relevant combinations of Gasser–Leutwyler constants L_4, L_5, L_6 and L_8 are estimated.

1 Introduction

The low energy dynamics of strong interactions in the pseudo-Goldstone boson sector of QCD is constrained by the non-linear realization of spontaneously broken chiral symmetry [1]. In an expansion in powers of momenta and light quark masses a few low energy constants – the Gasser–Leutwyler constants – appear which parameterize the strength of interactions in the low energy chiral Lagrangian [2]. The Gasser–Leutwyler constants are free parameters which can be constrained by analyzing experimental data. In the framework of lattice regularization they can be determined from first principles by numerical simulations. In experiments one can investigate processes with different momenta but the quark masses are, of course, fixed by nature. In numerical simulations there is, in principle, much more freedom because, besides the possibility of changing momenta, one can also freely change the masses of the quarks. This allows for a precise determination of the Gasser–Leutwyler constants – once the simulations reach high precision. First steps towards this goal have recently been done by several authors [3–6] including our Collaboration [7–9].

The main difficulty for numerical simulations in lattice QCD is to reach the regime of light quark masses where ChPT is applicable. The reason is the critical slowing down of simulation algorithms for small quark masses and lattice spacings. We apply the two-step multi-boson (TSMB) algorithm [10] which allows one to perform simulations with small quark masses within the range of applicability of next-to-leading order (NLO) ChPT [7, 8].

Another important aspect of investigating the quark mass dependence in numerical simulations is the possibility to use ChPT for the extrapolation of the results to the physical values of u- and d-quark masses which would be very difficult to reach otherwise. In fact, ChPT can be extended by changing the *valence quark masses* in quark propagators independently from the *sea quark masses* in virtual quark loops which are represented in the path integral by the *quark determinant*. In this way one arrives at partially quenched chiral perturbation theory (PQChPT) [11–13]. The freedom of changing valence and sea quark masses substantially contributes to the power of lattice QCD both in performing quark mass extrapolations and in determining the values of the Gasser–Leutwyler constants [14].

For a fast convergence of numerical results to the continuum limit it is important to explicitly deal with the leading $\mathcal{O}(a)$ lattice artifacts. An often used method is the application of the $\mathcal{O}(a)$ improved lattice action [15]. We apply an alternative technique [16] which in the pseudo-Goldstone boson sector is equivalent to the $\mathcal{O}(a)$ improvement of the lattice action. In this method the (unimproved) Wilson action is used in the Monte Carlo generation of gauge configurations and the $\mathcal{O}(a)$ effects are compensated in PQChPT itself. This means that we apply *chiral perturbation theory for the Wilson lattice action*. Our calculations showed that in practice this method gives results with good precision [9].

The plan of this paper is as follows: in the next two sections we collect the NLO (PQ)ChPT formulas for ratios of pseudo-scalar meson masses and decay constants. In Sect. 2 a discussion of the general form of the NNLO tree-

graph corrections is also included. In Sect. 4 the results of numerical simulations is presented. The last section is devoted to a summary and discussion.

2 Valence quark mass dependence

In this paper we use the notation introduced in [9] which slightly differ from those of [14,16]. The dimensionless variables for quark masses and $\mathcal{O}(a)$ lattice artifacts are denoted, respectively, by

$$\chi_A \equiv \frac{2B_0 m_q}{f_0^2} \ , \qquad \rho_A \equiv \frac{2W_0 a c_{\rm SW}}{f_0^2} \ . \tag{1}$$

Here m_q is the quark mass, a the lattice spacing, B_0 and W_0 are parameters of dimension mass and (mass)^3, respectively, which appear in the leading order (LO) chiral effective Lagrangian, $c_{\rm SW}$ is the coefficient of the $\mathcal{O}(a)$ chiral symmetry breaking term and f_0 is the value of the pion decay constant at zero quark mass. (Its normalization is such that the physical value is $f_0 \simeq 93\,\mathrm{MeV}$.) For fixed sea quark mass $\chi_{\rm S}$ the dependence of the pseudo-scalar meson mass and decay constant on the valence quark mass $\chi_{\rm SV}$ can be described by the variables

$$\xi \equiv \frac{\chi_{\rm SV}}{\chi_{\rm S}} \ , \qquad \eta_{\rm S} \equiv \frac{\rho_{\rm S}}{\chi_{\rm S}} \ . \tag{2}$$

For instance, in case of a number of $N_{\rm s}$ equal mass sea quarks the ratios of decay constants are given by

$$\begin{aligned} Rf_{\rm VV} \ &\equiv \frac{f_{\rm VV}}{f_{\rm SS}} = 1 + 4(\xi-1)\chi_{\rm S} L_{\rm S5} \\ &- \frac{N_{\rm s}\chi_{\rm S}}{64\pi^2}(1+\xi+2\eta_{\rm S}) \log\frac{1+\xi+2\eta_{\rm S}}{2} \\ &+ \frac{N_{\rm s}\chi_{\rm S}}{32\pi^2}(1+\eta_{\rm S})\log(1+\eta_{\rm S}) \ , \end{aligned} \tag{3}$$

and similarly

$$\begin{aligned} Rf_{\rm VS} \equiv \frac{f_{\rm VS}}{f_{\rm SS}} &= 1 + 2(\xi-1)\chi_{\rm S} L_{\rm S5} \\ &+ \frac{\chi_{\rm S}}{64N_{\rm s}\pi^2}(\xi-1) - \frac{\chi_{\rm S}}{64N_{\rm s}\pi^2}(1+\eta_{\rm S}) \log\frac{\xi+\eta_{\rm S}}{1+\eta_{\rm S}} \\ &- \frac{N_{\rm s}\chi_{\rm S}}{128\pi^2}(1+\xi+2\eta_{\rm S}) \log\frac{1+\xi+2\eta_{\rm S}}{2} \\ &+ \frac{N_{\rm s}\chi_{\rm S}}{64\pi^2}(1+\eta_{\rm S})\log(1+\eta_{\rm S}) \ . \end{aligned} \tag{4}$$

$L_{{\rm S}k}$ ($k=5$) denotes the relevant Gasser–Leutwyler coefficient at the scale $f_0\sqrt{\chi_{\rm S}}$. This is related to $\bar{L}_k$ defined at the scale f_0 and L'_k defined at the generic scale μ according to

$$L_{{\rm S}k} = \bar{L}_k - c_k \log(\chi_{\rm S}) = L'_k - c_k \log\left(\frac{f_0^2}{\mu^2}\chi_{\rm S}\right) \ . \tag{5}$$

with the constants c_k ($k = 4,5,6,8$) given below. Similarly, the corresponding relations for the coefficients $W_{{\rm S}k}$ introduced in [16] are

$$W_{{\rm S}k} = \bar{W}_k - d_k \log(\chi_{\rm S}) = W'_k - d_k \log\left(\frac{f_0^2}{\mu^2}\chi_{\rm S}\right) \ . \tag{6}$$

The constants in (5) and (6) are given by

$$\begin{aligned} c_4 &= \frac{1}{256\pi^2} \ , \qquad c_5 = \frac{N_{\rm s}}{256\pi^2} \ , \\ c_6 &= \frac{(N_{\rm s}^2+2)}{512N_{\rm s}^2\pi^2} \ , \qquad c_8 = \frac{(N_{\rm s}^2-4)}{512N_{\rm s}\pi^2} \ , \end{aligned} \tag{7}$$

respectively,

$$\begin{aligned} d_4 &= \frac{1}{256\pi^2} \ , \qquad d_5 = \frac{N_{\rm s}}{256\pi^2} \ , \\ d_6 &= \frac{(N_{\rm s}^2+2)}{256N_{\rm s}^2\pi^2} \ , \qquad d_8 = \frac{(N_{\rm s}^2-4)}{256N_{\rm s}\pi^2} \ . \end{aligned} \tag{8}$$

For the valence quark mass dependence of the (squared) pseudo-scalar meson masses one can consider, similarly to (3) and (4), the ratios

$$Rm_{\rm VV} \equiv \frac{m_{\rm VV}^2}{m_{\rm SS}^2} \ , \qquad Rm_{\rm VS} \equiv \frac{m_{\rm VS}^2}{m_{\rm SS}^2} \ . \tag{9}$$

In the present paper we prefer to divide these ratios by the tree level dependences and consider

$$\begin{aligned} Rn_{\rm VV} \equiv \frac{m_{\rm VV}^2}{\xi m_{\rm SS}^2} &= 1 - \eta_{\rm S}\frac{(\xi-1)}{\xi} \\ &+ 8(\xi-1)\chi_{\rm S}(2L_{\rm S8} - L_{\rm S5}) \\ &+ 8N_{\rm s}\frac{(\xi-1)}{\xi}\eta_{\rm S}\chi_{\rm S}(L_{\rm S4} - W_{\rm S6}) \\ &+ \frac{\chi_{\rm S}}{16N_{\rm s}\pi^2}\frac{(\xi-1)}{\xi}(\xi+\eta_{\rm S}) \\ &- \frac{\chi_{\rm S}}{16N_{\rm s}\pi^2}(1+2\eta_{\rm S})\log(1+\eta_{\rm S}) \\ &+ \frac{\chi_{\rm S}}{16N_{\rm s}\pi^2}\frac{(2\xi^2-\xi-\eta_{\rm S}+3\eta_{\rm S}\xi)}{\xi}\log(\xi+\eta_{\rm S}) \ , \end{aligned} \tag{10}$$

and

$$\begin{aligned} Rn_{\rm VS} \ &\equiv \frac{2m_{\rm VS}^2}{(\xi+1)m_{\rm SS}^2} = 1 - \eta_{\rm S}\frac{(\xi-1)}{(\xi+1)} \\ &+ 4(\xi-1)\chi_{\rm S}(2L_{\rm S8} - L_{\rm S5}) \\ &+ 8N_{\rm s}\frac{(\xi-1)}{(\xi+1)}\eta_{\rm S}\chi_{\rm S}(L_{\rm S4} - W_{\rm S6}) \\ &- \frac{\chi_{\rm S}}{16N_{\rm s}\pi^2}(1+2\eta_{\rm S})\log(1+\eta_{\rm S}) \\ &+ \frac{\chi_{\rm S}}{16N_{\rm s}\pi^2}\frac{(\xi^2+\xi+\eta_{\rm S}+3\eta_{\rm S}\xi)}{(\xi+1)}\log(\xi+\eta_{\rm S}) \ . \end{aligned} \tag{11}$$

A useful quantity is the double ratio of decay constants [17] which does not depend on any of the NLO coefficients. In other words there one can see the chiral logarithms alone. The NLO expansion for this quantity is

$$RRf \equiv \frac{f_{\rm VS}^2}{f_{\rm VV} f_{\rm SS}} = 1 + \frac{\chi_{\rm S}}{32 N_{\rm s} \pi^2}(\xi - 1) - \frac{\chi_{\rm S}}{32 N_{\rm s} \pi^2}(1+\eta_{\rm S}) \log \frac{\xi + \eta_{\rm S}}{1+\eta_{\rm S}} \; . \tag{12}$$

The double ratio of the pion mass squares [18] corresponding to (10) and (11) has the NLO expansion

$$\begin{aligned} RRn \equiv & \frac{4\xi m_{\rm VS}^4}{(\xi+1)^2 m_{\rm VV}^2 m_{\rm SS}^2} = 1 - \frac{\eta_{\rm S}(\xi-1)^2}{\xi(\xi+1)} \\ & + \frac{\chi_{\rm S}(\xi^2 + \xi + \eta_{\rm S} + 3\eta_{\rm S}\xi^2)\log(\xi+\eta_{\rm S})}{16 N_{\rm s}\pi^2 \xi(\xi+1)} \\ & - \frac{\chi_{\rm S}(2\eta_{\rm S}+1)\log(1+\eta_{\rm S})}{16 N_{\rm s}\pi^2} \\ & - \frac{\chi_{\rm S}(\xi-1)(\xi+\eta_{\rm S})}{16 N_{\rm s}\pi^2 \xi} \\ & + \frac{8 N_{\rm s}\chi_{\rm S}\eta_{\rm S}(\xi-1)^2}{\xi(\xi+1)}(L_{\rm S4} - W_{\rm S6}) \; . \end{aligned} \tag{13}$$

2.1 Quadratic corrections

A complete NNLO (i. e. two-loop) calculation in PQChPT for our physical quantities is not yet available. Nevertheless, the general form of NNLO tree-graph ("counterterm insertion") contributions can be given [19][1]. For instance, one has for the pion mass square:

$$\begin{aligned} \frac{\delta m_{AB}^2}{m_{AB}^2} = & \; \alpha_1 \chi_{\rm S}^2 + \alpha_2 \chi_{\rm S}(\chi_A + \chi_B) \\ & + \alpha_3(\chi_A + \chi_B)^2 + \alpha_4(\chi_A^2 + \chi_B^2) \; . \end{aligned} \tag{14}$$

(Here A and B denote generic quark indices: S is the label for the sea quarks, V for valence quarks.) For the pion decay constant there is a similar expression. This information is very useful in order to estimate the importance of the NNLO terms in our present range of quark masses.

The general characteristic of the NNLO terms is that they are proportional to the quark mass square: $\chi_{\rm S}^2$. (Here we only consider terms in the continuum limit and hence neglect lattice artifacts. This will be to some extent justified a posteriori by the observed smallness of the $\mathcal{O}(a)$ terms.) Neglecting loop contributions, which are at the NLO order relatively small, the dependence on the quark mass ratio ξ is at most quadratic and can, therefore, be represented by terms proportional to $(\xi-1)$ and $(\xi-1)^2$. Therefore, these contributions have the generic form

$$D_X \chi_{\rm S}^2(\xi-1) + Q_X \chi_{\rm S}^2(\xi-1)^2 \; . \tag{15}$$

[1] We thank the authors for communicating us the content of this paper prior to publication

Here X denotes an index specifying the considered ratio as, for instance, $X = f{\rm VV}$, $n{\rm VS}$ etc. for the single ratios and $X = fd$ and $X = nd$ for the double ratios RRf and RRn, respectively. The NLO tree-graph contributions for the single ratios Rf and Rn are also proportional to $(\xi{-}1)$. These can be parametrized as $L_X \chi_{\rm S}(\xi{-}1)$ (for instance, we have $L_{f{\rm VV}} \equiv 4L_5$ and $L_{n{\rm VV}} \equiv 8(2L_8 - L_5)$). The inclusion of D_X-type terms is equivalent to a linear dependence of the effective L_X for fixed $\chi_{\rm S}$:

$$L_X^{\rm eff} = L_X + D_X \chi_{\rm S} \; . \tag{16}$$

At this point one has to remember that mathematically speaking – in order to completely remove the effect of higher order terms – L_X is defined in the limit $\chi_{\rm S} \to 0$.

The NNLO coefficients are not all independent but satisfy the relations

$$\begin{aligned} D_{f{\rm VS}} &= \frac{1}{2} D_{f{\rm VV}} \; , \qquad D_{n{\rm VS}} = \frac{1}{2} D_{n{\rm VV}} \; , \\ D_{fd} &= 0 \; , \qquad D_{nd} = 0 \; , \\ Q_{fd} &= 2Q_{f{\rm VS}} - Q_{f{\rm VV}} + \frac{1}{4} L_{f{\rm VV}}^2 \; , \\ Q_{nd} &= 2Q_{n{\rm VS}} - Q_{n{\rm VV}} + \frac{1}{4} L_{n{\rm VV}}^2 \; . \end{aligned} \tag{17}$$

The first line is a consequence of the general structure of the NNLO tree-graph contributions. The last two lines follow from the definition of RRf and RRn if one only considers NLO and NNLO tree-graph contributions.

We shall see in Sect. 4 that in our range of quark masses the NNLO tree-graph contributions of the form (15) are important but can be approximately determined by global fits. In this way the NLO constants L_k are better determined. Observe that a determination of the D_X is only possible in our analysis if different sea quark masses are included (see below).

2.2 $\mathcal{O}(a^2)$ corrections

The idea of including leading lattice artifacts in the low energy effective Lagrangian for the Wilson lattice action can be extended to higher orders in lattice spacing. Indeed, in writing this paper we have seen two recent publications about the inclusion of $\mathcal{O}(a^2)$ corrections [20,21]. The general formulas derived in these papers for the $\mathcal{O}(a^2)$ terms imply that in the formulas for the pion mass-squared ratios (10), (11) and (13) there are only very little changes. In fact, the changes can be summarized by the replacement

$$\begin{aligned} \eta_{\rm S}(L_{\rm S4} - W_{\rm S6}) \; \longrightarrow \; & \eta_{\rm S}(L_{\rm S4} - W_{\rm S6}) \\ & + \frac{\eta_{\rm S}^2}{N_{\rm s}}(N_{\rm s} W_{\rm S4} + W_{\rm S5} - 2N_{\rm s} W'_{\rm S6} - 2W'_{\rm S8}) \; . \end{aligned} \tag{18}$$

Here $W'_{\rm S6}$ and $W'_{\rm S8}$ denote some new low energy constants appearing in the $\mathcal{O}(a^2)$ part of the effective Lagrangian. This means that fitting the valence quark mass

dependence with our formulas (10), (11) and (13) effectively takes into account also $\mathcal{O}(a^2)$ corrections.

Concerning the ratios of the pion decay constants in (3), (4) and (12) the situation is expected to be similar but there, in addition to the $\mathcal{O}(a^2)$ terms, also new types of $\mathcal{O}(am_q)$ terms may appear.

3 Sea quark mass dependence

The dependence on the sea quark mass can be treated similarly to the valence quark mass dependence considered in Sect. 2. Here one chooses a "reference value" of the sea quark mass $\chi_{\rm R}$ and determines the ratios of the coupling and decay constant as a function of

$$\sigma \equiv \frac{\chi_{\rm S}}{\chi_{\rm R}} \ , \qquad \tau \equiv \frac{\rho_{\rm S}}{\rho_{\rm R}} \ . \tag{19}$$

Instead of τ one can also use

$$\eta_{\rm S} \equiv \frac{\rho_{\rm S}}{\chi_{\rm S}} \ , \qquad \eta_{\rm R} \equiv \frac{\rho_{\rm R}}{\chi_{\rm R}}, \tag{20}$$

which satisfy

$$\frac{\tau}{\sigma} = \frac{\eta_{\rm S}}{\eta_{\rm R}} \ . \tag{21}$$

With this we have for the decay constants

$$\begin{aligned} Rf_{\rm SS} \ &\equiv \frac{f_{\rm SS}}{f_{\rm RR}} = 1 + 4(\sigma-1)\chi_{\rm R}(N_{\rm s}L_{\rm R4} + L_{\rm R5}) \\ &+4(\eta_{\rm S}\sigma - \eta_{\rm R})\chi_{\rm R}(N_{\rm s}W_{\rm R4} + W_{\rm R5}) \\ &-\frac{N_{\rm s}\chi_{\rm R}}{32\pi^2}\sigma(1+\eta_{\rm S})\log[\sigma(1+\eta_{\rm S})] \\ &+\frac{N_{\rm s}\chi_{\rm R}}{32\pi^2}(1+\eta_{\rm R})\log(1+\eta_{\rm R}) \end{aligned} \tag{22}$$

and for the mass squares

$$\begin{aligned} Rn_{\rm SS} \ &\equiv \frac{m^2_{\rm SS}}{\sigma m^2_{\rm RR}} = 1 + \eta_{\rm S} - \eta_{\rm R} \\ &+8(\sigma-1)\chi_{\rm R}(2N_{\rm s}L_{\rm R6}+2L_{\rm R8}-N_{\rm s}L_{\rm R4}-L_{\rm R5}) \\ &+8(\eta_{\rm S}\sigma - \eta_{\rm R})\chi_{\rm R}(2N_{\rm s}W_{\rm R6} + 2W_{\rm R8} \\ &-N_{\rm s}W_{\rm R4} - W_{\rm R5} - N_{\rm s}L_{\rm R4} - L_{\rm R5}) \\ &+\frac{\chi_{\rm R}}{16\pi^2 N_{\rm s}}\sigma(1+2\eta_{\rm S})\log[\sigma(1+\eta_{\rm S})] \\ &-\frac{\chi_{\rm R}}{16\pi^2 N_{\rm s}}(1+2\eta_{\rm R})\log(1+\eta_{\rm R}) \ . \end{aligned} \tag{23}$$

Of course, the coefficients $L_{{\rm R}k}$ and $W_{{\rm R}k}$ ($k = 4,5,6,8$) are now defined at the scale $f_0\sqrt{\chi_{\rm R}}$ therefore in the relations (5) and (6) $\chi_{\rm S}$ is replaced by $\chi_{\rm R}$.

The logarithmic dependence of the $L_{{\rm S}k}$ and $W_{{\rm S}k}$ have to be taken into account also in simultaneous fits of the valence quark mass dependence at several sea quark mass values. Choosing a fixed *reference sea quark mass* $\chi_{\rm R}$ we have from (5) and (6) with $\mu = f_0\sqrt{\chi_{\rm R}}$

$$L_{{\rm S}k} = L_{{\rm R}k} - c_k \log\sigma \ , \quad W_{{\rm S}k} = W_{{\rm R}k} - d_k \log\sigma \ . \tag{24}$$

The NLO PQChPT formulas for the valence quark mass dependence in terms of the reference sea quark mass are obtained by the following substitutions in (3), (4), (10)–(13):

$$\begin{aligned} \chi_{\rm S} \to \sigma\chi_{\rm R} \ , \quad L_{{\rm S}k} \to L_{{\rm R}k} \ , \quad W_{{\rm S}k} \to W_{{\rm R}k} \ , \\ \log(1+\eta_{\rm S}) \to \log[\sigma(1+\eta_{\rm S})] \ , \\ \log(\xi+\eta_{\rm S}) \to \log[\sigma(\xi+\eta_{\rm S})] \ , \\ \log(1+\xi+2\eta_{\rm S}) \to \log[\sigma(1+\xi+2\eta_{\rm S})] \ . \end{aligned} \tag{25}$$

An important feature of both the valence and sea quark mass dependences considered in the present work is that they are ratios taken at a fixed value of the gauge coupling (β). These are renormalization group invariants independent from the Z-factors of multiplicative renormalization since the Z-factors only depend on the gauge coupling and not on the quark mass. Taking ratios of pion mass squares and pion decay constants at varying quark masses has, in general, the advantage that quark mass independent corrections – for instance of $\mathcal{O}(a)$ and/or $\mathcal{O}(a^2)$ – cancel.

4 Numerical simulations

We performed Monte Carlo simulations with $N_{\rm s} = 2$ degenerate sea quarks on a 16^4 lattice at $\beta = 5.1$ and three values of κ: $\kappa_0 = 0.176$, $\kappa_1 = 0.1765$ and $\kappa_2 = 0.177$. For the *reference sea quark mass* we choose $\kappa_{\rm R} \equiv \kappa_0 = 0.176$. A summary of the simulation points is reported in Table 1, where also the set-up of the TSMB algorithm for the different simulation points can be found. The gauge field configurations collected for the evaluation of the physical quantities are separated by 10 TSMB update cycles consisting out of boson field and gauge field updates and noisy correction steps. It turned out that these configurations were statistically independent from the point of view of almost all secondary quantities considered. Exceptions are r_0/a and M_r (see below) where autocorrelation lengths of 2–5 units in the configuration sequences appear.

We investigated for each simulation point the valence quark mass dependence of the pseudo-Goldstone boson spectrum and decay constants; the values of the valence κ considered for each simulation point are reported in Table 2. In these intervals the valence quark masses are approximately changing in the range $\frac{1}{2}m_{\rm sea} \le m_{\rm valence} \le 2m_{\rm sea}$.

A rough estimate of the sea quark mass range can be obtained by considering the quantity $M_r \equiv (r_0 m_\pi)^2$, which for the strange quark gives $M_r \approx 3.1$. (Here $r_0 \approx 0.5\,$fm is the Sommer scale parameter which characterizes the distance scale intrinsic to the gauge field.) In our simulation points the value of M_r ranges between $M_r \approx 2.10$ and $M_r \approx 1.09$, corresponding to about $\frac{2}{3}$ and $\frac{1}{3}$ of the

Table 1. Parameters of the simulations: all simulations were done at $\beta = 5.10$ with determinant breakup $N_f = 1 + 1$. The other TSMB-parameters are the interval of polynomial approximasions $[\epsilon, \lambda]$ and the polynomial orders $n_{1,2,3}$ [10]

Run	κ	Configurations	ϵ	λ	n_1	n_2	n_3
0	0.1760	1811	$4.50 \cdot 10^{-4}$	3.0	40	210	220
1	0.1765	746	$2.50 \cdot 10^{-4}$	3.0	40–44	280	260–340
2	0.1770	1031	$3.75 \cdot 10^{-5}$	3.0	54	690	840

Table 2. Values of the valence quark hopping parameter

Run	0	1	2
$\kappa_{\rm sea}$	0.1760	0.1765	0.1770
$\kappa_{\rm valence}$	0.1685	0.1710	0.1743
	0.1705	0.1718	0.1747
	0.1720	0.1726	0.1751
	0.1730	0.1734	0.1754
	0.1735	0.1742	0.1759
	0.1745	0.1750	0.1763
	0.1750	0.1758	0.1767
	0.1770	0.1772	0.1775
	0.1775	0.1778	0.1779
	0.1785	0.1785	0.1783
	0.1790	0.1791	0.1787
	0.1800	0.1797	0.1791

value for the strange quark mass. Since the valence quark masses roughly go down to $m_{\rm valence} \simeq \frac{1}{2} m_{\rm sea}$, they reach $m_{\rm valence} \simeq \frac{1}{6} m_{\rm s}$. In our configuration samples we did not encounter problems with "exceptional gauge configurations" – in spite of the smallness of the valence quark mass. This means that the quark determinant effectively suppresses such configurations.

Standard methods for the extraction of the relevant physical quantities have been applied (a more detailed description is given in our previous paper [7] and in [22]). Statistical errors have been obtained by the *linearization method* [23, 24] which we found more reliable than jackknifing on bin averages.

Within a mass independent scheme of renormalization – defined at zero quark mass – the Z-factors of multiplicative renormalization depend only on the gauge coupling (β) and not on the quark mass (κ). Similarly, the lattice spacing a is also a function of the gauge coupling alone [25]. Therefore, since our simulation points are at fixed gauge coupling $\beta = 5.1$, the ratios of the sea quark masses can be obtained by taking ratios of the measured bare quark masses in lattice units $Z_q a m_q$. Here Z_q is the multiplicative renormalization factor for the quark mass which is the ratio of the Z-factors of the pseudo-scalar density and axial-vector current ($Z_q = Z_{\rm P}/Z_{\rm A}$) because we determine the quark mass by the PCAC-relation: $m_q \equiv m_q^{\rm PCAC}$ [7]. (Of course, in the valence quark ratios the factor $Z_q a$ also cancels trivially.) The obtained values of the sea quark mass ratios $\sigma_i \equiv m_{qi}/m_{q0}$ $(i = 1, 2)$ are given in Table 3 together with some other basic quantities.

Table 3. The values of some basic quantities in our simulation points. Statistical errors in last digits are given in parentheses. We define $M_r = (r_0 m_\pi)^2$ and $\sigma_i = m_{qi}/m_{q0}$

κ	κ_0	κ_1	κ_2
r_0/a	2.149(15)	2.171(88)	2.395(52)
am_π	0.6747(14)	0.6211(22)	0.4354(68)
M_r	2.103(26)	1.824(41)	1.088(47)
$Z_q a m_q$	0.07472(32)	0.06247(51)	0.03087(36)
σ_i	1.0	0.8361(52)	0.4132(34)

Note that by identifying the quark mass ratios in the ChPT formulas with the ratios of the PCAC quark masses ("axial-vector Ward identity quark masses") one assumes that these two kinds of renormalized quark masses are proportional to each other. As it is shown, for instance, by (48) in [21] this is indeed the case – apart from lattice artifacts of $\mathcal{O}(am_q)$ and $\mathcal{O}(a^2)$. The quark mass independent part of the $\mathcal{O}(a^2)$ terms are cancelled by taking ratios. The remaining quark mass dependent lattice artifacts are neglected in the present paper.

The critical value of the hopping parameter where the quark mass vanishes can be estimated by a quadratic extrapolation using the values of $\sigma_{1,2}$:

$$\sigma_i \equiv \frac{m_{qi}}{m_{q0}} = \frac{(\kappa_i^{-1} - \kappa_{\rm cr}^{-1}) + d_\sigma (\kappa_i^{-1} - \kappa_{\rm cr}^{-1})^2}{(\kappa_0^{-1} - \kappa_{\rm cr}^{-1}) + d_\sigma (\kappa_0^{-1} - \kappa_{\rm cr}^{-1})^2} \,. \qquad (26)$$

The values of $\sigma_{1,2}$ in Table 3 give the solution $\kappa_{\rm cr}$=0.1773(1) and $d_\sigma = -11.2(8)$. (The relatively large absolute value of d_σ shows that the quadratic term in the extrapolation is important.)

The value of the lattice spacing a can be inferred from the value of r_0/a at $\kappa = \kappa_{\rm cr}$. This can also be determined by a quadratic extrapolation of the values of r_0/a given in Table 3 with the result: $r_0(\kappa_{\rm cr})/a = 2.65(7)$. Taking, by definition, $r_0(\kappa_{\rm cr}) = 0.5\,{\rm fm}$ this gives for the lattice spacing: $a = 0.189(5)\,{\rm fm}$.

The physical volume following from the lattice spacing is comfortably large: $L \simeq 3.0\,{\rm fm}$. Since the minimal value of the pion mass in lattice units in our points is $am_\pi^{\rm min} \simeq 0.43$ for sea quarks and $am_\pi^{\rm min} \simeq 0.30$ for the lightest valence quark, we have $Lm_\pi \geq 4.8$.

Another piece of information given by the values of M_r is an estimate of the quark mass parameter $\chi_{\rm S}$ in the ChPT formulas. For instance, in the reference point we have from $r_0 f_0 \simeq 0.23$ [26]: $\chi_{\rm R}^{\rm estimate} \approx M_r/(r_0 f_0)^2 \simeq 39.8$.

4.1 Valence quark mass dependence

For a fixed value of the sea quark mass $\chi_{\rm S}$ the valence quark mass dependence of the ratios $Rf_{\rm VV,VS}$, $Rn_{\rm VV,VS}$, RRf and RRn is determined by five parameters:

$$\chi_{\rm S}\ , \quad \eta_{\rm S}\ , \quad \chi_{\rm S}L_{\rm S5}\ ,$$
$$\chi_{\rm S}L_{\rm S4W6} \equiv \chi_{\rm S}(L_{\rm S4} - W_{\rm S6})\ ,$$
$$\chi_{\rm S}L_{\rm S85} \equiv \chi_{\rm S}(2L_{\rm S8} - L_{\rm S5}). \qquad (27)$$

The dependence is non-linear in $\eta_{\rm S}$ and linear in the rest.

After performing such fits of the data we realized that the sea quark mass dependence is not consistent with the NLO PQChPT formulas. In particular, the best fit values of the $\chi_{\rm S}$ have ratios considerably closer to 1 than $\sigma_{1,2}$ in Table 3 and the change of the L_k with $\chi_{\rm S}$ is also not consistent with (24). This shows that NNLO effects are important and, therefore, we tried fits including NNLO tree-graph terms of the form given in (15). The list of the relevant NNLO-parameters is

$$\chi_{\rm R}^2 D_{f{\rm VV},n{\rm VV}}\ , \quad \chi_{\rm R}^2 Q_{f{\rm VV},f{\rm VS},fd,n{\rm VV},n{\rm VS},nd}\ . \qquad (28)$$

Q_{fd} and Q_{nd} have to satisfy the quadratic relations given in the last line of (17) but in order to keep linearity we did not impose these relations and fitted the eight parameters in (28) independently. After performing the fits one can check how well the relations for Q_{fd} and Q_{nd} are fulfilled.

The global fit of the valence quark mass dependence for several values of the sea quark mass has twelve linear parameters: the linear parameters in (27) with $\chi_{\rm S}$ replaced by $\chi_{\rm R}$

$$\chi_{\rm R}\ , \quad \chi_{\rm R}L_{\rm R5}\ ,$$
$$\chi_{\rm R}L_{\rm R85} \equiv \chi_{\rm R}(2L_{\rm R8} - L_{\rm R5})\ ,$$
$$\chi_{\rm R}L_{\rm R4W6} \equiv \chi_{\rm R}(L_{\rm R4} - W_{\rm R6}) \qquad (29)$$

and the eight in (28). In addition there are the non-linear parameters, in our case three of them: $\eta_{\rm S} = \eta_{0,1,2}$.

Multi-parameter linear fits are easy and, except for degenerate situations, the chi-square always has a unique well-defined minimum. Non-linear fits involving the η are more problematic; therefore, we adopted the following procedure: performing non-linear fits at individual sea quark mass values we obtained the starting values of $\eta_{0,1,2}$. Then for fixed values of $\eta_{0,1,2}$ we performed a linear fit of the twelve parameters in (28) and (29) and looked for a minimum of the chi-square as a function of $\eta_{0,1,2}$. For the sea quark masses we imposed the relation $\chi_{\rm S} = \sigma\chi_{\rm R}$ and for the NLO-parameters the relations in (24) with the values of $\sigma_{1,2}$ given in Table 3. (The possible dependence of the NNLO-parameters D and Q on σ has been neglected.) The minimum of the chi-square after the non-linear minimization is near

$$\eta_0 = 0.07\ , \qquad \eta_1 = 0.03\ , \qquad \eta_2 = 0.02\ . \qquad (30)$$

The minimum as a function of $\eta_{0,1,2}$ is rather shallow but definitely within the bounds $0 \le \eta_{0,1,2} \le 0.10$. The minimization of the chi-square of the linear fit does not change the η substantially: already the starting values are close to (30). This confirms the small value of $\eta_{\rm S}$ found in our previous paper at $\beta = 4.68$ [9].

Table 4. Values of best fit parameters for the valence quark mass dependence. Quantities directly used in the fitting procedure are in bold face

$\boldsymbol{\chi_{\rm R}}$	33.5(2.4)		
$\boldsymbol{\chi_{\rm R}L_{\rm R4W6}}$	$5.24(38)\cdot10^{-2}$	$L_{\rm R4W6}$	$1.564(71)\cdot10^{-3}$
$\boldsymbol{\chi_{\rm R}^2 Q_{nd}}$	$6.5(1.8)\cdot10^{-3}$	Q_{nd}	$5.80(79)\cdot10^{-6}$
$\boldsymbol{\chi_{\rm R}L_{\rm R5}}$	$10.06(44)\cdot10^{-2}$	$L_{\rm R5}$	$3.00(19)\cdot10^{-3}$
$\boldsymbol{\chi_{\rm R}^2 D_{f{\rm VV}}}$	$-9.3(1.7)\cdot10^{-2}$	$D_{f{\rm VV}}$	$-8.3(1.9)\cdot10^{-5}$
$\boldsymbol{\chi_{\rm R}^2 Q_{f{\rm VV}}}$	$-2.80(19)\cdot10^{-2}$	$Q_{f{\rm VV}}$	$-2.50(50)\cdot10^{-5}$
$\boldsymbol{\chi_{\rm R}^2 Q_{f{\rm VS}}}$	$-2.197(45)\cdot10^{-2}$	$Q_{f{\rm VS}}$	$-1.96(29)\cdot10^{-5}$
$\boldsymbol{\chi_{\rm R}^2 Q_{fd}}$	$-0.99(14)\cdot10^{-2}$	Q_{fd}	$-0.89(45)\cdot10^{-5}$
$\boldsymbol{\chi_{\rm R}L_{\rm R85}}$	$-2.10(12)\cdot10^{-2}$	$L_{\rm R85}$	$-6.25(52)\cdot10^{-4}$
$\boldsymbol{\chi_{\rm R}^2 D_{n{\rm VV}}}$	$-1.67(20)\cdot10^{-1}$	$D_{n{\rm VV}}$	$-1.49(10)\cdot10^{-4}$
$\boldsymbol{\chi_{\rm R}^2 Q_{n{\rm VV}}}$	$-8.44(67)\cdot10^{-2}$	$Q_{n{\rm VV}}$	$-7.53(48)\cdot10^{-5}$
$\boldsymbol{\chi_{\rm R}^2 Q_{n{\rm VS}}}$	$-4.05(25)\cdot10^{-2}$	$Q_{n{\rm VS}}$	$-3.61(29)\cdot10^{-5}$

In contrast to the stable values of the η there are large fluctuations in the basic parameter $\chi_{\rm R}$: one can obtain values in the range $13 \le \chi_{\rm R} \le 40$ depending on the set of functions fitted, on the fit interval etc. This is presumably the effect of our small number (only three) of sea quark masses. In order to obtain more stable results we fixed $\eta_{0,1,2}$ according to (30) and first determined in a linear fit the three parameters $\chi_{\rm R}$, $\chi_{\rm R}L_{\rm R4W6}$ and $\chi_{\rm R}^2 Q_{nd}$ from RRn. These parameters were then used as an input in the linear fit of the remaining nine parameters.

All 18 valence quark mass dependences considered can be reasonably well fitted. The best fit is shown by Figs. 1 and 2. The sum of the chi-squares of the linear fits is $\chi^2 \simeq 300$ for a number of degrees of freedom n.d.f. $= 18\cdot12 - 12 = 204$. Most of the chi-squares comes from the points with largest and smallest valence quark masses where there are obviously some systematic deviations, too. The parameters of best fit are given in Table 4. The values in the table show that there are some discrepancies in both relations in the last line of (17), but the deviations are not very large. The first and second relation give $-0.89(49)\cdot10^{-5} \simeq 2.05(39)\cdot10^{-5}$ and $0.52(9)\cdot10^{-5} \simeq 0.92(8)\cdot10^{-5}$, respectively.

The values of the NLO- and NNLO-parameters themselves are also shown in the right hand part of Table 4, with errors determined (as always) by the linearization method. With the help of the formulas in (5) and (6) one can also transfer these results to the corresponding L and W at some other renormalization scale different from $f_0\sqrt{\chi_{\rm R}}$. Going to the conventional renormalization scale $\mu = 4\pi f_0$ and multiplying by an overall factor $128\pi^2$ one obtains the values of α_k and ω_k shown in Table 5.

Due to the unexpected smallness of the $\mathcal{O}(a)$ contributions it is interesting to try a linear fit of the valence quark mass dependences setting all $\mathcal{O}(a)$ terms to zero: $\eta_0 = \eta_1 = \eta_2 = 0$. This is a fit with eleven parameters because in the formulas $L_{\rm S4W6}$ is always multiplied by $\eta_{\rm S}$. The result is a reasonable fit but the chi-square is

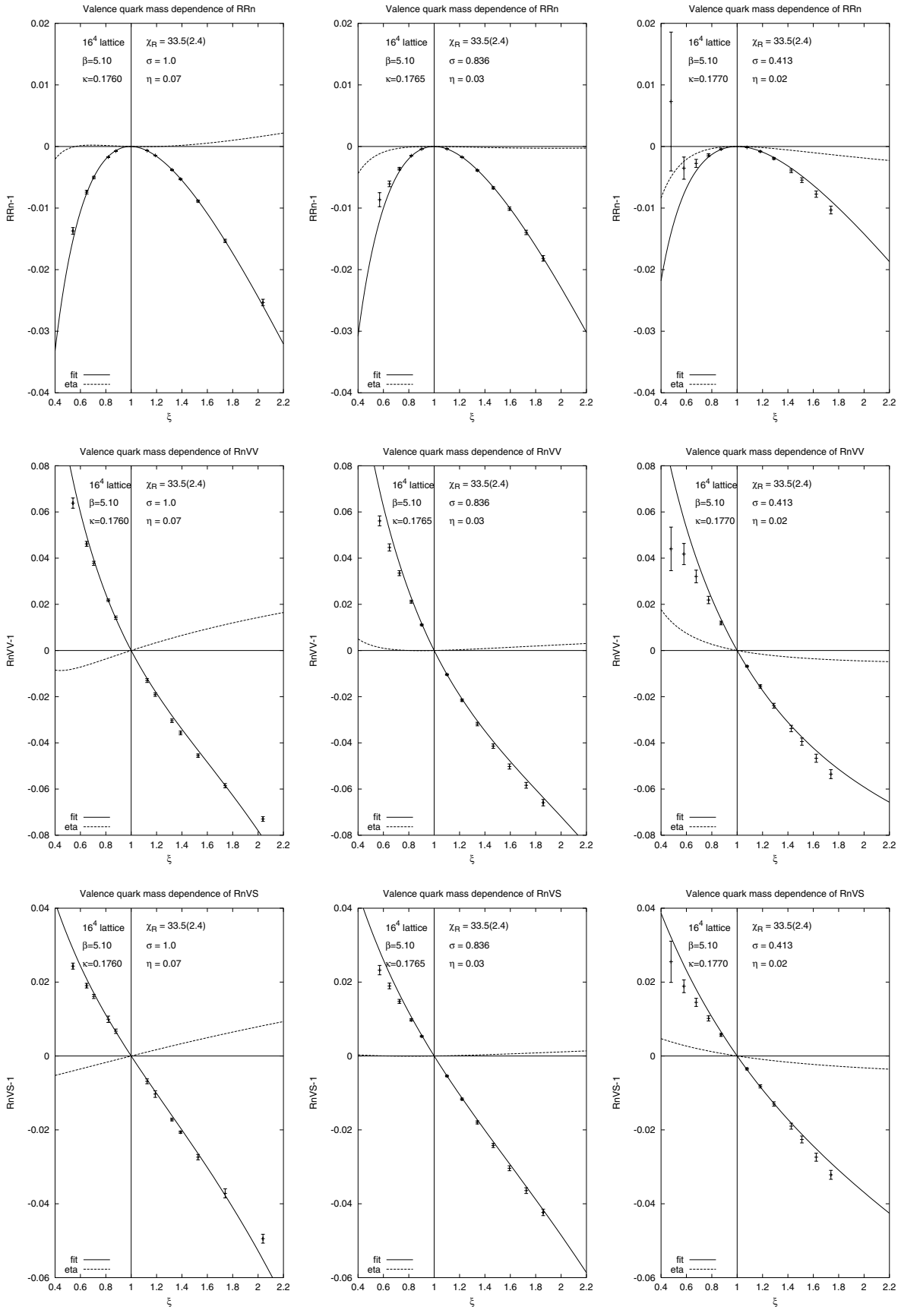

Fig. 1. $(RRn-1)$, $(Rn_{\rm VV}-1)$ and $(Rn_{\rm VS}-1)$ for the three different sea quark mass values (full lines). Beside the fit the unphysical contribution (proportional to $\eta_{\rm S}$) is separately shown (broken lines)

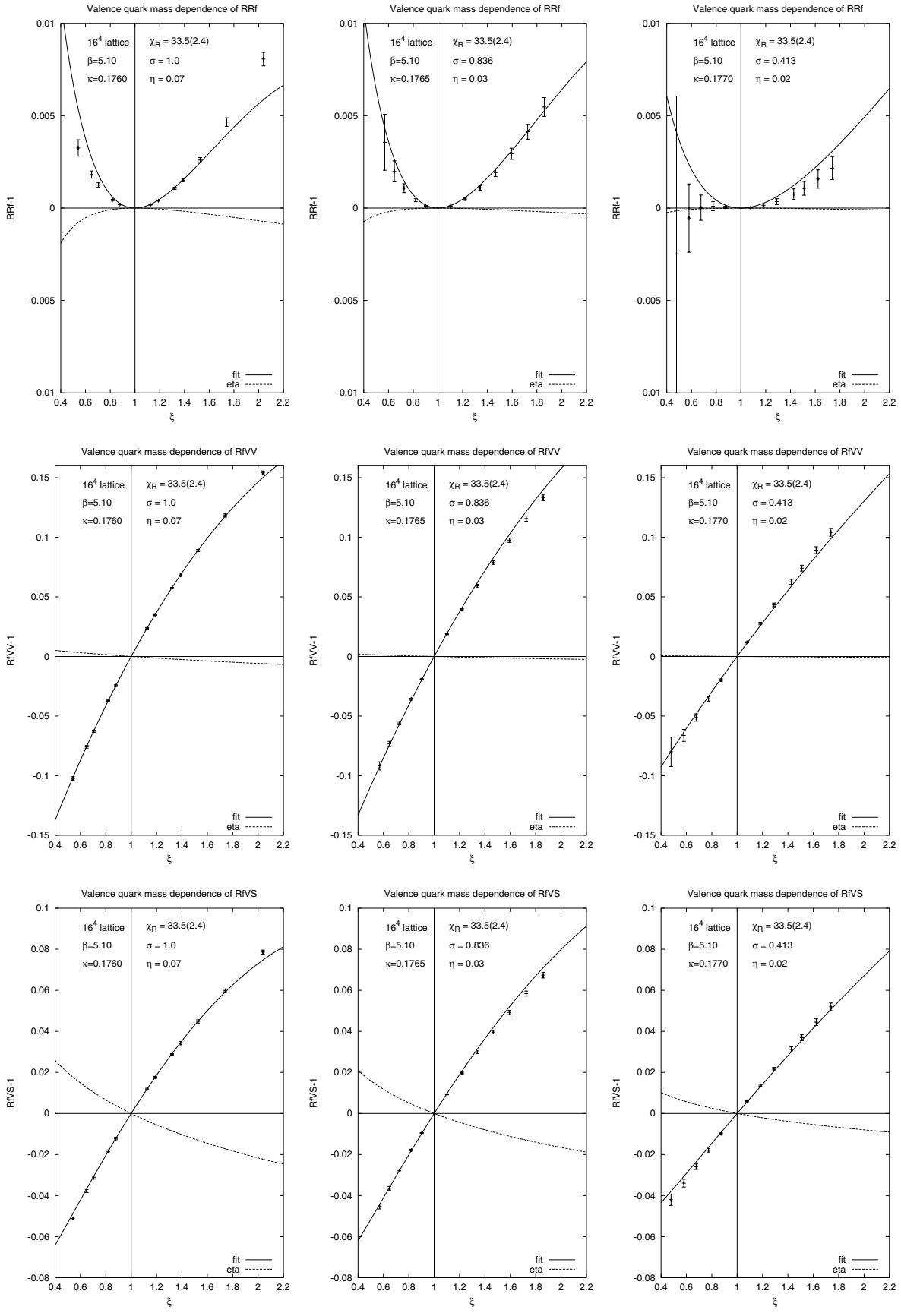

Fig. 2. $(RRf-1)$, $(Rf_{\rm VV}-1)$ and $(Rf_{\rm VS}-1)$ for the three different sea quark mass values (full lines). Beside the fit the unphysical contribution (proportional to $\eta_{\rm S}$) is separately shown (broken lines)

Table 5. Values of combinations of the α_k obtained from the best fit values in Table 4 and 6

α_5	2.24(20)				
$\alpha_{85} \equiv (2\alpha_8 - \alpha_5)$	0.762(49)			$(\alpha_4 - \omega_6)$	2.36(9)
$\alpha_{45} \equiv (2\alpha_4 - \alpha_5)$	2.40(26)	Λ_4/f_0	22.9(1.5)	ω_{45}	−1.7(1.8)
$\alpha_{6845} \equiv (4\alpha_6 + 2\alpha_8 - 2\alpha_4 - \alpha_5)$	0.658(86)	Λ_3/f_0	6.51(57)	ω_{6845}	−5.43(60)

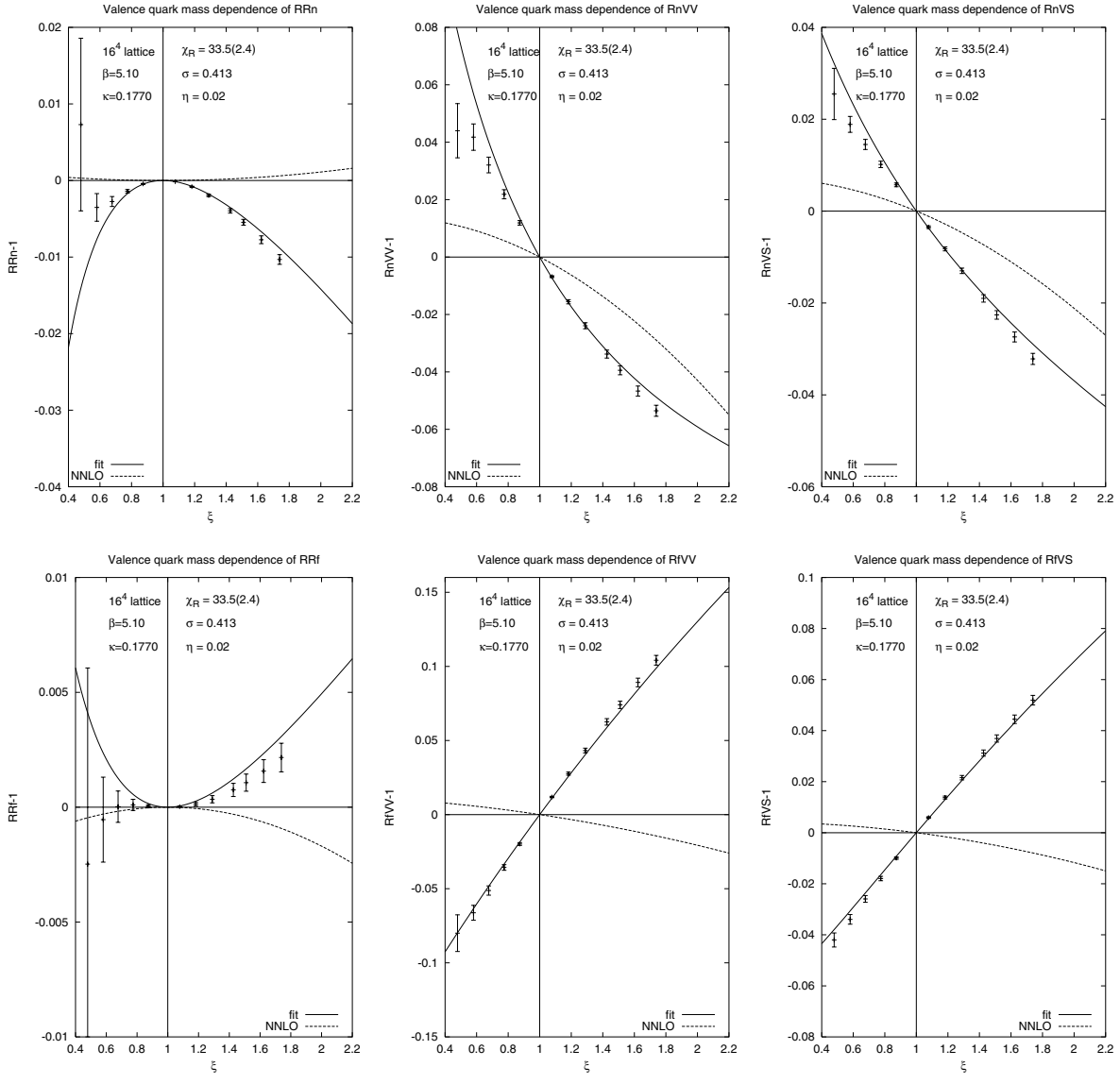

Fig. 3. NNLO tree-graph contribution at $\kappa_2 = 0.1770$ where the sea quark mass is given by $M_r \simeq 1$ (broken lines). The full lines represent the total fits shown also in Figs. 1 and 2 which are the sums of the continuum NLO, the $\mathcal{O}(a)$ and NNLO terms

by about 10% larger then in the case of $\eta_{0,1,2} \neq 0$. The best fit values of the main parameters are in this case $\chi_{\rm R} = 36.1(1.0)$, $\alpha_5 = 2.08(14)$, $\alpha_{85} = 0.502(46)$.

The NNLO tree-graph contributions are rather important especially at $\kappa = 0.176$. From the point of view of the NLO formulas the situation becomes better at $\kappa = 0.177$ but NNLO is still not negligible there; see Fig. 3. (At $\kappa = 0.1765$ we have, of course, an intermediate situation between $\kappa = 0.176$ and $\kappa = 0.177$.) In general, the NNLO contributions are more important in the ratios $R_{n\rm VV}$ and $R_{n\rm VS}$ than in $R_{f\rm VV}$ and $R_{f\rm VS}$. In fact, the ratios $R_{n\rm VV}$ and $R_{n\rm VS}$ at $\kappa = 0.176$ are dominated by NNLO. The relative importance of NNLO terms is stronger for $\xi > 1$ than for $\xi < 1$. In the double ratios RRn and RRf the NNLO terms are relatively unimportant.

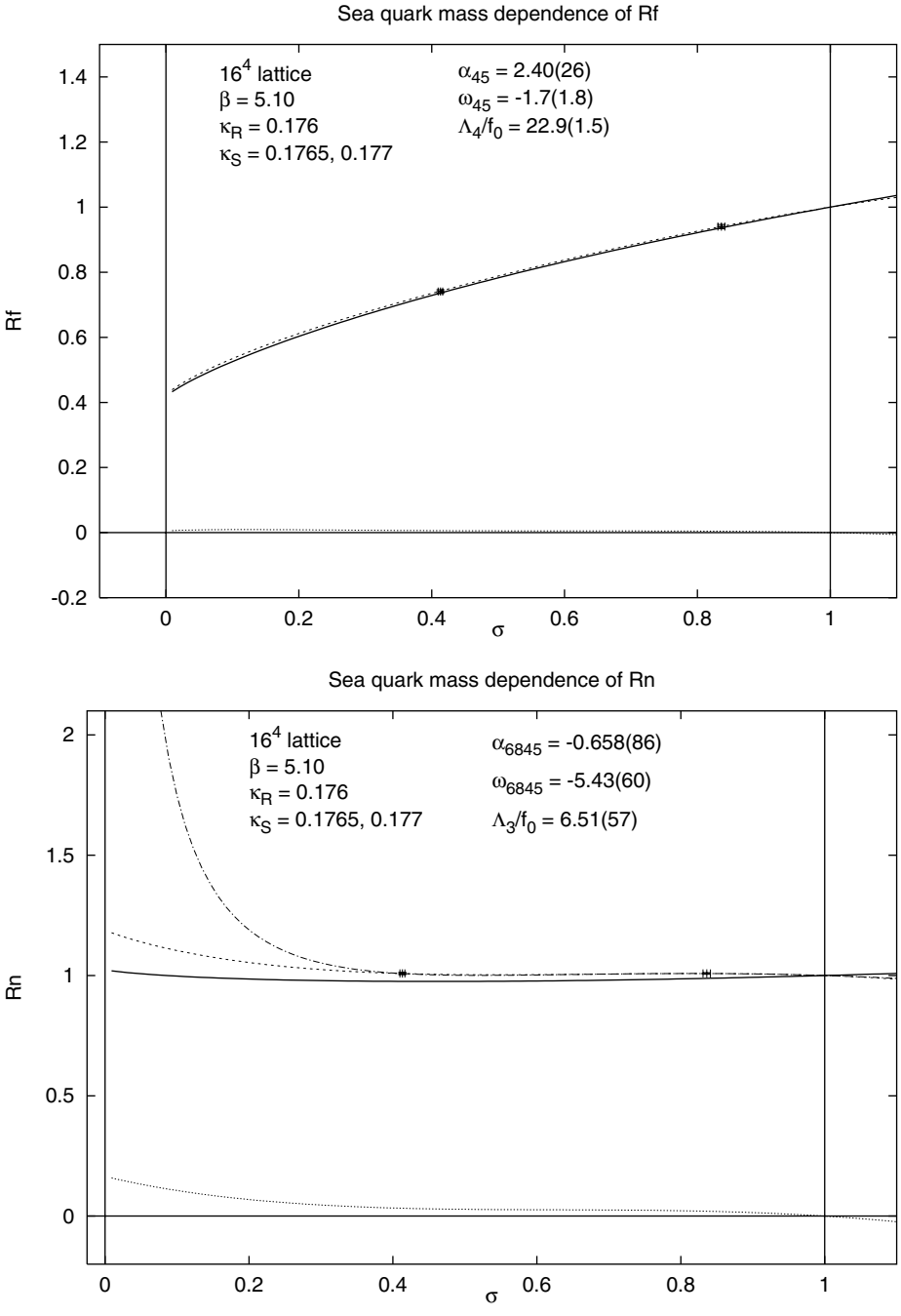

Fig. 4. $Rf_{\rm SS}$ and $Rn_{\rm SS}$. The full lines show the estimate of continuum contributions – without $\mathcal{O}(a)$ terms. The broken lines near zero show the unphysical contributions (proportional to $\eta_{\rm S}$). The other lines are different extrapolations of the measured values including $\mathcal{O}(a)$ terms (see text)

4.2 Sea quark mass dependence

The results from the fit of the valence quark mass dependence can also be used in the investigation of the sea quark mass dependence according to (22) and (23). In particular, the values (and errors) of $\chi_{\rm R}$ and $\eta_{0,1,2}$ are relevant there. Besides these values and the known ratios of the sea quark masses $\sigma_{1,2}$ (see Table 3) two extra parameter pairs appear, namely, for $N_{\rm s} = 2$,

$$L_{\rm R45} \equiv 2L_{\rm R4} + L_{\rm R5}\ , \quad W_{\rm R45} \equiv 2W_{\rm R4} + W_{\rm R5} \qquad (31)$$

in (22) and

$$\begin{aligned} L_{\rm R6845} &\equiv 4L_{\rm R6} + 2L_{\rm R8} - 2L_{\rm R4} - L_{\rm R5}\ , \\ W_{\rm R6845} &\equiv 4W_{\rm R6} + 2W_{\rm R8} - 2W_{\rm R4} - W_{\rm R5} \end{aligned} \qquad (32)$$

in (23).

Since we only have three sea quark mass values and therefore two independent values of $Rf_{\rm SS}$ and $Rn_{\rm SS}$ a "fit" actually means solving for the four unknowns. The results are collected in Table 6. The corresponding values of the

Table 6. Results for the parameters of the sea quark mass dependence. Quantities directly used in the fitting procedure are in bold face

$\boldsymbol{L_{\mathrm{R45}}}$	$4.34(28)\cdot 10^{-3}$	$Rf_{(\sigma=0)}$	0.415(19)
$\boldsymbol{W_{\mathrm{R45}}}$	$1.1(1.4)\cdot 10^{-3}$		
$\boldsymbol{L_{\mathrm{R6845}}}$	$-9.1(6.4)\cdot 10^{-5}$	$Rn_{(\sigma=0)}$	1.025(17)
$\boldsymbol{W_{\mathrm{R6845}}}$	$-5.52(48)\cdot 10^{-3}$		

α and ω are contained in Table 5. In this table also the values of the *universal low energy scales* $\Lambda_{3,4}$ are given. (For the definitions see [26, 27] or (10) in [9].) Once the parameters L_{R45} and L_{R6845} are known it is possible to extrapolate the continuum NLO curves (without the $\mathcal{O}(a)$ contributions) for Rf_{SS} and Rn_{SS} to zero sea quark mass; see Fig. 4. The values of these curves at $\sigma = 0$ are also given in Table 6.

The extrapolation of the full measured ratios, including $\mathcal{O}(a)$ contributions, requires an extrapolation of η_{S} as a function of σ which has, of course, a considerable uncertainty. The behavior of the extrapolated curve is especially sensitive to the assumed form of the η_{S}-extrapolation for Rn_{SS} near zero. For instance, if the magnitude of the $\mathcal{O}(a)$ contribution given by $\rho_{\mathrm{S}} = \eta_{\mathrm{S}}\chi_{\mathrm{S}}$ is finite at zero, which is reasonable to assume, then $Rn_{\mathrm{SS}} = m_{\mathrm{SS}}^2/(\sigma m_{\mathrm{RR}}^2)$ has a σ^{-1} singularity near zero. This is a manifestation of the fact that different definitions of the "critical line" in the (β,κ)-plane, for instance by $m_\pi^2 = 0$ or $m_q^{\mathrm{PCAC}} = 0$, in general differ by lattice artifacts (in our case by $\mathcal{O}(a)$). If, however, $\eta_{\mathrm{S}} = \rho_{\mathrm{S}}/\chi_{\mathrm{S}}$ would have a finite value at $\sigma = 0$ then there would be no such singularity. The two extrapolations shown in the lower part of Fig. 4 are examples of these two cases.

Concerning the results on the parameters obtained from the sea quark mass dependence (Table 6 and the second half of Table 5) one has to remark that the assumption of a quark mass independent lattice spacing a has an important effect on them. Assuming a quark mass independent Sommer scale parameter r_0 would change these results substantially. (There would be small changes in the first half of Table 5 due to the somewhat different values of the quark mass ratios $\sigma_{1,2}$, too.) For instance, the values of Λ_4/f_0 and Λ_3/f_0 would come out to be 16.1(1.1) and 30.4(2.9), respectively, instead of the values given in the tables. As it has been discussed above, the choice of a quark mass independent renormalization scheme requires a quark mass independent lattice spacing and is not consistent with a quark mass independent r_0 [25,28]. Nevertheless, it is plausible that in the continuum limit and in the limit of very small sea quark masses r_0/a becomes independent from the sea quark mass and the differences between the values for constant r_0 and a disappear.

5 Summary and discussion

The results obtained in this paper for the Gasser–Leutwyler constants (see Tables 4, 5 and 6) can only be taken as estimates of the values in continuum. In order to deduce continuum values with controlled error estimates the left out lattice artifacts have to be removed by performing simulations at increasing β values and extrapolating the results to $a = 0$. Reasonable next steps would be to tune the lattice spacing to $a \simeq 0.13\,\mathrm{fm}$ on $24^3\cdot 48$ and $a \simeq 0.10\,\mathrm{fm}$ on $32^3\cdot 64$ lattices. This would require with the TSMB algorithm by a factor of about 10 and 100 more computer time, respectively. Our calculations near $a \simeq 0.20\,\mathrm{fm}$ should be improved by going from 16^4 to $16^3\cdot 32$ lattices in order to improve the extraction of the physical quantities of interest. The number of sea quark masses considered should be increased to 5–6 towards smaller values. This will decrease the overall statistical errors considerably. We hope to reach sea quark masses about $m_{\mathrm{sea}} \simeq \frac{1}{6}m_{\mathrm{s}}$ on $16^3\cdot 32$ lattices in the near future.

General conclusions of the present work are the following.
(1) Compensating $\mathcal{O}(a)$ effects in the pseudo-Goldstone boson sector by introducing $\mathcal{O}(a)$ terms in the PQCh-Lagrangian itself is a viable alternative to the $\mathcal{O}(a)$-improvement of the lattice action. An extension to also treat $\mathcal{O}(a^2)$ effects in the PQCh-Lagrangian is possible [20, 21] and has been partially taken into account also in the present paper.
(2) The observed $\mathcal{O}(a)$ contributions in the pseudo-Goldstone boson sector are surprisingly small. The ratios of the $\mathcal{O}(a)$-parameters in the NLO PQCh-Lagrangian to the quark masses $\eta_{\mathrm{S}} \equiv \rho_{\mathrm{S}}/\chi_{\mathrm{S}}$ are in our present range of quark masses ($\frac{1}{3}m_{\mathrm{s}} \le m_{\mathrm{sea}} \le \frac{2}{3}m_{\mathrm{s}}$) at the few percent level.
(3) Taking ratios of pion mass squares and pion decay constants at fixed gauge coupling and varying quark masses has the advantage that the Z-factors of multiplicative renormalization as well as all sorts of quark mass independent corrections cancel.
(4) NNLO contributions in PQChPT are in our present sea quark mass range rather important. In fact, they are more important than the $\mathcal{O}(a)$ lattice artifacts. This introduces new parameters in the multi-parameter fits which makes the fitting procedure more difficult. The situation will be better at smaller sea quark masses where the importance of NNLO terms diminishes.

The present results strengthen the observation already made in our previous paper [9] that the expected behavior dictated by PQChPT sets in rather early – at relatively large lattice spacings – once the quark masses are small enough. Our present cut-off $a^{-1} \simeq 1\,\mathrm{GeV}$ is already a "high energy scale" from the point of view of the pion dynamics. As a consequence, it seems to us that the numerical study of the pseudo-Goldstone boson sector of QCD is perhaps the easiest field for obtaining new quantitative results about hadron physics by lattice simulations.

Acknowledgements. The computations were performed on the APEmille systems installed at NIC Zeuthen, the Cray T3E systems at NIC Jülich, the PC cluster at DESY Hamburg, and the Sun Fire SMP-Cluster at the Rechenzentrum - RWTH Aachen. Parts of the simulations were performed at the Eötvös University parallel PC cluster supported by Hungarian Science Foundation grants OTKA-T349809/ T37615.

We thank Steve Sharpe for correspondence on the structure of the NNLO terms in the PQChPT formulas and Marteen Golterman and Oliver Bär for helpful discussions. We thankfully acknowledge the contributions of Claus Gebert in the early stages of this work.

References

1. S. Weinberg, Phys. Rev. **166**, 1568 (1968)
2. J. Gasser, H. Leutwyler, Annals Phys. **158**, 142 (1984)
3. ALPHA Collaboration, J. Heitger et al., Nucl. Phys. B **588**, 377 (2000), hep-lat/0006026
4. UKQCD Collaboration, A.C. Irving et al., Phys. Lett. B **518**, 243 (2001), hep-lat/0107023
5. G.T. Fleming, D.R. Nelson, G.W. Kilcup, Nucl. Phys. Proc. Suppl. **106**, 221 (2002), hep-lat/0110112
6. G.T. Fleming, D.R. Nelson, G.W. Kilcup, hep-lat/0209141
7. qq+q Collaboration, F. Farchioni, C. Gebert, I. Montvay, L. Scorzato, Eur. Phys. J. C **26**, 237 (2002), hep-lat/0206008
8. qq+q Collaboration, F. Farchioni, C. Gebert, I. Montvay, L. Scorzato, hep-lat/0209142
9. qq+q Collaboration, F. Farchioni, C. Gebert, I. Montvay, E. Scholz, L. Scorzato, Phys. Lett. B **561**, 102 (2003), hep-lat/0302011
10. I. Montvay, Nucl. Phys. B **466**, 259 (1996), hep-lat/9510042
11. C.W. Bernard, M.F.L. Golterman, Phys. Rev. D **49**, 486 (1994), hep-lat/9306005
12. S.R. Sharpe, Phys. Rev. D **56**, 7052 (1997), hep-lat/9707018, Erratum D **62**, 099901 (2000)
13. M.F.L. Golterman, K.-Ch. Leung, Phys. Rev. D **57**, 5703 (1998), hep-lat/9711033
14. S.R. Sharpe, N. Shoresh, Phys. Rev. D **62**, 094503 (2000), hep-lat/0006017
15. B. Sheikholeslami, R. Wohlert, Nucl. Phys. B **259**, 572 (1985)
16. G. Rupak, N. Shoresh, Phys. Rev. D **66**, 054503 (2002), hep-lat/0201019
17. JLQCD Collaboration, S. Hashimoto et al., hep-lat/0209091
18. JLQCD Collaboration, S. Aoki et al., Nucl. Phys. Proc. Suppl. **106**, 224 (2002), hep-lat/0110179
19. S.R. Sharpe, R. Van de Water, poster presented at the Tsukuba Lattice Conference 2003, to be published in the Proceedings, hep-lat/030810
20. O. Baer, G. Rupak, N. Shoresh, hep-lat/0306021
21. S. Aoki, hep-lat/0306027
22. C. Gebert, Ph.D. Thesis, Hamburg University, 2002
23. ALPHA Collaboration, R. Frezzotti, M. Hasenbusch, U. Wolff, J. Heitger, K. Jansen, Comput. Phys. Commun. **136**, 1 (2001), hep-lat/0009027
24. U. Wolff, hep-lat/0306017
25. S. Aoki, Nucl. Phys. Proc. Suppl. **94**, 3 (2001), hep-lat/0011074
26. S. Dürr, hep-lat/0208051
27. H. Leutwyler, Nucl. Phys. Proc. Suppl. **94**, 108 (2001), hep-ph/0011049
28. R. Sommer, talk presented at the Tsukuba Lattice Conference 2003, to be published in the Proceedings

[Chi-3]

Quark mass dependence of pseudoscalar masses and decay constants on a lattice

Eur. Phys. J. C37 197-204 (2004)

Eur. Phys. J. C 37, 197–204 (2004)
Digital Object Identifier (DOI) 10.1140/epjc/s2004-01984-0

THE EUROPEAN PHYSICAL JOURNAL C

Quark mass dependence of pseudoscalar masses and decay constants on a lattice

The $qq+q$ Collaboration
F. Farchioni[1], I. Montvay[2], E. Scholz[2]

[1] Westfälische Wilhelms-Universität Münster, Institut für Theoretische Physik, Wilhelm-Klemm-Strasse 9, 48149 Münster, Germany
[2] Deutsches Elektronen-Synchrotron DESY, Notkestr. 85, 22603 Hamburg, Germany

Received: 19 March 2004 /
Published online: 24 August 2004 –

Abstract. Our previous calculations of the sea- and valence-quark mass dependence of the pseudoscalar meson masses and decay constants is repeated on a $16^3 \cdot 32$ lattice, which allows for a better determination of the quantities in question. The conclusions are similar as before on the 16^4 lattice [1]. The two light dynamical quark flavours we simulate have masses in the range $m_s/4 < m_{u,d} < 2m_s/3$. The sea quark mass dependence of f_π and m_π^2/m_q is well described by the next-to-leading order (NLO) chiral perturbation theory (ChPT) formulas and clearly shows the presence of chiral logarithms. The valence quark mass dependence requires the presence of NNLO contributions in partially quenched ChPT (PQChPT)—in addition to the NLO terms. The $\mathcal{O}(a)$ lattice artifacts in these quantities turn out to be small.

1 Introduction

In Quantum Chromodynamics (QCD) – the theory of strong interactions – there are two very light quarks and one moderately light quark (u, d and s, respectively). The strong interaction dynamics at low energies can be formulated by an *effective chiral Lagrangian*, which incorporates the symmetry constraints following from the spontaneously broken chiral symmetry of the light quarks. In this low-energy effective theory, the interactions are described by a simultaneous expansion in powers of momenta and light quark masses [2,3]. The coefficients of the interaction terms in the effective chiral Lagrangian – the *Gasser-Leutwyler constants* – are free parameters, which can be constrained by experimental data and also calculated from the underlying basic QCD Lagrangian in the framework of the nonperturbative lattice regularization.

In numerical lattice QCD simulations, the quark masses are free parameters. Changing these parameters gives an excellent opportunity to precisely determine the Gasser-Leutwyler constants. In fact, chiral perturbation theory (ChPT) based on the chiral Lagrangian can be extended by changing the *valence quark masses* in quark propagators independently from the *sea quark masses* in virtual quark loops. This leads to partially quenched chiral perturbation theory (PQChPT) [4].

The aim of numerical simulations in QCD is to reach the regime of light quark masses where next-to-leading order (NLO) chiral perturbation theory gives a good approximation. In previous papers [5,6,1], our collaboration started a series of simulations with two equal-mass light quarks (qq) with the goal of extracting the values of the Gasser-Leutwyler constants conventionally denoted by L_k, $(k = 1, 2, \ldots)$. Later on, it will be possible to extend these calculations by also including the s-quark ($qq+q$).

In our previous paper [1], we started some larger scale simulations on a 16^4 lattice at the gauge coupling $\beta = 5.1$, which corresponds to a lattice spacing of $a \simeq 0.2\,\mathrm{fm}$. Because it became clear that interesting results can be obtained already at this relatively rough discretization scale, we decided to repeat and extend these simulations on a $16^3 \cdot 32$ lattice, which is better suited for extracting quantities like the pseudoscalar (pion) mass (m_π) and decay constant (f_π). Our work profited from the valuable experience of previous simulations by other collaborations [7–9].

Because the present work is on the same topics as [1], we shall often only refer to it without repeating its full content. In general, we use the conventions and notations of [1,6,5]. Nevertheless, we also try to make the present paper easily understandable for the reader and therefore repeat the main definitions and relations. In the next section, we deal with the sea quark mass dependence of f_π and m_π. In Sect. 3, the valence quark mass dependence is considered and the question of the magnitude of leading lattice artifacts is investigated. Section 4 is a short summary of our experience with the Monte Carlo updating algorithm. The last section contains the summary and discussion.

2 Sea quark mass dependence

We performed Monte Carlo simulations with $N_s = 2$ degenerate sea quarks on a $16^3 \cdot 32$ lattice at gauge coupling $\beta = 5.1$ and four values of the hopping parameter κ: $\kappa_0 = 0.176$, $\kappa_1 = 0.1765$, $\kappa_2 = 0.1768$ and $\kappa_3 = 0.177$. Three of these points have also been simulated previously on the 16^4 lattice in [1]. The point at $\kappa_2 = 0.1768$ is new. We collected 950–1000 gauge configurations per point, which are typically separated by 10 update cycles consisting of boson-field and gauge-field updates and noisy correction steps. (Some observations about the algorithm will be summarized in Sect. 4.)

A collection of the values of some basic quantities in these simulation points is given in Table 1: the Sommer scale-parameter in lattice units, r_0/a; the pion mass in lattice units, am_π; the quark mass parameter, $M_r = (r_0 m_\pi)^2$; the bare PCAC quark mass $Z_q a m_q$, including the multiplicative renormalization factor, $Z_q = Z_P/Z_A$; the ratio of the PCAC quark masses σ_i with respect to the *reference sea quark mass* at $\kappa = \kappa_0$ and the pion decay constant in lattice units, af_π divided by the renormalization factor Z_A. (The normalization of the pion decay constant is such that the physical value is $f_\pi \simeq 93\,\mathrm{MeV}$.)

Comparing Table 1 to the corresponding one (Table 3) in [1], one can see that these quantities extracted on the $16^3 \cdot 32$ lattice differ considerably from those extracted on the 16^4 lattice. The change of r_0/a is about 2–5%. The difference in am_π increases from 3% at κ_0 to about 16% at κ_3, whereas $Z_q a m_q$ differs at κ_0 by 5% and at κ_3 already by about 28%. However, as we shall see later on, considering ratios of the pion mass-square and of the pion decay constant as a function of the ratios of PCAC quark masses (denoted by σ for sea quark masses and ξ for valence quark masses), it turns out that almost all changes between the 16^4 and $16^3 \cdot 32$ lattices cancel.

In Table 1, the bare quark mass obtained from the PCAC relation is shown: $m_q \equiv m_q^{PCAC}$. (For details of its numerical determination, see Sect. 3.1.1 in [5].) Another possibility to define the quark mass is to take $am_{ren} \equiv \mu_{ren} \equiv Z_m(\mu_0 - \mu_{cr})$, where $\mu_0 = 1/(2\kappa) - 4$ is the bare quark mass in the Wilson–fermion action, μ_{cr} is its critical value corresponding to zero quark mass and Z_R is an appropriate multiplicative renormalization factor. The values of μ_0 corresponding to $\kappa_0, ..., \kappa_3$ are $\mu_{0(0)} = -1.1590909...$, $\mu_{0(1)} = -1.1671388...$, $\mu_{0(2)} = -1.1719457...$, $\mu_{0(3)} = -1.1751412...$, respectively. Comparing the values of $Z_q a m_q$ or σ_i in Table 1 to the values $\mu_{0(i)}$, one can see that the relation between them is highly nonlinear. This implies the same also for the relation between the (ratios of) m_q^{PCAC} and m_{ren}. The nonlinear terms in this relation are lattice artifacts, which have to vanish in the continuum limit, but they are large at our lattice spacings.

A consequence of the strongly nonlinear relation between σ and μ_0 is that the determination of μ_{cr} (or κ_{cr}) has large uncertainty. In fact, with our four points only, we could not find a convincing extrapolation of σ to zero. A crude quadratic extrapolation gives $\mu_{cr} = -1.180(4)$ or $\kappa_{cr} = 0.1773(2)$. The uncertainty in the critical point implies an uncertainty in the extrapolation of physical quantities, too, which is necessary in a quark mass-independent renormalization scheme. In case of the lattice spacing, which can be obtained from the extrapolation of r_0/a to the critical point, Table 1 shows that the values of r_0/a increase between κ_0 and κ_2, but between κ_2 and κ_3, they are within error constants. Therefore, we take this constant value as the extrapolated one: $[r_0/a]_{cr} = 2.57(5)$. This gives, with $r_0 \equiv 0.5\,\mathrm{fm}$, for the quark mass independent lattice spacing $a = 0.195(4)\,\mathrm{fm}$.

In the ChPT formulas, the quark mass can be represented by the dimensionless quantity

$$\chi \equiv \frac{2B_0 m_q}{f_0^2}, \tag{1}$$

where B_0 is a conventional parameter with dimension mass and f_0 is the value of the pion decay constant at zero quark mass. (Its normalization here is such that the physical value is $f_0 \simeq 93\,\mathrm{MeV}$.) In what follows, we shall identify the quark mass m_q in χ with the PCAC quark mass m_q^{PCAC}. According to the previous discussion, this is a nontrivial choice because the lattice artifacts in (ratios of) the quark mass are rather different for am_q^{PCAC} than, for instance, for am_{ren}.

The sea quark mass dependence of the ratio of the pion decay constant in NLO of ChPT is:

$$Rf_{SS} \equiv \tfrac{f_{SS}}{f_{RR}} = 1 + 4(\sigma - 1)\chi_R(N_s L_{R4} + L_{R5}) - \frac{N_s \chi_R}{32\pi^2}\sigma \log \sigma + \mathcal{O}(\chi_R^2). \tag{2}$$

Here f_{SS} is the pion decay constant of a pion consisting of two sea quarks with mass χ_S and f_{RR} is its

Table 1. The values of some basic quantities in our simulation points. Statistical errors in last digits are given in parentheses

κ	κ_0	κ_1	κ_2	κ_3
r_0/a	2.229(63)	2.212(44)	2.621(46)	2.528(51)
am_π	0.6542(10)	0.5793(17)	0.3919(46)	0.3657(24)
$M_r = (r_0 m_\pi)^2$	2.13(12)	1.642(72)	1.055(36)	0.855(34)
$Z_q a m_q$	0.07092(27)	0.05571(30)	0.02566(27)	0.02208(21)
$\sigma_i = m_{qi}/m_{q0}$	1.0	0.7856(56)	0.3618(44)	0.3113(31)
$Z_A^{-1} a f_\pi$	0.2819(15)	0.2590(14)	0.2008(17)	0.1936(16)

value at some *reference quark mass* χ_R. N_s is the number of mass-degenerate sea quarks (actually $N_s = 2$), L_{Rk} $(k = 4, 5, \ldots)$ are Gasser-Leutwyler constants at the scale $\mu = f_0\sqrt{\chi_R}$ and the ratio of sea quark masses to the reference quark mass is

$$\sigma \equiv \frac{\chi_S}{\chi_R}. \tag{3}$$

The analogous formula for the pion mass squares is:

$$\begin{aligned} Rn_{SS} \equiv \frac{m_{SS}^2}{\sigma m_{RR}^2} = 1 + 8(\sigma-1)\chi_R \cdot \\ \cdot(2N_s L_{R6} + 2L_{R8} - N_s L_{R4} - L_{R5}) \\ + \frac{\chi_R}{16\pi^2 N_s}\sigma\log\sigma + \mathcal{O}(\chi_R^2). \end{aligned} \tag{4}$$

Note that instead of the scale-dependent combinations (at $N_s = 2$),

$$\begin{aligned} L_{R45} &\equiv 2L_{R4} + L_{R5}\ , \\ L_{R6845} &\equiv 4L_{R6} + 2L_{R8} - 2L_{R4} - L_{R5}, \end{aligned} \tag{5}$$

one can also use the *universal low-energy scales* $\Lambda_{3,4}$ defined by [10].

$$\begin{aligned} \Lambda_3 &= 4\pi f_0 \exp(-\alpha_{6845})\ , \\ \alpha_{6845} &= 128\pi^2 L_{R6845} - \frac{1}{2}\log\frac{\chi_R}{16\pi^2} \\ \Lambda_4 &= 4\pi f_0 \exp(\alpha_{45}/4)\ , \\ \alpha_{45} &= 128\pi^2 L_{R45} + 2\log\frac{\chi_R}{16\pi^2}. \end{aligned} \tag{6}$$

The free parameters in Rf_{SS} and Rn_{SS} are χ_R, $\chi_R L_{R45}$ and $\chi_R L_{R6845}$. With the small number of points we have, the linear fit with these parameters gives a good chi-square but relatively large errors: $\chi^2 = 0.8$ and

$$\begin{aligned} \chi_R &= 30.8(9.4), \\ \chi_R L_{R45} &= 0.1398(86), \\ \chi_R L_{R6845} &= -0.0078(22). \end{aligned} \tag{7}$$

This corresponds to

$$\begin{aligned} L_{R45} = 4.5(1.1)\cdot 10^{-3},\ \frac{\Lambda_4}{f_0} = 23.3(8.2), \\ L_{R6845} = -2.54(21)\cdot 10^{-4},\ \frac{\Lambda_3}{f_0} = 7.64(14). \end{aligned} \tag{8}$$

Consistent results with smaller errors can be obtained if one takes the value of $\chi_R = 35.8(3.3)$ from the fit of the valence quark mass dependences (see next section) and performs two linear fits with the parameters $\chi_R L_{R45}$ and $\chi_R L_{R6845}$, respectively. The resulting parameters are

$$\begin{aligned} \chi_R L_{R45} &= 0.1443(15), \\ L_{R45} = 4.03(37)\cdot 10^{-3},\ \frac{\Lambda_4}{f_0} &= 21.4(1.5), \\ \chi_R L_{R6845} &= -0.00896(86), \\ L_{R6845} = -2.50(34)\cdot 10^{-4},\ \frac{\Lambda_3}{f_0} &= 8.21(27) \end{aligned} \tag{9}$$

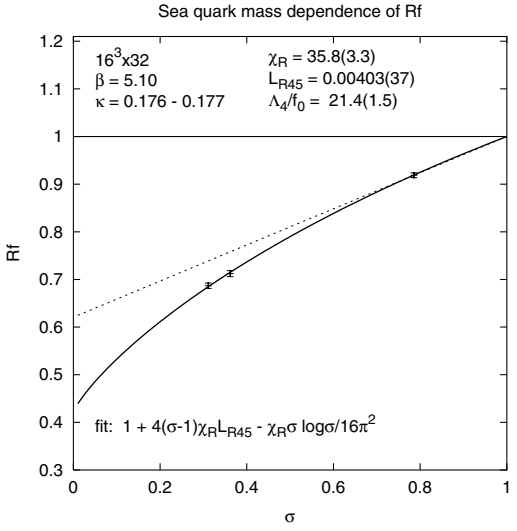

Fig. 1. Sea quark mass dependence of the pion decay constant. The straight dashed line connects the first two points

and the fits are shown in Figs. 1 and 2.

As these figures show, both Rf_{SS} and Rn_{SS} can be well fitted with the NLO ChPT formula. The fit parameters are within the expected range. For instance, the value of χ_R is rather close to the tree-level estimate $\chi_R^{estimate} \approx M_r/(r_0 f_0)^2 \simeq 40.3$. (Here we used $r_0 f_0 \simeq 0.23$.) The presence of a *chiral logarithm*, which causes the curvature, is clearly displayed in Fig. 1, where a straight line connecting the first two points is also shown. In Rn_{SS}, the measured points are consistent with the presence of a chiral logarithm but the relative errors are large because all the values including the ChPT fit are very close to 1. This implies that the deviation from the tree-level behaviour $m_{SS}^2 \propto \chi_S$ is rather small. The results for the parameters in (9) are close to the ones reported in [1]: the values for

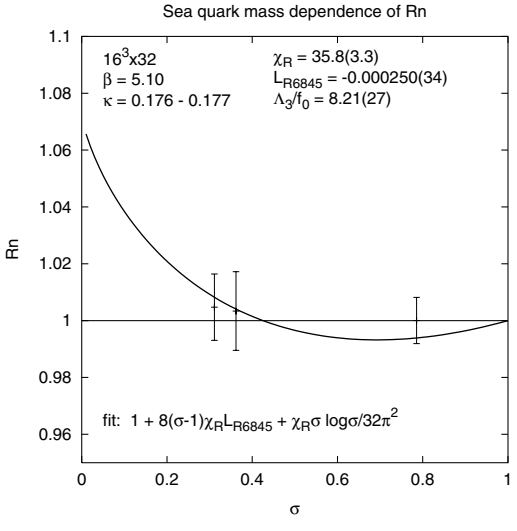

Fig. 2. Sea quark mass dependence of the pion mass-squared divided by the quark mass

Λ_4/f_0 practically coincide and the value of Λ_3/f_0 is only slightly higher now.

The extrapolated values of Rf_{SS} and Rn_{SS} at zero quark mass are, respectively:

$$Rf_0 = 0.4228(60), \qquad Rn_0 = 1.0717(69). \tag{10}$$

The value of Rf_0 together with $Z_A^{-1} a f_\pi$ from Table 1 and $r_0 = 0.5\,\mathrm{fm}$ imply, for the pion decay constant, at zero quark mass (f_0)

$$Z_A^{-1} f_0 = 121(5)\,\mathrm{MeV}. \tag{11}$$

This result for $N_s = 2$ light quarks compares well with the phenomenological value $f_0 = 93\,\mathrm{MeV}$ if, as expected, $Z_A = \mathcal{O}(1)$.

3 Valence quark mass dependence

We consider, for fixed sea quark mass χ_S, the valence quark mass dependence of f_π and m_π^2 as a function of the quark mass ratio

$$\xi \equiv \frac{\chi_V}{\chi_S}. \tag{12}$$

In our numerical data, we determined the pseudoscalar mass and decay constant in relatively wide ranges of the valence quark mass ratios, typically $\frac{1}{2} \le \xi \le 2$. At the smaller quark masses ($\kappa = \kappa_{2,3}$), however, for $\xi < 1$ *exceptional gauge configurations* appear, which blow up the statistical errors and clearly influence the mean values themselves. Therefore, in most cases, we restrict our fits to valence quark masses larger than the sea quark mass ($\xi > 1$).

In the partially quenched situation, several types of ratios can be constructed because the pseudoscalar meson can be the bound state of two valence quarks (VV) and also a valence quark and a sea quark (VS). The PQChPT formulas for the ratios of decay constants are:

$$\begin{aligned} Rf_{VV} \equiv \frac{f_{VV}}{f_{SS}} &= 1 + 4(\xi-1)\chi_S L_{S5} \\ &\quad - \frac{N_s \chi_S}{64\pi^2}(1+\xi)\log\frac{1+\xi}{2} \\ &\quad + D_{fVV}\chi_S^2(\xi-1) + Q_{fVV}\chi_S^2(\xi-1)^2 \\ &\quad + \mathcal{O}(\chi_S^2\log\xi, \chi_S^3) \end{aligned} \tag{13}$$

and

$$\begin{aligned} Rf_{VS} \equiv \frac{f_{VS}}{f_{SS}} &= 1 + 2(\xi-1)\chi_S L_{S5} \\ &\quad + \frac{\chi_S}{64 N_s \pi^2}(\xi - 1 - \log\xi) \\ &\quad - \frac{N_s \chi_S}{128\pi^2}(1+\xi)\log\frac{1+\xi}{2} \\ &\quad + \frac{1}{2} D_{fVV}\chi_S^2(\xi-1) + Q_{fVS}\chi_S^2(\xi-1)^2 \\ &\quad + \mathcal{O}(\chi_S^2\log\xi, \chi_S^3). \end{aligned} \tag{14}$$

The analogous formulas for the valence quark mass dependence of the (squared) pseudoscalar meson masses are:

$$\begin{aligned} Rn_{VV} \equiv \frac{m_{VV}^2}{\xi m_{SS}^2} &= 1 + 8(\xi-1)\chi_S(2L_{S8} - L_{S5}) \\ &\quad + \frac{\chi_S}{16 N_s \pi^2}[\xi - 1 + (2\xi-1)\log\xi] \\ &\quad + D_{nVV}\chi_S^2(\xi-1) + Q_{nVV}\chi_S^2(\xi-1)^2 \\ &\quad + \mathcal{O}(\chi_S^2\log\xi, \chi_S^3) \end{aligned} \tag{15}$$

and

$$\begin{aligned} Rn_{VS} \equiv \frac{2m_{VS}^2}{(\xi+1)m_{SS}^2} &= 1 + 4(\xi-1)\chi_S(2L_{S8} - L_{S5}) \\ &\quad + \frac{\chi_S}{16 N_s \pi^2}\xi\log\xi \\ &\quad + \frac{1}{2} D_{nVV}\chi_S^2(\xi-1) + Q_{nVS}\chi_S^2(\xi-1)^2 \\ &\quad + \mathcal{O}(\chi_S^2\log\xi, \chi_S^3). \end{aligned} \tag{16}$$

In these formulas the Gasser-Leutwyler coefficients, L_{Sk} ($k = 4, 5, \ldots$), are defined at the scale $f_0\sqrt{\chi_S}$ and, in addition to the NLO terms, also the tree-graph (i.e. counterterm) contributions of the NNLO are included. Their general form is taken from [11] and is discussed in more detail in Sect. 2.1 of [1]. The left-out terms of NNLO, which come from two-loop integrals, are generically denoted here by $\mathcal{O}(\chi_S^2\log\xi)$.

In addition to the *single ratios*, Rf_{VV}, Rf_{VS}, Rn_{VV} and Rn_{VS}, it is useful to consider the so-called *double ratios*, which do not depend on any of the NLO coefficients L_{Sk}. The PQChPT formulas for the double ratios are:

$$\begin{aligned} RRf \equiv \frac{f_{VS}^2}{f_{VV} f_{SS}} &= 1 + \frac{\chi_S}{32 N_s \pi^2}(\xi - 1 - \log\xi) \\ &\quad + Q_{fd}\chi_S^2(\xi-1)^2 + \mathcal{O}(\chi_S^2\log\xi, \chi_S^3) \end{aligned} \tag{17}$$

and

$$\begin{aligned} RRn \equiv \frac{4\xi m_{VS}^4}{(\xi+1)^2 m_{VV}^2 m_{SS}^2} &= 1 - \frac{\chi_S}{16 N_s \pi^2}(\xi - 1 - \log\xi) \\ &\quad + Q_{nd}\chi_S^2(\xi-1)^2 + \mathcal{O}(\chi_S^2\log\xi, \chi_S^3). \end{aligned} \tag{18}$$

In the PQChPT formulas (13)-(18), there are altogether 11 parameters. Three of them appear at NLO, namely with $N_s = 2$,

$$\chi_R\,, \qquad \chi_R L_{R5}\,, \qquad \chi_R L_{R85} \equiv \chi_R(2L_{R8} - L_{R5}), \tag{19}$$

and the rest in NNLO:

$$\chi_R^2 D_{fVV,nVV}\,, \qquad \chi_R^2 Q_{fVV,fVS,fd,nVV,nVS,nd}. \tag{20}$$

At the smallest quark mass, fits with the NLO formulas are reasonable but for the larger quark masses the NNLO contributions are required unless the fits are restricted to a small range around $\xi = 1$.

An acceptable global fit with 11 parameters can be achieved if the valence quark mass dependence at all four sea quark masses is simultaneously considered. In this case, one has to choose a *reference sea quark mass*, χ_R, and take into account the relation between the NLO parameters

$$L_{Sk} = L_{Rk} - c_k \log \frac{\chi_S}{\chi_R}, \tag{21}$$

where the relevant constants are:

$$c_5 = \frac{1}{128\pi^2}\ , \qquad c_{85} \equiv 2c_8 - c_5 = -\frac{1}{128\pi^2}. \tag{22}$$

Fitting all six valence quark mass dependences, (Rf_{VV}, Rf_{VS}, RRf, Rn_{VV}, Rn_{VS}, RRn), there are reasonably good 11 parameter (linear) fits with $\chi^2 \simeq 200 \simeq$ degrees of freedom. A typical set of the resulting fit parameters is shown in Table 2.

Comparing Table 2 with the corresponding one (Table 4) in [1], one can see that most values are, within statistical errors, the same. This is also true for the NLO

Table 2. Values of best fit parameters for the valence quark mass dependence. Quantities directly used in the fitting procedure are in boldface

$\boldsymbol{\chi_R}$	35.8(3.3)		
$\boldsymbol{\chi_R L_{R5}}$	0.1003(76)	L_{R5}	$2.80(39)\cdot 10^{-3}$
$\boldsymbol{\chi_R L_{R85}}$	−0.0256(12)	L_{R85}	$-0.714(65)\cdot 10^{-3}$
$\boldsymbol{\chi_R^2 D_{fVV}}$	−0.109(42)	D_{fVV}	$-8.5(4.4)\cdot 10^{-5}$
$\boldsymbol{\chi_R^2 Q_{fVV}}$	−0.014(29)	Q_{fVV}	$-1.1(2.3)\cdot 10^{-5}$
$\boldsymbol{\chi_R^2 Q_{fVS}}$	−0.0177(94)	Q_{fVS}	$-1.39(81)\cdot 10^{-5}$
$\boldsymbol{\chi_R^2 Q_{fd}}$	−0.0180(31)	Q_{fd}	$-1.41(13)\cdot 10^{-5}$
$\boldsymbol{\chi_R^2 D_{nVV}}$	−0.134(21)	D_{nVV}	$-10.46(93)\cdot 10^{-5}$
$\boldsymbol{\chi_R^2 Q_{nVV}}$	−0.087(13)	Q_{nVV}	$-6.77(30)\cdot 10^{-5}$
$\boldsymbol{\chi_R^2 Q_{nVS}}$	−0.0394(44)	Q_{nVS}	$-3.07(24)\cdot 10^{-5}$
$\boldsymbol{\chi_R^2 Q_{nd}}$	0.0077(48)	Q_{nd}	$0.60(26)\cdot 10^{-5}$

parameters defined at the scale $4\pi f_0$, which are now

$$\alpha_5 \equiv 128\pi^2 L_{R5} + \log\frac{\chi_R}{16\pi^2} = 2.06(42),$$
$$\alpha_{85} \equiv 2\alpha_8 - \alpha_5 \equiv 128\pi^2 L_{R85} - \log\frac{\chi_R}{16\pi^2} = 0.583(45). \tag{23}$$

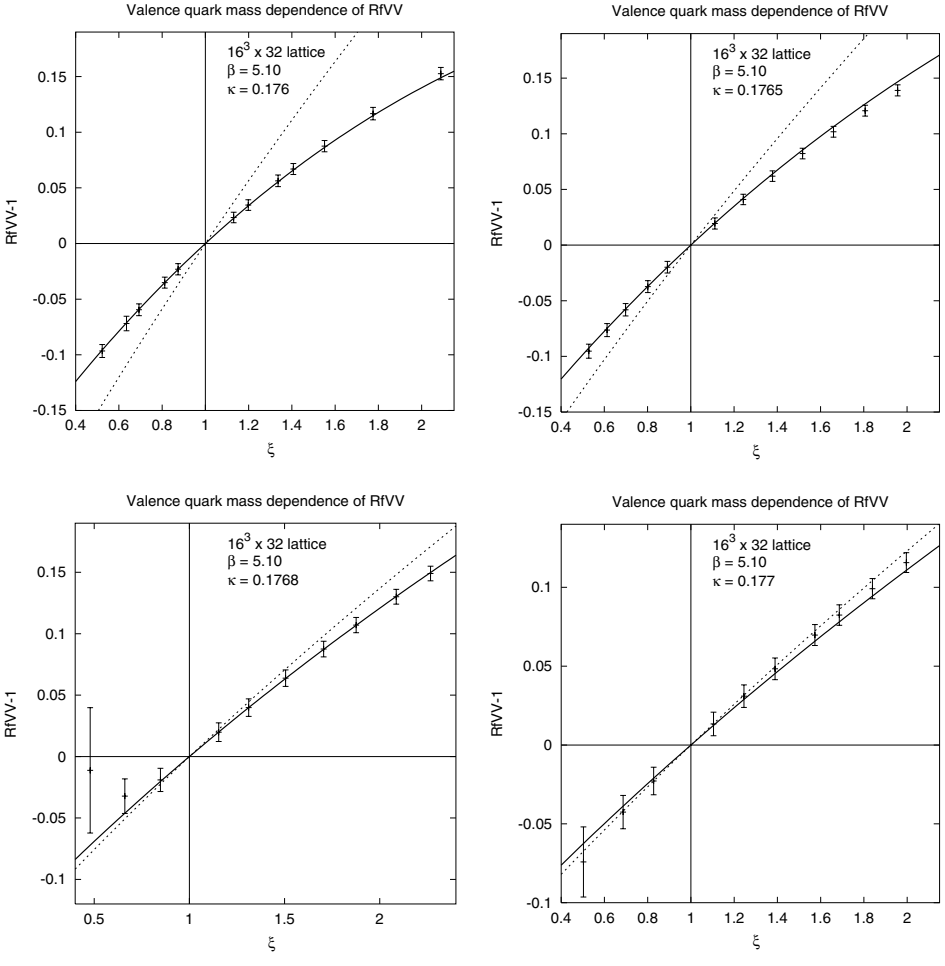

Fig. 3. The linear fit for Rf_{VV} for different sea quark masses. The NLO contributions alone are shown by dashed lines

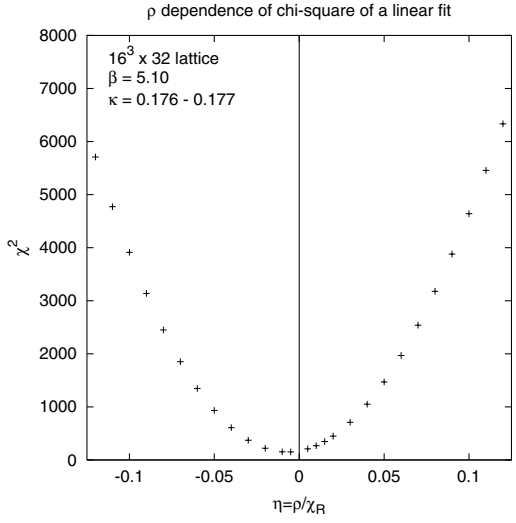

Fig. 4. χ^2 of the linear fit of the ratios Rf_{VV}, Rf_{VS}, RRf, Rn_{VV}, Rn_{VS} and RRn for all four sea quark masses at fixed values of the $\mathcal{O}(a)$ parameter ρ in the chiral Lagrangian

The value of α_5 is practically the same as in Table 5 of [1], whereas α_{85} is slightly smaller now.

The tree-graph NNLO contributions play an important role in the global fits of the valence quark dependences, especially at the two larger sea quark masses ($\kappa = \kappa_0$ and $\kappa = \kappa_1$). At the two smaller sea quark masses, NNLO is substantially less important. This is illustrated in Fig. 3, where the 11 parameter fit for Rf_{VV} is shown together with the NLO contributions alone.

3.1 $\mathcal{O}(a)$ terms

The fits above have been performed with the continuum formulas – without $\mathcal{O}(a)$ or any other lattice artifacts. The fits are reasonably good and the resulting parameters are quite similar to those obtained in [1], where the $\mathcal{O}(a)$ terms have been taken into account in the (PQ)ChPT Lagrangian according to [12]. It has been observed already in [1] that the parameter in the chiral Lagrangian characterizing the magnitude of $\mathcal{O}(a)$ effects,

$$\rho \equiv \frac{2W_0 a c_{SW}}{f_0^2}, \tag{24}$$

is rather small compared with the quark mass parameter χ in (1). Fitting the ratio $\eta_S \equiv \rho_S/\chi_S$ separately for the individual sea quark mass values, we obtained increasing values for increasing sea quark masses: $0.02 \le \eta_S \le 0.07$.

The parameter ρ should be independent of the quark mass because the quark masses are the other expansion parameters in the chiral Lagrangian. This means that a quark mass dependent ρ_S incorporates some higher order effects proportional to some power of am_q. (For instance, a linearly increasing value of η_S corresponds to $\rho_S \propto (am_q)^2$.) Because the observed values of ρ are small anyway, it is interesting to consider the behaviour of the chi-square as a function of ρ if the linear fits are performed for fixed ρ . Because of the presence of another new parameter describing $\mathcal{O}(a)$ effects in the chiral Lagrangian, the linear fit has 12 parameters for $\rho \neq 0$ (instead of 11 for $\rho = 0$). As is shown by Fig. 4, the χ^2 of the fit has a minimum near $\rho = \eta = 0$ and becomes extremely large already at $|\eta| \simeq 0.1$. where the absolute value of ρ is 10% of the value of the reference quark mass parameter χ_R. Another way to investigate the importance of $\mathcal{O}(a)$ effects in our data is to consider the following combination of double ratios:

$$RRn + 2\,RRf - 3 = (Q_{nd} + 2Q_{fd})\chi_S^2(\xi-1)^2 + \mathcal{O}(\chi_S^2 \log\xi, \chi_S^3). \tag{25}$$

As this formula shows, this combination vanishes in next-to-leading order and only NNLO and higher orders contribute to it. On the lattice, there could also be $\mathcal{O}(a)$ contributions, which can be parametrized as

$$\begin{aligned} RRn + 2\,RRf - 3 = {} & 16\rho\, L_{S4W6}\frac{(\xi-1)^2}{\xi(\xi+1)} - \rho\,\frac{(\xi-1)^2}{\chi_S\xi(\xi+1)} \\ & + \rho\,\frac{[2(1-\xi^2)+\log\xi+3\xi^2\log\xi]}{32\pi^2\xi(\xi+1)} \\ & + \rho\,\frac{(\xi-1-\xi\log\xi)}{32\pi^2\xi} \\ & + \mathcal{O}(\rho^2,\chi^2). \end{aligned} \tag{26}$$

Here only the linear piece of the $\eta_S = \rho/\chi_S$-dependence is kept because η_S is small. $L_{S4W6} \equiv L_{S4} - W_{S6}$ is a new parameter appearing in the $\mathcal{O}(a)$ terms of the chiral Lagrangian [12].

The linear fits with $\chi_S^2 Q_{n2f} \equiv \chi_S^2(Q_{nd}+2Q_{fd})$ in (25) and with ρ in (26), respectively, are shown in case of the smallest sea quark mass ($\kappa = \kappa_3$) by Fig. 5. As this figure shows, the NNLO fit with $\chi_S^2 Q_{n2f}$ is better ($\chi^2 = 1.3$) than the one with the leading $\mathcal{O}(a)$ term proportional to ρ ($\chi^2 = 7.2$). For simplicity, the parameters $\chi_S = 11.7$ and

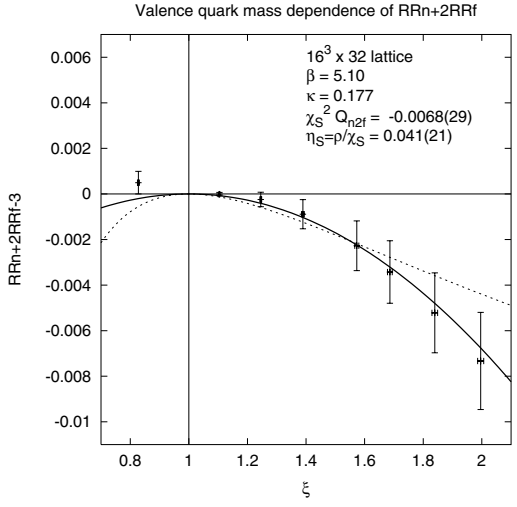

Fig. 5. Comparing the NNLO fit (full line) with the leading $\mathcal{O}(a)$ fit (dashed line) for $(RRn + 2\,RRf - 3)$ at $\kappa = \kappa_3$

$L_{S4W6} = 0.001$ are fixed in this latter case, but taking other values does not change the qualitative picture.

At the larger sea quark mass values, the fits with the leading $\mathcal{O}(a)$ terms behave similarly to Fig. 5. This supports the fact that the $\mathcal{O}(a)$ terms are not important in our numerical data. As shown by Fig. 4, good fits can only be obtained at rather small values of $\eta = \rho/\chi$. In contrast, the NNLO contributions are very important, especially at our larger sea quark masses.

4 Studies of the updating algorithm

The numerical simulations have been performed by the two-step multi-boson (TSMB) algorithm [13]. This dynamical fermion update algorithm is based on the *multiboson representation* of the fermion determinant [14], and in its present form, it incorporates several modern ideas of fermionic updating: the *global correction step* in the update [15], the final *reweighting correction* [16] and the *determinant breakup* [17].

Our error analysis is based on measuring the autocorrelations of the quantities in question [18,19], therefore, we can estimate the *computation cost* based on the integrated autocorrelations $\tau_{\rm int}$. In our previous papers [5,20, 21], we proposed an approximate formula for the cost,

$$C_{\tau_{\rm int}} \simeq F\,(am_q)^{-2}\,\Omega, \tag{27}$$

where am_q is the quark mass in lattice units and Ω the number of lattice points. The overall factor F depends on the quantity under investigation. If we count the cost in terms of the number of floating-point operations necessary to perform an update sequence with length $\tau_{\rm int}$, then the present simulations on $16^3 \cdot 32$ lattice are consistent with

$$F_{\rm plaquette} \simeq 7 \cdot 10^6, \qquad F_{m_\pi} \simeq 10^6, \qquad F_{f_\pi} < 4 \cdot 10^5. \tag{28}$$

In case of f_π, we only have an upper limit on $\tau_{\rm int}$ because the gauge configurations stored for the measurements were statistically independent. These numbers are somewhat smaller than our previous estimates in [5,20,21], which is due to a better tuning of algorithmic parameters. In particular, these simulations were done with a determinant breakup $N_b = 4$, which means that the fermion determinant of the two degenerate flavours ($N_f = 2$) were reproduced by $4 \otimes (N_f = \frac{1}{2})$ flavours. Another important point is the frequent call of the global heatbath update of the multiboson fields, which every time gives a statistically independent boson configuration.

If we take the plaquette expectation value as the worst case, then at the present quark masses and lattice spacing, this cost estimate is similar to previous estimates (see, for instance, the formula of A. Ukawa [22]), but considering the more interesting cases of m_π or f_π, there is a substantial improvement by an order of magnitude or more. In addition, toward large volumes, smaller quark masses and/or smaller lattice spacings, the scaling of the cost estimate in (27) is better: for fixed lattice spacing, the cost increases as $m_q^{-2}\Omega$ and decreasing the lattice spacing and keeping the physical parameters fixed, the cost behaves as a^{-6}. This has to be compared with the estimated behaviour in [22], $m_q^{-3}\Omega^{5/4}$ and a^{-7}, respectively.

5 Summary

The quark mass dependence of the pseudoscalar mass and decay constant in our numerical data can be well fitted with the continuum (PQ)ChPT formulas. It has been already observed on the 16^4 lattice in [1] that the $\mathcal{O}(a)$ lattice artifacts at our gauge coupling $\beta = 5.1$, corresponding to a lattice spacing $a \simeq 0.2\,$fm, are small and one can obtain reasonable fits by omitting them. This conclusion is strengthened by the new $16^3 \cdot 32$ data and, therefore, here we based our estimates of the chiral Lagrangian parameters on fits with the continuum formulas.

The use of the ratios of the PCAC quark mass as the variable in comparing the simulation data to chiral perturbation theory is essential. Taking other quark mass definitions, for instance $\mu_{ren} \equiv Z_m(\mu_0 - \mu_{cr})$, would be the source of large lattice artifacts at our lattice spacing.

The sea quark mass dependence of f_π and m_π^2/m_q can be well described in our quark mass range $0.855 \le M_r \le 2.13$, which roughly corresponds to $\frac{1}{4}m_s \le m_q \le \frac{2}{3}m_s$, by the NLO ChPT formulas. The obtained estimates of the relevant Gasser-Leutwyler constants are, according to Sect. 2,

$$\frac{\Lambda_3}{f_0} = 8.21(27), \qquad \frac{\Lambda_4}{f_0} = 21.4(1.5). \tag{29}$$

The functional dependence of the ratio of f_π as a function of the ratio of quark masses clearly shows the presence of chiral logarithms (see Fig. 1). This observation is in agreement with the results in a recent paper of the UKQCD Collaboration [23], which came out during the writing of this paper.

In the valence quark mass dependence of the same quantities, in addition to the NLO terms, the higher order NNLO contributions appear to be important – especially at our two larger sea quark masses. But, as shown by Fig. 3, the importance of the NNLO terms is considerably reduced at the two lighter sea quark masses. Our best estimates for the relevant Gasser-Leutwyler constants at the scale $4\pi f_0$ are, according to (23).

$$\alpha_5 = 2.06(42), \qquad 2\alpha_8 - \alpha_5 = 0.583(45). \tag{30}$$

The errors quoted in (29) and (30) are only the statistical ones. In order to decrease the systematic errors, simulations at still smaller sea quark masses would be useful. Because our lattice volume is relatively large ($L \simeq 3\,$fm), finite volume effects can be expected to be small (see [24, 25]). For the moment, we have no direct handle on the magnitude of the remaining nonzero lattice spacing effects. These should be determined by performing simulations at smaller lattice spacings.

Acknowledgements. The computations were performed on the APEmille systems installed at NIC Zeuthen, the Cray T3E

systems at NIC Jülich, the PC clusters at DESY Hamburg and at the University of Münster and the Sun Fire SMP-Cluster at the Rechenzentrum – RWTH Aachen.

We thank Stephan Dürr, Karl Jansen and Gernot Münster for helpful suggestions and discussions. We thankfully acknowledge the contributions of Luigi Scorzato in the early stages of this work.

References

1. qq+q Collaboration, F. Farchioni, I. Montvay, E. Scholz, L. Scorzato, Eur. Phys. J. C **31**, 227 (2003); hep-lat/0307002
2. S. Weinberg, Physica A **96**, 327 (1979)
3. J. Gasser, H. Leutwyler, Annals Phys. **158**, 142 (1984)
4. C.W. Bernard, M.F.L. Golterman, Phys. Rev. D **49**, 486 (1994); hep-lat/9306005
5. qq+q Collaboration, F. Farchioni, C. Gebert, I. Montvay, L. Scorzato, Eur. Phys. J. C **26**, 237 (2002); hep-lat/0206008
6. qq+q Collaboration, F. Farchioni, C. Gebert, I. Montvay, E. Scholz, L. Scorzato, Phys. Lett. B **561**, 102 (2003); hep-lat/0302011
7. ALPHA Collaboration, J. Heitger, et al., Nucl. Phys. B **588**, 377 (2000); hep-lat/0006026
8. UKQCD Collaboration, A.C. Irving, et al., Phys. Lett. B **518**, 243 (2001); hep-lat/0107023
9. G.T. Fleming, D.R. Nelson, G.W. Kilcup, Nucl. Phys. Proc. Suppl. **106**, 221 (2002); hep-lat/0110112; hep-lat/0209141
10. H. Leutwyler, Nucl. Phys. Proc. Suppl. **94**, 108 (2001); hep-ph/0011049
11. S.R. Sharpe, R.S. Van de Water, Nucl. Phys. Proc. Suppl. **129**, 245 (2004); hep-lat/0308010, Phys. Rev. D **69**, 054027 (2004); hep-lat/0310012
12. G. Rupak, N. Shoresh, Phys. Rev. D **66**, 054503 (2002); hep-lat/0201019
13. I. Montvay, Nucl. Phys. B **466**, 259 (1996); hep-lat/9510042
14. M. Lüscher, Nucl. Phys. B **418**, 637 (1994); hep-lat/9311007
15. A. Borici, Ph. de Forcrand, Nucl. Phys. B **454**, 645 (1995); hep-lat/9505021
16. R. Frezzotti, K. Jansen, Phys. Lett. B **402**, 328 (1997); hep-lat/9702016
17. A. Hasenfratz, A. Alexandru, Phys. Rev. D **65**, 114506 (2002); hep-lat/0203026
18. ALPHA Collaboration, R. Frezzotti, M. Hasenbusch, U. Wolff, J. Heitger, K. Jansen, Comput. Phys. Commun. **136**, 1 (2001); hep-lat/0009027
19. U. Wolff, Comput. Phys. Commun. **156**, 143 (2004); hep-lat/0306017
20. qq+q Collaboration, F. Farchioni, C. Gebert, I. Montvay, L. Scorzato, hep-lat/0209142
21. qq+q Collaboration, F. Farchioni, C. Gebert, I. Montvay, E. Scholz, L. Scorzato, Nucl. Phys. Proc. Suppl. **129**, 179 (2004); hep-lat/0309094
22. A. Ukawa, Nucl. Phys. Proc. Suppl. **106**, 195 (2002)
23. UKQCD Collaboration, C.R. Allton, et al., hep-lat/0403007
24. G. Colangelo, S. Dürr, Eur. Phys. J. C **33**, 543 (2004); hep-lat/0311023
25. D. Becirevic, G. Villadoro, Phys. Rev. **D69**, 054010 (2004); hep-lat/0311028

[Wil-1]

Twisted mass quarks and the phase structure of lattice QCD

Eur. Phys. J. C39 421-433 (2005)

Eur. Phys. J. C 39, 421–433 (2005)
Digital Object Identifier (DOI) 10.1140/epjc/s2004-02078-9

THE EUROPEAN PHYSICAL JOURNAL C

Twisted mass quarks and the phase structure of lattice QCD

F. Farchioni[1], R. Frezzotti[2], K. Jansen[3], I. Montvay[4], G.C. Rossi[3,5], E. Scholz[4], A. Shindler[3,a], N. Ukita[4], C. Urbach[3,6], I. Wetzorke[3]

[1] Universität Münster, Institut für Theoretische Physik, Wilhelm-Klemm-Strasse 9, 48149 Münster, Germany
[2] INFN, Sezione di Milano and Dipartimento di Fisica, Università di Milano "Bicocca", Piazza della Scienza 3, 20126 Milano, Italy
[3] NIC/DESY Zeuthen, Platanenallee 6, 15738 Zeuthen, Germany
[4] Deutsches Elektronen-Synchrotron DESY, Notkestr. 85, 22603 Hamburg, Germany
[5] Dipartimento di Fisica, Università di Roma "Tor Vergata" and INFN, Sezione di Roma 2, Via della Ricerca Scientifica, 00133 Roma, Italy
[6] Freie Universität Berlin, Institut für Theoretische Physik, Arnimallee 14, 14196 Berlin, Germany

Received: 24 August 2004 / Revised version: 29 October 2004 /
Published online: 25 January 2005 –

Abstract. The phase structure of zero temperature twisted mass lattice QCD is investigated. We find strong metastabilities in the plaquette observable in correspondence of which the untwisted quark mass assumes positive or negative values. We provide interpretations of this phenomenon in terms of chiral symmetry breaking and the effective potential model of Sharpe and Singleton.

1 Introduction

As a consequence of (soft) chiral symmetry breaking, nature has arranged itself such that three of the pseudo-scalar mesons are light, with masses around 140 MeV. This lightness of the pion mass becomes important also when we think of numerical simulations in lattice QCD. Approaching the "physical point", at which the pion mass assumes its value as measured in experiment, the algorithms used in lattice simulations suffer from a substantial slowing down [1, 2] which restricts present simulations to rather high and unphysical values of the quark mass.

In addition to this slowing down of the algorithms for Wilson fermions, the quark mass does not act as an infrared regulator allowing thus for the appearance of very small unphysical eigenvalues of the lattice Wilson–Dirac operator. These eigenvalues render the simulations more difficult and sometimes even impossible.

Staggered fermions solve this problem, but it is not clear how to use this approach to simulate $N_f = 2$ or odd number of flavors [3]. Overlap fermions [4] also solve the problem, but they are computationally very demanding and, unless new algorithms are invented, they are very difficult to use for dynamical simulations.

An elegant way out may be the use of so-called twisted mass fermions [5, 6]. This formulation of lattice QCD (tmQCD) is obtained when the Wilson term and the physical quark mass term are taken not parallel in flavor chiral space, but rotated by a relative twist angle ω. If the Wilson term is given the usual form, such a chiral rotation leads to a *twisted mass* parameter μ, in addition to the standard Wilson quark mass m_0 ("untwisted" quark mass). Lattice QCD with a twisted mass was first employed for $\mathcal{O}(a)$-improved Wilson fermions with the nice feature that the improvement coefficients and the renormalization constants are the same as for $\mathcal{O}(a)$-improved Wilson fermions without twisted mass and hence they did not need to be recalculated [7]. The main advantage of the twisted mass fermions is that the twisted quark mass provides a natural infrared cut-off and avoids problems with accidental small eigenvalues, rendering therefore the simulations safe. Of course, the slowing down of the algorithms when approaching small quark masses will remain, although it is expected to be less severe.

Later on it was realized that a full $\mathcal{O}(a)$-improvement of correlation functions can be obtained by using the twisted mass alone *without additional improvement terms* when, as a special case, m_0 is set to the critical value $m_{\rm crit}$ and the above mentioned twist angle is equal to $\omega = \pi/2$ [8]. In this way the demanding computation of many improvement coefficients can be avoided rendering the simulations much easier both from a conceptual as well as from a practical point of view.

The Wilson twisted mass formulation has been tested numerically in the quenched approximation already [9]. The results are very encouraging. The $\mathcal{O}(a)$ corrections appear indeed to be cancelled and even higher order effects seem to be small, at least for the quantities and the value of the quark mass considered in [9].

A word of caution has to be added at this point. Although, as mentioned above, the twisted quark mass can be decreased towards zero without simulations breaking

[a] e-mail: andrea.shindler@desy.de

down due to exceptional configurations, there is an important interplay between the lattice cut-off, $\Lambda = a^{-1}$ with a the lattice spacing, and the quark mass m_q (see (10) below). In the continuum in the presence of spontaneous chiral symmetry breaking the chiral symmetry is not realized à la Wigner and, as the quark mass goes to zero, the chiral phase of the vacuum is driven by the phase of the quark mass term. The same must be true on the lattice; thus the scaling limit $a \to 0$ should be taken before letting $m_q \to 0$. As a result, taking the chiral limit is a numerically delicate matter.

In order to ensure in practice that on the lattice the chiral phase of the vacuum is determined by the quark mass term, proportional to m_q, and not by the Wilson term, the lattice parameters should satisfy the order of magnitude inequality [8]

$$m_q \Lambda_{\rm QCD}^{-1} \gg a \Lambda_{\rm QCD}. \tag{1}$$

This same condition emerges from many different corners of the lattice theory when the physical world is approached. A very simple argument leading to the bound (1) is obtained by comparing the magnitude of the critical Wilson term to that of the quark mass term and requiring the first to be negligibly small compared to the second one, in order to be sure that lattice physics matches the requirements of the continuum theory. From the order of magnitude inequality $a(\Lambda_{\rm QCD})^5 \ll m_q(\Lambda_{\rm QCD})^3$, one immediately gets the condition (1). It is important to observe, however, that the less restrictive condition

$$m_q \Lambda_{\rm QCD}^{-1} \gg (a \Lambda_{\rm QCD})^2 \tag{2}$$

may be sufficient if one is dealing with $\mathcal{O}(a)$-improved quantities.

It should be remarked that, since $a\Lambda_{\rm QCD}$ can be (non-perturbatively) expressed in terms of g_0^2, (1) and (2) are actually (order of magnitude) conditions for the values of the dimensionless bare lattice parameters am_q and g_0^2. Contact with dimensionful quantities can be made by comparing simulation data with physical inputs.

What is in practice important is to know for which range of the bare lattice parameters one can avoid troubles from chiral breaking cut-off effects, even if parametrically of order a^2 or higher. This issue has to be settled by numerical investigations aimed at establishing both the structure of the phase diagram of the lattice model in study and the size of residual scaling violations on the physical observables.

In this perspective, twisted mass fermions offer a unique opportunity to explore the phase diagram of Wilson fermions. By fixing the twisted mass parameter μ, one may vary $(m_0 - m_{\rm crit})$ from positive to negative values. In this way, the phase diagram of zero temperature lattice QCD can be explored. It should be emphasized that, on large lattices, such an investigation would be very difficult without having $\mu \neq 0$, since else the algorithms would slow down dramatically approaching the critical quark mass.

In this work we have performed simulations to explore the phase diagram of zero temperature QCD. As it will be shown in the following, we find strong metastabilities in the plaquette expectation value. We determined in both metastable branches a number of quantities such as the (untwisted) PCAC quark mass and pseudo-scalar meson masses. The results presented in this paper are obtained at only one value of $\beta = 5.2$, with β related to the bare gauge coupling g_0 by $\beta = 6/g_0^2$. Since the value of $\beta = 5.2$ corresponds to a rather coarse value of the lattice spacing ($a \approx 0.16\,\mathrm{fm}$) our work can only be considered as a starting point for a more detailed investigation of the phase diagram of lattice QCD. In particular, the β dependence of the strength of the observed metastabilities has to be determined. We believe that a qualitative and even quantitative understanding of the phase diagram is a necessary prerequisite for phenomenologically relevant numerical simulations.

This paper is organized as follows. In Sect. 2 we introduce Wilson twisted mass fermions and give our notation. This is followed by a short discussion of the algorithms used. In Sect. 3 we provide our evidence for metastabilities by hysteresis effects and long-living metastable states. There, we also show results for a selected set of physical quantities. In Sect. 4, we give a possible interpretation of these results in terms of chiral symmetry breaking and the Sharpen–Singleton effective potential model. We conclude finally in Sect. 5. In the appendix some details of the applied update algorithms are explained.

2 Lattice action and basic variables

2.1 Lattice action

Let us start by writing the Wilson tmQCD action as

$$S[U,\chi,\bar\chi] = \bar\chi\,(D[U] + m_0 + \mu \mathrm{i}\gamma_5\tau_3)\,\chi. \tag{3}$$

In (3) m_0 is the *quark mass* parameter and μ is the *twisted quark mass* parameter. The operator $D[U]$ is given by

$$\begin{aligned}\bar\chi\, D[U]\,\chi = a^4 \sum_x \Bigg\{ & \frac{4r}{a}\bar\chi(x)\chi(x) \\ & - \frac{1}{2a}\bar\chi(x)\sum_{\mu=1}^{4}\Big(U(x,\mu)(r+\gamma_\mu)\chi(x+a\hat\mu) \\ & + U^\dagger(x-a\hat\mu,\mu)(r-\gamma_\mu)\chi(x-a\hat\mu)\Big)\Bigg\},\end{aligned} \tag{4}$$

with r the Wilson parameter which will be set to $r = 1$ in our simulations.

The action as it stands in (3) can, of course, be studied in the full parameter space (m_0, μ). A special case arises, however, when m_0 is tuned towards a critical bare quark mass $m_{\rm crit}$. In such, and only in such a situation all physical quantities are, or can easily be, $\mathcal{O}(a)$-improved. It is hence natural to rewrite

$$m_0 = m_{\rm crit} + \tilde m, \tag{5}$$

with $\tilde m$ an offset quark mass. The values of $m_{\rm crit}$ need only to be known with $\mathcal{O}(a)$ accuracy [8] and can be, for instance, taken from the pure Wilson theory at $\mu = 0$.

For standard Wilson fermions usually the hopping parameter representation is taken in the numerical simulations. This representation is easily obtained from (3) by a rescaling of the fields

$$\chi \to \frac{\sqrt{2\kappa}}{a^{3/2}}\chi, \qquad \bar{\chi} \to \frac{\sqrt{2\kappa}}{a^{3/2}}\bar{\chi}, \qquad \kappa = \frac{1}{2am_0 + 8r}. \quad (6)$$

We then obtain the form of the action that is actually used in our simulations

$$\begin{aligned} S[\chi,\bar{\chi},U] = \sum_x \Bigg\{ & \bar{\chi}(x)\,(1 + 2\mathrm{i}a\mu\kappa\gamma_5\tau_3)\,\chi(x) \\ & -\kappa\bar{\chi}(x)\sum_{\mu=1}^{4}\Big(U(x,\mu)(r+\gamma_\mu)\chi(x+a\hat{\mu}) \\ & + U^\dagger(x-a\hat{\mu},\mu)(r-\gamma_\mu)\chi(x-a\hat{\mu})\Big)\Bigg\}. \end{aligned} \quad (7)$$

Although not needed for the discussion of the numerical data presented below, we give for completeness here the action in the so-called *physical basis*. This action is obtained by introducing new fields $\psi(x)$ and $\bar{\psi}(x)$ which are related to the fields in (3) by a chiral transformation

$$\begin{aligned} \psi(x) &\equiv \mathrm{e}^{\mathrm{i}\frac{\omega}{2}\gamma_5\tau_3}\chi(x) = \Big(\cos\frac{\omega}{2} + \mathrm{i}\gamma_5\tau_3\sin\frac{\omega}{2}\Big)\,\chi(x)\,, \\ \bar{\psi}(x) &\equiv \bar{\chi}(x)\mathrm{e}^{\mathrm{i}\frac{\omega}{2}\gamma_5\tau_3} = \bar{\chi}(x)\Big(\cos\frac{\omega}{2} + \mathrm{i}\gamma_5\tau_3\sin\frac{\omega}{2}\Big)\,. \end{aligned} \quad (8)$$

The action then reads

$$\begin{aligned} S[\psi,\bar{\psi},U] = a^4\sum_x \Bigg\{ & m_q\bar{\psi}(x)\psi(x) \\ & -\frac{1}{2a}\bar{\psi}(x)\mathrm{e}^{-\mathrm{i}\omega\gamma_5\tau_3}\Bigg[\sum_{\mu=1}^{4}\Big(rU(x,\mu)\psi(x+a\hat{\mu}) \\ & \quad +rU^\dagger(x-a\hat{\mu},\mu)\psi(x-a\hat{\mu})\Big) \\ & \quad -(2am_{\mathrm{crit}}+8r)\psi(x)\Bigg] \\ & -\frac{1}{2a}\bar{\psi}(x)\sum_{\mu=1}^{4}\Big(U(x,\mu)\gamma_\mu\psi(x+a\hat{\mu}) \\ & \quad -U^\dagger(x-a\hat{\mu},\mu)\gamma_\mu\psi(x-a\hat{\mu})\Big)\Bigg\}, \end{aligned} \quad (9)$$

where we have identified

$$m_q\cos\omega = m_0 - m_{\mathrm{crit}} = \tilde{m}, \qquad m_q\sin\omega = \mu. \quad (10)$$

2.2 Simulation algorithms

In our numerical simulations we used two different optimized updating algorithms for producing samples of gauge configurations: the hybrid Monte Carlo (HMC) algorithm with up to three pseudo-fermion fields as suggested in [10, 11] and the two-step multi-boson (TSMB) algorithm [12].

In the standard HMC algorithm we used even–odd preconditioning, which in presence of a twisted mass is only a slight modification of the standard preconditioning technique [13]. We give the relevant equations in Appendix A.1 of this paper. As a subsequent improvement of the algorithm, we implemented the idea of [10] and used shifted fermion matrices to "precondition" the original fermion matrix. These shifted matrices are treated by introducing additional pseudo-fermion fields. In the shifted fermion matrix we simply used larger values of the twisted mass parameter than the value of μ that is to be simulated. Using two pseudo-fermion fields we experienced a substantial improvement of the HMC algorithm by at least a factor of two. The addition of a third pseudo-fermion field gave only another 10–20% improvement. Again we list the relevant equations, how the shifted matrices are implemented, in Appendix A.1. As a further algorithmic trick we used the Sexton–Weingarten leap-frog integrator as proposed in [14].

Our alternative algorithm, the TSMB algorithm [12], is based on the multi-boson representation of the fermion determinant [15]. Optimized polynomial approximations are used, both in the first update step and in the second global accept-reject correction step, for reproducing the dynamical effect of fermions on the gauge field. We apply high order least-square optimization and obtain the necessary polynomials using high precision arithmetics [16]. Concerning the optimization of TSMB for QCD see, for instance, [17].

A useful improvement of the TSMB update algorithms can again be achieved by even–odd preconditioning. This can be implemented in TSMB for twisted mass quarks along the lines of [18]. For the even–odd preconditioning of the TSMB update the flavor indices of the quark fields have to be kept. This means that the multi-boson fields have 24 components per lattice site (2 for flavor, 3 for color and 4 for Dirac spinor indices). Correspondingly, the polynomials are approximating the function $x^{-\frac{1}{2}}$ as in the case of a single Dirac flavor with untwisted quark mass. We give some more details of our even–odd implementation of the TSMB algorithm in Appendix A.2.

In the region of light quarks an important part of the numerical effort has to be spent on equilibrating the gauge configuration in a new simulation point. This is particularly relevant in studies of the phase structure where many different points in the parameter space have to be investigated. In case of TSMB the equilibration time is substantially longer than the autocorrelation of relevant physical quantities in equilibrium: on our lattices equilibration can take ten or more times the autocorrelation time of the plaquette observable. The autocorrelation times in equilibrium themselves are similar but most of the time by factors of 2–3 shorter with our twisted quark masses than with untwisted quark masses of similar magnitude. For an approximate formula of the computational cost see [19].

The use of two different optimized update algorithms was very helpful in checking our results. We did not try to obtain a precise performance comparison. Qualitatively, we did not see a noticeable difference in the speed once equi-

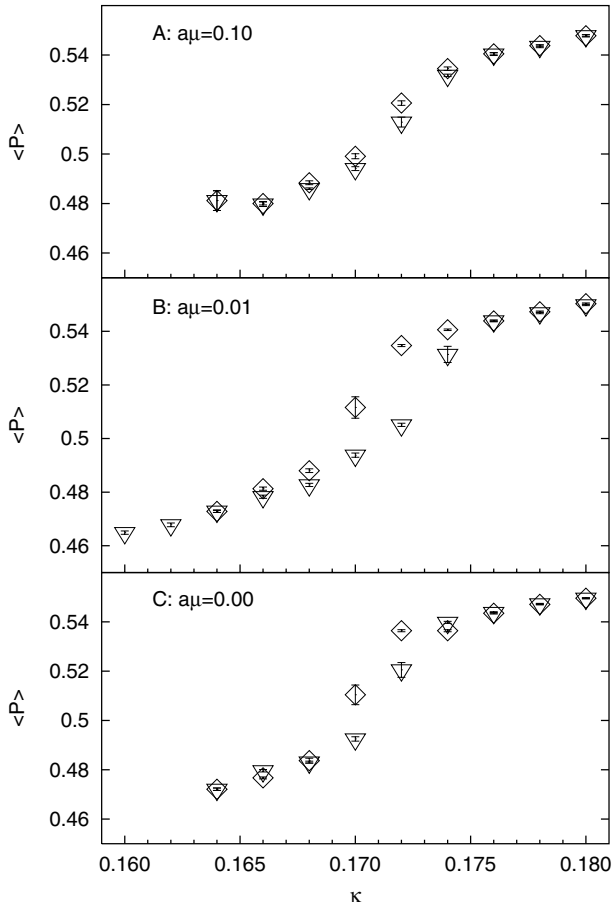

Fig. 1. Thermal cycles in κ on $8^3 \times 16$ lattices at $\beta = 5.2$. The plaquette expectation value is shown for: $a\mu = 0.1$ (A); $a\mu = 0.01$ (B); $a\mu = 0$ (C). The triangles ($\triangledown$) refer to increasing κ-values, the diamonds ($\diamond$) to decreasing ones

librium was reached, but the HMC algorithm with multiple pseudo-fermion fields (MPHMC) turned out to be faster in the equilibration process. In particular, crossing the transition region below and above the metastability region is faster with MPHMC. Nevertheless, the extension in κ of the metastability region is the same with both algorithms.

The data used for preparing the figures in this publication were obtained with MPHMC, except for the upper four panels in Fig. 2, which were obtained with TSMB. The thermal cycles in Fig. 1 were only run with MPHMC. In the other figures the results of the TSMB runs, whenever performed, were always consistent within errors with the shown MPHMC results.

3 Numerical results

In this section we give our numerical evidence for the phenomenon of metastability mentioned in the introduction. As a first step and for an orientation we have investigated thermal cycles in the hopping parameter κ. We then discuss metastable states in the plaquette expectation value. Finally we determine quantities such as the pion mass and the untwisted PCAC quark mass in the metastable branches in order to obtain a picture of the physical properties in the different states. In most cases we perform the simulations at a twisted mass $a\mu = 0.01$, but in a few cases we also put $a\mu = 0$, which is possible on the lattice sizes we consider.

3.1 Thermal cycles

We started our investigation of the phase diagram of zero temperature lattice QCD by performing thermal cycles in κ while keeping fixed $\beta = 5.2$ and the value of the twisted mass parameter $a\mu$. These cycles are performed such that a starting value of $\kappa_{\rm start}$ is chosen and then κ is incremented, without performing further intermediate thermalization sweeps, until a final value of $\kappa_{\rm final}$ is reached. At this point the procedure is reversed and κ is decremented until the starting value $\kappa_{\rm start}$ is obtained back. At each value of κ 150 configurations are produced and averaged over.

In Fig. 1 we show three such thermal cycles, performed at $a\mu = 0$, $a\mu = 0.01$ and $a\mu = 0.1$ from bottom to top. In the cycles signs of hysteresis effects can be seen for $a\mu = 0$ and $a\mu = 0.01$ while for the largest value of $a\mu = 0.1$ such effects are hardly visible. Hysteresis effects in thermal cycles *may be* signs of the existence of a first order phase transition. However, they should only be taken as first indications. Nevertheless, they provide most useful hints for further studies to search for metastable states.

3.2 Metastability

Guided by the results from the thermal cycles, we next performed simulations at fixed values of $a\mu$ and κ, starting with ordered and disordered configurations, staying again at $\beta = 5.2$. In Fig. 2 we show the Monte Carlo time evolution of the plaquette expectation value, in most cases on a $12^3 \times 24$ lattice. For several values of κ we find coexisting branches with different average values of the plaquette. The gap (the "latent heat") appears to be rather large. At $\kappa = 0.1717$ we show the history of the plaquette expectation value also on a larger ($16^3 \times 32$) lattice. It seems that the gap in the plaquette expectation value does not depend much on the lattice size, suggesting that the metastability we observe here is not a finite volume effect. In most cases the twisted mass is $a\mu = 0.01$, except for the picture left in the bottom line where it is $a\mu = 0$.

The lifetime of a metastable state, i.e. the time before a tunneling to the stable branch occurs, depends on the algorithm used. In fact, one may wonder, whether the appearance of the metastable states seen in Fig. 2 may not be purely an artefact of our algorithms. We cannot completely exclude this possibility but we believe it is very unlikely: we employed two very different kinds of algorithms in our simulations as explained in Sect. 2.2. We observe the metastable states with both of them. We also interchanged configurations between the two algorithms: a configuration generated with the algorithm A was iterated further with algorithm B and vice versa. We find that in such situations the plaquette expectation value remains in the state where it has been before the interchange of configurations took

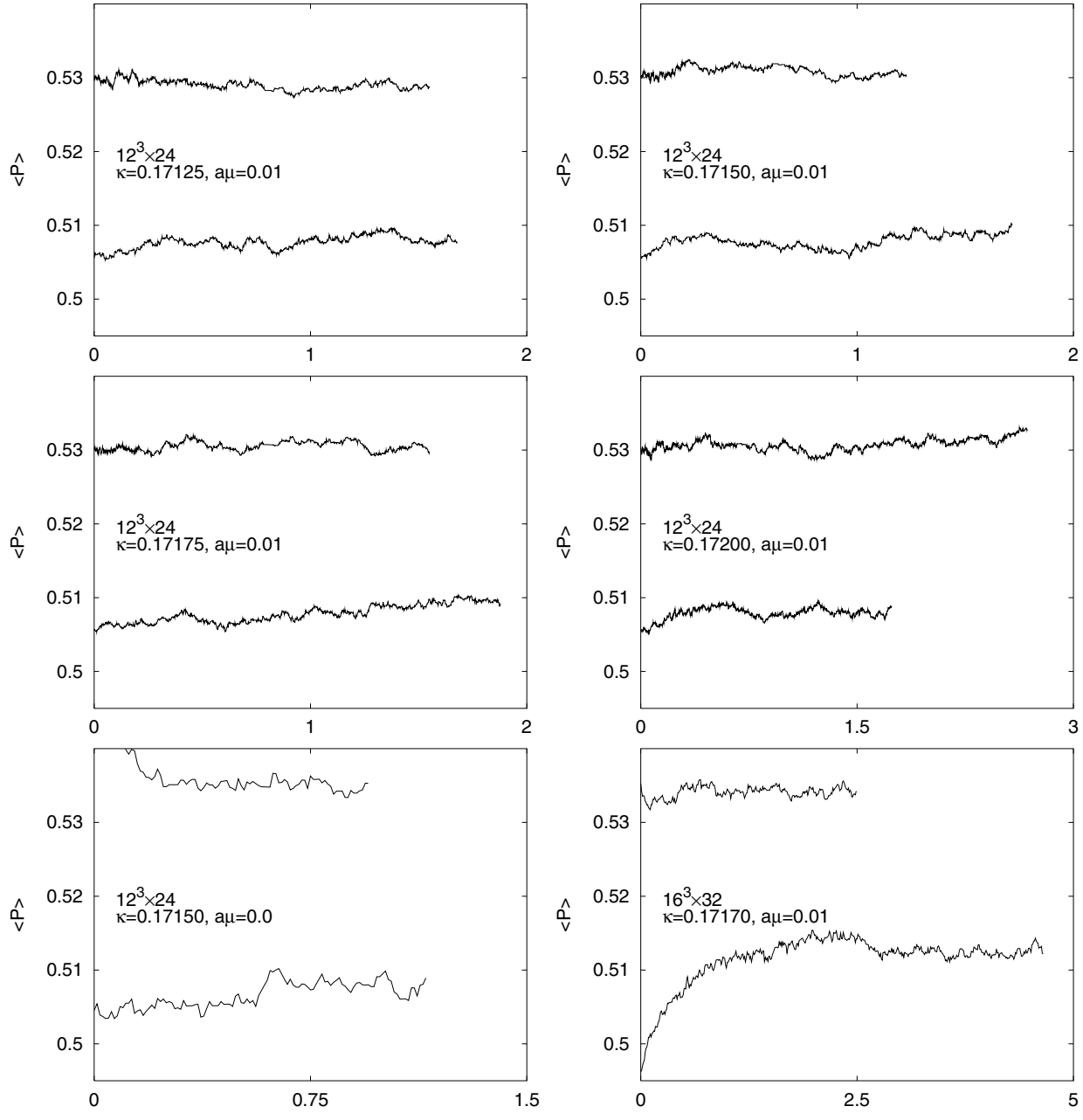

Fig. 2. Metastable states at $\beta = 5.2$. The number of sweeps is given in thousands. The lattice size is $12^3 \times 24$, except for the right panel in the bottom line where it is $16^3 \times 32$. The twisted mass is $a\mu = 0.01$, except for the left panel in the bottom line where it is $a\mu = 0$

place. In addition, as we shall see below, the two states can be characterized by well defined and markedly different values of basic quantities. We therefore conclude that the metastable states are a generic phenomenon of lattice QCD in our formulation.

3.3 Pion and quark masses

By selecting separately configurations with high and with low plaquette expectation value, we measured the pion mass and the untwisted PCAC quark mass to study the physical properties in the two metastable states.

We obtained the pseudo-scalar ("pion") mass from suitable correlation functions. These are constructed from the standard composite fields defined in terms of the fields $\bar{\psi}$ and ψ in (9):

$$S^0(x) = \bar{\psi}(x)\psi(x), \quad P^\alpha(x) = \bar{\psi}(x)\gamma_5 \frac{\tau_\alpha}{2}\psi(x),$$
$$A^\alpha_\mu(x) = \bar{\psi}(x)\gamma_\mu\gamma_5 \frac{\tau_\alpha}{2}\psi(x),$$
$$V^\alpha_\mu(x) = \bar{\psi}(x)\gamma_\mu \frac{\tau_\alpha}{2}\psi(x). \qquad (11)$$

Here $\tau_\alpha,\ \alpha = 1, 2, 3$ are the usual Pauli matrices in isospin space. The corresponding composite fields in terms of the

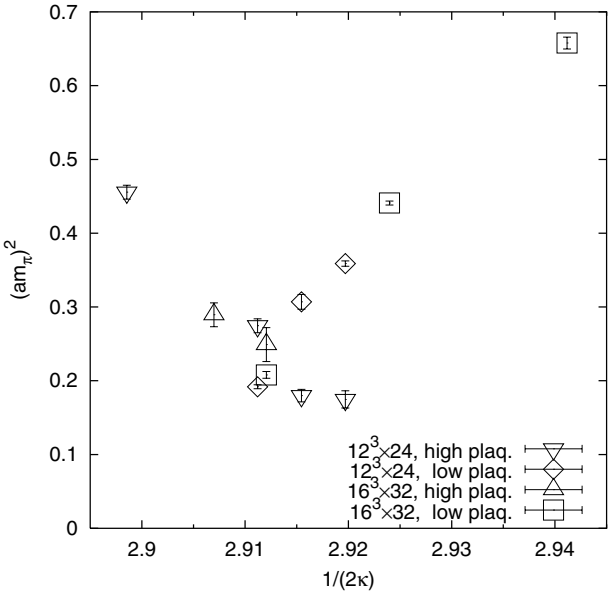

Fig. 3. The pion mass squared in lattice units on two lattice sizes measured separately on configurations in the two metastable states. These runs were made at $\beta = 5.2$ and $a\mu = 0.01$

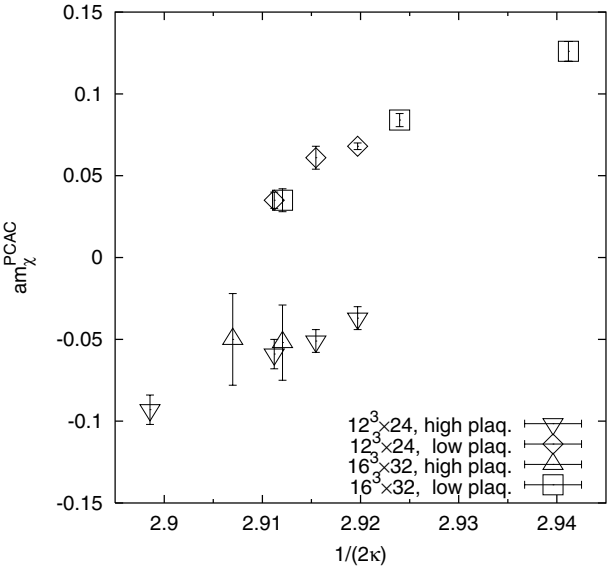

Fig. 4. The quark mass in lattice units $m_\chi^{\rm PCAC}$ as defined in (12) on two lattice sizes measured separately on configurations in the two metastable states. The values of $\beta = 5.2$ and $a\mu = 0.01$ are fixed

quark fields χ and $\bar\chi$ of (3) are then given by the transformation in (8). For instance, for $\alpha = 1, 2$ ("charged pions") the pseudo-scalar density has the same form in the χ-basis as in the ψ-basis. Therefore, the mass of the charged pions can be extracted from correlators in the χ-basis in the usual way. The charged axial vector and vector currents are rotated into each other by the angle ω in such a way that at $\omega = \pi/2$ they are interchanged. (For more details see the literature, e.g. [5, 8].)

Besides the pion mass, we measured the PCAC quark mass from the axial vector current in the χ-basis:

$$m_\chi^{\rm PCAC} \equiv \frac{\left\langle \partial^*_\mu \bar\chi \gamma_\mu \gamma_5 \frac{\tau^\pm}{2} \chi(x)\, \hat O^\mp(y) \right\rangle}{2 \left\langle \bar\chi \frac{\tau^\pm}{2} \gamma_5 \chi(x)\, \hat O^\mp(y) \right\rangle}. \qquad (12)$$

Here $\hat O^\mp$ is a suitable operator that we have chosen to be the pseudo-scalar density $\hat O^\mp = \bar\chi \frac{\tau^\mp}{2} \gamma_5 \chi(x)$, ∂^*_μ is the lattice backward derivative defined as usual and $\tau^\pm = \tau_1 \pm i\tau_2$. One can show that in the limit $a \to 0$ the quantity $m_\chi^{\rm PCAC}$ is asymptotically proportional, through finite renormalization constants, to $\tilde m$.

In Fig. 3 we show the pion mass squared in lattice units as function of $(2\kappa)^{-1}$. We observe that the pion mass is rather large and the most striking effect in the graph is that it can have two different values at the same κ. If we consider the quark mass $m_\chi^{\rm PCAC}$ in Fig. 4, we see that in the states with a low plaquette expectation value the mass is positive while for high values of the plaquette expectation it is negative. These quark masses with opposite sign coexist for some values of κ. Plotting the pion mass versus $m_\chi^{\rm PCAC}$ one obtains Fig. 5.

Figures 2–4 clearly reveal that for small enough μ metastabilities show up in the quantities we have investigated, such as m_π, $m_\chi^{\rm PCAC}$ and the average plaquette, if m_0 is

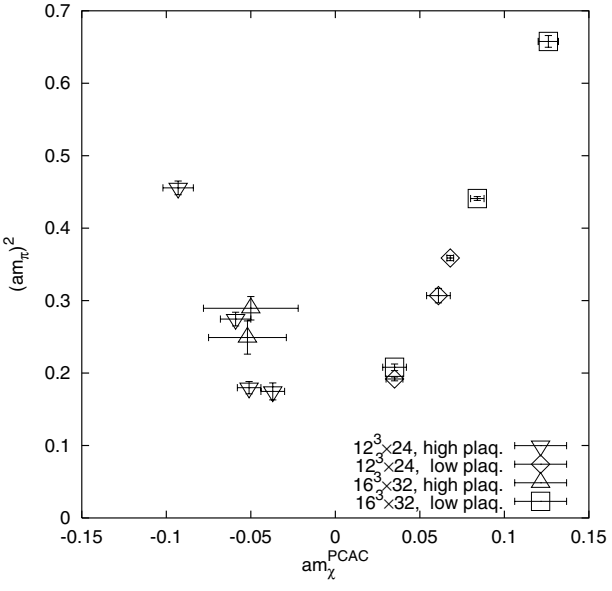

Fig. 5. The pion mass squared in lattice units from Fig. 3 plotted against the untwisted PCAC quark mass in Fig. 4

close to its critical value. What "small enough μ" means is likely to change with β. Simulations at larger values of β are in progress. As a matter of fact, when m_0 is significantly larger (smaller) than $m_{\rm crit}$ we find $m_\chi^{\rm PCAC}$ to be positive (negative) and no signal of metastabilities. The remark that metastabilities take place for m_0 close to its critical value will be important both in Sect. 4.1 to understand why they affect also a purely gluonic observable such as the plaquette and in Sect. 4.3, where it leads to a plausible explanation of the observed metastability phenomena in terms of spectral properties of the lattice tmQCD Dirac

matrix (suppression of the "eigenvalue cloud crossing" phenomenon by the fermionic determinant).

The remarks in Sect. 4.1 may provide further insight also on the similar metastability phenomena reported in [20] for the $N_f = 3$ untwisted Wilson theory and on the reason why they "disappear" when changing the gluonic action or details, e.g. $c_{\rm SW}$-value, of the fermionic action. A possible reason is that these changes might shift the range of m_0 where metastabilities appear to values where no data are yet available.

4 Physical interpretation

The observed strong metastabilities discussed in the previous section clearly suggest that we are working either directly at a first order phase transition or at least very close to it such that we see the remnants of a close-by first order phase transition. With the present data we cannot really differentiate between these two scenarios and in the following we will therefore discuss both of them.

4.1 Jump in the plaquette and chiral symmetry breaking

Generally speaking, a jump in the plaquette as seen in our data can arise owing to the lack of chiral symmetry for chirally non-invariant formulations of lattice QCD. The argument relies on the key observation that, when working with chirally twisted Wilson fermions, there are two distinct sources of chirality breaking. The first source is the combination of the untwisted Wilson and mass terms

$$\bar\chi\, M[U]\,\chi = a^4 \sum_x \Bigg\{ \bar\chi(x) \left(\frac{4r}{a} + m_0 \right) \chi(x) - \frac{r}{2a} \bar\chi(x) \sum_{\mu=1}^{4} \Big(U(x,\mu)\chi(x+a\hat\mu) - U^\dagger(x-a\hat\mu,\mu)\chi(x-a\hat\mu) \Big) \Bigg\}. \qquad (13)$$

The second source of chirality breaking is the twisted mass term $\mu\bar\chi{\rm i}\gamma_5\tau_3\chi$. As pointed out in Sect. 2, one may trade the bare parameters m_0 and μ in (3) for the equivalent bare parameters m_q and ω of (9). The latter are best suited to discuss the connection with continuum QCD physics, as ω is an unphysical parameter, while m_q represents the bare quark mass. Assuming spontaneous chiral symmetry breaking in infinite volume, the pion mass squared is expected to vanish linearly in m_q (up to lattice artifacts) as $m_q \to 0$. Moreover in the continuum limit the physical scalar condensate is expected to show a discontinuity and changes sign as m_q passes through zero:

$$\lim_{m_q\to 0^+} \langle \left[\bar\psi\psi\right]_{\rm R} \rangle = - \lim_{m_q\to 0^-} \langle \left[\bar\psi\psi\right]_{\rm R} \rangle \neq 0\,, \qquad (14)$$

where by $[\bar\psi\psi]_{\rm R}$ we mean the appropriately subtracted and renormalized scalar density. We recall that for $\omega \neq 0$ this is a non-trivial linear combination of $\bar\chi\chi$, $\bar\chi{\rm i}\gamma_5\tau_3\chi$ and the constant field (see below for details).

In order to make contact with the observed metastability phenomena in the regime of spontaneous chiral symmetry breaking, two further remarks are important.
(1) At non-zero lattice spacing the twisted mass term $\mu\bar\chi{\rm i}\gamma_5\tau_3\chi$ induces the twisted condensate $\langle[\bar\chi{\rm i}\gamma_5\tau_3\chi]_{\rm R}\rangle$, while the untwisted mass terms $\bar\chi M[U]\chi$ of (13) determine the untwisted condensate $\langle[\bar\chi\chi]_{\rm R}\rangle$.
(2) The local plaquette field

$$\phi(x) \equiv \frac{1}{12} \sum_{\mu\neq\nu} \frac{1}{3} {\rm tr}\left[U_\mu(x) \times U_\mu^\dagger(x+a\hat\nu) U_\nu^\dagger(x) \right] \qquad (15)$$

admits on the basis of lattice symmetries an operator expansion of the form

$$\phi(x) = \left[b_0\, \mathbb{1} + b_{4g}\, a^4 F\cdot F \right] + b_3\, a^3 \left[\bar\chi\chi\right]_{\rm sub} + b_4\, a^4 \mu \left[\bar\chi{\rm i}\gamma_5\tau_3\chi\right]_{\rm sub} + \mathcal{O}(a^5), \qquad (16)$$

with $[\ldots]_{\rm sub}$ denoting a subtracted, multiplicatively renormalizable, operator and F the continuum gauge field strength tensor. The plaquette expectation value $P(r, am_0, a\mu)$ can be correspondingly written in the form

$$P(r,am_0,a\mu) = \left[b_0 + b_{4g}\, a^4 \langle F\cdot F\rangle_{(r,am_0,a\mu)} \right] + b_3\, a^3 \langle \left[\bar\chi\chi\right]_{\rm sub} \rangle_{(r,am_0,a\mu)} + b_4\, a^4 \mu \langle \left[\bar\chi{\rm i}\gamma_5\tau_3\chi\right]_{\rm sub} \rangle_{(r,am_0,a\mu)} + \mathcal{O}(a^5). \qquad (17)$$

The important point about the representation (17) is that it shows that P is actually sensitive to the value of the subtracted condensates $\langle[\bar\chi{\rm i}\gamma_5\tau_3\chi]_{\rm sub}\rangle$ and $\langle[\bar\chi\chi]_{\rm sub}\rangle$.

Before continuing it is useful to pause a moment and discuss the structure of (16) and (17) and the nature of the various terms appearing in it.
– We first notice that the contributions from the identity and the $F\cdot F$ operator are put together within a square parenthesis in (16) and (17) to remind us that there is no unambiguous way to subtract from the latter its power divergent mixing with the identity. Ultimately this is due to the fact that, unlike the chiral condensates, the vacuum expectation value of $F\cdot F$ is not an order parameter of any symmetry.
– For the reason we have just recalled, it is instead perfectly possible to unambiguously define, in the massless limit, multiplicatively renormalizable operators $[\bar\chi\chi]_{\rm sub}$ and $[\bar\chi{\rm i}\gamma_5\tau_3\chi]_{\rm sub}$, by following the procedure outlined in [21]. More generally, such quark bilinears can be defined as finite operators even at non-vanishing masses, though not uniquely. This can be done by setting, for instance,

$$\left[\bar\chi\chi\right]_{\rm sub} = \bar\chi\chi - a^{-3} C_{S^0}(r, a\tilde m, a\mu), \qquad (18)$$

$$\left[\bar\chi{\rm i}\gamma_5\tau_3\chi\right]_{\rm sub} = \bar\chi{\rm i}\gamma_5\tau_3\chi - a^{-2}\mu\, C_P(r, a\tilde m, a\mu), \qquad (19)$$

with the dimensionless coefficient functions C_{S^0} and C_P determined at some finite space-time volume $V = V_0$ by the conditions

$$\langle \left[\bar\chi\chi\right]_{\rm sub} \rangle_{(r,m_0,\mu)} = 0,\ \ V = V_0, \qquad (20)$$

$$\langle[\bar{\chi}\mathrm{i}\gamma_5\tau_3\chi]_{\mathrm{sub}}\rangle_{(r,m_0,\mu)} = 0,\ \ V = V_0. \tag{21}$$

Both the coefficients C_{S^0} and C_P admit a finite polynomial expansion in $a\tilde{m}$ and $a\mu$ (actually in $(a\mu)^2$ for parity reasons).
(3) In terms of $[\bar{\chi}\chi]_{\mathrm{sub}}$ and $[\bar{\chi}\mathrm{i}\gamma_5\tau_3\chi]_{\mathrm{sub}}$, the renormalized scalar density in the physical basis, $[\bar{\psi}\psi]_{\mathrm{R}}$, reads

$$\begin{aligned}&\left[\bar{\psi}\psi\right]_{\mathrm{R}} \\ &= Z_M^{-1}(\omega)Z_P[\cos\omega\,[\bar{\chi}\chi]_{\mathrm{sub}} + \sin\omega\,[\bar{\chi}\mathrm{i}\gamma_5\tau_3\chi]_{\mathrm{sub}}],\end{aligned} \tag{22}$$

where $z_m = Z_P/Z_{S^0}$, $Z_M = [z_m^2\cos^2\omega + \sin^2\omega]^{1/2}$ and Z_Γ denotes the renormalization constant of $\bar{\chi}\Gamma\chi$ in the standard Wilson regularization computed in a mass independent renormalization scheme[1]. Consistently with the general arguments given above, we remark that only the leading a^{-3} divergent subtraction is uniquely fixed by the symmetries of the theory (WTI's and spurionic transformations). Consequently these properties can be used to make the chiral scalar condensate, $\bar{\psi}\psi$, multiplicative renormalizable in the massless limit, by defining it, e.g., as the Wilson average over the expectation values computed with opposite values of the coefficient of the Wilson term [8, 22].

After this little digression let us go back and discuss the implications of (17). If we are on the lattice and take the action of (3) for values of μ or $\tilde{m}$ much larger than $\mathcal{O}(a\Lambda_{\mathrm{QCD}}^2)$, the condensates $\langle[\bar{\chi}\mathrm{i}\gamma_5\tau_3\chi]_{\mathrm{sub}}\rangle$ or $\langle[\bar{\chi}\chi]_{\mathrm{sub}}\rangle$ are expected to show no metastability and thus the same should be true for the plaquette expectation value. However, if μ is smaller than $\mathcal{O}(a\Lambda_{\mathrm{QCD}}^2)$ the physical scalar condensate signaling spontaneous chiral symmetry breaking is not simply given by $\langle[\bar{\chi}\mathrm{i}\gamma_5\tau_3\chi]_{\mathrm{sub}}\rangle$, but has in general also an untwisted component, $\langle[\bar{\chi}\chi]_{\mathrm{sub}}\rangle$. Both components have an impact on the value of the plaquette (see (17)). When $\tilde{m}$ passes from positive to negative values the expectation value of the untwisted operator $[\bar{\chi}\chi]_{\mathrm{sub}}$ should also change sign and, at non-vanishingly small values of μ, eventually become very small for almost critical values of m_0. In this situation, owing to the presence of the chiral symmetry breaking term (13) in the action, the tmQCD sample of gauge configurations is expected to include configurations where $\langle[\bar{\chi}\chi]_{\mathrm{sub}}\rangle_U$ is positive and configurations where $\langle[\bar{\chi}\chi]_{\mathrm{sub}}\rangle_U$ is negative, corresponding to whether m_χ^{PCAC} is positive or negative, respectively. (By $\langle\ldots\rangle_U$ we mean the fermionic Wick contraction on a fixed gauge background U.) Since the coefficient $b_3 = b_3(r, am_0, a\mu)$ does not vanish at $m_0 = m_{\mathrm{crit}}$[2], the value of the plaquette on the configurations where $\langle[\bar{\chi}\chi]_{\mathrm{sub}}\rangle_U$ is positive should be different – on the basis of the operator expansion (16) – from that on the configurations where $\langle[\bar{\chi}\chi]_{\mathrm{sub}}\rangle_U$ is negative. The observed jumps of the plaquette expectation value can hence be regarded as a combined effect of spontaneous chiral symmetry breaking and the explicit breaking of this symmetry due to the Wilson term in (13).

4.2 Effective potential model

The scenario of a jump in the scalar condensate for Wilson fermions on the lattice has actually been given already some time ago by Sharpe and Singleton [23]. As it has been shown in that work, the phase structure of lattice QCD for $\mu = 0$ with Wilson-type quarks can be understood in the low energy chiral theory of pseudo-Goldstone bosons if the influence of leading lattice artifacts of $\mathcal{O}(a)$ and $\mathcal{O}(a^2)$ is taken into account.

There are two alternatives: either there exists an *Aoki phase* [22] or there is a first order phase transition between the phases with positive and negative quark mass and the Aoki phase does not exist.

The relevant part of the effective potential is written in [23] as

$$\mathcal{V}_\chi = -c_1 A + c_2 A^2. \tag{23}$$

Here A denotes the flavor singlet component of the SU(2) matrix valued field Σ in the low energy effective chiral Lagrangian:

$$\Sigma = A + \mathrm{i}\sum_{r=1}^{3} B_r\tau_r. \tag{24}$$

Because of the relation $1 = A^2 + \sum_{r=1}^3 B_r B_r$ the variable A is constrained to lie between -1 and $+1$ inclusive. In the vicinity of the critical quark mass the constant $c_2 = \mathcal{O}(a^2)$ and the other parameter c_1 is proportional to the bare quark mass (in our notation $c_1 \propto \tilde{m}$).

In order to find the ground state ("vacuum") the effective potential has to be minimized. Without repeating the details of the discussion in [23] let us just summarize the result.

In case of positive c_2 there exists an Aoki phase in the region of bare quark masses defined by $-2c_2 \le c_1 \le 2c_2$. At the boundaries $c_1 = \pm 2c_2$ all three pion masses vanish. Inside the Aoki phase the charged pions are massless because they are the Goldstone bosons of spontaneous flavor symmetry breaking but the neutral pion is massive. Outside the Aoki phase ($|c_1| > 2c_2$) the flavor symmetry is preserved by the ground state and the three degenerate pions are massive (see Fig. 6).

The other alternative is that c_2 is negative. In this case the flavor symmetry is preserved everywhere but there exists a minimal pion mass because the pion mass is given by

$$m_\pi^2 = f_\pi^{-2}\left(|c_1| + 2|c_2|\right). \tag{25}$$

At $c_1 = 0$ the vacuum expectation value jumps from $\Sigma = A = +1$ to $\Sigma = A = -1$. Since the jump of this "order parameter" happens at non-zero pion mass (i.e. finite correlation length) the thermodynamical description of the behavior near $c_1 = 0$ corresponds to a *first order phase transition.*

An interesting intermediate situation is defined by $c_2 = 0$. In this case the vacuum expectation value jumps between

[1] The relations between renormalized and subtracted operators in the χ-basis are $[\bar{\chi}\chi]_{\mathrm{R}} = Z_{S^0}[\bar{\chi}\chi]_{\mathrm{sub}}$ and $[\bar{\chi}\mathrm{i}\gamma_5\tau_3\chi]_{\mathrm{R}} = Z_P[\bar{\chi}\mathrm{i}\gamma_5\tau_3\chi]_{\mathrm{sub}}$.

[2] Using the spurionic invariances of the action (3), it is possible to show that b_3 is odd under $(r \to -r) \times (m_0 \to -m_0)$, or equivalently, since $m_c(-r) = -m_c(r)$, under $(r \to -r) \times (\tilde{m} \to -\tilde{m})$. We expect hence a contribution to b_3 odd in r and even in $\tilde{m}$.

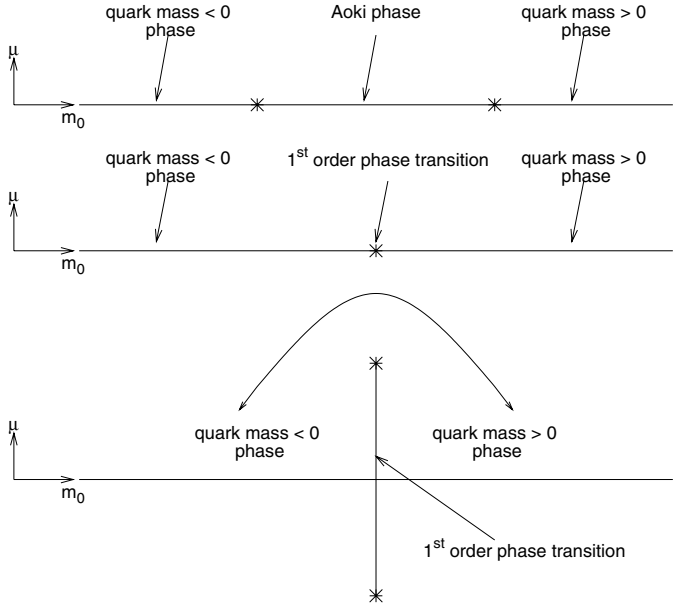

Fig. 6. The alternatives of the phase structure in the (m_0, μ) plane: *Upper part*: Aoki phase at $\mu = 0$ if $c_2 > 0$, *middle part:* first order phase transition point if $c_2 = 0$, *lower part:* first order phase transition line if $c_2 < 0$. In the latter case the two phases are connected with each other as it is shown by the curve with arrows at both ends

$\Sigma = A = +1$ and $\Sigma = A = -1$ at a single first order phase transition point. This limiting case is the ideal situation, when the phase structure in the Sharpe–Singleton model is identical to the expected one in the continuum. It can be characterized either by saying that the Aoki phase has zero extension or that the minimal pion mass is zero (see Fig. 6). Of course, this behavior is valid only up to $\mathcal{O}(a^3)$ effects, neglecting higher orders in the chiral expansion.

4.3 Scenarios

Our numerical results reveal that we clearly observe metastabilities in various quantities. Thus our conclusion is that at least for vanishing twisted mass parameter, i.e. for the standard Wilson lattice theory, *there is a first order phase transition.* For non-vanishing values of μ we can have two scenarios.

The first is that the first order phase transition persists for $\mu \neq 0$ but sufficiently small in absolute value. For large μ the theory approaches the quenched limit with a constant quark determinant and therefore it is plausible that no phase transition is expected. This scenario suggests that the first order phase transition line in the (m_0, μ) plane has an end point: the two phases with positive and negative quark masses are analytically connected (see Fig. 6). The situation is in this sense analogous to the phase structure of the SU(2) fundamental Higgs model (see Chap. 6 of [24] and references therein).

The second scenario is that for any non-vanishing value of μ the first order phase transition disappears. In this scenario, when varying m_0, one passes at some small distance from the first order phase transition at $\mu = 0$ and just feels this close-by phase transition.

We can at present not differentiate between these two scenarios. From the numerical side we would need to know better the μ and β dependence of the metastability phenomena. From the analytical side an analysis à la Sharpe and Singleton including the twisted mass parameter μ is helpful.[3]

The first order phase transition between the phases with positive and negative quark masses observed in the previous section is consistent with the *no-Aoki-phase* alternative ($c_2 < 0$) of Sharpe and Singleton.

Our exclusion of the Aoki phase is in agreement with the results of a recent paper [25] which suggests that in case of the unimproved Wilson action the Aoki phase is restricted to the region of strong gauge couplings ($\beta \leq 4.6$). Note that in an early paper on QCD thermodynamics with Wilson quarks [26] a first order "bulk" phase transition has also been observed at $\beta = 4.8$ which is consistent both with [25] and with our observations. For further numerical work on the Aoki phase, see [27].

The rather strong metastability of the two phases with positive and negative quark mass can be understood on the basis of the properties of the eigenvalue spectrum of the (non-hermitean) Wilson-fermion matrix in the twisted mass basis corresponding to (3). For zero twisted mass ($\mu = 0$) at small positive quark masses there is a "cloud" of eigenvalues close to the origin near the real axis. (For a numerical study see Sect. 4 of [17].) In order to reach negative quark masses this "cloud" has to cross near the origin to the other side with negative real parts. This *eigenvalue cloud crossing* is strongly suppressed by the zero of the determinant. This, we believe, is the reason at the microscopical level for the observed strong metastability. For non-zero twisted mass there is a strip of width $2|\mu|$ around the real axis where there are no eigenvalues. If this strip is wide enough the eigenvalues are sufficiently far away from the origin and the first order phase transition disappears.

As it was already emphasized in [23], the sign of the coefficient c_2 in the low energy pion effective potential is not universal, it depends on the way the action is discretized. Therefore a clever choice of the lattice action may weaken the first order phase transition and, for instance, decrease the minimal pion mass at it. Previous results of the JLQCD Collaboration [20] support the conjecture that changing the gauge action alone has an important effect. If, indeed, one could find some parameter in the lattice gauge action which at some value would change the sign of c_2 an appealing possibility would be to tune the lattice action to this value. The features of a discretization with $c_2 = 0$ seem to be quite favorable from the point of view of light quark simulations when, up to $\mathcal{O}(a^2)$, there would be just a single point in the (m_0, μ) plane with vanishing pion mass – an ideal situation corresponding to the expected phase structure in the continuum.

[3] We thank Gernot Münster for discussions on this and for communicating us his results before publication.

5 Conclusion

In this paper we have explored Wilson twisted mass fermions restricting ourselves to simulations at only one value of $\beta = 5.2$. By fixing the twisted mass parameter μ and changing the untwisted Wilson quark mass m_0, or equivalently the hopping parameter κ, we encountered strong metastabilities in the plaquette expectation value, visible both in thermal cycles as well as in long-living metastable states. At the same time, the pion mass does not vanish but has a minimum at a rather large value. The PCAC quark mass $m_\chi^{\rm PCAC}$ in the different metastable branches is positive for the branch with low plaquette expectation value and it is negative for the branch with high plaquette expectation value.

The detection of these metastabilities became possible by employing a twisted mass term. Only a non-vanishing value of μ allowed us to cross the critical quark mass. We showed that for lattice theories that break chiral symmetry explicitly the jump of the scalar condensate, when changing the sign of the quark mass, induces a jump of the plaquette expectation value with associated signs of metastability. For $\mu = 0$ these metastabilities find a natural interpretation in the effective potential model of Sharpe and Singleton, arising from spontaneous symmetry breaking and using a low energy effective Lagrangian which also describes lattice artifacts. The agreement with the Sharpe–Singleton model is remarkable because in the continuum limit in this model the phase structure of lattice QCD with Wilson quarks approaches fast – at a rate $\mathcal{O}(a^2)$ – the expected phase structure of QCD near zero quark mass. This is an important property which has to be required from any lattice regularization of QCD.

It should be clear that our work can only represent a first step in a detailed understanding of the QCD phase diagram at zero temperature near vanishing quark masses. Clearly, substantially more work has to be done to resolve this phase structure and its behavior in the continuum limit. For instance, at present for $\mu \neq 0$ we are unable to differentiate between a scenario where the first order phase transition persists and another one where at $\mu \neq 0$ only a remnant of the phase transition at $\mu = 0$ is seen. In this respect an analysis like in [23] for $\mu \neq 0$ is very helpful [28].

Among the many open questions there are: How fast does the gap vanish when the continuum limit at higher values of β is approached? How are the signs of metastability related to the ones observed using the Wilson plaquette action and clover-improved Wilson fermions? How precisely do the eigenvalues re-arrange when the critical quark mass is crossed? Do different gauge actions change the couplings of the effective potential and may hence lead to avoid the phenomena of metastability and reproduce the ideal phase structure at vanishing quark mass already for non-zero lattice spacing?

The most important question is, of course, how phenomenology can be done given the metastability phenomenon seen in our present results, i.e.: What is the lowest value of the quark mass that can be reached before one enters the regime of metastabilities and how does this change with decreasing value of the lattice spacing?

Acknowledgements. We thank Gernot Münster, Luigi Scorzato and Stephen Sharpe for helpful discussions. The computations were performed on the APEmille systems installed at NIC Zeuthen and INFN Milano, the IBM-JUMP computer at NIC Jülich, IBM pSeries 690 Supercomputer at HLRN, the PC clusters at DESY Hamburg, NIC Zeuthen, University of Münster, Forschungszentrum Karlsruhe and the Sun Fire SMP-Cluster at the Rechenzentrum - RWTH Aachen. This work was supported by the DFG Sonderforschungsbereich/Transregio SFB/TR9-03. G.C.R. wishes to thank the Humboldt Foundation for financial support while this work was prepared.

A Appendix

A.1 Even–odd preconditioning for the HMC algorithm

Let us start with the Dirac operator in the hopping parameter representation in the twisted basis written as

$$S\left[\chi,\bar{\chi},U\right] \equiv \sum_{xy} \bar{\chi}(x)\, M_{xy}\, \chi(y), \tag{26}$$

where the matrix M can be easily read from (7). Using M one can define the hermitian operator

$$Q \equiv \gamma_5 M = \begin{pmatrix} Q_+ & 0 \\ 0 & Q_- \end{pmatrix}, \tag{27}$$

where the submatrices $Q_\pm$ can be factorized as follows:

$$\begin{aligned} Q_\pm &= \gamma_5 \begin{pmatrix} 1 \pm \mathrm{i}\tilde{\mu}\gamma_5 & M_{\rm eo} \\ M_{\rm oe} & 1 \pm \mathrm{i}\tilde{\mu}\gamma_5 \end{pmatrix} \\ &= \gamma_5 \begin{pmatrix} M_{\rm ee}^{\pm} & M_{\rm eo} \\ M_{\rm oe} & M_{\rm oo}^{\pm} \end{pmatrix} \\ &= \begin{pmatrix} \gamma_5 M_{\rm ee}^{\pm} & 0 \\ \gamma_5 M_{\rm oe} & 1 \end{pmatrix} \begin{pmatrix} 1 & (M_{\rm ee}^{\pm})^{-1} M_{\rm eo} \\ 0 & \gamma_5 (M_{\rm oo}^{\pm} - M_{\rm oe}(M_{\rm ee}^{\pm})^{-1} M_{\rm eo}) \end{pmatrix}, \end{aligned} \tag{28}$$

and we have defined $\tilde{\mu} \equiv 2\kappa\mu$. Note that $(M_{\rm ee}^{\pm})^{-1}$ can be easily computed to be

$$(1 \pm \mathrm{i}\tilde{\mu}\gamma_5)^{-1} = \frac{1 \mp \mathrm{i}\tilde{\mu}\gamma_5}{1 + \tilde{\mu}^2}.$$

Using $\det(Q) = \det(Q_+)\det(Q_-)$ one can now derive the following relation (an equation apart from an irrelevant factor):

$$\begin{aligned} \det(Q_\pm) \;&\propto\; \det(\hat{Q}_\pm) \\ \hat{Q}_\pm &:= \gamma_5 (M_{\rm oo}^{\pm} - M_{\rm oe}(M_{\rm ee}^{\pm})^{-1} M_{\rm eo}), \end{aligned} \tag{29}$$

where $\hat{Q}_\pm$ is only defined on the odd sites of the lattice. In the HMC algorithm the determinant is stochastically estimated using pseudo-fermion fields $\phi_{\rm o}$:

$$\begin{aligned} \det(\hat{Q}_+\hat{Q}_-) \;&=\; \int D\left[\phi_{\rm o}, \phi_{\rm o}^\dagger\right] \exp(-S_b), \\ S_b &:= \phi_{\rm o}^\dagger (\hat{Q}_+\hat{Q}_-)^{-1} \phi_{\rm o}, \end{aligned}$$

where the fields $\phi_{\rm o}$ are defined only on the odd sites of the lattice. In order to compute the force corresponding to the effective action S_b we need the variation of S_b with respect to the gauge fields (using $\delta(A^{-1}) = -A^{-1}\delta A A^{-1}$):

$$\begin{aligned}\delta S_b &= -\Big[\phi_{\rm o}^\dagger(\hat{Q}_+\hat{Q}_-)^{-1}\delta\hat{Q}_+\hat{Q}_+^{-1}\phi_{\rm o} \\ &\quad + \phi_{\rm o}^\dagger\hat{Q}_-^{-1}\delta\hat{Q}_-(\hat{Q}_+\hat{Q}_-)^{-1}\phi_{\rm o}\Big] \\ &= -\left[X_{\rm o}^\dagger\delta\hat{Q}_+Y_{\rm o} + Y_{\rm o}^\dagger\delta\hat{Q}_-X_{\rm o}\right], \end{aligned} \tag{30}$$

with $X_{\rm o}$ and $Y_{\rm o}$ defined on the odd sites as

$$X_{\rm o} = (\hat{Q}_+\hat{Q}_-)^{-1}\phi_{\rm o}, \quad Y_{\rm o} = \hat{Q}_+^{-1}\phi_{\rm o} = \hat{Q}_-X_{\rm o}\ , \tag{31}$$

where $\hat{Q}_\pm^\dagger = \hat{Q}_\mp$ has been used. The variation of $\hat{Q}_\pm$ reads

$$\delta\hat{Q}_\pm = \gamma_5\left(-\delta M_{\rm oe}(M_{\rm ee}^\pm)^{-1}M_{\rm eo} - M_{\rm oe}(M_{\rm ee}^\pm)^{-1}\delta M_{\rm eo}\right), \tag{32}$$

and one finds

$$\begin{aligned}\delta S_b &= -(X^\dagger\delta Q_+Y + Y^\dagger\delta Q_-X) \\ &= -(X^\dagger\delta Q_+Y + (X^\dagger\delta Q_+Y)^\dagger), \end{aligned} \tag{33}$$

where X, Y is now defined over the full lattice as

$$X = \begin{pmatrix} -(M_{\rm ee}^-)^{-1}M_{\rm eo}X_{\rm o} \\ X_{\rm o}\end{pmatrix}, \quad Y = \begin{pmatrix} -(M_{\rm ee}^+)^{-1}M_{\rm eo}Y_{\rm o} \\ Y_{\rm o}\end{pmatrix}. \tag{34}$$

In addition, $\delta Q_+ = \delta Q_-$, $M_{\rm eo}^\dagger = \gamma_5 M_{\rm oe}\gamma_5$ and $M_{\rm oe}^\dagger = \gamma_5 M_{\rm eo}\gamma_5$ has been used. Since the bosonic part is quadratic in the $\phi_{\rm o}$ fields, the $\phi_{\rm o}$ are generated at the beginning of each molecular dynamics trajectory with

$$\phi_{\rm o} = \hat{Q}_+R, \tag{35}$$

where R is a random spinor field taken from a Gaussian distribution with norm one.

A.1.1 Hasenbusch trick

The trick first presented in [10] is based on the observation that writing

$$\det[Q_+Q_-] = \det[W_+W_-]\cdot\det[(Q_+Q_-)/(W_+W_-)] \tag{36}$$

is advantageous for the HMC, if the condition number of W_+W_- and of $(Q_+Q_-)/(W_+W_-)$ is significantly reduced compared to the condition number of only (Q_+Q_-). In order to achieve this we define

$$\begin{aligned} Q_\pm &= \gamma_5 D_W \pm {\rm i}\tilde{\mu}, \\ W_\pm &= \gamma_5 D_W \pm {\rm i}\tilde{\mu}_2. \end{aligned} \tag{37}$$

With $\tilde{\mu}_2 = \tilde{\mu} + \Delta\tilde{\mu}$ it follows immediately that the condition number of W_+W_- is lower than the one of Q_+Q_- if for $\lambda_{\rm min}$ and $\lambda_{\rm max}$ the lowest and the largest eigenvalue of Q_+Q_-, respectively, $|\lambda_{\rm min}| \ll \tilde{\mu}_2^2 \ll |\lambda_{\rm max}|$ holds: the condition number of W_+W_- is $|\lambda_{\rm max}|/\tilde{\mu}_2^2$ while the one of $(W_+W_-)^{-1}(Q_+Q_-)^2$ contrariwise is $\tilde{\mu}_2^2/|\lambda_{\rm min}|$. We can take $\tilde{\mu}$, which is a lower bound for $|\lambda_{\rm min}|$, to write down the following estimates for the condition numbers k:

$$k_{W_+W_-} = \frac{|\lambda_{\rm max}|}{\tilde{\mu}_2^2}\ , \quad k_{(Q_+Q_-)/(W_+W_-)} \le \frac{\tilde{\mu}_2^2}{\tilde{\mu}^2}\ ,$$

which leads to an optimal choice for $\tilde{\mu}_2^2 = \sqrt{|\lambda_{\rm max}|\cdot\tilde{\mu}^2}$. As has been shown in [11] also the force contribution coming from $(Q_+Q_-)/(W_+W_-)$ is reduced. This is true also for tmQCD and can be seen in the following way: noticing that

$$Q_+Q_- = Q^2 + \tilde{\mu}^2$$

and

$$\begin{aligned} W_+W_- &= Q^2 + \tilde{\mu}_2^2 = Q^2 + \tilde{\mu}^2 + \tilde{\mu}_2^2 - \tilde{\mu}^2 \\ &= Q_+Q_- + \tilde{\mu}_2^2 - \tilde{\mu}^2, \end{aligned} \tag{38}$$

it follows that

$$W_+W_-(Q_+Q_-)^{-1} = 1 + (\tilde{\mu}_2^2 - \tilde{\mu}^2)(Q_+Q_-)^{-1}. \tag{39}$$

Since the corresponding effective action reads

$$S_F = \phi^\dagger(1 + (\tilde{\mu}_2^2 - \tilde{\mu}^2)(Q_+Q_-)^{-1})\phi \tag{40}$$

one can see that one gets an explicit factor $(\tilde{\mu}_2^2 - \tilde{\mu}^2) \ll 1$ multiplying the force contribution compared to the original effective action which will reduce the force and therefore lead to a smoother evolution of the algorithm.

Let us remark that the procedure explained above can be immediately applied to the even–odd preconditioned system. Furthermore the trick can be iterated to two or even more additional operators.

In Fig. 7 the cost C in units of CG iterations and the acceptance rate P_A is plotted versus $\tilde{\mu}_2 = 2\kappa\mu_2$ at fixed HMC stepsize and trajectory length. One can see that as expected the acceptance rate increases by introducing an additional operator and reaches a maximum around $\tilde{\mu} = 0.2$. Of course also the costs increase when compared to the HMC without additional operators. But the costs are still much less than what is needed to reach an acceptance rate of about 90% without the additional operator (see the dashed line in Fig. 7). One can see that the gain in the costs is about a factor of two.

A.2 Even–odd preconditioning for the TSMB algorithm

In this appendix even–odd preconditioning is derived for the TSMB algorithm. The even–odd subspace decomposition of the fermion matrix in the twisted basis can be written as

$$Q^\chi = \begin{pmatrix} \mu_1 + {\rm i}\gamma_5\tau_3\mu & -\frac{1}{2}M_{\rm eo} \\ -\frac{1}{2}M_{\rm oe} & \mu_1 + {\rm i}\gamma_5\tau_3\mu\end{pmatrix}, \tag{41}$$

where indices start by zero = even, the lattice spacing is set to $a = 1$ and the abbreviation $\mu_1 \equiv m_0 + 4r = (2\kappa)^{-1}$ is

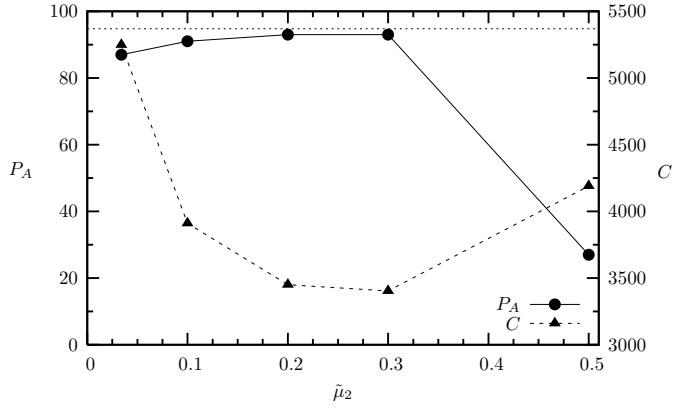

Fig. 7. Acceptance rate P_A and cost C in units of CG iterations versus $\tilde{\mu}_2 = 2\kappa\mu_2$ at fixed HMC stepsize and trajectory length. The dashed line represents the cost required to obtain about 90% acceptance rate without the additional operator. The parameters are: 8^4 lattice, $\beta = 5.2$, $\kappa = 0.17$, $\mu = 0.01$

introduced. The *hermitean* fermion matrix $\tilde{Q} = \gamma_5\tau_1 Q^\chi = \tilde{Q}^\dagger$ is then

$$\tilde{Q} = \begin{pmatrix} \gamma_5\tau_1\mu_1 + \tau_2\mu & -\frac{1}{2}\gamma_5\tau_1 M_{\rm eo} \\ -\frac{1}{2}\gamma_5\tau_1 M_{\rm oe} & \gamma_5\tau_1\mu_1 + \tau_2\mu \end{pmatrix}. \tag{42}$$

Using the notation

$$\begin{aligned} t_5 &\equiv (\gamma_5\tau_1\mu_1 + \tau_2\mu)^{-1}\gamma_5\tau_1 \\ &= (\mu_1 - \mathrm{i}\gamma_5\tau_3\mu)(\mu_1^2 + \mu^2)^{-1} \end{aligned} \tag{43}$$

one can write $\tilde{Q}$ as the following product:

$$\begin{aligned} \tilde{Q} = &\begin{pmatrix} \gamma_5\tau_1\mu_1 + \tau_2\mu & 0 \\ 0 & \gamma_5\tau_1\mu_1 + \tau_2\mu \end{pmatrix} \\ &\times \begin{pmatrix} 1 & 0 \\ -\frac{1}{2}t_5 M_{\rm oe} & 1 \end{pmatrix} \\ &\times \begin{pmatrix} 1 & 0 \\ 0 & 1 - \frac{1}{4}t_5 M_{\rm oe} t_5 M_{\rm eo} \end{pmatrix} \begin{pmatrix} 1 & -\frac{1}{2}t_5 M_{\rm eo} \\ 0 & 1 \end{pmatrix}. \end{aligned} \tag{44}$$

This can be used for preconditioned inversion of $\tilde{Q}$ because the inverse of all the factors but the third one is trivial. Of course, the third factor is expected to have a smaller condition number than $\tilde{Q}$ itself.

Multi-boson (MB) updating can be set up following [18]. Since the determinant of the above triangular matrices is equal to 1 we have

$$\begin{aligned} &\det\tilde{Q} \\ &= \det\begin{pmatrix} \gamma_5\tau_1\mu_1 + \tau_2\mu & 0 \\ 0 & \gamma_5\tau_1\mu_1 + \tau_2\mu - \frac{1}{4}\gamma_5\tau_1 M_{\rm oe} t_5 M_{\rm eo} \end{pmatrix} \\ &= \det_{\rm e}\left(\gamma_5\tau_1\mu_1 + \tau_2\mu\right) \\ &\quad \times \det_{\rm o}\left(\gamma_5\tau_1\mu_1 + \tau_2\mu - \frac{1}{4}\gamma_5\tau_1 M_{\rm oe} t_5 M_{\rm eo}\right), \end{aligned} \tag{45}$$

where $\det_{\rm e}$ and $\det_{\rm o}$ denote determinants in the even and odd subspaces, respectively. The first factor does not depend on the gauge field and therefore it can be omitted. In the second factor we have the hermitean matrix defined on odd sites

$$\begin{aligned} \bar{Q} &= \gamma_5\tau_1\mu_1 + \tau_2\mu \\ &\quad -\frac{1}{4}\gamma_5\tau_1 M_{\rm oe}(\gamma_5\tau_1\mu_1 + \tau_2\mu)^{-1}\gamma_5\tau_1 M_{\rm eo} \\ &= \gamma_5\tau_1\mu_1 + \tau_2\mu \\ &\quad -\frac{1}{4}\gamma_5\tau_1 M_{\rm oe}(\gamma_5\tau_1\mu_1 + \tau_2\mu)(\mu_1^2 + \mu^2)^{-1}\gamma_5\tau_1 M_{\rm eo} \\ &= \bar{Q}^\dagger. \end{aligned} \tag{46}$$

The hermiticity of $\bar{Q}$, which can be called *hermitean preconditioned fermion matrix*, follows from

$$\gamma_5\tau_1 M_{\rm oe}^\dagger \gamma_5\tau_1 = M_{\rm eo}. \tag{47}$$

In MB updating one can start with the identity

$$\det Q = \det\tilde{Q} \propto \det_{\rm o}\bar{Q} = \left(\det_{\rm o}\bar{Q}^2\right)^{\frac{1}{2}} \simeq \frac{1}{\det_{\rm o} P_{\frac{1}{2}}(\bar{Q}^2)} \tag{48}$$

where the $P_{\frac{1}{2}}$ is a polynomial approximation satisfying

$$P_{\frac{1}{2}}(x) \simeq \frac{1}{x^{\frac{1}{2}}} \tag{49}$$

in an interval $x \in [\epsilon, \lambda]$ covering the spectrum of $\bar{Q}^2$. (Note that for $\mu \neq 0$ $\det Q$ and $\det\bar{Q}$ are positive.)

The rest is the same as usual: one writes the polynomial with the help of the square roots of its roots ρ_j, $j = 1, 2, \ldots$ as

$$P_{\frac{1}{2}}(\bar{Q}^2) \propto \prod_j (\bar{Q} - \rho_j^*)(\bar{Q} - \rho_j). \tag{50}$$

Then using the identity

$$\det\begin{pmatrix} A_{\rm ee} & A_{\rm eo} \\ A_{\rm oe} & A_{\rm oo} \end{pmatrix} = \det_{\rm e} A_{\rm ee} \cdot \det_{\rm o}\left(A_{\rm oo} - A_{\rm oe}A_{\rm ee}^{-1}A_{\rm eo}\right) \tag{51}$$

one obtains

$$\begin{aligned} \det_{\rm o}(\bar{Q} - \rho_j) = &\det_{\rm e}(\gamma_5\tau_1\mu_1 + \tau_2\mu)^{-1} \\ &\times \det\begin{pmatrix} \gamma_5\tau_1\mu_1 + \tau_2\mu & -\frac{1}{2}\gamma_5\tau_1 M_{\rm eo} \\ -\frac{1}{2}\gamma_5\tau_1 M_{\rm oe} & \gamma_5\tau_1\mu_1 + \tau_2\mu - \rho_j \end{pmatrix}. \end{aligned} \tag{52}$$

Denoting the projector on the odd subspace by $P_{\rm o}$ we finally obtain the multi-boson representation

$$\begin{aligned} &\left(\det_{\rm o}\bar{Q}^2\right)^{\frac{1}{2}} \\ &\propto \prod_j \frac{1}{\det\left[(\tilde{Q} - P_{\rm o}\rho_j^*)(\tilde{Q} - P_{\rm o}\rho_j)\right]} \\ &\propto \int [\mathrm{d}\Phi] \exp\left\{ -\sum_j \Phi_j^\dagger(\tilde{Q} - P_{\rm o}\rho_j^*)(\tilde{Q} - P_{\rm o}\rho_j)\Phi_j \right\}. \end{aligned} \tag{53}$$

References

1. C. Bernard et al., Nucl. Phys. Proc. Suppl. **106**, 199 (2002)
2. K. Jansen, Nucl. Phys. Proc. Suppl. **129**, 3 (2004); hep-lat/0311039
3. B. Bunk, M. Della Morte, K. Jansen, F. Knechtli, Nucl. Phys. B **697**, 343 (2004); hep-lat/0403022
4. H. Neuberger, Phys. Lett. B **417**, 141 (1998); hep-lat/9707022; for reviews, see F. Niedermayer, Nucl. Phys. Proc. Suppl. **73**, 105 (1999); hep-lat/9810026; P. Hernandez, Nucl. Phys. Proc. Suppl. **106**, 80 (2002); hep-lat/0110218
5. R. Frezzotti, P.A. Grassi, S. Sint, P. Weisz, Nucl. Phys. Proc. Suppl. **83**, 941 (2000); hep-lat/9909003
6. R. Frezzotti, P.A. Grassi, S. Sint, P. Weisz [Alpha Collaboration], JHEP **0108**, 058 (2001); hep-lat/0101001
7. R. Frezzotti, S. Sint, P. Weisz, JHEP **0107**, 048 (2001); hep-lat/0104014; M. Della Morte, R. Frezzotti, J. Heitger, S. Sint [ALPHA Collaboration], JHEP **0110**, 041 (2001); hep-lat/0108019
8. R. Frezzotti, G.C. Rossi, JHEP **0408**, 007 (2004); hep-lat/0306014; Nucl. Phys. Proc. Suppl. **128**, 193 (2004); hep-lat/0311008
9. K. Jansen, A. Shindler, C. Urbach, I. Wetzorke [XLF Collaboration], Phys. Lett. B **586**, 432 (2004); hep-lat/0312013
10. M. Hasenbusch, Phys. Lett. B **519**, 177 (2001); hep-lat/0107019
11. M. Hasenbusch, K. Jansen, Nucl. Phys. B **659**, 299 (2003); hep-lat/0211042
12. I. Montvay, Nucl. Phys. B **466**, 259 (1996); hep-lat/9510042
13. T.A. DeGrand, P. Rossi, Comput. Phys. Commun. **60**, 211 (1990)
14. J.C. Sexton, D.H. Weingarten, Nucl. Phys. B **380**, 665 (1992)
15. M. Lüscher, Nucl. Phys. B **418**, 637 (1994); hep-lat/9311007
16. C. Gebert, I. Montvay, hep-lat/0302025
17. F. Farchioni, C. Gebert, I. Montvay, L. Scorzato [qq+q Collaboration], Eur. Phys. J. C **26**, 237 (2002); hep-lat/0206008
18. B. Jegerlehner, Nucl. Phys. Proc. Suppl. **53**, 959 (1997); hep-lat/9612013
19. F. Farchioni, I. Montvay, E. Scholz [qq+q Collaboration], Eur. Phys. J. C **37**, 197 (2004); hep-lat/0403014
20. S. Aoki et al. [JLQCD Collaboration], Nucl. Phys. Proc. Suppl. **106**, 263 (2002); hep-lat/0110088
21. M. Bochicchio, L. Maiani, G. Martinelli, G.C. Rossi, M. Testa, Nucl. Phys. B **262**, 331 (1985); JHEP **9804**, 002 (1998)
22. S. Aoki, Phys. Rev. D **30**, 2653 (1984); Phys. Rev. Lett. **57**, 3136 (1986)
23. S.R. Sharpe, R. Singleton, Jr., Phys. Rev. D **58**, 074501 (1998); hep-lat/9804028
24. I. Montvay, G. Münster, Quantum fields on a lattice, Cambridge monographs on mathematical physics (Cambridge University Press, Cambridge 1994)
25. E.M. Ilgenfritz, W. Kerler, M. Müller-Preussker, A. Sternbeck, H. Stuben, Phys. Rev. D **69**, 074511 (2004); hep-lat/0309057
26. T. Blum et al., Phys. Rev. D **50**, 3377 (1994); hep-lat/9404006
27. S. Aoki, A. Gocksch, Phys. Rev. D **45**, 3845 (1992); S. Aoki, Prog. Theor. Phys. **122**, 179 (1996); S. Aoki, A. Ukawa, T. Umemura, Phys. Rev. Lett. **76**, 873 (1996); Y. Iwasaki, K. Kanaya, S. Sakai, T. Yoshie, Nucl. Phys. Proc. Suppl. **30**, 327 (1993), **34**, 314 (1994); S. Aoki, Nucl. Phys. Proc. Suppl. A **60**, 206 (1998)
28. G. Münster, JHEP **0409**, 035 (2004); hep-lat/0407006

[Wil-2]

Lattice spacing dependence of the first order phase transition for dynamical twisted mass fermions

Phys. Lett. B624 324-333 (2005)

Available online at www.sciencedirect.com
SCIENCE DIRECT®
Physics Letters B 624 (2005) 324–333
PHYSICS LETTERS B
www.elsevier.com/locate/physletb

Lattice spacing dependence of the first order phase transition for dynamical twisted mass fermions

F. Farchioni [a], K. Jansen [b], I. Montvay [c], E.E. Scholz [c], L. Scorzato [d], A. Shindler [b], N. Ukita [c], C. Urbach [b,e], U. Wenger [b], I. Wetzorke [b]

[a] *Institut für Theoretische Physik, Universität Münster, Wilhelm-Klemm-Str. 9, 48149 Münster, Germany*
[b] *NIC, Platanenallee 6, 15738 Zeuthen, Germany*
[c] *DESY, Notkestr. 85, 22607 Hamburg, Germany*
[d] *Institut für Physik, Humboldt Universität zu Berlin, Newtonstr. 15, 12489 Berlin, Germany*
[e] *Institut für Theoretische Physik, Freie Universität Berlin, Arnimallee 14, 14195 Berlin, Germany*

Received 14 July 2005; accepted 8 August 2005

Available online 18 August 2005

Editor: L. Alvarez-Gaumé

Abstract

Lattice QCD with Wilson fermions generically shows the phenomenon of a first order phase transition. We study the phase structure of lattice QCD using Wilson twisted mass fermions and the Wilson plaquette gauge action in a range of β values where such a first order phase transition is observed. In particular, we investigate the dependence of the first order phase transition on the value of the lattice spacing. Using only data in one phase and neglecting possible problems arising from the phase transition we are able to perform a first scaling test for physical quantities using this action.

1. Introduction

Understanding the phase structure of lattice QCD is an important pre-requisite before starting large scale simulations. Indeed, our collaboration found that when working at lattice spacings of about 0.15 fm there can be strong first order phase transitions at small quark masses, at least when a combination of Wilson plaquette action and Wilson fermions is used [1,2]. The phenomenon appears also when a small twisted mass term is switched on. This has serious consequences, since in such a scenario the pion mass m_{PS} cannot be made arbitrarily small but assumes a minimal value, $m_{\mathrm{PS}}^{\mathrm{min}}$, which may be about 500 MeV and hence it becomes impossible to work close to the physical value of the pion mass.

The presence of the first order phase transition for pure Wilson fermions is in accordance with predic-

E-mail address: carsten.urbach@physik.fu-berlin.de (C. Urbach).

0370-2693/$ – see front matter
doi:10.1016/j.physletb.2005.08.018

tions from chiral perturbation theory [3], which have been extended later to the case of adding a twisted mass [4–8]. Let us, for completeness, also mention that for values of the lattice spacing much coarser than $a = 0.15$ fm the first order phase transition turns into a second order one from the normal QCD phase to the so-called Aoki phase [9–11]. The generic phase structure of lattice QCD according to our present understanding is discussed and illustrated in Refs. [1,2,12].

In Refs. [1,2] we have studied only one value of the inverse gauge coupling $\beta = 6/g_0^2$ in order to demonstrate the existence of the first order phase transition, leaving the question of the β-dependence open. Since lattice chiral perturbation theory predicts a weakening of the first order phase transition towards the continuum limit, it is interesting to check this prediction and, in particular, to investigate quantitatively how fast the transition weakens when the continuum limit is approached. The answer to the latter question will naturally depend on the choice of the actions that are used for the gauge and the fermion fields.

In this Letter we will present results using Wilson twisted mass fermions and the Wilson plaquette gauge action for three values of β. At each of these β values we have performed simulations at a number of quark masses on both sides of the first order phase transition. This allows to study the β-dependence of the phase transition itself and, in addition, the lattice spacing dependence of physical observables computed separately in the two phases. We have performed such a scaling test for the pion mass, the pion decay constant and the ratio of the pion to the vector meson mass. For a scaling test of Wilson twisted mass fermions and other recent results in the quenched approximation see Refs. [13–15].

2. Wilson twisted mass fermions

In this Letter we will work with Wilson twisted mass fermions [16] that can be arranged to be $O(a)$ improved without employing specific improvement terms [17]. The Wilson tmQCD action in the twisted basis can be written as

$$S[U,\chi,\bar{\chi}] = a^4 \sum_x \bar{\chi}(x)(D_{\mathrm{W}} + m_0 + i\mu\gamma_5\tau_3)\chi(x), \tag{1}$$

where the Wilson–Dirac operator D_{W} is given by

$$D_{\mathrm{W}} = \sum_{\mu=0}^{3} \frac{1}{2}\big[\gamma_\mu\big(\nabla_\mu^* + \nabla_\mu\big) - a\nabla_\mu^*\nabla_\mu\big], \tag{2}$$

and ∇_μ and ∇_μ^* denote the usual covariant forward and backward derivatives and the Wilson parameter r was set to 1.

The situation of full twist and hence automatic $O(a)$ improvement arises when m_0 in Eq. (1) is tuned towards a critical bare quark mass m_{crit}. We use for our simulations the hopping representation of the Wilson–Dirac operator with $\kappa = (2am_0 + 8)^{-1}$.

We extract the pseudo scalar mass m_{PS} and the vector meson mass m_{V} from the usual correlation functions:

$$C_{PP}(x_0) = a^3 \sum_{\mathbf{x}} \big\langle P^+(x) P^-(0)\big\rangle,$$
$$C_{VV}(x_0) = \frac{a^3}{3} \sum_{k=1}^{3} \sum_{\mathbf{x}} \big\langle V_k^+(x) V_k^-(0)\big\rangle, \tag{3}$$

where we consider the local bilinears $P^\pm = \bar{\chi}\gamma_5\frac{\tau^\pm}{2}\chi$ and $V_\mu^\pm = \bar{\chi}\gamma_\mu\frac{\tau^\pm}{2}\chi$. Here we used $\tau^\pm = (\tau_1 \pm i\tau_2)$ with $\tau_{1,2}$ the first two Pauli matrices. Similarly one can define the correlation function C_{AP} with the local bilinear $A_\mu^\pm = \bar{\chi}\gamma_\mu\gamma_5\frac{\tau^\pm}{2}\chi$.

The bare pseudo scalar decay constant f_χ^{PS} in the twisted basis can be obtained from (cf. [18,19])

$$f_\chi^{\mathrm{PS}} = m_{\mathrm{PS}}^{-1} r_{AP} \langle 0|P^+(0)|\pi\rangle, \tag{4}$$

where the ratio

$$r_{AP} = \frac{\langle 0|A_0^+(0)|\pi\rangle}{\langle 0|P^+(0)|\pi\rangle} \tag{5}$$

can be extracted from the asymptotic behavior of

$$\frac{C_{AP}(x_0)}{C_{PP}(x_0)} = r_{AP}\tanh\big[m_{\mathrm{PS}}(T/2 - x_0)\big]. \tag{6}$$

The bare PCAC quark mass m_χ^{PCAC} in the twisted basis can then be computed from the ratio

$$m_\chi^{\mathrm{PCAC}} = \frac{f_\chi^{\mathrm{PS}}}{2\langle 0|P^+(0)|\pi\rangle} m_{\mathrm{PS}}^2. \tag{7}$$

The sign of m_χ^{PCAC} and f_χ^{PS} is determined by the sign of r_{AP} and therefore, the corresponding values can be negative. One has to keep in mind that m_χ^{PCAC} and f_χ^{PS},

since measured in the twisted basis, do not correspond to the physical quark mass and the physical pseudo scalar decay constant, respectively. While the quark mass is given by a combination of the (renormalized) values of $m_\chi^{\rm PCAC}$ and μ, the pseudo scalar decay constant can be computed by the help of $f_\chi^{\rm PS}$ and the twist angle, as long as $f_\chi^{\rm PS} \neq 0$ and the value of the twist angle is different from $\pi/2$.

Note that the purpose of the present Letter is *not* to work at full twist nor to extract physical quantities, but rather to study the lattice spacing dependence of the first order phase transition. For the same reason, we also do not address the question of the choice of the critical quark mass in order to stay at full twist here, see Refs. [14,15] for recent quenched simulations addressing this point.

3. The phase transition as a function of the lattice spacing

In order to study the lattice spacing dependence of the phase transition we have chosen three values of β: $\beta = 5.1$, $\beta = 5.2$ and $\beta = 5.3$. We scaled the volumes and the values of μ such that the physical volume is larger than 2 fm, roughly constant and that $r_0\mu \approx 0.03$, where r_0 is the Sommer scale [20] fixed to be $r_0 = 0.5$ fm. Note that the value of r_0/a depends on the value of the quark mass and therefore we had to choose a reference value for r_0/a as will be explained below. The parameters are summarized in Table 1.

In practice it turned out that a very direct way of detecting the presence of a first order phase transition in lattice QCD is to monitor the behavior of the plaquette expectation value $\langle P\rangle$, e.g. as a function of κ for fixed twisted mass parameter μ. In such a situation, starting at identical parameter values from "hot" (random) or "cold" (ordered) configurations, $\langle P\rangle$ can assume different, co-existing values. In Fig. 1 we show $\langle P\rangle$ as a function of $1/(2\kappa)$ for the three values of β. The picture is typical for the behavior of a first order phase transition with meta-stable branches, one with a low value of $\langle P\rangle$ and one with a high value of $\langle P\rangle$. We will denote in the following these branches as high ("H") and low ("L") plaquette phases, respectively.

The β-dependence shows that the gap in the plaquette expectation value ΔP decreases substantially

Table 1
Simulation points for Wilson plaquette gauge action. For the three values of β we give the lattice extent, the value for $a\mu$ and the value of the lattice spacing in fm, determined using $r_0 = 0.5$ fm at the reference point (see text), where $(r_0 m_{\rm PS})^2 = 1.5$

β	$L^3 \times T$	$a\mu$	a [fm]
5.1	$12^3 \times 24$	0.013	0.200(2)
5.2	$12^3 \times 24$	0.010	0.160(4)
5.3	$16^3 \times 32$	0.008	0.138(8)

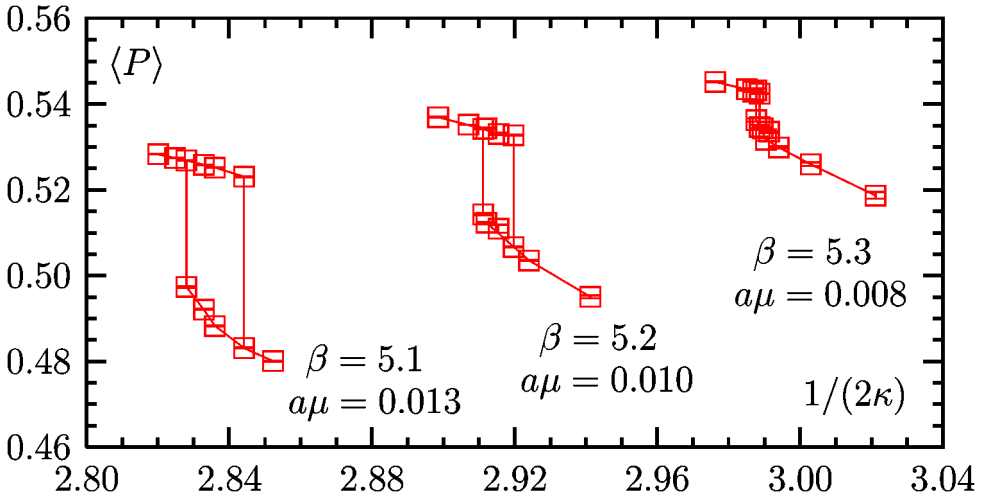

Fig. 1. The plaquette expectation value $\langle P\rangle$ as a function of $1/(2\kappa)$ at the three values of β we have simulated. We also indicate the values of $a\mu$ which are scaled with β such that $r_0\mu$ is roughly constant. The lines just connect the data points and only serve to guide the eye. For this study we have more simulations points than in the next figures and than in Tables 4, 5 and 6.

when moving from $\beta = 5.1$ ($a \approx 0.20$ fm) to $\beta = 5.3$ ($a \approx 0.14$ fm), which is presumably due to the mixing with the chiral condensate as discussed in [1]. One possible definition for the quantity ΔP is the difference between low and high phase plaquette expectation value at the smallest value of κ where a meta-stability occurs.

Let us remark that the first order phase transition exists also in the continuum limit at zero quark mass where the scalar condensate has a jump as a consequence of spontaneous chiral symmetry breaking. This means, of course, that in the continuum limit the phase transition occurs only for $\mu = 0$.

We give our simulation parameters, the statistics of the Monte Carlo runs and the results for $am_{\rm PS}$, $af_\chi^{\rm PS}$, $am_\chi^{\rm PCAC}$ and r_0/a in Tables 4, 5 and 6.

The meta-stability phenomenon observed in $\langle P \rangle$ can also be seen in fermionic quantities. As an example, we show in Fig. 2 the values of the PCAC quark mass as obtained in the branches with high and low plaquette expectation values of Fig. 1 for the three values of β. Again we observe that with increasing β the gap between positive (low plaquette phase) and negative (high plaquette phase) quark masses shrinks. Also, the meta-stability region in $1/(2\kappa)$ gets much narrower with increasing β.

The effects of the first order phase transition can also be seen in the pion mass and the value of the force parameter r_0. We plot in Fig. 3 an example of the pion mass as a function of the PCAC quark mass at $\beta = 5.3$. The most intriguing observation here is that due to the presence of the first order phase transition, the pion mass, say for positive quark masses, does not go to zero but rather reaches a minimal value, and jumps then to the phase with negative quark mass. This is, of course, just another manifestation of the jump in the PCAC quark mass in Fig. 2.

In Fig. 4 we also show the values of r_0/a in the low and high plaquette phases at $\beta = 5.3$. Note that the values of r_0/a are quite different when determined in the low and the high plaquette phases, which is a generic feature also for other values of β and even for different gauge actions, see Ref. [12].

An interesting question is, at which value of the lattice spacing a the minimal pion mass $m_{\rm PS}^{\rm min}$ assumes a value of, say, 300 MeV where contact to chiral perturbation could be established.

The pion mass assumes two different values for a fixed quark mass, once this quark mass lies inside the meta-stability region. These two values for the pion masses correspond to the two phases that for a certain interval of quark masses co-exist. The precise determination of the meta-stability region is, of course, very difficult. We can, however, give an interval in κ, $[\kappa_1, \kappa_2]$, that can be read from Tables 4, 5 and 6 for the three different β values, where meta-stabilities occur in our simulation. In the following, we will mainly concentrate on the low plaquette phase since this is

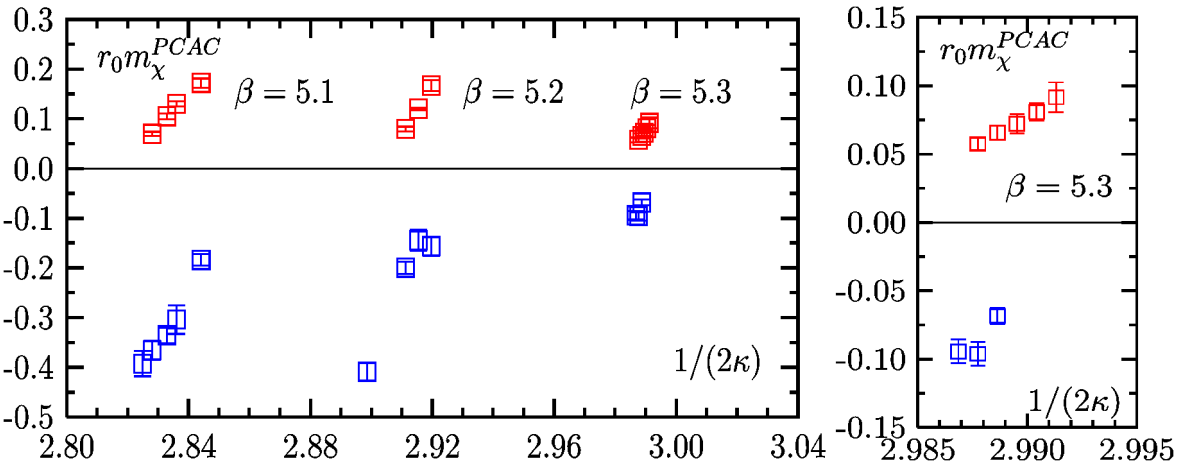

Fig. 2. In the graph on the left the PCAC quark mass is plotted as a function of $1/(2\kappa)$ at the three values of β we have simulated. Positive values correspond to the low plaquette phase while negative values correspond to the high plaquette phase. The statistical errors are on this scale for most of the points smaller than the symbols. In the right plot we give a closeup of the $\beta = 5.3$ results.

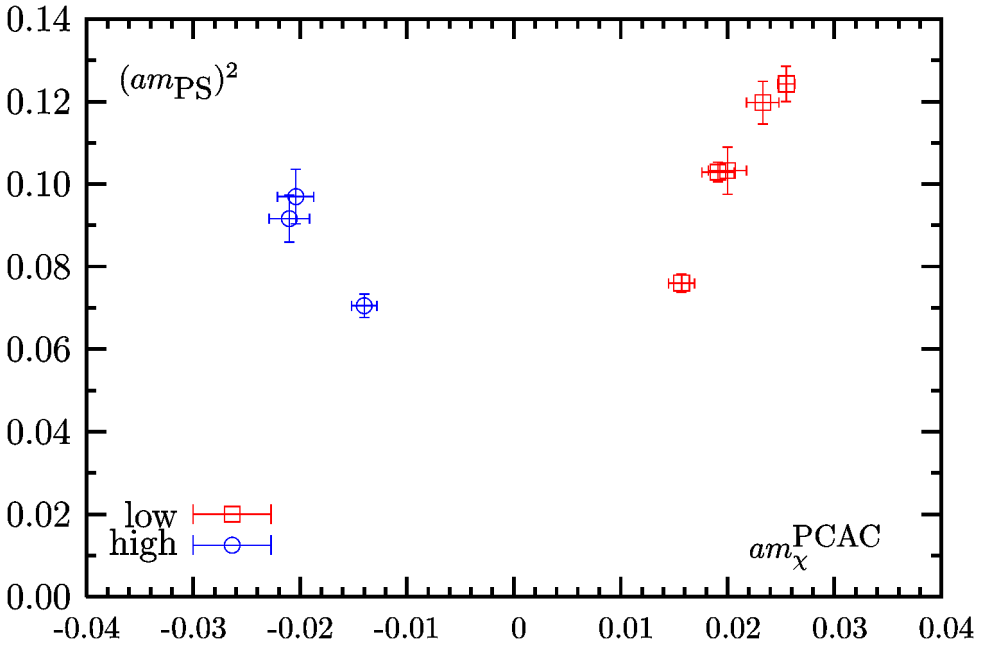

Fig. 3. The squared pion mass as a function of the PCAC quark mass at $\beta = 5.3$.

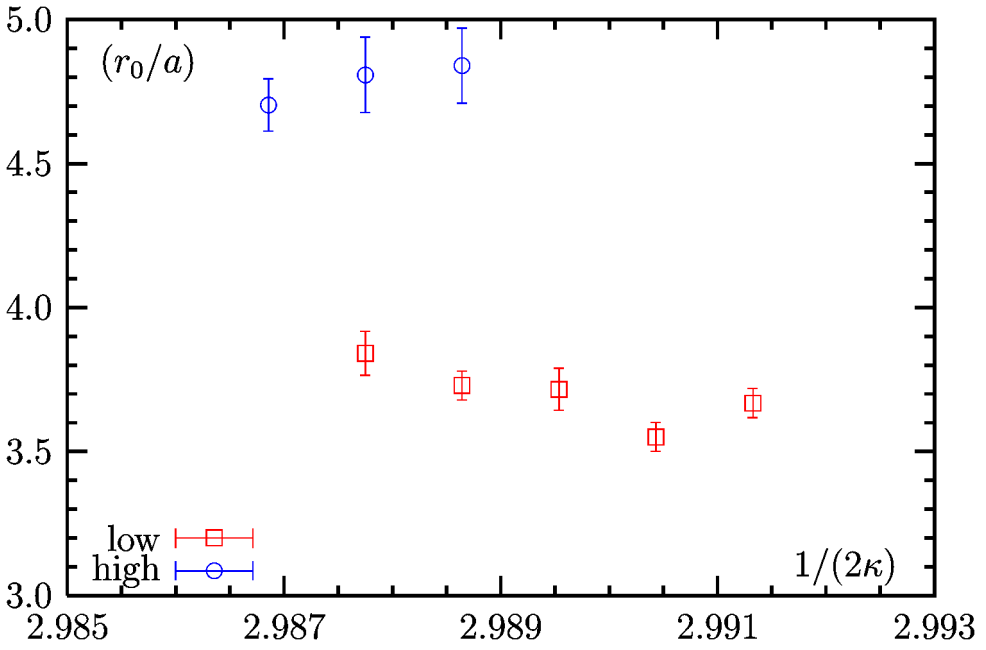

Fig. 4. r_0/a as a function of $1/(2\kappa)$ at $\beta = 5.3$.

the natural choice for studying lattice QCD. Being interested only in the low plaquette phase we determine then a lower bound for the minimal pion mass as computed at the lower end of this interval, i.e. κ_1, in the low plaquette phase. We give in Table 2 the values of the minimal pion masses in the low plaquette phase in

Table 2
Minimal pion mass $m_{\rm PS}^{\rm min}$ in physical units in the low plaquette phase and ΔP for the three β values. To set the scale we used $r_0 = 0.5$ fm and the value of r_0/a measured for the corresponding simulation point

β	$m_{\rm PS}^{\rm min}$ [MeV]	ΔP
5.1	$\gtrsim 600$	0.0399(1)
5.2	$\gtrsim 630$	0.0261(1)
5.3	$\gtrsim 470$	0.0077(4)

physical units. In addition, we provide the value for the gap in the plaquette expectation value ΔP.

In principle, it would be interesting to extrapolate the minimal pion mass and the gap in $\langle P \rangle$ as a function of the lattice spacing. However, our present data do not allow for a reliable and safe extrapolation. First of all, the determination of the minimal pion mass has a large ambiguity in itself since we do not know exactly for which value of the quark mass the meta-stability will disappear. A substantially larger statistics would be necessary to answer this question and to check whether tunneling from one phase to the other occurs. Second, the only three values of β we have used give a too short lever arm to perform a trustworthy extrapolation. And, third, the values of r_0/a are very different in the two phases, as can be seen in Fig. 4, which makes it particularly difficult to follow the gap in $\langle P \rangle$ as a function of a/r_0.

Nevertheless, an estimate on a more qualitative level yields a value of the lattice spacing of $a \sim 0.07$ fm–0.1 fm where simulations with pion masses of about 300 MeV can be performed without being affected by the first order phase transition.

4. Lattice spacing dependence of physical observables

Although the present simulations are not at full twist, the fact that we have results at three values of β with roughly constant $r_0\mu$ allows us to check for the size of lattice artifacts. In order to perform such an investigation it is advantageous to express physical quantities in dimensionless variables. To this end, let us first define a reference pion mass through $(r_0 m_{\rm PS})^2 = 1.5$. We have chosen this particular value in order to be able to interpolate for the values of $\beta = 5.1$ and $\beta = 5.3$, and to perform only a short extrapolation for $\beta = 5.2$ to this point.

Table 3
Reference values for $am_\chi^{\rm PCAC}$, $af_\chi^{\rm PS}$ and r_0/a. The reference point is chosen such that $(r_0 m_{\rm PS})^2 = 1.5$. The errors include the interpolation errors

β	$am_\chi^{\rm PCAC}\vert_{\rm ref}$	$af_\chi^{\rm PS}\vert_{\rm ref}$	$(r_0/a)\vert_{\rm ref}$
5.1	0.035(2)	0.195(06)	2.497(29)
5.2	0.025(4)	0.139(15)	3.124(85)
5.3	0.022(1)	0.122(07)	3.628(60)

At the aforementioned reference pion mass, a corresponding reference value of r_0/a and a reference quark mass can be determined, the latter leading to a variable σ,

$$\sigma = \frac{m_\chi^{\rm PCAC}}{m_\chi^{\rm PCAC}\vert_{\rm ref}}. \tag{8}$$

Similarly, we can define ratios for a quantity O,

$$R_O = \frac{O}{O\vert_{\rm ref}}, \tag{9}$$

where $O\vert_{\rm ref}$ is the quantity as determined at the reference pion mass. The values for several quantities at the reference point can be found in Table 3.

In order to determine the reference values for $m_\chi^{\rm PCAC}$, $f_\chi^{\rm PS}$ and r_0, in a first step we interpolated $m_\chi^{\rm PCAC}$ linearly as a function of $(r_0 m_{\rm PS})^2$ to the point where $(r_0 m_{\rm PS})^2 = 1.5$ and extracted the reference value for $m_\chi^{\rm PCAC}$. Then we determined the reference values for $f_\chi^{\rm PS}$ and r_0 by quadratically interpolating the data as a function of $m_\chi^{\rm PCAC}$ to the reference value of $m_\chi^{\rm PCAC}$. We repeated the latter step with a linear interpolation finding agreement within the errors. The fits to the data have been performed with the ROOT and MINUIT packages from CERN (cf. [21,22]), taking the errors on both axis into account. We remark that for the quantity $r_0 m_{\rm PS}$ we have neglected the correlation of the data between r_0/a and $am_{\rm PS}$.

For a given observable O, R_O is a universal function of σ for fixed value of μ in physical units that allows for a direct comparison of results obtained at different values of β and, in principle, even for different actions. Deviations of results at different β values provide then a direct measure of scaling violations. In Fig. 5 we show $R_{m_{\rm PS}^2}$ as a function of σ. Note that for

Table 4
Parameters and physical observables for the simulations with $\beta = 5.1$. The lattice size in these runs was set to $12^3 \times 24$ and the twisted mass parameter to $a\mu = 0.013$. We give the values for κ and the number of measurements $N_{\rm meas}$ performed. We indicate with "L" or "H" whether the plaquette expectation assumes a low or a high value. Moreover, we give the values for $m_{\rm PS}$, $f_\chi^{\rm PS}$, $m_\chi^{\rm PCAC}$ and r_0 in lattice units. For r_0 we give in addition to the statistical error two systematic errors, the first of them coming from possible excited state contaminations and the second from the necessary interpolation of the force in r

κ		$N_{\rm meas}$	$am_{\rm PS}$	$af_\chi^{\rm PS}$	$am_\chi^{\rm PCAC}$	r_0/a
0.1758	L	160	0.7015(031)	+0.2856(60)	+0.0799(12)	2.178(8)(4)(20)
0.1763	L	160	0.6155(040)	+0.2538(56)	+0.0597(12)	2.258(8)(0)(8)
0.1765	L	160	0.5353(068)	+0.2201(76)	+0.0446(16)	2.370(12)(4)(26)
0.1768	L	160	0.4468(051)	+0.1683(82)	+0.0268(13)	2.625(19)(22)(1)
0.1758	H	160	0.5323(126)	−0.2065(119)	−0.0496(25)	3.926(26)(12)(10)
0.1763	H	160	0.6771(116)	−0.2351(227)	−0.0777(50)	4.087(56)(4)(0)
0.1765	H	160	0.7231(111)	−0.2595(232)	−0.0864(26)	4.053(18)(17)(3)
0.1768	H	160	0.7377(119)	−0.2302(136)	−0.0926(38)	4.139(35)(16)(2)
0.1770	H	160	0.7530(189)	−0.2212(189)	−0.0977(59)	4.045(28)(10)(4)

Table 5
Parameter and physical observables for the simulations with $\beta = 5.2$. The lattice size in these runs was set to $12^3 \times 24$ and the twisted mass parameter to $a\mu = 0.01$. See Table 4 for further explanations

κ		$N_{\rm meas}$	$am_{\rm PS}$	$af_\chi^{\rm PS}$	$am_\chi^{\rm PCAC}$	r_0/a
0.17125	L	320	0.6057(025)	+0.2289(35)	+0.0650(08)	2.618(20)(5)(49)
0.17150	L	459	0.5066(050)	+0.1968(38)	+0.0452(08)	2.800(17)(9)(4)
0.17175	L	320	0.4189(071)	+0.1540(84)	+0.0292(17)	3.038(28)(14)(4)
0.17125	H	320	0.4173(111)	−0.1571(166)	−0.0352(43)	4.796(63)(65)(15)
0.17150	H	318	0.4220(126)	−0.1566(219)	−0.0349(50)	4.282(61)(16)(0)
0.17175	H	320	0.4985(088)	−0.1770(119)	−0.0494(28)	4.418(23)(23)(0)
0.17250	H	320	0.6462(131)	−0.1974(087)	−0.0874(24)	4.767(51)(7)(3)

Table 6
Parameter and physical observables for the simulations with $\beta = 5.3$. The lattice size in these runs was set to $16^3 \times 32$ and the twisted mass parameter to $a\mu = 0.008$. For further explanations see Table 4

κ		$N_{\rm meas}$	$am_{\rm PS}$	$af_\chi^{\rm PS}$	$am_\chi^{\rm PCAC}$	r_0/a
0.16715	L	100	0.3525(061)	+0.1349(111)	+0.0255(18)	3.668(34)(9)(8)
0.16720	L	101	0.3460(075)	+0.1259(063)	+0.0233(15)	3.551(47)(2)(1)
0.16725	L	180	0.3213(088)	+0.1211(078)	+0.0200(18)	3.716(49)(24)(0)
0.16730	L	243	0.3208(037)	+0.1160(063)	+0.0191(15)	3.730(35)(6)(9)
0.16735	L	160	0.2757(040)	+0.0887(084)	+0.0157(12)	3.841(47)(28)(1)
0.16730	H	388	0.2656(054)	−0.1037(093)	−0.0140(12)	4.84(10)(2)(1)
0.16735	H	100	0.3114(106)	−0.1291(128)	−0.0204(17)	4.808(95)(33)(3)
0.16740	H	100	0.3027(094)	−0.1237(137)	−0.0210(19)	4.703(90)(0)(1)

the scaling analysis we take the data in the low plaquette phase only since this corresponds to the standard lattice QCD situation. We also remark that some of the points taken in this analysis might be meta-stable. Nevertheless, we assume here that these data can serve for checking scaling violations. Besides the data from the present work, we added also results from simulations at $\beta = 5.6$ [23], which were obtained, however, at vanishing twisted mass parameter $\mu = 0$.

A rather amazing consequence of Fig. 5 is that, despite the fact that we are using coarse lattices, we cannot detect any scaling violation, at least within the (large) statistical errors of our data. Even more, the results of our present simulations at small values of

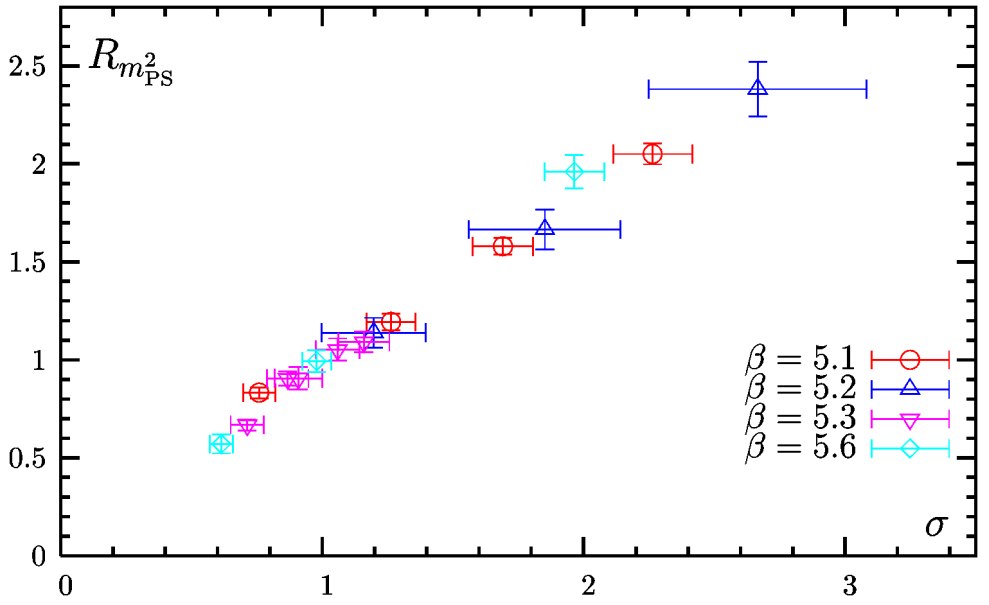

Fig. 5. The dependence of the pion mass on the quark mass, i.e. $R_{m_{\rm PS}^2}$ as a function of σ. Besides the data of this work, we added in the plot also results from Wilson fermion simulations at $\beta = 5.6$ [23] which were obtained at $\mu = 0$.

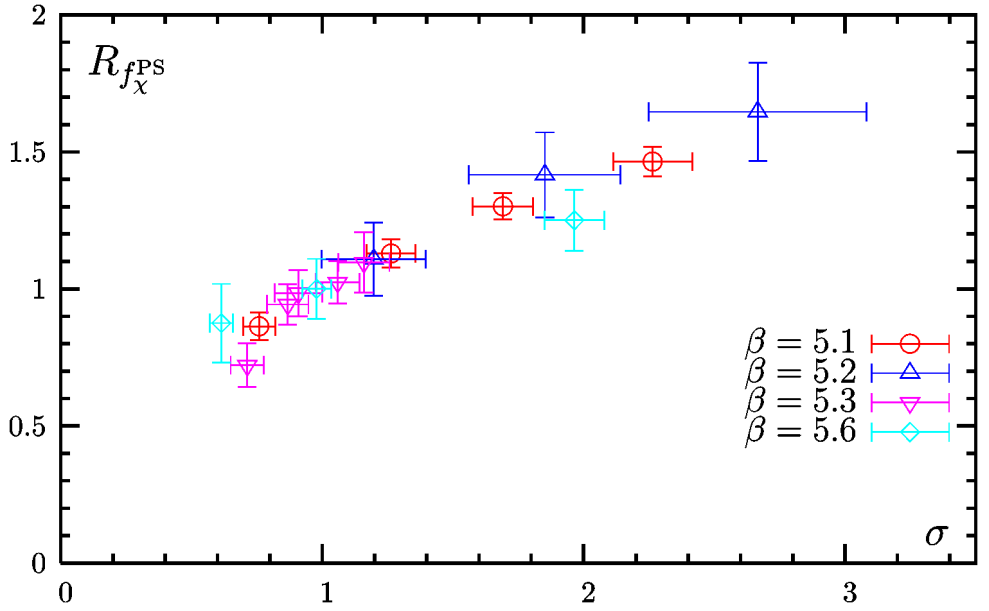

Fig. 6. The ratio $R_{f_\chi^{\rm PS}}$ for the pseudo scalar decay constant as a function of σ. We also added results from Wilson fermion simulations for $R_{f_{\rm PS}}$ at $\beta = 5.6$ [23] obtained with $\mu = 0$.

β agree with results from simulations with pure Wilson fermions at $\beta = 5.6$ setting $\mu = 0$. The same observation is made for $R_{f_\chi^{\rm PS}}$, see Fig. 6 and the ratio $m_{\rm PS}/m_{\rm V}$, see Fig. 7. These results indicate that the lattice artifacts and the effect of a non-vanishing twisted mass parameter μ are surprisingly small. We

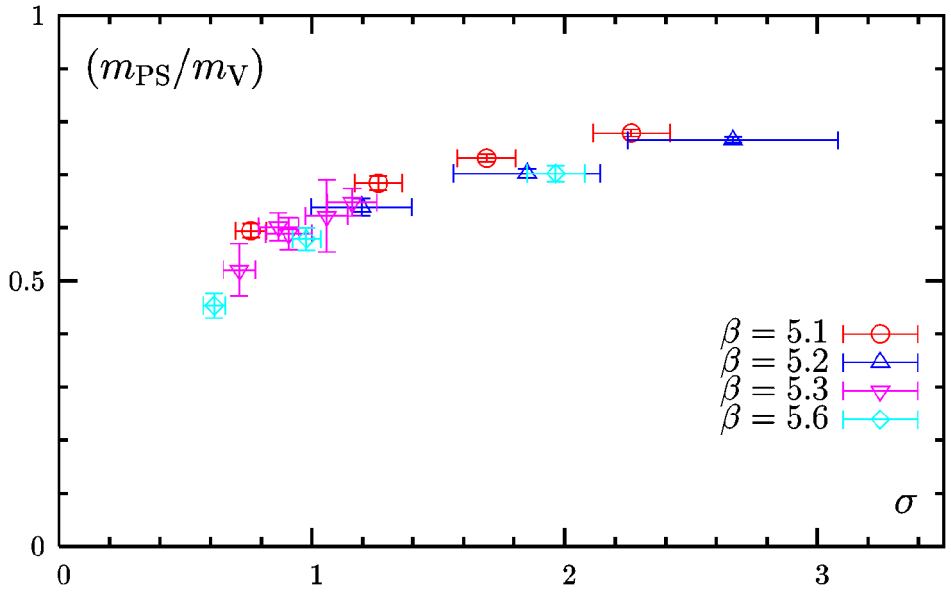

Fig. 7. The ratio $m_{\rm PS}/m_{\rm V}$ as a function of σ. Again, we also added results from Wilson fermion simulations at $\beta = 5.6$ [23].

remark here that in the case of the ratios like $R_{m_{\rm PS}^2}$ and $R_{f_\chi^{\rm PS}}$ one could have cancellation of mass independent cutoff effects. One has also to have in mind that, due to the presence of the first order phase transition, the simulated pion masses are still larger than 500 MeV. Whether our findings also hold when one is approaching the chiral limit is certainly an interesting but open question. However, in a set-up with Wilson twisted mass fermions and Wilson plaquette gauge action this question cannot be answered at these values of the lattice spacing.

5. Conclusions

In this Letter we have investigated dynamical Wilson twisted mass fermions employing the Wilson plaquette gauge action. We have performed simulations at three values of $\beta = 5.1, 5.2, 5.3$, corresponding to values of the lattice spacing of $a \approx 0.20, 0.16, 0.14$ fm, respectively. The non-zero values of the twisted mass parameter μ were chosen such that $r_0\mu \approx 0.03$ for all of the three β values. At these rather coarse lattice spacings we find clear signals of first order phase transitions that manifest themselves in a meta-stable behavior of the plaquette expectation value and fermionic quantities, such as the PCAC quark mass and the pion mass.

We clearly observe that the gaps in quantities sensitive to the phase transition, such as the plaquette expectation value and the PCAC quark mass decrease substantially when β is increased. Unfortunately, with our present set of simulations, we are not able to quantitatively locate the value of the lattice spacing, where the effects of the first order phase transition becomes negligible and where a minimal pion mass of, say, 300 MeV can be reached. As an estimate of such a value of the lattice spacing we give a range of $a \approx 0.07$ fm–0.1 fm. Of course, this would mean that a continuum extrapolation of physical results obtained on lattices with linear extent of at least $L = 2$ fm would be very demanding, since the starting point for such simulations would already require large lattices. It is therefore very important to find alternative actions such that the value of the lattice spacing can be lowered without running into problems with the first order phase transition. One candidate for such an action, the DBW2 gauge action, is discussed in Ref. [12] where it has indeed been found that modifying the gauge action alone can substantially reduce the strength of the first order phase transition. We are presently investigating another possibility, the tree-level Symanzik improved gauge action [24,25].

Despite the problems arising from the presence of a first order phase transition, we performed a scaling analysis for the pion mass, the pion decay constant and the ratio $m_{\rm PS}/m_{\rm V}$ for the data obtained at the three values of β where we performed simulations. To this end, we only analyzed data from the low plaquette phase, since this is the natural choice for QCD simulations.

By defining a reference pion mass at $(r_0 m_{\rm PS})^2 = 1.5$, we computed the ratio of $m_{\rm PS}$ and $f_\chi^{\rm PS}$ to the corresponding reference values as a function of the PCAC quark mass, again measured with respect to the corresponding reference quark mass. We find that for these ratios the scaling violations are remarkably small and cannot be detected with the present precision of our data. Even more, when adding data from simulations of Wilson fermions with $\mu = 0$ at $\beta = 5.6$, then these data fall on the same scaling curve as our results on much coarser lattices and with twisted mass parameter switched on. This indicates that not only the lattice artifacts but also the effect of switching on a twisted mass of the order of $r_0\mu \approx 0.03$ are small, at least for the rather large pion masses simulated here. This finding is surprising since it suggests that continuum values of physical quantities can be already estimated from simulations at not too small lattice spacings. Of course, our scaling results suffer from the fact that they are obtained using data that might be meta-stable as a consequence of the presence of the first order phase transition. Hence, a scaling test with an action that does not lead to significant effects of the first order phase transition is mandatory to check the results presented in this Letter.

Acknowledgements

We thank R. Frezzotti, G. Münster, G.C. Rossi and S. Sharpe for many useful discussions. The computer centers at NIC/DESY Zeuthen, NIC at Forschungszentrum Jülich and HLRN provided the necessary technical help and computer resources. We are indebted to R. Hoffmann and J. Rolf for leaving us a MatLab program to check our fits. This work was supported by the DFG Sonderforschungsbereich/Transregio SFB/TR9-03.

References

[1] F. Farchioni, et al., Eur. Phys. J. C 39 (2005) 421, hep-lat/0406039.
[2] F. Farchioni, et al., Nucl. Phys. B (Proc. Suppl.) 140 (2005) 240, hep-lat/0409098.
[3] S.R. Sharpe, R. Singleton Jr., Phys. Rev. D 58 (1998) 074501, hep-lat/9804028.
[4] G. Münster, JHEP 0409 (2004) 035, hep-lat/0407006.
[5] L. Scorzato, Eur. Phys. J. C 37 (2004) 445, hep-lat/0407023.
[6] S.R. Sharpe, J.M.S. Wu, Phys. Rev. D 71 (2005) 074501, hep-lat/0411021.
[7] S.R. Sharpe, J.M.S. Wu, Phys. Rev. D 70 (2004) 094029, hep-lat/0407025.
[8] S. Aoki, O. Bär, Phys. Rev. D 70 (2004) 116011, hep-lat/0409006.
[9] S. Aoki, Phys. Rev. D 30 (1984) 2653.
[10] E.-M. Ilgenfritz, W. Kerler, M. Müller-Preussker, A. Sternbeck, H. Stüben, Phys. Rev. D 69 (2004) 074511, hep-lat/0309057.
[11] A. Sternbeck, E.-M. Ilgenfritz, W. Kerler, M. Müller-Preussker, H. Stüben, Nucl. Phys. B (Proc. Suppl.) 129 (2004) 898, hep-lat/0309059.
[12] F. Farchioni, et al., Eur. Phys. J. C 42 (2005) 73, hep-lat/0410031.
[13] χLF Collaboration, K. Jansen, A. Shindler, C. Urbach, I. Wetzorke, Phys. Lett. B 586 (2004) 432, hep-lat/0312013.
[14] A.M. Abdel-Rehim, R. Lewis, R.M. Woloshyn, Phys. Rev. D 71 (2005) 094505, hep-lat/0503007.
[15] χLF Collaboration, K. Jansen, M. Papinutto, A. Shindler, C. Urbach, I. Wetzorke, Phys. Lett. B 619 (2005) 184, hep-lat/0503031.
[16] ALPHA Collaboration, R. Frezzotti, P.A. Grassi, S. Sint, P. Weisz, JHEP 0108 (2001) 058, hep-lat/0101001.
[17] R. Frezzotti, G.C. Rossi, JHEP 0408 (2004) 007, hep-lat/0306014.
[18] UKQCD Collaboration, R.M. Baxter, et al., Phys. Rev. D 49 (1994) 1594, hep-lat/9308020.
[19] F. Farchioni, C. Gebert, I. Montvay, L. Scorzato, Eur. Phys. J. C 26 (2002) 237, hep-lat/0206008.
[20] R. Sommer, Nucl. Phys. B 411 (1994) 839, hep-lat/9310022.
[21] The ROOT system home page, http://root.cern.ch/.
[22] MINUIT home page, http://seal.web.cern.ch/seal/snapshot/work-packages/mathlibs/minuit/home.html.
[23] C. Urbach, K. Jansen, A. Shindler, U. Wenger, hep-lat/0506011.
[24] P. Weisz, Nucl. Phys. B 212 (1983) 1.
[25] P. Weisz, R. Wohlert, Nucl. Phys. B 236 (1984) 397.

[dbW-1]

The phase structure of lattice QCD with Wilson quarks and renormalization group improved gluons

Eur. Phys. J. C42 73-87 (2005)

Eur. Phys. J. C 42, 73–87 (2005)
Digital Object Identifier (DOI) 10.1140/epjc/s2005-02262-5

THE EUROPEAN PHYSICAL JOURNAL C

The phase structure of lattice QCD with two flavors of Wilson quarks and renormalization group improved gluons

F. Farchioni[1], K. Jansen[2], I. Montvay[3,a], E. Scholz[3], L. Scorzato[4], A. Shindler[2], N. Ukita[3], C. Urbach[2,5], I. Wetzorke[2]

[1] Universität Münster, Institut für Theoretische Physik, Wilhelm- Klemm-Strasse 9, 48149 Münster, Germany
[2] NIC/DESY Zeuthen, Platanenallee 6, 15738 Zeuthen, Germany
[3] Deutsches Elektronen-Synchrotron DESY, Notkestr. 85, 22603 Hamburg, Germany
[4] Institut für Physik, Humboldt Universität zu Berlin, 12489 Berlin, Germany
[5] Freie Universität Berlin, Institut für Theoretische Physik, Arnimallee 14, 14196 Berlin, Germany

Received: 29 October 2004 / Revised version: 7 March 2005 /
Published online: 31 May 2005 –

Abstract. The effect of changing the lattice action for the gluon field on the recently observed [F. Farchioni, R. Frezzotti, K. Jansen, I. Montvay, G.C. Rossi, E. Scholz, A. Shindler, N. Ukita, C. Urbach, I. Wetzorke, Eur. Phys. J. C **39**, 421 (2005); hep-lat/0406039] first order phase transition near zero quark mass is investigated by replacing the Wilson plaquette action by the DBW2 action. The lattice action for quarks is unchanged: it is in both cases the original Wilson action. It turns out that Wilson fermions with the DBW2 gauge action have a phase structure where the minimal pion mass and the jump of the average plaquette are decreased, when compared to Wilson fermions with Wilson plaquette action at similar values of the lattice spacing. Taking the DBW2 gauge action is advantageous also from the point of view of the computational costs of numerical simulations.

1 Introduction

A basic feature of the low-energy dynamics in quantum chromodynamics (QCD) is the spontaneous chiral symmetry breaking implying the existence of light pseudo-Goldstone (pseudoscalar) bosons. The associated phase structure near zero quark masses has to be reproduced in the continuum limit by the lattice-regularized formulations but it is in general modified by lattice artifacts at non-vanishing lattice spacing. In lattice theories based on Wilson-type quark actions the possible phase structures have been investigated up to $\mathcal{O}(a^2)$ in the lattice spacing a by Sharpe and Singleton [2] in the framework of low-energy chiral Lagrangians [3,4] and using the effective continuum description of cut-off effects [5,6]. Their results allow for two possible "scenarios": the existence of the Aoki phase [7] or, alternatively, a first order phase transition near zero quark mass.

In a recent numerical simulation [1,8] the phase structure of lattice QCD with Wilson fermions and Wilson gauge action has been investigated with the help of the twisted mass Wilson fermion formulation [9,10]. For fixed values of a, smaller than $a \approx 0.2\,\mathrm{fm}$, evidence for a first order phase transition line, near zero quark mass in the plane of untwisted and twisted quark mass, has been found corresponding to the "second scenario" of [2]. It is important to remark that this line is finite and ends at a particular value of the twisted quark mass μ_c. This implies metastability and a non-zero minimum of the absolute value of quark- (and pion-) masses. These are lattice artifacts which are expected to vanish in the continuum limit where $\mu_c = 0$ and the first order phase transition line shrinks to a singular point. (For generalizations of the results of [2] for non-zero twisted mass see [11–13].) Considering, besides the bare quark masses, the bare gauge coupling, too, near the continuum limit the first order phase transition spans a surface, as it is schematically shown by Fig. 1.

It might be speculated that at the microscopic level the occurrence of the first order phase transition at $a > 0$ is accompanied by a massive rearrangement of small eigenvalues of the Wilson–Dirac operator. The detailed properties and, in particular, the strength of the first order phase transition does probably depend on the number and distribution of these eigenvalues. It is known that some type of small eigenvalues, especially real ones, are associated with small topological dislocations of the gauge field. A high probability of these dislocations and of the corresponding small eigenvalues is presumably a cut-off effect which can be diminished by an appropriate choice of the lattice action. In fact, it is known [14–17] that the small topological dislocations can, indeed, be suppressed by taking renormalization group improved (RGI) gauge actions as the Iwasaki action [18] or the DBW2 action [19].

[a] e-mail: montvay@mail.desy.de

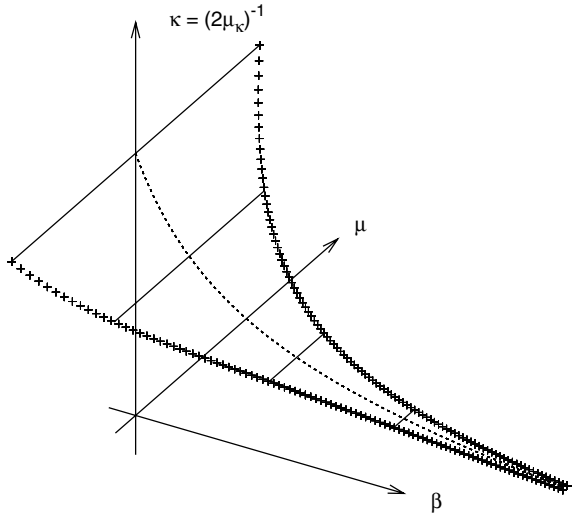

Fig. 1. The schematic view of the first order phase transition surface in the (β, κ, μ) space close to the continuum limit. (β is the bare gauge coupling, κ is the hopping parameter, μ is the bare twisted quark mass, $\mu_\kappa \equiv (2\kappa)^{-1}$ is the bare untwisted quark mass.) The crosses mark the second order boundary line of the first order phase transition surface. The strong coupling region near $\beta = 0$ is not shown in this figure

In the present paper we try to answer the question whether the combination of RGI gauge actions with the Wilson fermion action does shrink the first order phase transition line near zero quark mass. Here we restrict ourselves to the study of the DBW2 gauge action which has been successfully applied also in dynamical domain wall fermion simulations [20]. The goal of the present paper is to qualitatively show how a change of the gauge action will modify the phase structure. Hence, we do not aim here at a high precision study.

The Iwasaki action is often used in dynamical quark simulations by the CP-PACS and JLQCD Collaborations, in particular, in combination with the Sheikholeslami–Wohlert clover improved Wilson fermion action [6]. Earlier results of the JLQCD Collaborations indicate [21] that, indeed, a metastability seen in the average plaquette can be suppressed by replacing the Wilson plaquette action by the Iwasaki action. (See also [22], and for a review of earlier results on the phase structure of QCD, see [23]. An early discussion of the phase structure of QCD can also be found in [24].)

The plan of this paper is as follows: in the next section the lattice action and some parameters of the update algorithm are defined. In Sect. 3 we present the results of the numerical simulations. Section 4 is devoted to the investigation of the eigenvalue spectrum of the Wilson–Dirac operator near the origin. The last section contains some discussion and concluding remarks.

2 Lattice action and simulation algorithm

2.1 Lattice action

We apply for quarks the lattice action of Wilson fermions, which can be written as

$$S_q = \sum_x \left\{ \left(\overline{\chi}_x [\mu_\kappa + \mathrm{i}\gamma_5 \tau_3 \mu] \chi_x \right) - \frac{1}{2} \sum_{\mu=\pm 1}^{\pm 4} \left(\overline{\chi}_{x+\hat{\mu}} U_{x\mu} [r + \gamma_\mu] \chi_x \right) \right\} . \quad (1)$$

Here the ("untwisted") bare quark mass in lattice units is denoted by

$$\mu_\kappa \equiv a m_0 + 4r = \frac{1}{2\kappa} , \quad (2)$$

r is the Wilson parameter, set in our simulations to $r = 1$, am_0 is another convention for the bare quark mass in lattice units and κ is the conventional hopping parameter. In (1) the twisted mass μ is also introduced. $U_{x\mu} \in \mathrm{SU}(3)$ is the gauge link variable and we also defined $U_{x,-\mu} = U^\dagger_{x-\hat{\mu},\mu}$ and $\gamma_{-\mu} = -\gamma_\mu$.

For the SU(3) Yang–Mills gauge field we apply the DBW2 lattice action [19] which belongs to a one-parameter family of actions obtained by renormalization group considerations. These actions also include, besides the usual (1×1) Wilson loop plaquette term, planar rectangular (1×2) Wilson loops:

$$S_g = \beta \sum_x \left(c_0 \sum_{\mu<\nu;\, \mu,\nu=1}^{4} \left\{ 1 - \frac{1}{3} \mathrm{Re}\, U^{1\times 1}_{x\mu\nu} \right\} + c_1 \sum_{\mu\neq\nu;\, \mu,\nu=1}^{4} \left\{ 1 - \frac{1}{3} \mathrm{Re}\, U^{1\times 2}_{x\mu\nu} \right\} \right) , \quad (3)$$

with the normalization condition $c_0 = 1 - 8c_1$. (The notation $c_{0,1}$ is conventional. Of course, c_1 should not be confused with the parameter c_1 in the effective potential of [2,1].) The coefficient c_1 in (3) takes different values for various choices of RGI actions, for instance,

$$c_1 = \begin{cases} -0.331 & \text{Iwasaki action,} \\ -1.4088 & \text{DBW2 action.} \end{cases} \quad (4)$$

Clearly, $c_1 = 0$ corresponds to the original Wilson gauge action with the plaquette term only. Note that for $c_1 = -1/12$ one obtains the tree-level improved action in the Symanzik improvement scheme [25].

2.2 Twist angle

An important quantity is the twist angle ω, the polar angle in the plane of the untwisted and twisted mass (μ_κ, μ). We present here a method which allows one to determine the twist angle only on the basis of symmetry of the correlators defined in a given point of bare parameter space (see also [8]).

Following [10], we introduce the twist angle ω as the chiral rotation angle between the renormalized (physical) vector and axialvector currents $\hat{V}^a_{x\mu}$, $\hat{A}^a_{x\mu}$ and the bare bilinears of the χ-fields $V^a_{x\mu}$, $A^a_{x\mu}$:

$$V^a_{x\mu} \equiv \overline{\chi}_x \frac{1}{2}\tau_a\gamma_\mu\chi_x \ , \qquad A^a_{x\mu} \equiv \overline{\chi}_x \frac{1}{2}\tau_a\gamma_\mu\gamma_5\chi_x \ . \tag{5}$$

With the renormalization constants Z_V and Z_A we have

$$\hat{V}^a_{x\mu} = Z_V V^a_{x\mu} \cos\omega + \epsilon_{ab}\, Z_A A^b_{x\mu} \sin\omega \ , \tag{6}$$

$$\hat{A}^a_{x\mu} = Z_A A^a_{x\mu} \cos\omega + \epsilon_{ab}\, Z_V V^b_{x\mu} \sin\omega \, , \tag{7}$$

where only charged currents are considered ($a = 1, 2$).

The twist angle ω is related to the ratio of the renormalized twisted and untwisted masses entering the chiral Ward identities [10]. (In [10] this definition of the twist angle was called α.) We define, in addition, the two auxiliary angles

$$\begin{aligned} \omega_V &= \arctan(Z_A Z_V^{-1} \tan\omega) \ , \\ \omega_A &= \arctan(Z_V Z_A^{-1} \tan\omega) \ . \end{aligned} \tag{8}$$

In terms of ω_V, ω_A (6) and (7) are written as

$$\hat{V}^a_{x\mu} = \mathcal{N}_V \left(\cos\omega_V V^a_{x\mu} + \epsilon_{ab} \sin\omega_V A^b_{x\mu}\right) , \tag{9}$$

$$\hat{A}^a_{x\mu} = \mathcal{N}_A \left(\cos\omega_A A^a_{x\mu} + \epsilon_{ab} \sin\omega_A V^b_{x\mu}\right) \tag{10}$$

where the overall multiplicative renormalization is ($X = V, A$):

$$\mathcal{N}_X = \frac{Z_X}{\cos\omega_X \sqrt{1 + \tan\omega_V \tan\omega_A}} \ . \tag{11}$$

From (8) it follows that

$$\omega = \arctan\left(\sqrt{\tan\omega_V \tan\omega_A}\right) \ . \tag{12}$$

As shown by the relations in (8) and (12), the values of ω, ω_V and ω_A coincide for $|\omega| = 0, \pi/2$. However, for other angles they are, in general, different and the difference goes to zero in the continuum limit only as fast as $Z_V/Z_A \to 1$.

A possibility to determine ω_V and ω_A is to impose the vector and axialvector Ward identities, respectively, with a suitable insertion operator $\hat{O}_x$. For instance, in the vector case one can use the Ward identity

$$\sum_{\boldsymbol{x},\boldsymbol{y}} \langle \partial^*_\mu \hat{V}^+_{x\mu}\, \hat{O}^-_y \rangle = 0 \implies \tan\omega_V = \frac{-\mathrm{i}\sum_{\boldsymbol{x},\boldsymbol{y}} \langle \partial^*_0 V^+_{x0}\, \hat{O}^-_y \rangle}{\sum_{\boldsymbol{x},\boldsymbol{y}} \langle \partial^*_0 A^+_{x0}\, \hat{O}^-_y \rangle} \ . \tag{13}$$

Here the indices + and − refer to the charged components $\tau_\pm \equiv \tau_1 \pm \mathrm{i}\tau_2$ and ∂^*_μ denotes the backward lattice derivative.

Another possibility for determining the twist angles ω_V, ω_A and ω is to impose parity conservation for suitable matrix elements, for instance with the pseudoscalar density $P^\pm_x = \bar{\chi}_x \frac{\tau^\pm}{2}\gamma_5\chi_x$:

$$\sum_{\boldsymbol{x},\boldsymbol{y}} \langle \hat{A}^+_{x0}\, \hat{V}^-_{y0} \rangle \ = \ \sum_{\boldsymbol{x},\boldsymbol{y}} \langle \hat{V}^+_{x0}\, P^-_y \rangle \ = \ 0 \ . \tag{14}$$

These equations admit the solution

$$\tan\omega_V = \frac{-\mathrm{i}\sum_{\boldsymbol{x},\boldsymbol{y}} \langle V^+_{x0}\, P^-_y \rangle}{\sum_{\boldsymbol{x},\boldsymbol{y}} \langle A^+_{x0}\, P^-_y \rangle} \ , \tag{15}$$

$$\tan\omega_A = \frac{\mathrm{i}\sum_{\boldsymbol{x},\boldsymbol{y}} \langle A^+_{x0}\, V^-_{y0} \rangle + \tan\omega_V \sum_{\boldsymbol{x},\boldsymbol{y}} \langle A^+_{x0}\, A^-_{y0} \rangle}{\sum_{\boldsymbol{x},\boldsymbol{y}} \langle V^+_{x0}\, V^-_{y0} \rangle - \mathrm{i}\tan\omega_V \sum_{\boldsymbol{x},\boldsymbol{y}} \langle V^+_{x0}\, A^-_{y0} \rangle} \ . \tag{16}$$

In (14) one can also take the derivatives of the currents instead of the currents themselves. For instance, taking the divergence of the vector current in the second equality gives the same equations as (13) with $\hat{O} = P$.

Once ω_V and ω_A are determined, the twist angle ω can be obtained by (12). This method for determining the twist angle can also be used in case of simulations with partially quenched twisted mass quarks. The estimate of ω is, of course, affected by $\mathcal{O}(a)$ ambiguities. For non-zero twisted mass $\mu \neq 0$ the critical bare untwisted quark mass $\mu_\kappa = \mu_{\kappa_{\rm cr}}$, or the critical hopping parameter $\kappa_{\rm cr} = (2\mu_{\kappa_{\rm cr}})^{-1}$, is signaled by $|\omega| = \pi/2$.

2.3 Updating algorithm

Concerning updating in our numerical simulations, we apply the two-step multi-boson (TSMB) algorithm [26], which has been tuned to QCD simulations with Wilson quarks in previous works [1, 27–30]. (For details and references see in these papers.) In [27] there is an approximate formula for the computational cost of an update cycle in terms of matrix-vector-multiplications (MVMs):

$$\frac{N_{\rm MVM}}{\rm cycle} \ \simeq \ 6(n_{\rm B} n_1 N_\Phi + N_U) + 2 n_{\rm B}(n_2 + n_3) N_{\rm C} + I_{\rm G} F_{\rm G} \ . \tag{17}$$

Here $n_{1,2,3}$ are the orders of polynomials used in the two approximation steps, $n_{\rm B}$ gives the multiplicity in determinant breakup, N_Φ is the number of local bosonic sweeps per update cycle, N_U the number of local gauge sweeps, $N_{\rm C}$ the number of global Metropolis accept–reject correction steps, and $I_{\rm G}$ and $F_{\rm G}$ give the number of MVMs in the global boson heatbath and its frequency, respectively.

The number of MVMs can also be converted into the number of floating point operations by noting that in our code, for vanishing twisted mass, we have

$$1 \text{ MVM} \ \simeq \ 1.2 \cdot 10^3 \, \Omega \, \text{flop} \ , \tag{18}$$

where Ω is the number of lattice points. For non-zero twisted mass there is an additional factor 2 due to the flavor index. (This does, however, not mean that twisted mass fermions are a factor of two more expensive since in this case the two flavors are incorporated in one fermion matrix and the polynomial approximations have lower orders; see Appendix A.2 of [1].)

Measuring the integrated autocorrelations $\tau_{\rm int}$ as a function of the quark mass in lattice units am_q and of the lattice volume Ω, previous experience tells that one

can approximate the computational cost of a number of update cycles equal to $\tau_{\rm int}$ by the simple formula

$$C_{\tau_{\rm int}} \simeq F\,(am_q)^{-z}\,\Omega\ . \tag{19}$$

According to [27], in case of combining the Wilson fermion action with the Wilson plaquette gauge action, the power of the inverse quark mass is close to $z = 2$. The overall factor F depends on the quantity under investigation. For Wilson quarks with Wilson gauge action the previous results can be summarized, for instance, for the average plaquette and for the pion mass determined with a randomly chosen source by [30]

$$F_{\rm plaq} \simeq 7 \cdot 10^6\,{\rm flop}\ , \qquad F_{m_\pi} \simeq 10^6\,{\rm flop}\ . \tag{20}$$

Let us note that the approximate formula in (19) has been, up to now, verified only for some fixed values of the gauge coupling β. The β-dependence of F has not yet been systematically investigated.

3 Numerical simulation results

Our aim is to compare the phase structure of two-flavor ($N_f = 2$) QCD near zero quark mass for Wilson lattice fermion action and DBW2 gauge action with the one observed in [1,8] for Wilson fermion action and Wilson (plaquette) gauge action. Since the phase structure obviously depends on the lattice spacing, we have to find the values of the bare parameters (β, μ_κ) in the lattice action (1)–(3) which correspond to quark mass $m_q \simeq 0$ and to the same lattice spacing as in [1,8], namely $a \simeq 0.2\,{\rm fm}$. For having a fair comparison, the lattice volume has to be kept constant, too, because the metastability phenomenon does also depend on it. Therefore, we shall compare the results on $12^3 \times 24$ lattices.

A possibility for facilitating the parameter tuning is to explore the position of the high-temperature phase transition on lattices with time extension $N_t = 4$ and $N_t = 6$ for small quark masses, which mark $a = 0.25$–$0.30\,{\rm fm}$ and $a = 0.17$–$0.20\,{\rm fm}$, respectively. (This method with $N_t = 4$ has been applied, for instance, in [27].) A useful first orientation is also provided by the quenched studies. (For a useful collection of data on RGI gauge actions see [31] and references therein). For specifying the actual value of the lattice spacing we determine the Sommer scale parameter in lattice units r_0/a [32], which we set by definition to be $r_0 \equiv 0.5\,{\rm fm}$, independently from the quark mass.

In order to localize the $N_t = 4$ high-temperature phase transition we fixed the gauge coupling at $\beta = 0.55$ and changed the bare quark mass μ_κ (or, equivalently, the hopping parameter $\kappa = (2\mu_\kappa)^{-1}$). The results on an $8^3 \times 4$ lattice for the absolute value of the Polyakov line and average plaquette are given in Fig. 2. As it is shown by the figure, the transition with the DBW2 action is rather smooth, barely visible. This has to be contrasted with the strong and sudden increase of both Polyakov line and average plaquette in case of the Wilson plaquette action, which is also shown for comparison in Fig. 2.

Table 1. Bare couplings and parameters of the TSMB algorithm in runs with the DBW2 gauge action. The determinant breakup multiplicity is $n_{\rm B} = 4$ in all runs. Small letters label runs on $8^3 \times 16$ lattices at $\beta = 0.55$ whereas capital letters stand for runs on $12^3 \times 24$ lattices at $\beta = 0.67$. The suffix l and h denote "low" and "high" plaquette phase, respectively. Those runs with a calligraphic letter are performed with an additional twisted mass term ($\mu = 0.01$). The number of analyzed configurations is given in the last column. An asterix on these numbers denotes that a few configurations have very low ($\ll 1$) reweighting factors. The analyzed gauge configurations are separated by 10 update cycles, except for runs (a) and ($\mathcal{A}_{\rm l}$), where they are separated by 100 and 2 update cycles, respectively

run	κ	n_1	n_2	n_3	λ	ϵ	$N_{\rm conf}$
(a)	0.184	22	100	102	24	$2.4{\cdot}10^{-3}$	116
(b)	0.186	22	200	220	23	$5.8{\cdot}10^{-4}$	381
(c)	0.188	24	500	520	23	$5.7{\cdot}10^{-5}$	165
(d)	0.190	30	900	940	22	$1.1{\cdot}10^{-5}$	66*
(e)	0.192	30	1400	1440	22	$2.7{\cdot}10^{-6}$	159*
(f)	0.193	26	650	680	22	$2.7{\cdot}10^{-5}$	192
(g)	0.194	22	300	320	21	$2.1{\cdot}10^{-4}$	111
($A_{\rm l}$)	0.165	28	210	220	26	$1.3 \cdot 10^{-3}$	82
($C_{\rm l}$)	0.167	28	500	510	25	$1.3 \cdot 10^{-4}$	62
($C_{\rm h}$)	0.167	30	1100	1200	25	$1.3 \cdot 10^{-5}$	220
($D_{\rm l}$)	0.168	30	1100	1200	25	$1.2 \cdot 10^{-5}$	82*
($D_{\rm h}$)	0.168	30	1100	1200	25	$1.2 \cdot 10^{-5}$	211
($E_{\rm h}$)	0.170	28	900	920	24	$4.8 \cdot 10^{-5}$	194
($F_{\rm h}$)	0.172	28	500	510	24	$1.2 \cdot 10^{-4}$	151
($G_{\rm h}$)	0.175	28	500	510	23	$1.1 \cdot 10^{-4}$	78*
($\mathcal{A}_{\rm l}$)	0.165	16	250	270	24	$1.2 \cdot 10^{-3}$	540
($\mathcal{B}_{\rm l}$)	0.166	18	420	460	24	$3.6 \cdot 10^{-4}$	58
($\mathcal{C}_{\rm h}$)	0.167	18	420	460	24	$3.6 \cdot 10^{-4}$	139
($\mathcal{D}_{\rm h}$)	0.168	18	420	460	24	$3.6 \cdot 10^{-4}$	321
($\mathcal{E}_{\rm h}$)	0.170	18	420	460	24	$3.6 \cdot 10^{-4}$	100

A similar analysis on $12^3 \times 6$ lattices at $\beta = 0.67$ gives qualitatively similar results but there the difference between the DBW2 and the Wilson plaquette action is smaller because the transition for the Wilson plaquette action becomes weaker.

3.1 Results on an $8^3 \times 16$ lattice at $\beta = 0.55$

The runs on an $8^3 \times 16$ lattice at $\beta = 0.55$ and $\mu = 0$ were started from the low-temperature phase by taking four copies in the time direction of some of the $8^3 \times 4$ lattices. The parameters of these runs are specified in the first part of Table 1.

Besides the hopping parameter κ also some parameters of the TSMB updating algorithm are specified: the orders of the polynomials used $n_{1,2,3}$ and the interval covering the eigenvalues of the squared preconditioned hermitean quark matrix $[\epsilon, \lambda]$.

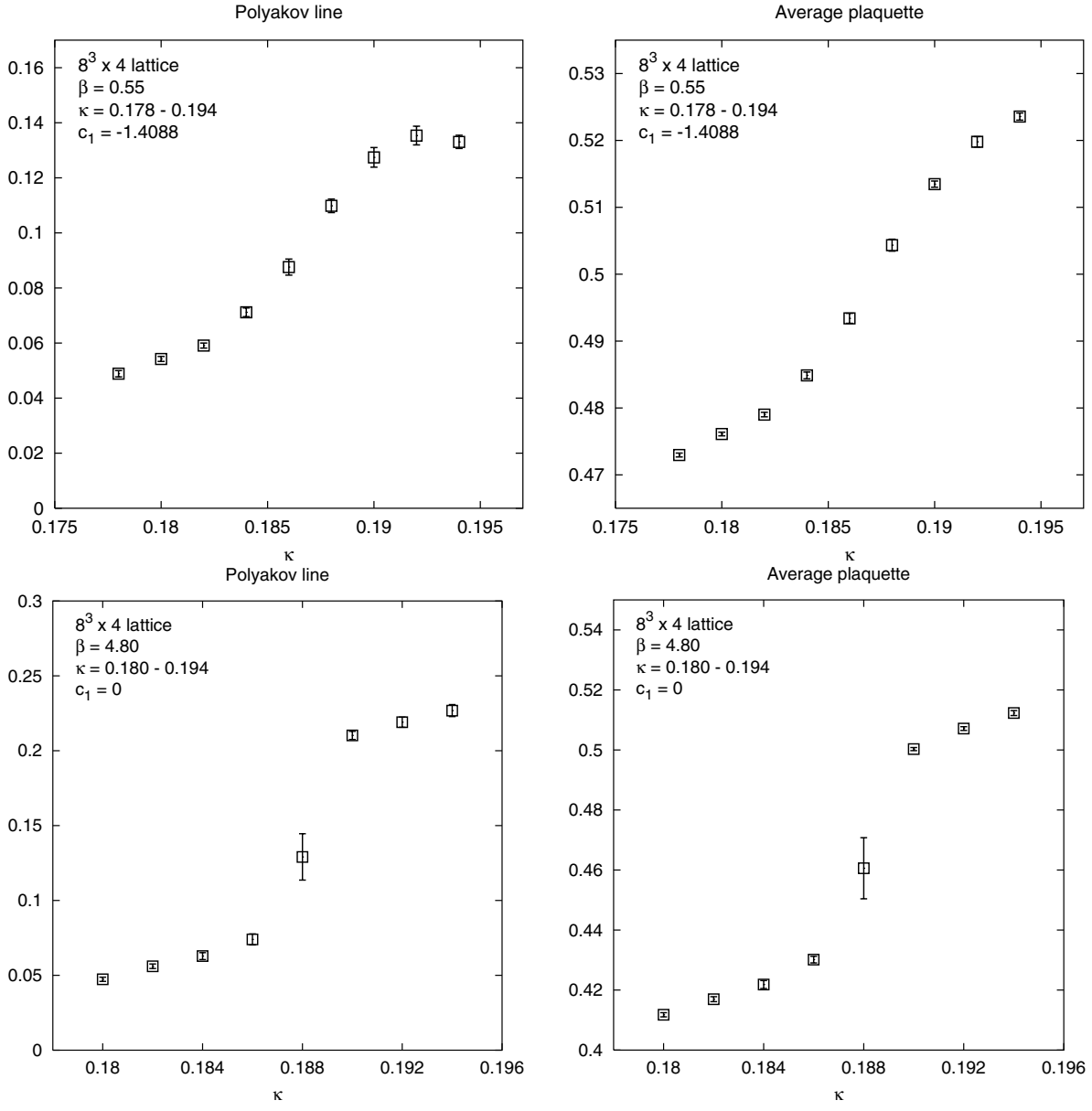

Fig. 2. Upper panels: the signals of the $N_t = 4$ non-zero temperature transition on an $8^3 \times 4$ lattice with the DBW2 gauge action. Lower panels: the same with Wilson gauge action. Left panels: absolute value of the Polyakov line, right panels: average plaquette, both as a function of κ

In the $8^3 \times 16$ runs we looked for signals of metastability but we did not find any. The results for some interesting quantities are collected in the first part of Table 2: the pion (i.e. pseudoscalar meson) and ρ-meson masses and the bare quark mass in lattice units $am_\chi^{\rm PCAC}$. Some of these quantities are also shown in Fig. 3. The scale parameter in lattice units r_0/a was also determined. We note in passing that at this small value of β and with our partly low statistics the evaluation of r_0 is rather difficult. Nevertheless, in order to estimate quantities also in physical units, we performed a purely statistical analysis for r_0, being aware of the fact that systematic effects can be large.

The bare quark mass $am_\chi^{\rm PCAC}$ is defined by the PCAC relation containing the axialvector current $A^a_{x\mu}$ in (5) and the pseudoscalar density insertion:

$$am_\chi^{\rm PCAC} \equiv \frac{\langle \partial^*_\mu A^+_{x\mu}\, P^-_y \rangle}{2\langle P^+_x\, P^-_y \rangle}\ . \tag{21}$$

Since for the moment we do not determine the Z-factors of multiplicative renormalization, the bare quark mass $am_\chi^{\rm PCAC}$ contains an unknown $\mathcal{O}(1)$ Z-factor $Z_q \equiv Z_P/Z_A$. In the following analysis we extracted the quark mass with the method detailed in [27]; see Sect. 3.1.1 there.

In agreement with the absence of a signal for metastability, the μ_κ-dependence of the pion mass and quark

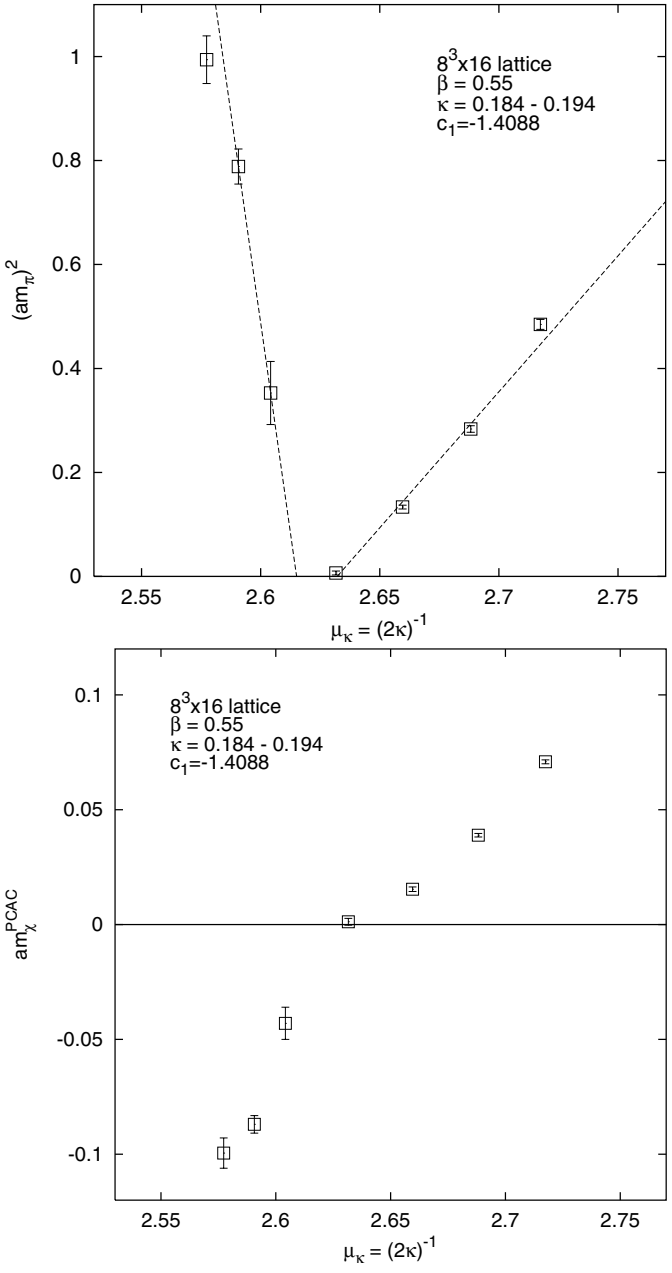

Fig. 3. Results of the numerical simulation on an $8^3 \times 16$ lattice at $\beta = 0.55$: upper panel the square of the pion mass $(am_\pi)^2$, lower panel the PCAC quark mass $am_\chi^{\rm PCAC}$. In the upper panel the dashed lines are extrapolations to zero pion mass: at the right it is a linear fit of four points, at the left a straight line connecting two points with small quark mass

mass in Fig. 3 is consistent with the absence of a first order phase transition at this gauge coupling ($\beta = 0.55$). A rough estimate for the value of the lattice spacing is $a \simeq 0.30\,\mathrm{fm}$ in the positive quark mass phase and $a \simeq 0.23\,\mathrm{fm}$ in the negative quark mass phase. The upper panel in Fig. 3 suggests the existence of a short interval ($\mu_\kappa \in [2.62, 2.63]$ or $\kappa \in [0.190, 0.191]$) of an Aoki phase near zero quark- and pion masses. This behavior is qualitatively similar to the one for the Wilson plaquette action which also shows the existence of the Aoki phase at strong gauge coupling [33].

Table 2. Results of runs specified in Table 1 for different quantities

run	am_π	am_ρ	m_π/m_ρ	$am_\chi^{\rm PCAC}$
(a)	0.6962(69)	1.0015(75)	0.6952(37)	0.07086(85)
(b)	0.5325(60)	0.9013(75)	0.5908(57)	0.03890(75)
(c)	0.3652(49)	0.840(26)	0.435(13)	0.0154(10)
(d)	0.081(24)	0.62(38)	0.130(78)	0.0012(15)
(e)	0.594(51)	1.80(30)	0.355(42)	−0.0430(70)
(f)	0.888(19)	1.794(30)	0.495(13)	−0.0870(38)
(g)	0.997(23)	1.820(59)	0.548(17)	−0.0995(66)
$(A_{\rm l})$	0.454(04)	0.724(25)	0.627(18)	0.0414(05)
$(C_{\rm l})$	0.343(07)	0.735(32)	0.466(21)	0.0222(11)
$(C_{\rm h})$	0.313(22)	0.776(125)	0.403(67)	−0.0222(28)
$(D_{\rm l})$	0.153(12)	0.445(109)	0.344(91)	0.0053(17)
$(D_{\rm h})$	0.380(31)	1.144(88)	0.332(37)	−0.0335(54)
$(E_{\rm h})$	0.644(15)	1.324(75)	0.487(27)	−0.0834(38)
$(F_{\rm h})$	0.840(23)	1.468(52)	0.572(25)	−0.1295(77)
$(G_{\rm h})$	1.005(44)	1.801(81)	0.558(28)	−0.1585(103)
$(\mathcal{A}_{\rm l})$	0.4641(45)	0.7228(58)	0.6421(53)	0.03803(81)
$(\mathcal{B}_{\rm l})$	0.341(05)	0.634(55)	0.538(45)	0.0177(22)
$(\mathcal{C}_{\rm h})$	0.291(12)	0.607(232)	0.480(178)	−0.0149(22)
$(\mathcal{D}_{\rm h})$	0.472(07)	1.035(72)	0.456(32)	−0.0469(16)
$(\mathcal{E}_{\rm h})$	0.712(14)	1.136(65)	0.627(34)	−0.0946(72)

3.2 Results on a $12^3 \times 24$ lattice at $\beta = 0.67$

With a short investigation of the high-temperature phase transition on a $12^3 \times 6$ lattice one can easily localize the gauge coupling β and bare quark mass $\mu_\kappa = (2\kappa)^{-1}$ where the lattice spacing is about a factor 3/2 smaller than at $\beta = 0.55$. It turned out that one can take $\beta = 0.67$ and $\kappa \simeq 0.17$. Fixing $\beta = 0.67$ and changing κ we performed several runs on a $12^3 \times 24$ lattice. In this way the physical volume of the lattice is approximately the same as the one of an $8^3 \times 16$ lattice at $\beta = 0.55$. In order to be able to compare with the results of [1], besides the runs with $\mu = 0$, at this β we also considered a non-vanishing twisted mass $\mu = 0.01$.

First we looked also here at $\mu = 0$ for a signal of metastability in the average plaquette and we found it near $\kappa = 0.167$–0.168, as it is shown by the upper panel of Fig. 4. Note that the average plaquette values are substantially higher here than at $\beta = 5.2$ with the Wilson plaquette gauge action in [1]: $A_{\rm plaq} \equiv \langle \frac{1}{3} \mathrm{Re}\,\mathrm{Tr}\, U_{\rm plaq} \rangle \simeq 0.59$ instead of $A_{\rm plaq} \simeq 0.52$. This qualitatively shows that the gauge field with DBW2 is smoother.

We also determined the pion, ρ-meson and quark masses, with the results given in Table 2. (For a graphical representation of some of these results see also the upper panels of Fig. 5.) For the extraction of r_0/a we performed

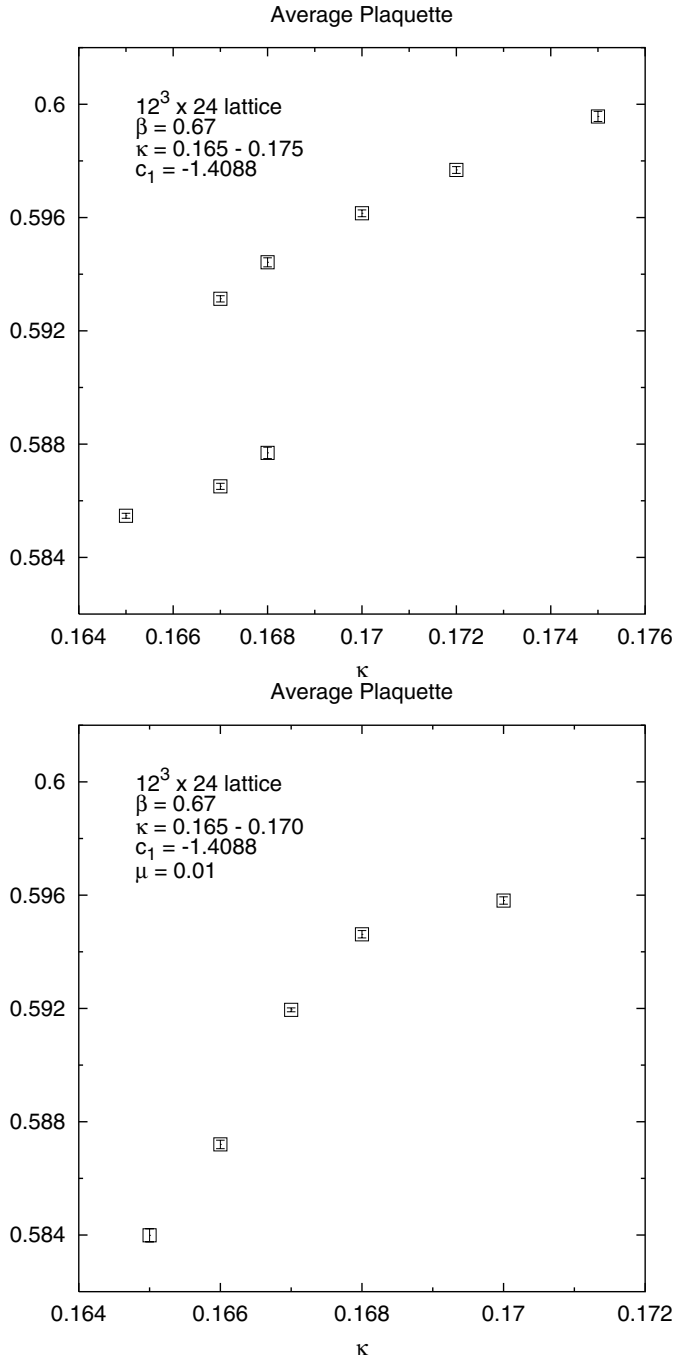

Fig. 4. The average plaquette at $\beta = 0.67$ on a $12^3 \times 24$ lattice as a function of the hopping parameter κ: upper panel $\mu = 0$ and lower panel $\mu = 0.01$, respectively

only a statistical analysis also here, neglecting the systematic effects. Let us give a range of values for the runs in Table 2. For A_l to D_l we find $2.37 < r_0/a < 2.76$ in the low and for C_h to G_h $2.72 < r_0/a < 3.17$ in the high plaquette phases, respectively. For $\mathcal{A}_\mathrm{l}, \mathcal{B}_\mathrm{l}$ we find $2.39 < r_0/a < 2.54$ in the low and for $\mathcal{C}_\mathrm{h}$ to $\mathcal{E}_\mathrm{h}$ we find $2.89 < r_0/a < 3.07$ in the high plaquette phase.

From the values of the scale parameter r_0/a we determined the lattice spacing, and found $a \simeq 0.18$–$0.21\,\mathrm{fm}$ in the positive and $a \simeq 0.16$–$0.18\,\mathrm{fm}$ in the negative quark mass phase, respectively. This is quite close to the values obtained in both phases with the Wilson plaquette gauge action at $\beta = 5.2$ in [1].

Going to the positive twisted mass $\mu = 0.01$, the metastability in the average plaquette disappears on our $12^3 \times 24$ lattice, as it is shown by the lower panel of Fig. 4. Having in mind the strong metastability signal in the average plaquette observed on a $12^3 \times 24$ lattice at $\beta = 5.2$ and $\mu = 0.01$ with the Wilson plaquette gauge action in [1], the absence of the metastability here signals a dramatic improvement of the phase structure due to the DBW2 gauge action. The presence of metastability at $\mu = 0$ and the absence of it at $\mu = 0.01$ indicates the existence of a rather short first order phase transition line near the origin in the (μ_κ, μ)-plane. Of course, for a precise localization of the first order phase transition line a detailed study of the infinite volume limit is required, which is beyond the scope of this paper.

An important question is the minimal value of the pion mass $m_\pi^{\min}$ associated to the first order phase transition line. A precise definition of $m_\pi^{\min}$ could be the value of the infinite volume pion mass just at the position of the first order phase transition, defined by the equal depth of the two free energy minima in the infinite volume limit. To obtain this would be rather demanding. Although the volume dependence could be studied beyond our volume extension of $L \simeq 2.4\,\mathrm{fm}$, for instance on a $16^3 \times 32$ lattice, the precise comparison of the free energy minima would be quite difficult. An approximate determination of $m_\pi^{\min}$ can be obtained by requiring the equality of the pion mass in lattice units am_π in the two phases on our $12^3 \times 24$ lattices. For this a linear extrapolation of $(am_\pi)^2$ from the points on both sides of the phase transition can be considered. As shown in the upper left panel of Fig. 5, our result at $\mu = 0$ is $(am_\pi)^2 = 0.0881$. This implies, with the range of r_0 values given above, that $m_\pi^{\min} \simeq 251\,\mathrm{MeV}$ in the positive quark mass phase and $m_\pi^{\min} \simeq 374\,\mathrm{MeV}$ in the phase with negative quark mass.

The minimal charged pion mass at $\mu = 0.01$ is $m_\pi^{\min} \simeq 360\,\mathrm{MeV}$ (see the lower left panel of Fig. 5). This originates from the non-zero value of the twisted quark mass and not from the presence of a first order phase transition.

In the right panels of Fig. 5 the bare quark mass in lattice units is shown. The dashed lines are linear fits to the points with positive and negative quark mass, respectively. At zero twisted mass (upper panel) the metastability region near the first order phase transition is clearly displayed. At $\mu = 0.01$ (lower panel) the difference between the two dashed lines is smaller. This difference may be interpreted as a consequence of a cross-over in the continuation of the first order phase transition line. In the figure there is also a linear fit to all points shown (full line) which goes reasonably close to every point. The two dashed lines also give lower and upper bound estimates for the critical hopping parameter: $0.1661 \leq \kappa_\mathrm{cr} \leq 0.1689$.

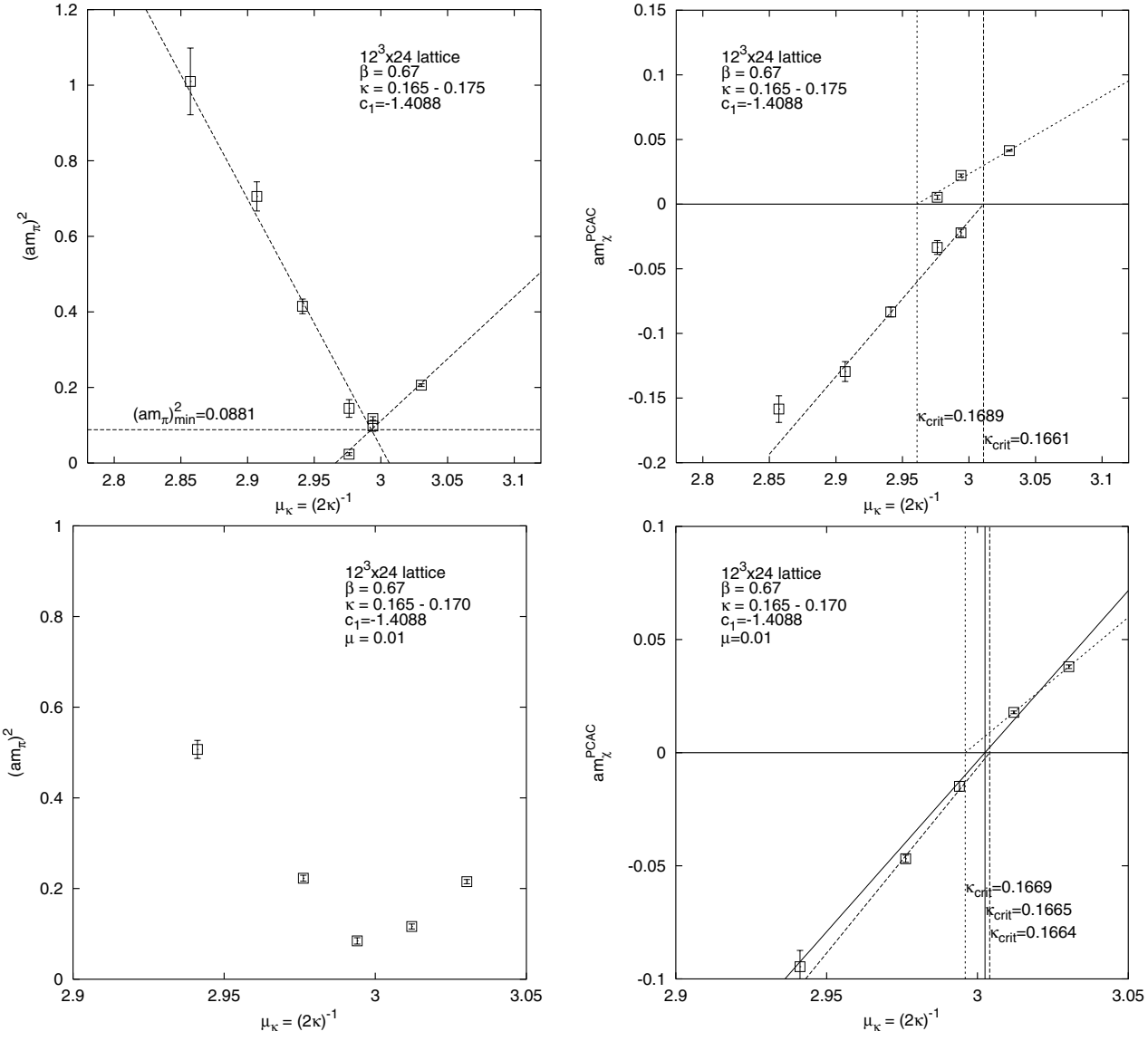

Fig. 5. Results of the numerical simulation on a $12^3 \times 24$ lattice at $\beta = 0.67$ as a function of $\mu_\kappa = (2\kappa)^{-1}$: upper panels $\mu = 0$, lower panels $\mu = 0.01$. Left panels: $(am_\pi)^2$, right panels: the bare PCAC quark mass am_χ^{PCAC}. The dashed straight lines are fits to the points in the positive and negative quark mass phase, respectively. The horizontal line in the upper left panel shows the estimated value of the minimal pion mass in lattice units. The straight lines in the right panels are explained in the text

Another way to estimate the critical hopping parameter (i.e. critical bare untwisted quark mass) is to determine the twist angle and find $\kappa_{\mathrm{cr}} = (2\mu_{\kappa_{\mathrm{cr}}})^{-1}$ where it equals $\pi/2$. Considering, for definiteness, the twist angle ω_V defined in Sect. 2.2, the fit in Fig. 6 gives $\kappa_{\mathrm{cr}} = 0.16651(2)$, in good agreement with the previous estimate. (Actually the numbers in Fig. 6 come from the vector Ward identity (13) but, within errors, (15) gives compatible results.) The Z-parameter appearing in this fit for ω_V is $Z_{oV} \equiv Z_A Z_S/(Z_V Z_P)$ (see Sect. 2.2 and [10]). According to Fig. 6 we have $Z_{oV} = 0.959(30)$. Since from an analogous fit to ω_A one could determine $Z_{oA} \equiv Z_V Z_S/(Z_A Z_P)$, this also offers a relatively easy way to obtain the Z-parameter combinations Z_A/Z_V and Z_P/Z_S.

The quantities $(r_0 m_\pi)^2$ and am_χ^{PCAC} can also be plotted against each other (see Figs. 7 and 8 for $\mu = 0$ and $\mu = 0.01$, respectively). Figure 7 and the data in Table 2 show that at $\mu = 0$, in the metastable region beyond the minimal pion mass, one can also reach values close to the physical value $m_\pi \simeq 140\,\mathrm{MeV}$.

3.3 Topological charge

The RGI gauge actions, and in particular the DBW2 action, are known to slow down the transitions between different topological sectors both in quenched [16] and in dynamical domain wall simulations [20]. In order to check this we determined the topological charge Q_{top} in some of

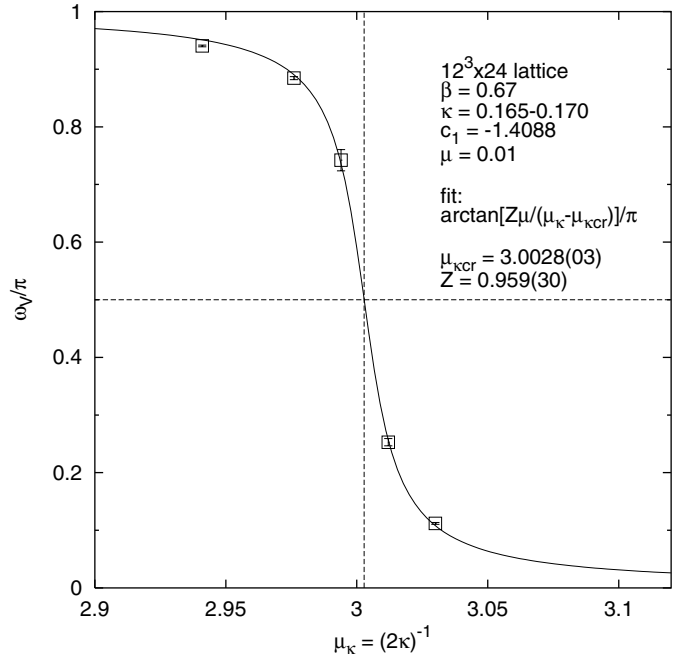

Fig. 6. The dependence of the twist angle ω_V on the bare untwisted quark mass $\mu_\kappa = (2\kappa)^{-1}$ at $\beta = 0.67$, $\mu = 0.01$ on a $12^3 \times 24$ lattice. The fit determines the critical hopping parameter to be $\kappa_{\rm cr} = (2\mu_{\kappa_{\rm cr}})^{-1} = 0.16651(2)$

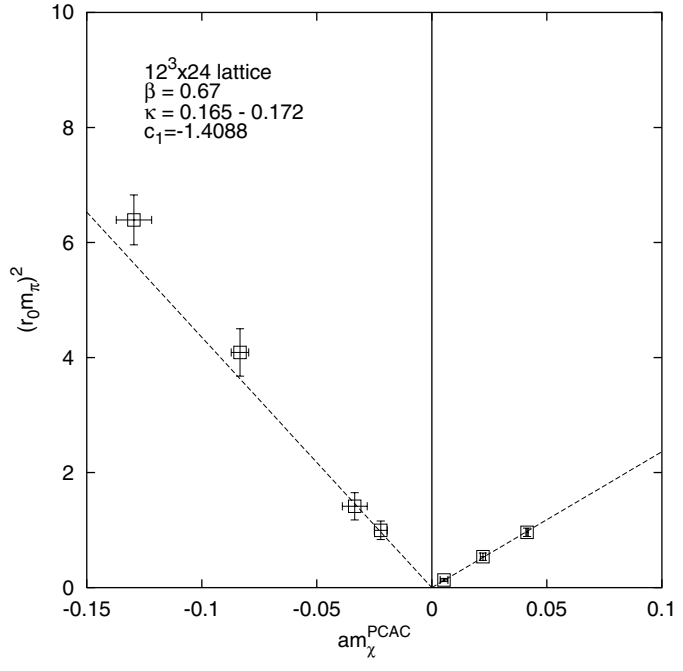

Fig. 7. The dependence of $(r_0 m_\pi)^2$ on $am_\chi^{\rm PCAC}$ at $\beta = 0.67$, $\mu = 0$ on a $12^3 \times 24$ lattice. The dashed lines are linear fits of the form $A|am_\chi^{\rm PCAC}|$. At the right all three points are included in the fit, at the left only two of them with the smallest quark masses. The fit parameter is for positive and negative quark mass $A = 23.6$ and $A = 43.5$, respectively

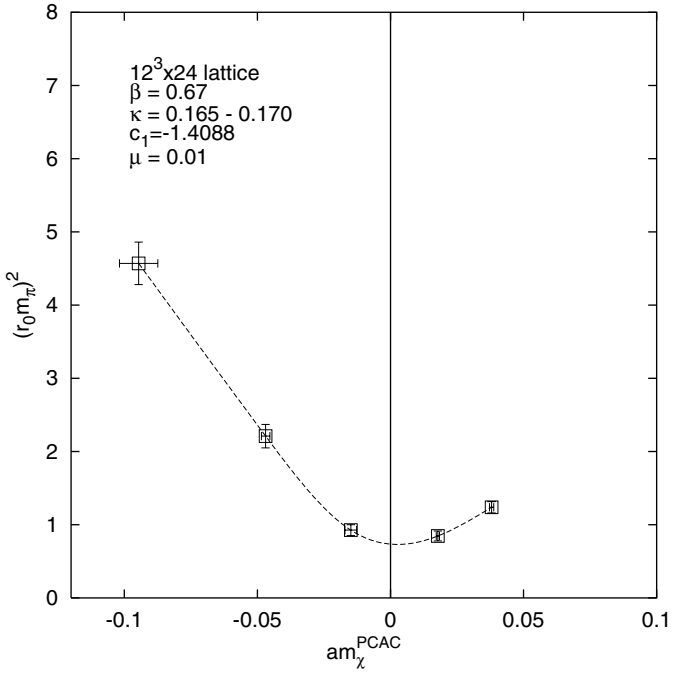

Fig. 8. The dependence of $(r_0 m_\pi)^2$ on am_χ^{PCAC} at $\beta = 0.67$, $\mu = 0.01$ on a $12^3 \times 24$ lattice. The dashed line is a spline interpolation for guiding the eyes

the runs using a cooling method [34]. In the following we denote the result from the cooling analysis by "topological charge", being aware of the fact that this definition contains some degree of arbitrariness. However, for our aim of testing the autocorrelation time this definition is sufficient.

In the run with label ($\mathcal{C}_{\rm h}$) ($12^3 \times 24$ lattice, $\beta = 0.67$, $\mu = 0.01$, $\kappa = 0.167$) the history of the topological charge is shown in the upper panel of Fig. 9. (The lower panel is a histogram of $Q_{\rm top}$.) The analyzed configurations are separated by 10 TSMB update cycles. In this point, according to Table 2, the quark mass is about $m_q \simeq 0.3\, m_{\rm strange}$ and the pion mass $m_\pi \simeq 380\,$MeV. As the figure shows, the topological charge is often changed. Its integrated autocorrelation in this run is $\tau_{\rm int}^{\rm top} \simeq 180$, but there is obviously a long tail of the autocorrelation which is not yet properly taken into account in a run of this length. In any case, $\tau_{\rm int}^{\rm top}$ is substantially longer than those of the average plaquette ($\tau_{\rm int}^{\rm plaq} \simeq 22$) or of the pion mass ($\tau_{\rm int}^{m_\pi} \simeq 6$) in Table 3.

In another run, the one with label ($C_{\rm l}$) ($12^3 \times 24$ lattice, $\beta = 0.67$, $\mu = 0$, $\kappa = 0.167$), where the quark mass is about $m_q \simeq 0.18\, m_{\rm strange}$ and the pion mass $m_\pi \simeq 295\,$MeV, the general picture is similar to Fig. 9. The integrated autocorrelation here comes out to be $\tau_{\rm int}^{\rm top} \simeq 70$, but this value is even less reliable because the run is shorter.

In spite of these relatively long autocorrelations, it is clear that in a sufficiently long run, say of length $1000\,\tau_{\rm int}^{m_\pi}$, which would be needed anyway for a good statistics on other quantities, the different topological sectors could be properly sampled by the TSMB algorithm. Therefore, at these bare parameter values, there is no problem with the

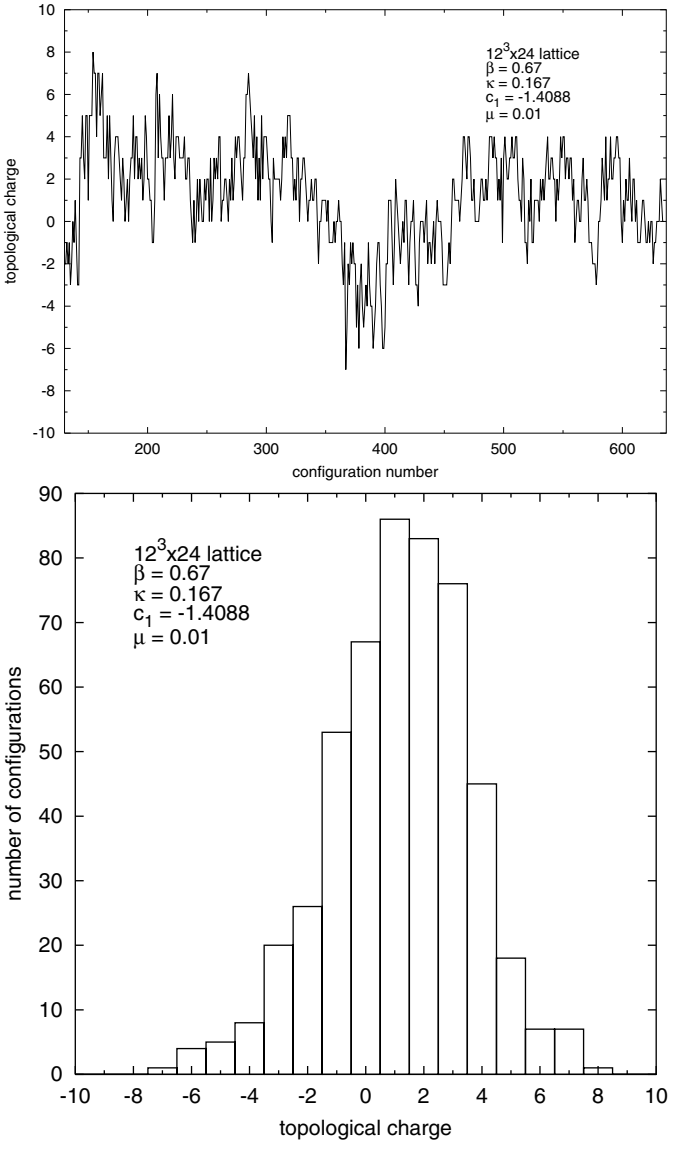

Fig. 9. The topological charge on a $12^3 \times 24$ lattice at $\beta = 0.67$, $\mu = 0.01$, $\kappa = 0.167$. Upper panel: the run history, with configurations separated by 10 TSMB update cycles. Lower panel: the distribution of the topological charge in this run

suppression of the transitions between different topological sectors.

3.4 Results about the update algorithm

In this paper we applied the TSMB update algorithm [26]. The estimates of the autocorrelations in different runs and the cost estimates obtained using (17) are given in Table 3. Since in our relatively short runs the autocorrelations can only be estimated, say, within a factor of two, the numbers in Table 3 give only a first orientation.

Qualitatively speaking, the $12^3 \times 24$ runs with "low plaquette" (positive quark mass) have lower costs than the corresponding runs with "high plaquette" (negative quark mass): at the same absolute value of the bare quark mass the runs in the negative quark mass phase have in most cases at least by an order of magnitude higher costs than those in the positive quark mass phase. The reason of the higher cost at negative quark mass is that the smallest eigenvalues fluctuate more frequently to very small values.

Table 3. The cost of an update cycle $C_{\rm cycle}$ in thousands of MVMs according to (17) and the estimated integrated autocorrelation lengths in update cycles obtained from runs specified by Table 1. The suffix plaq and m_π refer to the average plaquette and the pion mass, respectively. The last two columns give the factors F calculated from (19) with $z = 2$

run	$C_{\rm cycle}$	$\tau_{\rm int}^{\rm plaq}$	$\tau_{\rm int}^{m_\pi}$	$F_{\rm plaq}/10^6$	$F_{m_\pi}/10^6$
(a)	13	152		11.9	
(b)	19	100	20	3.5	0.7
(c)	30	147	< 5	1.3	< 0.04
(d)	48		12		0.001
(e)	65	167	< 5	24	< 0.7
(f)	38	95	9	33	3.1
(g)	25	32	< 5	9.5	< 1.5
$(A_{\rm l})$	19	21	< 5	0.8	< 0.2
$(C_{\rm l})$	29	18	15	0.3	0.3
$(C_{\rm h})$	50	53	33	1.5	0.9
$(D_{\rm l})$	51	77	< 5	0.1	< 0.01
$(D_{\rm h})$	51	113	7	7.8	0.5
$(E_{\rm h})$	43	61	11	22	3.9
$(F_{\rm h})$	30	56	< 5	33.4	< 3.0
$(G_{\rm h})$	31	52	6	48.4	5.6
$(\mathcal{A}_{\rm l})$	12	143	13	5.9	0.5
$(\mathcal{B}_{\rm l})$	21	41	9	0.6	0.1
$(\mathcal{C}_{\rm h})$	21	22	6	0.2	0.1
$(\mathcal{D}_{\rm h})$	21	72	8	7.8	0.9
$(\mathcal{E}_{\rm h})$	21	29	7	12.8	3.1

There is also a general tendency that the overall factors F decrease for decreasing absolute value of the quark mass. In fact, the data on F show that in the small quark mass region an inverse quark mass power $z = 1$ is a better approximation than $z = 2$, which has been observed in previous simulations with the Wilson plaquette gauge action [27–30,9]. At $\mu = 0$ the overall factor for the average plaquette $F_{\rm plaq}$ in the parameterization

$$C_{\tau_{\rm int}} \simeq F\,(am_q)^{-1}\,\Omega \tag{22}$$

turns out to be $F_{\rm plaq} \simeq 2 \cdot 10^7$ in the positive quark mass phase and $F_{\rm plaq} \simeq (2\text{–}3) \cdot 10^8$ at negative quark mass. The corresponding numbers at $\mu = 0.01$ are between these two values.

Let us note that at the smallest quark masses a final reweighting correction has to be applied because the smallest eigenvalues cannot be always kept in the interval of polynomial approximations. Sometimes they fluctuate below the lower limit ϵ.

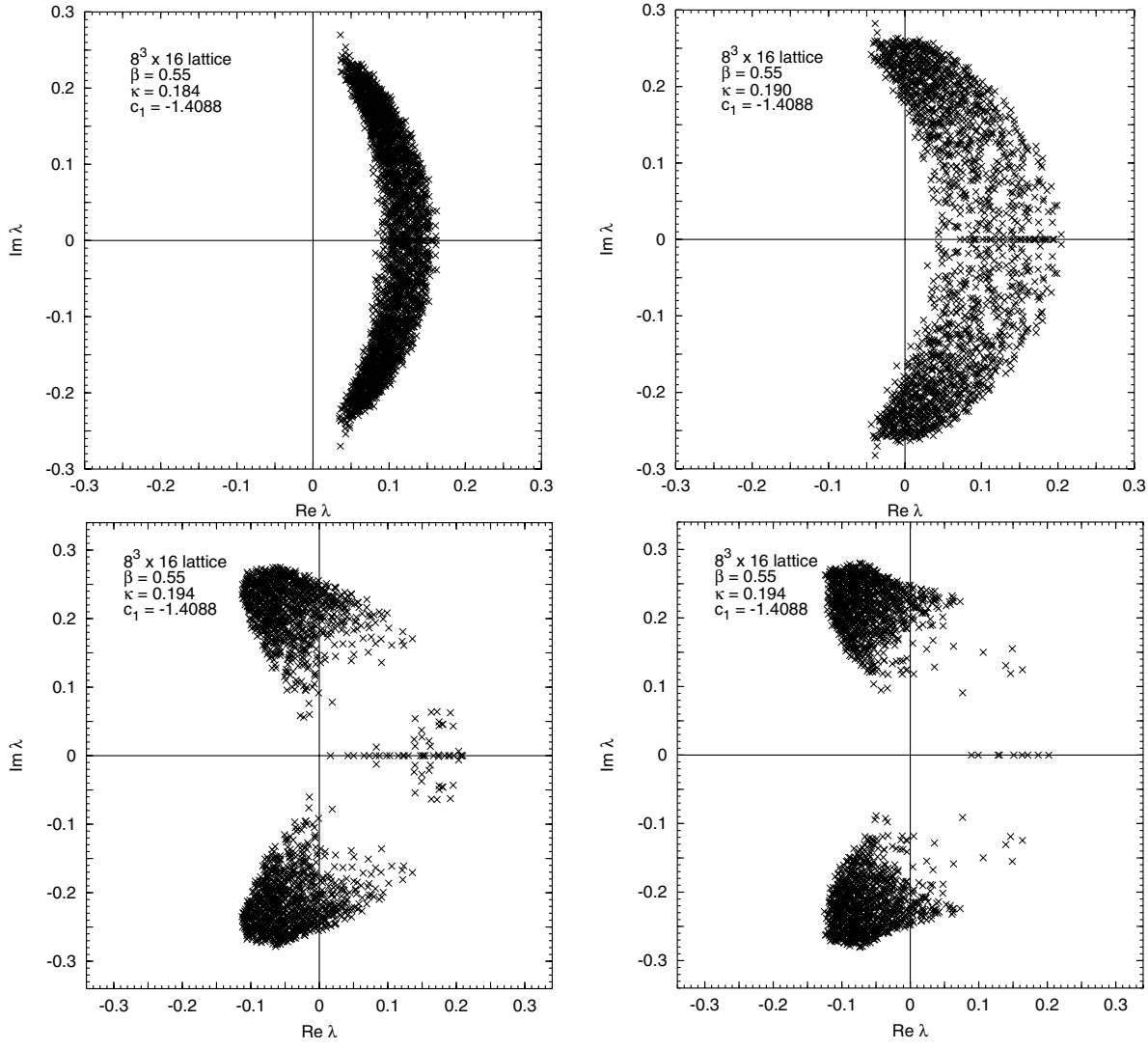

Fig. 10. Eigenvalues of the Wilson–Dirac fermion matrix (1) with small absolute value for $\mu = 0$, $\beta = 0.55$ on an $8^3 \times 16$ lattice. Upper left panel: $\kappa = 0.184$. Upper right panel: $\kappa = 0.190$. Lower panels: $\kappa = 0.194$ at the beginning of equilibration (left panel) and after equilibration (right panel)

4 Eigenvalue spectra

Looking at the eigenvalue spectra of the Wilson–Dirac fermion matrix (1) at small (untwisted) quark masses (see, for instance, in Sect. 4 of [27]) it seems plausible that near zero quark mass there has to be a massive rearrangement of eigenvalues. This is because in the path integral small eigenvalues are strongly supressed by the zero of the fermion determinant. At the sign change of the quark mass the eigenvalues have to somehow avoid the zero of the determinant at the origin. It is plausible that this eigenvalue rearrangement is related to the phase transition at zero quark mass.

An interesting question is how the behavior of eigenvalues in the small quark mass region is influenced by a non-zero twisted mass term.

We investigated the eigenvalue spectra by the Arnoldi method on $8^3 \times 16$ and $12^3 \times 24$ lattices in some of the runs listed in Table 1. Typically 100–200 eigenvalues were determined on 10–30 independent gauge field configurations. The parameters of the Arnoldi code were set for searching the eigenvalues with the smallest absolute value.

The results at $\mu = 0$ on an $8^3 \times 16$ lattice are shown by Fig. 10. In the upper panels of the figure, where the quark mass is positive, typical "half-moons" filled with eigenvalues can be seen, which correspond to the figures in [27]. At negative quark mass – in the lower part of Fig. 10 – an almost empty segment in the middle of the "half-moon" appears. Comparing the two figures at negative quark mass one can also see how this segment is gradually emptied during equilibration.

It is remarkable that even after equilibration there are some real ("zero-mode") eigenvalues on the positive axis. Our Arnoldi code did not find in these configurations any negative real eigenvalues. In addition, it is quite surprising that, apart from the empty segment in the middle,

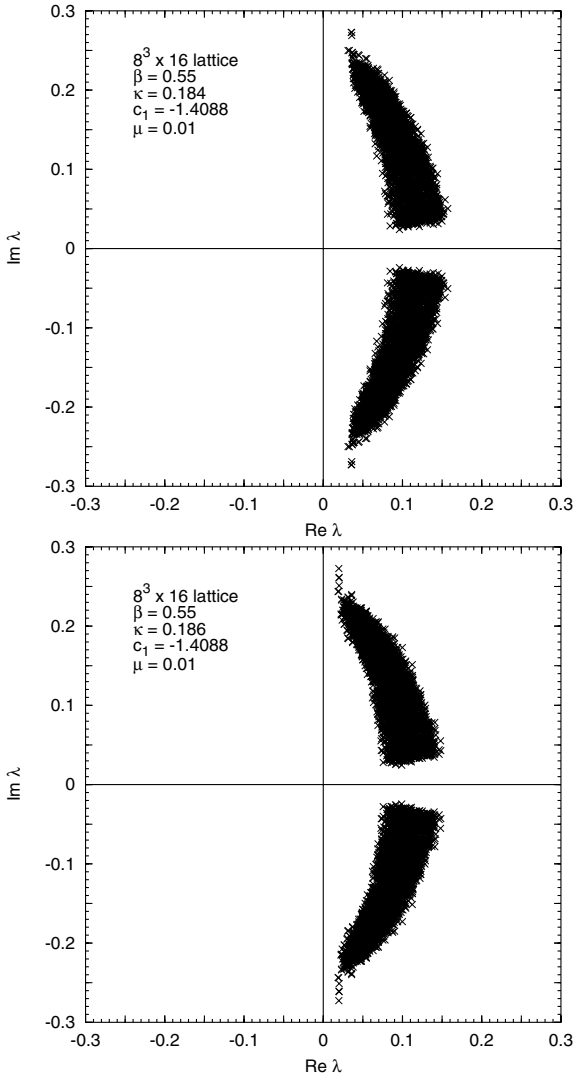

Fig. 11. Eigenvalues of the Wilson–Dirac fermion matrix (1) with small absolute value for $\mu = 0.01$, $\beta = 0.55$ on an $8^3 \times 16$ lattice. Upper panel: $\kappa = 0.184$, lower panel: $\kappa = 0.186$

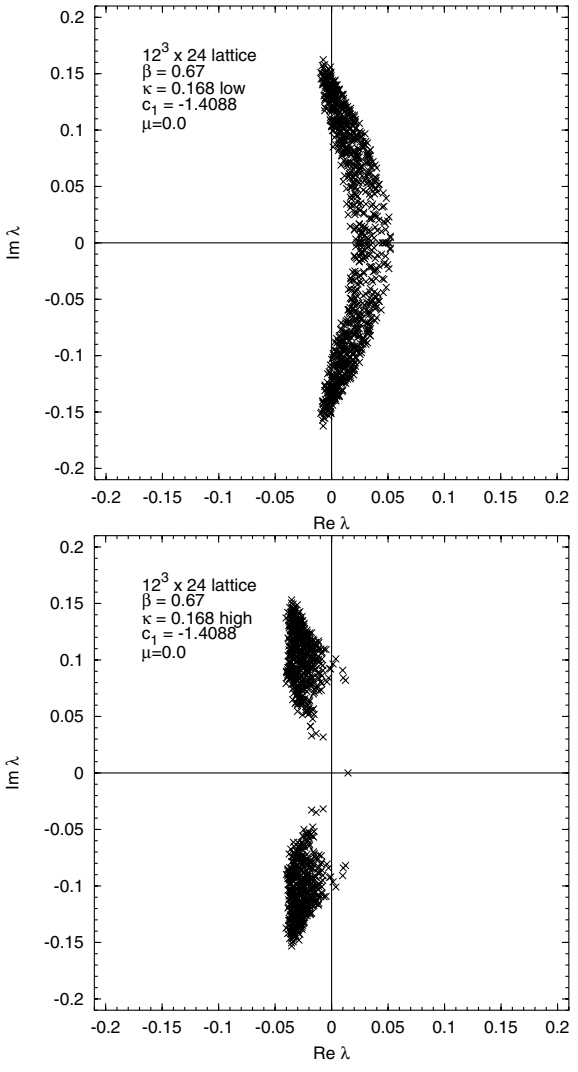

Fig. 12. Eigenvalues of the Wilson–Dirac fermion matrix (1) with small absolute value at $\beta = 0.67$, $\kappa = 0.168$ on a $12^3 \times 24$ lattice. Upper panel: $\mu = 0$, "low plaquette"; lower panel: $\mu = 0$, "high plaquette"

the half-moon-shaped deformation of the eigenvalue region observed at small positive quark masses does not disappear for small negative quark masses either.

The effect of a non-zero twisted mass on the eigenvalue spectrum on an $8^3 \times 16$ lattice is illustrated by Fig. 11. It can be seen that the strip around the real axis $-\mu \leq \mathrm{Im}(\lambda) \leq +\mu$ is free from eigenvalues. Let us remark that also in presence of a non-zero twisted mass we studied the spectrum of the operator of (1), which corresponds to the so-called "twisted basis". In the "physical basis" [35], for $\omega = \pi/2$, the spectrum of the Dirac operator lies in a vertical line parallel to the imaginary axis and is shifted from the origin by μ (exactly as in the continuum).

Going to larger β (smaller lattice spacing) the visible difference is that the "half-moons" are straightened and come closer to the origin; see Fig. 12. Otherwise most qualitative features are unchanged. There is, however, a marked difference in the number of real eigenvalues (for $\mu = 0$): in the upper panels of Fig. 10 there are lots of them, whereas at larger β, in the upper panel of Fig. 12, their number is substantially reduced.

The effect of changing the gauge action can be seen by comparing Fig. 12 with the eigenvalue spectra in case of the Wilson plaquette gauge action at a similar lattice spacing $a \simeq 0.2\,\mathrm{fm}$ in Fig. 13. The fact that in the case of using the Wilson gauge action the pion mass is larger than in the case of the DBW2 action is reflected by a movement of the "half-moons" farther away from the origin.

5 Conclusion

The main conclusion of this paper is that, indeed, exchanging the Wilson plaquette gauge action with the (renormalization group improved) DBW2 action shows substantial effects on the phase structure. We performed a qualitative

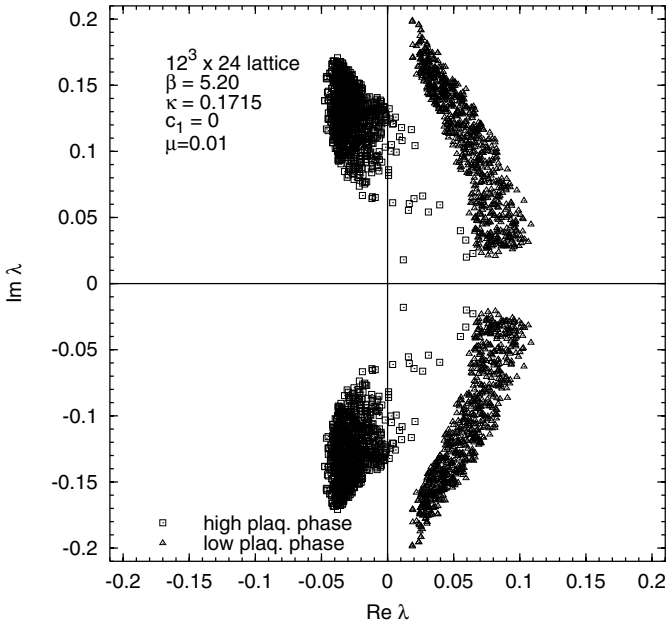

Fig. 13. Eigenvalues of the Wilson–Dirac fermion matrix with small absolute value in case of the Wilson plaquette action at $\beta = 5.20,\ \mu = 0.01,\ \kappa = 0.1715$ on a $12^3 \times 24$ lattice. Both "high plaquette" and "low plaquette" spectra are shown

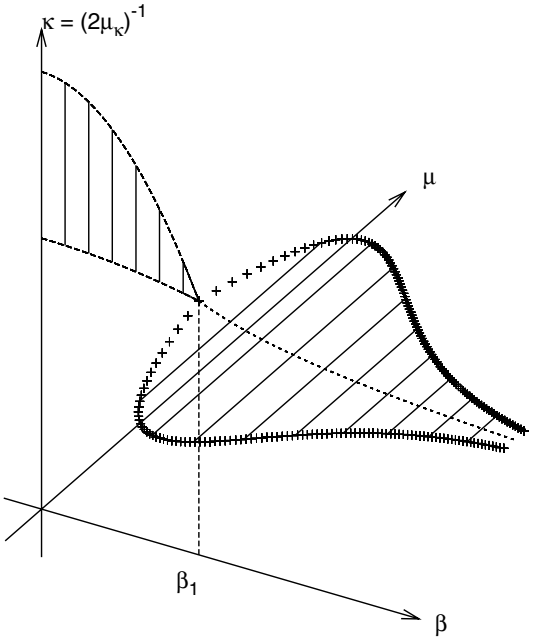

Fig. 14. The schematic view of the phase transitions in the (β, κ, μ) space for Wilson quarks with both DBW2 and Wilson plaquette gauge action (β is the bare gauge coupling, κ is the hopping parameter, μ is the bare twisted quark mass, and $\mu_\kappa \equiv (2\kappa)^{-1}$ is the bare untwisted quark mass.) The crosses mark the second order boundary line of the first order phase transition surface. At strong gauge coupling there is the surface containing the Aoki phase, which ends at a point denoted by $\beta = \beta_1$. The figure does not extend down to $\beta = 0$ and only one "finger" of the Aoki phase is shown

study of the phase structure of lattice QCD by changing the gauge action and compared the Wilson plaquette and DBW2 actions at a lattice spacing $a \simeq 0.2\,\mathrm{fm}$ in the positive quark mass phase and $a \simeq 0.17\,\mathrm{fm}$ in the phase with negative quark mass. This means: at $\beta = 5.2$ for the Wilson plaquette action and $\beta = 0.67$ for the DBW2 action. At this comparable situation the metastability signaled by the existence of long living states with different average plaquette value and quark masses with opposite sign becomes weaker and the minimal pion mass and the jump in the average plaquette between the phases with positive and negative quark mass decrease.

For vanishing twisted mass $\mu = 0$ the metastability occurs in the hopping parameter range $0.167 \leq \kappa \leq 0.168$. Going to the twisted mass value $\mu = 0.01$, which is the same as in the numerical simulations of [1,8], the metastability disappears on our $12^3 \times 24$ lattices. It might reappear on larger lattices, but our $12^3 \times 24$ data indicate that the jump in the average plaquette is at least by a factor of ten smaller than the one observed in [1].

At a lower β value, $\beta = 0.55$, which corresponds to lattice spacings $a \simeq 0.30\,\mathrm{fm}$ and $a \simeq 0.23\,\mathrm{fm}$ for positive and negative quark mass, respectively, our simulation data are consistent with the existence of the Aoki phase. This is similar to the situation for $\beta \leq 4.6$ in case of the Wilson plaquette action [33]. The schematic picture of the suggested phase diagram in the (β, κ, μ) space, both for DBW2 and Wilson plaquette gauge actions, is shown by Fig. 14.

The minimal pion mass in a stable phase can be estimated from our simulation data at $\beta = 0.67$ and vanishing twisted mass on a $12^3 \times 24$ lattice to be $m_\pi^{\min} \simeq 250\,\mathrm{MeV}$ in the positive quark mass phase and $m_\pi^{\min} \simeq 375\,\mathrm{MeV}$ in the phase with negative quark mass. On larger lattices this value is expected to be 10–20% smaller due to the finite volume effects which are non-negligible on the $12^3 \times 24$ lattice, especially in the negative quark mass phase where the lattice extension is only $L \simeq 2.0\,\mathrm{fm}$. At positive twisted mass $\mu = 0.01$ the estimate for the minimal charged pion mass is $m_\pi^{\min} \simeq 360\,\mathrm{MeV}$, a value entirely due to the non-zero twisted mass and not to the first order phase transition.

Besides the pion- and ρ-meson masses, at non-vanishing twisted mass, we also determined the twist angle ω_V as a function of the bare untwisted quark mass μ_κ. The μ_κ-dependence of ω_V can be well described by the expected arctan-function (see Fig. 6). From the fit one obtains the value of the critical hopping parameter $\kappa_{\mathrm{cr}} = 0.16651(2)$ and an estimate of a combination of Z-factors.

In some of the simulation runs we also monitored the history of the topological charge (see, for instance, Fig. 9). Although the autocorrelation of the topological charge is markedly longer than those of the average plaquette or of the pion mass, in a good statistics run with, say, thousand times the integrated autocorrelation length of the pion mass, the different topological sectors could be properly sampled.

In order to illustrate the rearrangement of the small eigenvalues near the zero quark mass phase transition we investigated in some detail the eigenvalue spectrum of the non-hermitean fermion matrix defined in (1). To our surprise, the transition from positive to negative quark mass is signaled in the eigenvalue spectrum by the opening up of an almost empty segment in the "half-moon" occupied by the eigenvalues near the origin. The introduction of a non-vanishing twisted mass causes the appearance of an empty strip $[-\mu, +\mu]$ on both sides of the real axis. The effect of larger β is to straighten the "half-moon" occupied by the small eigenvalues. At the same time the small real eigenvalues at zero twisted mass, which are causing the problem of the so-called "exceptional gauge configurations" in partially quenched simulations, occur much less frequently.

A welcome side-effect of introducing the RGI gauge action is the speed-up of the TSMB update algorithm. (This presumably also applies to other update algorithms, but in this paper we only used TSMB.) This can be qualitatively understood by the reduction of the probability for small size "dislocations" in the gauge field and for the less frequent occurrence of small real eigenvalues. (This is qualitatively similar to the conclusions of [36], obtained in another setup.) The computational cost as a function of the quark mass can be better approximated in the small quark mass region by an inverse power behavior of only $(am_q)^{-1}$ than by the behavior $(am_q)^{-2}$ observed previously with the Wilson plaquette action.

The results of the present paper indicate that the combination of $N_f = 2$ Wilson quarks with the DBW2 gauge action leads to a phase structure with a weaker first order phase transition than $N_f = 2$ Wilson quarks with the plaquette gauge action at a comparable value of the lattice spacing. For the moment we have no detailed information on the dependence of the phase structure on the parameter c_1 in the gauge action which multiplies the rectangular Wilson loops. It is possible that the optimal choice is different from $c_1 = -1.4088$, for instance, $c_1 = -0.331$ for to the Iwasaki action or $c_1 = -1/12$ for the tree-level improved Symanzik action. The best choice of c_1 might also be influenced by the positivity problem of improved actions [31] and/or by the convergence rate of lattice perturbation theory [37].

An important open question, which remains to be investigated in the future, is the β-dependence of the phase structure for Wilson-type lattice fermions. It is expected that closer to the continuum limit the minimal pion mass and the jump in the average plaquette become smaller and finally, in the continuum, the first order phase transition line in the plane of untwisted and twisted quark mass shrinks to a first order phase transition point. The faster this actually happens the better it is for phenomenologically relevant numerical QCD simulations with Wilson-type quarks.

Another important question is whether the DBW2 gauge action in combination with Wilson twisted mass fermions shows a good scaling behavior. To this end, a simulation at a higher value of β than the one used here is necessary. For the scaling studies previous experience in the quenched approximation [38] will be very helpful. Both questions mentioned above are presently investigated by our collaboration.

Acknowledgements. We thank Roberto Frezzotti, Gernot Münster and Giancarlo Rossi for helpful discussions, Stanislav Shcheredin for giving us his cooling code as well as Silvia Necco and Urs Wenger for their advice and help in evaluating the scale parameter r_0.

The computations were performed on the IBM-JUMP computer at NIC Jülich and the PC clusters at DESY Hamburg, NIC Zeuthen, Forschungszentrum Karlsruhe, University of Münster and the Sun Fire SMP-Cluster at the Rechenzentrum - RWTH Aachen. This work was supported by the DFG Sonderforschungsbereich/Transregio SFB/TR9-03.

References

1. F. Farchioni, R. Frezzotti, K. Jansen, I. Montvay, G.C. Rossi, E. Scholz, A. Shindler, N. Ukita, C. Urbach, I. Wetzorke, Eur. Phys. J. C **39**, 421 (2005); hep-lat/0406039
2. S.R. Sharpe, R. Singleton, Jr., Phys. Rev. D **58**, 074501 (1998); hep-lat/9804028
3. S. Weinberg, Physica A **96**, 327 (1979)
4. J. Gasser, H. Leutwyler, Annals Phys. **158**, 142 (1984)
5. K. Symanzik, Nucl. Phys. B **226**, 187 (1983)
6. B. Sheikholeslami, R. Wohlert, Nucl. Phys. B **259**, 72 (1985)
7. S. Aoki, Phys. Rev. D **30**, 2653 (1984); Phys. Rev. Lett. **57**, 3136 (1986)
8. F. Farchioni, C. Urbach, R. Frezzotti, K. Jansen, I. Montvay, G.C. Rossi, E. Scholz, A. Shindler, N. Ukita, I. Wetzorke, Nucl. Phys. Proc. Suppl. **140**, 240 (2005); hep-lat/0409098
9. R. Frezzotti, P.A. Grassi, S. Sint, P. Weisz, Nucl. Phys. Proc. Suppl. **83**, 941 (2000); hep-lat/9909003
10. ALPHA Collaboration, R. Frezzotti, P.A. Grassi, S. Sint, P. Weisz, JHEP **0108**, 058 (2001); hep-lat/0101001
11. G. Münster, JHEP **0409**, 035 (2004); hep-lat/0407006
12. S.R. Sharpe, J.M.S. Wu, Phys. Rev. D **70**, 094029 (2004); hep-lat/0407025; Nucl. Phys. Proc. Suppl. **140**, 323 (2005); hep-lat/0407035
13. L. Scorzato, Eur. Phys. J. C **37**, 445 (2004); hep-lat/0407023
14. CP-PACS Collaboration, A. Ali Khan et al., Phys. Rev. D **63**, 114504 (2001); hep-lat/0007014
15. RBC Collaboration, K. Orginos, Nucl. Phys. Proc. Suppl. **106**, 721 (2002); hep-lat/0110074
16. Y. Aoki et al., Phys. Rev. D **69**, 074504 (2004); hep-lat/0211023
17. K. Jansen, K. Nagai, JHEP **0312**, 038 (2003); hep-lat/0305009
18. Y. Iwasaki, UTHEP-118 (1983), unpublished.
19. T. Takaishi, Phys. Rev. D **54**, 1050 (1996); QCD-TARO Collaboration, P. de Forcrand et al., Nucl. Phys. Proc. Suppl. **53**, 938 (1997); hep-lat/9608094
20. RBC Collaboration, C. Dawson, Nucl. Phys. Proc. Suppl. **128**, 54 (2004); **129**, 167 (2004); hep-lat/0310055; RBC Collaboration, T. Izubuchi, Nucl. Phys. Proc. Suppl. **129**,

266 (2004); hep-lat/0310058; L. Levkova, R. Mawhinney, Nucl. Phys. Proc. Suppl. **129**, 399 (2004); hep-lat/0309122
21. JLQCD Collaboration, S. Aoki et al., Nucl. Phys. Proc. Suppl. **106**, 263 (2002); hep-lat/0110088
22. JLQCD Collaboration, S. Aoki et al., hep-lat/0409016
23. A. Ukawa, Nucl. Phys. Proc. Suppl. **53**, 106 (1997); hep-lat/9612011
24. M. Creutz, Talk given at RHIC Summer Study 96; hep-lat/9608024
25. P. Weisz, Nucl. Phys. B **212**, 1 (1983); P. Weisz, R. Wohlert, Nucl. Phys. B **236**, 397 (1984)
26. I. Montvay, Nucl. Phys. B **466**, 259 (1996); hep-lat/9510042
27. qq+q Collaboration, F. Farchioni, C. Gebert, I. Montvay, L. Scorzato, Eur. Phys. J. C **26**, 237 (2002); hep-lat/0206008
28. qq+q Collaboration, F. Farchioni, C. Gebert, I. Montvay, E Scholz, L. Scorzato, Phys. Lett. B **561**, 102 (2003); hep-lat/0302011
29. qq+q Collaboration, F. Farchioni, I. Montvay, E. Scholz, L. Scorzato, Eur. Phys. J. C **31**, 227 (2003); hep-lat/0307002
30. qq+q Collaboration, F. Farchioni, I. Montvay, E. Scholz, Eur. Phys. J. C **37**, 197 (2004); hep-lat/0403014
31. S. Necco, Nucl. Phys. B **683**, 137 (2004); hep-lat/0309017
32. R. Sommer, Nucl. Phys. B **411**, 839 (1994); hep-lat/9310022
33. E.M. Ilgenfritz, W. Kerler, M. Müller-Preussker, A. Sternbeck, H. Stüben, Phys. Rev. D **69**, 074511 (2004); hep-lat/0309057
34. E.M. Ilgenfritz, M.L. Laursen, G. Schierholz, M. Müller-Preussker, H. Schiller, Nucl. Phys. B **268**, 693 (1986)
35. R. Frezzotti, Nucl. Phys. Proc. Suppl. **119**, 140 (2003); hep-lat/0210007
36. M. Della Morte, R. Hoffmann, F. Knechtli, U. Wolff, Nucl. Phys. Proc. Suppl. **140**, 862 (2005); hep-lat/0409005
37. QCDSF Collaboration, R. Horsley et al., Nucl. Phys. B **693**, 3 (2004); hep-lat/0404007
38. K. Jansen, A. Shindler, C. Urbach, I. Wetzorke, Phys. Lett. B **586**, 432 (2004); hep-lat/0312013

[dbW-2]

Numerical simulations with two flavors of twisted-mass Wilson quarks and DBW2 gauge action

Eur. Phys. J. C47 453-472 (2006)

Eur. Phys. J. C 47, 453–472 (2006)
Digital Object Identifier (DOI) 10.1140/epjc/s2006-02549-y

THE EUROPEAN PHYSICAL JOURNAL C

Numerical simulations with two flavours of twisted-mass Wilson quarks and DBW2 gauge action

F. Farchioni[1], P. Hofmann[1], K. Jansen[2], I. Montvay[3,a], G. Münster[1], E.E. Scholz[3,b], L. Scorzato[4], A. Shindler[2], N. Ukita[3,c], C. Urbach[2,5,d], U. Wenger[2,e], I. Wetzorke[2]

[1] Universität Münster, Institut für Theoretische Physik, Wilhelm-Klemm-Strasse 9, 48149 Münster, Germany
[2] NIC/DESY Zeuthen, Platanenallee 6, 15738 Zeuthen, Germany
[3] Deutsches Elektronen-Synchrotron DESY, Notkestr. 85, 22603 Hamburg, Germany
[4] Institut für Physik, Humboldt Universität zu Berlin, 12489 Berlin, Germany
[5] Freie Universität Berlin, Institut für Theoretische Physik, Arnimallee 14, 14196 Berlin, Germany

Received: 19 December 2005 / Revised version: 21 March 2006 /
Published online: 7 June 2006 –

Abstract. Discretisation errors in two-flavour lattice QCD with Wilson quarks and DBW2 gauge action are investigated by comparing numerical simulation data at two values of the bare gauge coupling. Both non-zero- and zero-twisted-mass values are considered. The results, including also data from simulations using the Wilson plaquette gauge action, are compared to next-to-leading order chiral perturbation theory formulas.

1 Introduction

The singular point of QCD at vanishing quark masses is distorted in Wilson-type lattice formulations: as a result of lattice artefacts, in the region of small quark masses an extended phase structure is developed. This phase structure can be predicted and classified in chiral perturbation theory (ChPT) [1] if lattice artefacts are taken into account [2]. If, in addition to the usual quark mass parameter, a twisted quark mass is introduced [3, 4] then in the plane of untwisted and twisted quark mass a first order phase transition line with second order endpoints appears. Depending on the sign of the leading term representing lattice artefacts, the first order phase transition line is either on the untwisted quark mass axis ("Aoki phase scenario" [3]) or perpendicular to it ("normal scenario") [5–7].

In numerical simulations it pays off to try to reduce lattice artefacts at fixed (non-vanishing) lattice spacing by an appropriate choice of the lattice action. An important issue in this respect is to bring the phase structure at small quark masses as close as possible to the point-like singularity appearing in the continuum limit. In fact, the strong first order phase transition observed earlier in numerical simulations with Wilson-type quarks [8–10] presents a serious obstacle for QCD simulations with light quarks.

In previous work we systematically investigated the phase structure of lattice QCD with twisted-mass Wilson-type quarks (for a recent review see [11]). In [12] we have shown that at lattice spacings near $a \simeq 0.2\,\mathrm{fm}$ the phase structure with Wilson quarks and Wilson plaquette gauge action is consistent with the "normal scenario" of ChPT. This differs from the situation in the strong coupling regime, where the "Aoki phase scenario" has been previously observed [13].

A consequence of the "normal scenario" is that for fixed gauge coupling (β) the mass of charged pions have a positive lower bound ($m_\pi^{\min}$). The numerical simulation data in [12] have shown that this lower bound is at $a \simeq 0.2\,\mathrm{fm}$ quite high, namely about 600 MeV. Such a high lower bound would prohibit the study of light quarks. Therefore, an important question is the behaviour of this lower bound as a function of the gauge coupling (or lattice spacing) towards the continuum limit. In a subsequent paper it has been shown [14] that, as expected, the lower bound becomes clearly smaller for decreasing lattice spacing. Its decrease in the range $0.20\,\mathrm{fm} \geq a \geq 0.14\,\mathrm{fm}$ is roughly consistent with the prediction of next-to-leading order (NLO) ChPT [2, 5–7, 15], namely $m_\pi^{\min} \propto a$ (at $a\mu = 0$). A minimal pion mass of $m_\pi^{\min} \simeq 300\,\mathrm{MeV}$ is estimated to occur near $a \approx 0.07$–$0.10\,\mathrm{fm}$, but this estimate is rather uncertain and has to be checked in future simulations if the Wilson gauge action ought to be used. The question arises whether

[a] e-mail: montvay@mail.desy.de
[b] *Present address*: Physics Department, Brookhaven National Laboratory, Upton, NY 11973 USA
[c] *Present address*: Institute of Physics, University of Tsukuba, Tsukuba, Ibaraki 305-8571, Japan and Department of Physics, The University of Tokyo, Hongo 7-3-1, Bunkyo-ku, Tokyo 113-0033, Japan
[d] *Present address*: Theoretical Physics Division, Dept. of Mathematical Sciences, University of Liverpool, Liverpool L69 3BX, UK
[e] *Present address*: Institute for Theoretical Physics, ETH Zürich, 8093 Zürich, Switzerland

one could lower $m_\pi^{\min}$ by a suitable change of the lattice action.

An early observation by the JLQCD Collaboration has been [9] that the strength of the first order phase transition near zero quark mass is sensitive to a change of the gauge action. Following this hint, we have shown in a previous paper [16] that combining two flavours ($N_f = 2$) of Wilson quarks with the DBW2 gauge action [17] leads to a phase structure near zero quark mass with substantially weaker first order phase transition. As a consequence, the minimal pion mass is at least by a factor of two lower compared to the plaquette gauge action at similar lattice spacings.

This implies that numerical simulations with light quarks become possible on coarser lattices and hence with much less computational costs if the DBW2 gauge action is used. Of course, for the choice of the gauge action also other criteria may be relevant. For instance, it has been reported in quenched studies [18, 19] that in some quantities strong scale breaking effects appear if the DBW2 action is used. Another problem could be the late convergence of lattice perturbation theory, implied by the results of the QCDSF Collaboration [20].

In general, the question of the scaling behaviour of the results obtained by a given lattice action is very important. In case of the Wilson twisted-mass formulation of lattice QCD it has been shown [21] that the leading lattice artefacts are of $\mathcal{O}(a^2)$ if the bare quark masses are appropriately tuned. Detailed investigations have shown [22–24] that in the quenched approximation excellent scaling behaviour can be achieved, indeed, also at light quark masses. The same question in the full theory with dynamical quarks is obviously very important.

In the present paper we perform first exploratory scaling tests for the combination of Wilson fermion lattice action with the DBW2 gauge action by comparing numerical simulation data at two values of the gauge coupling, namely $\beta = 0.67$ and $\beta = 0.74$. We consider data points with both vanishing and non-vanishing value of the twisted mass. Moreover, since one can extract useful information on multiplicative renormalisation factors from the dependence of matrix elements on the twist angle in the plane of untwisted and twisted quark mass, we exploit this method and derive from our simulation data the values of Z_V, Z_A and Z_P/Z_S. In addition, we compare the NLO-ChPT formulas of [5–7, 15, 25] to the results of the numerical simulations. For comparison, ChPT fits of the data obtained by the Wilson plaquette gauge action [14] are also considered.

The outline of the paper is as follows: in the next section, after specifying the lattice action and the simulation algorithms, the numerical simulation runs are discussed and some scaling tests are presented. Section 3 is devoted to a detailed description of the results on the twist angle in the plane of untwisted and twisted quark mass together with an explanation how the aforementioned multiplicative renormalisation Z-factors can be determined. The knowledge of the twist angle and Z-factors makes it possible to obtain results on physical quantities, such as the quark mass and the pion decay constant. In Sect. 4 the ChPT fits of the data with DBW2 gauge action are presented. Section 5 contains a discussion and a summary. In an appendix alternative chiral fits of the DBW2 data are shown and compared to similar ChPT fits of Wilson plaquette data.

2 Numerical simulations

The lattice action and simulation algorithms are defined here for the reader's convenience. The notation is similar to the one in [16].

2.1 Lattice action and simulation algorithms

We apply for quarks the lattice action of Wilson fermions, which can be written as

$$S_{\rm q} = \sum_x \left\{ \left(\overline{\chi}_x [\mu_\kappa + {\rm i}\gamma_5 \tau_3 a\mu] \chi_x \right) - \frac{1}{2} \sum_{\mu=\pm 1}^{\pm 4} \left(\overline{\chi}_{x+\hat{\mu}} U_{x\mu} [r + \gamma_\mu] \chi_x \right) \right\} . \quad (1)$$

Here the ("untwisted") bare quark mass in lattice units is denoted by

$$\mu_\kappa \equiv a m_0 + 4r = \frac{1}{2\kappa} , \quad (2)$$

r is the Wilson parameter, set in our simulations to $r = 1$, am_0 is another convention for the bare quark mass in lattice units and κ is the conventional hopping parameter. The twisted mass in lattice units is denoted here by $a\mu$. (This differs from the notation in [16] where μ has been defined without the lattice spacing factor a in front.) $U_{x\mu} \in SU(3)$ is the gauge link variable and we also defined $U_{x,-\mu} = U^\dagger_{x-\hat{\mu},\mu}$ and $\gamma_{-\mu} = -\gamma_\mu$.

For the $SU(3)$ Yang–Mills gauge field we apply the DBW2 lattice action [17] which belongs to a one-parameter family of actions obtained by renormalisation group considerations. Those actions also include, besides the usual (1×1) Wilson loop plaquette term, planar rectangular (1×2) Wilson loops:

$$S_g = \beta \sum_x \left(c_0 \sum_{\mu<\nu;\, \mu,\nu=1}^{4} \left\{ 1 - \frac{1}{3} {\rm Re}\, U^{1\times 1}_{x\mu\nu} \right\} + c_1 \sum_{\mu\neq\nu;\, \mu,\nu=1}^{4} \left\{ 1 - \frac{1}{3} {\rm Re}\, U^{1\times 2}_{x\mu\nu} \right\} \right) , \quad (3)$$

with the condition $c_0 = 1 - 8c_1$. For the DBW2 action we have $c_1 = -1.4088$.

For preparing the sequences of gauge configurations two different updating algorithms were used: the hybrid Monte Carlo (HMC) algorithm [26] with multiple time scale integration and mass preconditioning as described in [27] and the two-step multi-boson (TSMB) algorithm [28] which has been tuned for QCD applications following [12, 29].

2.2 Simulation parameters and a first scaling test

In our numerical simulations we considered two values of the gauge coupling, namely $\beta = 0.67$ and $\beta = 0.74$. The simulations at the lower β-value have been performed on a $12^3 \cdot 24$ lattice as in [16]. The higher β-value ($\beta = 0.74$) was chosen in such a way that the physical volume of the $16^3 \cdot 32$ lattice remains approximately the same; that is, $a(\beta = 0.74) \simeq \frac{3}{4} a(\beta = 0.67)$. The value of the lattice spacing was defined by extrapolating the Sommer scale parameter in lattice units r_0/a [30] to zero quark mass and assuming $r_0 \equiv 0.5\,\mathrm{fm}$. The simulation parameters and the amount of statistics are specified in Table 1.

As Table 1 shows, both zero- and non-zero-twisted-mass points were simulated. The non-zero values of the twisted mass were also chosen according to the assumed scale ratio; that is, $a\mu(\beta = 0.74) = \frac{3}{4}\, a\mu(\beta = 0.67) = 0.0075$. In other words, the bare twisted mass μ is kept (approximately) constant.

In several points of the parameter space simulation runs have been performed with both the HMC and the TSMB updating algorithms. Having run the two algorithms in the same points allowed one to compare their performance. It turned out that the optimised HMC algorithm of [27] is substantially faster than TSMB. For instance, in long runs at the simulation point (A) ($16^3 \cdot 32$ lattice, $\beta = 0.74$, $\kappa = 0.1580$, $a\mu = 0$) HMC with multiple time scale integration and mass preconditioning is almost by a factor of 10 faster. Therefore, in the majority of simulation points the final data analysis is based on HMC runs. Results from TSMB updating were only used in the runs of the first part of Table 1 (those at $\beta = 0.67$ and $a\mu = 0$). Even if results with both updating algorithms were available in several other points, in the final analysis we never mixed results from different updating procedures.

Table 1. Run parameters: the gauge coupling (β), the twisted mass in lattice units ($a\mu$), the hopping parameter (κ) and the lattice size. The last column shows the number of gauge configurations used in the data analysis

run	β	$a\mu$	κ	$L^3 \times T$	N_{conf}
(a)	0.67	0	0.1650	$12^3 \times 24$	4514
(b)	0.67	0	0.1655	$12^3 \times 24$	2590
(c)	0.67	0	0.1660	$12^3 \times 24$	2589
(d)	0.67	0	0.1665	$12^3 \times 24$	1721
(a')	0.67	0.01	0.1650	$12^3 \times 24$	600
(b')	0.67	0.01	0.1655	$12^3 \times 24$	620
(c')	0.67	0.01	0.1660	$12^3 \times 24$	509
(d')	0.67	0.01	0.1665	$12^3 \times 24$	570
(e')	0.67	0.01	0.1670	$12^3 \times 24$	584
(f')	0.67	0.01	0.1675	$12^3 \times 24$	499
(g')	0.67	0.01	0.1680	$12^3 \times 24$	606
(A)	0.74	0	0.1580	$16^3 \times 32$	1319
(B)	0.74	0	0.1585	$16^3 \times 32$	419
(A')	0.74	0.0075	0.1580	$16^3 \times 32$	430
(B')	0.74	0.0075	0.1585	$16^3 \times 32$	296
(C')	0.74	0.0075	0.1590	$16^3 \times 32$	353
(D')	0.74	0.0075	0.1595	$16^3 \times 32$	352

The results for some basic quantities are collected in Tables 2 and 3. The pseudoscalar meson ("pion") mass am_π is obtained from the correlator of the charged pseudoscalar density

$$P_x^{\pm} = \bar{\chi}_x \frac{\tau^{\pm}}{2} \gamma_5 \chi_x \,, \tag{4}$$

Table 2. The results for the scale parameter (r_0/a), the pseudoscalar ("pion") mass am_π and the vector-meson ("ρ-meson") mass am_ρ

run	r_0/a	am_π	am_ϱ	m_π/m_ϱ	$r_0 m_\pi$	$(r_0 m_\pi)^2$
(a)	2.305(36)	0.4468(30)	0.7025(44)	0.6359(51)	1.030(19)	1.061(38)
(b)	2.391(56)	0.4085(55)	0.7007(79)	0.5831(66)	0.977(23)	0.954(44)
(c)	2.351(27)	0.3619(27)	0.629(10)	0.5747(84)	0.850(11)	0.724(19)
(d)	2.652(38)	0.235(12)	0.595(22)	0.396(18)	0.623(30)	0.389(37)
(a')	2.347(26)	0.4540(24)	0.7026(46)	0.6461(47)	1.065(12)	1.135(25)
(b')	2.415(24)	0.3981(40)	0.6808(66)	0.5847(61)	0.9618(25)	0.925(18)
(c')	2.503(29)	0.3449(40)	0.662(11)	0.520(10)	0.863(11)	0.745(18)
(d')	2.867(29)	0.2793(26)	0.654(45)	0.426(30)	0.801(16)	0.641(26)
(e')	3.127(31)	0.2937(32)	0.807(64)	0.363(29)	0.918(14)	0.844(25)
(f')	3.279(36)	0.3706(50)	0.913(72)	0.403(33)	1.215(23)	1.477(57)
(g')	3.261(31)	0.4514(84)	1.013(82)	0.444(36)	1.472(30)	2.168(88)
(A)	3.563(33)	0.3038(15)	0.5256(37)	0.5780(41)	1.082(11)	1.172(23)
(B)	3.741(90)	0.2250(29)	0.491(14)	0.457(13)	0.843(22)	0.711(36)
(A')	3.467(51)	0.3107(24)	0.5354(71)	0.5803(78)	1.077(17)	1.161(36)
(B')	3.78(10)	0.2429(36)	0.537(21)	0.451(18)	0.920(25)	0.846(46)
(C')	3.87(10)	0.1954(22)	0.57(14)	0.337(79)	0.756(31)	0.572(48)
(D')	4.148(65)	0.2620(38)	0.639(73)	0.409(48)	1.086(24)	1.181(52)

Table 3. The results for the PCAC quark mass ($am_\chi^{\rm PCAC}$) and pseudoscalar ("pion") decay constant ($af_{\chi\pi}$)

run	$am_\chi^{\rm PCAC}$	$r_0 m_\chi^{\rm PCAC}$	$af_{\chi\pi}$	$r_0 f_{\chi\pi}$
(a)	0.03884(22)	0.0895(14)	0.18567(90)	0.4279(62)
(b)	0.03224(71)	0.0771(18)	0.1798(17)	0.4301(98)
(c)	0.02247(80)	0.0528(20)	0.1553(27)	0.3653(75)
(d)	0.00972(43)	0.0258(11)	0.1369(65)	0.363(18)
(a')	0.03801(63)	0.0892(16)	0.05774(88)	0.1355(25)
(b')	0.02791(65)	0.0674(16)	0.0520(11)	0.1257(28)
(c')	0.01846(99)	0.0462(22)	0.0442(20)	0.1107(44)
(d')	0.00505(82)	0.0145(22)	0.0174(26)	0.0499(75)
(e')	−0.0109(2)	−0.0341(37)	−0.0354(37)	−0.110(12)
(f')	−0.0252(18)	−0.0829(62)	−0.0562(44)	−0.184(15)
(g')	−0.0409(17)	−0.1336(56)	−0.0683(30)	−0.2229(98)
(A)	0.02313(23)	0.0824(10)	0.1243(12)	0.4429(58)
(B)	0.01251(43)	0.0469(24)	0.1124(37)	0.420(22)
(A')	0.02247(33)	0.0779(16)	0.03645(60)	0.1264(28)
(B')	0.01093(49)	0.0414(21)	0.0266(12)	0.1007(46)
(C')	−0.00120(18)	−0.0046(29)	−0.0043(18)	−0.016(11)
(D')	−0.01635(66)	−0.06783(29)	−0.0361(16)	−0.1500(71)

where $\tau_\pm \equiv \tau_1 \pm \mathrm{i}\tau_2$. In case of the vector meson ("ρ-meson") mass am_ρ, for generic values of the bare untwisted and twisted quark mass, the correlators of both vector ($V^a_{x\mu}$) and axial-vector ($A^a_{x\mu}$) bilinears of the χ-fields can be used:

$$V^a_{x\mu} \equiv \overline{\chi}_x \frac{1}{2}\tau_a \gamma_\mu \chi_x \,,$$
$$A^a_{x\mu} \equiv \overline{\chi}_x \frac{1}{2}\tau_a \gamma_\mu \gamma_5 \chi_x \quad (a = 1, 2)\,. \tag{5}$$

The reason is that the physical vector current is, in general, a linear combination of $V^a_{x\mu}$ and $A^a_{x\mu}$ (see Sect. 3). In a given simulation point we determined am_ρ from the correlator possessing the better signal.

In Table 3 the values of the bare (untwisted) PCAC quark mass $am_\chi^{\rm PCAC}$ are also given. It is defined by the PCAC-relation containing the axial-vector current $A^a_{x\mu}$ in (5) and the pseudoscalar density $P^\pm_x$:

$$am_\chi^{\rm PCAC} \equiv \frac{\langle \partial^*_\mu A^+_{x\mu} P^-_y \rangle}{2\langle P^+_x P^-_y \rangle}\,. \tag{6}$$

Here ∂^*_μ denotes, as usual, the backward lattice derivative.

Besides $am_\chi^{\rm PCAC}$, Table 3 also contains the values of the bare "untwisted" pseudoscalar decay constant $af_{\chi\pi}$ defined by

$$af_{\chi\pi} \equiv (am_\pi)^{-1} \langle 0 \left| A^+_{x=0,0} \right| \pi^- \rangle\,. \tag{7}$$

The relation of the bare (untwisted) quantities $am_\chi^{\rm PCAC}$ and $af_{\chi\pi}$ to the corresponding physical quantities will be discussed in the following section.

The squared ratio of the pion mass to the ρ-meson mass is plotted in Fig. 1 as a function of $(r_0 m_\pi)^2$, both of which are expected to be approximately proportional to the quark mass for small quark masses. (This holds if the effect of the "chiral logarithms" is negligible in the quark mass depedence of m_π^2 and if r_0 is approximately constant near zero as a function of the quark mass.) The straight line in the figure connects the origin and the point with the physical values $m_\pi = 140$ MeV, $m_\rho = 770$ MeV and $r_0 =$

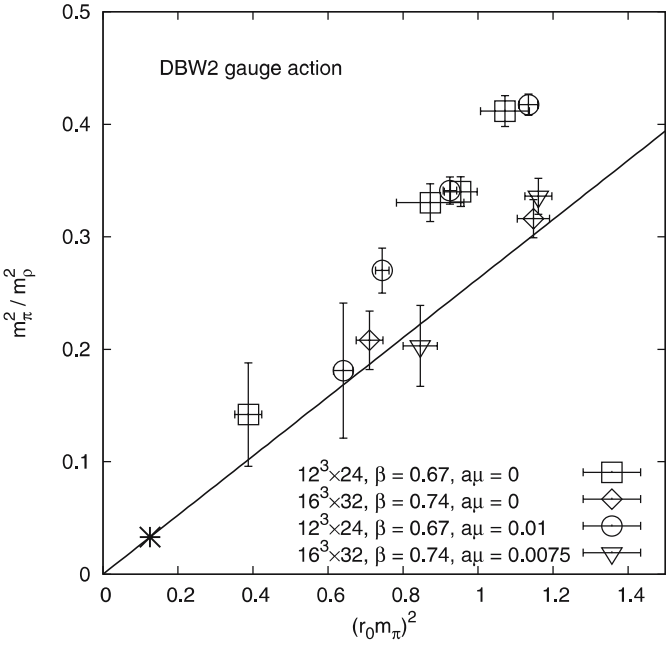

Fig. 1. The squared pion to ρ-meson mass ratio $(m_\pi/m_\rho)^2$ versus $(r_0 m_\pi)^2$. Only simulation points with positive quark mass are considered. The physical point is shown by an *asterisk*. The *straight line* connecting the origin with it is the continuum expectation for small quark masses where both quantities are approximately proportional to the quark mass

0.5 fm. As the figure shows, in this plot there are observable scale breaking effects between $\beta = 0.67$ and $\beta = 0.74$, but the $\beta = 0.74$ points are already close to the continuum expectation. Within the (large) statistical errors there is no noticeable difference between the points with vanishing and non-vanishing twisted mass. (According to Table 9 the twisted-mass values are given by $r_0\mu = 0.02845(68)$ and $r_0\mu = 0.0283(15)$ for $\beta = 0.67$ and $\beta = 0.74$, respectively.)

3 Twist angle and renormalisation factors

3.1 Twist angle

In this section we discuss the determination of the twist angle ω. For given $(\mu_\kappa, a\mu)$ this is defined as the rotation angle relating twisted-mass QCD (TMQCD) to the physical theory QCD. An important point is that the connection can be made only after (lattice) renormalisation of the theory. The renormalisation of the local bilinears in the Wilson twisted-mass formulation is therefore involved. Some of the arguments of this section were already discussed in previous publications of this collaboration [16, 31].

Following [32] we operationally define [16, 31] the twist angle ω as the chiral rotation angle between the renormalised (physical) chiral currents and the corresponding bilinears of the twisted formulation. We denote with $\hat{V}^a_{x\mu}$ and $\hat{A}^a_{x\mu}$ the physical vector and axial-vector currents, while $V^a_{x\mu}$ and $A^a_{x\mu}$ are the bilinears of the χ-fields defined in (5). In order to establish the correspondence with the physical currents, the bilinears of the χ-fields have to be properly renormalised. This is obtained, as in QCD, by multiplying them by the respective renormalisation constants Z_V and Z_A. In a mass independent scheme these are functions of β alone and coincide with the analogous quantities in Wilson lattice QCD for the same value of β. So the relation reads

$$\hat{V}^a_{x\mu} = Z_V V^a_{x\mu} \cos\omega + \epsilon_{ab} Z_A A^b_{x\mu} \sin\omega \,, \tag{8}$$

$$\hat{A}^a_{x\mu} = Z_A A^a_{x\mu} \cos\omega + \epsilon_{ab} Z_V V^b_{x\mu} \sin\omega \,, \tag{9}$$

where only charged currents are considered ($a = 1, 2$) and ϵ_{ab} is the antisymmetric unit tensor.

The conserved vector current of the χ-fields

$$\tilde{V}^a_{x\mu} \equiv \frac{1}{4}\left(\overline{\chi}_{x+\mu}\tau_a\, U_{x\mu}(\gamma_\mu + r)\chi_x + \overline{\chi}_x \tau_a\, U^\dagger_{x\mu}(\gamma_\mu - r)\chi_{x+\mu}\right) \tag{10}$$

satisfies by construction the correct Ward–Takahashi identity of the continuum. In this case (8) and (9) apply with Z_V replaced by 1; in particular,

$$\hat{A}^a_{x\mu} = Z_A\, A^a_{x\mu} \cos\omega + \epsilon_{ab} \tilde{V}^b_{x\mu} \sin\omega \,. \tag{11}$$

In practical applications it is useful to define two further angles ω_V and ω_A:

$$\begin{aligned} \omega_V &= \arctan(Z_A Z_V^{-1} \tan\omega) \,, \\ \omega_A &= \arctan(Z_V Z_A^{-1} \tan\omega) \,. \end{aligned} \tag{12}$$

In terms of ω_V and ω_A, (8) and (9) read

$$\hat{V}^a_{x\mu} = \mathcal{N}_V \left(\cos\omega_V V^a_{x\mu} + \epsilon_{ab} \sin\omega_V A^b_{x\mu}\right) , \tag{13}$$

$$\hat{A}^a_{x\mu} = \mathcal{N}_A \left(\cos\omega_A A^a_{x\mu} + \epsilon_{ab} \sin\omega_A V^b_{x\mu}\right) . \tag{14}$$

The unknown multiplicative renormalisations are now contained in an overall factor ($X = V, A$):

$$\mathcal{N}_X = \frac{Z_X}{\cos\omega_X \sqrt{1 + \tan\omega_V \tan\omega_A}} \,. \tag{15}$$

From the definition (12) it follows that

$$\omega = \arctan\left(\sqrt{\tan\omega_V \tan\omega_A}\right) \tag{16}$$

$$\frac{Z_A}{Z_V} = \sqrt{\tan\omega_V / \tan\omega_A} \,. \tag{17}$$

As already proposed in [16, 31], we determine the twist angle ω by imposing parity-restoration (up to $\mathcal{O}(a)$ precision) for matrix elements of the physical currents. Due to the presence of unknown lattice renormalisations, two conditions are required. The most suitable choice in the case of the vector current is

$$\sum_{\mathbf{x}} \left\langle \hat{V}^+_{x0}\, P^-_y \right\rangle = 0 \,. \tag{18}$$

Indeed, for asymptotic times, the pion state dominates the matrix element[1] and the condition reads

$$\left\langle 0 \middle| \hat{V}^+_{x0} \middle| \pi^- \right\rangle = 0 \,. \tag{19}$$

In case of the axial-vector current we choose the condition[2]

$$\sum_{\mathbf{x},i} \left\langle \hat{A}^+_{xi} \hat{V}^-_{xi} \right\rangle = 0 \tag{20}$$

or asymptotically

$$\left\langle 0 \middle| \hat{A}^+_{xi} \middle| \rho^- \right\rangle = 0 \,. \tag{21}$$

In terms of (13) and (14), (18) and (20) admit the solution

$$\tan\omega_V = -\mathrm{i} \frac{\sum_{\mathbf{x}} \left\langle V^+_{x0} P^-_y \right\rangle}{\sum_{\mathbf{x}} \left\langle A^+_{x0} P^-_y \right\rangle} \,, \tag{22}$$

$$\tan\omega_A = \frac{-\mathrm{i} \sum_{\mathbf{x},i} \left\langle A^+_{xi} V^-_{yi} \right\rangle + \tan\omega_V \sum_{\mathbf{x},i} \left\langle A^+_{xi} A^-_{yi} \right\rangle}{\sum_{\mathbf{x},i} \left\langle V^+_{xi} V^-_{yi} \right\rangle + \mathrm{i} \tan\omega_V \sum_{\mathbf{x},i} \left\langle V^+_{xi} A^-_{yi} \right\rangle} \,. \tag{23}$$

[1] At small time separations, due to the $\mathcal{O}(a)$ breaking of parity, intermediate states with "wrong" parity may still play a role.

[2] In [16, 31] the use of the temporal component for the currents was proposed. This choice is however not optimal: a scalar state with positive parity dominates in this case the matrix element in the continuum limit, but at finite lattice spacing the $\mathcal{O}(a)$ breaking of parity introduces contamination by pion intermediate states which eventually dominate for light quark masses.

Equations (16), (17), (22) and (23) allow for the numerical determination of ω and of the ratio Z_A/Z_V.

It is obvious that the definition of the twist angle in the lattice theory is subject to $\mathcal{O}(a)$ ambiguities. Different choices of the parity-restoration conditions, including also the form of the lattice currents, result in different definitions of the twist angle differing by $\mathcal{O}(a)$ terms. The situation of full twist corresponds to $\omega = \omega_V = \omega_A = \pi/2$. Numerically it is most convenient to use $\omega_V = \pi/2$ as a criterion. The reason is that a safe determination of the twist angle is obtained in the asymptotic regime where the lightest particle dominates as intermediate state. This is the pseudoscalar state in the case of ω_V which, as one would expect, delivers a better signal than the vector meson in case of ω_A. Therefore we impose [16, 31]

$$\omega_V = \frac{\pi}{2} \Longleftrightarrow \sum_{\mathbf{x}} \left\langle A^+_{x0} P^-_y \right\rangle = 0 \tag{24}$$

or asymptotically

$$\left\langle 0|A^+_{x0}|\pi^-\right\rangle = 0\,, \tag{25}$$

and we denote by $\mu_{\kappa \mathrm{cr}}$ the corresponding value of μ_κ for the given μ.

Another possible determination of ω_V is obtained by replacing in (22) the currents with their divergences. For simplicity, we consider the case of the conserved vector current which avoids the introduction of a renormalisation constant:

$$\cot\tilde{\omega}_V = \mathrm{i}\frac{\sum_{\mathbf{x}} \left\langle \partial^*_\mu A^+_{x\mu} P^-_y \right\rangle}{\sum_{\mathbf{x}} \left\langle \partial^*_\mu \tilde{V}^+_{x\mu} P^-_y \right\rangle} = \frac{m_\chi^{\mathrm{PCAC}}}{\mu}\,. \tag{26}$$

Here in the last step [7, 15] the Ward identity for the conserved vector current

$$\partial^*_\mu \tilde{V}^+_{x\mu} = 2\mathrm{i}\mu P^+_x \tag{27}$$

and the definition (6) of the "untwisted" PCAC quark mass m_χ^{PCAC} have been used. If the local vector current defined in (5) is used for the determination of ω_V instead of the conserved one, in (26) the introduction of the renormalisation constant Z_V is required. In this case one has

$$\cot\omega_V = \mathrm{i}\frac{\sum_{\mathbf{x}} \left\langle \partial^*_\mu A^+_{x\mu} P^-_y \right\rangle}{\sum_{\mathbf{x}} \left\langle \partial^*_\mu V^+_{x\mu} P^-_y \right\rangle} = Z_V \frac{m_\chi^{\mathrm{PCAC}}}{\mu}\,, \tag{28}$$

where Z_V is determined as explained in the next subsection. Using the definition (12) for ω_V one arrives at the following relation involving this time the twist angle ω:

$$\cot\omega = Z_A \frac{m_\chi^{\mathrm{PCAC}}}{\mu}\,. \tag{29}$$

Notice that the factor Z_V cancels in this relation, which is, therefore, independent of the choice for the vector current employed for the determination of the twist angle ω.

One can simply show that the two determinations of ω_V given by (22) and (28) coincide under the assumption that the ratio of the correlators is independent of the time separation; this is in particular true for asymptotic times where the pion dominates.

To have an effective automatic $\mathcal{O}(a)$ improvement, meaning without large $\mathcal{O}(a^2)$ effects, the critical line $(\mu_{\kappa\mathrm{cr}}(a,\mu),\mu)$ has to be fixed in such a way that the lattice definition of the untwisted quark mass (e.g. m_χ^{PCAC} defined above) is free, on that line, from mass independent $\mathcal{O}(a)$ errors. For a definition of the critical line where this condition is not necessarily satisfied, one has to make sure that $\mu > a\Lambda^2$.

The issue of the choice of the critical untwisted mass has been raised by the work of Aoki and Bär [33] and by the numerical results obtained in [34]. This problem has been further analysed in several aspects [15, 35, 36]. In [15, 33, 36] the theoretical framework is twisted-mass chiral perturbation theory (tmChPT) [25] where the cutoff effects are included in the chiral lagrangian along the lines of [2, 46]. The works [15, 33] agree on the fact that choosing the critical mass by imposing $m_\chi^{\mathrm{PCAC}} = 0$ (or $\omega_V = \pi/2$) allows one to have automatic $\mathcal{O}(a)$ improvement down to quark masses that fulfill $\mu \simeq a^2\Lambda^3$. In [35] a Symanzik expansion was performed (in an approach different from that of [15, 33], cf. [15] for a discussion) confirming the results of [15, 33]. For a discussion of these issues in numerical studies within the quenched approximation see [22–24] and the review [11].

3.2 Determination of Z_V

We adopt here the procedure well known in QCD which relies on the non-renormalisation property of the conserved current $\tilde{V}_{x\mu}$ [38]. A possible determination of Z_V in TMQCD is given by

$$Z_V^{(1)} = \frac{\left\langle 0|\tilde{V}^+_{x=0,0}|\pi^-\right\rangle}{\left\langle 0|V^+_{x=0,0}|\pi^-\right\rangle}\,. \tag{30}$$

Note that in TMQCD the time component of the vector current couples the vacuum to the pseudoscalar particle: in the most interesting region near full twist this coupling is maximal. (Note that at $a\mu = 0$ the analogous procedure has to rely on the noisier matrix element with the vector particle or on three point functions.) Alternatively Z_V can be determined without direct use of the conserved current by exploiting the (exact) Ward identity for the vector current. This implies [39]

$$\left\langle 0|\tilde{V}^+_{x=0,0}|\pi^-\right\rangle = \frac{-2\mathrm{i}\mu}{m_\pi}\left\langle 0|P^+_{x=0}|\pi^-\right\rangle\,. \tag{31}$$

Inserting the above relation in (30) a second determination of Z_V is obtained:

$$Z_V^{(2)} = \frac{-2\mathrm{i}\mu\left\langle 0|P^+_{x=0}|\pi^-\right\rangle}{m_\pi\left\langle 0|V^+_{x=0,0}|\pi^-\right\rangle}\,. \tag{32}$$

$Z_V^{(1)}$ and $Z_V^{(2)}$ (differing by $\mathcal{O}(a)$ terms) are mass dependent renormalisations. We obtain a mass independent

determination of Z_V by extrapolating $Z_V^{(i)}$ to full twist ($m_\chi^{\rm PCAC}=0$). In this situation the theory is $\mathcal{O}(a)$ improved and the $Z_V^{(i)}$ deliver an estimate of Z_V with $\mathcal{O}(a^2)$ error (also including $\mathcal{O}((\mu a)^2)$ terms).

3.3 Physical quantities

The knowledge of the twist angle ω allows for the derivation of physical quantities of interest in QCD for a generic choice of $(\mu_\kappa, a\mu)$. Let us consider the case of the quark mass and the pion decay constant. It is convenient [22, 39, 40] here to use the conserved vector current since it possesses already the right continuum normalisation. The physical PCAC quark mass $m_q^{\rm PCAC}$ can be obtained from the Ward identity for the physical axial-vector current:

$$\left\langle \partial^*_\mu \hat{A}^+_{x\mu} P^-_y \right\rangle = 2am_q^{\rm PCAC} \left\langle P^+_x P^-_y \right\rangle . \tag{33}$$

We use (8) in order to eliminate $A^a_{x\mu}$ in (11) for $\omega \neq 0$

$$\hat{A}^a_{x\mu} = -\epsilon_{ab}\hat{V}^b_{x\mu}\cot\omega + \epsilon_{ab}\tilde{V}^b_{x\mu}(\sin\omega)^{-1} \tag{34}$$

and insert the result in the Ward identity (33) using isospin invariance for $\hat{V}^a_{x\mu}$. As a result we obtain

$$am_q^{\rm PCAC} = \frac{-{\rm i}}{2\sin\omega}\frac{\left\langle \partial^*_\mu \tilde{V}^+_{x\mu} P^-_y \right\rangle}{\left\langle P^+_x P^-_y \right\rangle} = \frac{\mu}{\sin\omega} , \tag{35}$$

where in the last step we used once again the Ward identity (27). Inserting (29) into the last expression in the above equation, we arrive at the following relation for the untwisted quark mass:

$$m_\chi^{\rm PCAC} = m_q^{\rm PCAC} Z_A^{-1}\cos\omega . \tag{36}$$

In the remainder we shall also make use of a definition of the untwisted quark mass which already incorporates the renormalisation factor of the axial current:

$$\bar{m}_\chi^{\rm PCAC} = m_q^{\rm PCAC}\cos\omega = Z_A m_\chi^{\rm PCAC} . \tag{37}$$

Analogously, for the physical pion decay constant f_π we use

$$\begin{aligned} af_\pi &= (am_\pi)^{-1}\left\langle 0|\hat{A}^+_{x=0,0}|\pi^-\right\rangle \\ &= -{\rm i}(am_\pi\sin\omega)^{-1}\left\langle 0|\tilde{V}^+_{x=0,0}|\pi^-\right\rangle . \end{aligned} \tag{38}$$

Also here the matrix element on the right hand side can be replaced by the matrix element of the pseudoscalar density as in (31) giving

$$af_\pi = \frac{-2a\mu}{(am_\pi)^2\sin\omega}\left\langle 0|P^+_{x=0}|\pi^-\right\rangle . \tag{39}$$

Let us note that here the normalisation of f_π corresponds to a phenomenological value ≈ 130 MeV. If the local vector current is used in (38) instead of the conserved one, a factor Z_V is missing:

$$\begin{aligned} af_{v\pi} &= -{\rm i}(am_\pi\sin\omega)^{-1}\left\langle 0|V^+_{x=0,0}|\pi^-\right\rangle , \\ f_{v\pi} &= Z_V^{-1} f_\pi . \end{aligned} \tag{40}$$

3.4 Results

In Fig. 2 the local determination of ω_V and ω_A is shown as a function of the time separation for a specific simulation point at positive untwisted quark mass. The numerical values of the twist angles ω_V, ω_A and ω are reported in Table 4. Notice that the simulation point at $\beta=0.74$ and $\kappa=0.159$ is almost at full twist.

Figures 3 and 4 show the determinations of $\mu_{\kappa{\rm cr}}$ by extrapolating $m_\chi^{\rm PCAC}$ and $\cot\omega_V$ to zero. The theoretical dependence of the twist angle upon the untwisted bare quark mass μ_κ can be obtained [16] by starting from [37]

$$\cot\omega = \frac{m_{\chi{\rm R}}}{\mu_{\rm R}} + \mathcal{O}(a) , \tag{41}$$

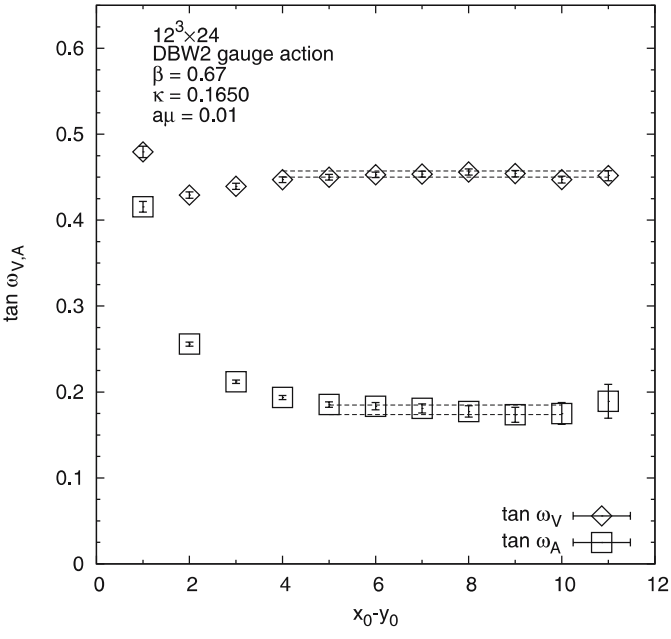

Fig. 2. Determination of $\tan\omega_V$ and $\tan\omega_A$ as in (22) and (23) for the point (a'). The *lines* represent the fitted values

Table 4. The twist angles ω, ω_V and ω_A, as defined in (8), (9) and (12), determined by (22), (23) and (16)

β	$a\mu$	κ	ω_V/π	ω_A/π	ω/π
0.67	$1.0\cdot10^{-2}$	0.1650	0.1352(13)	0.0564(17)	0.0883(13)
0.67	$1.0\cdot10^{-2}$	0.1655	0.1772(29)	0.0771(27)	0.1190(25)
0.67	$1.0\cdot10^{-2}$	0.1660	0.2412(62)	0.1069(41)	0.1661(54)
0.67	$1.0\cdot10^{-2}$	0.1665	0.411(12)	0.229(17)	0.334(17)
0.67	$1.0\cdot10^{-2}$	0.1670	0.678(12)	0.622(16)	0.647(11)
0.67	$1.0\cdot10^{-2}$	0.1675	0.8053(86)	0.826(13)	0.8137(80)
0.67	$1.0\cdot10^{-2}$	0.1680	0.8709(43)	0.843(23)	0.857(11)
0.74	$7.5\cdot10^{-3}$	0.1580	0.1542(26)	0.0722(38)	0.1076(31)
0.74	$7.5\cdot10^{-3}$	0.1585	0.2613(66)	0.1393(96)	0.1963(77)
0.74	$7.5\cdot10^{-3}$	0.1590	0.532(12)	0.582(37)	0.5544(92)
0.74	$7.5\cdot10^{-3}$	0.1597	0.7966(49)	0.790(15)	0.794(12)

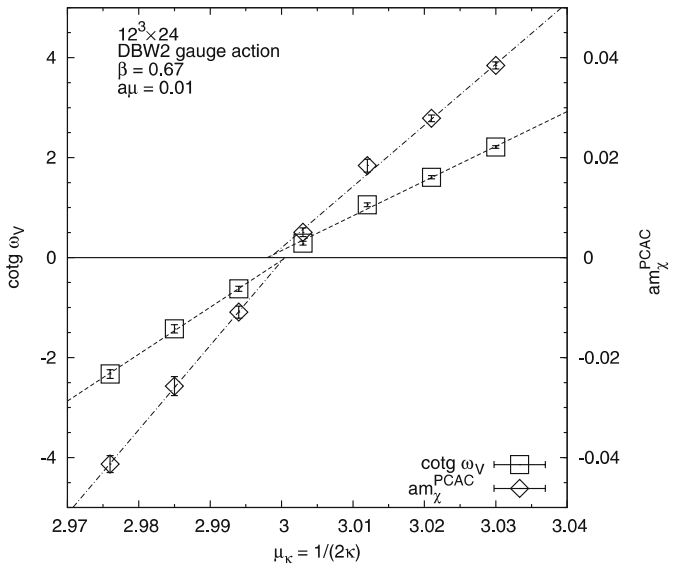

Fig. 3. Determination of $\mu_{\kappa \mathrm{cr}}$ at $\beta = 0.67$, $a\mu = 0.01$ by parity-restoration and by extrapolating the untwisted PCAC quark mass m_χ^{PCAC} to zero

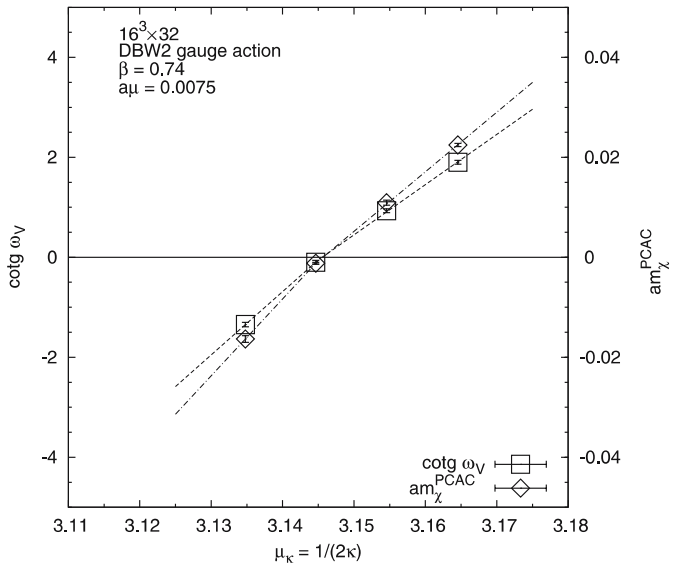

Fig. 4. Determination of $\mu_{\kappa \mathrm{cr}}$ at $\beta = 0.74$, $a\mu = 0.0075$ by parity-restoration and by extrapolating the untwisted PCAC quark mass m_χ^{PCAC} to zero

where μ_{R} and $m_{\chi \mathrm{R}}$ are the renormalised twisted and untwisted quark masses in the continuum limit

$$\mu_{\mathrm{R}} = Z_P^{-1}\mu\,, \tag{42}$$

$$m_{\chi \mathrm{R}} = a^{-1} Z_S^{-1}(\mu_\kappa - \mu_{\kappa \mathrm{cr}})\,. \tag{43}$$

Observe that the relation (41) holds up to $\mathcal{O}(a)$ terms because the right hand side of the relation corresponds to a different definition of the twist angle compared to the one given in Sect. 3.1. The two definitions only coincide in the continuum limit. By using the first of equations (12) one obtains for ω_V [16]

$$\cot\omega_V = (Z_{oV}\mu)^{-1}(\mu_\kappa - \mu_{\kappa \mathrm{cr}}) + \mathcal{O}(a) \tag{44}$$

$$Z_{oV} = Z_S Z_A Z_P^{-1} Z_V^{-1}\,. \tag{45}$$

Note that the angular coefficient of the linear fit gives the finite combination of renormalisation factors Z_{oV}. Using as an input the determination of Z_A/Z_V in (17) one can obtain from this the combination Z_P/Z_S.

We use (44) for a linear fit to $\mu_{\kappa \mathrm{cr}}$ and Z_{oV}; see Table 5 for the results. As expected from the discussion in Sect. 3.1, the condition $m_\chi^{\mathrm{PCAC}} = 0$ gives results very close to those from the parity-restoration condition $\cot\omega_V = 0$. We conclude that the two methods are essentially equivalent also from the numerical point of view. A discrepancy is observed between the extrapolation from positive and negative quark masses for the simulation point $\beta = 0.67$: we interpret this as a residual effect of the first order phase transition at the given value of the lattice spacing. (Whether first order phase transition or "cross-over" can only be decided in a study of the infinite volume limit.) Observe also that the Z_{oV} comes out different for the two different signs of the quark mass: this is due to the breaking of symmetry under reflection of the untwisted quark mass induced by $\mathcal{O}(a)$ terms [36]. The numerical discrepancy shows that these $\mathcal{O}(a)$ corrections are relevant. An $\mathcal{O}(a)$-improved estimate of Z_{oV} is simply obtained by averaging the determinations for negative and positive quark masses, corresponding to a Wilson average for the quantity under study. An analogous observation can be done for

Table 5. Determination of $\mu_{\kappa \mathrm{cr}}$ by requiring $\omega = \pi/2$, $\mu_{\kappa \mathrm{cr}}(\omega_V)$, or $m_\chi^{\mathrm{PCAC}} = 0$, $\mu_{\kappa \mathrm{cr}}(m_\chi^{\mathrm{PCAC}})$. The *plus* and *minus* signs indicate extrapolations from positive or negative untwisted quark masses m_χ^{PCAC}, avg denotes the average

β	$a\mu$	sign	$\mu_{\kappa \mathrm{cr}}(\omega_V)$	$\mu_{\kappa \mathrm{cr}}(m_\chi^{\mathrm{PCAC}})$	Z_{oV}
0.67	$1.0 \cdot 10^{-2}$	+	2.99800(9)	2.99839(12)	1.438(33)
0.67	$1.0 \cdot 10^{-2}$	−	3.00059(13)	3.00043(17)	1.065(61)
0.67	$1.0 \cdot 10^{-2}$	avg	2.99930(11)	2.99941(15)	1.251(47)
0.74	$7.5 \cdot 10^{-3}$	+	3.145528(52)	3.145645(22)	1.328(36)
0.74	$7.5 \cdot 10^{-3}$	−	3.145441(52)	3.145435(21)	1.055(49)
0.74	$7.5 \cdot 10^{-3}$	avg	3.145484(52)	3.145540(22)	1.191(42)

Table 6. Renormalisation constants of the vector and axial-vector currents. The ratio Z_A/Z_V is determined from the analysis of the twist angles, cf. (16); two different determinations of the vector current Z_V are reported: $Z_V^{(1)}$ from (30) and $Z_V^{(2)}$ from (32); the renormalisation constant of the axial-vector current is derived by combining the results for Z_A/Z_V and $Z_V^{(1)}$

β	$a\mu$	κ	Z_A/Z_V	$Z_V^{(1)}$	$Z_V^{(2)}$	Z_A
0.67	$1.0 \cdot 10^{-2}$	0.1650	1.589(26)	0.5910(13)	0.5810(16)	0.939(15)
0.67	$1.0 \cdot 10^{-2}$	0.1655	1.587(28)	0.5813(11)	0.5761(25)	0.923(16)
0.67	$1.0 \cdot 10^{-2}$	0.1660	1.649(28)	0.5766(12)	0.5708(38)	0.951(16)
0.67	$1.0 \cdot 10^{-2}$	0.1665	1.979(68)	0.5689(10)	0.5657(39)	1.126(39)
0.67	$1.0 \cdot 10^{-2}$	0.1670	0.815(58)	0.5705(14)	0.5666(46)	0.465(33)
0.67	$1.0 \cdot 10^{-2}$	0.1675	1.087(47)	0.5716(32)	0.5688(38)	0.623(27)
0.67	$1.0 \cdot 10^{-2}$	0.1680	0.894(78)	0.5851(33)	0.5754(43)	0.518(46)
0.74	$7.5 \cdot 10^{-3}$	0.1580	1.508(35)	0.6379(12)	0.6315(32)	0.963(22)
0.74	$7.5 \cdot 10^{-3}$	0.1585	1.515(59)	0.6294(11)	0.6294(38)	0.953(37)
0.74	$7.5 \cdot 10^{-3}$	0.1590	1.65(45)	0.62595(95)	0.6241(38)	1.04(28)
0.74	$7.5 \cdot 10^{-3}$	0.1597	0.972(73)	0.6291(25)	0.6242(40)	0.612(46)

other combinations of renormalisation constants (see the following).

Table 6 reports the determination of the renormalisation constants of the vector and axial-vector currents Z_V and Z_A. The ratio Z_A/Z_V comes from the analysis of the the twist angles, (17). Using the direct estimate of Z_V by (30) we can also determine Z_A. Observe that the full twist extrapolations of Z_A/Z_V from the two quark mass signs present large discrepancies, which in this case cannot be attributed to $\mathcal{O}(a)$ effects (these should disappear at full twist). A possible explanation of the discrepancy could reside in the relatively bad quality of the data in the negative mass region. The discrepancies in Z_A and Z_P/Z_S are a consequence of that for Z_A/Z_V. In the light of these considerations we rely on the determinations for positive quark masses.

The full twist extrapolations of Z_V are shown in Figs. 5 and 6: the values from the two signs of the quark mass are rather close, compatible with each other within statistical uncertainty. For the case $\beta = 0.74$ the extrapolation is very short, see Table 7 for the numerical values with comparison with one-loop perturbative estimates [41]. Table 7 also includes the determinations of the ratio Z_P/Z_S from Z_{oV} (see (44) and (45)). This quantity is of particular interest for simulations [42] of the theory with an additional mass-split doublet describing the strange and charm quarks [43].

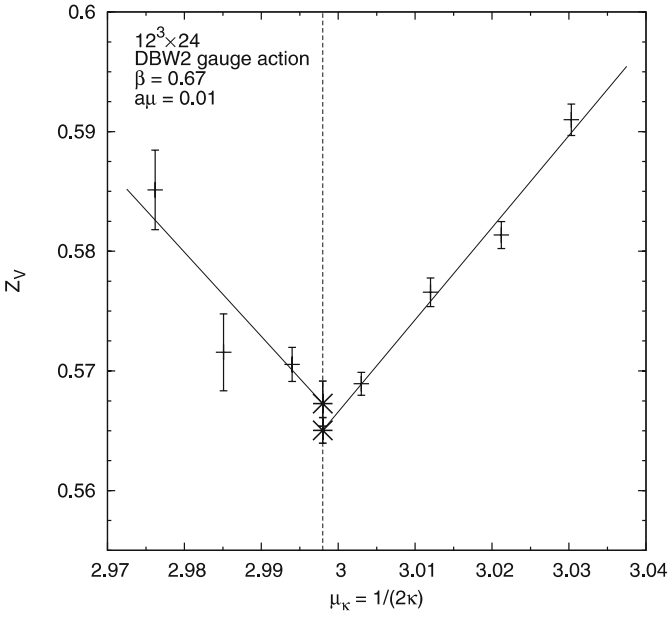

Fig. 5. Full twist extrapolation of $Z_V^{(1)}$ at $\beta = 0.67$, $a\mu = 0.01$

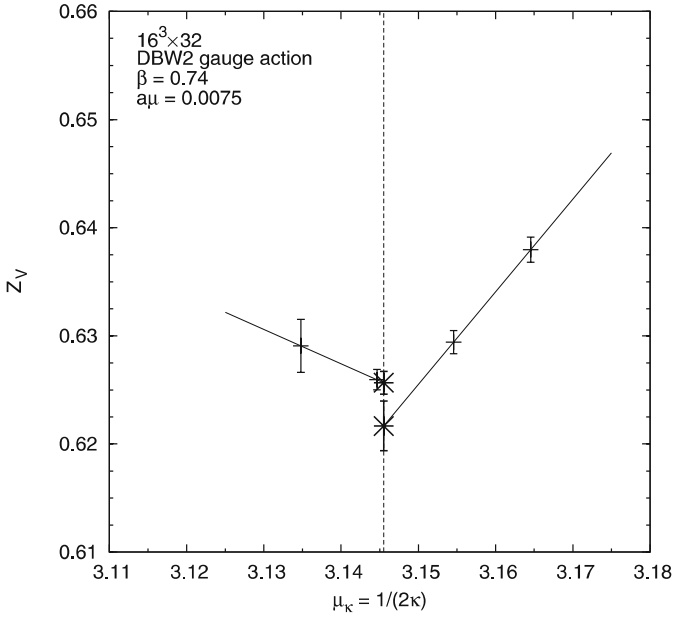

Fig. 6. Full twist extrapolation of $Z_V^{(1)}$ at $\beta = 0.74$, $a\mu = 0.0075$

Table 7. Full twist extrapolations for Z_V, Z_A and the ratio Z_A/Z_V (see text for explanation) with comparison with one-loop perturbative estimates (PT) and tadpole-improved perturbative estimates (TI) [41]. The ratio Z_P/Z_S is also reported, determined from Z_{oV} (see (44) and (45))

β	$a\mu$	Sign	Op.	Z	Z(PT)	Z(TI)
0.67	$1.0 \cdot 10^{-2}$	+	V	0.5650(11)	0.6089	0.6531
0.67	$1.0 \cdot 10^{-2}$	–	V	0.5673(19)	0.6089	0.6531
0.74	$7.5 \cdot 10^{-3}$	+	V	0.6217(23)	0.6459	0.6892
0.74	$7.5 \cdot 10^{-3}$	–	V	0.6257(10)	0.6459	0.6892
0.67	$1.0 \cdot 10^{-2}$	+	A	0.952(30)	0.7219	0.7176
0.67	$1.0 \cdot 10^{-2}$	–	A	0.49(4)	0.7219	0.7176
0.74	$7.5 \cdot 10^{-3}$	+	A	0.944(74)	0.7482	0.7735
0.74	$7.5 \cdot 10^{-3}$	–	A	0.612(46)	0.7482	0.7735
0.67	$1.0 \cdot 10^{-2}$	+	A/V	1.683(52)	1.1130	0.9696
0.67	$1.0 \cdot 10^{-2}$	–	A/V	0.867(70)	1.1130	0.9696
0.74	$7.5 \cdot 10^{-3}$	+	A/V	1.52(12)	1.1023	0.9747
0.74	$7.5 \cdot 10^{-3}$	–	A/V	0.972(73)	1.1023	0.9747
0.67	$1.0 \cdot 10^{-2}$	+	P/S	1.17(6)	0.8157	0.9407
0.67	$1.0 \cdot 10^{-2}$	–	P/S	0.81(11)	0.8157	0.9407
0.74	$7.5 \cdot 10^{-3}$	+	P/S	1.14(12)	0.8302	0.9444
0.74	$7.5 \cdot 10^{-3}$	–	P/S	0.92(10)	0.8302	0.9444

Defining r_{cs} as the mass ratio m_c/m_s, the positivity of the fermionic measure in the strange–charm sector imposes

$$\frac{Z_P}{Z_S} > \frac{r_{cs}-1}{r_{cs}+1}\,. \tag{46}$$

The most stringent condition considering the experimental bounds [44] for m_s and m_c is

$$\frac{Z_P}{Z_S} > 0.89\,. \tag{47}$$

Our results and the tadpole improved perturbative determinations for Z_P/Z_S (for $N_f = 2$) seem to indicate that already at our values of β this condition is satisfied.

The results for the physical PCAC quark mass and pion decay constant f_π obtained from (35) and (38) are listed in Table 8. In Figs. 7 and 8 the pion decay constant is plotted as a function of the quark mass. The simulation points for negative quark masses are not taken into account in the present discussion. The figures also include the determination of f_π by the axial-vector current $A^a_{x\mu}$: a formula similar to (38) applies in this case where, however, the factor $1/\sin\omega$ is replaced by $1/\cos\omega$. In the interesting region near full twist this introduces large fluctuations in the estimate of f_π, as one can see from the figures. Moreover in the case of the axial-vector current, the decay constant has not yet the right normalisation of the continuum: a Z_A-factor

Table 8. Physical PCAC quark mass $am_q^{\rm PCAC}$ and pion decay constant af_π obtained from (35) and (38), respectively. The last two columns show $a\bar{m}_\chi^{\rm PCAC} \equiv \cos(\omega)\, am_q^{\rm PCAC}$ and the unrenormalised pion decay constant calculated with the local current $af_{v\pi}$, respectively

β	$a\mu$	κ	$am_q^{\rm PCAC}$	af_π	$a\bar{m}_\chi^{\rm PCAC}$	$af_{v\pi}$
0.67	$1.0 \cdot 10^{-2}$	0.1650	0.03652(53)	0.1672(25)	0.03511(54)	0.2936(63)
0.67	$1.0 \cdot 10^{-2}$	0.1655	0.02739(55)	0.1541(25)	0.02549(59)	0.2750(73)
0.67	$1.0 \cdot 10^{-2}$	0.1660	0.02006(59)	0.1447(23)	0.01739(69)	0.2549(84)
0.67	$1.0 \cdot 10^{-2}$	0.1665	0.01154(11)	0.1192(18)	0.00575(71)	0.2113(62)
0.67	$1.0 \cdot 10^{-2}$	0.1670	0.01117(38)	0.1085(37)	−0.00497(43)	0.1932(80)
0.67	$1.0 \cdot 10^{-2}$	0.1675	0.01810(69)	0.1203(44)	−0.01508(82)	0.219(13)
0.67	$1.0 \cdot 10^{-2}$	0.1680	0.0230(17)	0.1146(95)	−0.0207(18)	0.202(14)
0.74	$7.5 \cdot 10^{-3}$	0.1580	0.02262(45)	0.1170(25)	0.02133(66)	0.1833(57)
0.74	$7.5 \cdot 10^{-3}$	0.1585	0.01297(44)	0.0999(26)	0.01057(54)	0.1625(83)
0.74	$7.5 \cdot 10^{-3}$	0.1590	0.007611(38)	0.0874(15)	−0.00129(22)	0.1400(56)
0.74	$7.5 \cdot 10^{-3}$	0.1595	0.01245(61)	0.0867(39)	−0.00992(78)	0.137(10)

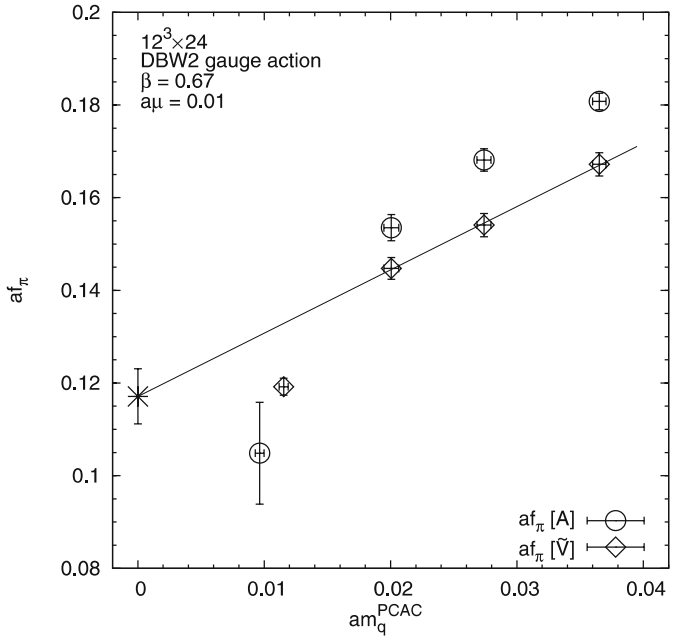

Fig. 7. The pion decay constant af_π as a function of the PCAC quark mass $am_q^{\rm PCAC}$ at $\beta = 0.67$, $a\mu = 0.01$

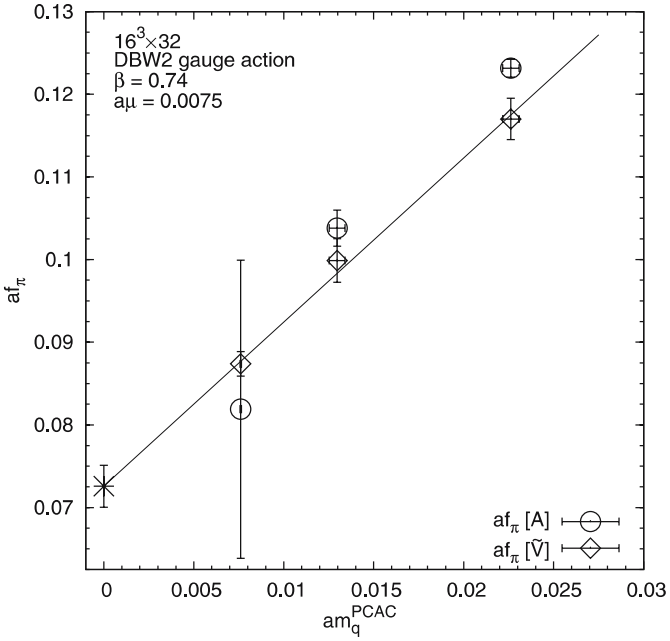

Fig. 8. The pion decay constant af_π as a function of the PCAC quark mass $am_q^{\rm PCAC}$ at $\beta = 0.74$, $a\mu = 0.0075$

is still missing. On the contrary, in the case of the conserved vector current f_π has automatically the physical normalisation [22, 39, 40]. If we exclude the lightest point at $\beta = 0.67$, which is likely to be under the influence of residual metastabilities, f_π seems to be characterised by a linear dependence upon the quark mass. On the basis of this observation we try a simple linear extrapolation to the chiral limit $m_q^{\rm PCAC} = 0$; see Table 9 for the numerical results. Of course, deviations from this linear behaviour could be present for lighter quark masses where chiral logarithms play a role.

In order to check the scaling between the two β-values we need to fix the lattice spacing. This can be accomplished by extrapolating the value of r_0 to $m_q^{\rm PCAC} = 0$. Also in this case we obtain two different values for the two different signs of the untwisted quark mass, again due to $\mathcal{O}(a)$ effects. As for Z_{oV} we take the average of the two values, which delivers an $\mathcal{O}(a)$-improved estimate of r_0 in the chiral limit. The results are reported in Table 9. We obtain for the lattice spacing (assuming $r_0 = 0.5\,\text{fm}$): $a(0.67) = 0.1757(41)\,\text{fm}$, $a(0.74) = 0.1326(70)\,\text{fm}$. Denoting the zero quark mass limit of the pion decay constant by

$$f_0 \equiv \lim_{m_q^{\rm PCAC}=0} f_\pi\,, \tag{48}$$

we obtain $f_0 r_0(0.67) = 0.333(10)$, $f_0 r_0(0.74) = 0.274(20)$. These values are not far from the phenomenological value $(f_0 r_0)_{\rm phen} = 0.308$. (The errors here are only statistical. Systematic errors of the chiral extrapolation are not included.)

4 Fits to chiral perturbation theory

Chiral perturbation theory (ChPT) is an expansion around the limit of massless quarks in QCD [1]. It describes the dependency of physical quantities on the quark masses in terms of expansions in powers of quark masses, modified by logarithms. In nature, however, quark masses have fixed values. The question of how observables depend on them functionally is experimentally unaccessible. Lattice gauge theory, on the other hand, offers the possibility to vary quark masses. Therefore it represents the ideal field of application of chiral perturbation theory. On the one

Table 9. Chiral extrapolation ($m_q^{\rm PCAC} = 0$) of the Sommer scale parameter r_0 and pion decay constant f_π. (This latter is denoted by $f_0 \equiv \lim_{m_q^{\rm PCAC}=0} f_\pi$.) The scale independent combination $f_0 r_0$ is also reported. Only data with positive twisted quark masses have been used for the extrapolations, with the exception of the point at $a\mu = 0.0075$ and $\kappa = 0.1590$ which is almost at full twist

β	$a\mu$	r_0/a	a [fm]	$a\,f_0$	$f_0\,r_0$
0.67	$1.0\cdot10^{-2}$	2.845(66)	0.1757(41)	0.1171(59)	0.333(10)
0.74	$7.5\cdot10^{-3}$	3.77(20)	0.1326(70)	0.0726(25)	0.274(20)

hand, chiral perturbation theory allows one to extrapolate results from numerical simulations of QCD into the region of small physical values for the up- and down-quark masses. On the other hand, lattice QCD can provide values for the low-energy constants of chiral perturbation theory.

In chiral perturbation theory the effects of the non-zero lattice spacing a can be taken into account in form of an expansion in powers of a [2, 45–48]. For the case of the Wilson twisted-mass formulation of lattice QCD this has been worked out in next-to-leading order in [6, 15, 25, 49].

The major purpose of the present paragraph is to provide a set of formulas derived from lattice chiral perturbation theory that can be used to analyse physical quantities such as the pion mass, decay constants and amplitudes. The novelty here is that these quantities have to be described across or nearby a phase transition.

The ChPT formulas are expected to be applicable at sufficiently small values of the lattice spacing and quark mass. It is thus far from obvious whether the data obtained with the DBW2 action in this work can be described by them, hence it is interesting to confront the simulation data at our quark masses and lattice spacings with these formulas. Let us emphasise that we consider this investigation mainly as a methodological study that does not aim to extract physical values of the low-energy constants in the first place.

Properly determined parameters of the ChPT formulas in the continuum limit are independent of the lattice action. The parameters describing the dependence on the lattice spacing do, however, depend on it. Therefore, in an appendix we also present ChPT fits of some simulation data obtained previously with the Wilson plaquette gauge action [14].

The quark masses in chiral perturbation theory always appear multiplied by $2B_0$, where B_0 is a low-energy constant. A connection to lattice regularisation can be established by considering the renormalised quark masses defined in (42), (43) and

$$m_{\chi R}^{\mathrm{PCAC}} = \frac{Z_A}{Z_P} m_{\chi}^{\mathrm{PCAC}} \,. \tag{49}$$

A common renormalisation factor $1/Z_P$ in $m_{\chi R}^{\mathrm{PCAC}}$ and μ_{R} can be absorbed into B_0. However, since the multiplicative renormalisation of m_{χ}^{PCAC} and μ differs by a factor Z_A, this has to be taken into account when fitting lattice data (see below).

The lattice spacing enters chiral perturbation theory in the combination

$$\rho = 2W_0 a \,, \tag{50}$$

where W_0 is another low-energy constant.

For the low-energy constants of lattice QCD in next-to-leading order [46, 48] with two quark flavours we use the notation

$$\begin{aligned} L_{54} &= 2L_4 + L_5, & L_{86} &= 2L_6 + L_8 \,, \\ W_{54} &= 2W_4 + W_5, & W_{86} &= 2W_6 + W_8 \,, \end{aligned} \tag{51}$$

$$W = \frac{1}{2}(W_{86} - 2L_{86}), \quad W' = \frac{1}{2}(W'_{86} - W_{86} + L_{86}) \,,$$
$$\widetilde{W} = \frac{1}{2}(W_{54} - L_{54}) \,. \tag{52}$$

Experience in untwisted lattice QCD shows [50] that lattice artefacts are considerably reduced when observables are considered as functions of the PCAC quark mass instead of the renormalised lattice quark mass. (A possible reason is that the PCAC quark mass reabsorbs leading $\mathcal{O}(a)$ effects.) Therefore, in our case, instead of using $m_{\chi\mathrm{R}}$ as a variable, we re-expand the physical quantities in terms of the PCAC quark mass in the twisted basis $m_{\chi R}^{\mathrm{PCAC}}$. Including the relevant prefactor we define

$$\chi'_{\mathrm{PCAC}} = 2B_0 m_{\chi R}^{\mathrm{PCAC}} \,. \tag{53}$$

For the purpose of fitting data at constant μ it is convenient to define the combination

$$\bar{\chi} = 2B_0 \sqrt{\left(m_{\chi R}^{\mathrm{PCAC}}\right)^2 + \mu_{\mathrm{R}}^2} \,. \tag{54}$$

(The attentive reader is certainly realising that we use the symbols χ for different quantities. Nevertheless, both the notation for the fermion field of twisted-mass fermions and the mass parameters in ChPT are standard in the literature and we do not want to change either of them in this paper.) Then, for the charged pion masses, chiral perturbation theory at next-to-leading order including lattice terms of order a gives

$$\begin{aligned} m_{\pi\pm}^2 = \bar{\chi} &+ \frac{1}{32\pi^2 F_0^2}\bar{\chi}^2 \ln\frac{\bar{\chi}}{\Lambda^2} \\ &+ \frac{8}{F_0^2}\Big\{(-L_{54}+2L_{86})\bar{\chi}^2 + 2(W-\widetilde{W})\rho\chi'_{\mathrm{PCAC}}\Big\} \,. \end{aligned} \tag{55}$$

Similarly for the pion decay constant and the one-pion matrix element of the pseudoscalar density:

$$\frac{F_\pi}{F_0} = 1 - \frac{1}{16\pi^2 F_0^2}\bar{\chi}\ln\frac{\bar{\chi}}{\Lambda^2} + \frac{4}{F_0^2}\Big\{L_{54}\bar{\chi} + 2\widetilde{W}\rho\frac{\chi'_{\mathrm{PCAC}}}{\bar{\chi}}\Big\} \,, \tag{56}$$

$$\begin{aligned} \frac{G_\pi}{F_0 B_0} = 1 &- \frac{1}{32\pi^2 F_0^2}\bar{\chi}\ln\frac{\bar{\chi}}{\Lambda^2} \\ &+ \frac{4}{F_0^2}\Big\{(-L_{54}+4L_{86})\bar{\chi} + (4W-2\widetilde{W})\rho\frac{\chi'_{\mathrm{PCAC}}}{\bar{\chi}}\Big\} \,. \end{aligned} \tag{57}$$

In the ChPT formulas the pion decay constant at zero quark mass (F_0) appears. In the conventional normalisation its phenomenological value is $F_0 \approx 86\,\mathrm{MeV}$. This is related to $f_0 \approx 122\,\mathrm{MeV}$ used in the previous section by $F_0 \equiv f_0/\sqrt{2}$. Similarly, F_π and G_π denote the pion decay constant and the one-pion matrix element of the pseudoscalar density, respectively, in this normalisation convention.

The renormalisation scale Λ appearing in the one-loop contributions is taken to be $\Lambda = 4\pi F_0$ as usual. Taking into

account the renormalisation factors, when using these expressions for fitting the lattice data, one writes

$$\bar{\chi} = 2B\sqrt{(m_\chi^{\rm PCAC})^2 + Z_A^{-2}\mu^2}\,, \tag{58}$$

where $B = B_0 Z_A/Z_P$.

4.1 Fit procedure

For fitting the data as a function of $m_\chi^{\rm PCAC}$ (55)–(57) are going to be used. The data for m_π, F_π and G_π, as well as that for $m_\chi^{\rm PCAC}$ are afflicted with numerical errors. Therefore, a fit procedure has to be used which takes into account errors in both coordinates. The method with effective variances [51] treats the coordinates on unequal footings but is numerically not so convenient. We have decided to use the more appropriate method of generalised least-squares fits [52].

Consider a data set containing N "measured" values for each of the D variables. They are collected in the vector $\mathbf{y} = (\mathbf{y_1}, \ldots, \mathbf{y_N})$, where each element $\mathbf{y_i}$ is itself a column vector with D elements $\mathbf{y_i} = \{y_{i,j}\}\,,\ j = 1, \ldots, D$. The true values for each data point, which have to be estimated together with the parameters, will be collected in the same way in a vector $\mathbf{x} = (\mathbf{x_1}, \ldots, \mathbf{x_N})$ with entries $\mathbf{x_i} = \{x_{i,j}\}\,,\ j = 1, \ldots, D$. Now the set of measured data points $\{y_{i,j}\}$ represents a single realisation of an experiment which occurs with a probability given by a joint distribution called "likelihood". The likelihood is specified by a multivariate normal distribution L with mean values given by the exact values $\mathbf{x}$ and a $ND \times ND$ covariance matrix $\sigma = \left\{\sigma_{(i,j),(k,l)}\right\}\,,\ i,k = 1, \ldots, N;\ j,l = 1, \ldots, D$:

$$L = \frac{1}{(2\pi)^{\frac{ND}{2}}} \frac{1}{\sqrt{\det \sigma}} \exp\left[-\frac{1}{2}\,(\mathbf{x}-\mathbf{y})\,\sigma^{-1}\,(\mathbf{x}-\mathbf{y})^{\rm T}\right]. \tag{59}$$

The process of data analysis amounts to the constrained maximisation of this likelihood through the estimation of the values of $\mathbf{x}$ based on the knowledge of $\mathbf{y}$, where the constraints enter through the fit-functions. Instead of maximising L it is more convenient to minimise its negative logarithm. The only non-constant term is given by

$$L' = \frac{1}{2}\,(\mathbf{x}-\mathbf{y})\,\sigma^{-1}\,(\mathbf{x}-\mathbf{y})^{\rm T}\,. \tag{60}$$

The fit-functions are given by a number F of model-functions G_i, which can be incorporated as, generally non-linear, constraints on the relationship between the exact values collected in $\mathbf{x}$. These functions also depend on a set of P parameters $\alpha = (\alpha_1, \ldots, \alpha_P)$, whose values are to be determined. They can be written in the compact form $\mathbf{G}\,(\mathbf{x}, \alpha) = \mathbf{0}$ with the F-dimensional column vector $\mathbf{G} = (G_1, \ldots, G_F)$.

Maximisation of the likelihood L under the constraints $\mathbf{G}\,(\mathbf{x}, \alpha) = \mathbf{0}$ is now equivalent to the unconstrained minimisation of $\mathcal{L}$ given by

$$\mathcal{L} = \frac{1}{2}\,(\mathbf{x}-\mathbf{y})\,\sigma^{-1}\,(\mathbf{x}-\mathbf{y})^{\rm T} + \lambda\mathbf{G}\,, \tag{61}$$

where λ is the F-dimensional row-vector of Lagrange multipliers. We implemented the minimisation of $\mathcal{L}$ using the Maple algorithm NLPSolve, which is based on routines provided by the numerical algorithms group (NAG).

In the present case the N different points of measurement correspond to different values of the hopping parameter κ, which are completely independent of each other. Therefore we can assume the covariance matrix to be diagonal, $\sigma_{(i,j),(i,j)} = (\Delta y_{i,j})^2$, where $\Delta y_{i,j}$ denotes the statistical error of $y_{i,j}$.

The errors of the model parameters α_i are calculated using a Monte Carlo approach. In K steps of an artificial Monte Carlo procedure a new set of normally distributed values $\left\{y_{i,j}^{\rm mc}\right\}_k\,,\ k = 1, \ldots, K$, is generated using the values of $\{y_{i,j}\}$ as means and $\sigma_{i,j}$ as the variances. Now for every k an independent estimate for the parameters is calculated yielding $\alpha_{{\rm mc};i}^k$ in each step. Finally the errors $\Delta\alpha_i$ are given by the standard deviation of the set of $\left\{\alpha_{{\rm mc},i}^k\right\}\,,\ k = 1, \ldots, K$.

4.2 Results

At $\beta = 0.67$ and at $\beta = 0.74$ results for m_π, F_π, G_π and $m_\chi^{\rm PCAC}$ are available both for non-vanishing and for vanishing twist mass μ. At $\mu = 0$ only part of the data, namely for $m_0 - m_{\rm cr} > 0$, is reliable and is being used.

By using the results in Table 9 for the values of r_0/a extrapolated to the chiral limit, we express all quantities in units of MeV. For the value of the Sommer scale we assume $r_0 \equiv 0.5\,{\rm fm} = (394.6\,{\rm MeV})^{-1}$. This allows us to compare and to combine the results from the different values of β.

It is important to observe that the lattice spacing $a(\beta)$ is obtained from extrapolation of r_0/a to the chiral limit. In presence of both positive and negative masses we take the average. This is a strong constraint on the fits, since the data have to reproduce the scaling behaviour dictated by r_0. If the purpose is the determination of the low-energy constants, matching ratios like m_π/F_π with ChPT would be preferable. However, in this exploratory study, we find it interesting to check that the scaling behaviour of different quantities is indeed consistent.

We made combined fits of the three quantities as functions of $m_\chi^{\rm PCAC}$ for both values of β, including lattice terms of order a. For the pion masses the expressions for the $\mathcal{O}(a^2)$ lattice terms are known, but they cannot be fitted meaningfully. The value of Z_A, entering the fit-functions, has been taken as input from the Monte Carlo data. As it varies with β, we denote the corresponding values $Z_A(\beta)$. The fits include data both for non-zero- and zero-twisted mass μ.

The low-energy constants resulting from the fits are shown in Table 10. In the first case data points with both positive and negative values of $m_\chi^{\rm PCAC}$ are fitted, whereas in the second case only those with $m_\chi^{\rm PCAC} > 0$. (This latter choice corresponds to the procedure in Sect. 3 where also only points with $m_\chi^{\rm PCAC} > 0$ have been taken into account in the chiral extrapolation of f_π.) We also made single fits for the three quantities, which are not displayed here. As

Table 10. Results of the ChPT fits with DBW2 gauge action. Upper part: fit with both positive and negative values of $am_\chi^{\rm PCAC}$. Lower part: fit with only positive values of $am_\chi^{\rm PCAC}$

	Input Z_A			Fitted Z_A		
	$\beta = 0.67$	$\beta = 0.74$	both β	$\beta = 0.67$	$\beta = 0.74$	both β
$Z_A(0.67)$	0.952(30)	–	0.952(30)	0.8658(90)	–	0.852(14)
$Z_A(0.74)$	–	0.944(74)	0.944(74)	–	0.868(18)	0.909(31)
F_0 [MeV]	80.7(3.6)	68.6(5.2)	73.7(4.8)	78.9(3.2)	66.0(4.4)	72.0(3.0)
$B(0.67)$ [GeV]	3.20(13)	–	3.20(12)	3.09(10)	–	3.063(94)
$B(0.74)$ [GeV]	–	3.31(30)	3.16(38)	–	3.12(19)	3.18(15)
$L_{54} \cdot 10^3$	0.98(26)	0.96(26)	1.17(28)	0.50(15)	0.80(23)	0.74(12)
$L_{86} \cdot 10^3$	0.78(13)	0.81(11)	0.94(14)	0.554(84)	0.76(10)	0.709(61)
$W_0 \cdot W \cdot 10^{-3}$ [MeV^3]	50(15)	−21(16)	18(17)	35(12)	−30(14)	6.6(8.0)
$W_0 \cdot \tilde{W} \cdot 10^{-3}$ [MeV^3]	89(19)	21(38)	64(29)	62(14)	−9(22)	35(12)
Λ_3/F_0	6.1(2.8)	5.5(2.3)	5.1(2.5)	5.9(1.7)	5.0(2.0)	5.3(1.1)
Λ_4/F_0	17.1(1.4)	17.0(1.4)	18.2(1.6)	14.74(69)	16.2(1.1)	16.86(59)
$\mathcal{L}_{\rm min}$/d.o.f.	12.8(3.5)	12.3(4.9)	13.1(7.2)	9.2(1.6)	11.6(2.4)	9.4(1.6)
$Z_A(0.67)$	0.952(30)	–	0.952(30)	0.888(10)	–	0.896(11)
$Z_A(0.74)$	–	0.944(74)	0.944(74)	–	0.910(18)	0.880(23)
F_0 [MeV]	80.3(3.4)	91.2(5.4)	83.9(4.4)	79.3(3.4)	89.9(4.2)	82.2(2.6)
$B(0.67)$ [GeV]	2.92(11)	–	2.95(11)	2.85(10)	–	2.864(84)
$B(0.74)$ [GeV]	–	3.46(22)	3.52(38)	–	3.39(15)	3.39(11)
$L_{54} \cdot 10^3$	1.39(33)	1.04(53)	1.32(28)	0.86(17)	0.82(23)	0.80(13)
$L_{86} \cdot 10^3$	0.92(16)	0.71(20)	0.81(15)	0.70(11)	0.64(13)	0.649(77)
Λ_3/F_0	7.1(4.1)	7.7(6.4)	7.7(4.0)	6.4(2.2)	6.9(3.0)	6.7(1.7)
Λ_4/F_0	19.5(2.0)	17.4(2.9)	18.6(1.6)	16.47(88)	16.3(1.2)	16.19(69)
$\mathcal{L}_{\rm min}$/d.o.f.	10.1(4.9)	2.7(6.5)	5.8(7.9)	7.0(2.0)	2.6(2.4)	4.5(1.6)

they are each based on less data, their results are less valuable, but consistent with the combined fits.

In addition to the single-β fits we also made a global fit including the data from both values of β. The results are also contained in Table 10. The fits at the two single values of β and the global fit are roughly consistent with each other. The differences in the numbers for the low-energy constants give an indication of the size of the uncertainties.

Instead of using Z_A as input from the numerical calculations, it can alternatively be left as an additional fit parameter. The corresponding fit results are shown in the right hand side of the table. The fitted Z_A is in rough agreement with its Monte Carlo estimate. Also, the low-energy coefficients are consistent with the ones from the other fits.

In addition to the combinations of Gasser–Leutwyler coefficients L_k, the table includes the values of the invariant scale parameters [53]

$$\Lambda_3 = 4\pi F_0 \exp(128\pi^2(L_{54} - 2L_{86}))\,,$$
$$\Lambda_4 = 4\pi F_0 \exp(32\pi^2 L_{54})\,. \qquad (62)$$

The results for Λ_3, Λ_4 are close to phenomenological estimates (see the discussion). The W-parameters have large errors but their magnitude is reasonable, as W_0 is expected to be of order $\Lambda_{\rm QCD}^3$ and the other W's of the same order as the L's.

The fit curves for m_π, F_π and G_π together with data points at $\beta = 0.67$ and $\beta = 0.74$ are shown in Figs. 9, 10, 11 and 12. In order to display the size of the leading-order

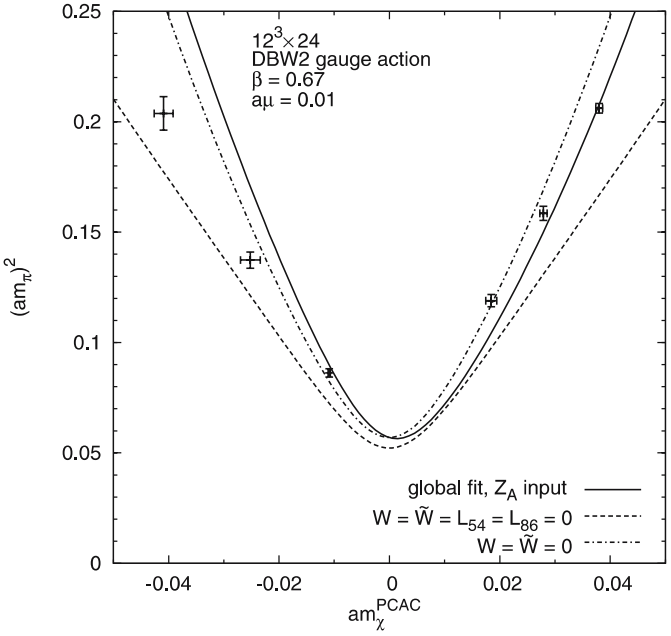

Fig. 9. The charged pion masses squared as a function of $am_\chi^{\rm PCAC}$ at $a\mu = 0.01$. The points represent the data at $\beta = 0.67$. The *solid line* displays the global fit with Z_A as input. The *dashed* and *dotted lines* show the fit with part of the L and W coefficients set to zero, in order to indicate the size of the NLO corrections

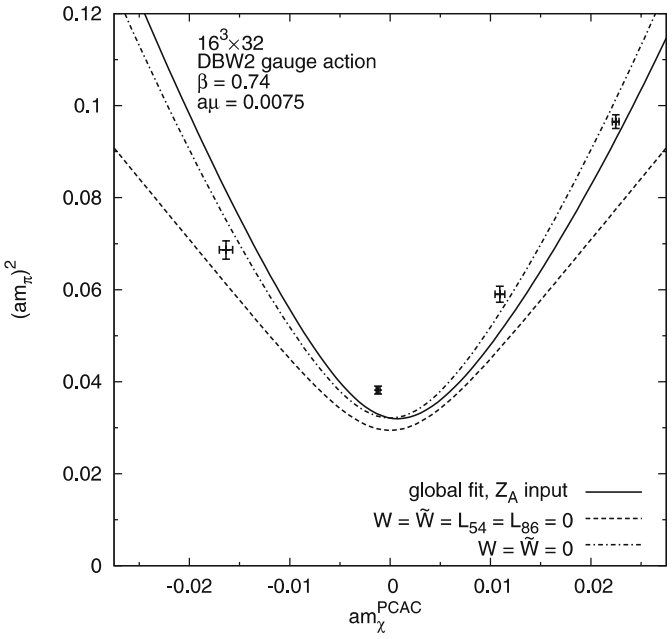

Fig. 10. The charged pion masses squared as a function of $am_\chi^{\rm PCAC}$ at $a\mu = 0.0075$. The points represent the data at $\beta = 0.74$. The *solid line* displays the global fit with Z_A as input. The *dashed* and *dotted lines* show the fit with part of the L and W coefficients set to zero, in order to indicate the size of the NLO corrections

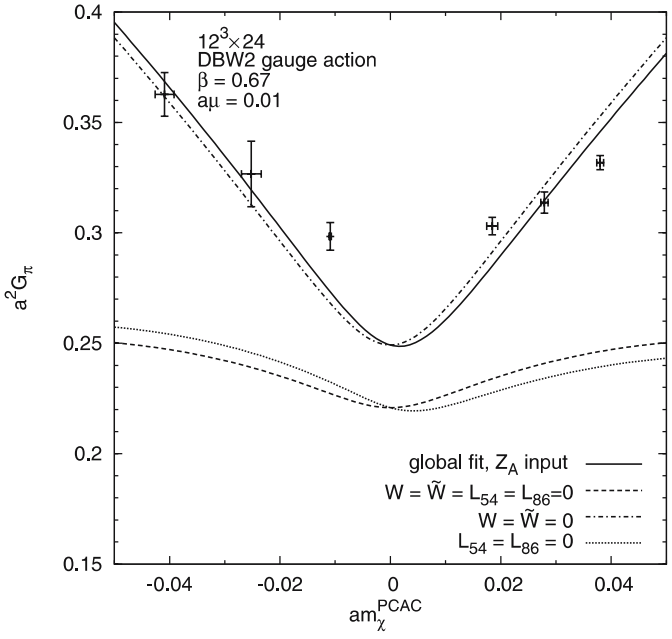

Fig. 12. The pseudoscalar matrix element $a^2 G_\pi$ as a function of $am_\chi^{\rm PCAC}$ at $\beta = 0.67$, $a\mu = 0.01$. The *solid line* displays the global fit with Z_A as input. The *dashed* and *dotted lines* show the fit with part of the L and W coefficients set to zero, in order to indicate the size of the NLO corrections

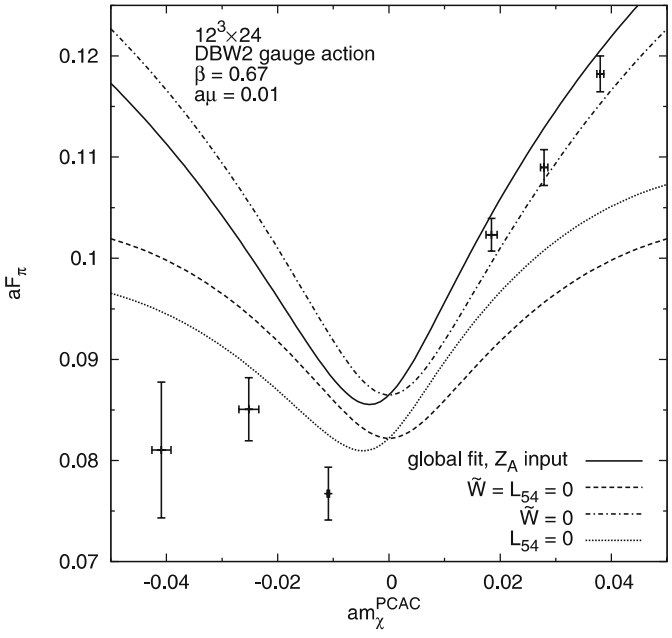

Fig. 11. The pion decay constant aF_π as a function of $am_\chi^{\rm PCAC}$ at $\beta = 0.67$, $a\mu = 0.01$. The *solid line* displays the global fit with Z_A as input. The *dashed* and *dotted lines* show the fit with part of the L and W coefficients set to zero, in order to indicate the size of the NLO corrections

contribution and the corrections, the figures contain additional curves representing the fit-functions with some of the low-energy constants being put to zero.

We have also investigated $m_\chi^{\rm PCAC}$ as a function of m_0. It can be fitted with the corresponding formula from chiral perturbation theory, which involves W, W' and $\widetilde{W}$ but no L-coefficients, but the resulting coefficients are unreliable owing to large errors.

In this section we stick to the definition of the untwisted bare PCAC quark mass $am_\chi^{\rm PCAC}$ in (6). As it is shown in the Appendix, the agreement with the ChPT formulas can be improved by taking $a\bar{m}_\chi^{\rm PCAC}$ of (37) as the quark mass variable, instead. In addition, ChPT fits to some previously obtained simulation data by the Wilson plaquette gauge action are also presented there.

5 Discussion

We compared in this paper the numerical simulation results with two flavours of twisted-mass Wilson quarks and DBW2 gauge action at two values of the lattice spacing corresponding to $\beta = 0.67$ and $\beta = 0.74$. The lattices were $12^3 \cdot 24$ and $16^3 \cdot 32$, respectively. The lattice spacing was defined by the value of the Sommer scale parameter r_0 extrapolated to zero quark mass and assuming $r_0 \equiv 0.5$ fm. The β-values were chosen in such a way that the lattice extensions were approximately equal: $L \simeq 2.11$ fm and $L \simeq 2.12$ fm, respectively. Also the bare twisted masses scaled approximately: $r_0\mu \simeq 0.0285$ and $r_0\mu \simeq 0.0283$, respectively.

The comparison of the observed quantities at two β-values allows for a first look at discretisation errors.

The outcome of these tests is reasonable, having in mind the coarse lattice spacings: $a \simeq 0.176\,\mathrm{fm}$ on the $12^3 \cdot 24$ and $a \simeq 0.133\,\mathrm{fm}$ on $16^3 \cdot 32$. For instance, the results for the pseudoscalar decay constant at zero quark mass are $f_\pi r_0 = 0.330(10)$ and $f_\pi r_0 = 0.274(20)$ at $\beta = 0.67$ and $\beta = 0.74$, respectively. These values also come close to the phenomenological value $(f_\pi r_0)_{\mathrm{phen}} = 0.308$ [55]. The situation is somewhat worse for the pseudoscalar–vector mass ratio, as Fig. 1 indicates. There are some noticeable scale breaking effects, especially for pseudoscalar masses near $m_\pi = r_0^{-1}$. Of course, one has to bear in mind that the ρ-meson mass in most of the points is quite close to the cutoff.

The prerequisite for the extraction of quantities as, for instance, f_π is the knowledge of the multiplicative renormalisation Z-factors for the currents. For obtaining the Z-factors one can exploit the twist-angle dependence in the plane of untwisted and twisted quark masses. As we have shown in Sect. 3, this is a rather powerful method for obtaining "finite" (according to perturbation theory) Z-factor combinations as Z_V, Z_A and Z_P/Z_S. Remarkably consistent results could be obtained even with our exploratory simulation data, without a dedicated choice of simulation points for this purpose.

We have also attempted to describe our numerical simulation data by a set of formulas derived from lattice chiral perturbation theory. Although the values of the lattice spacing and the quark mass are rather large in the simulations, it turned out that these formulas describe the behaviour of many physical quantities – even across the phase transition – surprisingly well, at least on a qualitative level. However, at the quantitative level our presently available data do neither allow one to make a quantitative extraction of the values of the ChPT parameters nor can we answer the question whether the lattice artifacts are well described by the lattice extension of ChPT. The achieved qualitatively correct ChPT fits of our simulation data makes us very optimistic that with new data we are working on at present – at smaller lattice spacings and small quarks masses – these questions will be answered. To achieve this the experience with the fits in this paper will be very helpful.

In Sect. 4 and the Appendix we used the NLO expressions of ChPT including terms describing $\mathcal{O}(a)$ lattice artefacts. In general, metastable points near the first order phase transition can be and have been included in the fits. (Note that the fits in [50] are also based on metastable points, as it has been discovered later.) Several setups were tried and were shown to give satisfactory and consistent fits. Nevertheless, there are probably some higher order effects (higher orders both in the quark mass and in lattice spacing) which are non-negligible in our parameter range. In addition, for the multi-parameter fits our data are not precise enough and the data points are too few and not optimally distributed in the parameter space. (In a dedicated investigation the inclusion of partially quenched data points could be very helpful.) Qualitatively speaking, the ChPT fits presented here support the choice of the PCAC quark mass as the preferred quark mass variable and show that the $\mathcal{O}(a)$ effects are not overwhelming because a fit without them is most of the time possible. Both these findings agree with those of [50].

The ChPT fits are also helpful in estimating the minimal pion mass at a given lattice spacing. For instance, the results at $\beta = 0.74 (a = 0.1326(70)\,\mathrm{fm})$ indicate that for fixed $a\mu = 0.0075$ we are above the end point of the first order phase transition line (see e.g. the smooth behaviour near $\mu_{\kappa\mathrm{cr}}$ in Fig. 4). The minimal value of the pion mass in Figs. 10 and 13 is about $m_\pi^{\min}(a\mu = 0.0075) \simeq 280\,\mathrm{MeV}$. This is an upper bound for the absolute minimum $m_\pi^{\min}$ at $\beta = 0.74$.

According to Table 10 the fits of the data with DBW2 gauge action suggest the following qualitative estimates for the values of the relevant ChPT parameters:

$$\begin{aligned} 2.9\,\mathrm{GeV} \le B \le 3.5\,\mathrm{GeV}\,, \\ 70\,\mathrm{MeV} \le F_0 \le 85\,\mathrm{MeV}\,, \\ 4.0 \le \Lambda_3/F_0 \le 8.0\,, \\ 16.0 \le \Lambda_4/F_0 \le 19.0\,. \end{aligned} \tag{63}$$

As Table 11 shows, the fits with the plaquette gauge action are roughly consistent with these values. The estimates of $\Lambda_{3,4}$ are close to previous estimates in [50]: $\Lambda_3/F_0 \approx 8$, $\Lambda_4/F_0 \approx 21$.

The values of the W-parameters describing $\mathcal{O}(a)$ effects are not well determined and are in most cases consistent with zero in our fits, if am_χ^{PCAC} (or $a\bar{m}_\chi^{\mathrm{PCAC}}$) is taken as the independent variable. Note that if one considers the relation of am_χ^{PCAC} and am_0, then W and W' are quite visible. An example is Fig. 2 in our previous proceedings contribution [56] where W gives the difference of the slope between positive and negative masses (W' turns out to be small).

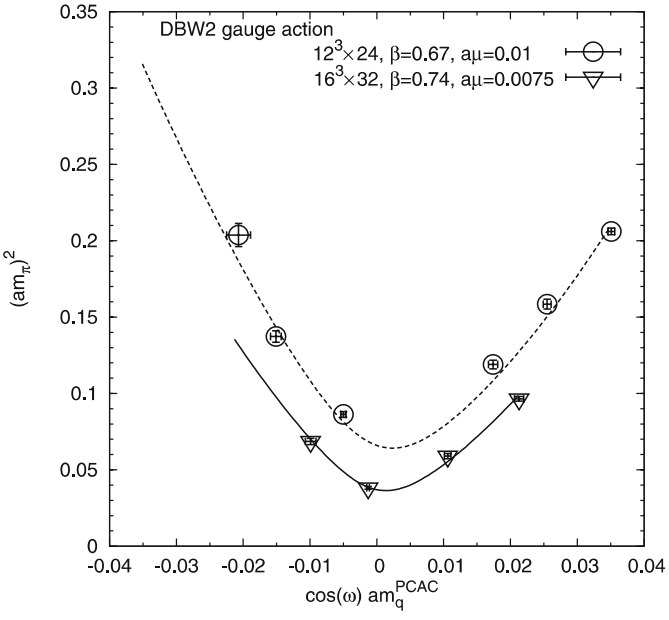

Fig. 13. Fit of the charged pion mass squared from DBW2 data at non-zero $a\mu$ as described in the Appendix. The *upper* (*lower*) *curve* belongs to $\beta = 0.67$ ($\beta = 0.74$)

Table 11. Results of the ChPT fits with plaquette gauge action. The columns correspond to different definitions of the currents for af_π and $am_\chi^{\rm PCAC}$. For the definitions see Sect. 3.3. Upper part: fit with both positive and negative values of $am_\chi^{\rm PCAC}$. Lower part: fit with only positive values of $am_\chi^{\rm PCAC}$

	$f_{v\pi}$ & $\bar{m}_\chi^{\rm PCAC}$	f_π & $\bar{m}_\chi^{\rm PCAC}$	$f_{v\pi}$ & $m_\chi^{\rm PCAC}$	f_π & $m_\chi^{\rm PCAC}$
B [GeV]	5.05	5.04	5.00	4.90
F_0 [MeV]	104.9	104.2	88.3	86.6
$L_{86}\cdot 10^3$	0.916	0.950	1.829	1.943
$L_{54}\cdot 10^3$	1.637	1.709	2.850	3.027
$W_0\cdot W\cdot 10^{-3}$ [MeV^3]	31.5	28.5	2.9	6.6
$W_0\cdot \tilde{W}\cdot 10^{-3}$ [MeV^3]	43.2	39.7	−3.6	−1.3
Λ_3/F_0	9.8	9.9	4.5	4.2
Λ_4/F_0	21.1	21.6	30.9	32.7
$(\sum {\rm dev}^2/\sigma^2)$/d.o.f.	2.08	2.19	4.25	4.16
B [GeV]	5.05	4.33	4.43	3.95
F_0 [MeV]	98.5	93.9	90.5	85.8
$L_{86}\cdot 10^3$	0.892	1.466	1.135	1.836
$L_{54}\cdot 10^3$	1.848	2.705	2.099	3.155
Λ_3/F_0	13.6	9.4	10.1	6.5
Λ_4/F_0	22.5	29.5	24.4	34.0
$(\sum {\rm dev}^2/\sigma^2)$/d.o.f.	1.36	2.24	1.26	1.77

If the data at the two β-values are fitted separately, as Table 10 shows, there is a remarkably good agreement of the corresponding parameter values. This agrees with expectations since the inclusion of $\mathcal{O}(a)$ terms in the formulas reduces the discretisation errors in the physical parameters. The consistency of the ChPT fits is supported by the agreement of the pion decay constant at zero quark mass F_0 with the value directly extracted from the data in Sect. 3: $f_0(\beta=0.74)/\sqrt{2}\simeq 76\,{\rm MeV}$. The estimates of the universal low-energy scales $\Lambda_{3,4}$ are within the bounds of their phenomenological values given in [55]: $\Lambda_3 = 0.6(+1.4,-0.4)\,{\rm GeV},\ \Lambda_4 = 1.2(+0.7,-0.4)\,{\rm GeV}$ that is $2.3\le\Lambda_3/F_0\le 23.3$, $9.3\le\Lambda_4/F_0\le 22.1$.

Acknowledgements. We thank H. Perlt for providing us with the perturbative estimates of the renormalisation constants of the quark bilinears. The computer centers at DESY Hamburg, NIC, DESY Zeuthen, NIC at Forschungszentrum Jülich and HLRN provided the necessary technical help and computer resources. This work was supported by the DFG Sonderforschungsbereich/Transregio SFB/TR9-03.

Appendix : Comparison with the fits to plaquette action data

It is interesting to compare the results obtained from the DBW2 gauge action with those presented in [14] resulting from the plaquette gauge action. As shown in the previous sections, chiral perturbation theory for Wilson lattice fermions (WChPT) offers a natural framework to perform such a comparison. In fact, if NLO-WChPT is applicable, the parameters B_0, F_0 and L_i entering (55)–(57) should already take their physical (continuum) values: lattice artefacts are expected to be taken into account by the W-parameters. The latter depend, in general, on the lattice action.

We remark that, having expressed all quantities (F_π, G_π and m_π) as functions of $m_\chi^{\rm PCAC}$, the parameter W' [7, 15] disappears, and the pion mass can apparently go to zero when $m_\chi^{\rm PCAC}\to 0$ and $\mu\to 0$. However, one should keep in mind that not all values of $m_\chi^{\rm PCAC}$ are accessible with

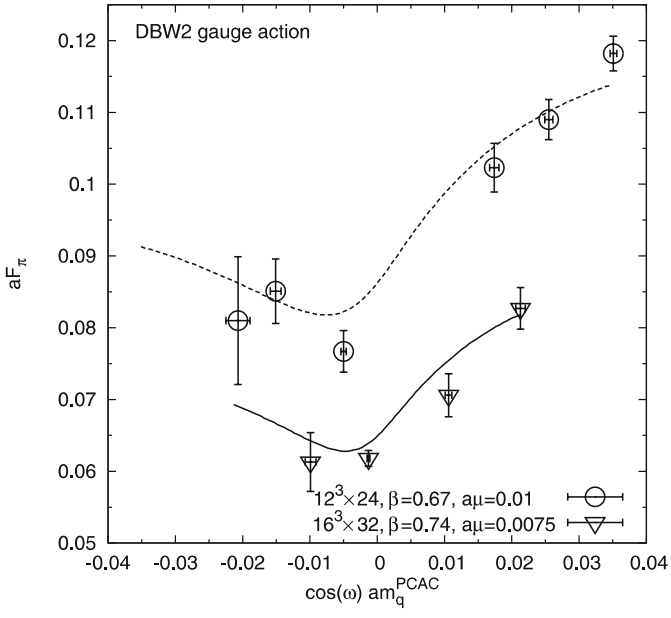

Fig. 14. Fit of the pion decay constant aF_π from DBW2 data at non-zero $a\mu$ as described in the Appendix. The *upper (lower) curve* belongs to $\beta=0.67$ ($\beta=0.74$)

stable simulation points. This parametrisation allows one to include in the ChPT fit also metastable points, where both m_π and $m_\chi^{\rm PCAC}$ are lower than it would be possible in a stable minimum of the effective potential. Since this is an interesting check, we exploit this possibility and we include also metastable points (from [14]) in the fit.

Given the larger amount of data points, we use a different fit procedure from the one described in Sect. 4.1. The χ^2 is defined as for the effective variances method [51, 52, 54], but minimised through the Matlab implementation of the Nelder–Mead simplex method. The variables a and $m_\chi^{\rm PCAC}$ are taken as independent variables, and F_π, G_π and m_π as dependent ones.

Besides using a fitting procedure different from the one in the previous Sects. 4.1–4.2, our fits to the plaquette gauge action data are restricted to data points with non-zero twisted mass ($a\mu > 0$) only. We also tried to use different independent variables instead of $am_\chi^{\rm PCAC}$, which correspond to different possible definitions of the untwisted component of the quark mass. It turned out that the fit quality is improving if one considers $a\bar{m}_\chi^{\rm PCAC}$ defined in (37). The difference implied by these changes compared to the analysis in Sects. 4.1–4.2 – i.e. different fitting procedure, restricting the fit to $a\mu > 0$ and using $a\bar{m}_\chi^{\rm PCAC}$ – is illustrated by Figs. 13, 14 and 15 which have to be compared to Figs. 9, 10, 11 and 12, respectively.

A consequence of considering $a\bar{m}_\chi^{\rm PCAC}$ instead of $am_\chi^{\rm PCAC}$ is that Z_A enters only indirectly – through the determination of ω; therefore, we do not need to fit them. As said before, the Z_P is included in the B-factor. However, when comparing different lattice spacings and different actions, we must allow for a β dependent Z_P. In practice we choose a reference β (corresponding to the smallest a which appears in the fit) and we fit a correction to Z_P for each different a. These are not given in the table, but they are always between 0.95 and 1.35.

We summarise our results for the plaquette gauge action data in Table 11. No statistical errors are quoted, since the systematic errors dominate, as the comparison of the results from the different fit setups shows. We perform fits

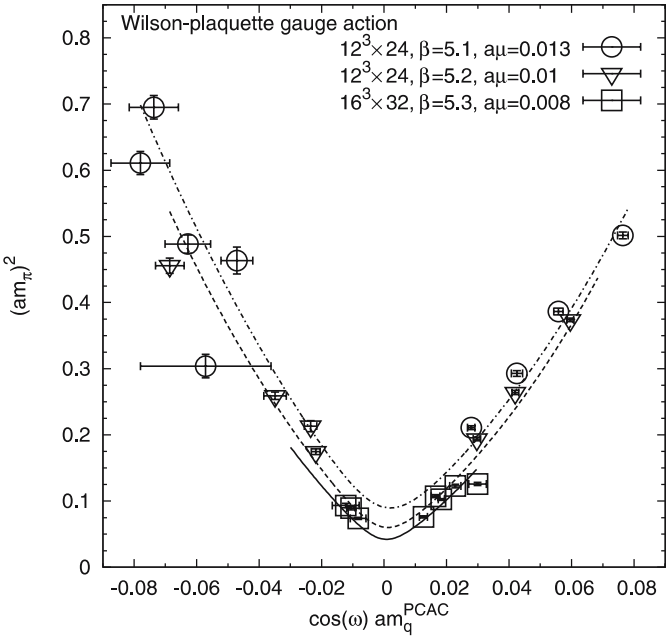

Fig. 16. Fit of the charged pion mass squared from plaquette data at non-zero $a\mu$. The *upper*, *intermediate* and *lower curves* refer to $\beta = 5.1$, $\beta = 5.2$ and $\beta = 5.3$, respectively

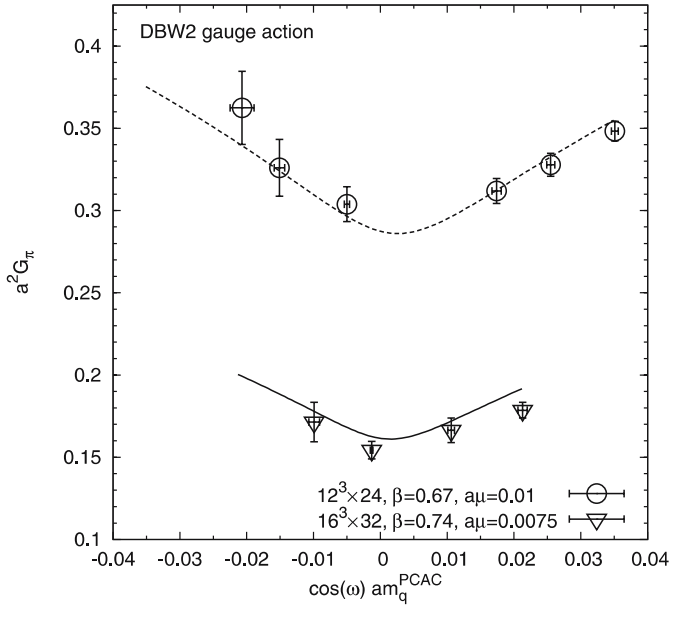

Fig. 15. Fit of $a^2 G_\pi$ from DBW2 data at non-zero $a\mu$ as described in the Appendix. The *upper (lower) curve* belongs to $\beta = 0.67$ ($\beta = 0.74$)

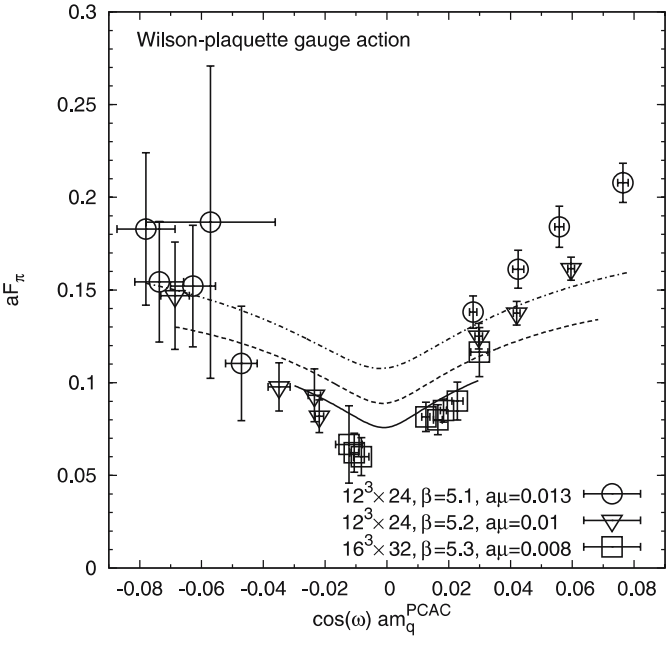

Fig. 17. Fit of the pion decay constant aF_π from plaquette data at non-zero $a\mu$. The *upper*, *intermediate* and *lower curves* refer to $\beta = 5.1$, $\beta = 5.2$ and $\beta = 5.3$, respectively

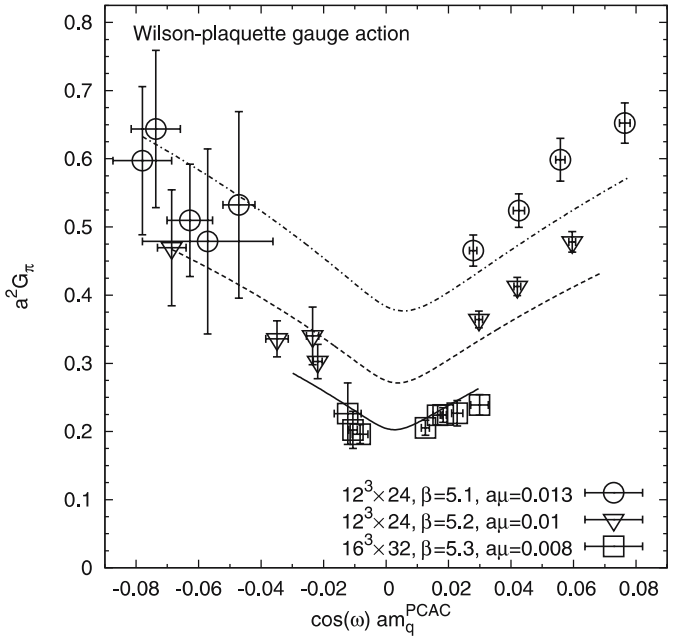

Fig. 18. Fit of a^2G_π from plaquette data at non-zero $a\mu$. The *upper*, *intermediate* and *lower curves* refer to $\beta = 5.1$, $\beta = 5.2$ and $\beta = 5.3$, respectively

including all data (top part of Table 11) or only data at positive mass (bottom part of Table 11). In this second case the W-parameters are set to zero.

In Figs. 16, 17 and 18 the fits of the plaquette gauge action data are presented. Similarly to the DBW2 fits, the W's are very unstable, depending on the chosen subset of data, and in general they are consistent with zero within errors. The physical combinations L_{54} and L_{86} are consistent with the values obtained by the DBW2 gauge action.

We also performed fits of all data and imposing $W = \widetilde{W} = 0$. The values of the physical quantities are still reasonable, however the curves fit the data worse. We have also attempted fits where all the NLO parameters are set to zero ($L_i = W = \widetilde{W} = 0$), or where only lattice artefacts are included ($L_i = 0$). Both these assumptions result in very poor fits, essentially because they cannot reproduce the curvature in F_π and G_π.

References

1. S. Weinberg, Physica A **96**, 327 (1979); J. Gasser, H. Leutwyler, Annals Phys. **158**, 142 (1984)
2. S.R. Sharpe, R. Singleton, Jr., Phys. Rev. D **58**, 074501 (1998) [hep-lat/9804028]
3. S. Aoki, Phys. Rev. D **30**, 2653 (1984); Phys. Rev. Lett. **57**, 3136 (1986)
4. R. Frezzotti, P.A. Grassi, S. Sint, P. Weisz, Nucl. Phys. Proc. Suppl. **83**, 941 (2000) [hep-lat/9909003]
5. G. Münster, JHEP **0409**, 035 (2004) [hep- lat/0407006]
6. L. Scorzato, Eur. Phys. J. C **37**, 445 (2004) [hep-lat/0407023]
7. S.R. Sharpe, J.M.S. Wu, Phys. Rev. D **70**, 094029 (2004) [hep-lat/0407025]
8. T. Blum et al., Phys. Rev. D **50**, 3377 (1994) [hep-lat/9404006]
9. JLQCD Collaboration, S. Aoki et al., Nucl. Phys. Proc. Suppl. **106**, 263 (2002) [hep-lat/0110088]
10. K. Jansen, Nucl. Phys. Proc. Suppl. **129**, 3 (2004) [hep-lat/0311039]
11. A. Shindler, PoS LAT2005 014 (2005) [hep-lat/0511002]
12. F. Farchioni, R. Frezzotti, K. Jansen, I. Montvay, G.C. Rossi, E. Scholz, A. Shindler, N. Ukita, C. Urbach, I. Wetzorke, Eur. Phys. J. C **39**, 421 (2005) [hep-lat/0406039]
13. E.M. Ilgenfritz, W. Kerler, M. Müller-Preussker, A. Sternbeck, H. Stüben, Phys. Rev. D **69**, 074511 (2004) [hep-lat/0309057]
14. F. Farchioni, K. Jansen, I. Montvay, E.E. Scholz, L. Scorzato, A. Shindler, N. Ukita, C. Urbach, U. Wenger, I. Wetzorke, Phys. Lett. B **624**, 324 (2005) [hep-lat/0506025]
15. S.R. Sharpe, J.M.S. Wu, Phys. Rev. D **71**, 074501 (2005) [hep-lat/0411021]
16. F. Farchioni, K. Jansen, I. Montvay, E. Scholz, L. Scorzato, A. Shindler, N. Ukita, C. Urbach, I. Wetzorke, Eur. Phys. J. C **42**, 73 (2005) [hep-lat/0410031]
17. T. Takaishi, Phys. Rev. D **54**, 1050 (1996); QCD-TARO Collaboration, P. de Forcrand et al., Nucl. Phys. Proc. Suppl. **53**, 938 (1997) [hep-lat/9608094]
18. S. Necco, Nucl. Phys. B **683**, 137 (2004) [hep-lat/0309017]
19. CP-PACS Collaboration, S. Takeda et al., Phys. Rev. D **70**, 074510 (2004) [hep-lat/0408010]
20. QCDSF Collaboration, R. Horsley et al., Nucl. Phys. B **693**, 3 (2004) [hep-lat/0404007]
21. R. Frezzotti, G.C. Rossi, JHEP **0408**, 007 (2004) [hep-lat/0306014]; Nucl. Phys. Proc. Suppl. **129**, 880 (2004) [hep-lat/0309157]
22. K. Jansen, A. Shindler, C. Urbach, I. Wetzorke, Phys. Lett. B **586**, 432 (2004) [hep-lat/0312013]
23. A.M. Abdel-Rehim, R. Lewis, R.M. Woloshyn, Phys. Rev. D **71**, 094505 (2005) [hep-lat/0503007]
24. K. Jansen, M. Papinutto, A. Shindler, C. Urbach, I. Wetzorke, JHEP **0509**, 071 (2005) [hep-lat/0507010]
25. G. Münster, C. Schmidt, Europhys. Lett. **66** (2004) 652 [hep-lat/0311032]
26. S. Duane, A.D. Kennedy, B.J. Pendleton, D. Roweth, Phys. Lett. B **195**, 216 (1987)
27. C. Urbach, K. Jansen, A. Shindler, U. Wenger, Comput. Phys. Commun. **174**, 87 (2006) [hep-lat/0506011]
28. I. Montvay, Nucl. Phys. B **466**, 259 (1996) [hep-lat/9510042]
29. qq+q Collaboration, F. Farchioni, C. Gebert, I. Montvay, L. Scorzato, Eur. Phys. J. C **26**, 237 (2002) [hep-lat/0206008]
30. R. Sommer, Nucl. Phys. B **411**, 839 (1994) [hep-lat/9310022]
31. F. Farchioni, C. Urbach, R. Frezzotti, K. Jansen, I. Montvay, G.C. Rossi, E.E. Scholz, A. Shindler, N. Ukita, I. Wetzorke, Nucl. Phys. Proc. Suppl. **140**, 240 (2005) [hep-lat/0409098]
32. ALPHA Collaboration, R. Frezzotti, P.A. Grassi, S. Sint, P. Weisz, JHEP **0108**, 058 (2001) [hep-lat/0101001]
33. S. Aoki, O. Bär, Phys. Rev. D **70**, 116011 (2004) [hep-lat/0409006]

34. XLF Collaboration, W. Bietenholz et al., JHEP **0412**, 044 (2004) [hep-lat/0411001]
35. R. Frezzotti, G. Martinelli, M. Papinutto, G.C. Rossi, hep-lat/0503034
36. S.R. Sharpe, Phys. Rev. D **72**, 074510 (2005) [hep-lat/0509009]
37. Alpha collaboration, R. Frezzotti, P.A. Grassi, S. Sint, P. Weisz, JHEP **0108**, 058 (2001) [hep-lat/0101001]
38. L. Maiani, G. Martinelli, Phys. Lett. B **178**, 265 (1986)
39. R. Frezzotti, S. Sint, Nucl. Phys. Proc. Suppl. **106**, 814 (2002) [hep-lat/0110140]
40. M. Della Morte, R. Frezzotti, J. Heitger, Nucl. Phys. Proc. Suppl. **106**, 260 (2002) [hep-lat/0110166]
41. H. Perlt (QCDSF Collaboration), private communication
42. This collaboration, work in progress
43. R. Frezzotti, G.C. Rossi, Nucl. Phys. Proc. Suppl. **128**, 193 (2004) [hep-lat/0311008]
44. S. Eidelman et al., Phys. Lett. B **592**, 1 (2004)
45. W. Lee, S. Sharpe, Nucl. Phys. B (Proc. Suppl.) **73** (1999) 240 [hep-lat/9809026]
46. G. Rupak, N. Shoresh, Phys. Rev. D **66**, 054503 (2002) [hep-lat/0201019]
47. S. Aoki, Phys. Rev. D **68**, 054508 (2003) [hep-lat/0306027]
48. O. Bär, G. Rupak, N. Shoresh, Phys. Rev. D **70**, 034508 (2004) [hep-lat/0306021].
49. G. Münster, C. Schmidt, E. Scholz, Europhys. Lett. **86**, 639 (2004) [hep-lat/0402003]
50. qq+q Collaboration, F. Farchioni, I. Montvay, E.E. Scholz, L. Scorzato, Eur. Phys. J. C **31**, 227 (2003) [hep-lat/030700]; qq+q Collaboration, F. Farchioni, I. Montvay, E. Scholz, Eur. Phys. J. C **37**, 197 (2004) [hep-lat/0403014]
51. J. Orear, Am. J. Phys. **50**, 912 (1982); Erratum, ibid. **52**, 278 (1984); Byron P. Roe, Probability and Statistics in Experimental Physics, 2nd ed. (Springer, Berlin, 2001)
52. S.L. Marshall, J.G. Blencoe, Am. J. Phys. **73**, 69 (2005)
53. H. Leutwyler, Nucl. Phys. Proc. Suppl. **94**, 108 (2001) [hep-ph/0011049]
54. W.H. Press, S.A. Teukolsky, W.T. Vetterling, B.P. Flannery, Numerical Recipes in C (Cambridge University Press, 1992)
55. S. Dürr, Eur. Phys. J. C **29**, 383 (2003) [hep-lat/0208051]
56. L. Scorzato et al., Nucl. Phys. Proc. Suppl. **153**, 283 (2006) [hep-lat/0511036]

[tIS-1]

Dynamical twisted mass fermions with light quarks

Phys. Lett. B650 304-311 (2007)

Available online at www.sciencedirect.com
ScienceDirect
Physics Letters B 650 (2007) 304–311
PHYSICS LETTERS B
www.elsevier.com/locate/physletb

Dynamical twisted mass fermions with light quarks

Ph. Boucaud [a], P. Dimopoulos [b], F. Farchioni [c], R. Frezzotti [b], V. Gimenez [d], G. Herdoiza [b], K. Jansen [e,*], V. Lubicz [f], G. Martinelli [g], C. McNeile [h], C. Michael [h], I. Montvay [i], D. Palao [d], M. Papinutto [f], J. Pickavance [h], G.C. Rossi [b], L. Scorzato [j], A. Shindler [e], S. Simula [f], C. Urbach [h], U. Wenger [k]

[a] *Laboratoire de Physique Théorique (Bât. 210), Université de Paris XI, Centre d'Orsay, 91405 Orsay-Cedex, France*
[b] *Dipartimento di Fisica, Università di Roma Tor Vergata and INFN, Sez. di Roma Tor Vergata, Via della Ricerca Scientifica, I-00133 Roma, Italy*
[c] *Universität Münster, Institut für Theoretische Physik, Wilhelm-Klemm-Strasse 9, D-48149 Münster, Germany*
[d] *Departamento de Física Teòrica and IFIC, Univ. de València, Dr. Moliner 50, E-46100 Burjassot, Spain*
[e] *NIC, DESY, Zeuthen, Platanenallee 6, D-15738 Zeuthen, Germany*
[f] *Dipartimento di Fisica, Università di Roma Tre and INFN, Sez. di Roma III, Via della Vasca Navale 84, I-00146 Roma, Italy*
[g] *Dipartimento di Fisica, Università di Roma "La Sapienza", and INFN, Sezione di Roma, P.le A. Moro 2, I-00185 Rome, Italy*
[h] *Theoretical Physics Division, Departament of Mathematical Sciences, University of Liverpool, Liverpool L69 7ZL, UK*
[i] *Deutsches Elektronen-Synchrotron DESY, Notkestr. 85, D-22607 Hamburg, Germany*
[j] *ECT* Strada delle Tabarelle 286, I-38050 Villazzano (TN), Italy*
[k] *Institute for Theoretical Physics, ETH Zürich, CH-8093 Zürich, Switzerland*

Received 30 January 2007; received in revised form 10 April 2007; accepted 21 April 2007

Available online 13 May 2007

Editor: A. Ringwald

Abstract

We present results of dynamical simulations of $N_f = 2$ degenerate Wilson twisted mass quarks at maximal twist in the range of pseudo scalar masses 300 MeV $\lesssim m_{\rm PS} \lesssim$ 550 MeV. Reaching such small masses was made possible owing to a recently developed variant of the HMC algorithm. The simulations are performed at one value of the lattice spacing $a \lesssim 0.1$ fm. In order to have $\mathcal{O}(a)$ improvement and aiming at small residual $\mathcal{O}(a^2)$ cutoff effects, the theory is tuned to maximal twist by requiring the vanishing of the untwisted quark mass. Precise results for the pseudo scalar decay constant and the pseudo scalar mass are confronted with chiral perturbation theory predictions and the low energy constants F, $\bar{l}_3$ and $\bar{l}_4$ are evaluated with small statistical errors.

1. Introduction

The Wilson twisted mass formulation of lattice QCD, though a rather recent approach, has been by now well established. It amounts to adding a twisted mass term to the standard, unimproved Wilson–Dirac operator [1] leading to so-called Wilson twisted mass fermions [2,3].

Besides being a theoretically sound formulation of lattice QCD, Wilson twisted mass fermions offer a number of advantages when tuned to maximal twist: (i) in this case automatic $\mathcal{O}(a)$ improvement is obtained by tuning only one parameter, the bare untwisted quark mass, while avoiding additional tuning of operator-specific improvement-coefficients; (ii) the mixing pattern in the renormalisation process can be significantly simplified; (iii) the twisted mass provides an infra-red regulator helping to overcome possible problems with ergodicity in molecular dynamics based algorithms.[1]

* Corresponding author.
E-mail address: karl.jansen@desy.de (K. Jansen).

[1] Although in the light of recent algorithmic developments [4–9] this property does not seem to be that important anymore, we consider it still to be an advantage to have an infra-red regulator in the theory which helps in stabilising the simulations. For a recent stability analysis of pure Wilson fermion simulations see Ref. [10].

0370-2693/$ – see front matter
doi:10.1016/j.physletb.2007.04.054

In the *quenched approximation*, these expectations—based on general field theoretical and chiral perturbation theory (χPT) related arguments [2,3,11–16]—could be verified in actual simulations [17–20]: $\mathcal{O}(a)$ improvement is indeed realised when the theory is tuned to maximal twist. Moreover, it has been shown that a particular realisation of maximal twist, requiring parity restoration, also suppresses the $\mathcal{O}(a^2)$ cut-off effects substantially, even at small quark masses corresponding to values of the pseudo scalar mass of $m_{\rm PS} \lesssim 300$ MeV. In addition, with the twisted mass parameter as an infra-red cut-off in place, substantially smaller quark masses could be obtained, compared to those reachable by standard or $\mathcal{O}(a)$ improved Wilson fermions which are plagued by so-called exceptional configuration problems in the quenched approximation. In Refs. [21–23] it was shown that "wrong chirality" mixing effects in the renormalisation process are substantially reduced. In Ref. [11] it was proved that all such mixings can be eliminated if a mixed action with maximally twisted sea quarks and appropriately chosen Osterwalder–Seiler valence fermions is employed. For a further discussion of the potential of twisted mass QCD on the lattice, see Refs. [24–27].

The main drawback of the twisted mass approach is the explicit breaking of parity and isospin symmetry which are only restored when the continuum limit is reached. However, due to $\mathcal{O}(a)$ improvement, this breaking is an $\mathcal{O}(a^2)$ effect as confirmed by simulations performed in the quenched approximation [28,29]. For recent reviews of the status of Wilson twisted mass fermions see Refs. [30–32] and references therein.

It is the main goal of our collaboration to compute a number of phenomenologically relevant quantities with *dynamical quarks*, *in the continuum limit* and at *small values of the pseudo scalar mass*. As a first step in this direction we here present results for $N_f = 2$ mass-degenerate quarks at a fixed lattice spacing $a \lesssim 0.1$ fm. We have so far concentrated on the pseudo scalar mass $m_{\rm PS}$, covering a range of values 300 MeV $\lesssim m_{\rm PS} \lesssim$ 550 MeV, the pseudo scalar decay constant $f_{\rm PS}$ and the static inter-quark force parameter r_0 at five values of the quark mass. A wider range of physical observables will be addressed in the future. The results for $m_{\rm PS}$ and $f_{\rm PS}$ are confronted with predictions of χPT which allows extracting the low-energy constants $\bar{l}_3$, $\bar{l}_4$, F and B_0 of the corresponding effective chiral Lagrangian. We also provide a determination of the size of isospin violation measured from the mass splitting between the lightest charged and neutral pseudo scalar particles. First accounts of our work were presented at recent conferences, see Refs. [33,34]. In this publication we will focus on the results of our present simulations obtained at one value of β and one volume. We shall provide, in a forthcoming paper [35], a comprehensive description of our analysis procedure and address systematic errors by including future runs on larger lattices, at different values of β and with extended statistics. Related works with Wilson fermions at similar small pseudo scalar meson masses are published in Refs. [36–38].

2. Choice of lattice action

The Wilson twisted mass fermionic lattice action for two flavours of degenerate quarks reads (in the so-called twisted basis [2] and fermion fields with continuum dimensions)

$$S_{\rm tm} = a^4 \sum_x \Bigg\{ \bar{\chi}_x \Big[m_0 + i\gamma_5\tau_3\mu + \frac{4r}{a} \Big] \chi_x + \frac{1}{2a} \sum_{\nu=1}^{4} \bar{\chi}_x \big[U_{x,\nu}(-r+\gamma_\nu)\chi_{x+\hat{\nu}} + U^{\dagger}_{x-\hat{\nu},\nu}(-r-\gamma_\nu)\chi_{x-\hat{\nu}} \big] \Bigg\}, \tag{1}$$

where am_0 is the bare untwisted quark mass and $a\mu$ the bare twisted mass, τ_3 is the third Pauli matrix acting in flavour space and r is the Wilson parameter, which we set to one in our simulations. Twisted mass fermions are said to be at *maximal twist* if the bare untwisted mass is tuned to its critical value, $m_{\rm crit}$. We will discuss later how this can be achieved in practise. Note that $m_{\rm crit}$ can be determined at each β-value at some suitably small value of the twisted mass parameter μ or even taken to be a function of μ itself. With the latter choice the line of maximal twist would become a non-trivial curve in parameter space.

In the gauge sector we use the so-called tree-level Symanzik improved gauge action (tlSym) [39], which includes besides the plaquette term $U^{1\times1}_{x,\mu,\nu}$ also rectangular (1×2) Wilson loops $U^{1\times2}_{x,\mu,\nu}$

$$S_g = \frac{\beta}{3} \sum_x \Bigg(b_0 \sum_{\substack{\mu,\nu=1 \\ 1\leqslant\mu<\nu}}^{4} \big\{ 1 - \mathrm{Re}\,\mathrm{Tr}\big(U^{1\times1}_{x,\mu,\nu}\big) \big\} + b_1 \sum_{\substack{\mu,\nu=1 \\ \mu\neq\nu}}^{4} \big\{ 1 - \mathrm{Re}\,\mathrm{Tr}\big(U^{1\times2}_{x,\mu,\nu}\big) \big\} \Bigg) \tag{2}$$

with β the bare inverse coupling, $b_1 = -1/12$ and the (proper) normalisation condition $b_0 = 1 - 8b_1$. Note that at $b_1 = 0$ this action becomes the usual Wilson plaquette gauge action.

2.1. $\mathcal{O}(a)$ improvement

As mentioned before, $\mathcal{O}(a)$ improvement can be obtained by tuning Wilson twisted mass fermions to maximal twist. In fact, it was first proved in Ref. [3] that parity even correlators are free from $\mathcal{O}(a)$ lattice artifacts at maximal twist by using spurionic symmetries of the lattice action. Later on it was realised [12,32] that a simpler proof is possible based on the parity symmetry of the continuum QCD action and the use of the Symanzik effective theory.

From this latter way of proving $\mathcal{O}(a)$ improvement, it becomes also clear how to define maximal twist: first, choose an operator odd under parity (in the physical basis) which has a zero expectation value in the continuum. Second, at a non-vanishing value of the lattice spacing tune the expectation value

of this operator to zero by adjusting the value of am_0. This procedure, which has been proposed in [40,41] and has been theoretically analysed in [12], is sufficient to define maximal twist independently of the chosen operator. To approach smoothly the continuum limit this tuning has to be performed at fixed physical situation while decreasing the lattice spacing.

It was shown in an extended scaling test in the quenched approximation, that $\mathcal{O}(a)$ improvement works extremely well for maximally twisted mass quarks [17–19]. In the context of this scaling test, the method of setting the so-called PCAC mass to zero was found to be very successful, in agreement with theoretical considerations [12,14,16]. Here the PCAC mass

$$m_{\mathrm{PCAC}} = \frac{\sum_{\mathbf{x}} \langle \partial_0 A_0^a(x) P^a(0) \rangle}{2 \sum_{\mathbf{x}} \langle P^a(x) P^a(0) \rangle}, \quad a = 1, 2 \tag{3}$$

is evaluated at large enough time separation, such that the pion ground state is dominant. To see that the procedure of defining am_{crit} from the vanishing of m_{PCAC} is the appropriate one, it is enough to recall that under that condition the multilocal operator $\sum_{\mathbf{x}} A_0^a(x) P^a(0)$ becomes, in the physical basis, the parity odd operator $\epsilon^{3ab} \sum_{\mathbf{x}} \bar{\psi} \gamma_0 \tau^b \psi(x) \bar{\psi} \gamma_5 \tau^a \psi(0)$.

In principle one could think of determining am_{crit} at each value of $a\mu$ at which simulations are performed, possibly followed by an extrapolation to vanishing $a\mu$. The strategy we are following in this Letter is, instead, to take the value of am_{crit} from the simulation at the lowest available value $a\mu_{\mathrm{min}} \ll a\Lambda_{\mathrm{QCD}}$. In this situation $\mathcal{O}(a)$ improvement is still guaranteed, because working at μ_{min} merely leads to $\mathcal{O}(a\mu_{\mathrm{min}}\Lambda_{\mathrm{QCD}})$ effects in m_{crit} and $\mathcal{O}(a^2\mu_{\mathrm{min}}\Lambda_{\mathrm{QCD}})$ relative corrections in physical quantities [12]. Although these theoretical arguments show that we are left with only $\mathrm{O}(a^2)$ lattice artifacts, numerical computations are required to determine the coefficient multiplying the a^2-term for the observables of interest. In the present Letter with data at only one value of the lattice spacing we cannot calculate these coefficients. However, for the observables we consider here, first results from our collaboration presented in Ref. [33,34] indicate that the $\mathcal{O}(a^2)$ errors are indeed small.

2.2. Phase structure

In order to understand our choice of the gauge action, it is important to realise that Wilson-type fermions have a non-trivial phase structure at finite lattice spacing: in a series of publications [30,40–44] the phase structure of lattice QCD was explored. For lattice spacings $a \geqslant 0.15$ fm clear signals of first order phase transitions at the chiral point were found. The strength of those phase transitions weakens when the continuum limit is approached. This phase transition was identified to be a *generic* property of Wilson-type fermions since the phenomenon takes place for the pure Wilson as well as the Wilson twisted mass formulation [2,3] of lattice QCD. Also the properties of physical quantities measured in both metastable branches of this first order phase transition were studied and compared to results of χPT [13,14,16,45–48] finding that (lattice) χPT describes the simulation data quite well. This is somewhat surprising since the simulation data were obtained at rather coarse values of the lattice spacing and at rather heavy pseudo scalar masses, where the applicability of χPT may be questionable.

A very important consequence of the first order phase transition phenomenon is that at non-vanishing lattice spacing, simulations cannot be performed with pseudo scalar mesons below a certain minimal mass value. From lattice χPT analyses it is expected that this minimal value of the pseudo scalar mass goes to zero with a rate of $\mathcal{O}(a)$. In different words, given a value of the pseudo scalar mass, m_{PS}, one can always find a value of the lattice spacing $a_{\mathrm{max}}(m_{\mathrm{PS}})$, such that simulations at $a < a_{\mathrm{max}}(m_{\mathrm{PS}})$ can be safely performed. For example, when the Wilson plaquette gauge action is used one finds $a_{\mathrm{max}} \approx 0.07$ fm to realise a pseudo scalar mass of about 300 MeV [44].

The phase structure of lattice QCD with Wilson-type fermions has previously been addressed: there have been investigations concerning the Aoki-phase [49] in Refs. [50,51] at large gauge couplings corresponding to values of the lattice spacing $a \geqslant 0.2$ fm. In other studies [52–54] signals of first order phase transitions were found for Wilson fermions with and without the clover term, see also Ref. [55]. In Ref. [56] a speculative picture of the phase structure of Wilson lattice QCD has been given and in Ref. [57] an analysis within the framework of χPT has been reported. A detailed understanding of the generic phase structure was obtained in the 2-dimensional Gross–Neveu model, see Refs. [58–60]. Of course, it is unclear how much these last results are applicable to 4-dimensional lattice QCD.

In order to choose a gauge action for our production simulations we studied the phase structure employing a number of different gauge actions: the standard Wilson plaquette gauge action [1] ($b_1 = 0$ in Eq. (2)), the DBW2 gauge action [61] ($b_1 = -1.4088$) and the tree-level Symanzik improved gauge action [39] ($b_1 = -1/12$). A marked dependence of the strength of the phase transition on the choice of the gauge action has been found. In particular, these investigations revealed that the DBW2 and the tlSym gauge actions substantially weaken the effect of the first order phase transition and in particular the value of a_{max} increases when the coefficient b_1 in Eq. (2) is moved away from zero [41,44]. We refer to Refs. [30,32] for summaries of these results.

The DBW2 gauge action appears to lead to a bad scaling behaviour [62–64] and a slow convergence of perturbation theory [65], whereas the tlSym gauge action is expected to show—by construction—a good scaling behaviour and a fast convergence of perturbation theory. Therefore, the tlSym gauge action looks like a good compromise between the Wilson gauge action which is most strongly affected by the first order phase transition and the DBW2 gauge action.

3. Numerical results

3.1. Set-up

In this Letter we will present results at a fixed value of the lattice spacing of $a \lesssim 0.1$ fm only. In Table 1 we provide the value of $a\mu_{\mathrm{min}}$ at which we imposed the vanishing of m_{PCAC} (Eq. (3)) and thus determined am_{crit}. In Table 2 we list the val-

Table 1
Simulation parameters. We denote by $a\mu_{\rm min}$ the smallest value of the twisted mass parameter $a\mu$ at which we have performed simulations. At this value of $a\mu$ we determined the critical mass $m_{\rm crit}$, or, equivalently the critical hopping parameter $\kappa_{\rm crit} = 1/(8 + 2am_{\rm crit})$. The value of r_0/a has been extrapolated to the physical point, where $m_{\rm PS} = 139.6$ MeV

β	$L^3 \cdot T$	$a\mu_{\rm min}$	$\kappa_{\rm crit}(a\mu_{\rm min})$	r_0/a
3.9	$24^3 \cdot 48$	0.004	0.160856	5.22(2)

Table 2
Results from simulations at $\beta = 3.9$ using the simulation parameters listed in Table 1. The measurements were started after 1500 equilibration trajectories and are based on 5000 equilibrated trajectories

$a\mu$	$am_{\rm PS}$	$af_{\rm PS}$	$am_{\rm PCAC}$	r_0/a	$\tau_{\rm int}(P)$
0.0040	0.13587(68)	0.06531(40)	−0.00001(27)	5.196(28)	55(17)
0.0064	0.16937(36)	0.07051(35)	−0.00009(17)	5.216(27)	23(07)
0.0085	0.19403(50)	0.07420(24)	−0.00052(17)	5.130(28)	13(03)
0.0100	0.21004(52)	0.07591(40)	−0.00097(26)	5.143(25)	15(04)
0.0150	0.25864(70)	0.08307(34)	−0.00145(42)	5.038(24)	06(02)

ues of the quark mass $am_{\rm PCAC}$, the pseudo scalar mass $am_{\rm PS}$, the pseudo scalar decay constant $af_{\rm PS}$, r_0/a and the plaquette integrated autocorrelation time at all values of the twisted mass parameter $a\mu$. All other parameters were kept fixed as specified in Table 1.

The algorithm we used is a HMC algorithm with mass preconditioning [4,66] and multiple time scale integration described in detail in Ref. [8]. The trajectory length τ was set to $\tau = 1/2$ in all our runs. Our estimates of the plaquette integrated autocorrelation time $\tau_{\rm int}(P)$ quoted in Table 2 are in units of $\tau = 1/2$. Note that our estimates of the autocorrelation times of quantities such as $am_{\rm PS}$ or $af_{\rm PS}$ are found to be substantially smaller, typically by a factor of 5–10, than those reported in the table for the plaquette.

As discussed above, maximal twist is realised in our simulations by tuning m_0 to obtain a vanishing PCAC quark mass $am_{\rm PCAC}$ at the smallest value $a\mu_{\rm min}$ of the twisted mass parameter $a\mu$. From Table 2 one can see that this condition has been numerically realised with good accuracy, which in this context means $m_{\rm PCAC}(\mu_{\rm min})/\mu_{\rm min} < a\Lambda_{\rm QCD}$ within statistical errors ($a\Lambda_{\rm QCD} \sim 0.1$ in our case). Once this is achieved, the (weak) μ-dependence of $m_{\rm PCAC}$, which is visible in Fig. 1(a), is an $\mathcal{O}(a)$ cutoff effect that merely modifies the $\mathcal{O}(a^2)$ artifacts in physical observables, as already mentioned in Section 2.1.

In order to make maximum use of the gauge configurations, we evaluate connected meson correlators using a stochastic method to include all spatial sources. The method involves a stochastic source (Z(2)-noise in both real and imaginary part) for all colour and spatial indices at one Euclidean time slice. By solving for the propagator from this source for each of the 4 spin components, we can construct zero-momentum meson correlators from any bilinear at the source and sink. Four inversions of the Dirac matrix per Euclidean time slice value are necessary, since we chose to use only one stochastic sample per gauge configuration. This "one-end" method is similar to that pioneered in Ref. [67] and implemented in Ref. [68]. We also employ a fuzzed source [69] of the extent of 6 lattice spacings to enable studying non-local meson creation and destruction operators. This allowed us to obtain very stable effective masses and to confirm the extraction of the pion ground state.

In general, we save a gauge configuration every second trajectory and analyse meson correlators as described above from a selection of different Euclidean time slice sources. To reduce autocorrelations, we only use the same time slice source every 8–10 trajectories. Our primary statistical error was obtained with the so-called Γ-method as described in Ref. [70] and cross-checked with a bootstrap analysis and a jack-knife analysis of blocked data. For a detailed description of our error analysis we refer to a forthcoming paper of our collaboration [35].

3.2. Force parameter r_0

In simulations of the quenched approximation of lattice QCD, the Sommer parameter r_0 [71] with a value of 0.5 fm, was widely used to set the lattice scale. While (r_0/a) is measurable to good accuracy in lattice QCD simulations it has the drawback that its value in physical units is not known very well. Therefore, it becomes necessary to determine the scale using other quantities which are experimentally accessible with high precision, such as m_π, f_π, $m_{\rm K}$, $f_{\rm K}$ or $m_{\rm K^*}$. In fact, in this Letter we attempt to determine the lattice scale by fitting χPT based formulae to our precise data for $f_{\rm PS}$ and $m_{\rm PS}$, using the physical values for m_π and f_π as inputs. From this analysis, we obtain a value of the lattice spacing which is 10% lower than the value obtained by setting $r_0 = 0.5$ fm.

Our results for (r_0/a) are reported in Table 2 and plotted in Fig. 1(b). Within the current errors the mass dependence of this quantity appears to be weak. Since r_0 is a pure gauge quantity, it should be a function of $(a\mu)^2$ and indeed, a linear fit in $(a\mu)^2$ describes the data rather well as shown in Fig. 1(b). From the fit we obtain a value for $r_0/a = 5.22(2)$ at the physical point, where $a\mu = a\mu_\pi$ (see below), as also quoted in Table 1.

3.3. $f_{\rm PS}$ and $m_{\rm PS}$ as a function of the quark mass

The *charged* pseudo scalar meson mass $am_{\rm PS}$ is as usual extracted from the time exponential decay of appropriate correlation functions.[2] In contrast to pure Wilson fermions, for maximally twisted mass fermions an exact lattice Ward identity allows to extract the (charged) pseudo scalar meson decay constant $f_{\rm PS}$ from the relation

$$f_{\rm PS} = \frac{2\mu}{m_{\rm PS}^2} \left| \langle 0 | P^1(0) | \pi \rangle \right|, \tag{4}$$

with no need to compute any renormalisation constant since $Z_P = 1/Z_\mu$ [2]. We give our results for $m_{\rm PS}$ and $f_{\rm PS}$ in Table 2.

We now discuss whether the continuum χPT formulae can reproduce the data in Table 2 for $am_{\rm PS}$ and $af_{\rm PS}$. In our χPT based analysis, we take into account finite size corrections because on our lattices at the lowest and next-to-lowest μ-values

[2] Concerning results on the neutral pion mass, $am_{\rm PS}^0$, see Section 3.4.

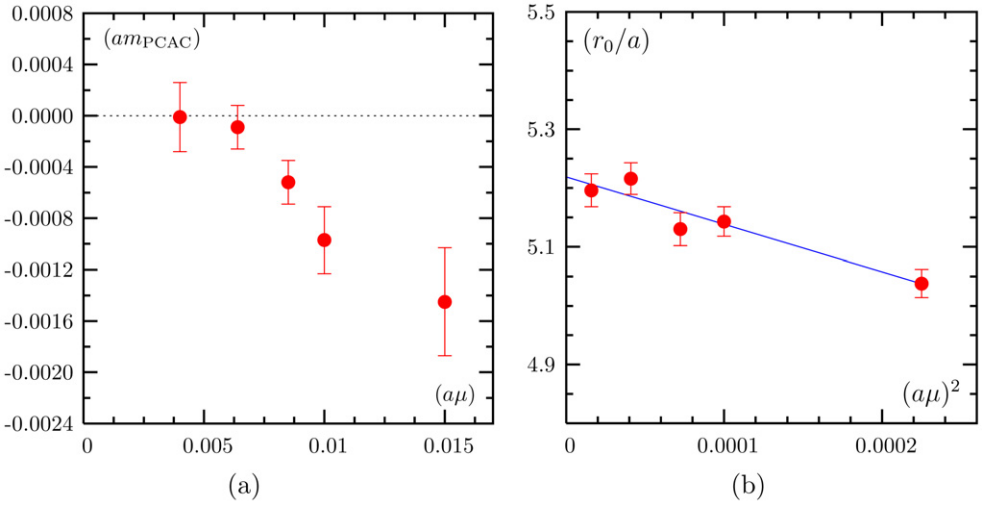

Fig. 1. (a) PCAC quark mass $am_{\rm PCAC}$ as function of $a\mu$ and (b) Sommer parameter (r_0/a) as functions of $(a\mu)^2$. The solid line in subfigure (b) represents a linear fit in $(a\mu)^2$ to the data.

they turn out to affect $am_{\rm PS}$ and, in particular, $af_{\rm PS}$ in a significant way. We have used continuum χPT to describe consistently the dependence of the data both on the finite spatial size (L) and on μ.

We fit the appropriate $(N_f = 2)$ χPT formulae [72,73]

$$m_{\rm PS}^2(L) = 2B_0\mu\left[1 + \frac{1}{2}\xi\tilde{g}_1(\lambda)\right]^2\left[1 + \xi\log\left(2B_0\mu/\Lambda_3^2\right)\right], \quad (5)$$

$$f_{\rm PS}(L) = F\left[1 - 2\xi\tilde{g}_1(\lambda)\right]\left[1 - 2\xi\log\left(2B_0\mu/\Lambda_4^2\right)\right], \quad (6)$$

to our raw data for $m_{\rm PS}$ and $f_{\rm PS}$ simultaneously. Here

$$\xi = 2B_0\mu/(4\pi F)^2, \qquad \lambda = \sqrt{2B_0\mu L^2}. \quad (7)$$

The finite size correction function $\tilde{g}_1(\lambda)$ was first computed by Gasser and Leutwyler in Ref. [72] and is also discussed in Ref. [73] from which we take our notation (except that our normalisation of f_π is 130.7 MeV). In Eqs. (5) and (6) NNLO χPT corrections are assumed to be negligible. The formulae above depend on four unknown parameters, B_0, F, Λ_3 and Λ_4, which will be determined by the fit. For $\mu = 0.004$ and $\mu = 0.0064$ we found the effect of finite size corrections to be 0.5% and 0.2% for the pseudo scalar mass and 2.2% and 0.9% for the pseudo scalar decay constant, respectively. For our larger values of μ the finite size corrections are negligible.

We determine $a\mu_\pi$, the value of $a\mu$ at which the pion assumes its physical mass, by requiring that the ratio $[\sqrt{[m_{\rm PS}^2(L=\infty)]}/f_{\rm PS}(L=\infty)]$ takes the value $(139.6/130.7) = 1.068$. From the knowledge of $a\mu_\pi$ we can evaluate $\bar{l}_{3,4} \equiv \log(\Lambda_{3,4}^2/m_\pi^2)$ and using f_π the value of the lattice spacing a in fm.

In order to estimate the statistical errors affecting our fit values we generate at each of the μ-values 1000 bootstrap samples for $m_{\rm PS}$ and $f_{\rm PS}$ extracted from the bare correlators, blocked with block-size of 32. For each sample (combining all masses) we then fit $m_{\rm PS}^2$ and $f_{\rm PS}$ simultaneously as a function of μ. From the 1000 fits we obtain 1000 bootstrap samples for $2aB_0$, aF, $\log(a^2\Lambda_{3,4}^2)$, $a\mu_\pi$, a and $\bar{l}_{3,4}$, respectively, from which we compute the corresponding error estimates, taking in this way the statistical correlation between $f_{\rm PS}$ and $m_{\rm PS}$ into account.

For our lightest four μ-values, we find an excellent fit to our data on $f_{\rm PS}$ and $m_{\rm PS}$ (see Figs. 2 and 3). The fitted values of the four parameters are

$$\begin{aligned} &2aB_0 = 4.99(6),\\ &aF = 0.0534(6),\\ &\log\left(a^2\Lambda_3^2\right) = -1.93(10),\\ &\log\left(a^2\Lambda_4^2\right) = -1.06(4). \end{aligned} \quad (8)$$

Our data are clearly sensitive to Λ_3 as visualised in Fig. 2(a). We obtain

$$a\mu_\pi = 0.00078(2), \qquad \bar{l}_3 = 3.65(12), \qquad \bar{l}_4 = 4.52(06) \quad (9)$$

which compares nicely with other determinations (for a review see Ref. [74]). Note that F, B_0, Λ_3 and Λ_4 were also determined in another setup for dynamical twisted mass fermions [43] with values in qualitative agreement, although those values could not be determined as precisely as in the present work. Including also our results from $a\mu = 0.0150$ in the fit gives an acceptable description of $m_{\rm PS}^2$ but misses the data for $f_{\rm PS}$, as shown in Figs. 2 and 3. Note, however, that in Eqs. (5), (6), and thus in the fit results (8), (9), a number of systematic errors as discussed below are not included.

The values presented here should hence be taken as a first estimate, the validity of which will be checked in the future. Nevertheless, the statistical accuracy we are able to achieve implies that there is a very good prospect of obtaining accurate and reliable values for the low-energy constants from Wilson twisted mass fermion simulations.

Since we have obtained an excellent description of our pseudo scalar mesons, we can use our fit to extract the lattice spacing. Based on the physical value of f_π, we get

$$a = 0.087(1)\ \text{fm}. \quad (10)$$

Using the value of r_0/a reported in Table 1, this lattice calibration method yields $r_0 = 0.454(7)$ fm.

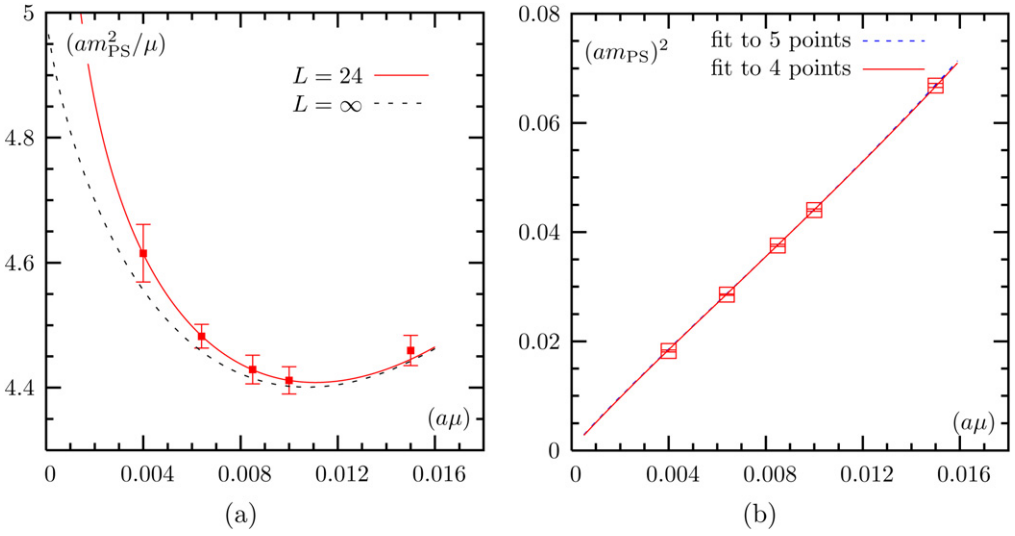

Fig. 2. In (a) we show $(am_{PS})^2/(a\mu)$ as a function of $a\mu$. We plot the χPT fit of Eq. (5) applied to the raw data on the $L = 24$ lattice from the lowest four μ-values. We represent the finite size correction by the dashed line. In (b) we show $(am_{PS})^2$ as a function of $a\mu$. Here we present two χPT fits with Eq. (5), one taking all data points and one leaving out the point at the largest value $a\mu = 0.015$. Also in figure (b) we show the $L = 24$ data points.

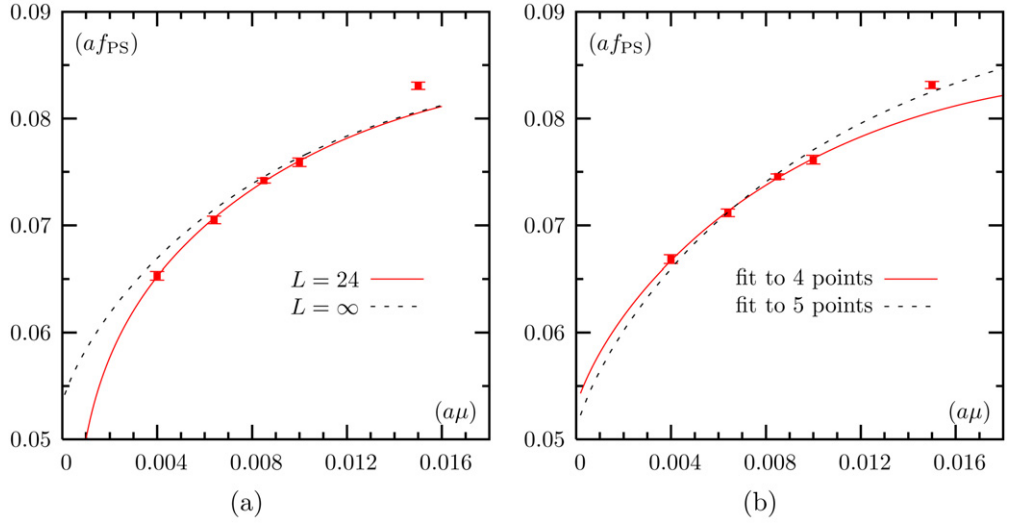

Fig. 3. We show af_{PS} as a function of $a\mu$ together with fits to χPT formula Eq. (6). In (a) we show the fit applied to the raw data on the $L = 24$ lattice at the 4 lowest values of $a\mu$. We represent the finite size correction by the dashed curve. In (b) we present two fits, one taking all data and one leaving out the point at the largest value $a\mu = 0.015$. Here we show only the finite size corrected ($L \to \infty$) data points.

We now discuss the possible sources of systematic error. Our analysis is based on lattice determinations of properties of pseudo scalar mesons with masses in the range 300 to 500 MeV on lattices with a spatial size slightly above 2 fm. Systematic errors can arise from several sources:

(i) Finite lattice spacing effects. Preliminary results at a smaller value of the lattice spacing that were presented in Refs. [33,34] suggest that $\mathcal{O}(a)$ improvement is nicely at work and that residual $\mathcal{O}(a^2)$ effects are small.

(ii) Finite size effects. In order to check that next to leading order (continuum) χPT adequately describes these, we are presently performing a run at $\beta = 3.9$ and $a\mu = 0.004$ on a $32^3 \cdot 64$ lattice.

(iii) Mass difference of charged and neutral pseudo scalar meson. In the appropriate lattice χPT power-counting for our values of the lattice spacing and quark masses, i.e. $a \sim \mu \sim p^2$, one gets the order of magnitude relation $(m_{PS})^2 - (m_{PS}^0)^2 = \mathcal{O}(a^2\Lambda_{QCD}^4) = \mathcal{O}(p^4)$, from which it follows that to the order we have been working the effects of the pion mass splitting do not affect, in particular, the finite size correction factors for m_{PS} and f_{PS}. In spite of these formal remarks, it is possible, however, that the fact that the neutral pion is lighter than the charged one (by about 20% at $a\mu = 0.0040$, see Section 3.4) makes inadequate the continuum χPT description of finite size effects adopted in the present analysis. This caveat represents a further motivation for simulations on larger lattices, which will eventually resolve the issue.

(iv) Extrapolation to physical quark masses. We are assuming that χPT at next to leading order for the $N_f = 2$ case is appropriate to describe the quark mass dependence of m_{PS}^2 and

$f_{\rm PS}$ up to ∼450–500 MeV. Our lattice data are consistent with this, but it would be useful to include higher order terms in the χPT fits as well as more values of $a\mu$ to check this assumption. The effect of strange quarks in the sea should also be explored.

3.4. Effects of isospin breaking

In this section we report the results of some quantitative investigation of the effects of isospin breaking in the twisted mass formulation of lattice QCD at finite lattice spacing. This effect is expected to be largest in the mass splitting between the lightest charged and uncharged pseudo scalar mesons. A first analysis at $a\mu = 0.004$, taking the disconnected contribution in the neutral channel fully into account, shows that the uncharged pseudo scalar meson is about 20% lighter than the charged one. We obtain

$$am_{\rm PS}^{\pm} = 0.1359(7), \qquad am_{\rm PS}^{0} = 0.111(11),$$

or, expressed differently, $r_0^2((m_{\rm PS}^0)^2 - (m_{\rm PS}^{\pm})^2) = c(a/r_0)^2$ with $c = -4.5(1.8)$. This coefficient is a factor of 2 smaller than the value found in quenched investigations [29]. Note that the uncharged pion being lighter than the charged one is compatible with predictions from lattice χPT if the first order phase transition scenario is realised [45,46,48]. For an investigation of isospin breaking effects in χPT see also Ref. [75]. From the value of c one may estimate the value of the endpoint, μ_c, of the first order phase transition, obtaining $a\mu_c \approx 0.0013$.

The disconnected correlations needed for the π^0 meson are evaluated using a stochastic (Gaussian) volume source with 4 levels of hopping-parameter variance reduction [76]. We use 24 stochastic sources per gauge configuration and evaluate the relevant propagators every 10th trajectory.

4. Summary

In this Letter we have presented results of simulations of lattice QCD with $N_f = 2$ maximally twisted Wilson quarks at a fixed value of the lattice spacing $a \lesssim 0.1$ fm. We reached a pseudo scalar meson mass of about 300 MeV. The numerical stability and smoothness of the simulations allowed us to obtain precise results for the pseudo scalar mass and decay constant which in turn led to determine the low energy constants of the effective chiral Lagrangian. In particular, we find for the pseudo scalar decay constant in the chiral limit $F = 121.3(7)$ MeV, and $\bar{l}_3 = 3.65(12)$ and $\bar{l}_4 = 4.52(6)$ where only statistical errors are given.

We do see effects of isospin breaking which are largest in the mass splitting of the neutral and charged pions and turn out to be about 20%. This is significantly smaller and opposite in sign than the corresponding splitting obtained in the quenched approximation.

Tuning to maximal twist had to be performed on lattices of the same size as those used for the calculation of physical quantities. The reason for this is that we need to single out cleanly the one pion sector in order to impose the vanishing of the PCAC quark mass (Eq. (3)) without being affected by finite size effects or excited state contributions. Thus the tuning step itself is rather expensive. But it has to be done only once, as is the case for the determination of action improvement coefficients in other Wilson based approaches. Note, however, that with twisted mass fermions we do not have to compute further operator-specific improvement coefficients.

The encouraging results presented here will be extended and checked by future simulations that will cover one coarser and one finer lattice spacing, double the statistics at one of our present simulation points ($\beta = 3.9$, $a\mu = 0.004$) and go to a larger, $32^3 \cdot 64$, volume at the latter simulation point. In this way, we will be able to obtain results in the continuum limit, cross-check our autocorrelation times, improve our error estimates and control the finite size effects in order to check χPT predictions. The preliminary results presented in Refs. [33,34] indicate a very good scaling behaviour already suggesting that automatic $\mathcal{O}(a)$ improvement is indeed working well.

Acknowledgements

The computer time for this project was made available to us by the John von Neumann-Institute for Computing on the JUMP and Jubl systems in Jülich and apeNEXT system in Zeuthen, by UKQCD on the QCDOC machine at Edinburgh, by INFN on the apeNEXT systems in Rome, by BSC on MareNostrum in Barcelona (www.bsc.es) and by the Leibniz Computer centre in Munich on the Altix system. We thank these computer centres and their staff for all technical advice and help. On QCDOC we have made use of Chroma [77] and BAGEL [78] software and we thank members of UKQCD for assistance. For the analysis we used among others the R language for statistical computing [79]. We gratefully acknowledge discussions with D. Bećirević, B. Blossier, N. Christian, G. Münster, O. Pène and A. Vladikas.

This work has been supported in part by the DFG Sonderforschungsbereich/Transregio SFB/TR9-03 and the EU Integrated Infrastructure Initiative Hadron Physics (I3HP) under contract RII3-CT-2004-506078. We also thank the DEISA Consortium (co-funded by the EU, FP6 project 508830), for support within the DEISA Extreme Computing Initiative (www.deisa.org). G.C.R. and R.F. thank MIUR (Italy) for partial financial support under the contract PRIN04. V.G. and D.P. thank MEC (Spain) for partial financial support under grant FPA2005-00711.

References

[1] K.G. Wilson, Phys. Rev. D 10 (1974) 2445.
[2] ALPHA, R. Frezzotti, P.A. Grassi, S. Sint, P. Weisz, JHEP 0108 (2001) 058, hep-lat/0101001.
[3] R. Frezzotti, G.C. Rossi, JHEP 0408 (2004) 007, hep-lat/0306014.
[4] M. Hasenbusch, Phys. Lett. B 519 (2001) 177, hep-lat/0107019.
[5] TrinLat, M.J. Peardon, J. Sexton, Nucl. Phys. B (Proc. Suppl.) 119 (2003) 985, hep-lat/0209037.
[6] QCDSF, A. Ali Khan, et al., Phys. Lett. B 564 (2003) 235, hep-lat/0303026.
[7] M. Lüscher, Comput. Phys. Commun. 165 (2005) 199, hep-lat/0409106.
[8] C. Urbach, K. Jansen, A. Shindler, U. Wenger, Comput. Phys. Commun. 174 (2006) 87, hep-lat/0506011.
[9] M.A. Clark, A.D. Kennedy, hep-lat/0608015.

[10] L. Del Debbio, L. Giusti, M. Lüscher, R. Petronzio, N. Tantalo, JHEP 0602 (2006) 011, hep-lat/0512021.
[11] R. Frezzotti, G.C. Rossi, JHEP 0410 (2004) 070, hep-lat/0407002.
[12] R. Frezzotti, G. Martinelli, M. Papinutto, G.C. Rossi, JHEP 0604 (2006) 038, hep-lat/0503034.
[13] G. Munster, C. Schmidt, Europhys. Lett. 66 (2004) 652, hep-lat/0311032.
[14] S.R. Sharpe, J.M.S. Wu, Phys. Rev. D 71 (2005) 074501, hep-lat/0411021.
[15] S.R. Sharpe, Phys. Rev. D 72 (2005) 074510, hep-lat/0509009.
[16] S. Aoki, O. Bär, Phys. Rev. D 70 (2004) 116011, hep-lat/0409006.
[17] $\chi_{\mathrm{L}}^{\mathrm{F}}$ Collaboration, K. Jansen, A. Shindler, C. Urbach, I. Wetzorke, Phys. Lett. B 586 (2004) 432, hep-lat/0312013.
[18] $\chi_{\mathrm{L}}^{\mathrm{F}}$ Collaboration, K. Jansen, M. Papinutto, A. Shindler, C. Urbach, I. Wetzorke, Phys. Lett. B 619 (2005) 184, hep-lat/0503031.
[19] $\chi_{\mathrm{L}}^{\mathrm{F}}$ Collaboration, K. Jansen, M. Papinutto, A. Shindler, C. Urbach, I. Wetzorke, JHEP 0509 (2005) 071, hep-lat/0507010.
[20] A.M. Abdel-Rehim, R. Lewis, R.M. Woloshyn, Phys. Rev. D 71 (2005) 094505, hep-lat/0503007.
[21] C. Pena, S. Sint, A. Vladikas, JHEP 0409 (2004) 069, hep-lat/0405028.
[22] ALPHA, M. Guagnelli, J. Heitger, C. Pena, S. Sint, A. Vladikas, JHEP 0603 (2006) 088, hep-lat/0505002.
[23] ALPHA, P. Dimopoulos, et al., Nucl. Phys. B 749 (2006) 69, hep-ph/0601002.
[24] D. Becirevic, et al., Phys. Rev. D 74 (2006) 034501, hep-lat/0605006.
[25] T. Chiarappa, et al., hep-lat/0606011.
[26] E.M. Ilgenfritz, et al., hep-lat/0610112.
[27] O. Bär, K. Jansen, S. Schaefer, L. Scorzato, A. Shindler, hep-lat/0609039.
[28] $\chi_{\mathrm{L}}^{\mathrm{F}}$ Collaboration, K. Jansen, et al., Phys. Lett. B 624 (2005) 334, hep-lat/0507032.
[29] F. Farchioni, et al., PoS LAT2005 (2006) 033, hep-lat/0509036.
[30] F. Farchioni, et al., PoS LAT2005 (2006) 072, hep-lat/0509131.
[31] L. Scorzato, et al., Nucl. Phys. B (Proc. Suppl.) 153 (2006) 283, hep-lat/0511036.
[32] A. Shindler, PoS LAT2005 (2006) 014, hep-lat/0511002.
[33] ETM, K. Jansen, C. Urbach, hep-lat/0610015.
[34] ETM, A. Shindler, hep-ph/0611264.
[35] ETM Collaboration, P. Boucaud et al., in preparation (2007).
[36] L. Del Debbio, L. Giusti, M. Lüscher, R. Petronzio, N. Tantalo, hep-lat/0610059.
[37] L. Del Debbio, L. Giusti, M. Lüscher, R. Petronzio, N. Tantalo, hep-lat/0701009.
[38] M. Gockeler, et al., PoS LAT2006 (2006) 179, hep-lat/0610066.
[39] P. Weisz, Nucl. Phys. B 212 (1983) 1.
[40] F. Farchioni, et al., Nucl. Phys. B (Proc. Suppl.) 140 (2005) 240, hep-lat/0409098.
[41] F. Farchioni, et al., Eur. Phys. J. C 42 (2005) 73, hep-lat/0410031.
[42] F. Farchioni, et al., Eur. Phys. J. C 39 (2005) 421, hep-lat/0406039.
[43] F. Farchioni, et al., Eur. Phys. J. C 47 (2006) 453, hep-lat/0512017.
[44] F. Farchioni, et al., Phys. Lett. B 624 (2005) 324, hep-lat/0506025.
[45] S.R. Sharpe, J.M.S. Wu, Phys. Rev. D 70 (2004) 094029, hep-lat/0407025.
[46] G. Münster, JHEP 0409 (2004) 035, hep-lat/0407006.
[47] G. Münster, C. Schmidt, E.E. Scholz, Nucl. Phys. B (Proc. Suppl.) 140 (2005) 320, hep-lat/0409066.
[48] L. Scorzato, Eur. Phys. J. C 37 (2004) 445, hep-lat/0407023.
[49] S. Aoki, Phys. Lett. B 190 (1987) 140.
[50] A. Sternbeck, E.-M. Ilgenfritz, W. Kerler, M. Müller-Preußker, H. Stüben, Nucl. Phys. B (Proc. Suppl.) 129 (2004) 898, hep-lat/0309059.
[51] E.-M. Ilgenfritz, W. Kerler, M. Müller-Preußker, A. Sternbeck, H. Stüben, Phys. Rev. D 69 (2004) 074511, hep-lat/0309057.
[52] T. Blum, et al., Phys. Rev. D 50 (1994) 3377, hep-lat/9404006.
[53] JLQCD, S. Aoki, et al., Nucl. Phys. B (Proc. Suppl.) 106 (2002) 263, hep-lat/0110088.
[54] JLQCD, S. Aoki, et al., Phys. Rev. D 72 (2005) 054510, hep-lat/0409016.
[55] K. Jansen, Nucl. Phys. B (Proc. Suppl.) 129 (2004) 3, hep-lat/0311039.
[56] M. Creutz, hep-lat/9608024.
[57] S.R. Sharpe, J.R. Singleton, Phys. Rev. D 58 (1998) 074501, hep-lat/9804028.
[58] S. Aoki, K. Higashijima, Prog. Theor. Phys. 76 (1986) 521.
[59] T. Izubuchi, J. Noaki, A. Ukawa, Phys. Rev. D 58 (1998) 114507, hep-lat/9805019.
[60] K.-I. Nagai, K. Jansen, Phys. Lett. B 633 (2006) 325, hep-lat/0510076.
[61] QCD-TARO, P. de Forcrand, et al., Nucl. Phys. B (Proc. Suppl.) 53 (1997) 938, hep-lat/9608094.
[62] T. DeGrand, A. Hasenfratz, T.G. Kovacs, Phys. Rev. D 67 (2003) 054501, hep-lat/0211006.
[63] S. Necco, Nucl. Phys. B 683 (2004) 137, hep-lat/0309017.
[64] S. Takeda, et al., Phys. Rev. D 70 (2004) 074510, hep-lat/0408010.
[65] QCDSF Collaboration, R. Horsley, H. Perlt, P.E.L. Rakow, G. Schierholz, A. Schiller, Nucl. Phys. B 693 (2004) 3, hep-lat/0404007.
[66] M. Hasenbusch, K. Jansen, Nucl. Phys. B 659 (2003) 299, hep-lat/0211042.
[67] UKQCD, M. Foster, C. Michael, Phys. Rev. D 59 (1999) 074503, hep-lat/9810021.
[68] UKQCD, C. McNeile, C. Michael, Phys. Rev. D 73 (2006) 074506, hep-lat/0603007.
[69] UKQCD, P. Lacock, A. McKerrell, C. Michael, I.M. Stopher, P.W. Stephenson, Phys. Rev. D 51 (1995) 6403, hep-lat/9412079.
[70] ALPHA, U. Wolff, Comput. Phys. Commun. 156 (2004) 143, hep-lat/0306017.
[71] R. Sommer, Nucl. Phys. B 411 (1994) 839, hep-lat/9310022.
[72] J. Gasser, H. Leutwyler, Phys. Lett. B 184 (1987) 83.
[73] G. Colangelo, S. Dürr, C. Haefeli, Nucl. Phys. B 721 (2005) 136, hep-lat/0503014.
[74] H. Leutwyler, hep-ph/0612112.
[75] A. Walker-Loud, J.M.S. Wu, Phys. Rev. D 72 (2005) 014506, hep-lat/0504001.
[76] UKQCD, C. McNeile, C. Michael, Phys. Rev. D 63 (2001) 114503, hep-lat/0010019.
[77] R.G. Edwards, B. Joo, Nucl. Phys. B (Proc. Suppl.) 140 (2005) 832, hep-lat/0409003.
[78] P. Boyle, http://www.ph.ed.ac.uk/~paboyle/bagel/Bagel.html.
[79] R Development Core Team, R: A Language and Environment for Statistical Computing, R Foundation for Statistical Computing, Vienna, Austria, ISBN 3-900051-07-0, 2005.

[tIS-2]

Numerical simulation of QCD with u, d, s and c quarks in the twisted-mass Wilson formulation

Eur. Phys. J. C50 373-383 (2007)

Eur. Phys. J. C 50, 373–383 (2007)
DOI 10.1140/epjc/s10052-006-0204-4

THE EUROPEAN PHYSICAL JOURNAL C

Regular Article – Theoretical Physics

Numerical simulation of QCD with u, d, s and c quarks in the twisted-mass Wilson formulation

T. Chiarappa[1], F. Farchioni[2], K. Jansen[3], I. Montvay[4,a], E.E. Scholz[5], L. Scorzato[6], T. Sudmann[2], C. Urbach[7]

[1] Università Milano Bicocca, Piazza della Scienza 3, 20126 Milano, Italy
[2] Universität Münster, Institut für Theoretische Physik, Wilhelm-Klemm-Strasse 9, 48149 Münster, Germany
[3] NIC, DESY, Zeuthen, Platanenallee 6, 15738 Zeuthen, Germany
[4] Deutsches Elektronen-Synchrotron DESY, Notkestr. 85, 22603 Hamburg, Germany
[5] Physics Department, Brookhaven National Laboratory, Upton, NY 11973, USA
[6] ECT*, strada delle tabarelle 286, 38050 Villazzano (TN), Italy
[7] Theoretical Physics Division, Dept. of Mathematical Sciences, University of Liverpool, Liverpool L69 3BX, UK

Received: 3 July 2006 / Revised version: 22 November 2006 /
Published online: 10 February 2007 –

Abstract. A first study of numerical Monte Carlo simulations with two quark doublets, a mass-degenerate one and a mass-split one, interpreted as u, d, s and c quarks, is carried out in the framework of the twisted mass Wilson lattice formulation. Tuning the bare parameters of this theory is explored on $12^3 \cdot 24$ and $16^3 \cdot 32$ lattices at lattice spacings $a \simeq 0.20$ fm and $a \simeq 0.15$ fm, respectively.

1 Introduction

In QCD the effect of virtual quark loops is most important for the three light quarks (u, d, s). In recent unquenched numerical simulations, besides the two lightest quarks u and d, the s quark is also included (see, for instance, [1–3]). The formulation of QCD with twisted-mass Wilson fermions [4] is based on chiral rotations of the bare mass (or, equivalently, of the Wilson term) within quark doublets. Therefore, in this formulation there are two possibilities for unquenched simulations with (u, d, s) quarks: either the s quark is taken alone and the twisted mass formulation is restricted to the (u, d) doublet or, in addition to the s quark, also the c quark is included in a mass-split doublet using the formulation in [5]. In the present paper we explore the latter possibility (for first results along this line see the proceedings contribution [6]).

Numerical simulations with twisted-mass Wilson fermions are usually performed at (or near) the critical (untwisted) bare quark mass, because there an *automatic* $\mathcal{O}(a)$ *improvement of the continuum limit* is expected [7, 8]. Our collaboration has performed several studies of twisted-mass QCD both in the quenched approximation [9–12] and in unquenched simulations with dynamical (u, d) quarks [13–16]. In the present paper we explore the possibility of numerical simulations of QCD with a degenerate doublet (u, d) and a mass-split doublet (c, s) of dynamical quarks in the twisted mass Wilson formulation.

The plan of this paper is as follows: in the next section we define the lattice action and describe the simulation algorithm. Section 3 is devoted to the introduction of physical fields and currents important for the interpretation of results. In Sect. 4 we present our numerical results. The last section contains a discussion and final remarks.

2 Lattice action and simulation algorithm

2.1 Lattice action

The notation for the lattice action of the *light* mass-degenerate (u, d) doublet, denoted by a subscript l, is the same as in our previous papers, for instance, [16]:

$$\begin{aligned} S_{\rm l} = \sum_x \Big\{ & (\overline{\chi}_{{\rm l},x}[\mu_{\kappa{\rm l}} + {\rm i}\gamma_5\tau_3\, a\mu_{\rm l}]\chi_{{\rm l},x}) \\ & - \frac{1}{2}\sum_{\mu=\pm 1}^{\pm 4} (\overline{\chi}_{{\rm l},x+\hat{\mu}} U_{x\mu}[r+\gamma_\mu]\chi_{{\rm l},x}) \Big\} \\ \equiv & \sum_{x,y} \overline{\chi}_{{\rm l},x} Q^{(\chi)}_{{\rm l},xy} \chi_{{\rm l},y}\,. \end{aligned} \tag{1}$$

Here, and in most cases below, colour-, spinor- and isospin indices are suppressed. For the isospin indices later on we shall also use a notation as, for instance, $\chi_{\rm l} \equiv (\chi_u\ \chi_d)$. The ("untwisted") bare quark mass of the light doublet in lattice units is denoted by

$$\mu_{\kappa{\rm l}} \equiv a m_{0{\rm l}} + 4r = \frac{1}{2\kappa_{\rm l}}\,, \tag{2}$$

[a] e-mail: istvan.montvay@desy.de

r is the Wilson parameter, set in our simulations to $r = 1$, $am_{0\mathrm{l}}$ is another convention for the bare quark mass in lattice units and κ_l is the conventional hopping parameter. The twisted mass of the light doublet in lattice units is denoted by $a\mu_\mathrm{l}$. $U_{x\mu} \in SU(3)$ is the gauge link variable, and we also defined $U_{x,-\mu} = U^\dagger_{x-\hat{\mu},\mu}$ and $\gamma_{-\mu} = -\gamma_\mu$.

Besides the quark doublet fields $\chi_\mathrm{l}, \overline{\chi}_\mathrm{l}$ in (1) it will turn out convenient to introduce other fields by the transformation

$$\psi_{\mathrm{l},x} \equiv \frac{1}{\sqrt{2}}(1 + \mathrm{i}\gamma_5\tau_3)\chi_{\mathrm{l},x}\,,$$
$$\overline{\psi}_{\mathrm{l},x} \equiv \overline{\chi}_{\mathrm{l},x}\frac{1}{\sqrt{2}}(1 + \mathrm{i}\gamma_5\tau_3)\,. \tag{3}$$

The *quark matrix on the χ basis* $Q^{(\chi)}_\mathrm{l}$ defined in (1) is

$$Q^{(\chi)}_{\mathrm{l},xy} = \delta_{xy}(\mu_{\kappa\mathrm{l}} + \mathrm{i}\gamma_5\tau_3\, a\mu_\mathrm{l}) - \frac{1}{2}\sum_{\mu=\pm1}^{\pm4}\delta_{x,y+\hat{\mu}}U_{y\mu}[r + \gamma_\mu] \tag{4}$$

or in a short notation, without the site indices,

$$Q^{(\chi)}_\mathrm{l} = \mu_{\kappa\mathrm{l}} + \mathrm{i}\gamma_5\tau_3 a\mu_\mathrm{l} + N + R\,, \tag{5}$$

with

$$N_{xy} \equiv -\frac{1}{2}\sum_{\mu=\pm1}^{\pm4}\delta_{x,y+\hat{\mu}}U_{y\mu}\gamma_\mu\,,$$
$$R_{xy} \equiv -\frac{r}{2}\sum_{\mu=\pm1}^{\pm4}\delta_{x,y+\hat{\mu}}U_{y\mu}\,. \tag{6}$$

On the ψ *basis* defined in (3) we have the quark matrix

$$Q^{(\psi)}_\mathrm{l} = \frac{1}{2}(1 - \mathrm{i}\gamma_5\tau_3)Q^{(\chi)}_\mathrm{l}(1 - \mathrm{i}\gamma_5\tau_3) = a\mu_\mathrm{l} + N - \mathrm{i}\gamma_5\tau_3(\mu_{\kappa\mathrm{l}} + R)\,. \tag{7}$$

As it has been shown by Frezzotti and Rossi in [5], a *real quark determinant* with a mass-split doublet can be obtained if the mass splitting is taken to be orthogonal in isospin space to the twist direction. One could take, for instance, the mass splitting in the τ_1 direction if the twist is in the τ_3 direction, as in (1). It is, however, more natural to exchange the two directions because then the bare mass is diagonal in isospin. In this case, the lattice action of the *heavy* mass-split (c, s) doublet, denoted by a subscript h, is defined as

$$S_\mathrm{h} = \sum_{x,y}\overline{\chi}_{\mathrm{h},x}Q^{(\chi)}_{\mathrm{h},xy}\chi_{\mathrm{h},y}\,, \tag{8}$$

with

$$Q^{(\chi)}_\mathrm{h} = \mu_{\kappa\mathrm{h}} + \mathrm{i}\gamma_5\tau_1 a\mu_\sigma + \tau_3 a\mu_\delta + N + R\,. \tag{9}$$

For the isospin indices later on we shall also use a notation as, for instance, $\chi_\mathrm{h} \equiv (\chi_c\ \chi_s)$. The ψ *basis* is introduced similarly to (3) by

$$\psi_{\mathrm{h},x} \equiv \frac{1}{\sqrt{2}}(1 + \mathrm{i}\gamma_5\tau_1)\chi_{\mathrm{h},x}\,,$$
$$\overline{\psi}_{\mathrm{h},x} \equiv \overline{\chi}_{\mathrm{h},x}\frac{1}{\sqrt{2}}(1 + \mathrm{i}\gamma_5\tau_1)\,, \tag{10}$$

and the *quark matrix on the ψ basis* is for the heavy mass-split doublet

$$Q^{(\psi)}_\mathrm{h} = \frac{1}{2}(1 - \mathrm{i}\gamma_5\tau_1)Q^{(\chi)}_\mathrm{h}(1 - \mathrm{i}\gamma_5\tau_1) = a\mu_\sigma + \tau_3 a\mu_\delta + N - \mathrm{i}\gamma_5\tau_1(\mu_{\kappa\mathrm{h}} + R)\,. \tag{11}$$

For the $SU(3)$ Yang–Mills gauge field we apply the *tree-level improved Symanzik* (tlSym) action which belongs to a one-parameter family of actions obtained by renormalisation group considerations and in the Symanzik improvement scheme [17]. Those actions also include, besides the usual (1×1) Wilson loop plaquette term, planar rectangular (1×2) Wilson loops:

$$S_g = \beta\sum_x\left(c_0\sum_{\mu<\nu;\mu,\nu=1}^{4}\left\{1 - \frac{1}{3}\,\mathrm{Re}\,U^{1\times1}_{x\mu\nu}\right\} + c_1\sum_{\mu\neq\nu;\mu,\nu=1}^{4}\left\{1 - \frac{1}{3}\,\mathrm{Re}\,U^{1\times2}_{x\mu\nu}\right\}\right), \tag{12}$$

with the condition $c_0 = 1 - 8c_1$. For the tlSym action we have $c_1 = -1/12$ [18–20].

2.2 Simulation algorithm

For preparing the sequences of gauge configurations a *polynomial hybrid Monte Carlo* (PHMC) updating algorithm was used. This algorithm is based on multi-step (actually two-step) polynomial approximations of the inverse fermion matrix with stochastic correction in the update chain as described in [21]. It is based on the PHMC algorithm as introduced in [22–24]. The polynomial approximation scheme and the stochastic correction in the update chain is taken over from the two-step multi-boson algorithm of [25]. (For an alternative updating algorithm in QCD with $N_f = 2+1+1$ quark flavours, which will be used for algorithmic comparisons in the future, see [26, 27].)

Table 1. Algorithmic parameters in two runs on a $16^3 \cdot 32$ lattice at $\beta = 3.35$, $\kappa_\mathrm{l} = \kappa_\mathrm{h} = \kappa$, $a\mu_\mathrm{l} = 0.0075$, $a\mu_\sigma = 0.2363$, $a\mu_\delta = 0.2138$ and with determinant break-up $n_\mathrm{B} = 2$. The first line for a given κ shows the pion mass and the parameters for the light doublet, the second line the kaon mass and the parameters for the heavy doublet

κ	$am_{\pi,K}$	ϵ	λ	n_1	$\bar{n}_1$	n_2	$\bar{n}_2$
0.1690	0.8237(13)	1.25e−2	25	70	110	120	160
	0.9231(11)	3.25e−2	26	50	80	90	130
0.1705	0.3433(52)	1.875e−4	25	220	320	800	930
	0.6503(18)	1.875e−2	26	60	100	120	160

For typical values of the approximation interval and polynomial orders on $16^3 \cdot 32$ lattices see Table 1. The notation is that of [21]: the approximation interval is $[\epsilon, \lambda]$, the orders of the polynomials $P_j (j = 1, 2)$ are n_j and those of $\bar{P}_j (j = 1, 2)$ are $\bar{n}_j$, respectively. The simulations have been done with *determinant break-up* $n_{\mathrm{B}} = 2$. On the $12^3 \cdot 24$, for similar values of the pseudoscalar masses in lattice units, the orders n_2 and $\bar{n}_2$ are the same and the values of n_1 and $\bar{n}_1$ are somewhat smaller.

3 Physical fields and currents

The *physical quark fields*, which in the continuum limit are proportional to the renormalised quark fields of both flavours in the doublets, are obtained [4] by a chiral rotation from the fields in the lattice action in (1) or from those defined in (3) for the light doublet, and similarly in (8)–(10) for the heavy doublet. On the χ basis we have

$$\psi^{\mathrm{phys}}_{\mathrm{l},x} = \mathrm{e}^{\frac{\mathrm{i}}{2}\omega_{\mathrm{l}}\gamma_5\tau_3}\chi_{\mathrm{l},x}\,, \quad \overline{\psi}^{\mathrm{phys}}_{\mathrm{l},x} = \overline{\chi}_{\mathrm{l},x}\mathrm{e}^{\frac{\mathrm{i}}{2}\omega_{\mathrm{l}}\gamma_5\tau_3}\,; \tag{13}$$

$$\psi^{\mathrm{phys}}_{\mathrm{h},x} = \mathrm{e}^{\frac{\mathrm{i}}{2}\omega_{\mathrm{h}}\gamma_5\tau_1}\chi_{\mathrm{h},x}\,, \quad \overline{\psi}^{\mathrm{phys}}_{\mathrm{h},x} = \overline{\chi}_{\mathrm{h},x}\mathrm{e}^{\frac{\mathrm{i}}{2}\omega_{\mathrm{h}}\gamma_5\tau_1}\,. \tag{14}$$

Since the transformations in (3) and (10) correspond to chiral rotations with $\omega_{\mathrm{l}} = \frac{\pi}{2}$ and $\omega_{\mathrm{h}} = \frac{\pi}{2}$, respectively, we have with

$$\bar{\omega}_{\mathrm{l}} \equiv \omega_{\mathrm{l}} - \frac{\pi}{2}\,, \quad \bar{\omega}_{\mathrm{h}} \equiv \omega_{\mathrm{h}} - \frac{\pi}{2} \tag{15}$$

the relations

$$\psi^{\mathrm{phys}}_{\mathrm{l},x} = \mathrm{e}^{\frac{\mathrm{i}}{2}\bar{\omega}_{\mathrm{l}}\gamma_5\tau_3}\psi_{\mathrm{l},x}\,, \quad \overline{\psi}^{\mathrm{phys}}_{\mathrm{l},x} = \overline{\psi}_{\mathrm{l},x}\mathrm{e}^{\frac{\mathrm{i}}{2}\bar{\omega}_{\mathrm{l}}\gamma_5\tau_3}\,; \tag{16}$$

$$\psi^{\mathrm{phys}}_{\mathrm{h},x} = \mathrm{e}^{\frac{\mathrm{i}}{2}\bar{\omega}_{\mathrm{h}}\gamma_5\tau_1}\psi_{\mathrm{h},x}\,, \quad \overline{\psi}^{\mathrm{phys}}_{\mathrm{h},x} = \overline{\psi}_{\mathrm{h},x}\mathrm{e}^{\frac{\mathrm{i}}{2}\bar{\omega}_{\mathrm{h}}\gamma_5\tau_1}\,. \tag{17}$$

Since the simulations are usually performed near *full twist* corresponding to $\omega_{\mathrm{l}} = \omega_{\mathrm{h}} = \frac{\pi}{2}$, the modified twist angles are close to zero:

$$\bar{\omega}_{\mathrm{l}} \simeq 0\,, \quad \bar{\omega}_{\mathrm{h}} \simeq 0\,. \tag{18}$$

Therefore, near full twist the ψ fields are approximately equal to the physical quark fields. At full twist the use of the ψ basis is advantageous because the formulas are simpler than in the χ basis.

The definition of the twist angles is not unique. There are different viable possibilities to define them and the *critical hopping parameters* corresponding to them (see, for instance, [10, 14, 28–33]).

Here, for the light doublet, we use the definition based on the requirement of parity conservation for some matrix element of the physical vector and axial-vector current, as first introduced in [14, 28] and numerically studied in detail in [16]. For this let us introduce the bare vector and axial-vector bilinears

$$V^a_{\mathrm{l},x\mu} \equiv \overline{\chi}_{\mathrm{l},x}\frac{1}{2}\tau_a\gamma_\mu\chi_{\mathrm{l},x}\,,$$
$$A^a_{\mathrm{l},x\mu} \equiv \overline{\chi}_{\mathrm{l},x}\frac{1}{2}\tau_a\gamma_\mu\gamma_5\chi_{\mathrm{l},x} \quad (a = 1, 2)\,. \tag{19}$$

The twist angle is introduced as the chiral rotation angle between the renormalised (physical) chiral currents:

$$\widehat{V}^a_{\mathrm{l},x\mu} = Z_{\mathrm{l}V}V^a_{\mathrm{l},x\mu}\cos\omega_{\mathrm{l}} + \epsilon_{ab}Z_{\mathrm{l}A}A^b_{\mathrm{l},x\mu}\sin\omega_{\mathrm{l}}\,, \tag{20}$$

$$\widehat{A}^a_{\mathrm{l},x\mu} = Z_{\mathrm{l}A}A^a_{\mathrm{l},x\mu}\cos\omega_{\mathrm{l}} + \epsilon_{ab}Z_{\mathrm{l}V}V^b_{\mathrm{l},x\mu}\sin\omega_{\mathrm{l}}\,, \tag{21}$$

where only charged currents are considered ($a = 1, 2$), ϵ_{ab} is the antisymmetric unit tensor and $Z_{\mathrm{l}V}$ and $Z_{\mathrm{l}A}$ are the multiplicative renormalisation factors of the vector and axial-vector current, respectively. The exact requirements defining ω_{l} (and also yielding the value of $Z_{\mathrm{l}A}/Z_{\mathrm{l}V}$) are taken to be

$$\big\langle 0\big|\widehat{V}^+_{\mathrm{l},x,\mu=0}\big|\pi^-\big\rangle = 0\,, \quad \big\langle 0\big|\widehat{A}^+_{\mathrm{l},x,\mu=1,2,3}\big|\rho^-\big\rangle = 0\,. \tag{22}$$

For the heavy doublet, in principle, one could translate and use this construction, too, but for applications in the kaon and D-meson sector it is more natural to consider bilinears between the light and the heavy doublet. In addition, inside the heavy doublet, due to the off-diagonal twist, one also would have to consider disconnected quark contributions which are absent in the light–heavy sector. Let us introduce the bare vector, axial-vector, scalar and pseudoscalar bilinears in the K^+ and D^0 sector as

$$V_{K^+,x\mu} \equiv \overline{\chi}_{s,x}\gamma_\mu\chi_{u,x}\,, \quad A_{K^+,x\mu} \equiv \overline{\chi}_{s,x}\gamma_\mu\gamma_5\chi_{u,x}\,, \tag{23}$$

$$S_{K^+,x} \equiv \overline{\chi}_{s,x}\chi_{u,x}\,, \quad P_{K^+,x} \equiv \overline{\chi}_{s,x}\gamma_5\chi_{u,x}\,, \tag{24}$$

$$V_{D^0,x\mu} \equiv \overline{\chi}_{c,x}\gamma_\mu\chi_{u,x}\,, \quad A_{D^0,x\mu} \equiv \overline{\chi}_{c,x}\gamma_\mu\gamma_5\chi_{u,x}\,, \tag{25}$$

$$S_{D^0,x} \equiv \overline{\chi}_{c,x}\chi_{u,x}\,, \quad P_{D^0,x} \equiv \overline{\chi}_{c,x}\gamma_5\chi_{u,x}\,, \tag{26}$$

and similarly for the K^0 and D^- sector by changing $u \to d$. Denoting the kaon and D-meson doublet by $K \equiv (K^+\ K^0)$ and $D \equiv (D^0\ D^-)$, respectively, and introducing $\check{K} \equiv (K^+\ -K^0)$ and $\check{D} \equiv (D^0\ -D^-)$, the renormalised vector and axial-vector currents of the kaon doublet are given by

$$\begin{aligned}\widehat{V}_{K,x\mu} = {} & \cos\frac{\omega_{\mathrm{l}}}{2}\cos\frac{\omega_{\mathrm{h}}}{2}Z_V V_{K,x\mu} + \sin\frac{\omega_{\mathrm{l}}}{2}\sin\frac{\omega_{\mathrm{h}}}{2}Z_V V_{\check{D},x\mu} \\ & + \mathrm{i}\sin\frac{\omega_{\mathrm{l}}}{2}\cos\frac{\omega_{\mathrm{h}}}{2}Z_A A_{\check{K},x\mu} \\ & - \mathrm{i}\cos\frac{\omega_{\mathrm{l}}}{2}\sin\frac{\omega_{\mathrm{h}}}{2}Z_A A_{D,x\mu}\,,\end{aligned} \tag{27}$$

$$\begin{aligned}\widehat{A}_{K,x\mu} = {} & \cos\frac{\omega_{\mathrm{l}}}{2}\cos\frac{\omega_{\mathrm{h}}}{2}Z_A A_{K,x\mu} + \sin\frac{\omega_{\mathrm{l}}}{2}\sin\frac{\omega_{\mathrm{h}}}{2}Z_A A_{\check{D},x\mu} \\ & + \mathrm{i}\sin\frac{\omega_{\mathrm{l}}}{2}\cos\frac{\omega_{\mathrm{h}}}{2}Z_V V_{\check{K},x\mu} \\ & - \mathrm{i}\cos\frac{\omega_{\mathrm{l}}}{2}\sin\frac{\omega_{\mathrm{h}}}{2}Z_V V_{D,x\mu}\,.\end{aligned} \tag{28}$$

Analogously for the scalar bilinears:

$$\begin{aligned}\hat{S}_{K,x} = {} & \cos\frac{\omega_{\mathrm{l}}}{2}\cos\frac{\omega_{\mathrm{h}}}{2}Z_S S_{K,x} - \sin\frac{\omega_{\mathrm{l}}}{2}\sin\frac{\omega_{\mathrm{h}}}{2}Z_S S_{\check{D},x} \\ & + \mathrm{i}\sin\frac{\omega_{\mathrm{l}}}{2}\cos\frac{\omega_{\mathrm{h}}}{2}Z_P P_{\check{K},x} + \mathrm{i}\cos\frac{\omega_{\mathrm{l}}}{2}\sin\frac{\omega_{\mathrm{h}}}{2}Z_P P_{D,x}\,,\end{aligned} \tag{29}$$

$$\begin{aligned}\hat{P}_{K,x} = {} & \cos\frac{\omega_{\mathrm{l}}}{2}\cos\frac{\omega_{\mathrm{h}}}{2}Z_P P_{K,x} - \sin\frac{\omega_{\mathrm{l}}}{2}\sin\frac{\omega_{\mathrm{h}}}{2}Z_P P_{\check{D},x} \\ & + \mathrm{i}\sin\frac{\omega_{\mathrm{l}}}{2}\cos\frac{\omega_{\mathrm{h}}}{2}Z_S S_{\check{K},x} + \mathrm{i}\cos\frac{\omega_{\mathrm{l}}}{2}\sin\frac{\omega_{\mathrm{h}}}{2}Z_S S_{D,x}\,.\end{aligned} \tag{30}$$

Similar relations hold in the D-meson doublet, too. Equations (27) and (28) show that near full twist, $\omega_{\mathrm{l,h}} \simeq \pi/2$, all four terms on the right hand sides have roughly equal coefficients.

The requirement of parity symmetry in the isotriplets (pions, rho mesons) allows one to fix the twist angle ω_{l}, cf. (22). In the case of the heavy–light isodoublet one has to take into account the mixing between the kaons and D mesons. In this case the twist angle ω_{h} (and ω_{l}) can be fixed by requiring conservation of parity and/or flavour symmetry.

The equations in (22) follow by considering [14, 16, 28] the (vanishing) vector-current–pseudoscalar and axial-vector-current–vector-current correlators, which turns out to be the most convenient choice for fixing the twist angle in the light sector. In the heavy–light sector the mixing patterns for currents and scalar bilinears are similar, so any combination of operators gives similar expressions. However, correlators only made up of scalar bilinears are expected to give a better signal, so we concentrate on this case for the discussion. Considering the upper components, the four bilinears P_{K^+}, P_{D^0}, S_{K^+}, S_{D^0} and the respective charge-conjugated versions must be included in the analysis. We define a four-dimensional vector of the multiplicatively renormalised bilinears:

$$\mathcal{V} = \begin{pmatrix} Z_P P_{K^+} \\ Z_P P_{D^0} \\ Z_S S_{K^+} \\ Z_S S_{D^0} \end{pmatrix},$$
$$\bar{\mathcal{V}} = (-Z_P P_{K^-}, -Z_P P_{\bar{D}^0}, Z_S S_{K^-}, Z_S S_{\bar{D}^0}), \quad (31)$$

and analogously the vector $\hat{\mathcal{V}}$ of the *fully* renormalised bilinears according to (29) and (30) (and the analogous equations for the D mesons). Equations (29) and (30) can be then reformulated in a compact notation as

$$\widehat{\mathcal{V}} = \mathcal{M}\mathcal{V}, \quad \bar{\widehat{\mathcal{V}}} = \bar{\mathcal{V}}\mathcal{M}^{-1}, \quad (32)$$

with the 4×4 matrix $\mathcal{M}$ given by

$$\mathcal{M}(\omega_{\mathrm{l}}, \omega_{\mathrm{h}}) = \begin{pmatrix} c_{\mathrm{l}}c_{\mathrm{h}} & -s_{\mathrm{l}}s_{\mathrm{h}} & \mathrm{i}s_{\mathrm{l}}c_{\mathrm{h}} & \mathrm{i}s_{\mathrm{h}}c_{\mathrm{l}} \\ -s_{\mathrm{l}}s_{\mathrm{h}} & c_{\mathrm{l}}c_{\mathrm{h}} & \mathrm{i}s_{\mathrm{h}}c_{\mathrm{l}} & \mathrm{i}s_{\mathrm{l}}c_{\mathrm{h}} \\ \mathrm{i}s_{\mathrm{l}}c_{\mathrm{h}} & \mathrm{i}s_{\mathrm{h}}c_{\mathrm{l}} & c_{\mathrm{l}}c_{\mathrm{h}} & -s_{\mathrm{l}}s_{\mathrm{h}} \\ \mathrm{i}s_{\mathrm{h}}c_{\mathrm{l}} & \mathrm{i}s_{\mathrm{l}}c_{\mathrm{h}} & -s_{\mathrm{l}}s_{\mathrm{h}} & c_{\mathrm{l}}c_{\mathrm{h}} \end{pmatrix}. \quad (33)$$

(Here we define for brevity $s_{\mathrm{l}} = \sin\frac{\omega_{\mathrm{l}}}{2}$, $s_{\mathrm{h}} = \sin\frac{\omega_{\mathrm{h}}}{2}$, $c_{\mathrm{l}} = \cos\frac{\omega_{\mathrm{l}}}{2}$, $c_{\mathrm{h}} = \cos\frac{\omega_{\mathrm{h}}}{2}$.) $\mathcal{M}$ is the unitary matrix describing the mixing pattern between the kaon and D-meson doublets. One can easily see that

$$\mathcal{M}^{\mathrm{T}} = \mathcal{M},$$
$$\mathcal{M}^{\dagger}(\omega_{\mathrm{l}}, \omega_{\mathrm{h}}) = \mathcal{M}^{*}(\omega_{\mathrm{l}}, \omega_{\mathrm{h}}) = \mathcal{M}(-\omega_{\mathrm{l}}, -\omega_{\mathrm{h}}) = \mathcal{M}^{-1}(\omega_{\mathrm{l}}, \omega_{\mathrm{h}}). \quad (34)$$

(The last equality is expected since reversing the sign of the angles corresponds to the inverse chiral transformation.) One can at this point define a *correlator matrix* in the kaon–D-meson sector by

$$\mathcal{C} = \langle \mathcal{V} \otimes \bar{\mathcal{V}} \rangle \quad (35)$$

(for example, $\mathcal{C}_{11} \equiv -Z_P^2 \langle P_{K^+} P_{K^-} \rangle$) and its fully renormalised version $\widehat{\mathcal{C}} = \langle \widehat{\mathcal{V}} \otimes \bar{\widehat{\mathcal{V}}} \rangle$. One has

$$\widehat{\mathcal{C}} = \mathcal{M}(\omega_{\mathrm{l}}, \omega_{\mathrm{h}}) \mathcal{C} \mathcal{M}^{-1}(\omega_{\mathrm{l}}, \omega_{\mathrm{h}}), \quad (36)$$
$$\mathcal{C} = \mathcal{M}^{-1}(\omega_{\mathrm{l}}, \omega_{\mathrm{h}}) \widehat{\mathcal{C}} \mathcal{M}(\omega_{\mathrm{l}}, \omega_{\mathrm{h}}). \quad (37)$$

Restoration of parity and flavour symmetry implies that $\widehat{\mathcal{C}}$ is a diagonal matrix with $\mathcal{M}(\omega_{\mathrm{l}}, \omega_{\mathrm{h}})$ the matrix realizing the diagonalisation. The off-diagonal elements of the matrix equation (36) can in principle be used to determine the angles ω_{l} and ω_{h}, while the diagonal elements give the physical correlators from which e.g. the masses can be obtained. Of course, in general, parity and flavour can only be restored up to $\mathcal{O}(a)$ violations.

Taking also into account the residual discrete symmetries possessed by the action defined by (1), (8) and (9), the only non-trivial conditions are obtained by imposing the vanishing of the flavour violating matrix elements $\widehat{\mathcal{C}}_{12}$, $\widehat{\mathcal{C}}_{34}$ and transposed:

$$\begin{aligned} \widehat{\mathcal{C}}_{12} + \widehat{\mathcal{C}}_{21} = {} & \left[(c_{\mathrm{l}}c_{\mathrm{h}})^2 + (s_{\mathrm{l}}s_{\mathrm{h}})^2\right](\mathcal{C}_{12} + \mathcal{C}_{21}) \\ & + \left[(s_{\mathrm{l}}c_{\mathrm{h}})^2 + (s_{\mathrm{h}}c_{\mathrm{l}})^2\right](\mathcal{C}_{34} + \mathcal{C}_{43}) \\ & - 2c_{\mathrm{l}}c_{\mathrm{h}}s_{\mathrm{l}}s_{\mathrm{h}}(\mathcal{C}_{11} + \mathcal{C}_{22} - \mathcal{C}_{33} - \mathcal{C}_{44}) \\ & + \mathrm{i}s_{\mathrm{h}}c_{\mathrm{h}}\left(s_{\mathrm{l}}^2 - c_{\mathrm{l}}^2\right)(\mathcal{C}_{13} - \mathcal{C}_{31} + \mathcal{C}_{24} - \mathcal{C}_{42}) \\ & + \mathrm{i}s_{\mathrm{l}}c_{\mathrm{l}}(s_{\mathrm{h}}^2 - c_{\mathrm{h}}^2)(\mathcal{C}_{23} - \mathcal{C}_{32} + \mathcal{C}_{14} - \mathcal{C}_{41}) \\ = {} & 0, \end{aligned} \quad (38)$$

$$\begin{aligned} \widehat{\mathcal{C}}_{34} + \widehat{\mathcal{C}}_{43} = {} & \left[(c_{\mathrm{h}}s_{\mathrm{l}})^2 + (c_{\mathrm{l}}s_{\mathrm{h}})^2\right](\mathcal{C}_{12} + \mathcal{C}_{21}) \\ & + \left[(c_{\mathrm{l}}c_{\mathrm{h}})^2 + (s_{\mathrm{l}}s_{\mathrm{h}})^2\right](\mathcal{C}_{34} + \mathcal{C}_{43}) \\ & + 2c_{\mathrm{l}}c_{\mathrm{h}}s_{\mathrm{l}}s_{\mathrm{h}}(\mathcal{C}_{11} + \mathcal{C}_{22} - \mathcal{C}_{33} - \mathcal{C}_{44}) \\ & - \mathrm{i}s_{\mathrm{h}}c_{\mathrm{h}}(s_{\mathrm{l}}^2 - c_{\mathrm{l}}^2)(\mathcal{C}_{13} - \mathcal{C}_{31} + \mathcal{C}_{24} - \mathcal{C}_{42}) \\ & - \mathrm{i}s_{\mathrm{l}}c_{\mathrm{l}}(s_{\mathrm{h}}^2 - c_{\mathrm{h}}^2)(\mathcal{C}_{23} - \mathcal{C}_{32} + \mathcal{C}_{14} - \mathcal{C}_{41}) \\ = {} & 0. \end{aligned} \quad (39)$$

The sum of the two above equations implies

$$\mathcal{C}_{12} + \mathcal{C}_{21} + \mathcal{C}_{34} + \mathcal{C}_{43} = 0. \quad (40)$$

A non-trivial relation for the renormalisation constants of the bilinears is obtained from (40):

$$Z_P^2/Z_S^2 = \frac{\langle S_{K^+} S_{\bar{D}^0} \rangle + \langle S_{D^0} S_{K^-} \rangle}{\langle P_{K^+} P_{\bar{D}^0} \rangle + \langle P_{D^0} P_{K^-} \rangle}, \quad (41)$$

which can be used for a non-perturbative determination of Z_P/Z_S.

Using (40), (38) (or (39)) can be restated in a compact way as a relation between $\cot\omega_{\mathrm{h}}$ and $\cot\omega_{\mathrm{l}}$:

$$\cot\omega_{\mathrm{h}} = \frac{\mathcal{C}_{11} + \mathcal{C}_{22} - \mathcal{C}_{33} - \mathcal{C}_{44} + \mathrm{i}(\mathcal{C}_{13} - \mathcal{C}_{31} + \mathcal{C}_{24} - \mathcal{C}_{42})\cot\omega_{\mathrm{l}}}{(\mathcal{C}_{12} + \mathcal{C}_{21} - \mathcal{C}_{34} - \mathcal{C}_{43})\cot\omega_{\mathrm{l}} - \mathrm{i}(\mathcal{C}_{23} - \mathcal{C}_{32} + \mathcal{C}_{14} - \mathcal{C}_{41})}. \quad (42)$$

This can be used to determine ω_{h} once ω_{l} is known. (ω_{l} can be obtained following the prescription of [14, 16, 28].)

This discussion suggests that, especially near full twist where the mixing is maximal, the analysis of the masses in the kaon–D-meson sector should be performed by considering the 4-dimensional correlator matrix $\mathcal{C}$.

For tuning the hopping parameters the *untwisted PCAC quark mass* is also very useful. In the light doublet it is defined by the PCAC relation containing the axial-vector current $A^a_{\mathrm{l},x\mu}$ in (19) and the corresponding pseudoscalar density $P^a_{\mathrm{l},x} = \overline{\chi}_{\mathrm{l},x}\frac{1}{2}\tau_a\gamma_5\chi_{\mathrm{l},x}$:

$$am_{\chi\mathrm{l}}^{\mathrm{PCAC}} \equiv \frac{\langle \partial^*_\mu A^+_{\mathrm{l},x\mu} P^-_{\mathrm{l},y}\rangle}{2\langle P^+_{\mathrm{l},x} P^-_{\mathrm{l},y}\rangle}\,, \tag{43}$$

where $\tau_\pm \equiv \tau_1 \pm \mathrm{i}\tau_2$. The condition of full twist in the light quark sector obtained from (22) by setting $\omega_\mathrm{l} = \pi/2$ coincides [16] with $m_{\chi\mathrm{l}}^{\mathrm{PCAC}} = 0$.

In the heavy sector one can define an untwisted PCAC quark mass $m_{\chi\mathrm{h}}^{\mathrm{PCAC}}$, too. A natural definition is obtained by considering the axial-vector Ward identity

$$\partial^*_\mu A^a_{\mathrm{h},x\mu} = 2am_{\chi\mathrm{h}}^{\mathrm{PCAC}} P^a_{\mathrm{h},x} + \begin{cases} 2\mathrm{i}Z_A^{-1}a\mu_\sigma S^0_{\mathrm{h},x}\,, & a=1\,,\\ 0\,, & a=2\,,\\ (-2\mathrm{i})Z_A^{-1}a\mu_\delta P^0_{\mathrm{h},x}\,, & a=3\,, \end{cases} \tag{44}$$

where, in analogy with the light sector in (19), we define

$$\begin{aligned} A^a_{\mathrm{h},x\mu} &\equiv \overline{\chi}_{\mathrm{h},x}\frac{1}{2}\tau_a\gamma_\mu\gamma_5\chi_{\mathrm{h},x} \quad (a=1,2,3)\,,\\ S^0_{\mathrm{h},x} &\equiv \overline{\chi}_{\mathrm{h},x}\chi_{\mathrm{h},x}\,, \quad P^0_{\mathrm{h},x} \equiv \overline{\chi}_{\mathrm{h},x}\gamma_5\chi_{\mathrm{h},x}\,. \end{aligned} \tag{45}$$

(Observe that for uniformity with the definition (43) we incorporate a factor Z_A^{-1} in the definition of the untwisted PCAC quark mass.) The above identity could in principle be used to tune ω_h to $\pi/2$ by imposing $am_{\chi\mathrm{h}}^{\mathrm{PCAC}} = 0$. However, as already mentioned, the presence of disconnected contributions in the heavy sector are likely not to allow for precise determinations.

One can consider also in this case the heavy–light sector. Here the axial-vector Ward identities read

$$\begin{aligned} \partial^*_\mu A_{K,x\mu} &= \big(am_{\chi s}^{\mathrm{PCAC}} + am_{\chi\mathrm{l}}^{\mathrm{PCAC}}\big)P_{K,x\mu}\\ &\quad + \mathrm{i}Z_A^{-1}a\mu_\mathrm{l}S_{\check{K},x\mu} + \mathrm{i}Z_A^{-1}a\mu_\sigma S_{D,x\mu}\,, \end{aligned} \tag{46}$$

$$\begin{aligned} \partial^*_\mu A_{D,x\mu} &= \big(am_{\chi c}^{\mathrm{PCAC}} + am_{\chi\mathrm{l}}^{\mathrm{PCAC}}\big)P_{D,x\mu}\\ &\quad + \mathrm{i}Z_A^{-1}a\mu_\mathrm{l}S_{\check{D},x\mu} + \mathrm{i}Z_A^{-1}a\mu_\sigma S_{K,x\mu}\,. \end{aligned} \tag{47}$$

The solution of the over-determined linear system, obtained by taking a suitable matrix element (for instance, $\langle\partial^*_\mu A_{K^+,x\mu}\,P_{K^-,y}\rangle$), allows one to determine numerically (together with (43)) the untwisted PCAC mass of the heavy quarks $m_{\chi c}^{\mathrm{PCAC}}$, $m_{\chi s}^{\mathrm{PCAC}}$ and the renormalisation factor Z_A. The condition of full twist in the heavy doublet can be written as

$$m_{\chi\mathrm{h}}^{\mathrm{PCAC}} \equiv m_{\chi c}^{\mathrm{PCAC}} + m_{\chi s}^{\mathrm{PCAC}} = 0\,. \tag{48}$$

The quark masses defined by (43), (46) and (47) are untwisted components of bare quark masses. The physical quark masses can be obtained by the corresponding PCAC relations of the renormalised currents and densities:

$$am_\mathrm{l}^{\mathrm{PCAC}} \equiv \frac{\langle \partial^*_\mu \widehat{A}^+_{\mathrm{l},x\mu}\hat{P}^-_{\mathrm{l},y}\rangle}{2\langle \hat{P}^+_{\mathrm{l},x}\hat{P}^-_{\mathrm{l},y}\rangle}\,, \tag{49}$$

$$am_s^{\mathrm{PCAC}} + am_\mathrm{l}^{\mathrm{PCAC}} \equiv \frac{\langle \partial^*_\mu \widehat{A}_{K^+,x\mu}\hat{P}_{K^-,y}\rangle}{\langle \hat{P}_{K^+,x}\hat{P}_{K^-,y}\rangle}\,, \tag{50}$$

$$am_c^{\mathrm{PCAC}} + am_\mathrm{l}^{\mathrm{PCAC}} \equiv \frac{\langle \partial^*_\mu \widehat{A}_{D^+,x\mu}\hat{P}_{D^-,y}\rangle}{\langle \hat{P}_{D^+,x}\hat{P}_{D^-,y}\rangle}\,. \tag{51}$$

They are related to the bare quark masses by

$$m_\mathrm{l}^{\mathrm{PCAC}} = Z_P^{-1}\sqrt{\big(Z_A m_{\chi\mathrm{l}}^{\mathrm{PCAC}}\big)^2 + \mu_\mathrm{l}^2}\,, \tag{52}$$

$$m_{c,s}^{\mathrm{PCAC}} = Z_P^{-1}\sqrt{\big(Z_A m_{\chi\mathrm{h}}^{\mathrm{PCAC}}\big)^2 + \mu_\sigma^2} \pm Z_S^{-1}\mu_\delta\,. \tag{53}$$

4 Numerical simulations

Our main goal in this work is to gain experience with the tuning of lattice parameters for future large scale simulations. Based on our recent work with $N_f = 2$ dynamical twisted mass Wilson fermion QCD simulations in [13–16, 34], the main emphasis is on the effects of the additional dynamical flavours s and c. As in the $N_f = 2$ case, we start with coarse lattices: lattice spacings about $a \simeq 0.2$ fm on a $12^3 \cdot 24$ lattice and $a \simeq 0.15$ fm on a $16^3 \cdot 32$ lattice. (This implies spatial lattice extensions of $L \simeq 2.4$ fm.) The parameters of our main runs are on the $12^3 \cdot 24$ lattice $\beta = 3.25$, $a\mu_\mathrm{l} = 0.01$, $a\mu_\sigma = 0.315$, $a\mu_\delta = 0.285$ and on the $16^3 \cdot 32$ lattice $\beta = 3.35$, $a\mu_\mathrm{l} = 0.0075$, $a\mu_\sigma = 0.2363$, $a\mu_\delta = 0.2138$. The statistics is between 500 and 1100 PHMC trajectories of length 0.4. (Of course, in order to find the appropriate parameters, we also had to perform at the beginning several additional short runs which we do not include here.)

The tuning to full twist of the theory with an additional heavy doublet is complicated by the fact that *two* independent parameters κ_l and κ_h must be set to their respective critical values, using e.g. for the heavy sector the procedure outlined in the previous section. However, it can be shown that in the continuum limit the deviation of the two critical hopping parameters $\kappa_{\mathrm{l,cr}}$ and $\kappa_{\mathrm{h,cr}}$ goes to zero as $\mathcal{O}(a)$. An argument is given in the appendix. This suggests that we tune κ_l to the value where $m_{\chi\mathrm{l}}^{\mathrm{PCAC}} = 0$ with $\kappa_\mathrm{h} = \kappa_\mathrm{l}$: in this situation $m_{\chi\mathrm{h}}^{\mathrm{PCAC}} = \mathcal{O}(a)$. Observe that since the average quark mass in the heavy sector is typically large, the $\mathcal{O}(a)$ error is expected not to affect the full twist improvement in the sense of [7, 8], while it is critical to have good tuning in the light quark sector. This can be checked by computing ω_h as suggested in the previous section and verifying $\omega_\mathrm{h} \approx \pi/2$.

In view of this, we have set the two hopping parameters to be equal in our main runs: $\kappa \equiv \kappa_\mathrm{l} = \kappa_\mathrm{h}$. (In a few additional runs we checked that small individual changes of κ_h by $\Delta\kappa_\mathrm{h} \simeq 0.001$ do not alter any of the qualitative conclusions.)

The average plaquette values as a function of the hopping parameter $\kappa_{\rm l} = \kappa_{\rm h} = \kappa$, for fixed values of the twisted masses, are shown by Figs. 1 and 2 on the $12^3 \cdot 24$ and $16^3 \cdot 32$ lattices, respectively. On the $12^3 \cdot 24$ lattice a strong metastability is observed for $0.1745 \leq \kappa \leq 0.1747$, which we interpret as the manifestation of a *first order phase transition*. This behaviour agrees with one of the scenarios predicted by ChPT including leading lattice artifacts [35–38]. It has also been observed in our previous simulations; for instance, in [13]. On the $16^3 \cdot 32$ lattice no metastability could be observed, although there is a sharp rise of the average plaquette value between $\kappa = 0.1705$ and $\kappa = 0.1706$. This may also signal a (weaker) first order phase transition or a *cross-over*. To decide among these two possibilities, in principle, an investigation of the infinite volume behaviour would be necessary. In practice, in a finite volume, the effects of a real first order phase transition and a cross-over are similar.

We emphasise that this observed behaviour is not related to some imperfection of the simulation algorithm. Due to the positive twisted masses the eigenvalues of the fermion matrix have a positive lower bound. Therefore, we could choose the HMC step size small enough in order that the molecular dynamical force does not become too large. The behaviour of the system when crossing the phase transition region is nicely illustrated by the run history in Fig. 3. One can recognise three stages in the plot: a metastable start at $m_{\chi l}^{\rm PCAC} > 0$; crossing; stable thermalization at $m_{\chi l}^{\rm PCAC} < 0$. A high concentration of small eigenvalues occurs during the crossing, because a large portion of the Dirac spectrum (actually all the physically relevant eigenvalues) is moving from the right half complex plane with $\mathrm{Re}\,\lambda > 0$ to the left one with $\mathrm{Re}\,\lambda < 0$.

We determined several quantities in both the pion and kaon sector. The values of some of them are collected in Tables 2 and 3 (see also Figs. 4 and 5). As in our previous work, we determined the lattice spacing from the quark force by the Sommer scale parameter [39] assuming $r_0 \equiv 0.5\,\mathrm{fm}$. Taking the values for positive untwisted PCAC quark masses ($am_{\chi l}^{\rm PCAC} > 0$), we get for $\beta = 3.25$ on the $12^3 \cdot 24$ lattice $a(\beta = 3.25) \simeq 0.20\,\mathrm{fm}$ and for $\beta = 3.35$ on the $16^3 \cdot 32$ lattice $a(\beta = 3.35) \simeq 0.15\,\mathrm{fm}$. These correspond to $a^{-1} \simeq 1.0\,\mathrm{GeV}$ and $a^{-1} \simeq 1.3\,\mathrm{GeV}$, respectively.

It follows from the data in Tables 2 and 3 that the pion, and hence the u- and d-quark masses, are not particularly small in our runs (see also Figs. 4 and 5). Considering only the points with positive untwisted PCAC quark mass ($am_{\chi \rm l}^{\rm PCAC} > 0$) outside the metastability region at $\beta = 3.25$ we have $m_\pi \geq 670\,\mathrm{MeV}$. At $\beta = 3.35$ the corresponding value is $m_\pi \geq 450\,\mathrm{MeV}$. (The points with $am_{\chi l}^{\rm PCAC} < 0$ have $m_\pi \geq 530\,\mathrm{MeV}$ and $m_\pi \geq 560\,\mathrm{MeV}$ for the two β values, respectively, but they are usually not considered for large scale simulations because of the strongly fluctuating small eigenvalues as shown, for instance, by Fig. 3.)

The kaon masses are also given in Tables 2 and 3 (see also Figs. 4 and 5). Let us note that, in the Frezzotti–Rossi formulation of the split-mass doublet we use, the masses in the kaon doublet (and D-meson doublet) are exactly degenerate. This follows from an exact symmetry of the lattice action defined in Sect. 2.1 (both in the χ and ψ basis of quark fields) namely, simultaneous multiplication by an

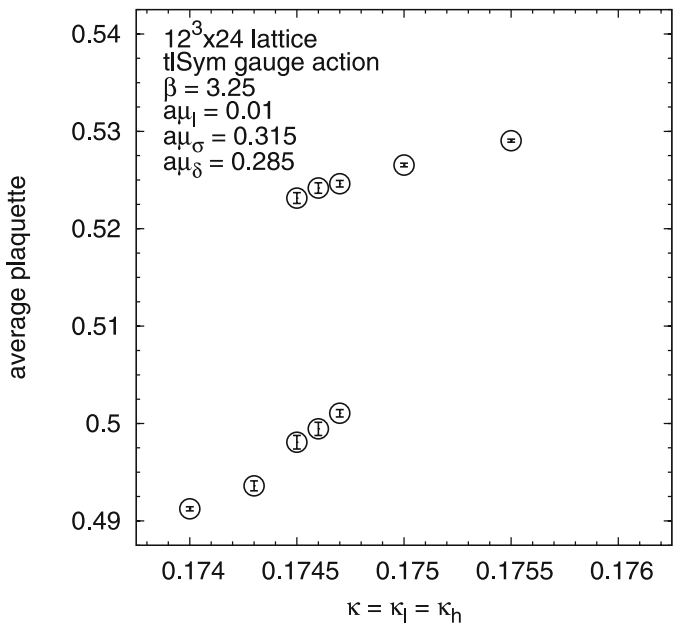

Fig. 1. The average plaquette on $12^3 \cdot 24$ lattice at $\beta = 3.25$, $a\mu_{\rm l} = 0.01$, $a\mu_\sigma = 0.315$, $a\mu_\delta = 0.285$ as a function of $\kappa \equiv \kappa_{\rm l} = \kappa_{\rm h}$

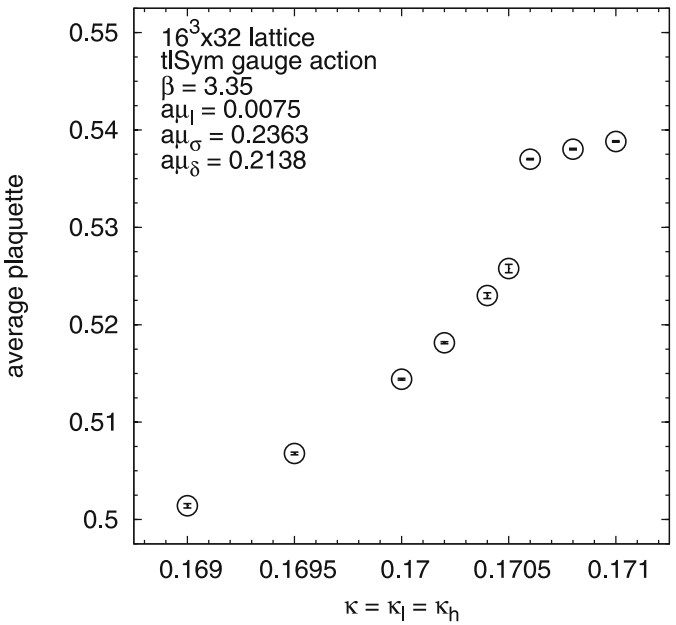

Fig. 2. The average plaquette on $16^3 \cdot 32$ lattice at $\beta = 3.35$, $a\mu_{\rm l} = 0.0075$, $a\mu_\sigma = 0.2363$, $a\mu_\delta = 0.2138$ as a function of $\kappa \equiv \kappa_{\rm l} = \kappa_{\rm h}$

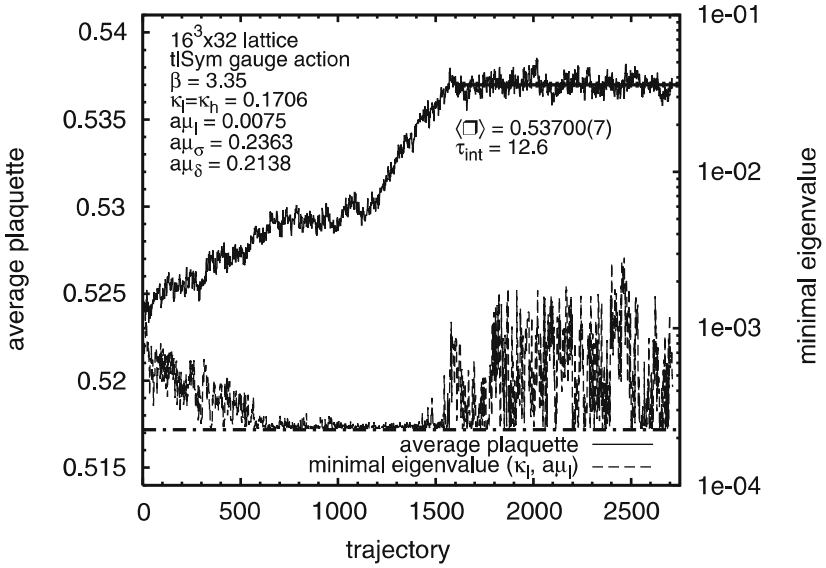

Fig. 3. Run history on a $16^3 \cdot 32$ lattice at $\beta = 3.35$, $a\mu_\mathrm{l} = 0.0075$, $a\mu_\sigma = 0.2363$, $a\mu_\delta = 0.2138$, $\kappa_\mathrm{l} = \kappa_\mathrm{h} = 0.1706$. This run started from a previous one at $\kappa = 0.1705$. On the *horizontal axis* the number of PHMC-trajectories (of length $\Delta\tau = 0.4$) is given. The average plaquette (*upper curve*, *left scale*) and the smallest eigenvalue of the squared preconditioned fermion matrix λ_min (*lower curve*, *right scale*) are shown. The *horizontal lines* indicate the average plaquette after equilibration and the absolute minimum of λ_min, respectively

Table 2. Selected results of the runs on a $12^3 \cdot 24$ lattice at $\beta = 3.25$, $a\mu_\mathrm{l} = 0.01$, $a\mu_\sigma = 0.315$, $a\mu_\delta = 0.285$. The subscript on $\kappa = \kappa_\mathrm{l} = \kappa_\mathrm{h}$ denotes L for "low" and H for "high" plaquette phase, respectively

$\kappa_\mathrm{l} = \kappa_\mathrm{h}$	r_0/a	am_π	am_ρ	am_K	am_D	$am_{\chi\mathrm{l}}^{\mathrm{PCAC}}$
0.1740_L	2.35(12)	0.7110(21)	0.9029(27)	0.9487(16)	1.4858(75)	0.08432(56)
0.1743_L	2.279(56)	0.6718(59)	0.8756(30)	0.9277(22)	1.4543(99)	0.07515(45)
0.1745_L	2.460(55)	0.5706(76)	0.7927(43)	0.8729(31)	1.4350(94)	0.0544(10)
0.1746_L	2.489(54)	0.5616(47)	0.7891(33)	0.8700(19)	1.433(23)	0.05205(81)
0.1747_L	2.457(48)	0.5303(74)	0.7566(75)	0.8566(38)	1.403(16)	0.04602(77)
0.1745_H	3.840(81)	0.3991(86)	1.0635(84)	0.8232(27)	1.096(16)	−0.0260(15)
0.1746_H	3.85(11)	0.481(11)	0.881(48)	0.8395(22)	1.055(37)	−0.0419(15)
0.1747_H	3.98(11)	0.456(13)	0.996(36)	0.8375(26)	1.028(42)	−0.0403(23)
0.1750_H	3.884(91)	0.531(18)	1.0936(97)	0.8690(46)	1.064(37)	−0.0525(24)
0.1755_H	4.02(10)	0.7012(97)	1.1056(99)	0.9186(27)	1.219(41)	−0.0868(17)

Table 3. Selected results of the runs on a $16^3 \cdot 32$ lattice at $\beta = 3.35$, $a\mu_\mathrm{l} = 0.0075$, $a\mu_\sigma = 0.2363$, $a\mu_\delta = 0.2138$

$\kappa_\mathrm{l} = \kappa_\mathrm{h}$	r_0/a	am_π	am_ρ	am_K	am_D	$am_{\chi\mathrm{l}}^{\mathrm{PCAC}}$
0.1690	2.222(54)	0.8237(13)	0.9684(20)	0.9231(11)	1.3192(87)	0.12113(40)
0.1695	2.503(41)	0.7329(11)	0.8916(15)	0.8652(11)	1.2827(58)	0.09738(34)
0.1700	2.812(48)	0.5857(18)	0.7631(35)	0.7739(12)	1.223(23)	0.06417(44)
0.1702	2.87(16)	0.5082(26)	0.7038(39)	0.7379(22)	1.187(21)	0.04837(30)
0.1704	3.28(12)	0.3695(22)	0.6041(44)	0.6553(21)	1.110(31)	0.02569(55)
0.1705	3.31(13)	0.3433(52)	0.5913(83)	0.6480(18)	1.080(35)	0.02117(53)
0.1706	4.50(20)	0.4331(74)	0.780(35)	0.6756(13)	0.943(46)	−0.0428(22)
0.1708	4.378(37)	0.4721(81)	0.843(15)	0.7004(18)	0.983(52)	−0.0492(31)
0.1710	4.59(16)	0.508(11)	0.812(16)	0.7216(17)	0.957(20)	−0.0569(26)

isospin matrix and space reflection:

$$S\colon \begin{cases} \text{light:} & \text{parity} \otimes \tau_1 \colon \begin{cases} u(x) \to \gamma_0 d(x_P)\,, \\ d(x) \to \gamma_0 u(x_P)\,, \end{cases} \\ \text{heavy:} & \text{parity} \otimes \tau_3 \colon \begin{cases} c(x) \to \gamma_0 c(x_P)\,, \\ s(x) \to -\gamma_0 s(x_P)\,. \end{cases} \end{cases} \tag{54}$$

This *exact* symmetry exchanges the u quark and the d quark; hence the equality of the masses within kaon and D-meson doublets follows.

Let us note that in a recent publication [40] a non-zero kaon mass splitting has been calculated in the quenched approximation using another formulation [41] of the mass-split doublet where both the twist and the mass splitting are in the same isospin direction. This formulation has,

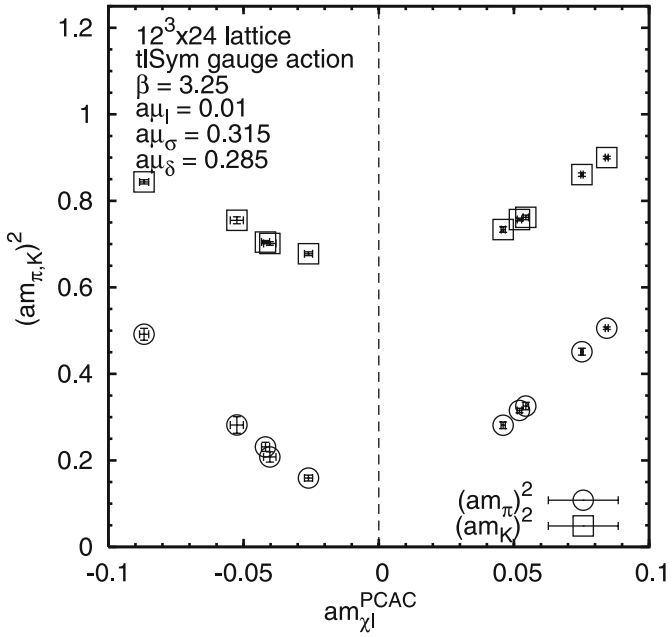

Fig. 4. The squared mass of the pion and kaon as a function of the untwisted PCAC quark mass on a $12^3 \cdot 24$ lattice at $\beta = 3.25$, $a\mu_\mathrm{l} = 0.01$, $a\mu_\sigma = 0.315$, $a\mu_\delta = 0.285$

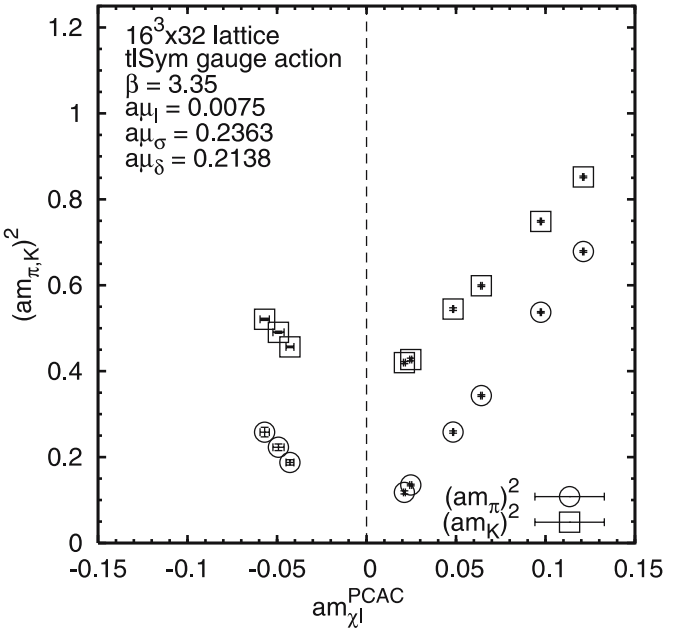

Fig. 5. The squared mass of the pion and kaon as a function of the untwisted PCAC quark mass on a $16^3 \cdot 32$ lattice at $\beta = 3.35$, $a\mu_\mathrm{l} = 0.0075$, $a\mu_\sigma = 0.2363$, $a\mu_\delta = 0.2138$

however, the disadvantage that the fermion determinant is non-real and therefore an unquenched computation is practically impossible at present. The difference in the presence and absence of the kaon mass splitting in the two formulations comes from the fact that the states with a given quark flavour correspond to different linear combinations here and there.

Similarly to the pion masses, the kaon masses in Tables 2 and 3 have also higher than the physical values. In the points cited above for the pion mass we have at $\beta = 3.25$ and $\beta = 3.35$ $m_K \geq 920\,\mathrm{MeV}$ and $m_K \geq 850\,\mathrm{MeV}$, respectively. The kaon mass can easily be lowered by tuning the mass parameters in the heavy doublet. In order to explore this we also performed simulations at $\beta = 3.35$, $a\mu_\mathrm{l} = 0.0075$ on the $16^3 \cdot 32$ lattice with $a\mu_\sigma = a\mu_\delta = 0.15$. For instance, at $\kappa_\mathrm{l} = \kappa_\mathrm{h} = 0.17$ we got $am_\pi = 0.4432(40)$ and $am_K = 0.5918(22)$. Comparing to the third line in Table 3 one can see that both the pion and the kaon mass become smaller. In particular, the kaon mass is smaller by a factor of about 3/4. This shows that the kaon mass can probably be tuned to its physical value if wanted. Another possibility is to do the chiral extrapolation by fixing, instead of m_K, the pion–kaon mass ratio m_π/m_K to its physical value.

The D-meson masses in Tables 2 and 3 are typically smaller than the physical value. In the points cited above for the pion and kaon masses we have at $\beta = 3.25$ and $\beta = 3.35$ $m_D \simeq 1450\,\mathrm{MeV}$ and $m_D \simeq 1400\,\mathrm{MeV}$, respectively. m_D can, in principle, also be tuned to its physical value. However, on coarse lattices the D-meson mass is close to the cut-off and, therefore, it is more reasonable to keep it smaller than the physical value in order to be well below the cut-off. In fact, in our runs the actual D-meson masses are already at the cut-off because we have $a^{-1} \simeq 1\,\mathrm{GeV}$ and $a^{-1} \simeq 1.3\,\mathrm{GeV}$ at $\beta = 3.25$ and $\beta = 3.35$, respectively. But on a fine lattice, say with $a^{-1} \simeq 4\,\mathrm{GeV}$, it will become possible to directly go to the physical value of m_D, too.

The machinery for the twist angle in the heavy doublet ω_h developed in Sect. 3 has been tested in a few runs, too. The formulas worked fine and the results turned out to be plausible. For instance, in the run at $\beta = 3.35$, $\kappa_\mathrm{l} = \kappa_\mathrm{h} = 0.1704$, $a\mu_\mathrm{l} = 0.0075$, $a\mu_\sigma = 0.2363$, $a\mu_\delta = 0.2138$ on a $16^3 \cdot 32$ lattice we obtained from 400 gauge configurations:

$$\begin{aligned} \omega_\mathrm{l}/\pi &= 0.0981(55)\,, & \omega_\mathrm{h}/\pi &= 0.490(25)\,, \\ Z_P/Z_S &= 0.5739(65)\,, & Z_A &= 0.897(11)\,, \\ Z_V &= 0.5490(12)\,. \end{aligned} \tag{55}$$

As one sees, ω_h is rather close to $\pi/2$ even if ω_l is still far from it. This is a consequence of $\mu_\sigma \gg \mu_\mathrm{l}$. Using the relation (valid in the continuum) $\cot(\omega_\mathrm{h})/\cot(\omega_\mathrm{l}) = \mu_\mathrm{l}/\mu_\sigma$ and the value of ω_l given above, one would get $\omega_\mathrm{h}/\pi = 0.468$. The situation is very similar in the runs on a $12^3 \cdot 24$ lattice, too. For instance, in the run with largest untwisted mass of Table 2 at $\kappa_\mathrm{l} = \kappa_\mathrm{h} = 0.1740_\mathrm{l}$ we obtained

$$\begin{aligned} \omega_\mathrm{l}/\pi &= 0.04298(34)\,, \quad \omega_\mathrm{h}/\pi = 0.4356(83)\,, \\ Z_P/Z_S &= 0.581(11)\,. \end{aligned} \tag{56}$$

These results imply that putting the untwisted quark mass equal in the two sectors gives an elegant solution for tuning to full twist: one can just do the same as in the $N_f = 2$ case. Due to the large twisted component in the heavy sector, the tuning of ω_h to $\pi/2$ is no problem at all: already at moderate values of ω_l, ω_h is almost equal to $\pi/2$.

Let us finally mention that using chiral perturbation theory (ChPT) formulas one can also extrapolate from

our simulation points to smaller pion and kaon masses. As a simple example, let us take the squared pion–kaon mass ratio in lowest order (LO) ChPT:

$$(m_\pi/m_K)^2 = \frac{2m_{ud}}{m_{ud}+m_s}\,. \tag{57}$$

In terms of our parameters we can set

$$\begin{aligned} m_{ud} &= \sqrt{\left(Z_A m_{\chi\mathrm{l}}^{\mathrm{PCAC}}\right)^2+\mu_\mathrm{l}^2}\,,\\ m_s &= \sqrt{\left(Z_A m_{\chi\mathrm{h}}^{\mathrm{PCAC}}\right)^2+(\mu_\sigma)^2}-\frac{Z_P}{Z_S}\mu_\delta\,, \end{aligned} \tag{58}$$

where Z_P/Z_S is a fitted relative renormalisation factor. In our fits we set, for simplicity, $Z_A = 0.897$ from (55), and we also assumed $m_{\chi\mathrm{h}}^{\mathrm{PCAC}} = m_{\chi\mathrm{l}}^{\mathrm{PCAC}}$, which corresponds to the assumption $\kappa_{\mathrm{h,cr}} = \kappa_{\mathrm{l,cr}}$. The results for both β values are shown in Fig. 6. Note that although these fits look rather good, clearly the validity of chiral perturbation theory in general has to be checked in further simulations at small values of a and m_π.

It turns out that the fitted values of Z_P/Z_S are well below 1, namely $Z_P/Z_S \simeq 0.45$, which implies that, as also directly shown by our simulation data, the kaon mass reacts relatively weakly to the change of the bare quark mass difference parameter $a\mu_\delta$. The deviation of Z_P/Z_S obtained in the LO-ChPT fit from the values in (55) and (56) might be due to lattice artifacts and/or to the fact that in (55) and (56) no extrapolation to zero quark masses is performed.

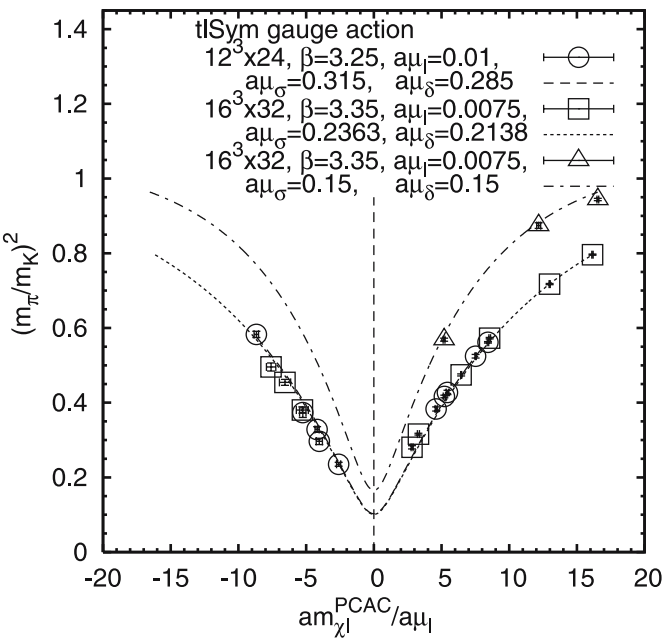

Fig. 6. Lowest order ChPT fit of the squared pion to kaon mass ratio as a function of the untwisted PCAC quark mass. *Squares* and *triangles* are data at $\beta = 3.35$, $a\mu_\mathrm{l} = 0.0075$ for $a\mu_\sigma = 0.2363$, $a\mu_\delta = 0.2138$ and $a\mu_\sigma = 0.15$, $a\mu_\delta = 0.15$, respectively. The fit to (57) and (58) gives $Z_P/Z_S = 0.446$. *Circles* are data at $\beta = 3.25$, $a\mu_\mathrm{l} = 0.01$, $a\mu_\sigma = 0.315$, $a\mu_\delta = 0.285$. The fit gives in this case $Z_P/Z_S = 0.457$

Note that the obtained values of Z_P/Z_S do not satisfy the bound derived in [5], which would ensure the positivity of the quark determinant, because in case of the (c,s) doublet this bound is $Z_P/Z_S > (m_c - m_s)/(m_c + m_s) \simeq 0.85$. This means that in simulations with $a\mu_\delta > a\mu_\sigma$ there might be some gauge configuration where the determinant of the (c,s) doublet is negative. However, such configurations have a very low probability, and hence they practically never occur in Monte Carlo simulations. In our runs (where actually $a\mu_\delta \le a\mu_\sigma$) this is shown by the eigenvalues of the fermion matrix which never come close to zero: for the (c,s) doublet they always satisfy $\lambda_{\mathrm{min,h}} > 0.01$. (This has to be compared to the minimal eigenvalues in the (u,d) doublet which only satisfy $\lambda_{\mathrm{min,l}} > 0.0001$.)

It is remarkable that the minimum value of the interpolated curves in Fig. 6 are not far away from the physical value $(m_\pi/m_K)^2 \simeq 0.082$. This raises the interesting question whether it would be possible to perform unconventional chiral extrapolations from simulation data at fixed twisted masses.

5 Discussion

The main conclusion of the present paper is that numerical simulations of QCD with unquenched u, d, s and c quarks are possible in the twisted-mass Wilson formulation.

The PHMC updating algorithm with multi-step polynomial approximations and stochastic correction during the update turned out to be effective even in difficult situations near a first order phase transition (or cross-over). The autocorrelations of the quantities given in Tables 2 and 3 are typically of $\mathcal{O}(1)$ in number of PHMC trajectories (most of the time of length 0.4); therefore, it is worth to analyse the gauge configurations after every trajectory.

At $\beta = 3.25$ (lattice spacing $a \simeq 0.20\,\mathrm{fm}$) on our $12^3 \cdot 24$ lattice we observed strong metastabilities suggesting a first order phase transition. This agrees with one of the scenarios predicted by ChPT including leading lattice artifacts [35–38] and has been observed previously in several QCD simulations with Wilson fermions [13, 42–44]. At $\beta = 3.35$ (lattice spacing $a \simeq 0.15\,\mathrm{fm}$) on our $16^3 \cdot 32$ lattice the phase transition becomes weaker but is still visible as a strong cross-over region with fast changes in several quantities. Compared to $N_f = 2$ runs at similar lattice spacings the first order phase transition becomes stronger for $N_f = 2+1+1$. (This agrees with the early observations in [43].)

The smallest simulated pion mass in a stable point with positive untwisted PCAC quark mass ($am_{\chi\mathrm{l}}^{\mathrm{PCAC}} > 0$) at $\beta = 3.25$ ($a \simeq 0.20\,\mathrm{fm}$) and $\beta = 3.35$ ($a \simeq 0.15\,\mathrm{fm}$) is $m_\pi \simeq 670\,\mathrm{MeV}$ and $m_\pi \simeq 450\,\mathrm{MeV}$, respectively. Our expectation based on the ChPT formulas and on our previous experience is that, for instance, on a $24^3 \cdot 48$ lattice with $a \simeq 0.10\,\mathrm{fm}$ the minimal pion mass at $a\mu = 0.005$ will be somewhere in the range $270\,\mathrm{MeV} < m_\pi^{\mathrm{min}} < 300\,\mathrm{MeV}$. This is because at vanishing twisted masses m_π^{min} is going to

zero as $\mathcal{O}(a)$ and for positive twisted mass the decrease is somewhat faster. (The lower value of the estimate corresponds to the minimum of the extrapolated curve in Fig. 6.)

The kaon mass in the present simulations is higher than the physical value but can probably be properly tuned by changing the twisted mass parameters in the (c, s) doublet. The D-meson mass is smaller than the physical value (i.e. the c–s mass splitting is smaller than in nature) but this is reasonable on coarse lattices in order to stay with it below the cut-off. On finer lattices (say, with $a \simeq 0.05$ fm) one can try to tune also the D-meson mass to its physical value. A possible difficulty in properly tuning the mass splittings in the (c, s) doublet can be caused by the relative insensitivity of the masses to the bare mass splitting parameter $a\mu_\delta$. This may imply the necessity of some extrapolations in the mass ratios.

If an extrapolation (or interpolation) in the s- and c-quark mass is necessary, one can consider dimensionless quantities as functions of the pseudoscalar mass ratios. For the strange quark mass one can take the ratio m_K/m_π, which is in nature $m_K/m_\pi \simeq 3.54$. In the $16^3 \cdot 32$ run at $\kappa = 0.1705$ of Table 3 we have $m_K/m_\pi = 1.888$ and, as Fig. 6 shows, in a future run on $24^3 \cdot 48$ lattice with $a \simeq 0.1$ fm, also discussed above, one can expect that this value can be tuned close to the physical value. As far as the ratio of the c- to s-quark mass is concerned, one can consider the variable m_D/m_K, which in the $\kappa = 0.1705$ run of Table 3, is $m_D/m_K \simeq 1.67$ (in nature it is $m_D/m_K \simeq 3.75$). Assuming that on the $24^3 \cdot 48$ lattice with $a \simeq 0.1$ fm the D-meson mass will be about 1 in lattice units, one will have $m_D/m_K \simeq 2.0$. This shows that the extrapolation in m_D/m_K will not be a big problem either, especially because the results will probably not depend very strongly on the heavy sea quark masses.

In case of the (c, s) doublet the mass splitting is rather large in nature because the renormalised quark masses satisfy $(m_c - m_s)/(m_c + m_s) \simeq 0.85$. Therefore it is important to take into account the mass splitting. For the (u, d) doublet, well above the scale of the u- and d-quark masses, the mass degeneracy can be considered as a good approximation, but even in this case we have in nature $(m_d - m_u)/(m_d + m_u) \simeq 0.28$. Hence also there, on a long run, the problem of the quark mass splitting within the doublet has to be tackled.

In summary, our experience in this paper is rather positive both for the twisted-mass Wilson fermion formulation and for the PHMC algorithm we are using. This opens the road for future large scale QCD simulations with dynamical u, d, s and c quarks.

Acknowledgements. We acknowledge helpful discussions with Roberto Frezzotti, Andrea Shindler and Urs Wenger. We thank the computer centers at DESY Hamburg and NIC at Forschungszentrum Jülich for providing us the necessary technical help and computer resources. This research has been supported by the DFG Sonderforschungsbereich/Transregio SFB/TR9-03 and in part by the EU Integrated Infrastructure Initiative Hadron Physics (I3HP) under contract RII3-CT-2004-506078 and also in part by the U.S. Department of Energy under contract number DE-AC02-98CH10886. The work of T.C. is supported by the DFG in the form of a Forschungsstipendium CH 398/1.

Appendix

In the $N_f = 2$ theory, one possible definition of the critical quark mass $m_{0\mathrm{cr}}(g_0, \mu)$ is given by the vanishing of the PCAC quark mass m_χ^{PCAC}. Due to chirality breaking the latter gets shifted:

$$m_\chi^{\mathrm{PCAC}} = m_0 - a^{-1} f(g_0, am_0, a\mu)\,, \tag{A.1}$$

with f a dimensionless function. On the basis of the symmetry of the action under parity $\times\,(\mu \to -\mu)$, one can show that the additive renormalisation of the quark mass is *even* in μ, and analyticity in turn implies

$$f(g_0, am_0, a\mu) = f(g_0, am_0) + \mathcal{O}(\mu^2 a^2)\,, \tag{A.2}$$

where $f(g_0, am_0)$ is the shift for ordinary $N_f = 2$ QCD without twisted mass term. So the twisted mass term in the action only produces an $\mathcal{O}(a)$ effect on the quark mass (with g_0 and m_0 held fixed):

$$m_\chi^{\mathrm{PCAC}} = m_0 - a^{-1} f(g_0, am_0) + \mathcal{O}(a)\,. \tag{A.3}$$

The above argument can easily be generalised to the $N_f = 2+1+1$ theory. Here one has to make a distinction between the two sectors:

$$m_{\chi\mathrm{l}}^{\mathrm{PCAC}} = m_{0\mathrm{l}} - a^{-1} f_{\mathrm{l}}(g_0, am_{0\mathrm{l}}, am_{0\mathrm{h}}, a\mu_{\mathrm{l}}, a\mu_\sigma, a\mu_\delta)\,, \tag{A.4}$$

$$m_{\chi\mathrm{h}}^{\mathrm{PCAC}} = m_{0\mathrm{h}} - a^{-1} f_{\mathrm{h}}(g_0, am_{0\mathrm{h}}, am_{0\mathrm{l}}, a\mu_\sigma, a\mu_{\mathrm{l}}, a\mu_\delta)\,. \tag{A.5}$$

The functions f_{l} and f_{h} are in this case even in μ_{l}, μ_{h} and μ_δ[1]: similarly to $N_f = 2$, the associated terms in the action only affect the additive renormalisation of the quark mass by $\mathcal{O}(a)$ terms. So we write

$$m_{\chi\mathrm{l}}^{\mathrm{PCAC}} = m_{0\mathrm{l}} - a^{-1} f(g_0, am_{0\mathrm{l}}, am_{0\mathrm{h}}) + \mathcal{O}(a)\,, \tag{A.6}$$

$$m_{\chi\mathrm{h}}^{\mathrm{PCAC}} = m_{0\mathrm{h}} - a^{-1} f(g_0, am_{0\mathrm{h}}, am_{0\mathrm{l}}) + \mathcal{O}(a)\,, \tag{A.7}$$

where on the r.h.s. we have now the mass shifts for the theory without twist and mass splitting ($N_f = 2+2$ QCD): here the distinction between the two sectors is immaterial. From (A.6) and (A.7) it follows immediately that

$$m_{0\mathrm{l}} = m_{0\mathrm{h}} = m_0 \Rightarrow m_{\chi\mathrm{h}}^{\mathrm{PCAC}} = m_{\chi\mathrm{l}}^{\mathrm{PCAC}} + \mathcal{O}(a)\,. \tag{A.8}$$

[1] An additional symmetry in the heavy sector is needed for the argument, namely $\chi_{\mathrm{h},x} \to \exp\{\mathrm{i}\frac{\pi}{2}\tau_1\}\chi_{\mathrm{h},x}$, $\bar\chi_{\mathrm{h},x} \to \chi_{\mathrm{h},x}\exp\{-\mathrm{i}\frac{\pi}{2}\tau_1\}$ composed with $\mu_\delta \to -\mu_\delta$.

References

1. Fermilab Lattice, MILC and HPQCD Collaboration, A.S. Kronfeld et al., PoS LAT2005, 206 (2005)
2. Fermilab Lattice, MILC and HPQCD Collaboration, A.S. Kronfeld et al., Int. J. Mod. Phys. A **21**, 713 (2006) [hep-lat/0509169]
3. JLQCD Collaborations, CP-PACS et al., PoS LAT2005, 057 (2005) [hep-lat/0509142]
4. R. Frezzotti, P.A. Grassi, S. Sint, P. Weisz, Nucl. Phys. Proc. Suppl. **83**, 941 (2000) [hep-lat/9909003]
5. R. Frezzotti, G.C. Rossi, Nucl. Phys. Proc. Suppl. **128**, 193 (2004) [hep-lat/0311008]
6. F. Farchioni et al., PoS LAT2005, 072 (2005) [hep-lat/0509131]
7. R. Frezzotti, G.C. Rossi, JHEP **0408**, 007 (2004) [hep-lat/0306014]
8. R. Frezzotti, G.C. Rossi, Nucl. Phys. Proc. Suppl. **129**, 880 (2004) [hep-lat/0309157]
9. XLF Collaboration, K. Jansen, A. Shindler, C. Urbach, I. Wetzorke, Phys. Lett. B **586**, 432 (2004) [hep-lat/0312013]
10. XLF Collaboration, W. Bietenholz et al., JHEP **0412**, 044 (2004) [hep-lat/0411001]
11. XLF Collaboration, K. Jansen, M. Papinutto, A. Shindler, C. Urbach, I. Wetzorke, Phys. Lett. B **619**, 184 (2005) [hep-lat/0503031]
12. XLF Collaboration, K. Jansen, M. Papinutto, A. Shindler, C. Urbach, I. Wetzorke, JHEP **0509**, 071 (2005) [hep-lat/0507010]
13. F. Farchioni et al., Eur. Phys. J. C **39**, 421 (2005) [hep-lat/0406039]
14. F. Farchioni et al., Eur. Phys. J. C **42**, 73 (2005) [hep-lat/0410031]
15. F. Farchioni et al., Phys. Lett. B **624**, 324 (2005) [hep-lat/0506025]
16. F. Farchioni et al., Eur. Phys. J. C **47**, 453 (2006) [hep-lat/0512017]
17. K. Symanzik, Nucl. Phys. B **226**, 187 (1983)
18. P. Weisz, Nucl. Phys. B **212**, 1 (1983)
19. P. Weisz, R. Wohlert, Nucl. Phys. B **236**, 397 (1984)
20. P. Weisz, R. Wohlert, Nucl. Phys. B **247**, 544 (1984) [Erratum]
21. I. Montvay, E. Scholz, Phys. Lett. B **623**, 73 (2005) [hep-lat/0506006]
22. R. Frezzotti, K. Jansen, Phys. Lett. B **402**, 328 (1997) [hep-lat/9702016]
23. R. Frezzotti, K. Jansen, Nucl. Phys. B **555**, 395 (1999) [hep-lat/9808011]
24. R. Frezzotti, K. Jansen, Nucl. Phys. B **555**, 432 (1999) [hep-lat/9808038]
25. I. Montvay, Nucl. Phys. B **466**, 259 (1996) [hep-lat/9510042]
26. T. Chiarappa, R. Frezzotti, C. Urbach, PoS LAT2005, 103 (2006) [hep-lat/0509154]
27. T. Chiarappa, R. Frezzotti, C. Urbach, work in preparation
28. F. Farchioni et al., Nucl. Phys. Proc. Suppl. **140**, 240 (2005) [hep-lat/0409098]
29. S. Aoki, O. Bär, Phys. Rev. D **70**, 116 011 (2004) [hep-lat/0409006]
30. S. Aoki, O. Bär, Phys. Rev. D **74**, 034 511 (2006) [hep-lat/0604018]
31. S.R. Sharpe, J.M.S. Wu, Phys. Rev. D **71**, 074 501 (2005) [hep-lat/0411021]
32. R. Frezzotti, G. Martinelli, M. Papinutto, G.C. Rossi, JHEP **0604**, 038 (2006) [hep-lat/0503034]
33. S.R. Sharpe, Phys. Rev. D **72**, 074 510 (2005) [hep-lat/0509009]
34. ETM Collaboration, Ph. Boucaud et al., hep-lat/0701012
35. S.R. Sharpe, R.L. Singleton, Phys. Rev. D **58**, 074 501 (1998) [hep-lat/9804028]
36. G. Münster, JHEP **0409**, 035 (2004) [hep-lat/0407006]
37. L. Scorzato, Eur. Phys. J. C **37**, 445 (2004) [hep-lat/0407023]
38. S.R. Sharpe, J.M.S. Wu, Phys. Rev. D **70**, 094 029 (2004) [hep-lat/0407025]
39. R. Sommer, Nucl. Phys. B **411**, 839 (1994) [hep-lat/9310022]
40. A.M. Abdel-Rehim, R. Lewis, R.M. Woloshyn, J.M.S. Wu, Phys. Rev. D **74**, 014 507 (2006) [hep-lat/0601036]
41. C. Pena, S. Sint, A. Vladikas, JHEP **0409**, 069 (2004) [hep-lat/0405028]
42. T. Blum et al., Phys. Rev. D **50**, 3377 (1994) [hep-lat/9404006]
43. JLQCD Collaboration, S. Aoki et al., Nucl. Phys. Proc. Suppl. **106**, 263 (2002) [hep-lat/0110088]
44. K. Jansen, Nucl. Phys. Proc. Suppl. **129**, 3 (2004) [hep-lat/0311039]

[SYM-1]

The supersymmetric Ward identities on the lattice

Eur. Phys. J. C23 719-734 (2002)

Eur. Phys. J. C 23, 719–734 (2002)
Digital Object Identifier (DOI) 10.1007/s100520200898

THE EUROPEAN PHYSICAL JOURNAL C

The supersymmetric Ward identities on the lattice

The DESY-Münster-Roma Collaboration

F. Farchioni[1,⋆], C. Gebert[1], R. Kirchner[1,⋆⋆], I. Montvay[1], A. Feo[2,⋆⋆⋆], G. Münster[2], T. Galla[3], A. Vladikas[4]

[1] Deutsches Elektronen-Synchrotron DESY, 22603 Hamburg, Germany
[2] Institut für Theoretische Physik, Universität Münster, Wilhelm-Klemm-Str. 9, 48149 Münster, Germany
[3] Department of Physics, University of Oxford, 1 Keble Road, Oxford OX1 3NP, UK
[4] INFN, Sezione di Roma 2, c/o Dipartimento di Fisica, Univ. di Roma "Tor Vergata", Via della Ricerca Scientifica 1, 00133 Rome, Italy

Received: 8 November 2001 / Revised version: 14 January 2001 /
Published online: 15 March 2002 –

Abstract. Supersymmetric (SUSY) Ward identities are considered for the N=1 SU(2) SUSY Yang-Mills theory discretized on the lattice with Wilson fermions (gluinos). They are used in order to compute non-perturbatively a subtracted gluino mass and the mixing coefficient of the SUSY current. The computations were performed at gauge coupling $\beta = 2.3$ and hopping parameter $\kappa = 0.1925$, 0.194, 0.1955 using the two-step multi-bosonic dynamical-fermion algorithm. Our results are consistent with a scenario where the Ward identities are satisfied up to $O(a)$ effects. The vanishing of the gluino mass occurs at a value of the hopping parameter which is not fully consistent with the estimate based on the chiral phase transition. This suggests that, although SUSY restoration appears to occur close to the continuum limit of the lattice theory, the results are still affected by significant systematic effects.

1 Introduction

A better understanding of non-perturbative phenomena in supersymmetric (SUSY) gauge theories could be gained in the framework of the lattice regularization. An immediate difficulty arises, however, because the lattice regularized theory is not supersymmetric as the Poincaré invariance, a sector of the superalgebra, is lost. This is evident if one considers the super-algebra in the canonical formalism (the notation is with Weyl spinors)

$$\{Q_\alpha, \bar{Q}_\beta\} \;=\; 2\,\sigma^\mu_{\alpha\beta}\,P_\mu \;. \qquad (1)$$

This relation cannot be fulfilled in a discrete space-time manifold, where momenta are not generators of infinitesimal space-time translations. More specific difficulties arise in the fermionic sector where spurious states may violate the balance between bosonic and fermionic degrees of freedom. In the standard approach to lattice gauge theories with Wilson fermions (for an approach using domain-wall fermions see [1]) the suppression of spurious states in the continuum limit is obtained by adding to the action an 'irrelevant' term (Wilson term) which explicitly breaks SUSY.

Some time ago Curci and Veneziano [2] proposed that in spite of this substantial SUSY breaking the Wilson discretization may be safely applied to SUSY gauge theories: the symmetry is recovered in the continuum limit by properly tuning the bare parameters of the action. They considered the simple example of the N=1 supersymmetric Yang-Mills theory (SYM). This is the supersymmetrized version of quantum gluodynamics where the N_c^2-1 gluons are accompanied by an equal number of fermionic partners (gluinos) in the same (adjoint) representation of the color group. The Wilson action for the N=1 SYM breaks SUSY by the Wilson term for the gluino action and by a gluino Majorana mass term. The lattice Ward identities (WIs), considered in [3] for the case of the chiral symmetry in QCD (see also [4,5]), provide a general theoretical framework for properly dealing with the problem of the restoration of the symmetry in the continuum limit. As a consequence of the SUSY breaking, similarly to QCD, the gluino mass is shifted: a tuning procedure on the bare mass is required in order to recover massless gluino and SUSY in the continuum limit.

The problem of the Monte Carlo simulation of the N=1 SU(2) SYM with Wilson fermions was considered by this collaboration in the past [6–10] (for a study in the quenched approximation see [11]). The theory with

⋆ *Address after October 1st:* Institut für Theoretische Physik, Universität Münster, Wilhelm-Klemm-Str. 9, 48149 Münster, Germany
⋆⋆ *Address after October 1st:* Universidad Autònoma de Madrid, Cantoblanco, Madrid 28049, Spain
⋆⋆⋆ Work supported by the Deutsche Forschungsgemeinschaft (DFG). *Address after November 1st:* School of Mathematics, Trinity College, Dublin 2, Ireland

dynamical gluino was simulated by the two-step multibosonic (TSMB) algorithm defined in [12,13]. The formulation of the algorithm, flexible with respect to the parameter N_f, allows to treat the gluino which is a Majorana fermion ($N_f = 1/2$). An extensive analysis of the low-energy aspects of the SU(2) SYM was performed.

An intricate point in the N=1 SYM is the tuning of the theory to the massless gluino limit. The straightforward spectroscopic method familiar in QCD cannot be applied in the case of the N=1 SYM since the theory possesses only an anomalous axial chiral symmetry and no Goldstone boson is available. The problem was considered in [9] by studying the behavior of the finite-volume gluino condensate as a function of the hopping parameter: the massless gluino is expected to correspond to two degenerate vacua with symmetric probability distribution of the gluino condensate. SUSY restoration can be also verified by direct inspection of the low-energy mass spectrum [10]: this is expected to reproduce the SUSY multiplets predicted by the low-energy effective Lagrangians [14,15]. An accurate analysis of the spectrum is however a non-trivial task from the computational point of view and an independent method for checking SUSY is welcome. A possibility [11] is to use the SUSY WIs to determine the gluino mass in the same way the chiral WIs are used in QCD to determine the quark mass. A great simplification consists in considering the on-shell regime. In addition the WI approach improves the insight in the renormalization of the lattice SUSY current. The properly renormalized current defines the supercharge and satisfies the appropriate superalgebra. The renormalization of the lattice SUSY current is more complicated compared to the chiral case since SUSY is more severely broken on the lattice. Explicit one-loop calculations in lattice perturbation theory may lead to a better understanding of this problem [16,17].

In this work we concentrate on the SUSY WI approach. As we shall see, two unknown parameters appear in the on-shell SUSY WIs. These are ratios of three coefficients entering the WIs: Z_S and Z_T multiplying the divergences of the SUSY current $\partial_\mu S_\mu(x)$ and of the mixing current $\partial_\mu T_\mu(x)$, and the subtracted gluino mass m_S. For $m_S = 0$, SUSY is expected to be restored in the continuum limit. As a result of the study we obtain a non-perturbative determination of the dimensionless ratios $am_S Z_S^{-1}$ and $Z_T Z_S^{-1}$. We consider the gauge coupling $\beta = 2.3$ on a $12^3 \times 24$ lattice and three values of the hopping parameter $\kappa = 0.1925$, 0.194, 0.1955, corresponding to decreasing gluino mass. Preliminary results were presented in [18–20].

The paper is organized as follows. In Sect. 2 the Curci-Veneziano approach is introduced in the case of the N=1 SYM. The lattice action is defined and its symmetries are pointed out (see also Appendix A). The latter play a special rôle in the analysis of the SUSY WIs. In Sect. 3 the formalism of the lattice WIs is reviewed. The fundamental issue in this context is the renormalization of the 'irrelevant' operator entering the WIs because of the explicit breaking of SUSY in the lattice model. A detailed account is given in Appendix B with an analysis based on the discrete hypercubic group. The result is that the SUSY WIs assume a specific lattice form. We discuss in this paper only the simplified case of the on-shell regime. Suitable gluino-glue insertion operators are discussed in Sect. 4. In Appendix C the rôle of the symmetries in this context is clarified. In Sect. 5 we give an account of the present setup of the TSMB algorithm. The parameters have been tuned in order to get good performance for light fermionic degrees of freedom. We also measure some quantities (smallest eigenvalue, sign of the Pfaffian, the scale r_0) which characterize the set of configurations under study. Sect. 6 is devoted to the numerical analysis of the SUSY WIs with an outline of the method and the presentation of the numerical results. Conclusions are finally drawn in Sect. 7.

2 The N=1 SYM on the lattice

We adopt the formulation of [2] for the lattice discretization of the N=1 SYM with N_c colors. The pure gauge action S_g is the standard plaquette one

$$S_g = \frac{\beta}{2} \sum_x \sum_{\mu \neq \nu} \left(1 - \frac{1}{N_c} \mathrm{Re}\,\mathrm{Tr}\, U_{\mu\nu}(x) \right) , \qquad (2)$$

where the plaquette is defined as

$$U_{\mu\nu}(x) \;=\; U_\nu^\dagger(x)\, U_\mu^\dagger(x+\hat{\nu})\, U_\nu(x+\hat{\mu})\, U_\mu(x) \;, \qquad (3)$$

and the bare gauge coupling is given by $\beta \equiv 2N_c/g_0^2$. For Wilson fermions the action (with Wilson parameter set to $r=1$) reads

$$\begin{aligned} S_f = \sum_x a^4\, \mathrm{Tr} \Bigg[& \frac{1}{2a} \sum_\mu \Big(\overline{\lambda}(x)\, (\gamma_\mu - 1)\, U_\mu^\dagger(x)\, \lambda(x+\hat{\mu}) \\ & \times U_\mu(x) - \overline{\lambda}(x+\hat{\mu})\, (\gamma_\mu + 1)\, U_\mu(x)\, \lambda(x)\, U_\mu^\dagger(x) \Big) \\ & + (m_0 + \frac{4}{a})\, \overline{\lambda}(x) \lambda(x) \Bigg] \;, \end{aligned} \qquad (4)$$

with a the lattice spacing and m_0 the gluino bare mass. The gluino field $\lambda(x)$ is a Majorana spinor transforming according to the adjoint representation of the gauge group. The symbol 'Tr' denotes the trace over the color indices. In this work we consider $N_c = 2$, for which the adjoint gluino field is expressed in terms of Pauli matrices σ_r

$$\lambda = \sum_{r=1}^{3} \frac{1}{2} \sigma_r \lambda^r \;. \qquad (5)$$

The following relation (Majorana condition) holds for an Euclidean Majorana field:

$$\lambda(x) = \lambda^C(x) \equiv C \overline{\lambda}^T(x) \;, \qquad (6)$$

where $C = \gamma_0 \gamma_2$ is the spinorial matrix associated with the charge-conjugation symmetry C. Boundary conditions

are taken to be periodic except for fermionic fields in the time direction, which are anti-periodic.

In Monte Carlo simulations a different parametrization is used. The hopping parameter κ is defined as

$$\kappa = \frac{1}{2(4+m_0 a)} \tag{7}$$

and the fermionic action is expressed in terms of the fermion matrix Q

$$S_f \;=\; \frac{a^3}{2\kappa}\sum_{xr,ys}\overline{\lambda}^s(y)Q_{ys,xr}\lambda^r(x) \tag{8}$$

(Dirac indices are implicit). The fermion matrix is given by

$$\begin{aligned} Q_{ys,xr} &\equiv Q_{ys,xr}[U] \\ &\equiv \delta_{yx}\delta_{sr} - \kappa\sum_{\mu=1}^{4}\Big[\delta_{y,x+\hat{\mu}}(1+\gamma_\mu)V_{sr,x\mu} \\ &\quad +\delta_{y+\hat{\mu},x}(1-\gamma_\mu)V^T_{sr,y\mu}\Big] \end{aligned} \tag{9}$$

with the adjoint link $V_{rs,x\mu}(x)$ defined as

$$\begin{aligned} V_{rs,x\mu} &\equiv V_{rs,x\mu}[U] \\ &\equiv \frac{1}{2}\,\mathrm{Tr}(U^\dagger_{x\mu}\sigma_r U_{x\mu}\sigma_s) = V^*_{rs,x\mu} = V^{-1T}_{rs,x\mu}\ . \end{aligned} \tag{10}$$

The action (2)-(4) is invariant under the discrete symmetries P (parity), T (time-reversal) and C (charge-conjugation). For the case under consideration the latter symmetry implies the following relation for the fermion matrix

$$Q^T_{xr,ys}[U] = CQ_{ys,xr}[U]C^{-1} \tag{11}$$

(transposition is intended on the suppressed Dirac indices). The discrete symmetries of the lattice action play an important rôle in the subsequent analysis of the WIs; their explicit definition is given in Appendix A.

3 Lattice SUSY Ward identities

SUSY is explicitly broken in the action (2)-(4) by the gluino mass term, by the Wilson term and by the lattice discretization. Using lattice SUSY WIs a soft-breaking subtracted gluino mass m_S can be defined. The expectation is that the vanishing of m_S, for asymptotically small lattice spacings, ensures the restoration of SUSY up to discretization effects. In this Section we discuss these issues, which were first introduced in [2], and have also been considered in [11] and [16].

Lattice SUSY transformations complying with gauge invariance, P, T and the Majorana nature of the gluino field are [21,16][1]:

$$\begin{aligned} \delta U_\mu(x) &= -\frac{ig_0 a}{2}\Big(\overline{\theta}(x)\gamma_\mu U_\mu(x)\lambda(x) \\ &\quad +\overline{\theta}(x+\hat{\mu})\gamma_\mu\lambda(x+\hat{\mu})U_\mu(x)\Big)\ , \\ \delta U^\dagger_\mu(x) &= \frac{ig_0 a}{2}\Big(\overline{\theta}(x)\gamma_\mu\lambda(x)U^\dagger_\mu(x) \\ &\quad +\overline{\theta}(x+\hat{\mu})\gamma_\mu U^\dagger_\mu(x)\lambda(x+\hat{\mu})\Big)\ , \\ \delta\lambda(x) &= \frac{1}{2}P^{(cl)}_{\mu\nu}(x)\sigma_{\mu\nu}\theta(x)\ , \\ \delta\overline{\lambda}(x) &= -\frac{1}{2}\overline{\theta}(x)\sigma_{\mu\nu}P^{(cl)}_{\mu\nu}(x)\ , \end{aligned} \tag{12}$$

where $\theta(x)$, $\overline{\theta}(x)$ are infinitesimal Majorana fermionic parameters. The lattice field tensor $P^{(cl)}_{\mu\nu}(x)$ is clover-symmetrized so as to comply with P and T:

$$P^{(cl)}_{\mu\nu}(x) = \frac{1}{4a}\sum_{i=1}^{4}\frac{1}{2ig_0 a}\left(U^{(i)}_{\mu\nu}(x) - U^{(i)\dagger}_{\mu\nu}(x)\right), \tag{13}$$

where

$$\begin{aligned} U^{(1)}_{\mu\nu}(x) &= U^\dagger_\nu(x)U^\dagger_\mu(x+\hat{\nu})U_\nu(x+\hat{\mu})U_\mu(x) \equiv U_{\mu\nu}(x)\ , \\ U^{(2)}_{\mu\nu}(x) &= U^\dagger_\mu(x)U_\nu(x+\hat{\mu}-\hat{\nu})U_\mu(x-\hat{\nu})U^\dagger_\nu(x-\hat{\nu})\ , \\ U^{(3)}_{\mu\nu}(x) &= U_\nu(x-\hat{\nu})U_\nu(x-\hat{\mu}-\hat{\nu}) \\ &\quad \times U^\dagger_\mu(x-\hat{\mu}-\hat{\nu})U^\dagger_\mu(x-\hat{\mu})\ , \\ U^{(4)}_{\mu\nu}(x) &= U_\mu(x-\hat{\mu})U^\dagger_\nu(x-\hat{\mu}) \\ &\quad \times U^\dagger_\mu(x-\hat{\mu}+\hat{\nu})U_\nu(x)\ . \end{aligned} \tag{14}$$

For any operator $Q(y)$ the expectation value $\langle Q(y)\rangle$ is invariant if in the functional integral a change of variables according to the above SUSY transformations is performed. In the case of a gauge invariant operator $Q(y)$ this results in the following WI

$$\begin{aligned} &\sum_\mu\left\langle\left(\nabla_\mu S^{(ps)}_\mu(x)\right)Q(y)\right\rangle \\ &\quad = m_0\left\langle\chi(x)Q(y)\right\rangle + \left\langle X^{(ps)}(x)Q(y)\right\rangle - \left\langle\frac{\delta Q(y)}{\delta\overline{\theta}(x)}\right\rangle\ . \end{aligned} \tag{15}$$

The SUSY current $S^{(ps)}_\mu(x)$ is point-split (ps) [16]

$$\begin{aligned} S^{(ps)}_\mu(x) = -\frac{1}{2}\sum_{\rho\sigma}\sigma_{\rho\sigma}\gamma_\mu\mathrm{Tr}\Big(&P^{(cl)}_{\rho\sigma}(x)U^\dagger_\mu(x)\lambda(x+\hat{\mu})U_\mu(x) \\ &+P^{(cl)}_{\rho\sigma}(x+\mu)U_\mu(x)\lambda(x)U^\dagger_\mu(x)\Big)\ , \end{aligned} \tag{16}$$

and the lattice derivative is the backward one $\nabla^b_\mu f(x) = (f(x) - f(x-\hat{\mu}))/a$. We recall that SUSY is broken by the presence of a non-zero bare mass in the action, by the Wilson term and by the discretization. The first type of SUSY breaking gives rise to the term of the WI (15) involving the operator $\chi(x)$:

$$\chi(x) = \sum_{\rho\sigma}\sigma_{\rho\sigma}\mathrm{Tr}\left(P^{(cl)}_{\rho\sigma}(x)\lambda(x)\right)\ . \tag{17}$$

[1] Our definition of the link variable $U_\mu(x)$ differs from that of [16] (see our definition of the plaquette (3)); the two definitions are related by Hermitian conjugation

The rest of the SUSY breaking results in the presence of the $X^{(ps)}(x)$ term. Its exact expression [16] is not needed in the following. It suffices to know that in the naive continuum limit $X_S(x) \approx aO_{11/2}(x)$, where $O_{11/2}(x)$ is a dimension-11/2 operator.

The last term in (15) is a contact term which vanishes when the distance $|x-y|$ is non-zero. This corresponds to the *on-shell* situation. We shall restrict ourselves to this regime in the numerical analysis of the WIs and contact terms will be consequently disregarded in the following discussions.

The definition of the SUSY current on the lattice is arbitrary up to terms which vanish in the continuum limit. Another choice is the local (*loc*) current

$$S_\mu^{(loc)}(x) = -\sum_{\rho\sigma} \sigma_{\rho\sigma}\gamma_\mu \mathrm{Tr}\Big(P_{\rho\sigma}^{(cl)}(x)\lambda(x)\Big) \ . \qquad (18)$$

This definition is preferable on the classical level [21] and is more convenient for analytic perturbative calculations. The local current $S_\mu^{(loc)}(x)$ satisfies a WI of the form (15), with a symmetric lattice derivative $\nabla_\mu^s f(x) = (f(x+\mu) - f(x-\hat{\mu}))/2a$ (required to preserve P and T) and a SUSY-breaking term $X^{(loc)} = X^{(ps)} + O(a)$.

3.1 Renormalization

The WI (15) is a relation between bare correlation functions. The rôle of the symmetry-breaking operator $X^{(ps)}(x)$ (or $X^{(loc)}(x)$) is of particular interest, as it is related to current normalization and gluino mass subtraction. Its treatment in the present case follows closely that of the axial WIs in QCD [3,5].

We consider the renormalization of the dimension-11/2 operator $O_{11/2}(x)$. According to the usual prescriptions, this implies mixing with operators of equal or lower dimensions d, which have the same transformation properties under the symmetries of the lattice action. A discussion of the mixing pattern on the basis of the discrete hypercubic group is carried out in Appendix B. The result is that no Lorentz-breaking mixing arises at least in the on-shell regime. The mixing pattern (involving operators with $7/2 \le d \le 11/2$) in the on-shell case is given by

$$\begin{aligned} O_{11/2}^R(x) = Z_{11/2}\Big[&O_{11/2}(x) + a^{-1}(Z_S - 1)\,\nabla_\mu S_\mu(x) \\ &+a^{-1}Z_T\,\nabla_\mu T_\mu(x) + a^{-2}Z_\chi\,\chi(x)\Big] \\ &+\sum_j Z_{11/2}^{(j)} O_{11/2}^{(j)\,R}(x) \ . \end{aligned} \qquad (19)$$

Since it is not relevant to the present discussion we have left unspecified the exact lattice form of the SUSY current (point-split or local) and derivative (backward or symmetric). The same applies to the other dimension-9/2 operator appearing in (19), namely the divergence of the mixing current $T_\mu(x)$. It may be defined in analogy to $S_\mu(x)$ as point-split

$$\begin{aligned} T_\mu^{(ps)}(x) = \sum_\nu \gamma_\nu \mathrm{Tr}\Big(&P_{\mu\nu}^{(cl)}(x)U_\mu^\dagger(x)\lambda(x+\hat{\mu})U_\mu(x) \\ &+P_{\mu\nu}^{(cl)}(x+\mu)U_\mu(x)\lambda(x)U_\mu^\dagger(x)\Big) \end{aligned} \qquad (20)$$

or local

$$T_\mu^{(loc)}(x) = 2\sum_{\mu\nu}\gamma_\nu \mathrm{Tr}\Big(P_{\mu\nu}^{(cl)}(x)\lambda(x)\Big) \ , \qquad (21)$$

with the lattice derivative chosen as in the case of the current $S_\mu(x)$. From the above discussion obviously follows that different lattice currents $S_\mu(x)$ and $T_\mu(x)$ are associated with different values of Z_S and Z_T.

The last term on the r.h.s. of (19) reflects the mixing of the operator $O_{11/2}(x)$ with other bare operators $O_{11/2}^{(j)}(x)$ of equal dimension. The reason (19) has been expressed in terms of the renormalized ones $O_{11/2}^{(j)\,R}(x)$ will become clear shortly. The multiplicative renormalization $Z_{11/2}$ and the mixing coefficients $Z_{11/2}^{(j)}$ are logarithmically divergent in perturbation theory. Solving (19) for $O_{11/2}(x)$ and substituting it in WI (15) one gets

$$\begin{aligned} &Z_S\,\langle(\nabla_\mu S_\mu(x))\,Q(y)\rangle + Z_T\,\langle(\nabla_\mu T_\mu(x))\,Q(y)\rangle \\ &\quad = m_S\,\langle\chi(x)Q(y)\rangle + O(a) \ , \end{aligned} \qquad (22)$$

where the subtracted mass m_S is given by

$$m_S = m_0 - a^{-1}Z_\chi \ . \qquad (23)$$

In deriving (22) we have relied on the vanishing in the continuum limit of the correlation

$$a\left\langle [Z_{11/2}^{-1}O_{11/2}^R(x) - \sum_j Z_{11/2}^{(j)}O_{11/2}^{(j)\,R}(x)]\,Q(y)\right\rangle = O(a) \ , \qquad (24)$$

which is valid on-shell, $x \neq y$ (recall that $Z_{11/2}$, $Z_{11/2}^{(j)}$ are only logarithmically divergent).

By using general renormalization group arguments (see e.g. [5]) one can show that Z_S, Z_T and Z_χ, being power-subtraction coefficients, do not depend on the renormalization scale μ defining the renormalized operator (19). Consequently dimensional considerations imply $Z_S = Z_S(g_0, m_0 a)$, $Z_T = Z_T(g_0, m_0 a)$, $Z_\chi = Z_\chi(g_0, m_0 a)$. The requirement of a well defined chiral limit of the theory implies in particular that the dependence of Z_S and Z_T on the gluino mass is vanishingly small in the continuum limit. In simulations at fixed lattice spacing this dependence is treated as an $O(a)$ effect.

In QCD the lattice chiral WI, a relation analogous to (22), leads to the definition of an axial current $\hat{A}_\mu(x) = Z_A A_\mu^{lat}(x)$ where $A_\mu^{lat}(x)$ is a generic discretization of the chiral current. A rigorous argument [3,5] shows that the current $\hat{A}_\mu(x)$ coincides with the correctly normalized continuum chiral current. It satisfies the appropriate current

algebra. It is tempting to associate by analogy the quantity $\hat{S}_\mu(x) = Z_S S_\mu(x) + Z_T T_\mu(x)$ with the correctly normalized continuum SUSY current. An attempt to reproduce in this case the QCD argument fails. This is because the proof in QCD relies on two key properties (cf. Sect. 3.1 of [5]):

1. The axial variation of the quark field is proportional to the field itself.
2. The gauge fixing term is invariant under axial transformations.

The above statements, valid for the axial symmetry, do not apply to SUSY. Thus, to the best of our knowledge, SUSY WIs cannot be used in a way analogous to the QCD chiral ones in order to prove the non-renormalization theorem for the current $\hat{S}_\mu(x)$. Explicit one-loop calculations in lattice perturbation theory may shed some light on this issue [16,17]. If the correctly normalized SUSY current coincides with $\hat{S}_\mu(x)$ (or is related to it by multiplicative renormalization), it is conserved when m_S vanishes. This is the restoration of SUSY in the continuum limit.

4 Insertion operators

In this Section we turn our attention to the insertion operator $Q(x)$ of the WI (22). The operators $\nabla_\mu S_\mu(x)$, $\nabla_\mu T_\mu(x)$ and $\chi(x)$, which will be in the following collectively denoted as 'sink operators', transform according to the bispinorial representation of the Poincaré group in the continuum. In order to get a non-trivial WI, the insertion operator $Q(x)$ is required to contain (at least) one non-zero spin-1/2 component. Thus, given a composite operator $\mathcal{O}$ which is a Majorana bispinor, $Q(x)$ may be chosen to be of the form

$$Q(x) = \bar{\mathcal{O}}^T(x) \equiv C^{-1}\mathcal{O}(x)\,. \tag{25}$$

Clearly this operator must also be gauge invariant.

We consider the zero spatial momentum WI obtained by summation over the spatial coordinates of (22)

$$\sum_{\vec{x}} \left\langle (\nabla_0 S_0(x))\, \bar{\mathcal{O}}^T(y) \right\rangle + Z_T Z_S^{-1} \sum_{\vec{x}} \left\langle (\nabla_0 T_0(x))\, \bar{\mathcal{O}}^T(y) \right\rangle = m_S Z_S^{-1} \sum_{\vec{x}} \left\langle \chi(x) \bar{\mathcal{O}}^T(y) \right\rangle + O(a)\,. \tag{26}$$

Note that in the above equation the three correlation functions are 4×4 matrices in Dirac indices. In numerical simulations these bare correlation functions can be computed at fixed lattice bare lattice parameters $\beta = 2N_c/g_0^2$ and κ. Thus by choosing two elements of the 4×4 matrices, a system of two equations can be solved for $m_S Z_S^{-1}$ and $Z_T Z_S^{-1}$.

One must clearly ensure that these two equations are non-trivial and independent. To do this, let us consider the correlations containing the SUSY current (identical considerations apply for the other two correlations). Written explicitly with its Dirac indices this reads

$$C^{(S,\mathcal{O})}_{\alpha\beta}(t) = a^{d_\mathcal{O}+9/2} \sum_{\vec{x}} \left\langle (\nabla_0 S_0)_\alpha(x)\, \bar{\mathcal{O}}_\beta(y) \right\rangle\,, \qquad t = x_0 - y_0\,. \tag{27}$$

We consider dimensionless correlations, since these are the quantities actually computed in simulations. The above 4×4 matrix can be expanded in the basis of the 16 Dirac matrices Γ

$$C^{(S,\mathcal{O})}_{\alpha\beta}(t) = \sum_\Gamma C^{(S,\mathcal{O})}_\Gamma(t)\, \Gamma_{\alpha\beta}\,. \tag{28}$$

Using discrete symmetries, see Appendix C, we can show that the only surviving contributions are (here Dirac indices are contracted)

$$C^{(S,\mathcal{O})}_{\mathbb{1}}(t) \equiv \sum_{\vec{x}} \left\langle \left(\overline{\nabla_0 S}_0(x)\mathcal{O}(y)\right)\right\rangle \tag{29}$$

$$C^{(S,\mathcal{O})}_{\gamma_0}(t) \equiv \sum_{\vec{x}} \left\langle \left(\overline{\nabla_0 S}_0(x)\gamma_0\mathcal{O}(y)\right)\right\rangle\,. \tag{30}$$

Due to the Majorana nature of the operators, the correlations $C^{(S,\mathcal{O})}_{\mathbb{1}}(t)$ and $C^{(S,\mathcal{O})}_{\gamma_0}(t)$ are real. In conclusion for a given insertion operator we determine the dimensionless quantities $am_S Z_S^{-1}$ and $Z_T Z_S^{-1}$ by solving the system of two equations

$$\begin{cases} C^{(S,\mathcal{O})}_{\mathbb{1}}(t) \;+\; (Z_T Z_S^{-1})\, C^{(T,\mathcal{O})}_{\mathbb{1}}(t) \\ \qquad\qquad = \; (am_S Z_S^{-1})\, C^{(\chi,\mathcal{O})}_{\mathbb{1}}(t) \\ C^{(S,\mathcal{O})}_{\gamma_0}(t) \;+\; (Z_T Z_S^{-1})\, C^{(T,\mathcal{O})}_{\gamma_0}(t) \\ \qquad\qquad = \; (am_S Z_S^{-1})\, C^{(\chi,\mathcal{O})}_{\gamma_0}(t)\,. \end{cases} \tag{31}$$

We now turn our attention to the choice of suitable insertion operators $Q(x)$. Practical considerations suggest the use of the lowest-dimensional insertion operators with the suitable symmetry properties. In our case this means the $d = 7/2$ gauge invariant bispinor

$$\mathrm{Tr}\left[P^{(cl)}_{\mu\nu}(x)\lambda(x)\right] \tag{32}$$

which is a tensor of 6 components in the Lorentz indices. Since the sink operators have spin-1/2, we must project out of the above Lorentz tensor the spin-1/2 components. Examples are S_0, T_0, χ and

$$\chi^{(sp)}(x) = \sum_{i<j} \sigma_{ij} \mathrm{Tr}\left[P^{(cl)}_{ij}\lambda(x)\right] \tag{33}$$

(only spatial plaquettes are taken into account). Since the Lorentz tensor of (32) has only two independent spin-1/2 components (see Appendix C for a detailed discussion), not all of the above operators can be independent. Indeed, they are related by

$$\chi(x) = \quad \gamma_0 T_0(x) - 2\chi^{(sp)}(x) \tag{34}$$

$$S_0(x) = 2\gamma_0(\gamma_0 T_0(x) - 2\chi^{(sp)}(x))\,. \tag{35}$$

We see that two independent systems of (31) exist for two choices of dimension-7/2 insertion operators O. This redundancy can in principle be used in order to check lattice artifacts.

Table 1. Parameters of the numerical simulations at $\beta = 2.3$. The run at $\kappa = 0.1925$ was performed in [10]. The notation is explained in the text

κ	$\epsilon \cdot 10^4$	λ	n_1	n_2	n_3	n_4	n_{HB}	n_{OB}	n_M	n_{NC}	updates	offset	N_{lat}
0.1925	3.0	3.7	32	150	220	400	1	3	1	1	216000	50	9
0.194 (a)	0.8	4.5	38	280	320	400	1	2	8	8	2250	50	9
0.194 (b)	1.0	4.5	24	160	200	400	1	2	8	8	2700	20	9
0.194 (c)	1.0	4.5	24	120	160	400	1	2	8	8	1620	20	9
0.194 (d)	1.0	4.5	28	160	210	400	2	2	8	8	35460	20	9
0.1955 (a)	0.2	5.0	32	420	560	840	2	10	4	4	5040	30	8
0.1955 (b)	0.125	5.0	32	480	640	960	2	10	4	4	27672	15	8
0.1955 (c)	0.125	5.0	32	480	640	960	6	6	12	12	33120	10	8

5 Simulation of the model with light gluinos

We simulate the N=1 SU(2) SYM on a $12^3 \times 24$ lattice at $\beta = 2.3$. This value of β corresponds to the lower end of the approximate scaling region in pure SU(2) lattice gauge theory. In the full theory virtual loops of gluinos contribute to the Callan-Symanzik β-function. The consequence is that, for fixed β, the lattice spacing is decreased.

The scaling properties of the model with dynamical gluinos were studied in detail in [10]. There values of κ up to $\kappa = 0.1925$ were considered. In that region of masses the observed effect coming from the dynamics of the gluinos was mainly the overall renormalization of the lattice spacing due to the fermionic virtual loops. The change of dimensionless ratios of masses and string tension where only moderate up to $\kappa \leq 0.1925$ where most of the simulations were performed.

The set of configurations for the lightest gluino produced in [10], κ=0.1925, is taken here as a starting point. We further simulate the model at lighter gluinos, at $\kappa =$ 0.194 and 0.1955. The largest of these hopping parameters coincides with the central value of the estimate of κ_c from the study of the finite volume gluino condensate, $\kappa_c = 0.1955(5)$ [9]. That determination was however obtained on a relatively small lattice ($6^3 \times 12$) and the value of κ_c is likely to be underestimated. In fact, anticipating results of the present study, the gluino mass starts decreasing significantly only for $\kappa \gtrsim 0.194$. For $\kappa = 0.1955$ the gluino mass is quite small but still appreciably different from zero. This is also evident in the simulation process.

Simulating light fermions in a reasonably large physical volume is a challenging task from the algorithmic point of view. The difficulty is related to very small eigenvalues of the fermion matrix. The relevant parameter in this context is the condition number of $\tilde{Q}^2$, where $\tilde{Q} \equiv \gamma_5 Q$ is the Hermitian fermion matrix[2]. For a given simulation volume the condition number gives an indication of the 'lightness' of the gluino. For the lightest gluino, at $\kappa = 0.1955$, we had condition numbers $\mathcal{O}(10^5)$. A direct comparison with the more familiar case of QCD is not possible since the simulation of SYM is generally less demanding.

[2] The condition number of a matrix is defined as the ratio between its largest and smallest eigenvalue

Another difficulty related to light fermions is the shrinking of the physical volume due to the renormalization of the lattice spacing by fermionic virtual loops. We expect that already at κ=0.194 the low energy bound-states mass spectrum is strongly affected by the finite-size scaling on our $12^3 \times 24$ lattice. (See also Sect. 5.5). The situation is different for the main subject of this work, the SUSY WIs. The WIs hold also on a finite volume with volume-dependent coefficients. These are however essentially renormalizations defined at the scale of the UV cutoff a^{-1}. Our volumes should be consequently large enough for an accurate determination.

All the numerical computations of this work were performed on the two 512-nodes CRAY-T3E machines at the John von Neumann Institute for Computing (NIC), Jülich, with 307.2 and 614.4 GFLOPS peak-performance respectively. The CPU cost of the simulation was $\sim$1 GFLOPS Year sustained ($\sim 3 \cdot 10^{16}$ f.p.o.) for each of the two simulation points of this work.

5.1 The TSMB algorithm: simulation parameters

The TSMB algorithm used in the simulations is defined in [12,13]. The multi-bosonic updating with the scalar pseudofermion fields was performed by heatbath and overrelaxation for the scalar fields and Metropolis sweeps for the gauge field; we refer to [10] for more details on the implementation of the TSMB algorithm in the case of the N=1 SU(2) SYM.

In Table 1 we report the parameters for the simulations performed in this work. We also include for reference the parameters for the simulation at $\kappa = 0.1925$ performed in [10]. We briefly explain the meaning of the various symbols (see also [10]);
$[\epsilon, \lambda]$ (columns 2 and 3) is the presumed domain of the eigenvalue spectrum of $\tilde{Q}^2$; this is also the domain of validity of the polynomial approximation of the fermionic measure; $n_{1,\ldots,4}$ (columns 4 to 7) are the orders of the polynomial approximations used in the simulation and measurement process; in particular, n_1 and n_2 are the orders of the polynomial approximations in the local update and in the global accept-reject step (noisy correction) respectively; n_3 is the order of the polynomial used for the generation of the noisy vector in the noisy correction; n_4 is the

Table 2. Exponential and integrated autocorrelation of the plaquette measured in update cycles. In square brackets the integrated autocorrelation is measured in no. of Dirac matrix multiplications. The data at $\kappa = 0.1925$ are taken from [10]

κ	run	τ_{exp}	τ_{int}	
0.1925	-	378(37)	675(200)	[1.15(34) 10^6]
0.194	d	249(68)	272(83)	[0.75(23) 10^6]
0.1955	b	220(50)	280(70)	[1.49(37) 10^6]
0.1955	c	210(40)	250(40)	[1.71(27) 10^6]
0.1955	b,c	260(30)	420(50)	

order of the polynomial used for the computation of the reweighting factors in the measurements; n_{HB}, n_{OB}, n_M (columns 8 to 10) indicate the heatbath, overrelaxation and Metropolis sweeps performed at each step of the local update; n_{NC} (column 11) is the number of Metropolis sweeps separating two consecutive global accept-reject steps; finally columns 12 to 14 report the total number of updates at equilibrium, the offset between measurements, and the number of independent lattices simulated.

5.2 Autocorrelations

Tuning the various parameters of the algorithm (ϵ, λ, $n_{1,2,3}$, n_{HB}, n_{OV}, etc.) is essential to get an optimized updating. As an optimization criterion we have considered the autocorrelation of the plaquette. In particular, the order of the first polynomial n_1 was increased until the acceptance probability in the noisy correction reached $\sim$50%. With this choice the two steps of the updating process equally contribute in shaping the distribution of gauge configurations. Larger values of n_1 have the effect of increasing autocorrelations with no substantial improvement of the algorithm. In the runs at $\kappa = 0.1955$ the update of the pseudofermionic fields was performed by iterating twice a sub-sequence of $n_{HB}/2$ heatbath and $n_{OB}/2$ overrelaxation sweeps. In Table 2 the integrated autocorrelations for the various runs are reported. The data for $\kappa = 0.1925$ are taken from [10]. A better tuning of the parameters of the algorithm allowed to keep autocorrelations down at low levels in spite of an increasingly light gluino.

5.3 Smallest eigenvalues and reweighting factors

To monitor the accuracy of the polynomial approximation in the updating process, we constantly checked the smallest and largest eigenvalue of $\tilde{Q}^2$. The distribution of the smallest eigenvalue for the two simulation points of this work is reported in Fig. 1. The vertical dashed line indicates the value of ϵ used in the simulation.

Extremely small eigenvalues can exceptionally occur without substantial harm. The corresponding configuration would then be suppressed at the measurement level by the reweighting. We calculated reweighting factors for subsamples of configurations. These turn out to be gaussian

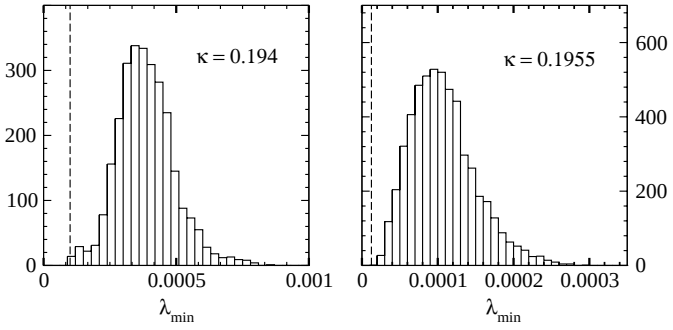

Fig. 1. Distribution of the smallest eigenvalue of $\tilde{Q}^2$ for the two simulation points of this work. The dashed line indicates the value of ϵ used in the simulation

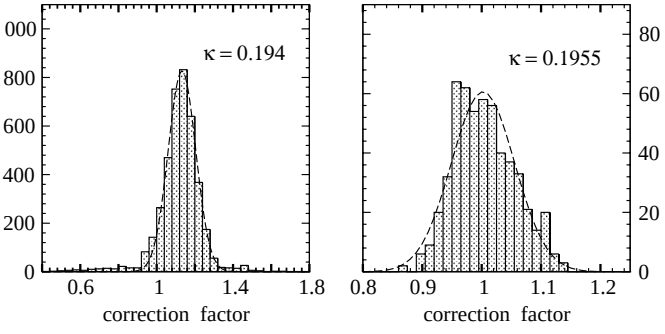

Fig. 2. Distribution of the reweighting factors with gaussian fit

distributed with average ~ 1, see Fig. 2. For $\kappa = 0.194$ we also observe a short tail towards small values. These distributions are consistent with the absence of extremely small eigenvalues in the ensembles. The effect of the reweighting turns out to be negligible compared to the statistical fluctuations for the quantities considered in this study. This confirms the overall accuracy of the simulation algorithm.

5.4 The sign of the Pfaffian

The fermionic measure implemented in the updating algorithm is given by $\sqrt{\det(Q)}$. The actual measure for Majorana fermions is instead given by the Pfaffian of the anti-symmetric matrix $M = CQ$

$$\mathrm{Pf}(M) = \sqrt{\det(Q)} \cdot \mathrm{sign}(\mathrm{Pf}(M)) \ . \qquad (36)$$

The previous formula implies that the configurations obtained by Monte Carlo updating should be further reweighted in the measurements by $\mathrm{sign}(\mathrm{Pf}(M))$. This could potentially introduce difficulties. Indeed, were positive and negative signs almost equally distributed in our ensembles, a cancellation could occur in the statistical averages. The significance of the samples would then be close to zero. This occurrence is know as 'the sign problem'. In the N=1 SYM with Wilson fermions the two signs are expected to be equally distributed for $\kappa > \kappa_c$. For $\kappa < \kappa_c$, sign-flips should be suppressed if the volume is large enough (the situation right at the critical point is still unclear).

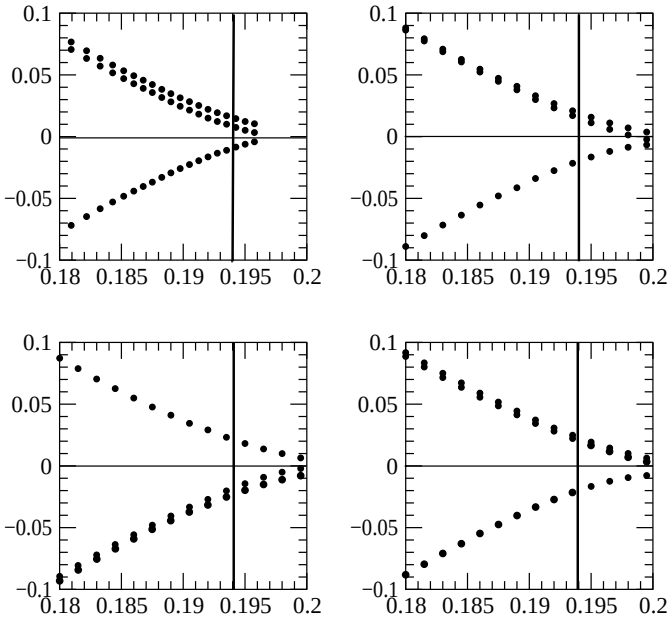

Fig. 3. The flow of eigenvalues as a function of the hopping parameter for different configurations produced at $\beta = 2.3$ and $\kappa = 0.194$. The vertical line indicates the hopping parameter of the simulation

We determined the sign of the Pfaffian for a subsample (10%) of configurations at κ=0.194 on our $12^3 \times 24$ lattice. We used the method explained in [10] consisting in following the flow of the eigenvalues of $\tilde{Q}$ as a function of the hopping parameter. A theorem ensures $\mathrm{sign}(\mathrm{Pf}(M)) = 1$ for small κ's. The sign of the Pfaffian flips whenever an eigenvalue crosses zero in the flow. We never found such zero-level crossings, implying that $\mathrm{sign}(\mathrm{Pf}(M))$ is always positive for the considered sub-sample. Examples of eigenvalue flows are given in Fig. 3. We conclude that statistically less than 0.5% of the configurations have negative sign. Negative Pfaffians were detected in [10] on a smaller lattice ($6^3 \times 12$) for $\kappa \geq 0.196$. Absence of sign-flip of the Pfaffian in our ensembles is also supported by the observation that extremely small eigenvalues do not occur and, consistently, the distribution of the reweighting factors does not extend to zero. Indeed each sign-flip under continuous modification of the gauge configuration would imply the crossing of a configuration with an exact fermionic zero-mode.

5.5 Determination of r_0/a

In [22] the scale parameter r_0 has been proposed as a reference scale for gauge configurations. It is defined by

$$r_0^2 F(r_0) = 1.65 \tag{37}$$

where $F(r)$ is the force between static fermionic color sources in the fundamental representation. In our case the determination of r_0/a allows us to monitor the reduction of the simulation volume with increasing κ.

Table 3. Determination of r_0/a for the sets of configurations considered in this study. We also report the ratio L_x/r_0 where L_x is the spatial lattice size

κ	r_0/a	L_x/r_0
0.1925	6.71(19)	1.79(5)
0.194	7.37(30)	1.63(7)
0.1955	7.98(48)	1.50(9)

We first calculated the static potential between color sources in the fundamental representation $V(\mathbf{r})$; this is needed only at intermediate distances. The potential can be estimated from Wilson loops $W(\mathbf{r}, t)$ by

$$V(\mathbf{r}, t) = \ln\left(\frac{W(\mathbf{r}, t)}{W(\mathbf{r}, t+1)}\right) . \tag{38}$$

To reduce the noise we used APE smearing [23] on the spatial links with $n_{APE} = 12$ iterations and $\epsilon_{APE} = 0.5$. Nevertheless the results get unstable for the larger Wilson loops, so we could not make an extrapolation to large t. We instead took the result for $t = 2$, calculated r_0/a for these values and added the difference to the result from $t = 3$ to the total error.

To get r_0/a from the potential we followed [24,25]. Their general procedure would be to make a fit to

$$V(\mathbf{r}) = V_0 + \sigma r - e\left[\frac{1}{\mathbf{r}}\right] + f\left(\left[\frac{1}{\mathbf{r}}\right] - \frac{1}{r}\right) \tag{39}$$

where

$$\left[\frac{1}{\mathbf{r}}\right] = 4\pi \int_{-\pi}^{\pi} \frac{\mathrm{d}^3 k}{(2\pi)^3} \frac{cos(\mathbf{k}\cdot\mathbf{r})}{4\sum_{j=1}^{3} \sin^2(k_j/2)} \tag{40}$$

removes lattice artifacts exactly to lowest order of perturbation theory. However it was not possible with our data to make fits to all four parameters. We therefore followed [24] and made a three parameter fit fixing $e = \pi/12$ and a two parameter fit fixing in addition $f = 0$. One can now extract r_0 as

$$r_0 = \sqrt{\frac{1.65 - e}{\sigma}} . \tag{41}$$

Our final estimate for r_0 comes from the three parameter fit, and the difference to the two parameter fit was again added to the Jackknife estimate for the error.

In Table 3 we report the results for r_0/a for the three sets of configurations considered in this study. From data in column 3 we see that the reduction of the physical lattice size is less than 20% for the lightest gluino in our simulations.

6 Numerical analysis of the SUSY WIs

In Sect. 4 we have shown how the quantities $am_S Z_S^{-1}$ and $Z_T Z_S^{-1}$ can be obtained by solving the system of (31) for

a given insertion operator. We have argued that there are two such independent dimension-7/2 operators. We choose the operators $\chi^{(sp)}(x)$ and $T_0^{(loc)}(x)$ defined in (33) and (21) for our analysis. Discrepancies between results obtained with these two operators signal the presence of systematic effects due to the lattice discretization.

In practice we use two methods to obtain $am_S Z_S^{-1}$ and $Z_T Z_S^{-1}$. The first method is the most straightforward, consisting simply in solving the system of (31) for each time-separation t. Results obtained in this way are reported in Figs. 4 and 5; they should be independent of t when contact terms are absent for large enough time-separations. The second method, explained in detail in Appendix D, consists in constructing an overdetermined system of equations for several consecutive time-separations (t_{min}, $\cdots$, $L_t/2$) and fitting simultaneously for all time-separations. Results obtained in this way are reported in Tables 4–7. Care should be taken in choosing t_{min} so as to avoid time-separations in which sink and insertion operators give rise to contact terms.

Previous experience with the mass spectrum [10] shows that point-like projection-operators give a poor signal for the correlations. This is mainly due to the gluonic content of both sink and insertion operators. The inconvenience is expected to be even more severe in the present case. Indeed sink operators involve time-derivatives which are subject to large statistical fluctuations. The problem was solved in [10,11] by smearing the projection-operator for the gluino-glue bound state. Combined APE [23] and Jacobi [26] smearing were performed on the gluon and gluino fields respectively. In the present case we apply the same procedure only for the insertion operator. We searched for the optimal smearing parameters by analyzing sub-samples of gauge configurations. The set of parameters employed in the final analysis was: N_{Jacobi}=18, K_{Jacobi}=0.2, N_{APE}=9, ϵ_{APE}=0.5 (set A). In one case ($\kappa = 0.1925$ and insertion operator $\chi^{(sp)}(x)$) we have also considered ϵ_{APE}=0.1 and remaining parameters as in set A (set B). The APE-Jacobi procedure is not completely satisfactory in the case of insertion operators extended in the time-direction such as $T_0^{(loc)}(x)$. In our case with dynamical gluinos, a multi-hit procedure [27] on the temporal links would not work since the noisy correction would be ineffective and anyway far too expensive.

The inversions of the fermion matrix Q required for the computation of the correlations were performed by the conjugate-gradient method. The number of iterations necessary for a good accuracy on the final result increases for light gluinos. Convergence was improved by preconditioning the Hermitian fermion matrix. The residuum for the conjugate-gradient was chosen by requiring that the final accuracy on the determination of $am_S Z_S^{-1}$ and $Z_T Z_S^{-1}$ was $\lesssim 5 \cdot 10^{-5}$. With this choice, ~ 1100 iterations were needed on average for the lightest gluino at $\kappa = 0.1955$. The computing power used was correspondingly $\sim 6 \cdot 10^{15}$ f.p.o.; this is about 20% of the amount employed for the generation of the gauge-fields. The site y of the insertion was chosen randomly for each configuration. We checked correlations in simulation time between propagators involved in the WIs. With the random choice of y the correlations between two consecutively measured propagators turns out to be negligible (less than 0.05). Consequently a naive jackknife procedure can be used for the error analysis on $am_S Z_S^{-1}$ and $Z_T Z_S^{-1}$.

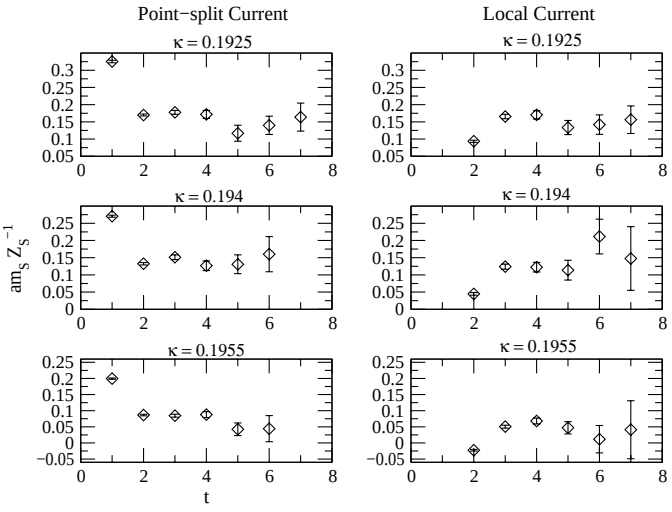

Fig. 4. $am_S Z_S^{-1}$ as a function of the time-separation t with insertion operator $\chi^{(sp)}(x)$

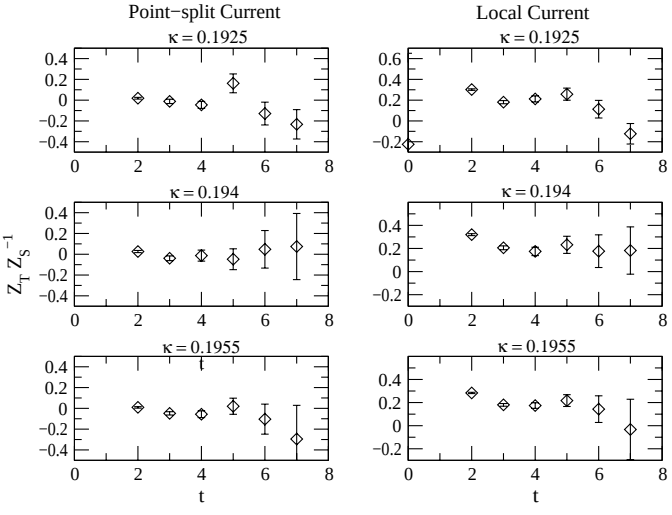

Fig. 5. $Z_T Z_S^{-1}$ as a function of the time-separation t with insertion operator $\chi^{(sp)}(x)$

At $\kappa = 0.1925$ we have also used a version of the operator $\chi^{(sp)}(x)$ defined as in (33) but with the lattice field tensor given by the simple plaquette

$$P_{\mu\nu}^{(pl)}(x) = \frac{1}{2ig_0a^2}\left(U_{\mu\nu}(x) - U_{\mu\nu}^{\dagger}(x)\right) \ . \qquad (42)$$

The drawback of this definition is that the properties of transformation under P and T are not the same as in the continuum. However comparison of results obtained with the two definitions of $\chi^{(sp)}(x)$ gives an indication of the size of discretization errors.

6.1 Results

In Figs. 4 and 5 we report the determinations of $am_S Z_S^{-1}$ and $Z_T Z_S^{-1}$ respectively, as a function of the time-separation t. The left column refers to the point-split SUSY current $S_\mu^{(ps)}(x)$ while the right one to the local current $S_\mu^{(loc)}(x)$. The insertion operator is $\chi^{(sp)}(x)$, which generally gives the best signal. A behavior consistent with a plateau can be observed for time-separations $t \geq 3$ for which there is no contamination from contact terms. The signal is rapidly washed-out by the statistical fluctuations for large time-separations.

The insertion operator $T_0^{(loc)}(x)$ containing links in the time direction gives larger fluctuations than the time-slice operator $\chi^{(sp)}(x)$. This is probably related to the poor performance of the Jacobi-APE smearing on operators extended in the time direction.

For a given insertion operator, $Z_T Z_S^{-1}$ is subject to larger statistical fluctuations than $am_S Z_S^{-1}$ as can be seen from Fig. 5 (notice the different scale). We have no theoretical justification for this outcome.

The results for $am_S Z_S^{-1}$ and $Z_T Z_S^{-1}$ from a global fit over a range of time-separations $t \geq t_{\min}$ are reported in Tables 4–7. Data are obtained by solving the overdetermined linear system as explained in Appendix D. An equivalent procedure consists in performing a least mean square fit on $am_S Z_S^{-1}(t)$ and $Z_T Z_S^{-1}(t)$ for $t \geq t_{\min}$ taking time correlations into account. This second procedure gives results consistent with the first one, with $\chi^2/d.o.f. \approx 1$ when contact terms are absent. For the final estimates we take $t_{\min} = 3$ for time-slice operators and $t_{\min} = 4$ for operators extended in the time-direction. This choice ensures absence of contact terms.

Discretization effects can be checked by comparing determinations obtained with the two independent insertions $\chi^{(sp)}(x)$ and $T_0^{(loc)}(x)$. For $\kappa = 0.1925$ one can also compare between different definitions of $\chi^{(sp)}(x)$ (simple plaquette definition of the lattice field tensor, (42), and different smearing parameters). It should be recalled at this point that different discretizations of the currents give different values for Z_S and Z_T. Consequently data from different discretizations should not be confronted.

An interesting point is the dependence of $Z_T Z_S^{-1}$ and $am_S Z_S^{-1}$ on the hopping parameter κ. This is reported in Fig. 6 and 7 respectively. Data refer to determinations obtained with $t_{min} = 3$ for insertion operator $\chi^{(sp)}(x)$ and $t_{min} = 4$ for insertion operator $T_0^{(loc)}(x)$. The definition of $\chi^{(sp)}(x)$ is the one with clover field tensor and smearing parameters of set A (cf. Tables 4–7). We see that the combination of renormalization factors $Z_T Z_S^{-1}$ shows no appreciable dependence on κ. We recall (see discussion in Sect. 3.1) that the latter is an $O(a)$ effect. Fitting these results (only for insertion $\chi^{(sp)}(x)$) with a constant in $1/\kappa$ we obtain $Z_T Z_S^{-1} = -0.039(7)$, for the point-split current, and $Z_T Z_S^{-1} = 0.185(7)$ for the local current. The renormalization is surprisingly small in the case of the point-split current. An estimate of $Z_T Z_S^{-1}$ for the point-split current at $\beta = 2.3$ can be obtained from the 1-loop perturbative calculation in [16]. At order g_0^2 one obtains $Z_T Z_S^{-1} \equiv Z_T|_{1-\text{loop}} = -0.074$.

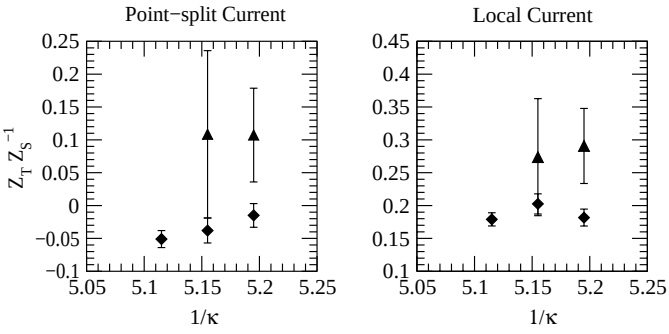

Fig. 6. $Z_T Z_S^{-1}$ as a function of $1/\kappa$ with the insertion operator $\chi^{(sp)}(x)$ (filled diamonds) and $T_0^{(loc)}(x)$ (filled triangles)

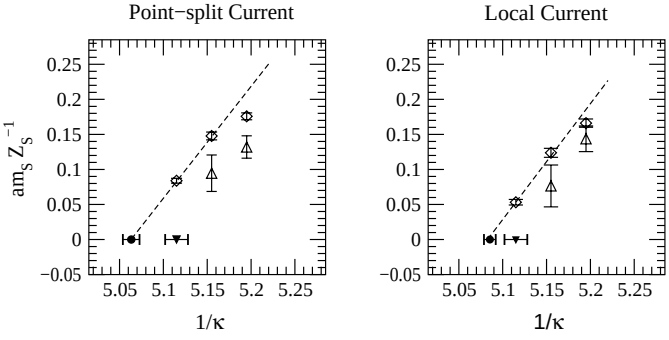

Fig. 7. $am_S Z_S^{-1}$ as a function of $1/\kappa$ with the insertion operator $\chi^{(sp)}(x)$ (diamonds) and $T_0^{(loc)}(x)$ (triangles). A linear extrapolation is also reported. The filled triangle indicates the determination of κ_c from the first order phase transition of [8]

Table 4. Summary of the results for $am_S Z_S^{-1}$ at $\beta = 2.3$ with point-split currents

κ	operator	$t_{min} = 3$	$t_{min} = 4$	$t_{\min} = 5$
0.1925	$\chi^{(sp)}$	0.176(5)	0.166(10)	0.135(14)
0.1925	$\chi^{(sp)}$ (*)	0.182(6)	0.152(11)	0.150(16)
0.1925	$\chi^{(sp)}$ (**)	0.1969(47)	0.168(9)	0.136(14)
0.1925	$T_0^{(loc)}$		0.132(16)	0.124(21)
0.194	$\chi^{(sp)}$	0.148(6)	0.130(11)	0.146(21)
0.194	$T_0^{(loc)}$		0.095(27)	0.090(27)
0.1955	$\chi^{(sp)}$	0.0839(35)	0.0820(7)	0.053(14)

* With plaquette field tensor.
** With plaquette field tensor and smearing parameters B.

In Fig. 7 the determination of $am_S Z_S^{-1}$ is reported as a function of the inverse hopping parameter. The expectation is that $am_S Z_S^{-1}$ vanishes linearly when $\kappa \to \kappa_c$. We see a clear decrease when κ is increased towards κ_c; $am_S Z_S^{-1}$ starts dropping abruptly at $\kappa \gtrsim 0.194$. We refer to data with insertion $\chi^{(sp)}(x)$. Given the weak dependence of the renormalization factors on the hopping parameter, the relative decrease of $am_S Z_S^{-1}$ as a function of κ should roughly compare with that of the gluino mass

Table 5. Summary of the results for $am_S Z_S^{-1}$ at $\beta = 2.3$ with local currents

κ	operator	$t_{min} = 3$	$t_{min} = 4$	$t_{\min} = 5$
0.1925	$\chi^{(sp)}$	0.166(6)	0.166(11)	0.146(16)
0.1925	$\chi^{(sp)}$ (*)	0.173(6)	0.155(11)	0.135(19)
0.1925	$\chi^{(sp)}$ (**)	0.1821(47)	0.173(11)	0.154(19)
0.1925	$T_0^{(loc)}$		0.144(18)	0.143(25)
0.194	$\chi^{(sp)}$	0.124(6)	0.126(12)	0.142(24)
0.194	$T_0^{(loc)}$		0.076(30)	0.098(35)
0.1955	$\chi^{(sp)}$	0.0532(40)	0.064(8)	0.047(15)

* With plaquette field tensor.
** With plaquette field tensor and smearing parameters B.

Table 6. Summary of the results for $Z_T Z_S^{-1}$ at $\beta = 2.3$ with point-split currents

κ	operator	$t_{min} = 3$	$t_{min} = 4$	$t_{\min} = 5$
0.1925	$\chi^{(sp)}$	−0.015(19)	−0.036(31)	0.045(56)
0.1925	$\chi^{(sp)}$ (*)	−0.044(16)	−0.096(33)	0.01(6)
0.1925	$\chi^{(sp)}$ (**)	−0.058(14)	−0.044(32)	−0.07(5)
0.1925	$T_0^{(loc)}$		0.11(7)	−0.03(7)
0.194	$\chi^{(sp)}$	−0.038(19)	−0.024(43)	−0.08(7)
0.194	$T_0^{(loc)}$		0.11(13)	0.02(13)
0.1955	$\chi^{(sp)}$	−0.051(13)	−0.064(26)	−0.05(5)

* With plaquette field tensor.
** With plaquette field tensor and smearing parameters B.

Table 7. Summary of the results for $Z_T Z_S^{-1}$ at $\beta = 2.3$ with local currents

κ	operator	$t_{min} = 3$	$t_{min} = 4$	$t_{\min} = 5$
0.1925	$\chi^{(sp)}$	0.183(14)	0.207(27)	0.19(5)
0.1925	$\chi^{(sp)}$ (*)	0.176(14)	0.184(28)	0.21(5)
0.1925	$\chi^{(sp)}$ (**)	0.146(11)	0.159(25)	0.139(45)
0.1925	$T_0^{(loc)}$		0.29(6)	0.22(6)
0.194	$\chi^{(sp)}$	0.202(15)	0.176(33)	0.186(6)
0.194	$T_0^{(loc)}$		0.27(9)	0.30(11)
0.1955	$\chi^{(sp)}$	0.179(10)	0.170(21)	0.170(45)

* With plaquette field tensor.
** With plaquette field tensor and smearing parameters B.

itself. In the case of the point-split current the latter almost halves when passing from $\kappa = 0.194$ to $\kappa = 0.1955$. In the case of the local current we get an even smaller mass at $\kappa = 0.1955$. Finally we obtain a determination κ_c by performing an extrapolation to zero gluino mass from two largest κ-values. The result is $\kappa_c = 0.19750(38)$ with the point-split current and $\kappa_c = 0.19647(27)$ with the local one. These values can be compared with the previous determination from the phase transition $\kappa_c = 0.1955(5)$ [8].

7 Summary and conclusions

The present study shows that the extraction of the ratios $am_S Z_S^{-1}$ and $Z_T Z_S^{-1}$ from the on-shell SUSY Ward identities is technically feasible with the computing resources at hand. The main technical difficulty (related to SUSY) is that high-dimensional operators with a mixed gluonic-fermionic composition must be considered, introducing relatively large statistical fluctuations. This difficulty can be handled with an appropriate smearing procedure. The non-perturbative determination of the ratio $am_S Z_S^{-1}$ can be used for a determination of the critical hopping parameter κ_c corresponding to massless gluinos. This can be compared to the independent determination of κ_c, based on the chiral phase transition [8]. The fact that the two determinations are not in full agreement can be explained by the presence of systematic effects. These are predominantly $O(a)$ effects in our case and finite volume effects in the determination of [8]. The discretization error in the present approach can be checked by comparing results from the two independent insertions. The statistical uncertainty is however relatively large (10-40%) for the insertion operator involving links in the time-direction. Our results for $am_S Z_S^{-1}$ and $Z_T Z_S^{-1}$ are consistent with the WIs (22) with $O(a)$ effects comparable to the statistical errors. The non-perturbative results here presented will be complemented by an analytical perturbative calculation [17].

The overall conclusion of our study is that lattice SUSY WIs can be implemented in the non-perturbative determination of the correctly subtracted SUSY current and provide a practicable method for the verification of SUSY restoration in this framework, once the proper SUSY current is identified and the usual lattice artefacts (most notably finite cutoff effects) are kept under control.

Acknowledgements. The numerical study presented here has been performed on the CRAY-T3E computers at the John von Neumann Institute for Computing (NIC), Jülich. We thank NIC and the staff at ZAM for their kind support. A.V. and C.G. wish to thank the DESY theory group and the INFN-Rome 2 respectively for their hospitality.

Appendix
A Discrete symmetries

The following Hermitian representation of the Euclidean γ-matrices is adopted:

$$\gamma_0 = \begin{pmatrix} 0 & \mathbb{1} \\ \mathbb{1} & 0 \end{pmatrix}, \quad \gamma_k = -i \begin{pmatrix} 0 & \sigma_k \\ -\sigma_k & 0 \end{pmatrix}, \qquad (43)$$

with anti-commutation property:

$$\{\gamma_\mu, \gamma_\nu\} = 2\,\delta_{\mu\nu}\ . \qquad (44)$$

The matrix γ_5 is defined as

$$\gamma_5 = \gamma_1\gamma_2\gamma_3\gamma_0 = \begin{pmatrix} \mathbb{1} & 0 \\ 0 & -\mathbb{1} \end{pmatrix} , \tag{45}$$

and the anti-Hermitian matrix $\sigma_{\mu\nu}$ reads

$$\sigma_{\mu\nu} = \frac{1}{2}[\gamma_\mu, \gamma_\nu] . \tag{46}$$

A.1 Parity P

Denoting with x_P the transformed coordinates, $x_P = (x_0, -x_1, -x_2, -x_3)$, the field transformations are:

$$\lambda^P(x) = \gamma_0\lambda(x_P) \tag{47}$$
$$\overline{\lambda}^P(x) = \overline{\lambda}(x_P)\gamma_0 \tag{48}$$
$$U_0^P(x) = U_0(x_P) \tag{49}$$
$$U_i^P(x) = U_i^\dagger(x_P - \hat{i}) . \tag{50}$$

A.2 Time reversal T

In this case $x_T = (-x_0, x_1, x_2, x_3)$, and the field transformations are:

$$\lambda^T(x) = \gamma_0\gamma_5\lambda(x_T) \tag{51}$$
$$\overline{\lambda}^T(x) = \overline{\lambda}(x_T)\gamma_5\gamma_0 \tag{52}$$
$$U_0^T(x) = U_0^\dagger(x_T - \hat{0}) \tag{53}$$
$$U_i^T(x) = U_i(x_T) . \tag{54}$$

The clover-symmetrized field tensor $P_{\mu\nu}^{(cl)}(x)$ of (13) has the same transformation properties under P and T as its continuum counterpart $F_{\mu\nu}(x)$. This does not apply to the simple plaquette lattice field tensor $P_{\mu\nu}^{(pl)}(x)$ of (42).

A.3 Charge conjugation C

The invariance of the gluino field under charge conjugation C (Majorana condition) reads

$$\begin{aligned} \lambda(x) = \lambda^C(x) &= C\overline{\lambda}^T(x) , \\ \overline{\lambda}(x) = \overline{\lambda}^C(x) &= \lambda^T(x)C^{-1} . \end{aligned} \tag{55}$$

The spinorial matrix C is defined as

$$C \equiv \gamma_0\gamma_2 = \begin{pmatrix} i\sigma_2 & 0 \\ 0 & -i\sigma_2 \end{pmatrix} , \tag{56}$$

with the properties

$$C^{-1} = -C = C^T \tag{57}$$

and

$$\begin{aligned} &C^{-1}\gamma_\mu C = -\gamma_\mu^T , \quad C^{-1}\sigma_{\mu\nu}C = -\sigma_{\mu\nu}^T , \\ &C^{-1}\gamma^5 C = \gamma^5 . \end{aligned} \tag{58}$$

B Renormalization of $O_{11/2}(x)$

We discuss here the renormalization of the composite operator $O_{11/2}(x)$ defining the continuum limit of $X(x)$ according to power-counting [2], see (19). In this context the particular lattice form of the operators is immaterial and continuum notation will be used for simplicity.

In the present work we consider gauge invariant correlation functions of the operator $O_{11/2}(x)$. In this case one can restrict the analysis to mixing with gauge invariant operators. These operators must have in addition the same transformation properties as $O_{11/2}(x)$ under the hypercubic group and the discrete symmetries C, P and T. Finally, dimensional considerations restrict the search to operators of dimension $d < 11/2$ (dimension-11/2 or higher mixing can be neglected as clarified in Sect. 3.1).

The operator $O_{11/2}(x)$ transforms under $O(4)$ like the gluino field

$$\lambda_\alpha(x) \to \sum_\beta S_{\alpha\beta}(R)\lambda_\beta(x)$$
$$S(R) = \exp\left\{-\frac{1}{2}\sum_{\mu<\nu}\omega_{\mu\nu}\sigma_{\mu\nu}\right\} . \tag{59}$$

The connection with $O(4)$ is given by

$$S(R)^{-1}\gamma_\mu S(R) = \sum_\nu R_{\mu\nu}\gamma_\nu . \tag{60}$$

The coefficient $\omega_{\mu\nu}$ represents the rotation angle in the plane (μ, ν); the hypercubic group, a discrete subgroup of O(4), is obtained by restricting these angles to multiples of $\pi/2$.

Gauge invariant operators are obtained by taking the trace in color space of products of fields in the adjoint representation. Available operators of this kind are the gluino field itself, the field tensor $F_{\mu\nu}(x)$ and the covariant derivative in the adjoint representation D_μ. Dirac and tensorial indices should be combined in such a way that the resulting operator transforms like (59) under hypercubic transformations. By using the algebra of the Γ-matrices

$$\Gamma = \{\mathbb{1}, \gamma^5, \gamma_\mu, \gamma^5\gamma_\mu, \sigma_{\mu\nu}\} \tag{61}$$

pairs of gluino fields can be assembled into bilinear expressions of the form

$$O_{\ldots}^{bilin}(x) = \overline{\lambda}(x)\Gamma_{\ldots}\lambda(x) \tag{62}$$

where Dirac indices are contracted and the dots indicate possible tensorial indices of the Γ-matrix. The transformation properties of the bilinears (62) depend on the Γ-matrix. They belong to irreducible representations of both $O(4)$ and the hypercubic group, see e.g. [28],

$\Gamma = \mathbb{1}, \gamma^5$: scalar, $I^{(+,-)}$ $(\tau_{1,4}^{(1)})$,
$\Gamma = \gamma_\mu, \gamma^5\gamma_\mu$: vectorial, $(1/2, 1/2)^{(+,-)}$ $(\tau_{1,4}^{(4)})$,
$\Gamma = \sigma_{\mu\nu}$: tensorial, $(1, 0) \oplus (0, 1)$ $(\tau_1^{(6)})$.

The representations of $O(4)$ are indicated in the notation of [28]. In parenthesis we report the corresponding representations of the hypercubic group in the notation used in [29] (see the following).

General classification. The general operator can be classified according to the number of contained gluino fields $\lambda(x)$, field tensors $F_{\mu\nu}(x)$ and covariant derivatives D_μ, n_λ, n_F and n_D. In the case of an even number of gluino fields, one can exploit the algebra of the Γ-matrices and build bilinears of the form (62) with no unpaired gluino field. Consequently all Dirac indices are contracted. Products made up by these bilinears $O^{bilin}_{\ldots}(x)$, field tensors $F_{\mu\nu}(x)$ and covariant derivatives $\overset{\ldots}{D}_\mu$ transform according to a general tensorial representation of the hypercubic group $O_{\mu_1,\ldots,\mu_n}$. An example is given by the dimension-4 operator

$$O_{\mu_1\mu_2} = \mathrm{Tr}\left[D_{\mu_1}(\overline{\lambda}(x)\gamma_{\mu_2}\lambda(x))\right] \ . \tag{63}$$

The decomposition into irreducible representations of the hypercubic group of tensorial representations has been studied in [29]. Of course the representation (59) cannot be contained in these representations[3]. One can consequently restrict the investigation to operators containing an odd number of gluino fields. An additional restriction to the possible structures of mixing operators comes from the general relation

$$\mathrm{Tr}\left[D_{\mu_1}\cdots D_{\mu_n}A(x)\right] \ = \ \partial_{\mu_1}\cdots\partial_{\mu_n}\mathrm{Tr}\left[A(x)\right] \ , \tag{64}$$

holding for a generic adjoint field $A(x)$. Since $\mathrm{Tr}[\lambda(x)] = 0$ relation (64) excludes cases where $n_\lambda = 1$ and $n_F = 0$. This leaves only three possibilities for $d \leq 9/2$:

a) $n_\lambda = 3$, $n_F = 0$, $n_D = 0$ $\quad (d = 9/2)$,
b) $n_\lambda = 1$, $n_F = 1$, $n_D = 1$ $\quad (d = 9/2)$,
c) $n_\lambda = 1$, $n_F = 1$, $n_D = 0$ $\quad (d = 7/2)$.

B.1 $n_\lambda = 3$, $n_F = 0$, $n_D = 0$

The most general gauge invariant three-gluino operator can be expressed as

$$O_{\alpha,\ldots}(x) = \mathrm{Tr}\left[(\overline{\lambda}(x)\Gamma_{\ldots}\lambda(x))\,(\Gamma'_{\ldots}\lambda(x))_\alpha\right] \ , \tag{65}$$

where as usual the dots indicate possible tensorial indices. Dirac indices are contracted in the bilinear. The transformation rule in the free Dirac index α is the right one given by (59). This Dirac index will be suppressed in the future notation. $O_{\alpha,\ldots}(x)$ defines a tensorial representation of $O(4)$ (and of the hypercubic group) in the remaining tensorial indices. Imposing invariance under $O(4)$ is equivalent to requiring that these indices are contracted so as to obtain a scalar. The procedure is standard and the result is

$$O_S(x)=\mathrm{Tr}\left[(\overline{\lambda}(x)\lambda(x))\lambda(x)\right] \tag{66}$$

$$O_P(x)=\mathrm{Tr}\left[(\overline{\lambda}(x)\gamma^5\lambda(x))\gamma^5\lambda(x)\right] \tag{67}$$

$$O_V(x)=\mathrm{Tr}\left[\sum_\mu(\overline{\lambda}(x)\gamma_\mu\lambda(x))\gamma_\mu\lambda(x)\right] \tag{68}$$

$$O_A(x)=\mathrm{Tr}\left[\sum_\mu(\overline{\lambda}(x)\gamma^5\gamma_\mu\lambda(x))\gamma^5\gamma_\mu\lambda(x)\right] \tag{69}$$

$$O_T(x)=\mathrm{Tr}\left[\sum_{\mu\nu}(\overline{\lambda}(x)\sigma_{\mu\nu}\lambda(x))\sigma_{\mu\nu}\lambda(x)\right] \ . \tag{70}$$

For Majorana fermions any three-gluino operator complying with $O(4)$ invariance, (66)-(70), vanishes. The Majorana condition (55) can be directly used to show vanishing of $O_S(x)$, $O_P(x)$ and $O_A(x)$:

$$O_S(x) = O_P(x) = O_A(x) = 0 \ . \tag{71}$$

Fierz rearrangements

$$O_V(x)=-O_A(x) \ = \ O_S(x) - O_P(x) \ , \tag{72}$$

$$O_T(x)=-O_S(x) - O_P(x) \tag{73}$$

imply vanishing of the remaining two operators $O_V(x)$ and $O_T(x)$.

The discussion is however not complete since the true symmetry of the lattice is the hypercubic one. So the question arises whether tensorial indices can be combined in (65) in a different way from (68)-(70), while still complying with the hypercubic invariance. The resulting operator would represent a potential Lorentz-breaking term in the renormalization of $O_{11/2}(x)$. The argument can be made more rigorous by considering that (65) defines tensorial representations of the hypercubic group. The question is whether singlet representations of the hypercubic group, which are not $O(4)$ scalars, are contained in the tensorial representations (65). We rely in this on the detailed discussion of the subject contained in [29].

Singlet representations of the hypercubic group which are not necessarily $O(4)$ scalars are contained in tensorial representations with even number of indices $n \geq 4$. In the classification (65) the only possible candidate is the operator with $\Gamma_{\mu\nu} = \Gamma'_{\mu\nu} = \sigma_{\mu\nu}$ containing four tensorial indices

$$\left(O^{(4)}_T\right)_{\mu_1\mu_2\mu_3\mu_4}(x) = \mathrm{Tr}\left[(\overline{\lambda}(x)\sigma_{\mu_1\mu_2}\lambda(x))\sigma_{\mu_3\mu_4}\lambda(x)\right] \ . \tag{74}$$

This means that $O(4)$-breaking versions of the operator $O_T(x)$, (70), are in principle possible. In order to decide the question we consider the general case of an operator with four tensorial indices $O^{(4)}_{\mu_1\mu_2\mu_3\mu_4}(x)$. One-dimensional representations of the hypercubic group which do not coincide with O(4) scalars are given by [29]

$$\sum_\mu O^{(4)}_{\mu,\mu,\mu,\mu}(x) \qquad \left(\tau_1^{(1)}\right) \ , \tag{75}$$

$$O^{(4)}_{\{0,1,2,3\}}(x) \qquad \left(\tau_2^{(1)}\right) \ . \tag{76}$$

[3] This is evident for example if one considers that a rotation of 2π according to (59) is not the identical transformation as in the tensorial representations. Relation (59) defines a double-valued irreducible representation of $O(4)$ and of the hypercubic group

The symbol {...} in (76) defines complete symmetrization on the Lorentz indices. In the case we are interested in, $(O_T^{(4)})_{\mu_1\mu_2\mu_3\mu_4}(x)$, antisymmetry of $\sigma_{\mu\nu}$ implies trivially vanishing of these new combinations of indices (combination (76) would have the wrong symmetry anyway). Consequently no three-gluino operators complying with hypercubic invariance can be built.

B.2 $n_\lambda = 1$, $n_F = 1$, $n_D = 1$

Gauge invariance imposes the form

$$O(x)_{\mu_1,\mu_2,\mu_3,\ldots} = \mathrm{Tr}\,[D_{\mu_1}\{F_{\mu_2\mu_3}(x)\Gamma_{\ldots}\,\lambda(x)\}]\ . \qquad (77)$$

The symbolic expression $D_\mu\{ABC\cdots\}$ is a collective representation of all the ways the covariant derivative D_μ can act on the products of the adjoint fields $A, B, C \ldots$. Since the adjoint covariant derivative satisfies the Leibniz rule, it is sufficient to consider only operators where D_μ acts on just one field $A, B, C \ldots$. Again, tensorial indices must be combined as to obtain singlets under the hypercubic group. $O(4)$-invariance and P leave only two possibilities

$$\mathrm{Tr}\,[D_\mu\{F_{\mu\nu}(x)\gamma_\nu\lambda(x)\}] \qquad (i) \qquad (78)$$
$$\mathrm{Tr}\,[\epsilon_{\mu\nu\rho\sigma}D_\mu\{F_{\nu\rho}(x)\gamma_5\gamma_\sigma\lambda(x)\}] \qquad (ii)\ . \qquad (79)$$

Also in this case new hypercubic-invariant combinations could come only from 4-index tensors, e.g.

$$O(x)_{\mu_1,\mu_2,\mu_3,\mu_4} = \mathrm{Tr}\,[D_{\mu_1}\{F_{\mu_2\mu_3}(x)\gamma_{\mu_4}\lambda(x)\}]\ . \qquad (80)$$

An analysis analogous to the one performed in the previous Subsection leads to the conclusion that no new, non-trivial operators arise from combinations (75),(76). In this case antisymmetry of $F_{\mu\nu}(x)$ plays the key rôle. So we concentrate on the Lorentz-conserving operators (78) and (79).

Case (i). The first possibility according to the Leibniz rule for the covariant derivative in (78)

$$\mathrm{Tr}\,[(D_\mu F_{\mu\nu}(x))\gamma_\nu\lambda(x)] \qquad (81)$$

vanishes on-shell. Indeed, using the equation of motion for $F_{\mu\nu}(x)$ it can be rewritten as a three-gluino operator, vanishing identically according to the previous discussion. The second possibility for the Leibniz rule

$$\mathrm{Tr}\,[F_{\mu\nu}(x)\gamma_\nu D_\mu\lambda(x)] \qquad (82)$$

is equivalent on shell to

$$\mathrm{Tr}\,[D_\mu(F_{\mu\nu}(x)\gamma_\nu\lambda(x))]\ , \qquad (83)$$

given the vanishing of (81). Using relation (64) we arrive at the operator $\partial_\mu T_\mu(x)$.

Case (ii). This goes along the same lines as case (i). The relation

$$\epsilon_{\mu\nu\rho\sigma}\gamma^5\gamma_\sigma = -\sigma_{\nu\rho}\gamma_\mu + (\delta_{\mu\rho}\gamma_\nu - \delta_{\mu\nu}\gamma_\rho) \qquad (84)$$

can be used. The part containing the γ_μ matrices reduces to the case (i) already considered. The new combination is:

$$\mathrm{Tr}\,[D_\mu\{F_{\nu\rho}(x)\sigma_{\nu\rho}\gamma_\mu\lambda(x)\}]\ . \qquad (85)$$

Again, there are essentially two possibilities:

$$\mathrm{Tr}\,[F_{\mu\nu}(x)\sigma_{\mu\nu}\not{D}\lambda(x)] \qquad (86)$$

and

$$\mathrm{Tr}\,[D_\mu(F_{\nu\rho}(x)\sigma_{\nu\rho}\gamma_\mu\lambda(x))]\ . \qquad (87)$$

On-shell, the first operator reduces to the lower dimensional operator $\chi(x)$ (17) due to the equation of motion for the field $\lambda(x)$, and can be neglected in this discussion. Rule (64) shows that the second operator is just the divergence of the SUSY current $\partial_\mu S_\mu(x)$.

In summary, the systematic scan of all possible dimension-9/2 operators with the required symmetry properties and the on-shell restriction leaves us with the two operators $\partial_\mu S_\mu(x)$ and $\partial_\mu T_\mu(x)$.

B.3 $n_\lambda = 1$, $n_F = 1$, $n_D = 0$

Using gauge invariance one gets of the general form

$$O(x)_{\mu_1,\mu_2,\ldots} = \mathrm{Tr}\,[F_{\mu_1\mu_2}(x)\Gamma_{\ldots}\lambda(x)]\ . \qquad (88)$$

The only hypercubic-invariant combination of indices is

$$\mathrm{Tr}\,[F_{\mu\nu}(x)\sigma_{\mu\nu}\lambda(x)] = \chi(x)\ . \qquad (89)$$

Again, no Lorentz-breaking combination appears.

This exhausts all possibilities for the power subtractions of $O_{11/2}(x)$ and implies the form (22) of the SUSY WIs.

C Insertion operators

In this Appendix we use for simplicity, as in the previous one, notions of the continuum. Even if the true symmetry of the lattice is the hypercubic one, the analysis is carried over by using the more restrictive Lorentz invariance. Indeed Lorentz breaking terms should not be considered, given that $O(a)$ effects are neglected.

Consider an insertion operator transforming under a generic representation of the Lorentz group (we restrict the discussion to operators depending on one coordinate). Due to the spinoral character of the SUSY WIs we need spinorial operators. Operators of this type are

$$\mathcal{O}_{\mu_1\ldots\mu_n,\alpha}(x) = T_{\mu_1\ldots\mu_n}(x)\,\psi_\alpha(x)\ , \qquad (90)$$

where $T_{\mu_1\ldots\mu_n}(x)$ is an operator transforming according to the tensorial representation of the Lorentz group and $\psi_\alpha(x)$ is a bispinor. Irreducible representations are projected-out by suitable (anti)symmetrizations, extraction of traces on the free indices. We consider zero spatial

momentum WIs (26). These are obtained by taking the vacuum expectation value of operators like e.g.

$$\mathcal{O}_{\mu_1\ldots\mu_n,\alpha\beta}(x_0,y_0) = \frac{1}{V_s}\int d\vec{x}d\vec{y}\,(\partial_0 S_0)_\alpha(\vec{x},x_0)\,\mathcal{O}_{\mu_1\ldots\mu_n,\beta}(\vec{y},y_0)\ . \quad (91)$$

The total angular momentum J of the above operator results from the composition of the spins of the two operators $\int d\vec{x}\,(\partial_0 S_0)_\alpha(\vec{x},x_0)$ and $\int d\vec{x}\,\mathcal{O}_{\mu_1\ldots\mu_n\beta}(\vec{x},y_0)$; the 'orbital' angular momentum is zero because of the summation on space coordinates. In order to get non-trivial WIs one must have of course $J=0$. Since the operator $\partial_\mu S_\mu(x)$ is a bispinor, the condition $J=0$ implies that the insertion operator must contain at least one spin-1/2 component. The irreducible representations of the Lorentz group[4] with this property are of the type $((S,S')\oplus(S',S))$, with $|S-S'|=1/2$.

The lowest dimensional gauge invariant operator has dimension $d=7/2$. It has the form (90) with tensorial part given by $F_{\mu\nu}(x)$ and $\psi(x)=\lambda(x)$. Its transformation properties under the Lorentz group are given by

$$\begin{aligned}&((1,0)\oplus(0,1))\otimes\left(\left(\frac{1}{2},0\right)\oplus\left(0,\frac{1}{2}\right)\right)\\ &=\left(\left(\frac{1}{2},0\right)\oplus\left(0,\frac{1}{2}\right)\right)\oplus\left(\frac{1}{2},\frac{1}{2}\right)\oplus\left(\frac{1}{2},\frac{1}{2}\right)\\ &\quad\oplus\left(\left(\frac{1}{2},1\right)\oplus\left(1,\frac{1}{2}\right)\right)\ .\end{aligned} \quad (92)$$

We see that two (and only two) representations on the r.h.s. of the above decomposition contain spin-1/2, namely $((\frac{1}{2},0)\oplus(0,\frac{1}{2}))$ and $((\frac{1}{2},1)\oplus(1,\frac{1}{2}))$. The first component is given by the operator $\chi(x)$, the second is present for example in $S_\mu(x)$ and $T_\mu(x)$ transforming like

$$\begin{aligned}&\left(\frac{1}{2},\frac{1}{2}\right)\otimes\left(\left(\frac{1}{2},0\right)\oplus\left(0,\frac{1}{2}\right)\right)\\ &=\left(\left(\frac{1}{2},0\right)\oplus\left(0,\frac{1}{2}\right)\right)\oplus\left(\left(\frac{1}{2},1\right)\oplus\left(1,\frac{1}{2}\right)\right)\ .\end{aligned} \quad (93)$$

Pure spin-1/2 operators are given by $\chi(x)$, $S_0(x)$ and $T_0(x)$, while $S_i(x)$ and $T_i(x)$ contain also spin-3/2 components. Equation (92) implies that any spin-1/2 component of any dimension-7/2 operator can be expressed as a linear combination of two operators chosen as a basis, for example $\chi(x)$ and $T_0(x)$ (see e.g. relations (34), (35)). Consequently only two operators give independent WIs at the lowest dimension.

For a given insertion operator the WIs consist of a number of independent equations which equals the number of rotational invariant (spin-0) components contained in the operatorial product (91). A straightforward analysis including also P reveals that these are two for $\mathcal{O}\equiv\chi(x), S_0(x), T_0(x)$, as given in (29) and (30). It should be stressed that considering other insertion operators like for example $S_i(x)$ or $T_i(x)$ would not give additional information to that given by e.g. $\chi(x)$, $T_0(x)$. One would get only different combinations of the same on-shell WIs.

The discrete symmetries T and C imply relations for the correlations involved in the SUSY WIs. For the correlations defined in (29), (30) these are

$$\mathsf{T}: \quad C^{(S,\mathcal{O})}(t) = \gamma_0\gamma_5 C^{(S,\mathcal{O})}(-t)\gamma_5\gamma_0 \quad (94)$$

$$\mathsf{C}: \quad C^{(S,\mathcal{O})}(t) = \gamma_0\gamma_2\gamma_5 (C^{(S,\mathcal{O})})^*(t)\gamma_5\gamma_2\gamma_0\ . \quad (95)$$

In terms of the components defined in (29), relation (94) reads

$$\begin{aligned}C^{(S,\mathcal{O})}_{\mathbb{1}}(-t) &= C^{(S,\mathcal{O})}_{\mathbb{1}}(t)\\ C^{(S,\mathcal{O})}_{\gamma_0}(-t) &= -C^{(S,\mathcal{O})}_{\gamma_0}(t)\ .\end{aligned} \quad (96)$$

In the case $\mathcal{O}\equiv S_0, T_0$ an extra minus sign must be included. Relation (95) ensures reality of the two components

$$\begin{aligned}C^{(S,\mathcal{O})}_{\mathbb{1}}(t) &= (C^{(S,\mathcal{O})}_{\mathbb{1}}(t))^*\\ C^{(S,\mathcal{O}}_{\gamma_0}(t) &= (C^{(S,\mathcal{O})}_{\gamma_0}(t))^*\ .\end{aligned} \quad (97)$$

Properties related to P and T apply unchanged for the lattice theory if the clover-symmetrized lattice field tensor $P^{(cl)}_{\mu\nu}(x)$ is used for the insertion operators. The simple discretization $P^{(pl)}_{\mu\nu}(x)$ breaks P and T and additional $O(a)$ pseudoscalar components are present in the correlations. In this case, for operators extended in the time-direction, the time-reflection properties (96) are violated.

D Linear fit

We perform a linear fit to solve the WI (31) for $Z_T Z_S^{-1}$ and $am_S Z_S^{-1}$ including several consecutive time-separations $(t_{min},\cdots,L_t/2)$. We define

$$A = Z_T Z_S^{-1},\quad B = am_S Z_S^{-1}\ , \quad (98)$$

and $x_{1,t}$, $y_{1,t}$ and $z_{1,t}$ as the different components of the correlation functions at different times (see (29),(30))

$$\begin{aligned}x_{1,t} = C^{(S,\mathcal{O})}_{\mathbb{1}}(t)\ ,\ y_{1,t} = C^{(T,\mathcal{O})}_{\mathbb{1}}(t)\ ,\ z_{1,t} = C^{(\chi,\mathcal{O})}_{\mathbb{1}}(t)\ ,\\ x_{2,t} = C^{(S,\mathcal{O})}_{\gamma_0}(t)\ ,\ y_{2,t} = C^{(T,\mathcal{O})}_{\gamma_0}(t)\ ,\ z_{2,t} = C^{(\chi,\mathcal{O})}_{\gamma_0}(t)\ .\end{aligned} \quad (99)$$

The overdetermined system reads

$$x_{i,t} + Ay_{i,t} = Bz_{i,t},\quad i=1,2\ ,\quad t=t_{min},\cdots,L_t/2\ . \quad (100)$$

We get the best estimates for $Z_T Z_S^{-1}$ and $am_S Z_S^{-1}$ (A and B) by minimizing the quantity

$$H = \sum_{i=1}^{2}\sum_{t=t_{min}}^{L_t/2}(x_{i,t}+Ay_{i,t}-Bz_{i,t})^2\ . \quad (101)$$

[4] As usual we take into account also P

With the conditions

$$\frac{\partial H}{\partial A} = \quad 2\sum_{i,t} y_{i,t}\left(x_{i,t} + Ay_{i,t} - Bz_{i,t}\right) = 0 \qquad (102)$$

$$\frac{\partial H}{\partial B} = -2\sum_{i,t} z_{i,t}\left(x_{i,t} + Ay_{i,t} - Bz_{i,t}\right) = 0 \qquad (103)$$

and the definition

$$\sum_{i,t} x_{i,t}\, y_{i,t} = \langle x, y\rangle \ , \qquad (104)$$

A and B are given by

$$A = \frac{\langle y,z\rangle\langle x,z\rangle - \langle x,y\rangle\langle z,z\rangle}{\langle y,y\rangle\langle z,z\rangle - \langle y,z\rangle^2} \ , \qquad (105)$$

$$B = \frac{\langle x,z\rangle\langle y,y\rangle - \langle x,y\rangle\langle y,z\rangle}{\langle y,y\rangle\langle z,z\rangle - \langle y,z\rangle^2} \ . \qquad (106)$$

References

1. D. B. Kaplan, M. Schmaltz, Chin. J. Phys. **38**, 543 (2000); G. Fleming, J. Kogut, P. Vranas, Phys. Rev. D **64**, 034510 (2001)
2. G. Curci, G. Veneziano, Nucl. Phys. B **292**, 555 (1987)
3. M. Bochicchio, L. Maiani, G. Martinelli, G. Rossi, M. Testa, Nucl. Phys. B **262**, 331 (1985)
4. L.H. Karsten, J. Smit, Nucl. Phys. B **183**, 111 (1981)
5. M. Testa, JHEP **9804**, 002 (1998)
6. I. Montvay, Nucl. Phys. Proc. Suppl. B **53**, 853 (1997)
7. G. Koutsoumbas, I. Montvay, A. Pap, K. Spanderen, D. Talkenberger, J. Westphalen, Nucl. Phys. Proc. Suppl. B **63**, 727 (1998)
8. R. Kirchner, S. Luckmann, I. Montvay, K. Spanderen, J. Westphalen, Nucl. Phys. Proc. Suppl. B **73**, 828 (1999)
9. R. Kirchner, S. Luckmann, I. Montvay, K. Spanderen, J. Westphalen, Phys. Letters B **446**, 209 (1999)
10. I. Campos, A. Feo, R. Kirchner, S. Luckmann, I. Montvay, G. Münster, K. Spanderen, J. Westphalen, Eur. Phys. J. C **11**, 507 (1999)
11. A. Donini, M. Guagnelli, P. Hernandez, A. Vladikas, Nucl. Phys. B **523**, 529 (1998)
12. I. Montvay, Nucl. Phys. B **466**, 259 (1996)
13. I. Montvay, Comput. Phys. Commun. **109**, 144 (1998)
14. G. Veneziano, S. Yankielowicz, Phys. Letters B **113**, 231 (1982)
15. G.R. Farrar, G. Gabadadze, M. Schwetz, Phys. Rev. D **58**, 015009 (1998)
16. Y. Taniguchi, Phys. Rev. D **63**, 014502 (2001)
17. F. Farchioni, A. Feo, T. Galla, C. Gebert, R. Kirchner, I. Montvay, G. Münster, Nucl. Phys. Proc. Suppl. B **94**, 791 (2001); F. Farchioni, A. Feo, T. Galla, C. Gebert, R. Kirchner, I. Montvay, G. Münster, R. Peetz, A. Vladikas, Nucl. Phys. Proc. Suppl. B **106**, 941 (2002)
18. F. Farchioni, A. Feo, T. Galla, C. Gebert, R. Kirchner, I. Montvay, G. Münster, A. Vladikas, Nucl. Phys. Proc. Suppl. B **94**, 787 (2001)
19. R. Kirchner, Ward Identities, Mass Spectrum of N=1 Super Yang-Mills Theory on the Lattice, PhD thesis, University of Hamburg, September 2000
20. F. Farchioni, A. Feo, T. Galla, C. Gebert, R. Kirchner, I. Montvay, G. Münster, A. Vladikas, Nucl. Phys. Proc. Suppl. B **106**, 938 (2002)
21. T. Galla, Supersymmetrische und Chirale Ward-Identitäten in einer diskretisierten N=1-SUSY-Yang-Mills-Theorie, Diploma Thesis, University of Münster, December 1999 (in german)
22. R. Sommer, Nucl. Phys. B **411**, 839 (1994)
23. M. Albanese et al., Phys. Letters B **192**, 163 (1987)
24. R. G. Edwards, U. M. Heller, T. R. Klassen, Nucl. Phys. B **517**, 377 (1998)
25. C. R. Allton et al. [UKQCD Collaboration], hep-lat/0107021
26. C. R. Allton et al. [UKQCD Collaboration], Phys. Rev. D **47**, 5128 (1993)
27. G.Parisi, R.Petronzio, F. Rapuano, Phys. Letters B **128**, 418 (1983)
28. J. E. Mandula, G. Zweig, J. Govaerts, Nucl. Phys. B **228**, 91 (1983)
29. M. Göckeler, R. Horsley, E.-M. Ilgenfritz, H. Perlt, P. Rakow, G. Schierholz, A. Schiller, Phys. Rev. D **54**, 5705 (1996)

[SYM-2]

The volume source technique for flavor singlets: A second look

Eur. Phys. J. C38 329-334 (2004)

Eur. Phys. J. C 38, 329–334 (2004)
Digital Object Identifier (DOI) 10.1140/epjc/s2004-02055-4

THE EUROPEAN PHYSICAL JOURNAL C

The volume source technique for flavor singlets: a second look

F. Farchioni[a], G. Münster, R. Peetz

Institut für Theoretische Physik, Universität Münster, Wilhelm-Klemm-Str. 9, 48149 Münster, Germany

Received: 14 May 2004 /
Published online: 26 November 2004 –

Abstract. We reconsider the volume source technique for the determination of flavor singlet quantities on the lattice. We point out a difficulty arising in the case of fermions in real representations of the gauge group and propose an improved version of the method (IVST) based on random gauge transformations of the background configuration. We compare the performance of IVST with the method based on stochastic estimators (SET). We consider the case of the $N = 1$ supersymmetric Yang–Mills theory, where just one fermionic flavor is present, the gluino in the adjoint representation, and only flavor singlet states are possible. This work is part of an inclusive analysis of the spectrum of the lightest particles of the theory, based on the simulation of the model on a $16^3 \cdot 32$ lattice with dynamical gluinos in the Wilson scheme.

1 Introduction

Supersymmetry (SUSY) is broken on the lattice owing to the finite lattice spacing a. We consider the $N = 1$ supersymmetric Yang–Mills theory (SYM) with gauge group SU(2) and Wilson discretization in the fermion sector. Here SUSY is also explicitly broken by the Wilson term. However, by properly tuning the (renormalized) gluino mass to zero, SUSY is expected to be recovered in the continuum limit [1] with exponentially small $O(a)$ deviations.

The manifestation of SUSY occurs at the non-perturbative level, the most interesting phenomenological implication being the expected ordering of the bound-states of the theory in supermultiplets. In the low-energy sector in particular, effective Lagrangians for SYM predict [2,3] two Wess–Zumino supermultiplets. The spin-0 particles are represented by meson-like bound states of the gluino and by glueballs, respectively, of opposite parity (this classification is of course only valid in the absence of mixings, which are however expected). The spin-$\frac{1}{2}$ particle of the multiplet is in both cases a gluino–glue bound-state.

We focus here on the problem of determining the masses of meson-like gluino bound states. Borrowing the terminology of QCD, these represent "flavor singlet" states. Indeed, SYM resembles $N_f = 1$ QCD, with the quark in the fundamental representation replaced by the gluino in the adjoint representation. The lattice computation of flavor singlet correlators is difficult because of the presence of disconnected diagrams (see [4] for a recent review on the topic). The exact evaluation of the correlator for these diagrams is not feasible since it requires the trace over color and space-time indices of the fermion propagator in the background of the gauge configuration, which in turn involves the solution of an "all-points to all-points" inversion problem *for any given gauge configuration*. The first approach to the subject was based on a volume source [5], the so-called "volume source technique" (VST). For a given background configuration the method delivers an estimate of the correlator which, however, contains spurious terms represented by non-closed loops. In [5], where QCD was considered, it was argued that these terms disappear in the ensemble-average on the basis of gauge invariance. In this paper we reconsider this argument more generally, showing that it is not applicable to models where the fermions are in real representations of the gauge group, as is the case for any representation of SU(2) and for the adjoint representation of SU(N_c). We propose a new formulation of the method, based on random gauge transformations of the background gauge configuration, which solves the problem. Due to the randomness introduced by the gauge transformation, IVST is analogous to the well known stochastic estimator technique SET [6]. In both cases the systematic error introduced by the computational procedure is converted into a statistical one and can be controlled by increasing the number of stochastic estimates. As a consequence IVST and SET can be directly compared.

This work represents the sequel of a long-standing project having the goal of a lattice verification of the non-perturbative low-energy properties of SYM. We refer to [7] and the references therein for the scope and goals of past studies. The model is simulated by means of the dynamical-gluino two-step multi-bosonic algorithm. Details on the algorithm can be found in [8]. The present analysis is based on a sample of configurations of SU(2) SYM on a $16^3 \cdot 32$ lattice. Partial results have been reported in [9].

In the next section we shall reconsider the theory of VST and propose the improved version of it, IVST. In Sect. 3 the numerical results will be presented, comparing IVST and SET; finally Sect. 4 contains our conclusions.

[a] e-mail: farchion@uni-muenster.de

2 The volume source technique revisited

In this section we consider lattice gauge theory with gauge group SU(N_c). The results of primary interest are for the gauge group SU(2) or for models with fermions in the adjoint representation of the gauge group. This includes SYM in particular. In the following, Greek letters denote Dirac indices, Latin letters color, Tr_d and Tr_c are the respective traces. With the usual bilinears $\bar{\psi}(x)\Gamma\psi(x)$ as insertion operators for the singlet mesonic states, where $\Gamma = 1$ or γ_5, the disconnected part of the mesonic correlator in the background of a gauge configuration $\{U\}$ can be written as

$$C_{\Gamma,\mathrm{disc}}[U](x_0 - y_0) = \frac{1}{V_s}\mathrm{Tr}_d\left[\Gamma S(x_0)\right]\,\mathrm{Tr}_d\left[\Gamma S(y_0)\right]\,, \quad (1)$$

where the time-slice sum $S(x_0)$ represents the trace over color and space indices of the inverse fermion-matrix, i.e. the propagator in the background of the gauge configuration $\{U\}$:

$$S_{\alpha\beta}(x_0) = \sum_{\mathbf{x}} \mathrm{Tr}_c\left[Q^{-1}_{x\alpha,x\beta}\right]\,. \quad (2)$$

VST delivers an estimate of $S_{\alpha\beta}(x_0)$ at the price of a single inversion for each value of the color and Dirac index. The inversion problem with the volume source ω_V reads

$$QZ = {\omega_V}^{[a,\alpha]}\,, \quad \left(\omega_V^{[a,\alpha]}\right)_{xb\beta} = \delta_{ab}\,\delta_{\alpha\beta}\,, \quad (3)$$

with solution

$$Z^{[a,\alpha]}_{xb\beta} = [Q^{-1}\omega_V^{[a,\alpha]}]_{xb\beta} = Q^{-1}_{xb\beta,xa\alpha} + \sum_{y\neq x} Q^{-1}_{xb\beta,ya\alpha} \quad (4)$$

When $Z^{[a,\alpha]}$ in the above equation is used to estimate the time-slice sum (2),

$$S_{\alpha\beta}(x_0) \to \tilde{S}_{\alpha\beta}(x_0) = \sum_{\mathbf{x},a} Z^{[a,\beta]}_{xa\alpha}\,, \quad (5)$$

the last term in (4) yields contributions to the disconnected part of the correlator (1) which represent non-closed loops. Such elements of the inverse fermion-matrix with $x \neq y$ are non-gauge-invariant and are canceled in the average over the gauge-ensemble (which is gauge-invariant). However, there are also contact terms in the correlator, which are potential sources of systematic errors.

In the original work [5], which introduced VST in the context of QCD, these unwanted terms were avoided by considering the correlator

$$\hat{C}_{\Gamma,\mathrm{disc}}[U](x_0-y_0) = \frac{1}{V_s}\mathrm{Tr}_d\left[\Gamma\tilde{S}(x_0)\right]\,\mathrm{Tr}_d\left[\Gamma\tilde{S}^\dagger(y_0)\right] \quad (6)$$

with one of the time slices conjugated. Owing to the fact that the product $\mathbf{3}\otimes\mathbf{3}$ of fundamental representations of SU(3) does not contain the trivial representation, a gauge-invariant contact term does not appear. The argument holds more generally for the fundamental representation of SU(N_c) for $N_c > 2$.

In the case of gauge group SU(2), which has real representations only, or in the case of the adjoint representation of SU(N_c), this prescription, however, does not help. For SU(2) the product of two fundamental representations contains the trivial one, which leads to non-vanishing contact terms again. The same is true for the adjoint representations of SU(N_c).

We now want to consider the gauge invariance of the contact terms in detail. We focus on the correlator (1); for (6) the discussion is analogous.

Consider the following average over gauge transformations $g(x)$ (*gauge-average*):

$$\left\langle \tilde{S}_{\alpha\beta}(x_0)\tilde{S}_{\gamma\delta}(y_0)\right\rangle_g = \left\langle \sum_{\mathbf{x},w,a} Q^{-1}_{xa\alpha,wa\beta}[U^g] \sum_{\mathbf{y},z,b} Q^{-1}_{yb\gamma,zb\delta}[U^g]\right\rangle_g\,. \quad (7)$$

The gauge-average induces an average over the gauge-orbit $\{U^g\}$. Using

$$Q^{-1}_{x,y}[U^g] = g^\dagger(x)Q^{-1}_{x,y}[U]g(y) \quad (8)$$

and the general formula

$$\left\langle g_{ab}(x)g^{-1}_{a'b'}(x')\right\rangle_g = A\,\delta_{xx'}\delta_{ab'}\delta_{a'b}\,, \qquad A = \begin{cases} \frac{1}{N_c}, & \text{fundamental} \\ \frac{1}{N_c^2-1}, & \text{adjoint} \end{cases} \quad (9)$$

(in the adjoint representation g are real orthogonal matrices of dimension $N_c^2 - 1$), the gauge-average of (7) reads for $x_0 \neq y_0$

$$\left\langle \tilde{S}_{\alpha\beta}(x_0)\tilde{S}_{\gamma\delta}(y_0)\right\rangle_g = \sum_{\mathbf{x}} \mathrm{Tr}_c\left[Q^{-1}_{x\alpha,x\beta}\right]\sum_{\mathbf{y}} \mathrm{Tr}_c\left[Q^{-1}_{y\gamma,y\delta}\right] + A\sum_{\mathbf{x},\mathbf{y}} \mathrm{Tr}_c\left[Q^{-1}_{x\alpha,y\beta}Q^{-1}_{y\gamma,x\delta}\right]\,. \quad (10)$$

The above expression represents the *gauge-invariant part* of $\tilde{S}_{\alpha\beta}(x_0)\tilde{S}_{\gamma\delta}(y_0)$.

Let us now consider the *ensemble-average* of $\tilde{S}_{\alpha\beta}(x_0)\times\tilde{S}_{\gamma\delta}(y_0)$. In the limit of infinite statistics any given gauge-orbit is completely covered, implying that the ensemble-average delivers in particular a gauge-average. Using the result in (10) this implies

$$\left\langle \tilde{S}_{\alpha\beta}(x_0)\tilde{S}_{\gamma\delta}(y_0)\right\rangle_U = \langle S_{\alpha\beta}(x_0)S_{\gamma\delta}(y_0)\rangle_U + A\left\langle \sum_{\mathbf{x},\mathbf{y}} \mathrm{Tr}_c\left[Q^{-1}_{x\alpha,y\beta}Q^{-1}_{y\gamma,x\delta}\right]\right\rangle_U\,. \quad (11)$$

We thus obtain that replacement (5) in (1) produces an error term for the *full* disconnected correlator

$$\tilde{C}_{\Gamma,\mathrm{disc}}(x_0 - y_0) = C_{\Gamma,\mathrm{disc}}(x_0 - y_0) + \Delta C_{\Gamma,\mathrm{disc}}(x_0 - y_0)\,, \quad (12)$$

$$\Delta C_{\Gamma,\mathrm{disc}}(x_0 - y_0) \qquad (13)$$
$$= A\,\frac{1}{V_s}\left\langle \sum_{\mathbf{x},\mathbf{y}} \mathrm{Tr}_c[\mathrm{Tr}_d\left[Q^{-1}_{x,y}\Gamma\right]\ \mathrm{Tr}_d\left[Q^{-1}_{y,x}\Gamma\right]]\right\rangle_U .$$

The conclusion is that the error term in (4) produces a systematic error in the correlator, *which does not vanish in the ensemble-average even in the limit of infinite statistics.* This error is due to gauge-invariant contact terms in the correlator, as shown above. The spurious term resembles the connected contribution

$$C_{\Gamma,\mathrm{conn}}[U](x_0 - y_0) = -f\,\frac{1}{V_s}\sum_{\mathbf{x},\mathbf{y}} \mathrm{Tr}_{cd}\left[Q^{-1}_{x,y}\Gamma\, Q^{-1}_{y,x}\Gamma\right] ,$$
$$f = \begin{cases} 1, & \text{fundamental} \\ 2, & \text{adjoint} \end{cases} \qquad (14)$$

the only difference being in the Dirac structure and the numerical factor. This outcome is not surprising considering that gauge invariance strongly constrains the space-time and color structure. We have checked the presence of the error term numerically for both types of correlators (1) and (6) for gauge group SU(2); see Sect. 3.

At this point we make the simple observation that the error is removed by using the gauge-average of $\tilde{S}_{\alpha\beta}(x_0)$ to determine the time-slice sums, since

$$\left\langle \tilde{S}_{\alpha\beta}(x_0)\right\rangle_g = S_{\alpha\beta}(x_0)\,. \qquad (15)$$

In practice this is obtained by averaging $\tilde{S}_{\alpha\beta}(x_0)$ over a sufficiently large number N_g of gauge configurations obtained from the original one by random gauge transformations [9][1] $g(x)$, namely with a flat probability distribution

$$\frac{\mathrm{d}p}{\mathrm{d}g} = 1\,, \qquad (16)$$

where $\mathrm{d}g$ denotes the Haar measure on the gauge group. Besides solving the problem of the error (13) in the correlator, the method brings the additional benefit of disentangling the systematic error inherent in VST from the statistical one: in the limit of an infinite number of random gauge transformations $N_g \to \infty$ the former goes to zero, only the second one surviving. In this view the improved version of VST is analogous to the techniques based on stochastic estimators, the randomness of the source being replaced by that of the gauge transformation.[2] This allows for a direct comparison of the two methods, which is carried out in the next section.

3 Numerical analysis

The simulation parameters of the gauge sample are $\beta = 2.3$ and $\kappa = 0.194$. The estimated value of the lattice spacing is, in QCD units, $a \approx 0.06\,\mathrm{fm}$ ($a^{-1} \approx 3.3\,\mathrm{GeV}$); there are indications [10] that the gluino is still relatively heavy ($m_{\tilde{g}} \gtrsim 200\,\mathrm{MeV}$ on the basis of QCD-inspired arguments). The set-up of the two-step multi-bosonic algorithm is the same as in [11], and ~ 4000 thermalized configurations were stored every 5 or 10 cycles. In order to obtain an estimate of the autocorrelation time of the disconnected part of the mesonic correlator, an analysis of the autocorrelation time of the smallest eigenvalue of the hermitian fermion-matrix was performed. The procedure is based on the expectation that the disconnected part of the mesonic correlator is strongly related to the infrared behavior of the fermion-matrix. After that, a subsample of 218 supposedly uncorrelated configurations was selected. This constitutes the sample for the numerical analysis.

3.1 Time-slice sums

For each configuration, 50 estimates of the time-slice sums (2) were performed, each obtained by applying a random gauge transformation on the original gauge configuration as explained in the previous section. The computations were performed in 64-bit arithmetic. Improved summation techniques were employed to ensure accuracy.

In the case of SYM the Majorana nature of the gluino field (invariance under charge conjugation) allows one to compute the inverse of the fermion-matrix for only half of the matrix-elements in Dirac space. This implies that, in the case of SU(2) SYM, only 6 fermion-matrix inversions must be performed for each configuration, compared to 12 inversions needed for QCD. So the total number of inversions N_{inv} required for a determination of the time-slice sum with N_{est} estimates is $N_{\mathrm{inv}} = 6N_{\mathrm{est}}$.[3]

As IVST is based on stochastic estimations, a comparison with stochastic-source methods SET suggests itself. We consider the SET variant with complex $\mathbf{Z}_2$ noise in the spin explicit variant SEM [12]. In this case each estimate of the time-slice sum is obtained by inverting the fermion-matrix with source $(\omega_S^{[\alpha]})_{xb\beta} = \delta_{\alpha\beta}\,\eta_{xb}^{[\alpha]}$, where $\eta_{xb}^{[\alpha]}$ are independent stochastic variables chosen at random among $\frac{1}{\sqrt{2}}(\pm 1 \pm \mathrm{i})$. For SET one has then $N_{\mathrm{inv}} = 2N_{\mathrm{est}}$. (Again a factor of 2 less comes from the symmetry of SYM.) We computed 165 estimates of the time-slice sums, in this case using 32-bit arithmetic.

In Fig. 1 the evolution of the estimated value of $\mathrm{Tr}[Q^{-1}\Gamma] \equiv \sum_{x_0} \mathrm{Tr}_d[S(x_0)\Gamma]$ for a chosen configuration is displayed as a function of the number of needed inversions N_{inv}. The error bounds represent the statistical uncertainty on the stochastic estimation. For both IVST and SET the value stabilizes after 150–200 inversions, with compatible results. This test on a single configuration only serves as a cross-check of the two methods, the physical information being contained in the ensemble-averages, Fig. 2. In the scalar case the two methods give compatible results after only 50 inversions. In the pseudoscalar case, fluctuations

[1] After the completion of this study we noticed that the use of random gauge transformations in VST was recently pointed out in [4].

[2] Actually on the basis of (8) IVST could be seen as a stochastic estimator method with a particular stochastic volume source.

[3] N_{est} coincides with N_g of previous section. The change of notation is for the sake of the homogeneity when comparing with SET.

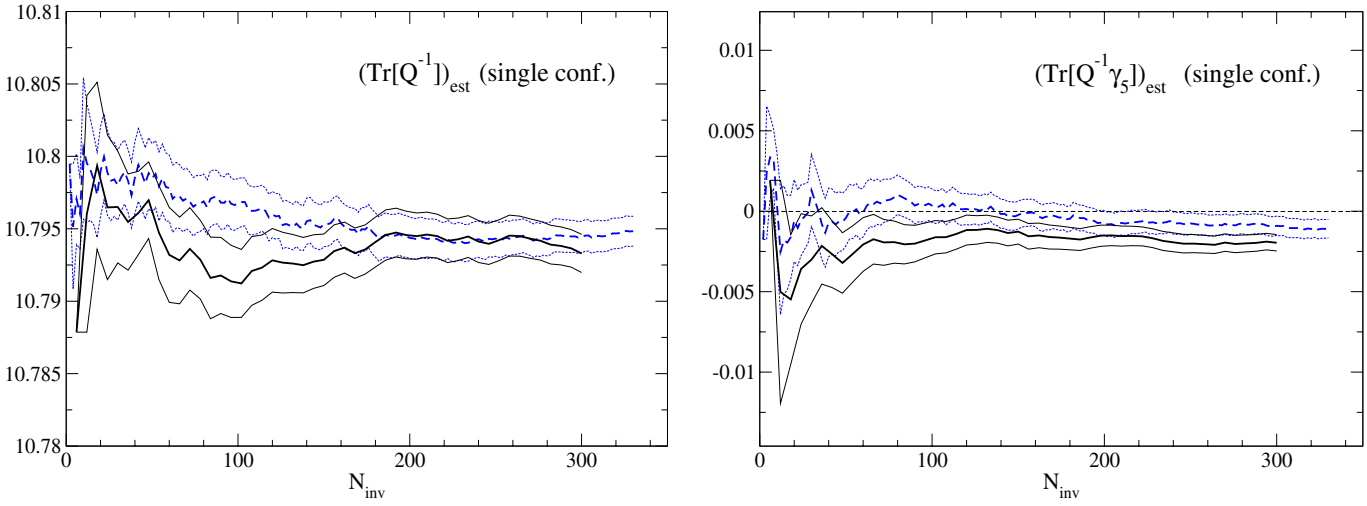

Fig. 1. Evolution of the estimated value of $\mathrm{Tr}[Q^{-1}]$ and $\mathrm{Tr}[Q^{-1}\gamma_5]$ for a chosen configuration as a function of the number of the needed inversions (with error bounds). Full lines: IVST, dashed lines: SET

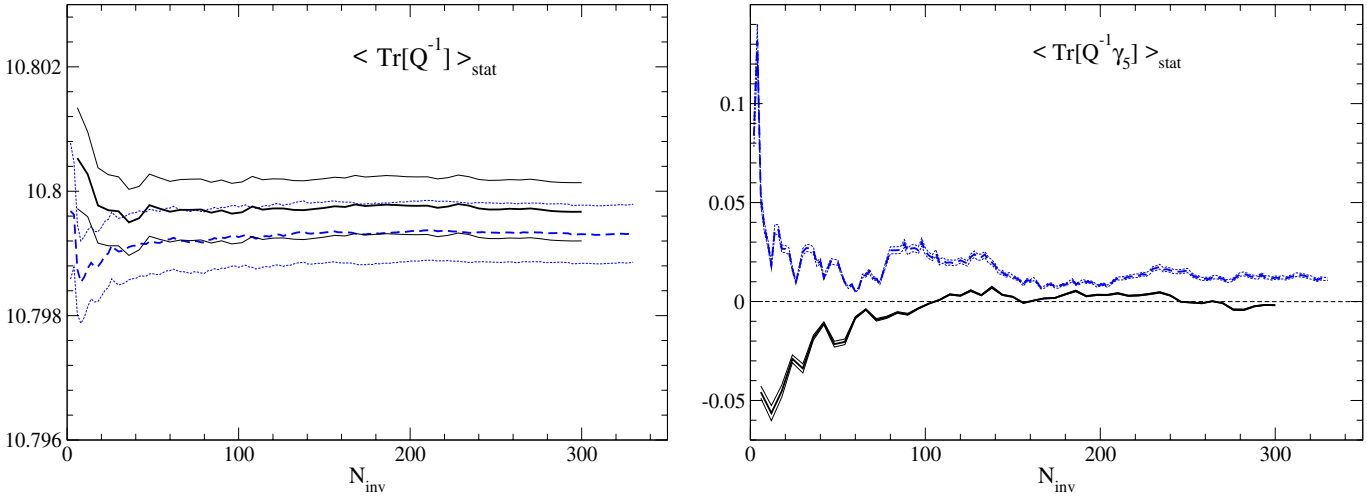

Fig. 2. Evolution of the average value of $\mathrm{Tr}[Q^{-1}]$ and $\mathrm{Tr}[Q^{-1}\gamma_5]$ over the complete sample as a function of the number of the needed inversions (with error bounds). Full lines: IVST, dashed lines: SET

much larger than the error bounds indicate additional effects. The fluctuations appear to be more relevant for SET, where 32-bit arithmetic was used. Moreover, in the latter case the estimate has an offset, while in the case of IVST the expected value (zero) is approached after ~ 100 inversions.

The evolution of the statistical error of the estimation for one configuration is displayed in Fig. 3, showing the a priori non-obvious result that the two methods introduce the same amount of stochastic uncertainty. The error in the estimation of the ensemble-average is shown in Fig. 4. We see that in both cases the error stabilizes after 100 inversions. In the pseudoscalar case, IVST seems to outperform SET, although the large instabilities prevent us from drawing firm conclusions.

3.2 Correlators and masses

In order to show the effect of the error term (13), we computed the disconnected correlator in two ways: (i) following the correct procedure according to (15) (IVST); (ii) performing the gauge-average as in (10). As one can see in Fig. 5 for the pseudoscalar meson, the error term produces a sizeable effect on the disconnected correlator. IVST and SET are in good agreement. The effective mass is shown in Fig. 6. The impact of the error on the effective mass is suppressed in the first time slices where the connected contribution (14) plays a larger role. However in the last time slices, where the disconnected contribution dominates, the effect of the error term shows-up in the form of a pronounced instability of the effective mass as a function of the time-separation (for $\Delta t = 13$ an estimate is not even possible). In the last few time-separations $\Delta t = 14, 15$, IVST delivers a better result compared to SET (no estimate is possible with SET for $\Delta t = 15$). Since the disconnected contribution to the mesonic correlator is essentially of infrared nature, the region of large time-separations is important for the determination of masses.

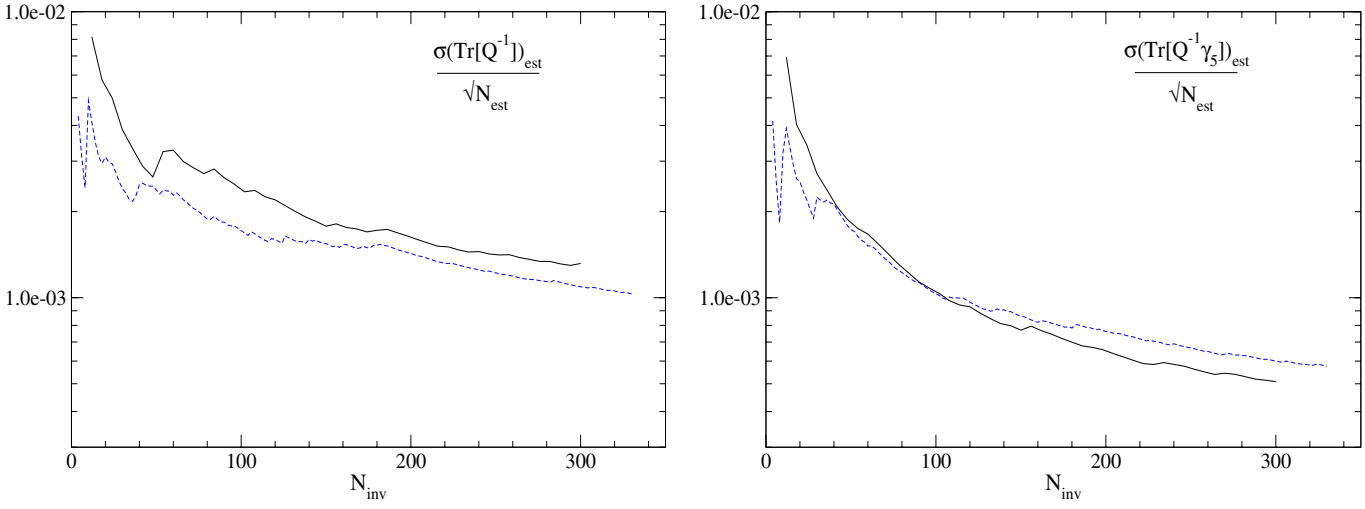

Fig. 3. Evolution of the statistical error of the estimated value of $\mathrm{Tr}[Q^{-1}]$ and $\mathrm{Tr}[Q^{-1}\gamma_5]$ for the same configuration as in Fig. 1, as a function of the number of the needed inversions. Full lines: IVST, dashed lines: SET

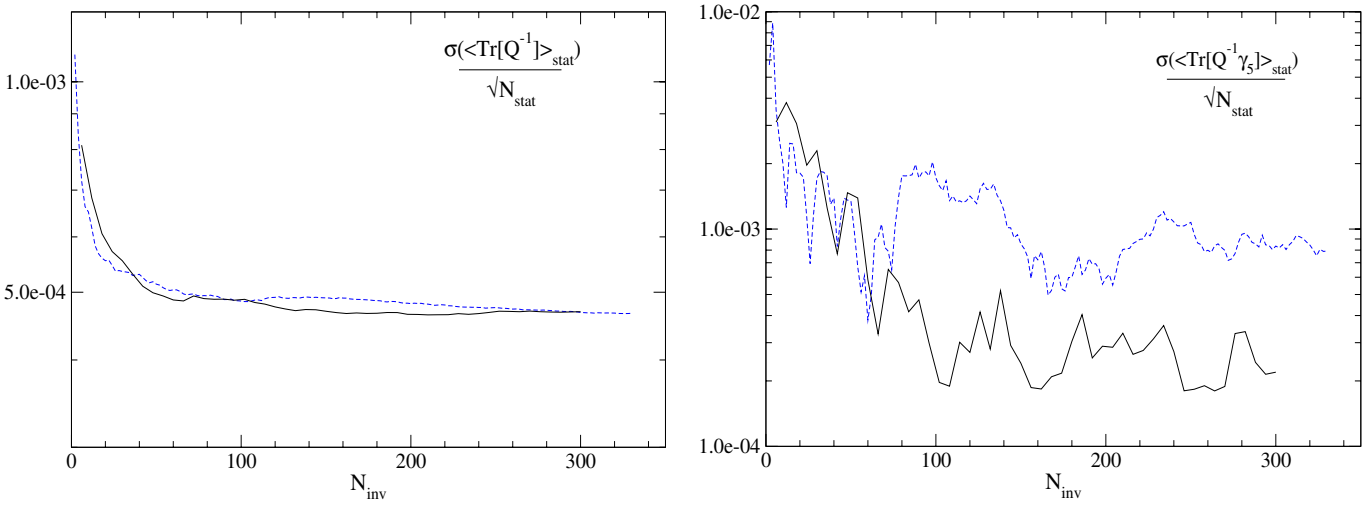

Fig. 4. Evolution of the statistical error on the average value of $\mathrm{Tr}[Q^{-1}]$ and $\mathrm{Tr}[Q^{-1}\gamma_5]$ over the complete sample as a function of the number of the needed inversions. Full lines: IVST, dashed lines: SET

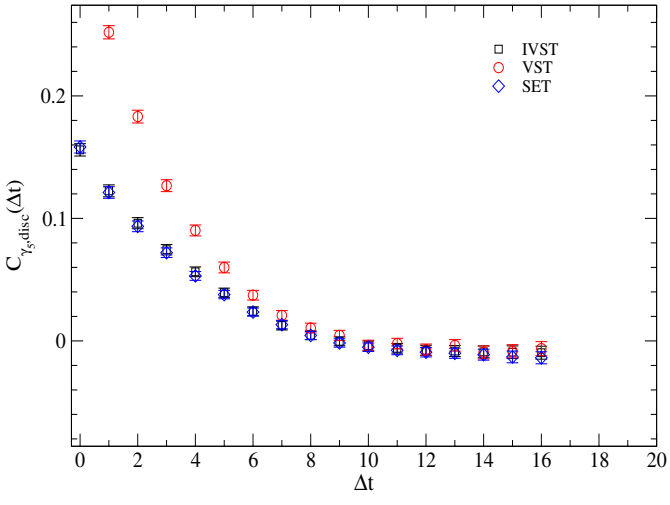

Fig. 5. The disconnected pseudoscalar correlator $C_{\Gamma,\mathrm{disc}}(\Delta t)$

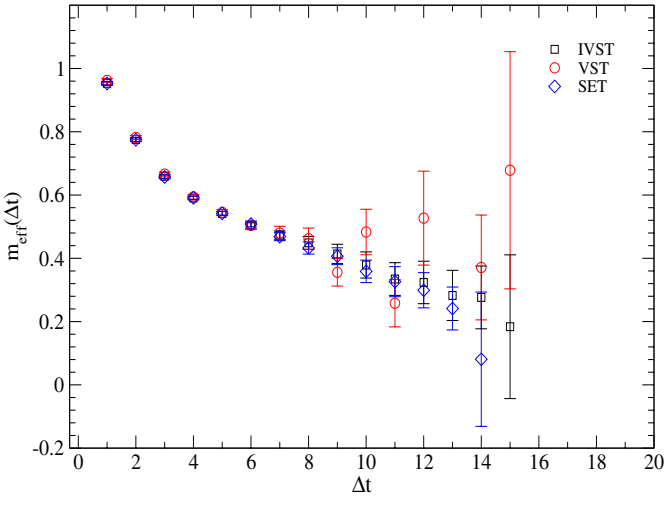

Fig. 6. The effective mass of the pseudoscalar meson

4 Conclusions

We propose an improved version of the volume source technique which eliminates erroneous contact terms in the case of fermions in real representations of the gauge group. The improved version is based on random gauge transformations and is analogous to stochastic estimator methods. Comparison between IVST and SET shows agreement and substantial equivalence. In few cases, e.g. for the determination of effective masses, IVST seems to give slightly better results. A study with higher statistical precision should put these observations on firmer ground.

Acknowledgements. The computations were performed on the Cray T3E and JUMP systems at NIC Jülich, the PC clusters at the ZIV of the University of Münster and the Sun Fire SMP-Cluster at the Rechenzentrum of the RWTH Aachen.

References

1. G. Curci, G. Veneziano, Nucl. Phys. B **292**, 555 (1987)
2. G. Veneziano, S. Yankielowicz, Phys. Lett. B **113**, 231 (1982)
3. G.R. Farrar, G. Gabadadze, M. Schwetz, Phys. Rev. D **58**, 015009 (1998)
4. K. Schilling, H. Neff, T. Lippert, hep-lat/0401005
5. Y. Kuramashi, M. Fukugita, H. Mino, M. Okawa, A. Ukawa, Phys. Rev. Lett. **72**, 3448 (1994)
6. S.J. Dong, K.F. Liu, Nucl. Phys. Proc. Suppl. **26**, 353 (1992); Phys. Lett. B **328**, 130 (1994)
7. I. Montvay, Int. J. Mod. Phys. A **17**, 2377 (2002)
8. I. Campos, A. Feo, R. Kirchner, S. Luckmann, I. Montvay, G. Münster, K. Spanderen, J. Westphalen, Eur. Phys. J. C **11**, 507 (1999)
9. R. Peetz, Ph.D. Thesis, University of Münster, 2003
10. F. Farchioni, R. Peetz, Eur. Phys. J. C (in press), hep-lat/0407036
11. F. Farchioni, A. Feo, T. Galla, C. Gebert, R. Kirchner, I. Montvay, G. Münster, A. Vladikas, Eur. Phys. J. C **23**, 719 (2002)
12. J. Viehoff et al. [SESAM Collaboration], Nucl. Phys. Proc. Suppl. **63**, 269 (1998)

[SYM-3]

The low-lying mass spectrum of the $\mathcal{N} = 1$ SU(2) SUSY Yang-Mills theory with Wilson fermions

Eur. Phys. J. C39 87-94 (2005)

Eur. Phys. J. C 39, 87–94 (2005)
Digital Object Identifier (DOI) 10.1140/epjc/s2004-02081-2

THE EUROPEAN PHYSICAL JOURNAL C

The low-lying mass spectrum of the N = 1 SU(2) SUSY Yang-Mills theory with Wilson fermions

F. Farchioni[a], R. Peetz

Institut für Theoretische Physik, Universität Münster, Wilhelm-Klemm-Str. 9, 48149 Münster, Germany

Received: 14 September 2004 / Revised version: 29 October 2004 /
Published online: 21 December 2004 –

Abstract. We analyze the low energy spectrum of bound states of the N = 1 SU(2) SUSY Yang-Mills Theory (SYM). This work continues the investigation of the non-perturbative properties of SYM by Monte Carlo simulations in the Wilson discretization with dynamical gluinos. The dynamics of the gluinos is included by the Two-Step Multi-Bosonic Algorithm (TSMB) for dynamical fermions. A new set of configurations has been generated on a $16^3 \cdot 32$ lattice at $\beta = 2.3$ and $\kappa = 0.194$. The analysis also includes sets of configurations previously generated on a smaller $(12^3 \cdot 24)$ lattice at $\kappa = 0.1925, 0.194$ and 0.1955. Guided by predictions from low energy Lagrangians, we consider spin-1/2, scalar and pseudoscalar particles. The spectrum of SYM is a challenging subject of investigation because of the extremely noisy correlators. In particular, meson-like correlators contain disconnected contributions. The larger time-extension of the $16^3 \cdot 32$ lattice allows to observe two-state signals in the effective mass. Finite-volume effects are monitored by comparing results from the two lattice sizes.

1 Introduction

The N = 1 SU(N_c) SUSY Yang-Mills (SYM) theory is the simplest instance of a SUSY gauge theory and presently the only one viable for large-scale numerical investigations. It describes N_c^2-1 gluons accompanied by an equal number of fermionic partners (gluinos) in the same (adjoint) representation of the color group. Veneziano and Yankielowicz [1] have shown how the assumption of confinement in combination with SUSY strongly constrains the low energy structure of the theory. The expected degrees of freedom dominating the low energy regime are composite operators of the gluon and gluino field which can be arranged into a chiral superfield. These are: the gluino scalar and pseudoscalar bilinears $\bar{\lambda}\lambda$, $\bar{\lambda}\gamma_5\lambda$, the corresponding gluonic quantities F^2, $\tilde{F}F$, and the spin-1/2 gluino-glue operator $\mathrm{tr}_c[F\sigma\lambda]$. However the program of including the purely gluonic operators ("glueballs") as dynamical degrees of freedom turns out to be non trivial [2–5]. In [2,4,5] the Veneziano-Yankielowicz low energy Lagrangian was extended so as to include all the desired low energy states, which are arranged into two Wess-Zumino supermultiplets. The authors of [3] pointed out on the other hand, that fulfillment of the program requires dynamical SUSY breaking and its consequent absence from the particle spectrum. In a situation where the theoretical framework seems to be still unsettled, a first-principles approach is welcome. This can be provided by lattice computations.

Our goal is to verify the low energy spectrum of SYM in the case of SU(2) gauge group by numerical techniques. By doing this we continue past projects, see [6] for a review. The direct approach to the spectrum of SYM consists in studying the time-dependence of correlators of operators having the expected quantum numbers of the low-lying particles. The simplest operators of this type are the glueball, gluino-glue and mesonic operators also entering the low energy Lagrangians. Since gluino bilinears and glueball operators of the same parity carry the same (conserved) quantum numbers of the theory, it is natural to expect mixing among them [2]. We have to stress here that when the dynamics of the gluinos is taken into account beyond the valence picture, the disentanglement of the "unmixed" states with identical quantum numbers is not possible: only the mixed physical states can be the object of investigation.[1] The result is the determination of the mass of the lightest particle with the same quantum numbers of the projecting operator: from this point of view glueball and mesonic operators are equivalent.

The action is discretized in the Wilson fashion [7][2] where, however, the gluino is a Majorana spinor in the adjoint representation:

$$S = S_G[U] + S_f\left[U, \bar{\lambda}, \lambda\right] ; \qquad (1)$$

[a] e-mail: farchion@uni-muenster.de

[1] In order to avoid confusion with the mass pattern of QCD we refrain to associate any name to the particle states of SYM and will refer to them according to their quantum numbers (spin and parity).

[2] First simulations with domain wall fermions were performed in [8].

$S_G[U]$ is the usual plaquette action and

$$S_f\left[U,\bar{\lambda},\lambda\right] = \frac{1}{2}\sum_x \bar{\lambda}(x)\lambda(x) - \frac{\kappa}{2}\sum_x\sum_\mu \big[\bar{\lambda}(x+\hat{\mu})V_\mu(x)(r+\gamma_\mu)\lambda(x) + \bar{\lambda}(x)V_\mu^T(x)(r-\gamma_\mu)\lambda(x+\hat{\mu})\big]\,; \tag{2}$$

r is the Wilson parameter set to $r = 1$ in our case. The gluino field satisfies the Majorana condition

$$\lambda = \lambda^{\mathcal{C}} = \mathcal{C}\bar{\lambda}^T\,, \tag{3}$$

where the charge conjugation in the spinorial representation is $\mathcal{C} = \gamma_0\gamma_2$; the gauge link in the adjoint representation reads:

$$[V_\mu(x)]_{ab} \equiv 2\,\mathrm{tr}[U_\mu^\dagger(x)T^a U_\mu(x)T^b] = \left[V_\mu^*(x)\right]_{ab} = \left[V_\mu^T(x)\right]^{-1}_{ab}\,, \tag{4}$$

where T^a are the generators of the color group.

The dynamics of the gluinos is included by adopting the two-step multi-bosonic algorithm (TSMB) for dynamical fermions [9]. The algorithm has the nice feature of accommodating any, even fractional, number of flavors. This is required for SYM since, schematically, the gluino has only half of the degrees of freedom of a Dirac fermion and consequently the fermion measure contains the square root of the fermion determinant: this corresponds to $N_f = 1/2$. In addition (cf. [10] for details) the design of TSMB is optimized to deal with light fermionic degrees of freedom, a critical factor when approaching the SUSY limit. Tests of the algorithm performance in QCD for light quark masses can be found in [11].

In the Wilson discretization SUSY is broken in a twofold way: explicitly by the Wilson term ensuring the correct balance between fermionic and bosonic degrees of freedom in the continuum limit, and softly by the gluino mass term. On the basis of the Ward identities [7, 12, 13], SUSY is expected to be recovered in the continuum limit by tuning the gluino mass to zero. (The situation is perfectly analogous to that of QCD, where chirality is recovered by tuning the quark mass to zero). However, $O(a)$ and $O(m_{\tilde{g}})$ SUSY violating effects are expected to distort the SUSY pattern in practical situations. A systematic analytical expansion in the gluino mass is missing in SYM; therefore it is not obvious how to set the scale for the $O(m_{\tilde{g}})$ breaking (something analogous to $\Lambda_\chi = 4\pi f_\pi$ in chiral perturbation theory). The only possibility, at least for the moment, to gain some information on the effective "heaviness" of the gluino is to force analogy with QCD. Needless to say, this procedure is only of heuristic value. The strategy we adopt is to gradually increase the hopping parameter κ in the Wilson action at fixed value of the gauge coupling $\beta = 2.3$ corresponding to a fairly small lattice size in QCD units ($a \approx 0.06$ fm), pushing the simulation towards a lighter and lighter gluino.

First large scale simulations of SYM were performed in [10] on a $12^3\cdot 24$ for $\kappa = 0.1925$. New sets of configurations were produced in [13] for $\kappa = 0.194$, 0.1955. We now turn to a $16^3\cdot 32$ lattice, whose larger time extension allows for a better analysis of the spectrum. We consider here $\kappa = 0.194$ (simulations at $\kappa = 0.1955, 0.196$ are in progress). The larger space extension allows us to monitor finite-volume effects in the spectrum.

The spectrum of SYM is challenging from the point of view of numerical analysis. The signal for the correlators of purely gluonic operators vanishes very rapidly (ideally one should use anisotropic lattices). The mixed gluonic-fermionic operators, typical for SUSY models, receive substantial fluctuations from the gluonic content. A better asymptotic behavior of the effective mass, however, can be obtained by combined smearing of the fermionic and gluonic degrees of freedom. Finally for mesonic operators, special techniques are required for the disconnected term in the correlator. Here we employ stochastic estimators (SET) [14]. Also, we apply an improved version [15] of the volume source technique (VST) [16]. For fermions in the real representation of the gauge group, as is the case for SYM, the original formulation in [16] cannot be used. The two independent techniques were tested in a comparative study for SYM in [15].

A description and some results of this study have been reported in [17].

The plan of the paper is as follows. In Sect. 2 we report details of the simulations and characterize the gauge sample, using analogy with QCD, by the Sommer scale parameter r_0 and the pseudo-pion mass; the gluino mass is obtained from the soft-breaking term in the SUSY Ward identities; Sect. 3 contains methodology and results for the spectrum; in Sect. 4 we discuss results and indicate possible directions of improvement.

2 The gauge sample

The gauge configurations were generated by the two-step multi-bosonic algorithm for dynamical gluinos [9]. We refer to [10] for a description of the algorithm. Table 1 reports an overview of the $\beta = 2.3$ ensembles used in this work; the set on the $16^3\cdot 32$ lattice with $\kappa = 0.194$ was newly generated. The setup of the TSMB was as follows. The local part of the updating procedure (one cycle) consisted of two steps of heat bath for the bosonic fields followed by two steps of over-relaxation; the updating for the gauge sector was obtained by 36 Metropolis sweeps. At the end of each cycle an accept-reject test was performed on the gauge configuration, along the lines of the general procedure described in [10]. Every five cycles a global heat-bath step was applied on the bosonic fields. The typical condition number of the squared hermitian fermion matrix was $\sim 10^4$. The integrated autocorrelation time for the smallest eigenvalue was ~ 240 cycles.

2.1 Static potential, string tension and Sommer scale parameter

We measured the potential between heavy sources in the fundamental representation. The results on the larger $16^3\cdot$

Table 1. Overview of the ensembles used in this work with determination of Sommer scale parameter and string tension. The fourth and fifth column, respectively, report the total number of configurations and of update cycles at equilibrium, the sixth column the number of replica lattices

reference	L_s	κ	$N_{\rm config}$	$N_{\rm cycle}$	$N_{\rm lat}$	r_0/a	$a\sqrt{\sigma}$
[10]	8	0.19	20768	1038400	32	5.41(28) [10]	0.22(1)
[10]	12	0.1925	4320	216000	9	6.71(19) [13]	0.176(4)
[13]	12	0.194	2034	42030	9	7.37(30) [13]	0.160(6)
this study	16	0.194	3890	25650	4	7.16(25)	0.165(9)
[13]	12	0.1955	4272	65832	8	7.98(48) [13]	0.147(8)

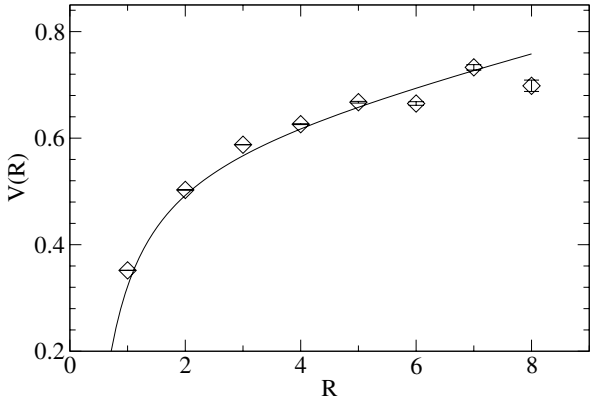

Fig. 1. Static potential between heavy sources in the fundamental representation on the $16^3 \cdot 32$ lattice, $\kappa = 0.194$; the line is the fit with lattice formulae

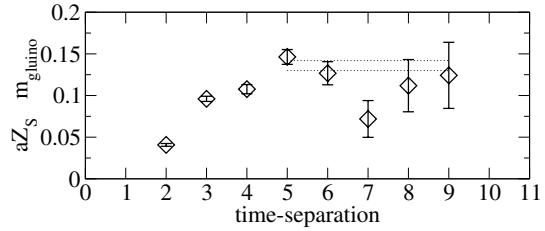

Fig. 2. The gluino mass as obtained from the SUSY Ward identities as a function of the time separation between current and insertion operator on the $16^3 \cdot 32$ lattice, $\kappa = 0.194$. The lines indicate bounds of the fit

32 lattice confirm the picture of confinement found in [10], see Fig. 1. The Sommer scale parameter r_0 and the string tension $\sqrt{\sigma}$ were measured by fitting the potential with the lattice formula [18]

$$V(\mathbf{r}) = V_0 + \sigma r - 4\pi e \int_{-\pi}^{\pi} \frac{\mathrm{d}^3 k}{(2\pi)^3} \frac{\cos(\mathbf{k}\cdot\mathbf{r})}{4\sum_{j=1}^{3}\sin^2(k_j/2)}\ ; \quad (5)$$

r_0 is given by

$$r_0 = \sqrt{\frac{1.65 - e}{\sigma}}\ . \quad (6)$$

The results are reported in Table 1.

Comparing the results on the two lattices, no finite-size effect beyond statistical uncertainty is visible in the Sommer scale parameter and the string-tension. Similarly to QCD, the Sommer scale parameter displays a sizeable gluino-mass dependence. A linear extrapolation to zero gluino mass is performed in the next subsection.

2.2 Massless gluino limit

In QCD the massless quark limit can be determined by inspection of the pion mass or use of the chiral Ward identities. In contrast, in SYM the $U(1)$ chiral symmetry is anomalous and the particle with the quantum numbers of the chiral current (namely the pseudoscalar particle) picks up a mass by the anomaly. However, theoretical arguments [1] (cf. also the discussion in [12]) support the picture that the anomaly is originated by OZI-rule violating diagrams, while the remaining ones determine spontaneous breaking of the chiral symmetry. The diagrams of the pseudoscalar correlator respecting the OZI-rule give rise to the connected (one loop) term, corresponding in QCD to the pion-correlator. The analogy with QCD suggests the name "adjoint-pion" $(a-\pi)$ for the associated pseudoparticle: in the above picture this is expected to be a soft-mode of the theory, the corresponding mass disappearing for $m_{\tilde{g}} \to 0$.

The gluino mass can be directly determined by studying the lattice SUSY Ward identities [7, 12, 13], where the former enters the soft breaking term. We refer to [13] for the illustration of the method and discussion of theoretical aspects. One can determine the combination $aZ_S^{-1}m_{\tilde{g}}$ where Z_S is the renormalization constant of the SUSY current, which is expected to be a (finite) function of the gauge coupling only. This quantity was determined in [13] for the $12^3 \cdot 24$ lattice. We repeat here the computation for the $16^3 \cdot 32$ lattice. The results are reported in Fig. 2, where the gluino mass is plotted against the time separation between current and insertion operator in the SUSY Ward identities. Compared to the $12^3 \cdot 24$ case of [13], the plateau establishes for larger values of the time separation (five compared to three); unfortunately, at these time separations the quality of the signal is already quite deteriorated. Table 2 contains the determinations of $aZ_S^{-1}m_{\tilde{g}}$ and $am_{a-\pi}$ in present and past works. Comparison of $12^3 \cdot 24$ and $16^3 \cdot 32$ results at $\kappa = 0.194$ reveals a sizeable finite volume effect for the adjoint-pion mass. It should be noted that the sign of the effect is opposite to the usual one (however this is no physical mass). The gluino mass comes in larger on the larger lattice, however within a 1-σ effect.

Table 2. Quantities determined in this and previous studies: the adjoint-pion mass, gluino mass from SUSY Ward identities (with local SUSY current, insertion operator $\chi^{(sp)}$, cf. Table 5 in [13]), spin-1/2, 0^+ and 0^- bound state masses

L_s	κ	$am_{a-\pi}$	$aZ_S^{-1}m_{\tilde{g}}$	spin-1/2	0^+(glueb.)	$0^-(\bar{\lambda}\gamma^5\lambda)$
8	0.19	0.71(2) [10]				
12	0.1925	0.550(1)	0.166(6) [13]	0.33(4)	0.53(10) [20]	0.52(10) [20]
12	0.194	0.470(4)	0.124(6) [13]	0.49(4)	0.40(11)	0.42(1)
16	0.194	0.484(1)	0.137(7)	0.43(1)		0.52(2)
12	0.1955	0.253(4)	0.053(4) [13]	0.35(4)	0.36(4)	0.24(2)

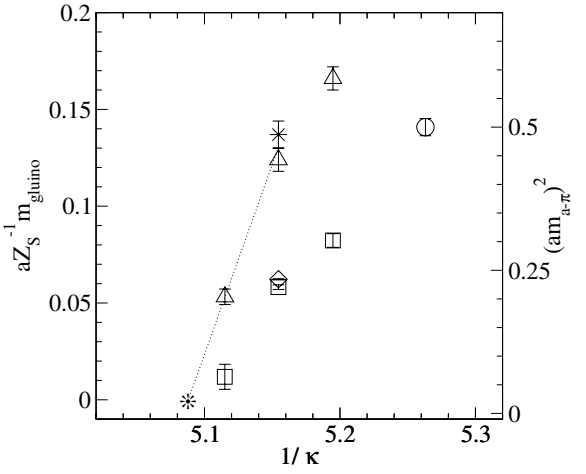

Fig. 3. The gluino mass from the SUSY Ward identities and the squared adjoint-pion mass $m_{a-\pi}$ as a function of $1/\kappa$ (from the present and past studies [10,13]); $aZ_S^{-1}m_{\tilde{g}}$ on the $12^3 \cdot 24$ lattice (triangles), the same quantity on the $16^3 \cdot 32$ lattice (star); squared adjoint-pion mass on $8^3 \cdot 16$ (circle), $12^3 \cdot 24$ (boxes), and $16^3 \cdot 32$ lattice (diamond). The burst indicates the extrapolated massless limit from the two lightest gluino masses

In Fig. 3 $aZ_S^{-1}m_{\tilde{g}}$ is shown together with the squared adjoint-pion mass. The two quantities appear to vanish for a common value of $\kappa \equiv \kappa_c$. The estimate of κ_c from the SUSY Ward identity gluino mass, $\kappa_c \approx 0.1965$ [13], is not changed by the inclusion of the point on the larger lattice. Using this value of κ_c we can now extrapolate the Sommer scale parameter in Table 1 to the massless gluino situation. A linear extrapolation results in $r_0/a(m_{\tilde{g}} = 0) = 8.4(4)$; the error takes into account the uncertainty in the determination of κ_c (assumed to be in the region κ=0.1965–0.1975 [13]). The Sommer scale parameter signals the degree of "smoothness" (or "coarseness") of the gauge sample. In QCD, the present value would correspond to $a \approx 0.06$ fm (3.3 GeV), a fairly fine lattice. Further, assuming that the adjoint-pion drives the low energy features of SYM, as the pion does in QCD, one can estimate the degree of soft-breaking of SUSY by considering the dimensionless quantity $M_r = (m_{a-\pi}r_0)^2$. In QCD, validity of NLO chiral perturbation theory requires [21] a $M_r \lesssim 0.8$ (corresponding to $m_{ud} \lesssim 1/4\, m_s$). In our case we have $M_r(\kappa = 0.194) \approx 16$ and $M_r(\kappa = 0.1955) \approx 4.5$; our lightest case would correspond in QCD to $m_{ud} \approx 1.5\, m_s$. Alternatively one can consider the gluino mass from the SUSY Ward identity neglecting $O(1)$ renormalizations, again fixing the scale by the Sommer parameter with QCD units. In this case we obtain for our lightest gluino $m_{\tilde{g}} \approx 174$ MeV in rough agreement with the previous estimate. Since QCD and SU(2) SYM are different theories, the above indications are of course of qualitative nature. On the other hand, the relatively large average condition numbers of the fermion matrix, $\sim 10^4$ for $\kappa = 0.194$ and $\sim 3.6\ 10^4$ for $\kappa = 0.1955$, point towards a lighter gluino.

3 The spectrum

As explained above, we concentrate our analysis of the spectrum on particles with spin = 0 (both parities) and spin = 1/2. We investigate the glueball operators, the gluino scalar and pseudoscalar bilinears (meson-type operators) and the gluino-glue operator.

3.1 Spin-1/2 bound states

We adopt here a lattice version [13] of the gluino-glue operator $\mathrm{tr}_c[F\sigma\lambda]$ where the field-strength tensor $F_{\mu\nu}(x)$ is replaced by the clover-plaquette operator $P_{\mu\nu}(x)$:

$$\mathcal{O}^{\alpha}_{\tilde{g}g}(x) = \sum_{i<j} \sigma_{ij}^{\alpha\beta}\, \mathrm{tr}_c \left[P_{ij}(x)\lambda^{\beta}(x)\right] \ ; \qquad (7)$$

only spatial indices are taken into account in order to avoid links in the time-direction. The clover-plaquette operator is defined to be

$$P_{\mu\nu}(x) = \frac{1}{8ig_0} \sum_{i=1}^{4} \left(U^{(i)}_{\mu\nu}(x) - U^{(i)\dagger}_{\mu\nu}(x) \right) \qquad (8)$$

with

$$\begin{aligned}
U^{(1)}_{\mu\nu}(x) &= U^{\dagger}_{\nu}(x) U^{\dagger}_{\mu}(x+\hat{\nu}) U_{\nu}(x+\hat{\mu}) U_{\mu}(x) \\
U^{(2)}_{\mu\nu}(x) &= U^{\dagger}_{\mu}(x) U_{\nu}(x-\hat{\nu}+\hat{\mu}) U_{\mu}(x-\hat{\nu}) U^{\dagger}_{\nu}(x-\hat{\nu}) \\
U^{(3)}_{\mu\nu}(x) &= U_{\nu}(x-\hat{\nu}) U_{\nu}(x-\hat{\nu}-\hat{\mu}) \\
&\quad \times U^{\dagger}_{\mu}(x-\hat{\nu}-\hat{\mu}) U^{\dagger}_{\mu}(x-\hat{\mu}) \\
U^{(4)}_{\mu\nu}(x) &= U_{\mu}(x-\hat{\mu}) U^{\dagger}_{\nu}(x-\hat{\mu}) U^{\dagger}_{\mu}(x+\hat{\nu}-\hat{\mu}) U_{\nu}(x) \ . \qquad (9)
\end{aligned}$$

The choice of the clover plaquette vs. the regular plaquette as the gluonic field-strength operator in (7) is motivated

by the correct behavior under parity and time reversal transformations as opposed to simply $U_{\mu\nu}(x)$. Because of the spinorial character of the gluino-glue, the correlator $C_{\tilde{g}g}(t)$ has a specific structure in Dirac space. On the basis of the symmetries of the theory, one can show [12] that only two components are linearly independent, $\mathrm{tr}_D[C_{\tilde{g}g}(x)]$ and $\mathrm{tr}_D[\gamma_0 C_{\tilde{g}g}(x)]$. In our experience, the latter gives the best signal. In order to get a better overlap with the ground state, we apply APE smearing [22] on the link-variables and Jacobi smearing [23] on the gluino field simultaneously.

3.2 0^- bound states

The meson-type correlators require a separate discussion because of the disconnected contribution. In the case of SYM one has (with Δ the gluino propagator):

$$\begin{aligned} C_{\mathrm{meson}}(x_0 - y_0) &= C_{\mathrm{conn}}(x_0 - y_0) - C_{\mathrm{disc}}(x_0 - y_0) \\ &= \frac{1}{V_s} \sum_{\boldsymbol{x}} \langle \mathrm{tr}[\Gamma \Delta_{x,y} \Gamma \Delta_{y,x}] \rangle \qquad (10) \\ &\quad - \frac{1}{2V_s} \sum_{\boldsymbol{x}} \langle \mathrm{tr}[\Gamma \Delta_{x,x}] \, \mathrm{tr}[\Gamma \Delta_{y,y}] \rangle \ , \end{aligned}$$

with $\Gamma \in \{1, \gamma_0\}$ (observe the factor 1/2 reflecting the Majorana nature of the gluino). The disconnected term requires the estimation of the time-slice sum of the gluino propagator

$$S_{\alpha\beta}(x_0) = \sum_{\boldsymbol{x}} \mathrm{tr}_c[\Delta_{x\alpha,x\beta}] \, . \qquad (11)$$

For this, we use the stochastic estimator technique (SET) [14] with complex Z_2 noise in the spin explicit variant SEM [19]. In this case each estimate of the time-slice sum is obtained by inverting the fermion-matrix with source $(\omega_S^{[\alpha]})_{xb\beta} = \delta_{\alpha\beta} \, \eta_{xb}^{[\alpha]}$ where $\eta_{xb}^{[\alpha]}$ are independent stochastic variables chosen at random from $\frac{1}{\sqrt{2}}(\pm 1 \pm i)$. Here we use point-like operators (i.e., no smearing on the gluino).

On the larger $16^3 \cdot 32$ lattice the computed meson correlator displays an offset: its long-time behavior is not purely exponential, since a constant term also appears. Such a constant term is theoretically excluded in the correlator by the symmetries of the theory. It is present in both SET and VST (see below) determinations of the disconnected contribution and does not decrease by increasing the number of the random estimators. In contrast, it is absent in the connected correlator. We conclude that its origin is to be traced to some cumulative numerical effect in the stochastic computation of the disconnected contribution.

In Fig. 4 we show the disconnected component of the pseudoscalar meson correlator after subtraction of the constant term. In Fig. 5 the ratio between the subtracted disconnected component and the connected one is reported. For a comparison with the same quantity in the case of QCD see e.g., [24,25]; we remark here that the case of SYM is quite different since the connected correlator is not related to a physical particle, but rather to the pseudoparticle $a - \pi$ discussed above.

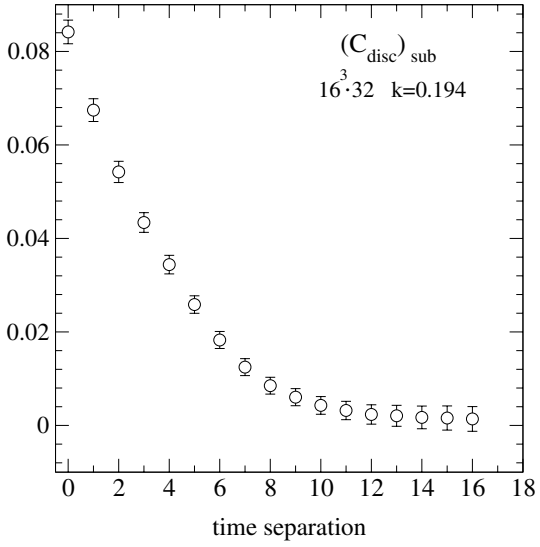

Fig. 4. The disconnected component of the pseudoscalar meson correlator after subtraction of the constant term on the $16^3 \cdot 32$ lattice, $\kappa = 0.194$ (SET)

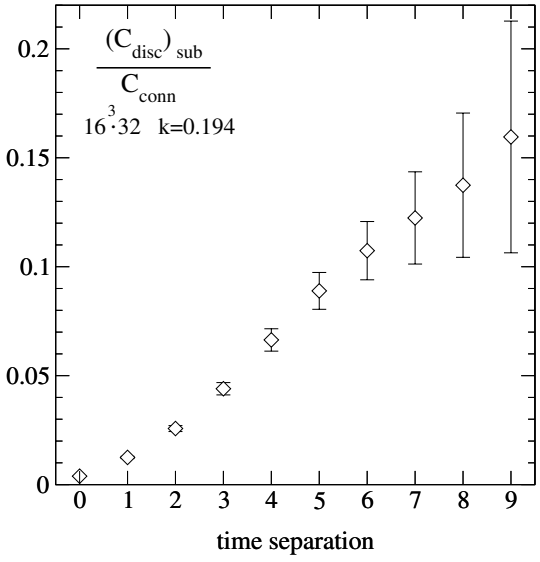

Fig. 5. Ratio of the disconnected (after subtraction) and connected components of the pseudoscalar meson correlator on the $16^3 \cdot 32$ lattice, $\kappa = 0.194$ (SET)

We cross-check the SET with the improved version [15] of the volume source technique (VST) [16], applying to fermions in real representations of the color group. The improvement consists in averaging the time-slice sums over random gauge transformations and therefore eliminating the gauge non-invariant spurious terms. The two methods deliver consistent results of comparable quality at similar computational cost. For the sake of brevity, we present here only those from SET.

Another operator with the right quantum numbers (0^-) is the pseudoscalar glueball operator. This is given by a linear combination of closed loops of link variables which cannot be rotated into their mirror image (cf. e.g., [10]). We considered the simplest loops of this kind. Unfortunately this operator does not give a clear signal on our samples.

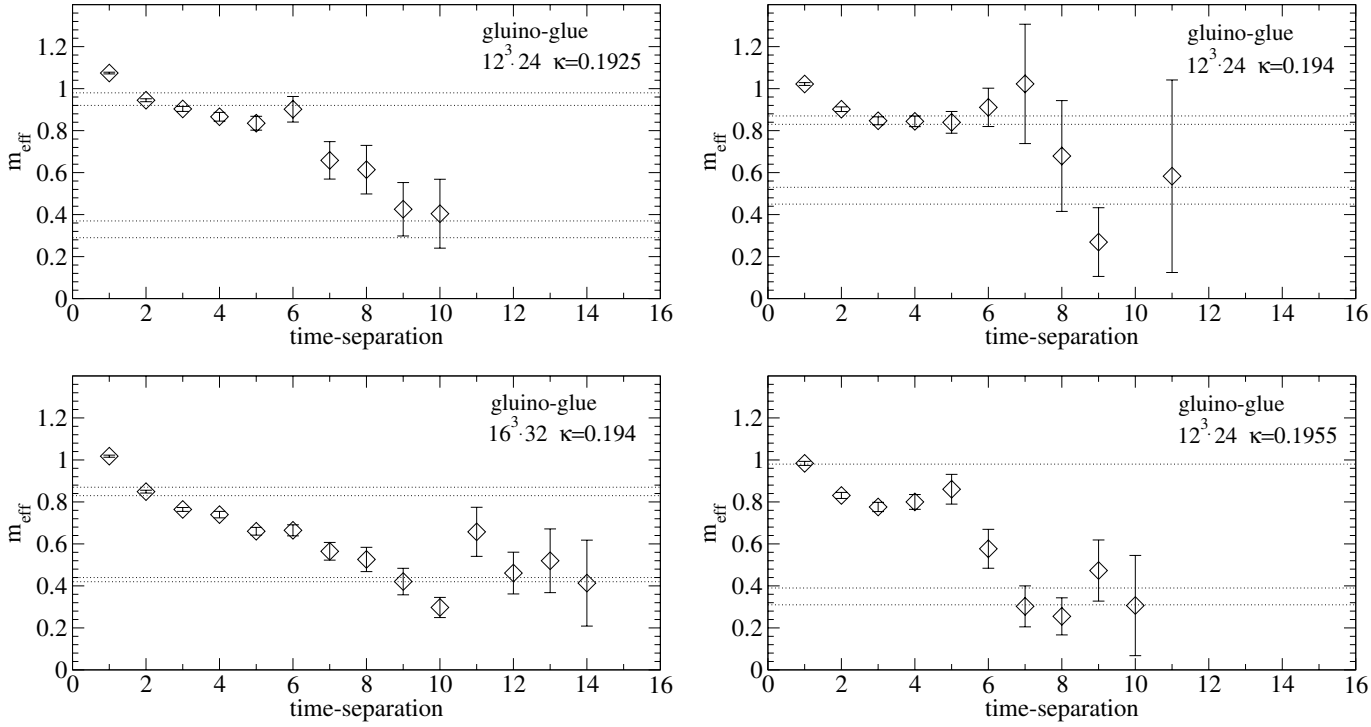

Fig. 6. The effective mass of the spin-1/2 particle (γ_0 component) for the different samples. Dotted lines are the bounds of the mass fits (ground and first excited state). In the last case only a rough indication of the first excited state mass could be obtained

3.3 0^+ bound states

Since the meson-type correlator does not show any appreciable signal for the 0^+ state, we turn to the scalar glueball operator. The standard operator in this case is

$$\mathcal{O}_{\text{glueball}}(x) = \text{tr}_c[U_{12}(x) + U_{23}(x) + U_{31}(x)]\,. \qquad (12)$$

We use fuzzy operators by applying APE smearing on the link variables.

3.4 Results

For all particles we measured the effective masses (Figs. 6–8). In many cases a clear plateau could not be determined. In order to get a better determination of the ground state mass, we used constrained two-mass fits (bounds in the figures). In some cases (the spin-1/2 particle on the larger lattice at $\kappa = 0.194$, Fig. 6, and the pseudoscalar particle at the same κ value, Fig. 7) the two-mass fit can be cross-checked against a plateau of the effective mass. We ensured the stability of the two-mass fits by systematically varying fit ranges (for details see [17]). The effective mass of the pseudoscalar meson on the $16^3 \cdot 32$ lattice, lower panel of Fig. 7, was determined after subtraction of the constant term in the correlator discussed in Sect. 3.2.

In the case of the scalar glueball operator, a decrease of the signal/noise ratio was observed on the larger lattice, as a consequence of which no determination of the mass was possible.

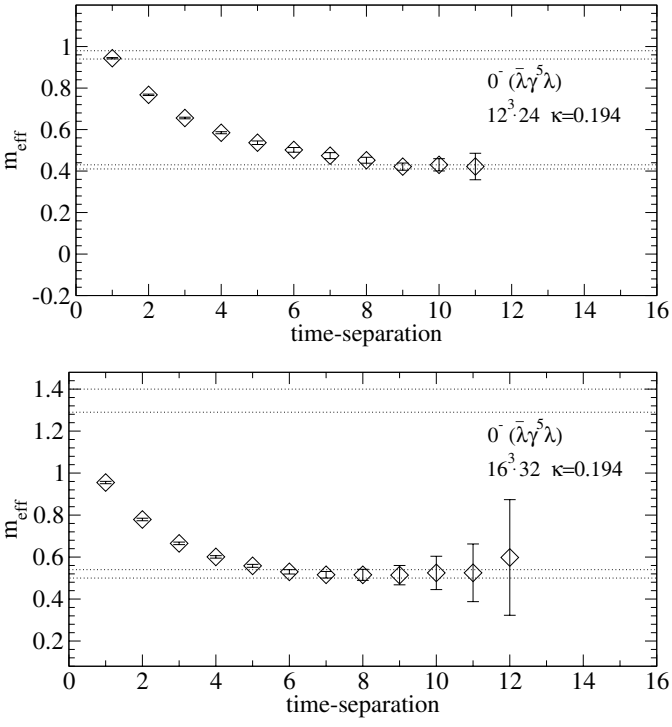

Fig. 7. The comparison of the effective mass of the pseudoscalar particle on the two lattices at $\kappa = 0.194$. Dotted lines are the bounds of the mass fits (ground and first excited state)

Results on the determinations of the ground state masses are reported in Table 2 and Fig. 9. A discussion of the results will be presented in the following section.

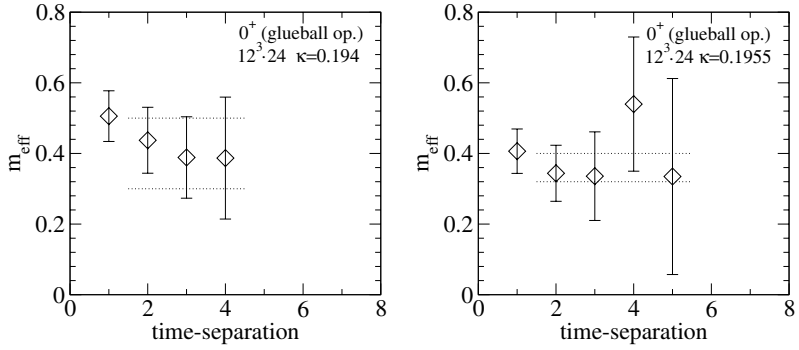

Fig. 8. The effective mass of the scalar particle with glueball operator on the $12^3 \cdot 24$ lattice at $\kappa = 0.194, 0.1955$. Dotted lines are the bounds of one-mass fits

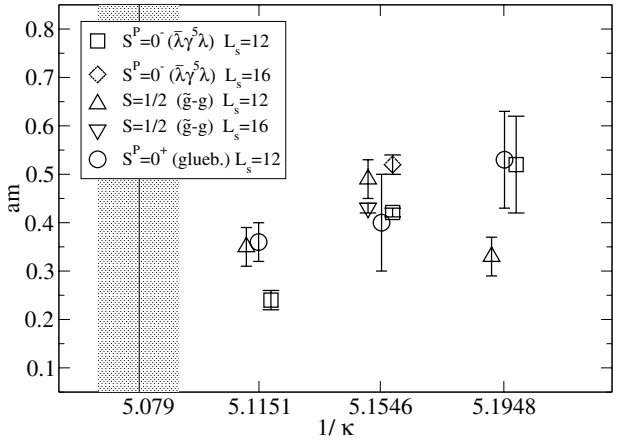

Fig. 9. Mass of lightest bound states of SYM determined in this work. The shaded region represents the presumed location of the massless gluino on the basis of the SUSY Ward identity analysis

4 Discussion

Our analysis of the low-lying spectrum of SYM shows a slow approach of the correlators to the asymptotic behavior where only the ground state dominates. This is evident in the case of the gluino-glue and mesonic correlators; in the case of the glueball correlator, the quality of the signal is not good enough to make definite statements. Excited states with masses comparable to that of the ground state are strongly coupled to these operators. In some cases a plateau of the effective mass emerged and consequently allowed us to cross-check the results of the two-mass fits. The situation can be improved by implementing optimized smearing on the operators (in the case of the gluino bilinears we use point-like operators).

The excited states which hamper the determination of the ground states are of physical interest by themselves. According to [2, 4, 5], the first excited states should be arranged in a second Wess-Zumino supermultiplet. The "higher masses" in our two-mass fits can give a first indication of the masses of these excited states: the ground state masses lie in the region 0.2–0.5 (in lattice units), while the higher masses are in the region 0.8–1. A more refined analysis of the excited states, however, could be obtained with matrix correlators. In the scalar sector, one would naturally include the gluino scalar bilinear in addition to the glueball operator. Given the large fluctuations observed on the former, the employment of variational methods would then be advisable. A similar analysis could be done in the pseudoscalar sector with the corresponding gluino bilinear and the pseudoscalar glueball operator.

A more fundamental question is whether the employed operators are optimal in the sense of maximal overlap with the low-lying bound states of SYM. Investigations could go in the direction of different operators and different quantum numbers [26].

In the following we restrict the discussion of our results to the ground states (Fig. 9). One of the goals of this study was to check finite volume effects by comparing lattices with different spatial extension. This can be done for our value of $\kappa = 0.194$ where two different lattice sizes are available, $L_s = 12$ and 16. The direct comparison shows, see Table 2, that a sizeable deviation is present for the pseudoscalar particle. Contrary to expectations, the particle comes in heavier on the larger lattice. For this lattice, however, an unexpected constant term is observed in the long-time behavior of the correlator, which could hint at some systematic effect in the stochastic determination of the disconnected correlator on large lattices. The pseudoscalar particle is the lightest particle for our lightest gluino ($\kappa = 0.1955$), though, in this case only data for the smaller lattice are available. The scalar and the spin-1/2 particle have comparable masses, compatible within errors.

Conclusions on the relevance of soft breaking terms require the control of finite lattice-spacing effects. Using analogy with QCD in absence of other indications, we argue that our mesh is relatively fine, while the gluino is still quite heavy. Next steps will be therefore to consider larger values of κ on large lattices.

Acknowledgements. We thank C. Gebert for participating in the early stages of this work, I. Montvay and G. Münster for stimulating discussions. The computations were performed on the Cray T3E and JUMP systems at NIC Jülich, the PC clusters at the ZIV of the University of Münster and the Sun Fire SMP-Cluster at the Rechenzentrum of the RWTH Aachen.

References

1. G. Veneziano, S. Yankielowicz, Phys. Lett. B **113**, 231 (1982)
2. G.R. Farrar, G. Gabadadze, M. Schwetz, Phys. Rev. D **58**, 015009 (1998)

3. L. Bergamin, P. Minkowski, hep-th/0301155
4. D.G. Cerdeno, A. Knauf, J. Louis, Eur. Phys. J. C **31**, 415 (2003)
5. P. Merlatti, F. Sannino, hep-th/0404251; A. Feo, P. Merlatti, F. Sannino, hep-th/0408214
6. I. Montvay, Int. J. Mod. Phys. A **17**, 2377 (2002)
7. G. Curci, G. Veneziano, Nucl. Phys. B **292**, 555 (1987)
8. G. Fleming, J. Kogut, P. Vranas Phys. Rev. D **64**, 034510 (2001)
9. I. Montvay, Nucl. Phys. B **466**, 259 (1996); Comput. Phys. Commun. **109**, 144 (1998)
10. I. Campos, A. Feo, R. Kirchner, S. Luckmann, I. Montvay, G. Münster, K. Spanderen, J. Westphalen, Eur. Phys. J. C **11**, 507 (1999)
11. F. Farchioni, C. Gebert, I. Montvay, L. Scorzato, Eur. Phys. J. C **26**, 237 (2002)
12. A. Donini, M. Guagnelli, P. Hernandez, A. Vladikas, Nucl. Phys. B **523**, 529 (1998)
13. F. Farchioni, A. Feo, T. Galla, C. Gebert, R. Kirchner, I. Montvay, G. Münster, A. Vladikas, Eur. Phys. J. C **23**, 719 (2002)
14. S.J. Dong, K.F. Liu, Phys. Lett. B **328**, 130 (1994)
15. F. Farchioni, G. Münster, R. Peetz, Eur. Phys. J. **C** (in press), hep-lat/0404004
16. Y. Kuramashi, M. Fukugita, H. Mino, M. Okawa, A. Ukawa, Phys. Rev. Lett. **72**, 3448 (1994)
17. R. Peetz, Ph.D. Thesis, University of Münster, 2003
18. R.G. Edwards, U.M. Heller, T.R. Klassen, Nucl. Phys. B **517**, 377 (1998)
19. J. Viehoff et al. [SESAM Collaboration], Nucl. Phys. Proc. Suppl. **63**, 269 (1998)
20. R. Kirchner, Ph.D. Thesis, University of Hamburg, 2000
21. S.R. Sharpe, N. Shoresh, Phys. Rev. D **62**, 094503 (2000)
22. M. Albanese et al., Phys. Letters B **192**, 163 (1987)
23. C.R. Allton et al. [UKQCD Collaboration], Phys. Rev. D **47**, 5128 (1993)
24. T. Struckmann et al. [TXL Collaboration], Phys. Rev. D **63**, 074503 (2001)
25. V.I. Lesk et al. [CP-PACS Collaboration], Phys. Rev. D **67**, 074503 (2003)
26. K. Johnson, Diploma Thesis, University of Münster, 2002; H. Schmalle, Diploma Thesis, University of Münster, 2004

[Nf1]

Hadron masses in QCD with one quark flavour

Eur. Phys. J. C52 305-314 (2007)

Eur. Phys. J. C 52, 305–314 (2007)
DOI 10.1140/epjc/s10052-007-0394-4

THE EUROPEAN PHYSICAL JOURNAL C

Regular Article – Theoretical Physics

Hadron masses in QCD with one quark flavour

F. Farchioni[1], I. Montvay[2,a], G. Münster[1], E.E. Scholz[3], T. Sudmann[1], J. Wuilloud[1]

[1] Universität Münster, Institut für Theoretische Physik, Wilhelm-Klemm-Strasse 9, 48149 Münster, Germany
[2] Deutsches Elektronen-Synchrotron DESY, Notkestr. 85, 22603 Hamburg, Germany
[3] Physics Department, Brookhaven National Laboratory, Upton, NY 11973, USA

Received: 9 July 2007 /
Published online: 6 September 2007 –

Abstract. One-flavour QCD – a gauge theory with SU(3) colour gauge group and a fermion in the fundamental representation – is studied by Monte Carlo simulations. The mass spectrum of the hadronic bound states is investigated in a volume with extensions of $L \simeq 4.4r_0$ ($\simeq 2.2$ fm) at two different lattice spacings: $a \simeq 0.37r_0$ ($\simeq 0.19$ fm) and $a \simeq 0.27r_0$ ($\simeq 0.13$ fm). The lattice action is a Symanzik tree-level improved Wilson action for the gauge field and an (unimproved) Wilson action for the fermion.

1 Introduction

QCD with one flavour of quarks is an interesting theoretical laboratory to study some aspects of the strong interaction dynamics, namely those not connected to spontaneous chiral symmetry breaking and to the existence of light pseudo-Goldstone bosons. As a consequence of a quantum anomaly, the U(1) axial symmetry of the classical Lagrangian is broken and in the limit of vanishing quark mass no massless Goldstone boson exists.

An intriguing possibility at negative quark masses is the spontaneous breakdown of parity and charge conjugation symmetry – a phenomenon first conjectured by Dashen [1] in the three-flavour theory. This has to do with the possible negative sign of the fermion determinant at negative quark masses, because under the assumption of the positiveness of the fermion determinant Vafa and Witten [2] proved the impossibility of this kind of spontaneous symmetry breaking.

A dramatic consequence of the absence of (broken) chiral symmetry is the difficulty to find a unique definition of the point with zero quark mass in parameter space [3–5]. (For an excellent summary and discussion of this problem see [6].)

Another line of recent theoretical developments is the relation between one-flavour ($N_f = 1$) QCD and supersymmetric Yang–Mills (SYM) theory with one supersymmetry charge ($\mathcal{N} = 1$) [7–10]. This connection is the consequence of *orientifold planar equivalence* in the limit of large number of colours ($N_c \to \infty$). This might imply approximate relations among hadron masses even at $N_c = 3$, for instance, the approximate degeneracy of scalar and pseudoscalar bound states of quarks [11] reflecting the properties of the Veneziano–Yankielovicz low-energy effective action of $\mathcal{N} = 1$ SYM [12] in the mass spectrum of $N_f = 1$ QCD. For instance, the ratio of the mass of the lowest pseudoscalar meson to the mass of the scalar meson is predicted, including $1/N_c$ corrections, to be $(N_c - 2)/N_c$ [13, 14]. Another prediction of orientifold equivalence is the size of the quark condensate in one-flavour QCD, which has recently been compared with numerical simulation results in [15].

In the present paper we start to explore the mass spectrum of hadronic states in one-flavour QCD by numerical Monte Carlo simulations. This requires reasonably large physical volumes at small quark masses and high statistics – especially for determining glueball masses and contributions of disconnected quark diagrams. We apply the Wilson lattice fermion action, which has recently been shown by several collaborations [16–20] to be well suited for such an investigation. We start our exploratory studies here on $12^3 \cdot 24$ and $16^3 \cdot 32$ lattices with lattice spacing $a \simeq 0.19$ fm and $a \simeq 0.13$ fm, respectively. This means that our present setup roughly corresponds to the earlier simulations of the qq+q Collaboration [16, 17], but we hope to continue these investigations in the near future closer to the continuum limit as in [18–20].

For setting the scale we use the Sommer parameter [21] r_0, which we set by definition to be $r_0 \equiv 0.5$ fm. In other words, whenever we speak about "1 fm" we always mean "$2r_0$" – having in mind that one-flavour QCD is a theory different from QCD realised in nature.

Since the sign of the quark determinant is a sensitive issue, we carefully determine it and take it into account in determining the expectation values. In the present paper we choose the quark mass to be sufficiently far away from zero on the positive side, where the effect of the determinant sign is not very strong. In spite of this, as we shall see, we can investigate quite small quark masses down to $m_q \simeq 12$ MeV (that is $m_q r_0 \simeq 0.03$), corresponding to a pion mass $m_\pi \simeq 270$ MeV.

[a] e-mail: montvay@mail.desy.de, istvan.montvay@desy.de

Let us mention that keeping the quarks sufficiently heavy (choosing the hopping parameter κ in the Wilson fermion action (2) below $\frac{1}{8}$) the problem of negative quark determinants can be avoided. (The thermodynamics of $N_f = 1$ QCD for heavy quarks has been investigated under this assumption in [22].) Our aim is, however, to reach small quark masses and therefore we have to deal with the possibly negative sign of the quark determinant.

For interpreting our results on the mass spectrum we find it useful to embed the $N_f = 1$ QCD theory in a *partially quenched* theory with more quark flavours. This embedding is particularly useful if the additional quenched *valence* quark flavours have the same mass as the dynamical *sea* quark because of the exact SU(N_F) flavour symmetry in the combined sea- and valence-sectors (N_F denotes here the total number of quenched and unquenched flavours). In most cases we consider the natural choice $N_F = 3$, which is closest to the situation realised in nature. We also work out some of the predictions of *partially quenched chiral perturbation theory* (PQChPT) and compare them to the numerical data.

The plan of this paper is as follows: in the next section we define the lattice action and briefly discuss the updating algorithm. In Sect. 3 the partially quenched viewpoint is introduced and PQChPT is considered for it. Section 4 is devoted to the presentation of our numerical simulation data. The last section contains a discussion and summary.

2 Lattice action and simulation algorithm

2.1 Lattice action

For the SU(3) Yang–Mills gauge field we apply, following [20], the *tree-level improved Symanzik* (tlSym) action, which is a generalisation of the Wilson plaquette gauge action. It belongs to a one-parameter family of actions obtained by renormalisation group considerations in the Symanzik improvement scheme [23]. Those actions also include, besides the usual (1×1) Wilson loop plaquette term, planar rectangular (1×2) Wilson loops:

$$S_g = \beta \sum_x \left(c_0 \sum_{\mu<\nu,\,\mu,\nu=1}^{4} \left\{ 1 - \frac{1}{3}\mathrm{Re} U^{1\times 1}_{x\mu\nu} \right\} + c_1 \sum_{\mu\neq\nu,\mu,\nu=1}^{4} \left\{ 1 - \frac{1}{3}\mathrm{Re} U^{1\times 2}_{x\mu\nu} \right\} \right) , \tag{1}$$

with the normalisation condition $c_0 = 1 - 8c_1$. For the tlSym action we have $c_1 = -1/12$ [24–26].

The fermionic part of the lattice action is the simple (unimproved) Wilson action:

$$S_f = \sum_x \left\{ \overline{\psi}^a_x \psi^a_x - \kappa \sum_{\mu=1}^{4} \left[\overline{\psi}^a_{x+\hat{\mu}}\, U_{ab,x\mu} (1+\gamma_\mu) \psi^b_x + \overline{\psi}^a_x\, U^\dagger_{ab,x\mu} (1-\gamma_\mu) \psi^b_{x+\hat{\mu}} \right] \right\} . \tag{2}$$

Here κ is the hopping parameter related to the bare quark mass in lattice units am_0 by

$$\frac{1}{2\kappa} = am_0 + 4 . \tag{3}$$

The Wilson parameter removing the fermion doublers in the continuum limit is fixed in (2)–(3) to $r = 1$.

2.2 Simulation algorithm

For preparing the sequences of gauge configurations a *Polynomial Hybrid Monte Carlo* (PHMC) updating algorithm was used, which is well suited for theories with an odd number of fermion species. This algorithm is based on multi-step (actually two-step) polynomial approximations of the inverse fermion matrix with stochastic correction in the update chain as described in [27, 28]. The starting point is the PHMC algorithm as introduced in [29–32]. The polynomial approximation scheme and the stochastic correction in the update chain are taken over from the two-step multi-boson algorithm of [33]. For details of the updating algorithm and for notation related to it see [27, 28].

In order to speed up the updating, *even–odd preconditioning* was used, which pushes the small eigenvalues of the (squared Hermitean) fermion matrix $Q[U]^2$ to larger values. The eigenvalues of $Q[U]^2$ are assumed to be covered on typical gauge configurations by the approximation interval $[\epsilon, \lambda]$. In exceptional cases some of the eigenvalues (typically just the smallest one) are outside this interval. In order to correct for this a *correction factor* $C[U]$ is associated with such configurations. The exact value of this correction factor can be written as

$$C[U] = \left\{ \prod_i \left[\lambda_i^{1/(2n_B)} P_1(\lambda_i) P_2(\lambda_i) \right] \right\}^{n_B} . \tag{4}$$

Here the product runs over the eigenvalues of $Q[U]^2$, the polynomial $P_1(x)$ is an approximation for $x^{-1/(2n_B)}$, $P_2(x)$ for $[x^{1/(2n_B)} P_1(x)]^{-1}$. The positive integer n_B defines the *determinant break-up* which means that in the path integral the fermions are represented by

$$\left[\left(\det Q[U]^2 \right)^{1/(2n_B)} \right]^{n_B} . \tag{5}$$

The part of the product in (4) where λ_i is inside the interval $[\epsilon, \lambda]$ can be effectively replaced by a stochastic estimator and then

$$C[U] = \left\{ \prod_j{}' \left[\lambda_j^{1/(2n_B)} P_1(\lambda_j) P_2(\lambda_j) \right] \times \frac{1}{N'} \sum_{n=1}^{N'} \exp\left[\eta_n^\dagger \Big(1 - P'(Q[U]^2) \Big) \eta_n \right] \right\}^{n_B} . \tag{6}$$

Here the $\prod'_j$ runs over the eigenvalues outside the interval $[\epsilon, \lambda]$, $P'(x)$ is a sufficiently good approximation

of $[x^{1/(2n_B)}P_1(x)P_2(x)]^{-1}$, N' is the arbitrary number of stochastic estimators and the η_n are Gaussian vectors in the subspace orthogonal to the eigenvectors corresponding to the eigenvalues λ_j. In practice, one can choose the polynomial $P_2(x)$ to be such a good approximation that the stochastic part in (6) has no noticeable effect on the expectation values and therefore can completely be neglected. In this case the correction factor is simply given by

$$C[U] = \left\{ \prod_j{}' \left[\lambda_j^{1/(2n_B)} P_1(\lambda_j) P_2(\lambda_j) \right] \right\}^{n_B} . \qquad (7)$$

Besides the correction factor $C[U]$, the sign $\sigma[U]$ of the fermion determinant $\det Q[U]$ has also to be included in the *reweighting* of the configurations and then the expectation value of a quantity A is given by

$$\langle A \rangle = \frac{\int \mathrm{d}[U]\sigma[U]C[U]A[U]}{\int \mathrm{d}[U]\sigma[U]C[U]} . \qquad (8)$$

This formula shows the dangerous *sign problem*, which can arise due to the fluctuation of the determinant sign because in case of strong fluctuations of $\sigma[U]$ both nominator and denominator on the right hand side may become small, spoiling the statistical accuracy. (Similarly, one can also lose statistics if the correction factors $C[U]$ are much smaller than 1 on many configurations.)

Typical values of the approximation interval and of the polynomial orders at the lightest quark mass simulated on $12^3 \cdot 24$ and $16^3 \cdot 32$ lattices, respectively, are collected in Table 1. As in [27, 28], the orders of the polynomials P_j, $(j = 1, 2)$ are denoted by n_j and those of $\bar{P}_j$, $(j = 1, 2)$ by $\bar{n}_j$, respectively. The simulations have been done with determinant break-up $n_B = 2$. (The polynomials $\bar{P}_j$ are approximating $(P_j)^{-\frac{1}{2}}$. For more details see [27, 28] and references therein.)

The last four columns of Table 1 show the values of the *deviation norm* δ, which is minimised for a given polynomial order n in the *least-square approximation* scheme we are using. Generically δ is defined as

$$\delta \equiv \left\{ \frac{\int_\epsilon^\lambda \mathrm{d}x w(x) \Big[f(x) - P_n(x) \Big]^2}{\int_\epsilon^\lambda \mathrm{d}x w(x) f(x)^2} \right\}^{\frac{1}{2}} . \qquad (9)$$

Here $f(x)$ is the function to be approximated and $w(x)$ is a positive weight function actually chosen in our case to be $w_1(x) = w_2(x) = x^{1/(2n_B)}$ and $\bar{w}_1(x) = \bar{w}_2(x) = 1$, respectively. The values of δ_1 in Table 1 are such that the average acceptance rate of the stochastic correction at the end of trajectory sequences is between 80%–90%. The other δ values are small enough to ensure practically infinite precision of the expectation values. For more details on the algorithmic setup in our runs see also Sect. 4.

3 Partially quenched viewpoint

Because the classical $\mathrm{U(1)_A}$ axial symmetry is anomalous, the single-flavour QCD theory does not have a continuous chiral symmetry apart from the U(1) quark number symmetry. Consequently it does not have spontaneous chiral symmetry breaking and hence no (pseudo-) Goldstone bosons and no easy definition of the quark mass [3–5]. In the lattice regularisation it is, however, possible to enhance the symmetry artificially by adding extra *valence quarks*, which are *quenched*, that is, are not taken into account in the Boltzmann weight of the gauge configurations by their fermion determinants. In principle, one might consider any number of quenched valence quarks with any mass values but, to remain close to QCD realised in nature, the most natural choice is to take two equal-mass valence quarks and to call them u and d quarks. The original dynamical quark can then be called s quark where "s" may stand for *sea* or *strange*. The theory with dynamical s quark and quenched u and d quarks is *partially quenched*. (Observe that this partially quenching is somewhat unconventional, since some of the valence quarks are quenched but taken degenerate with the sea quark.)

Using this terminology, for instance, the pseudoscalar bound state of s and $\bar{s}$ can be called η_s. The corresponding scalar state is then σ_s. The lowest baryon state consisting of s quarks, which has to have spin $\frac{3}{2}$ because of the Pauli principle, can be named Ω^- or e.g. Δ_s etc.

A theoretical description of partially quenched QCD can be obtained through the introduction of ghost quarks [36]. For each (quenched) valence quark a corresponding bosonic ghost quark is added to the model. The functional integral over the ghost quark fields then cancels the fermion determinant of the valence quarks and only the sea quark determinant remains in the measure. In our case there are 2 flavours of valence quarks and ghost quarks, each, with equal masses m_{V}, and a single flavour of sea quarks with mass m_{S}.

A particularly interesting point of the partially quenched theory is the one where all the three quark masses are equal. In this point there is an exact SU(3) vector-like flavour symmetry in the valence plus sea quark sector, and the hadronic bound states appear in exactly degenerate

Table 1. Algorithmic parameters in the runs with lightest quark mass on $12^3 \cdot 24$ (first line) and $16^3 \cdot 32$ (second line) lattice, respectively. For notation see the text and also [27, 28]

ϵ	λ	n_1	$\bar{n}_1$	n_2	$\bar{n}_2$	δ_1	$\bar{\delta}_1$	δ_2	$\bar{\delta}_2$
3.25×10^{-6}	2.6	350	550	1400	1600	4.9×10^{-4}	6.7×10^{-7}	9.9×10^{-7}	8.8×10^{-7}
1.20×10^{-5}	2.4	250	370	1000	1150	5.4×10^{-4}	8.2×10^{-7}	4.8×10^{-7}	3.1×10^{-7}

SU(3)-symmetric multiplets. For instance, there is a degenerate octet of pseudoscalar mesons – the "pions" (π^a, $a = 1, \ldots, 8$) satisfying an SU(3)-symmetric PCAC relation. With the help of the divergence of the axialvector current $A^a_{x\mu}$ and pseudoscalar density P^a_x one can define, as usual, the bare *PCAC quark mass* $am_{\rm PCAC}$ in lattice units:

$$am_{\rm PCAC} \equiv \frac{\langle \partial^*_\mu A^+_{x\mu} P^-_y \rangle}{2\langle P^+_x P^-_y \rangle} \,. \tag{10}$$

Here the indices + and − refer to the "charged" components corresponding to $\lambda_a \pm \mathrm{i}\lambda_b$ (with $\lambda_{a,b}$ some off-diagonal Gell-Mann matrices) and ∂^*_μ denotes the backward lattice derivative. Due to the exact SU(3) symmetry, the renormalised quark mass corresponding to $m_{\rm PCAC}$ can be defined by an SU(3)-symmetric multiplicative renormalisation:

$$m^{\rm R}_{\rm PCAC} = \frac{Z_{\rm A}}{Z_{\rm P}} m_{\rm PCAC} \,. \tag{11}$$

By tuning the bare quark mass on the lattice suitably, the masses of the "pions" can be made to vanish, as the numerical results indicate, and the renormalised quark mass vanishes, too. At this point the partially quenched theory has a graded $\mathrm{SU}(N_F|N_{\rm V})_{\rm L} \otimes \mathrm{SU}(N_F|N_{\rm V})_{\rm R}$ symmetry, which is broken spontaneously to a "flavour" $\mathrm{SU}(N_F|N_{\rm V})$. (Here $N_{\rm V}$ is the number of additional valence quark flavours and $N_F \equiv N_{\rm V} + N_f = N_{\rm V} + 1$.) In our case, with $N_{\rm V} = 2$ flavours of valence quarks, the symmetry is thus SU(3|2). The "pions" are the Goldstone bosons of the broken SU(3) subgroup.

Adding generic quark masses $m_{\rm V}$ and $m_{\rm S}$, the symmetry group is explicitly broken down to SU(2|2). In the special case $m_{\rm V} = m_{\rm S}$, considered here, the symmetry is still SU(3|2), and its subgroup SU(3) is the flavour symmetry mentioned above.

The "pions" are, of course, not physical particles in the spectrum of $N_f = 1$ QCD. Nevertheless, their properties such as masses and decay constants are well defined quantities, which can be computed on the lattice. The same is true of the PCAC quark mass $m^{\rm R}_{\rm PCAC}$, which is therefore a potential candidate for a definition of a quark mass of this theory.

The relation between the pion masses and the quark masses can be considered in partially quenched chiral perturbation theory [37–39], including effects of the lattice spacing a [40–44]. The pseudo-Goldstone fields are parameterized by a graded matrix,

$$U(x) = \exp\left(\frac{\mathrm{i}}{F_0}\Phi(x)\right) \tag{12}$$

in the supergroup SU(3|2). (Here the normalization of F_0 is such that its phenomenological value is $\simeq 86$ MeV.) The commuting elements of the graded matrix Φ represent the pseudo-Goldstone bosons made from a quark and an antiquark with equal statistics, and the anticommuting elements of Φ represent pseudo-Goldstone fermions that are built from one fermionic quark and one bosonic quark. The supertrace of Φ has to vanish, which can be implemented by a suitable choice of generators [45].

We have calculated the masses of the pseudo-Goldstone bosons in next-to-leading order of partially quenched chiral perturbation theory along the lines of [45], including $O(a)$ lattice effects [42]. The quark masses enter the expressions in the combinations

$$\chi_{\rm V} = 2B_0 m_{\rm V}, \quad \chi_{\rm S} = 2B_0 m_{\rm S} \,, \tag{13}$$

with the usual low-energy constant B_0, and the lattice spacing occurs as

$$\rho = 2W_0 a \,, \tag{14}$$

where W_0 is another, lattice-specific, low-energy constant. For the pion masses we obtain

$$\begin{aligned} m^2_{\rm VV} \equiv m^2_\pi = {} & \chi_{\rm V} + \rho + \frac{\chi_{\rm V}+\rho}{16\pi^2 F_0^2}\Big[\chi_{\rm V} - \chi_{\rm S} \\ & + (2\chi_{\rm V} - \chi_{\rm S} + \rho)\ln\left(\frac{\chi_{\rm V}+\rho}{16\pi^2 F_0^2}\right)\Big] \\ & + \frac{8}{F_0^2}\left[(2L_8 - L_5)\chi_{\rm V}^2 + (2L_6 - L_4)\chi_{\rm V}\chi_{\rm S}\right. \\ & + (2W_8 + W_6 - W_5 - W_4 - L_5)\rho\chi_{\rm V} \\ & \left. + (W_6 - L_4)\rho\chi_{\rm S}\right] , \end{aligned} \tag{15}$$

where the usual low-energy parameters L_i appear, together with additional ones (W_i) describing lattice artifacts.

The mixed mesons, whose masses $m_{\rm VS}$ we have also calculated, become degenerate with the pions in the special case $m_{\rm V} = m_{\rm S}$. In this case the expression reduces to

$$\begin{aligned} m^2_\pi = {} & \chi + \rho + \frac{(\chi+\rho)^2}{16\pi^2 F_0^2}\ln\left(\frac{\chi+\rho}{16\pi^2 F_0^2}\right) \\ & + \frac{8}{F_0^2}\Big[(2L_8 - L_5 + 2L_6 - L_4)\chi^2 \\ & + (2W_8 + 2W_6 - W_5 - W_4 - L_5 - L_4)\chi\rho\Big] . \end{aligned} \tag{16}$$

To leading order the PCAC quark mass obeys $2B_0 m^{\rm R}_{\rm PCAC} = \chi + \rho$, and we recognize the Gell-Mann–Oakes–Renner relation

$$m^2_\pi = 2B_0 m^{\rm R}_{\rm PCAC} + \mathrm{NLO} \,. \tag{17}$$

Including terms in next-to-leading (NLO) order, we can express m^2_π in terms of $m^{\rm R}_{\rm PCAC}$ as

$$\begin{aligned} m^2_\pi = {} & \chi_{\rm PCAC} + \frac{\chi^2_{\rm PCAC}}{16\pi^2 F_0^2}\ln\frac{\chi_{\rm PCAC}}{\Lambda^2} \\ & + \frac{8}{F_0^2}\left[(2L_8 - L_5 + 2L_6 - L_4)\chi^2_{\rm PCAC}\right. \\ & + (W_8 + W_6 - W_5 - W_4 \\ & \left. - 2L_8 + L_5 - 2L_6 + L_4)\chi_{\rm PCAC}\rho\right] , \end{aligned} \tag{18}$$

where we define

$$\chi_{\rm PCAC} = 2B_0 m^{\rm R}_{\rm PCAC} \,. \tag{19}$$

As a remark, in the case $m_{\rm V} = m_{\rm S}$ the masses can alternatively be obtained from the partially quenched theory

with symmetry SU(2|1) by considering mixed pions made from a valence quark and a degenerate sea quark. Indeed, calculating the masses in this model reproduces (16).

The η_s can be included in the analysis by relaxing the constraint of a vanishing supertrace [37, 45], and associating it with the field

$$\Phi_0(x) = \mathrm{sTr}\Phi(x). \tag{20}$$

The effective Lagrangian then contains additional terms depending on Φ_0:

$$\Delta\mathcal{L} = \alpha\partial_\mu\Phi_0\partial_\mu\Phi_0 + m_\Phi^2\Phi_0^2 + \mathcal{O}\left(\Phi_0^3\right) , \tag{21}$$

where α and m_Φ are free parameters in this context. We content ourselves with displaying only the leading-order expression for the mass of the η_s, which reads

$$m_{\eta_s}^2 = \frac{m_\Phi^2 + \chi_{\mathrm{PCAC}}}{1+\alpha}. \tag{22}$$

Our numerical results for m_{η_s} allow us to determine α and m_Φ.

4 Numerical simulations

After some preparatory search in the parameter space we concentrated our runs on the $12^3 \cdot 24$ lattice to $\beta = 3.8$ and those on $16^3 \cdot 32$ to $\beta = 4.0$. The parameter values, the number of analysed configurations, the average plaquette, its integrated autocorrelation and the value of the Sommer scale parameter in lattice units r_0/a are summarised in Table 2. As one can see, taking the values of r_0/a at the highest κ (smallest quark masses), the extensions of the 12^3 and 16^3 lattices are $L = 4.46\, r_0 = 2.23$ fm and $L = 4.29\, r_0 = 2.14$ fm, respectively. Since we fix $r_0 = 0.5$ fm by definition, these correspond to lattice spacings $a = 0.186$ fm and $a = 0.134$ fm, respectively.

In the update chain by the PHMC algorithm with stochastic correction [27, 28] a *sequence of PHMC trajectories* is followed by a Metropolis accept–reject step with a higher precision polynomial. The total length of the trajectory sequence in the runs in Table 2 was between 1.5 and 1.8. The sequences consisted out of 3–6 individual trajectories. The precision of the first step of polynomial approximations was tuned such that the acceptance of the PHMC trajectories was about 0.80–0.85. The total length of the trajectory sequence was chosen such that the acceptance of the Metropolis test was again 0.80–0.85. This ensured a relatively high total acceptance of 0.64–0.72. During the runs we tried to optimise the parameters of PHMC. The different values of the *integrated autocorrelation times* for the average plaquette in Table 2 are, in fact, mainly due to increasingly better optimisations and not so much to the dependence on the run parameters.

Table 2. Summary of the runs: $12^3 \cdot 24$ and $16^3 \cdot 32$ lattices have lowercase and uppercase labels, respectively. The number of gauge configurations, which were saved after every trajectory sequence, is N_{conf}. The average plaquette value, its autocorrelation in number of trajectory sequences τ_{plaq} and the value of r_0/a are also given

label	β	κ	N_{conf}	plaquette	τ_{plaq}	r_0/a
a	3.80	0.1700	5424	0.546041(66)	12.5	2.66(4)
b	3.80	0.1705	3403	0.546881(46)	4.6	2.67(5)
c	3.80	0.1710	2884	0.547840(67)	7.6	2.69(5)
A	4.00	0.1600	1201	0.581427(36)	4.3	3.56(5)
B	4.00	0.1610	1035	0.582273(36)	4.1	3.61(5)
C	4.00	0.1615	1005	0.582781(32)	3.3	3.73(5)

The second step approximations were more than good enough to ensure that the expectation values were completely unaffected by the remaining small imprecision. (See, for instance, the small relative deviations in Table 1.) This has also been explicitly checked by performing a final stochastic correction on a large sample of configurations with polynomials P' of order 2500 in the stochastic part of the right hand side of (6).

For the calculation of the expectation values the reweighting procedure according to (8) has to be carried out. For this, besides the correction factor $C[U]$ from (7), also the sign of the fermion determinant $\sigma[U]$ is needed. This we calculated by the *spectral flow* method [34]. For the κ-dependent computation of the low-lying eigenvalues of the hermitean fermion matrix $Q[U]$ we followed [35].

It turned out that the effect of the correction factors $\sigma[U]C[U]$ is in most cases negligible. For instance, in run b of Table 2 the average value of $\sigma[U]C[U]$ in the denominator is 0.9982. In run c it is 0.9842. In run b there are 34 configurations out of 3403, where some eigenvalue is outside the approximation interval $[\epsilon, \lambda]$ and out of them there is a single one with negative fermion determinant. In run c there are 167 from 2884 outside $[\epsilon, \lambda]$ and out of them there are 26 with negative correction factor due to $\sigma = -1$.

Since the sign of the fermion determinant was not determined on every configuration, the question arises whether perhaps some negative signs were missed. This is very improbable, because we determined the sign also on the neighbouring configurations in addition to those with small eigenvalues and out of the remaining configurations we have chosen 100 randomly for sign determination. None of these additional configurations turned out to have a negative determinant.

In the average plaquette and r_0/a the effect of the correction factors is completely negligible. For instance, in runs b and c the correction has an effect in the average value of r_0/a only in the fifth digit – whereas the statistical error is in the third digit. In all other runs besides b and c every eigenvalue is inside the approximation interval $[\epsilon, \lambda]$ and therefore, according to (7), the correction factor is equal to 1 on every configuration.

4.1 Results for hadron masses

Starting with the mesonic states, we consider the simplest interpolating operators in the pseudoscalar and scalar

sectors:

$$0^+: \quad P(x) = \bar{\psi}(x)\gamma_5\psi(x)\,, \tag{23}$$

$$0^-: \quad S(x) = \bar{\psi}(x)\psi(x)\,. \tag{24}$$

We denote by η_s and σ_s the corresponding hadron states at the lowest end of the energy spectrum (the usual notation J^P is used for the respective quantum numbers). The corresponding states in the QCD spectrum with the same quantum numbers are $\eta'(958)$ and $f_0(600)$ (or σ). (Note, however, that the states in QCD are linear combinations of $\bar{u}u$, $\bar{d}d$ and $\bar{s}s$ components – in contrast to the states in $N_f = 1$ QCD which are built out of a single quark flavour.)

In the case of the pseudoscalar mesons, invariance under the flavour group plays a special role when comparing with QCD states because of the U(1) axial anomaly. (This is not the case for baryons; see the following.)

Analogously to flavour singlet mesons in QCD, the correlators of the above interpolating operators contain disconnected diagrams. These were computed by applying stochastic estimator techniques (SET), and in particular the variant of [46] with Z_2 noise and spin dilution. The method was already applied to the case of SYM [47] (as mentioned in the introduction, SYM shares many similarities with $N_f = 1$ QCD). In order to optimise the computational load, taking also autocorrelations into account, every fifth configuration was typically analysed, with 20 stochastic estimates each.

Spin 0 states can also be build by purely gluonic operators. These are well known objects of investigation in lattice QCD were they should describe the glueballs. Due to the expected signal–noise ratio of their purely gluonic correlation they belong to the most notorious particles to measure. In particular the 0^{++} glueball has the same quantum numbers as the σ_s meson. As a consequence, these two states can also mix with each other but in this first investigation we neglect the mixing and consider only diagonal correlators for both states.

We used the single spatial plaquette to obtain the mass of the 0^{++} ground state. To increase the overlap of the operator with this state we used APE smearing and also performed variational methods to obtain optimal glueball operators from linear combinations of the basic operators.

We now come to the baryon sector. The simplest baryonic interpolating field which can be built out of one quark flavour is

$$\Delta_i(x) = \epsilon_{abc}\left[\psi_a(x)^{\mathrm{T}} C\gamma_i\psi_b(x)\right]\psi_c(x)\,. \tag{25}$$

The above operator also contains a spin 1/2 component, implying that the spin 3/2 component, on which we focus, must be projected out from the spinorial correlator,

$$G_{ji}(t) = \sum_{\mathbf{x}} \left\langle \Delta_j(\mathbf{x},t)\bar{\Delta}_i(0)\right\rangle\,. \tag{26}$$

We follow [48] and consider the spin-projected correlator

$$G_{3/2}(t) = \frac{1}{6}\mathrm{Tr}\left[G_{ji}(t)\gamma_j\gamma_i + G_{ii}(t)\right]\,. \tag{27}$$

The low-lying hadron state contributing to the above correlator is expected to have positive parity ($\frac{3}{2}^+$). This corresponds to the $\Delta(1232)^{++}$ of QCD if our dynamical fermion is interpreted as an u quark. If the dynamical fermion is taken to be the s quark then this would be the Ω^- baryon. (However, spin and parity of the corresponding particle have not yet been measured, so the identification of this state with the Ω^- baryon is still uncertain [49].) In correspondence to η_s and σ_s, in what follows we call this state Δ_s. (Here one can interpret the index s as referring to the "sea" quark.)

It should be noted at this point that the above QCD states are not flavour singlets in $N_f = 3$ QCD (and in the one flavour partially quenched theory). We recall here that interpolating fields corresponding to flavour singlet baryon states cannot be build in QCD if only quark fields are considered as ingredients.

The results of the hadron masses are reported in Table 3 and, as a function of the bare PCAC quark mass m_{PCAC}, in Fig. 1. In the figure the masses are multiplied by the Sommer scale parameter r_0; therefore, one can put the results for both lattice spacings in a single plot and check their scaling. (The expected small change of the multiplica-

Table 3. Results for light hadron masses in $N_f = 1$ QCD

run	am_{η_s}	am_{σ_s}	$am_{0^{++}}$	am_{Δ_s}
a	0.462(13)	0.660(39)	0.777(11)	1.215(20)
b	0.403(11)	0.629(29)	0.685(10)	1.116(38)
c	0.398(28)	0.584(55)	0.842(16)	1.204(57)
A	0.455(17)	0.607(57)	1.083(79)	1.006(15)
B	0.380(18)	0.554(52)	1.032(66)	0.960(15)
C	0.316(22)	0.613(67)	0.980(97)	0.876(26)

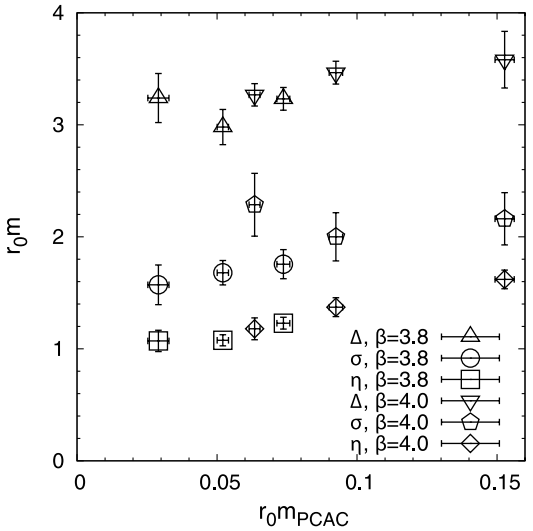

Fig. 1. The mass of the lightest physical particles in one-flavour QCD as a function of the PCAC quark mass. The masses are multiplied by the scale parameter r_0 in order to obtain dimensionless quantities

tive renormalisation factor of $m_{\rm PCAC}$ between $\beta = 3.8$ and $\beta = 4.0$ is neglected here.)

Only in the case of run c the measurement correction has a sizeable effect on the mass estimates. In this case configurations with negative determinant where singled out: the sign of the determinant has the effect of pushing the masses up by 7%–10%.

The errors on the glueball mass are rather large – especially on the $16^3 \cdot 32$ lattice at $\beta = 4.0$ – therefore, they are not shown in the figure. Obviously, our statistics is not sufficient for this purpose. In general a larger number of configurations would improve the determinations in the glueball sector. Since the computational load is in this case negligible, for future runs we plan a more frequent storage of the gauge configuration.

4.1.1 Valence analysis

The connected contribution to the meson correlators can be interpreted as a non-singlet meson made up of valence quarks in the partially quenched picture; see Sect. 3. The pseudoscalar channel corresponds in particular to the "valence" pion. Since the computation of the connected diagrams is less demanding, we could afford the analysis of the complete set of configurations.

In the baryon sector, one can define a "valence" nucleon, with the usual projector operator

$$N(x) = \epsilon_{abc}[\psi_a(x)^{\rm T} C \psi'_b(x)]\psi_c(x)\,, \tag{28}$$

where ψ' can be interpreted as the field of the valence quark.

The results concerning valence hadron masses are reported in Table 4 and Fig. 2. In addition, the bare PCAC quark mass according to the definition in (10) and the bare pion decay constant in lattice units af_π are also included. f_π and its renormalised counterpart $f_\pi^{\rm R}$ are defined as

$$\begin{aligned} af_\pi &= (am_\pi)^{-1}\langle 0|A^+_{x=0,\mu=0}|\pi^-(\mathbf{p}=0)\rangle\,, \\ f_\pi^{\rm R} &= Z_{\rm A} f_\pi\,, \end{aligned} \tag{29}$$

where $A^+_{x\mu}$ is the axialvector current as in (10) and $\pi^-(\mathbf{p}=0)$ is a pion state with zero momentum. (The normalisation of f_π is such that in nature we have $f_\pi^{\rm R} \simeq 130\,{\rm MeV}$.) The value of af_π on the lattice is obtained by the method described in [50]. In Fig. 2 the masses are multiplied by the scale parameter r_0 in order to obtain dimensionless variables.

Table 4. The PCAC quark mass $m_{\rm PCAC}$, the pion mass m_π and decay constant f_π, and the nucleon mass m_N in lattice units

run	$am_{\rm PCAC}$	am_π	af_π	$am_{\rm N}$
a	0.02771(45)	0.3908(24)	0.1838(11)	1.0439(54)
b	0.01951(39)	0.3292(25)	0.1730(15)	0.956(27)
c	0.0108(12)	0.253(10)	0.156(10)	1.011(51)
A	0.04290(36)	0.4132(21)	0.1449(9)	0.9018(44)
B	0.02561(31)	0.3199(22)	0.1289(10)	0.7978(53)
C	0.01700(30)	0.2635(24)	0.1188(12)	0.734(10)

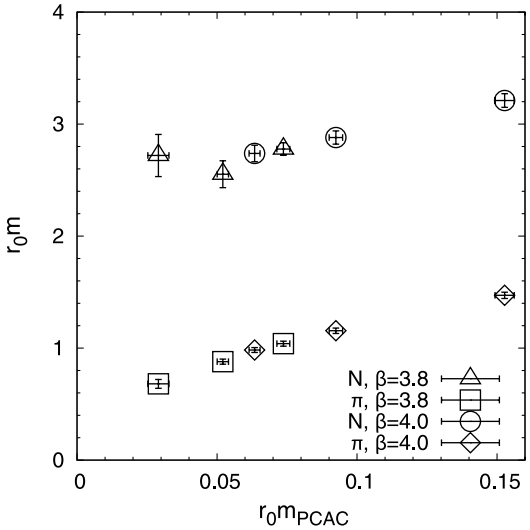

Fig. 2. The mass of the valence pion and nucleon as a function of the bare PCAC quark mass

4.1.2 Chiral perturbation theory fits

The properties of the valence pion (pion mass m_π and decay constant $f_\pi^{\rm R}$) can be analysed in partially quenched ChPT. We fit $a^2m_\pi^2$ and af_π simultaneously as a function of $am_{\rm PCAC}$ including the data at both values of β. There are not enough data to account for the lattice artifacts. Therefore the fit is done with the continuum formulae

$$\begin{aligned} m_\pi^2 &= \chi_{\rm PCAC} + \frac{\chi^2_{\rm PCAC}}{16\pi^2 F_0^2}\ln\frac{\chi_{\rm PCAC}}{\Lambda_3^2}\,, \\ \frac{f_\pi^{\rm R}}{F_0\sqrt{2}} &= 1 - \frac{\chi_{\rm PCAC}}{32\pi^2 F_0^2}\ln\frac{\chi_{\rm PCAC}}{\Lambda_4^2}\,, \end{aligned} \tag{30}$$

with the low-energy constants

$$\begin{aligned} \Lambda_3 &= 4\pi F_0 \exp\{64\pi^2(L_4+L_5-2L_6-2L_8)\}\,, \\ \Lambda_4 &= 4\pi F_0 \exp\{64\pi^2(L_4+L_5)\}\,. \end{aligned} \tag{31}$$

The changes of the renormalisation constants $Z_{\rm A}$ and $Z_{\rm P}$ between the two β values are neglected. The results are displayed in Figs. 3 and 4.

Owing to the fact that the number of degrees of freedom in the fit is small, the uncertainty of the fit parameters is relatively large. The determination of the universal low-energy scales Λ_3/F_0 and Λ_4/F_0 can be improved by considering the ratios [16, 17, 55]

$$\frac{m_\pi^2}{m_{\pi,{\rm ref}}^2}\,, \quad \frac{f_\pi}{f_{\pi,{\rm ref}}}\,, \tag{32}$$

in which some of the coefficients cancel. We consider the data on the larger lattice at $\beta = 4.0$ and take the quantities

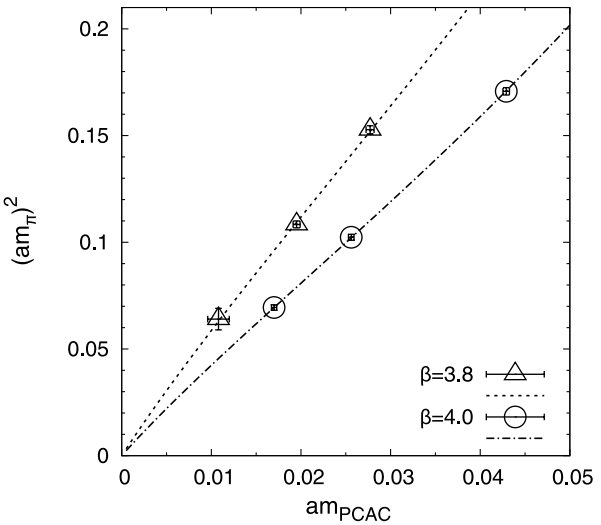

Fig. 3. Pion masses squared in lattice units and the results of the PQChPT fit

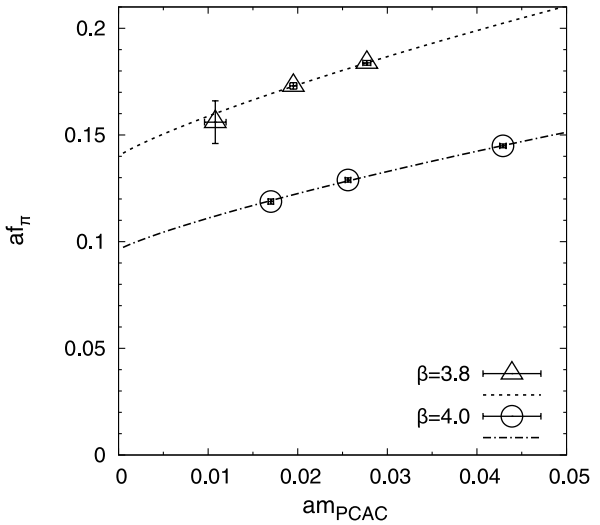

Fig. 4. Pion decay constants in lattice units and the results of the PQChPT fit

at $\kappa = 0.1615$ as reference. The fit yields

$$\frac{\Lambda_3}{F_0} = 10.0 \pm 2.6\,, \tag{33}$$

$$\frac{\Lambda_4}{F_0} = 31.5 \pm 14.3\,, \tag{34}$$

which is compatible with the phenomenological values from ordinary QCD [51, 52].

In order to estimate the parameters α and m_Φ, related to the mass of the η_s (see Sect. 3), we made a fit of m_π^2 and $m_{\eta_s}^2$ at $\beta = 4.0$ in leading-order ChPT. The result is

$$\alpha = -0.03(19)\,, \quad am_\Phi = 0.18(8)\,, \tag{35}$$

indicating the vanishing of α. Fixing $\alpha = 0$ in the fit yields

$$am_\Phi = 0.19(2) \quad \text{or} \quad r_0 m_\Phi = 0.72(10)\,, \tag{36}$$

where the value of r_0/a extrapolated to vanishing PCAC quark mass is used.

This constant, whose value in physical units is $m_\Phi = 284(40)$MeV, can be related to the quenched topological susceptibility $\chi_{\rm t}$ through the Witten–Veneziano formula [53, 54]

$$m_\Phi^2 = \frac{4N_f}{(f_\pi^{\rm R})^2}\chi_{\rm t}\,, \tag{37}$$

which is valid in leading order of the $1/N_c$ expansion. With $\chi_{\rm t} = (193 \pm 9\ {\rm MeV})^4$ [56] and our value for f_π^R we would obtain $m_\Phi = 426$ MeV.

5 Discussion

This first Monte Carlo investigation of the hadron masses in QCD with $N_f = 1$ dynamical quark flavour reveals the qualitative features of the low-lying particle spectrum in this theory. The spatial extensions of our $12^3 \cdot 24$ and $16^3 \cdot 32$ lattices are about $L \simeq 2.2$ fm (see Table 2).[1] This implies lattice spacings $a \simeq 0.19$ fm and $a \simeq 0.13$ fm, respectively. The (bare) quark masses are reasonably small – in a range 10–30 MeV and 25–60 MeV on the $12^3 \cdot 24$ and $16^3 \cdot 32$ lattice, respectively. The updating algorithm we use (PHMC with stochastic correction [27, 28]) works fine in this range, making the extension of the Monte Carlo investigations towards larger volumes, smaller quark masses and smaller lattice spacings straightforward. In the present runs the fluctuation of the eigenvalues of the fermion matrix towards exceptionally small (or negative) values can be easily handled by reweighting the configurations during the evaluation of the expectation values. In fact, except for the run with the smallest quark mass on the $12^3 \cdot 24$ lattice where the reweighting has a small effect, the reweighting is completely negligible or even unnecessary.

The lightest hadron is the pseudoscalar meson bound state of a quark and an antiquark – the η_s meson (see Table 3 and Fig. 1). The corresponding scalar bound state – the σ_s meson – is in our points by about a factor 1.5 heavier. Compared to the estimate in [13, 14] $m_{\sigma_s}/m_{\eta_s} \simeq N_c/(N_c - 2) = 3$ this result is too low, but the situation could be better in the zero quark mass limit that the prediction of [13, 14] applies to. The lightest baryon – the Δ_s baryon – is by a factor of about 3 heavier than the η_s meson. The lightest glueball lies between the σ_s meson and the Δ_s baryon, but its mass could not be properly measured on the $16^3 \cdot 32$ lattice with our statistics. In general, the mass measurements have relatively large errors – between 3%–10% – and no infinite volume and continuum limit extrapolations could be performed with our present data. We hope to return to these questions and to give more precise results in future publications.

An interesting aspect of $N_f = 1$ QCD is the possibility of a *partially quenched* extension with valence quarks. In

[1] In order to have some relation to the scales in real QCD, we set the Sommer scale parameter by definition to be $r_0 \equiv 0.5$ fm.

particular, adding two valence quarks, the model has similarities to QCD in nature with its three light (u, d and s) quark flavours. A theoretically interesting special case is if all three quarks, the dynamical one and the two valence ones, have exactly equal masses. In this case there is an exact SU(3) flavour symmetry. This can be exploited for the introduction of a quark mass by defining it as the PCAC quark mass in the partially quenched theory. In this extended model there exist the usual light hadron states well known from real QCD: the pseudoscalar pseudo-Goldstone bosons (pions etc.), the nucleon etc. The results for the masses of the lightest states and the decay constant of the pseudoscalar bosons are collected in Table 4 and also shown in Fig. 2.

Since the physical volumes of the 12^3 and 16^3 lattices are to a good approximation equal, the comparison of the results at the two different lattice spacings gives a hint for the magnitude of the deviations from the continuum limit. As one can see in Figs. 1 and 2, the scaling between $\beta = 3.8$ and $\beta = 4.0$ is reasonably good – especially for the lightest states η_s and π. However, for reliable continuum limit estimates more data at several lattice spacings are required.

In the pseudoscalar sector of the partially quenched model one can apply partially quenched chiral perturbation theory for fitting the mass and the decay constant. As Figs. 3 and 4 show, the NLO formulae give good fits but the number of degrees of freedom in the fits is small, and therefore the uncertainty of the fit parameters is relatively large.

Acknowledgements. We are grateful to Luigi Scorzato for valuable discussions and for helping us in the set-up of the programs for investigating the eigenvalue spectrum of the fermion matrix. We thank the computer centers at DESY Hamburg and NIC at Forschungszentrum Jülich for providing us the necessary technical help and computer resources. This work is supported in part by the Deutsche Forschungsgemeinschaft under grant Mu757/13-1. E.S. is supported by the U.S. Dept. of Energy under contract DE-AC02-98CH10886.

References

1. R.F. Dashen, Phys. Rev. D **3**, 1879 (1971)
2. C. Vafa, E. Witten, Nucl. Phys. B **234**, 173 (1984)
3. M. Creutz, Rev. Mod. Phys. **73**, 119 (2001) [hep-lat/0007032]
4. M. Creutz, hep-lat/0511052
5. M. Creutz, Phys. Rev. Lett. **92**, 201601 (2004) [hep-lat/0312018]
6. M. Creutz, Ann. Phys. **322**, 1518 (2007) [hep-th/0609187]
7. A. Armoni, M. Shifman, G. Veneziano, Nucl. Phys. B **667**, 170 (2003) [hep-th/0302163]
8. A. Armoni, M. Shifman, G. Veneziano, Phys. Rev. Lett. **91**, 191601 (2003) [hep-th/0307097]
9. A. Armoni, M. Shifman, G. Veneziano, Phys. Lett. B **579**, 384 (2004) [hep-th/0309013]
10. A. Armoni, M. Shifman, G. Veneziano, hep-th/0403071
11. P. Keith-Hynes, H.B. Thacker, Phys. Rev. D **75**, 085001 (2007) [hep-th/0701136]
12. G. Veneziano, S. Yankielowicz, Phys. Lett. B **113**, 231 (1982)
13. F. Sannino, M. Shifman, Phys. Rev. D **69**, 125004 (2004) [hep-th/0309252]
14. A. Armoni, E. Imeroni, Phys. Lett. B **631**, 192 (2005) [hep-th/0508107]
15. T. DeGrand, R. Hoffmann, S. Schaefer, Z. Liu, Phys. Rev. D **74**, 054501 (2006) [hep-th/0605147]
16. qq+q Collaboration, F. Farchioni, I. Montvay, E. Scholz, L. Scorzato, Eur. Phys. J. C **31**, 227 (2003) [hep-lat/0307002]
17. qq+q Collaboration, F. Farchioni, I. Montvay, E. Scholz, Eur. Phys. J. C **37**, 197 (2004) [hep-lat/0403014]
18. L. Del Debbio, L. Giusti, M. Lüscher, R. Petronzio, N. Tantalo, JHEP **0602**, 011 (2006) [hep-lat/0512021]
19. M. Göckeler et al., PoS **LAT2006**, 179 (2006) [hep-lat/0610066]
20. ETM Collaboration, P. Boucaud et al., Phys. Lett. B **650**, 304 (2007) [hep-lat/0701012]
21. R. Sommer, Nucl. Phys. B **411**, 839 (1994) [hep-lat/9310022]
22. C. Alexandrou, A. Borici, A. Feo, P. de Forcrand, A. Galli, F. Jegerlehner, T. Takaishi, Phys. Rev. D **60**, 034504 (1999) [hep-lat/9811028]
23. K. Symanzik, Nucl. Phys. B **226**, 187 (1983)
24. P. Weisz, Nucl. Phys. B **212**, 1 (1983)
25. P. Weisz, R. Wohlert, Nucl. Phys. B **236**, 397 (1984)
26. P. Weisz, R. Wohlert, Nucl. Phys. B **247**, 544 (1984)
27. I. Montvay, E. Scholz, Phys. Lett. B **623**, 73 (2005) [hep-lat/0506006]
28. E.E. Scholz, I. Montvay, PoS **LAT2006**, 037 (2006) [hep-lat/0609042]
29. R. Frezzotti, K. Jansen, Phys. Lett. B **402**, 328 (1997) [hep-lat/9702016]
30. R. Frezzotti, K. Jansen, Nucl. Phys. B **555**, 395 (1999) [hep-lat/9808011]
31. R. Frezzotti, K. Jansen, Nucl. Phys. B **555**, 432 (1999) [hep-lat/9808038]
32. P. de Forcrand, T. Takaishi, Nucl. Phys. Proc. Suppl. **53**, 968 (1997) [hep-lat/9608093]
33. I. Montvay, Nucl. Phys. B **466**, 259 (1996) [hep-lat/9510042]
34. R.G. Edwards, U.M. Heller, R. Narayanan, Nucl. Phys. B **535**, 403 (1998) [hep-lat/9802016]
35. T. Kalkreuter, H. Simma, Comput. Phys. Commun. **93**, 33 (1996) [hep-lat/9507023]
36. A. Morel, J. Phys. (Paris) **48**, 1111 (1987)
37. C.W. Bernard, M.F.L. Golterman, Phys. Rev. D **49**, 486 (1994) [hep-lat/9306005]
38. S.R. Sharpe, Phys. Rev. D **56**, 7052 (1997)
39. S.R. Sharpe, Phys. Rev. D **62**, 099901 (2000) [hep-lat/9707018]
40. S.R. Sharpe, R.L. Singleton, Phys. Rev. D **58**, 074501 (1998) [hep-lat/9804028]
41. W.J. Lee, S.R. Sharpe, Nucl. Phys. Proc. Suppl. **73**, 240 (1999) [hep-lat/9809026]
42. G. Rupak, N. Shoresh, Phys. Rev. D **66**, 054503 (2002) [hep-lat/0201019]
43. S. Aoki, Phys. Rev. D **68**, 054508 (2003) [hep-lat/0306027]
44. O. Bär, G. Rupak, N. Shoresh, Phys. Rev. D **70**, 034508 (2004) [hep-lat/0306021]
45. S.R. Sharpe, N. Shoresh, Phys. Rev. D **64**, 114510 (2001) [hep-lat/0108003]
46. TXL Collaboration, J. Viehoff et al., Nucl. Phys. Proc. Suppl. **63**, 269 (1998) [hep-lat/9710050]

47. F. Farchioni, R. Peetz, Eur. Phys. J. C **39**, 87 (2005) [hep-lat/0407036]
48. A.M. Abdel-Rehim, R. Lewis, R.M. Woloshyn, Phys. Rev. D **71**, 094 505 (2005) [hep-lat/0503007]
49. Particle Data Group, W.M. Yao et al., J. Phys. G **33**, 1 (2006)
50. F. Farchioni, C. Gebert, I. Montvay, L. Scorzato, Eur. Phys. J. C **26**, 237 (2002) [hep-lat/0206008]
51. J. Gasser, H. Leutwyler, Ann. Phys. **158**, 142 (1984)
52. S. Dürr, Eur. Phys. J. C **29**, 383 (2003) [hep-lat/0208051]
53. E. Witten, Nucl. Phys. B **156**, 269 (1979)
54. G. Veneziano, Nucl. Phys. B **159**, 213 (1979)
55. ALPHA Collaboration, J. Heitger, R. Sommer, H. Wittig, Nucl. Phys. B **588**, 377 (2000) [hep-lat/0006026]
56. S. Dürr, Z. Fodor, C. Hoelbling, T. Kurth, JHEP **0704**, 055 (2007) [hep-lat/0612021]